EARTHQUAKE RESPONSE OF LONG-SPAN SUSPENSION BRIDGES

by

Lawrence I. Rubin,
Ahmed M. Abdel-Ghaffar,
and Robert H. Scanlan

May, 1983

Report No. 83-SM-13

DEPARTMENT OF CIVIL ENGINEERING
PRINCETON UNIVERSITY
PRINCETON, NJ 08544

ACKNOWLEDGMENT

This report is based on the doctoral dissertation by Lawrence I. Rubin submitted to the Department of Civil Engineering of Princeton University on May 31, 1983 in partial fulfillment of the requirements for the Ph.D. degree. The study was directed by Ahmed M. Abdel-Ghaffar, Associate Professor of Civil Engineering and by Robert H. Scanlan, Professor of Civil Engineering. The research was supported by a grant (CEE-8017736) from the National Science Foundation (with Dr. John Scalzi as the manager) and the Department of Transportation (with Dr. James Cooper as the supervisor). Computer service support for some of the preliminary studies was provided by the School of Engineering and Applied Science and by the Department of Civil Engineering of Princeton University. The above noted support is gratefully scknowledged.

Any opinions, findings, and conclusions or recommendations expressed in this report are those of the authors and do not necessarily reflect the views of the National Science Foundation or the U.S. Department of Transportation.

TABLE OF CONTENTS

CHAPTER I

INTRODUCTION

I.1 GENERAL INTRODUCTION

The research work presented in this report is concerned, in general, with the earthquake response analysis of long-span suspension bridges when subjected to multiple-support seismic excitations. An earthquake dynamic-analysis methodology (which includes analytical and numerical methods; time and frequency domains; and deterministic and probabilistic techniques) for these structures is developed taking into account, among other things, the different seismic inputs at the support points of the bridge, the traveling wave effects, and the flexibility of the soils surrounding the foundations. The first phase of the investigation deals with the appropriate definition of seismic inputs (to permit estimation of relative motions between support points) taking into account the propagation, attenuation and phase characteristics of seismic waves as evident from existing and newly acquired strong-motion records [30]. The seismic inputs are time functions (such as time histories and cross-correlation functions) and/or frequency functions (such as power- and cross-spectral density functions). The form of these time and frequency functions is determined with the aid of available strong motion accelerograph records, random vibration theory and elastic wave propagation theory. In the second phase, the methodology of earthquake dynamic analyses of suspension bridges when subjected to multiple-support excitations is

developed utilizing analytical and numerical techniques (both including deterministic and probabilistic treatments). Earthquake response characteristics of three bridges selected to represent a wide band of suspension bridges are determined in the third phase and lead to definition of general earthquake resistance guidelines.

In the introductory chapter a comprehensive review is made of the literature related not only to the earthquake response of suspension bridges but also to their free-vibration dynamic-analysis methodologies. Existing publications on the characteristics of strong earthquake ground motions are also examined. And finally, a brief definition of the problem to be addressed in this report is made at the end of the chapter.

Before beginning the literature review, the following relevant observations and conclusions merit mentioning [19]:

1. The intensity of earthquake ground shaking attenuates with the distance from the causative fault more rapidly in the high frequency range than in the low frequencies. Consequently at considerable distances from the fault, structures which have long periods of vibration, such as long-span suspension bridges will be subjected to stronger shaking than will structures with short periods of vibration such as short-span bridges.
2. The effect of earthquake-induced differential motions of two or more foundations upon the dynamic response of the superstructure of a bridge is a little-understood problem which is of considerable interest in earthquake engineering [see 6, 17, 25, 24, 32, 42, 39, 106, 90-92]. The state-of-the-art does not yet offer a practicing earthquake engineer the means for making a good estimate of the differential pier and abutment (or anchorage)

displacement to be expected when a bridge is subjected to an earthquake. In all cases the definition of an appropriate ground-motion input is the most difficult and uncertain phase of the problem of predicting structural response to earthquakes. A common assumption in the usual treatment of earthquake excitations is that the same motion acts simultaneously at all points of the structure's foundation. If rotational motions are neglected, this assumption is equivalent to considering the foundation-soil to be rigid at least over a scale fully-enveloping the structure (though the soil may still be treated very locally as elastic). Another viewpoint of the same thing is that the wavelengths of the earthquake ground waves are long compared to the structural dimensions. Such a hypothesis is not wholly consistent with the concept of earthquake wave propagation; however, if the base dimensions of the structure are small relative to the vibration wavelength in the soil, the assumption is acceptable. For example, if the velocity of the wave propagation is 6,000 ft/sec, a sinusoidal wave of 3.0 Hz frequency will have a length of 2,000 ft, and a building with a base dimension of 100 ft will be subjected to essentially the same motions over its entire length. On the other hand, a long-span suspension bridge, which might have a length of several thousand feet, obviously would be subjected to drastically different motions at its foundations. No direct measurements have been taken of a bridge at two widely separated foundations during an earthquake; however during the 1971 San Fernando (California) earthquake (M_L = 6.3), the motions recorded by

instruments located in the basement of Millikan Library at one end of the campus of California Institute of Technology differed greatly from those of the instruments in the Caltech Athenaeum located approximately 800-1000 ft away at the other end [41]. Measurements taken during the 1979 Imperial Valley (California) earthquake (M_L = 6.6), by the instruments of the El Centro Array also emphasize the variation of ground motions with separation distance [30]. It is evident that the motions at the foundations of a long-span bridge must differ, and this difference could contribute significantly to the dynamic response of the structure; so it is important for design purposes to develop analytical procedures capable of establishing appropriate input motions and of dealing with multiple-support excitations.

In a study made by Abdel-Ghaffar [6,17], of the dynamic interaction, for incident plane SH-waves, between the soil of a half-space and a simple two-dimensional bridge model (supported by rigid end-abutments), it was found that the excitation of different modes of vibration of the bridge superstructure is related to the nature of foundation movement for different angles of incident SH-waves; in particular, it depends on the relative phase of motion for the two adjacent bridge supports. Even though the model studied was two-dimensional and therefore cannot be employed directly even with laterally elongated systems, knowledge about the interference phenomenon of waves scattered around different foundations and the different phasing of input motions along the extended structure may prove to be useful in clarifying some of the complexity of the dynamic

response of a more complicated three-dimensional system. The objective of such an investigation should not necessarily be to define all possible cases, but somehow to bound them in a reasoned way for design purposes.

3. The dynamic analysis of long-span suspension bridges under earthquake excitations has received some study to date [24, 34, 43, 44, 45, 50, 63, 87, 90-92, 106, and 103] but there remain aspects of it requiring further examination. For bridges of long span there are special features of the problem that differ significantly from the analysis of a typical multi-story building. Modern building codes have now been developed to the point where the basic earthquake-resistance requirements to be imposed on a standard building are specified adequately. A long-span bridge, however, is a vastly different structure from a typical building structure. The fundamental period of vibration of a suspension bridge, for instance, is usually long, and it is necessary to include a relatively large number of modes of vibration in order to obtain a reasonable representation of the response. Also, as discussed above, the piers or abutments of the bridge may be so far apart that the general motions at the two ends of the bridge are only partially correlated or are uncorrelated. In addition, bridges to date have not generally received the attention that buildings have with regard to full-scale testing, and to permanent earthquake-response instrumentation, which could provide data to correlate with linear or nonlinear response analyses.

4. Both theoretical dynamic analyses (including analytical and finite element techniques) and low-level full-scale ambient vibration tests of suspension bridges have indicated [1, 9, 24, 31, 43, 44, 87, 103] that modes of free-vibration of the structure can be separated into two groups. In one group, the displacements of the stiffening structures and cables are predominant, and in the other group, the displacements of the towers are predominant. Consequently, with proper attention to modeling, investigation of the earthquake response characteristics of different major parts of the suspension bridge may be made separately. For example, an earthquake-response analysis may be made in which the influences of the cables and suspended structures are represented by the proper masses and spring stiffnesses at the top or support points of the towers. Definition of the exact methodologies needed for such modeling of analysis can be extremely useful in design.

5. From the three-dimensional finite element analysis of San Francisco's Golden Gate Bridge by Baron and his co-worker [24], it was observed that the modes of vibrations of such a bridge can conveniently be grouped into four kinds of simply conceived oscillatory motions, namely: vertical, lateral, torsional and longitudinal. For certain bridges, especially those with straight and level decks, the vertical and torsional motions are quite well decoupled, if one considers only small vibrational amplitudes (linear theory). But for other bridges (the Ruck-a Chucky [35] or the Lions' Gate [31,67] designs, for example) such decoupling does not occur, due to geometric effects.

6. Assurance of the aerodynamic stability of suspension bridges does not in any way imply the safety of the structures during earthquake ground shaking. Both the inputs and the responses, as well as the possible modes of failure, are different for the two kinds of excitation. In particular, analysis of torsional and flexural-torsional vibrations is central to studies of the aerodynamic behavior of suspension bridges, whereas its importance to earthquake response analysis is less clear.

I.2. FREE-VIBRATION ANALYSIS OF SUSPENSION BRIDGES

The collapse of the Tacoma Narrows Suspension Bridge in 1940 attracted the attention of the engineering profession towards studying the vibrational characteristics of suspension bridges and their associated aerodynamic response. The slender bridge vibrated heavily in flexure and torsion and collapsed in a transverse wind of only 40 miles per hour. It was quite natural that the engineering profession concentrated its efforts upon the aerodynamic response of suspension bridges at this time, delaying the analysis of earthquake response of such structures until fairly recently. Researchers such as F. Bleich [26-28], T. Von Karman [96], G. Woodruff, C. McCullough, C. Scruton [74], G. Vincent [93-95], L. S. Moisseiff [60,61], F. Smith, F. Farquharson [33], D. B. Steinman [80-84],O. H. Ammann [20,21], A. Selberg [76-78], R. Frazer and R. H. Scanlan [72,73] are well-known for their work in the aerodynamic response of suspension bridges. Lately, the response of suspension bridges to other dynamic loadings, such as railway impact loadings (Hirai and Ito [36]), and seismic disturbances have been investigated with more enthusiasm.

The earliest treatments of the dynamic analysis of suspension bridges for their natural modes and associated natural frequencies began with Rohrs' [69] analysis in 1851 of an inextensible horizontal cable for the first two natural modes. Not much significant dynamic analysis occurred until the Tacoma Narrows collapse, at which time investigations by Rannie [68], Von Karman [96], and Vincent [79,94] analyzed the vibration of a three-span cable. In addition, in 1941-43, Steinman [81] proposed simpified formulae for the calculation of vertical and torsional frequencies and modes of vibration. Later, Bleich [26] proposed the analysis of free torsional and vertical vibration by the exact solution of the fourth order differential equations of motion. He also proposed a Rayleigh-Ritz procedure for obtaining the first few modes and frequencies of vertical and torsional vibration. Other formulae appeared by Smith and Vincent [79] but were misleading because the cable was assumed inextensible, and its gravity stiffness, which Pugsley had examined [64-66], had been ignored.

In the early 1960's, the dynamic analysis of suspension bridges received considerable attention by Konishi, Yamada, Takaoka, and other Japanese investigators [43-49,101-106]. These authors examined the vertical and lateral vibration of the bridge as well as the vibration of the tower-pier system using a lumped-mass matrix structural analysis approach. They pointed out that both the ground-acceleration and the ground-displacement are required as inputs for the computation of earthquake response of suspension bridges. They also suggested that since the modes of the suspended structure and the tower-piers are fairly well decoupled, the tower-pier vibration problem may be approximately analyzed separately from the suspended structure, as long as the elastic restraint at the top of the tower provided by the cables is accounted for properly.

In this manner, the effect of foundation-soil stiffness upon the tower-pier response can be examined rather efficiently. They indicated that in the first few modes of lateral vibration, the suspended structure and cables vibrate as a double pendulum, while in higher modes the system vibrates independently and there is no coincidence of nodal points of the cable and suspended structure.

Similar investigations were performed by Tezcan and Cherry [87,88] in 1969, considering the effect of geometric nonlinearity arising from large deflections of suspension bridges. An iteration scheme for the nonlinear static analysis was performed by means of tangent stiffness matrices, and these matrices were used to solve for the free vibration modes of the structure. The bridge was idealized as a three-dimensional lumped mass system subjected to three orthogonal and uniform ground motion components producing horizontal, vertical and torsional vibrations. A similar design analysis for the tower-piers of the Tagus River Bridge, using a lumped mass system which was interconnected by elements having shearing and bending stiffnesses, was pursued by Housner, Converse, and Clough [37]. In this work, the rotational stiffness of the foundation was also considered.

The most recent significant advances in the linear dynamic analysis of suspension bridge structures appeared in the 1970's through the work of Abdel-Ghaffar [1,5,6,9,13,18]. This involved methods of analyzing the free vibration of suspension bridges utilizing finite element methods and linearized deflection theory. Abdel-Ghaffar analyzed vertical, torsional, and lateral vibration of suspension bridges for natural frequencies, mode shapes, and energy storage capacities of different members of the structure. His methods were based upon specification of the potential and

kinetic energies of the vibrating members of the real continuous structure, derivation of the equations of motion for each type of vibration (vertical, lateral, and torsional), linearization of these equations for small amplitudes, finite element discretization of the structure, derivation of stiffness and inertia properties of the structure, and formulation of the matrix equations of motion and eigenvalue problems using Hamilton's principle. Detailed examples were presented by Abdel-Ghaffar, including an analysis of the free vibration modes of the Vincent-Thomas Bridge, in Los Angeles, California. The applicability of such methods was demonstrated by comparing analytical results with full-scale ambient vibration-test results [1,3,7,8]; an excellent agreement was attained. The effects of cable extensibility, tower stiffness, and suspended structure continuity were closely examined by Abdel-Ghaffar [1].

In the 1980's, Abdel-Ghaffar and Rubin investigated the large amplitude geometrically nonlinear coupled vertical-torsional vibrations of suspension bridges [10,11]. Their analysis involved a continuum approach for the nonlinear free coupled vertical-torsional vibrations of suspension bridges with horizontal decks. Approximate solutions to the nonlinear coupled equations were developed using the method of multiple scales (a perturbation technique), and compared to direct numerical integration of these equations of motion. The geometric nonlinearities included in the analysis arose from the large deflections of the cables, the axial stretching of the stiffening structure when hinges were immovable, and the nonlinear curvature of the stiffening structure. The amplitude-frequency relationships were investigated, and the exchange of energy between torsional and vertical modes closely-spaced in the frequency domain was observed. It was found that the geometric nonlinearities are only important under very high amplitude vibration. Therefore, in most cases, a geometrically linear analysis is appropriate for suspension bridges.

I.3. EARTHQUAKE RESPONSE ANALYSES OF SUSPENSION BRIDGES

During the last two decades, the seismic response of suspension bridges, using the concept of a discrete spring-mass system as well as the finite element approach, received considerable attention by Konishi, Yamada, Takoaka, Kuribayashi, and other Japanese authors [43-49,51-57,86,89 101-106]. In their approach the authors separated the bridge into the tower-pier system and the suspended structure system, each type of vibration to be studied separately. Thus, the response analysis of the tower-pier system was made separately from the vertical and lateral response of the suspended structure and cables by utilizing a partial model where the tower and physically equivalent effects of cables were considered in an approximately applicable manner. This enabled the response of the tower-pier system, the most critical element in the suspension bridge, to be examined more closely. For example, in 1969, Takaoka [86] examined the effect of foundation flexibility upon the dynamic response of the tower-pier. His results indicated that the flexibility of the foundation is very important in designing the tower-pier system of long-span suspension bridges that are founded on relatively soft soil. The flexibility affected the natural frequencies and modes of vibration of the tower, and increased the response bending stresses. In 1969, Konishi and Yamada [45] also pointed out that the rocking motion of the pier has a significant effect on the response stresses and bending moments in the tower, and thus the estimation of properties of the soil underlying the foundation is quite important. They suggested that if an accurate estimation of these soil properties is unavailable from field tests, a range of values must be considered in the design process. In the analysis of the response of the suspended structure and cables, Konishi and Yamada [43]

assumed the ground motion as a simple harmonic, and applied this motion to each support point (anchorages and tower-piers) separately. Since the towers and anchorages are connected by cables, both acceleration and displacement ground motion inputs were needed. Phase differences of ground motion at support points were accounted for by adding the response results graphically to obtain maximum bending moments and maximum stresses. It was found in both the vertical and lateral response studies that the higher mode contribution to the bending moment was fairly significant, that is, the inclusion of many modes was needed for an accurate determination of the response of suspension bridges.

In 1969, Tezcan and Cherry analyzed the three-dimensional response of suspension bridges to three orthogonal components of uniform earthquake ground motion [87]. They concluded that the vertical vibration of the tower and the longitudinal vibration of the bridge deck are small and thus may be neglected. They considered the torsional vibration of the bridge deck coupled with lateral vibration of the towers as well as the vertical vibration of the bridge deck coupled with the horizontal vibration of the towers in the longitudinal direction. In 1980, Irvine [40] proposed a simplified formula to calculate the peak additional cable tension that can be expected in a suspension bridge undergoing uniform earthquake excitations. In his analysis, the inputs to the cable were assumed in phase, so that the effect of longitudinal inputs cancelled each other, and only vertical inputs remained. With the phasing of inputs not considered, Irvine seriously underestimated the additional response cable tension. Also, the effects of the stiffening truss as well as the tower compliance were completely neglected in his analysis.

Abdel-Ghaffar and Rood [14,70] presented a simplified analysis to study the earthquake response of the suspension bridge tower using a continuum model. Their study consisted of two parts: the free vibration of the tower, and the earthquake response of the tower using selected earthquake ground motions. Also investigated was the influence of the suspended deck and the soil flexibility upon the alteration in modal configuration of the suspension bridge tower. The response stresses, displacements, and shear forces for the Golden Gate and Vincent-Thomas bridge towers were determined for a simplified model fixed at the base, using modal analysis, by both time integration and response spectra techniques. High values of live load earthquake-induced stresses were predicted by the simplified model. The main criticism of their method lies in the averaging of the properties of the tower over its height inherent in the continuum formulation as well as the neglect of the pier-foundation system. Usually, the properties of the tower vary considerably over its height, and hence a finite element formulation would be more appropriate. Also, the response was only evaluated for the fixed base case; that is, the effect of foundation flexibility was not considered. However, their study did show that the stresses expected in a suspension bridge tower during a seismic event are to be considered significant live loads in the design of such a structure.

I.4. MULTIPLE-SUPPORT SEISMIC INPUT PROBLEM

A common assumption in the usual treatment of earthquake excitations is that the same ground motion acts simultaneously at all points of the structure, which is equivalent to stating that the wavelengths of the ground waves are long compared to the structure's dimensions. For a long

extended-in-plane structure such as a suspension bridge, it is obvious that the structure would be subjected to different motions at its foundations. Konishi and Yamada [43] realized this when they accounted for phase differences at support points by graphically adding the results from each input to obtain maximum bending stresses. This method was rather crude however and the need to develop procedures capable of establishing appropriate input motions and of dealing with multiple-support excitations soon became apparent.

In 1965, Bogdanoff, Goldberg, and Schiff were among the first investigators to consider the transmission time of a seismic disturbance in considering the response of a long-span suspension bridge [29]. Their suspension bridge model was a simplified spring-mass arrangement, and they analyzed the random response in terms of extreme values, that is, in terms of return periods and probabilities of survival. They utilized a random input to the structure, which resembled a decaying sinusoid, and was assumed to propagate from left to right at constant velocity. Thus phase delays existed at the support points of the bridge (anchorages and tower piers). The equations of motion of the structure were derived using Lagrange's equations, with viscous damping included in the analysis. The results of this response analysis showed that the transmission time, and therefore the phasing of support motions, are very important in long-span structures. Their results showed that compared with the case of simultaneous support excitations, the propagating input resulted in a much more severe response. Therefore, the transmission time of a seismic disturbance cannot be ignored when considering the safety of long-span structures.

In 1976, Abdel-Ghaffar [2,4,17] studied the dynamic interaction, for incident plane SH-waves, of a simple two-dimensional bridge model with the soil half space. He found that the excitation of different modes of vibration of the bridge superstructure depends on the relative phase of motion for the two adjacent supports. Specifically, when two abutments move in phase there is a tendency to excite symmetric modes of girder vibration, and conversely, when the two abutments are moving out of phase the anti-symmetric modes are excited effectively. He also showed similar conclusions by studying a simply-supported horizontal beam subjected to sinusoidal motions of varying phase at its supports. Research work done by Masri [59,60] on the response of beams and cooling towers to propagating boundary excitations exhibited similar behavior.

In 1979, Werner, Lee, Wong and Trifunac [97-100] developed methods to analyze the three-dimensional response of simple bridge structures on an elastic halfspace subjected to incident P-waves, S-waves, and Rayleigh waves. Their results showed that the importance of traveling wave effects upon the response, becomes more pronounced when the wavelengths of the incident waves are equal to or less than the foundation dimensions. They noted that non-vertically incident SH-waves lead to the torsional excitation of the structure, non-vertically incident P-waves and SV-waves lead to rocking excitation, and traveling Rayleigh waves can excite all six components of response. They also pointed out the lack of suitable recorded strong-motion data necessary to specify spatially varying input motions for seismic analysis, and the lack of available engineering guidelines for assessing the behavior of structures subjected to traveling seismic waves. They concluded that phase differences in the input ground motions applied at the bridge foundations can have significant effects upon the bridge

response, and that it is important to consider traveling wave effects when designing earthquake resistant long-span structures, using real spatially varying ground motion records as inputs.

In 1976, Baron, Arikan, and Hamati [24] analyzed "The Effects of Seismic Disturbances on the Golden Gate Bridge." This report was intended to supplement the studies made by the designers of the bridge. They studied the response of the bridge to both uniform and propagating ground motions. He utilized the 1952 records of the Taft earthquake and an artificially-generated ground motion intended to be above 8.0 in Richter magnitude. The artificially-generated earthquake was used for the propagated ground motion, as well as a more basic type consisting of three consecutive sine waves propagating at a constant speed. They performed time-history and response spectra analyses for the uniform input case and time-history analyses for the propagating cases, calculating maximum values of response stresses for selected elements of the bridge. These calculations indicated that certain elements of the bridge (notably at the tower base) could be overstressed (exceed their yield value) during a strong earthquake (above 8.0 in Richter magnitude). Therefore, the earthquake loading of suspension bridges is most important for design purposes.

From the above-mentioned investigations it seems that the accuracy of calculated response characteristics for long-span bridge structures depends upon a sound knowledge of the expected ground motions at different supporting sites. Earthquake ground motions in the three orthogonal directions of a long-span bridge may be transmitted to the superstructure through the two tower bases (piers) and the two abutments or anchorages, as illustrated by Fig. I-1 for a suspension bridge. The bridge may be

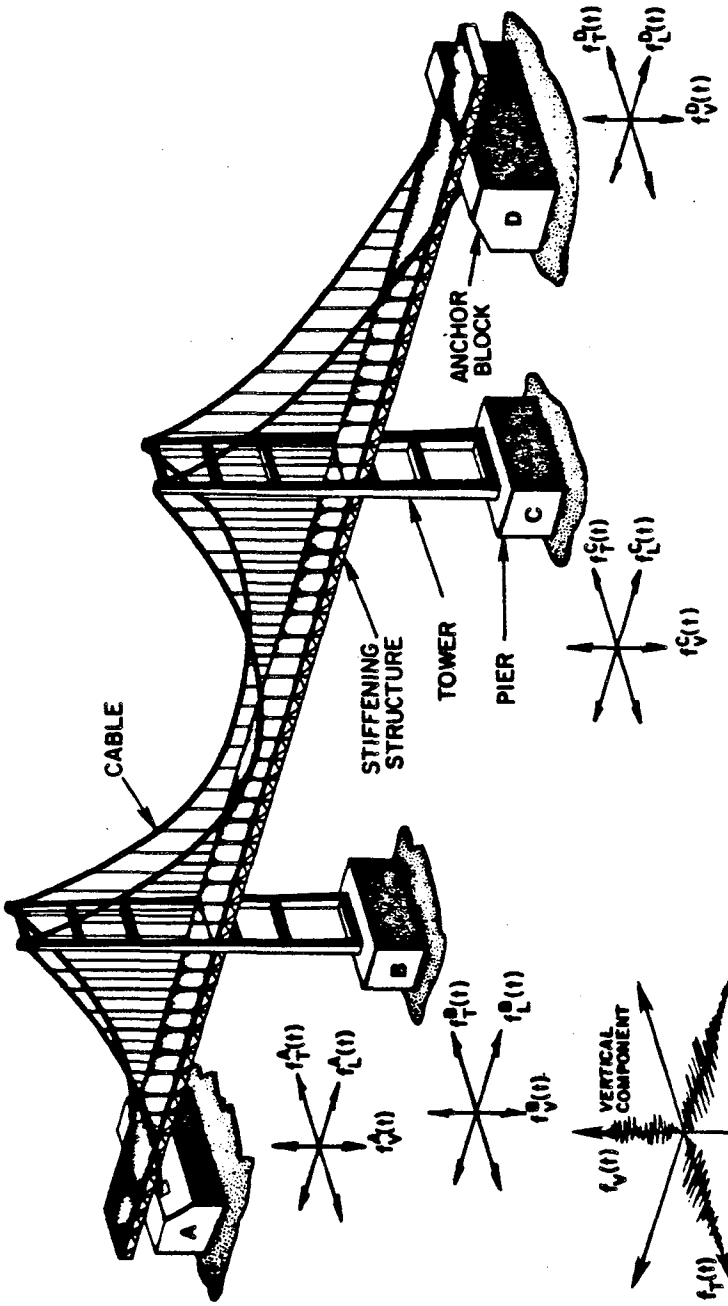

Fig. I-1. A typical three-dimensional suspension bridge subjected to multiple seismic input motions at its supporting points. (Ref. 19)

long with respect to the wavelengths of motion in the frequency range of importance to its earthquake response. Because of this fact, different portions of the bridge can be subjected to significantly different excitations, a problem not normally important for buildings. The essential feature of this problem is that the motion at the supporting points a given distance apart on the surface of the ground may receive long period earthquake motions that are nearly equal, but experience short period motions that are dissimilar and uncorrelated. In general, the correlation of the motion at these support points (Fig. I-1) is extremely complicated, particularly in the case of a long-span bridge, with different foundation conditions, subjected to seismic waves with different angles of incidence and different travel paths (reflections and refractions, etc.). In that case, marked differences in amplitude as well as phase could occur over distances of the order of a few wavelengths of the motion. However, when the dynamic behavior of a bridge structure subjected to multiple seismic excitations is investigated, some types of correlational relations (based on real observations or on reasonable assumptions) can be drawn between the seismic inputs.

For determining appropriate seismic inputs to be used in earthquake response analysis of these long structures, it may be suggested as a first step to adequately assess the differences that might occur at separate support points. First, the input motion has to be resolved into its apparent horizontal velocity and wavelength along the line determined by the points of concern. This resolution is necessary because waves of the same propagational speed may have different apparent velocities and wavelengths, depending on the angles of horizontal and vertical incidence. Secondly, estimation of the frequencies at which the problem

of phase and amplitude correlation may start to appear has to be made. This is perhaps best approached by examining the relation between wavelength and frequency (or period). For bridges located within the epicentral region (approximately 10-15 miles from the epicenter) the exciting shear motion comes directly from the fault slipping, while for bridges at some distance from the epicenter the exciting shear motion could result from propagating surface waves such as Love and Rayleigh waves; Fig. I-2 shows the different particle (or ground) motions in a typical earthquake. Assuming, as in the latter case, that the transverse support motion is due to a shear wave propagating in a direction parallel to the longitudinal axis of a long-span bridge (where particle motion is in the transverse direction) the uniformity of the support motion becomes a function of the span length as shown in Fig. I-3a. The shear wave velocity C_s in firm basement rocks ranges from 1000 to 2000 ft/sec, and the predominant earthquake period T_s causing maximum ground accelerations lies between 0.2 and 0.5 seconds [75]. Hence the wavelengths of the propagating waves (given by $\lambda = C_s T_s$) are of the order of 200 to 1000 ft and consequently for the case of earthquake motion approaching the bridge parallel to its axis, a span of or less than say 50 to 250 ft is necessary for a reasonable uniform base excitation [71]; (i.e., $\ell (\text{or } \ell_1) < \frac{\lambda}{4}$). Thus, if one-fourth of a wavelength is taken as a characteristic length beyond which significant differences in phase might occur, and if two wavelengths are taken as a representative length beyond which the motion may be poorly correlated in amplitude as well as phase (as suggested by Jennings, Ref. 41), the following relations result:

$$T_\theta = \frac{\ell}{2C} \quad \text{or} \quad \frac{\ell_1}{2C} \qquad \text{and} \qquad T_A = \frac{4\ell}{C} \quad \text{or} \quad \frac{4\ell_1}{C} \quad . \qquad \text{(I-1)}$$

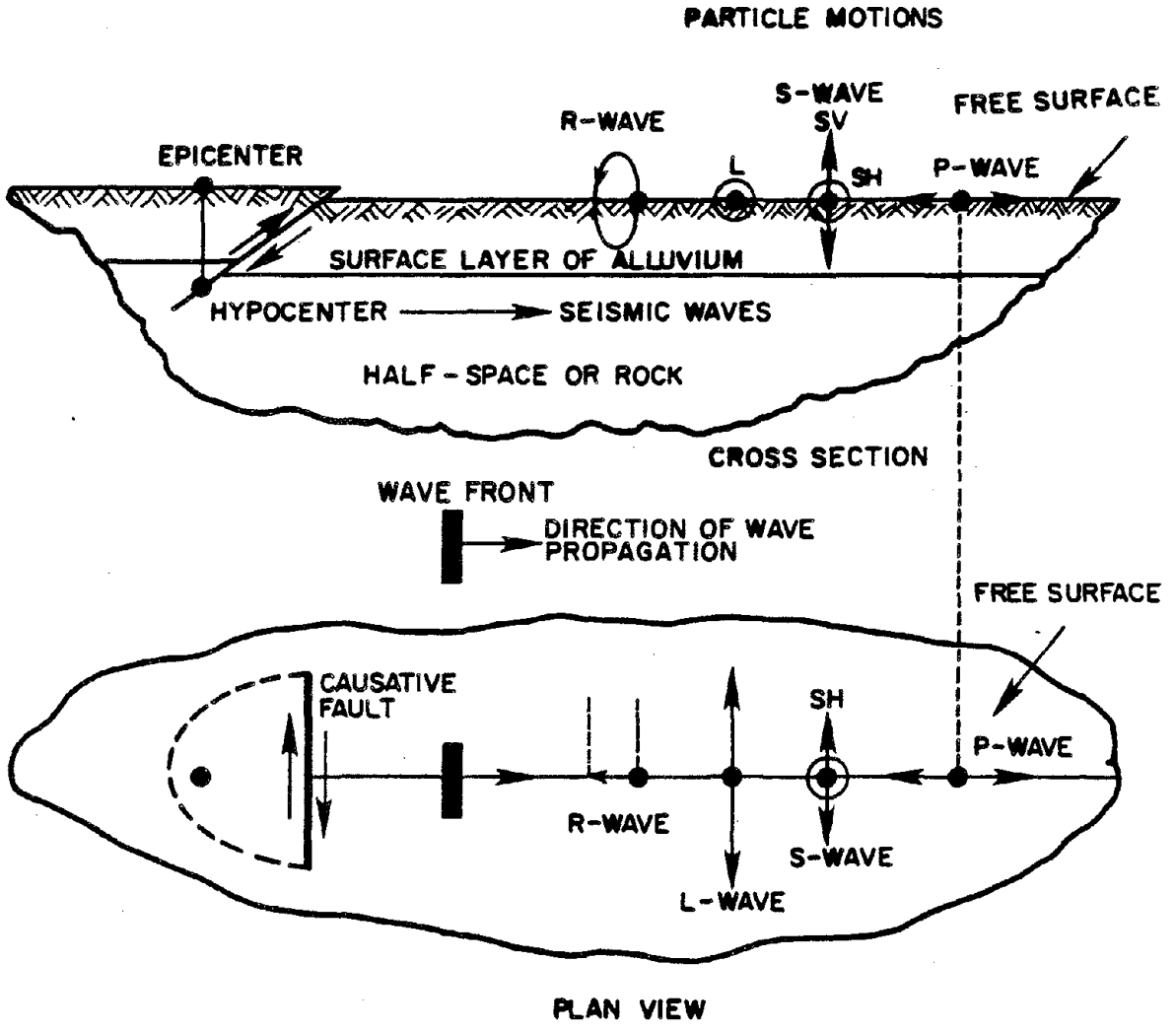

Fig. I-2. Particle (or ground) motions in a typical earthquake. (Ref. 19)

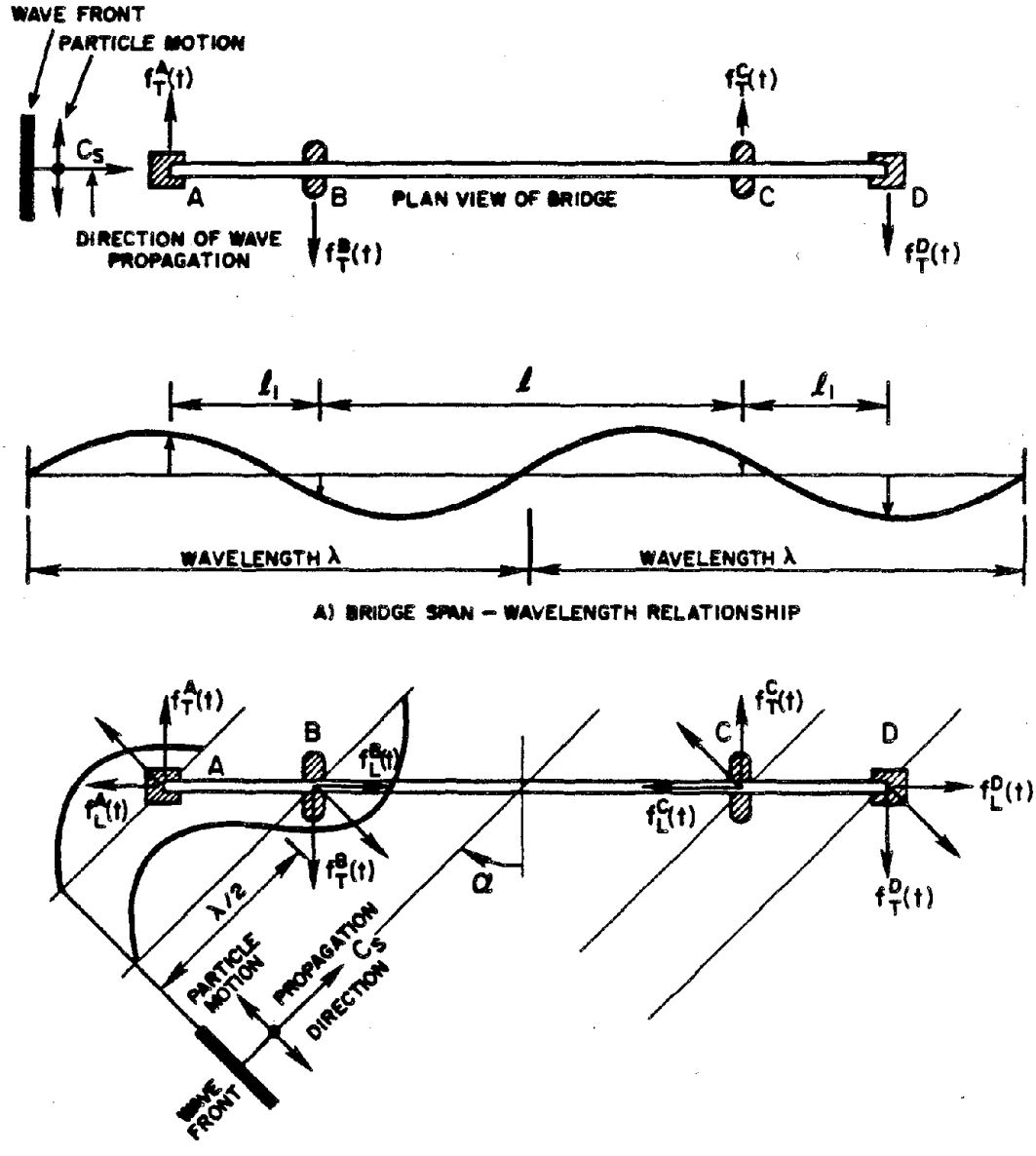

Fig. I-3. Phase difference resulting from incident earthquake waves (Ref. 19).

In these relations, T_θ is the period in seconds beyond which phase differences may be a problem, T_A is the period beyond which amplitude correlations may be weak, ℓ (or ℓ_1) is the separation distance of two support points (center or side span length), and C is the horizontal velocity of the assumed wave motion in the direction of concern.

An oblique angle of approach of a traveling shear wave, as shown in Fig. I-3b, raises the possibility of phase differences in the transverse (lateral) exciting motion when one considers the magnitude of the support length relative to the effective wavelength $\lambda/\cos\alpha$ in the transverse direction. Also, in such a case, as indicated by Fig. I-3b, longitudinal as well as lateral vibrations would be induced in the bridge. Phase differences in the support motions (in both transverse and longitudinal directions) would considerably influence the nature of the dynamic response of a bridge to an earthquake.

Based on the above discussion an effort may be made to consider the following cases in defining the seismic inputs [19]:

1. Earthquake motion is idealized as a single (non-dispersive) wave, propagating horizontally (as shown in Fig. I-3). In this case the differences in excitation at two separate support points are limited to differences in phase, and some amount of time delay between the support points has to be considered.
2. Earthquake motion is idealized (as either a single or train of wave(s)) such that the effects of topography, different angles of incidence, different travel paths and different local geology conditions are considered. In this case, marked differences in amplitude as well as phase are encountered. Steady-state excitations with different amplitudes and phases at different support points, could make a good approximation to examine this case.

3. Statistical study of some existing strong earthquake ground-motion records is pursued in this analysis (by using time and spectral analysis of classical random vibration theory). This step clarifies the differences between ground motions at one location and at another nearby (within the range of a bridge span) from the viewpoint of the propagation, attenuation and phasing of the seismic waves. And conditions are sought which most fully "exercise" the given structure, given the basic equation (or curve) spectra at the input points. The study does however require knowledge of the absolute time of the recorded traces to enable accurate synchronization of accelerographs located at any distance so that exact phase relationships can be established.

For a statistical description of appropriate ground shaking at different supporting points, well-recorded earthquakes such as the 1971 San Fernando (California) earthquake (M_L = 6.3) and the 1979 Imperial Valley (California) earthquake (M_L = 6.6), where numerous scattered records were recovered at different distances from the causative fault, are utilized as demonstrated by Fig. I-4a. Cross-correlation and cross-spectral density functions are produced indicating the probabilistic character of the multiple-seismic inputs of the earthquake problem. This procedure supports the view that the most appropriate procedure for selecting design earthquake ground motions is to extrapolate directly from comparable recorded accelerograms, or to use artificially simulated earthquakes conforming to the anticipated seismic exposure. In this analysis the above computed curves are smoothed and then

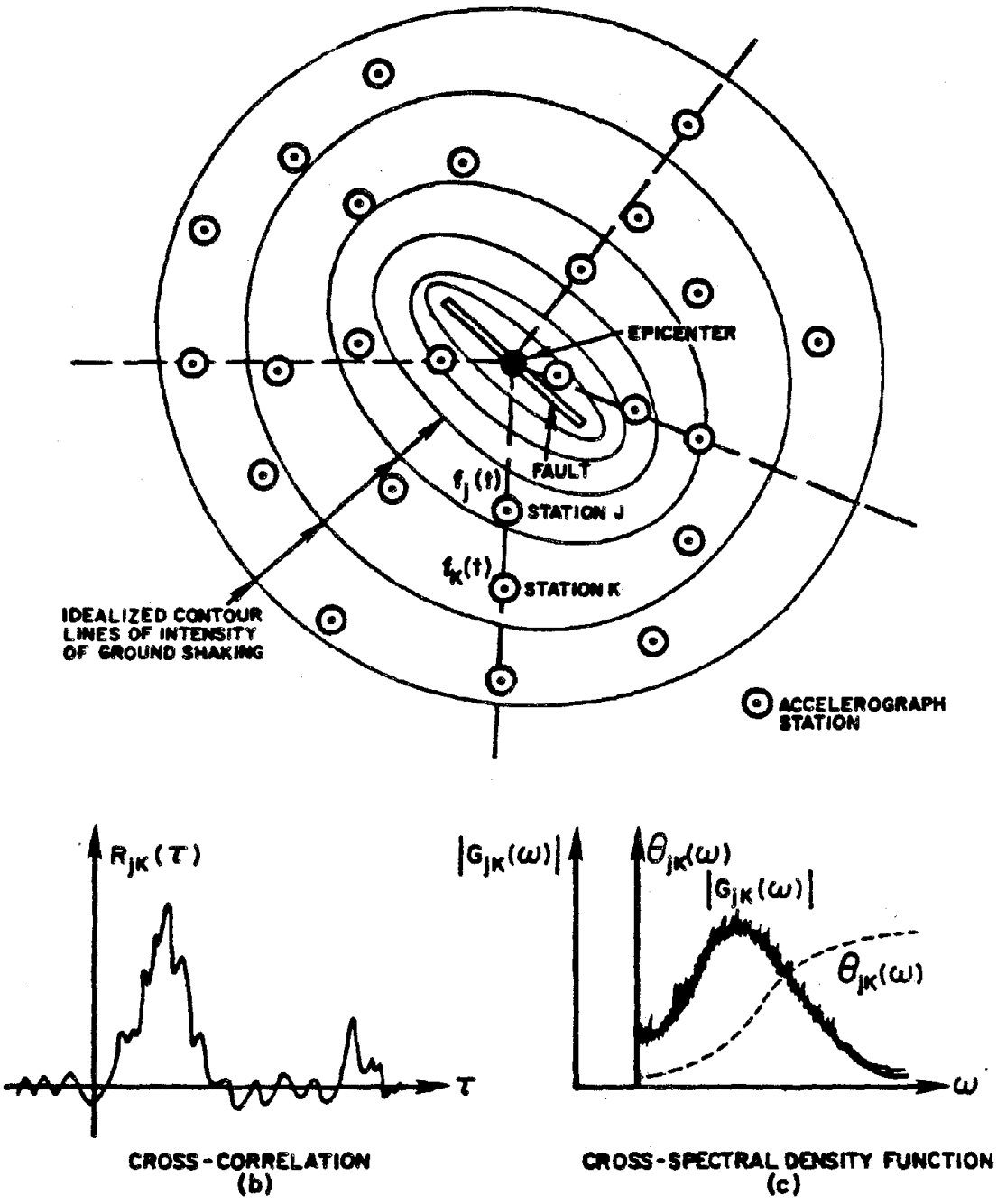

Fig. I-4. Time- and frequency-domain correlation study. (Ref. 19).

used in the earthquake response analysis. This family of curves could also be useful for studying the response of other extended structures, such as pipelines, power lines and large dams, to earthquakes.

It should be noted that in all three of the above cases certain sophistications of the design inputs should be included to allow for several parameters which, varying from site to site, could have a significant effect on the reliability of the proposed inputs; such parameters include: surface waves, oblique transmission of waves through the soil, the effect of reflection and refraction at the interfaces of different soil layers (or deposits) underlying the structure, the source mechanism of the earthquake producing the ground motion, the distance of the earthquake source from the site, and the local geology conditions of the supporting site. It also would be of use to statistically study the frequency of occurrence of strong earthquakes in zones where a wide class of suspension bridges are (or are planned to be) located. Even considering these factors, it must be remembered that the design ground shaking will not by itself predict how a specific suspension bridge will perform during a specific future earthquake, but it can be helpful in realistically creating and modifying the rules and regulations used in the design, strengthening or repair of bridge structures.

I.5. SCOPE OF PRESENT STUDY

The present study intends to investigate (analytically and numerically) the earthquake response of long-span suspension bridges when subjected to multiple-support seismic excitations. For many types of structures, the vertical component of ground motion may not be important; however,

for long-span suspension bridges vertical ground motion is important in itself as well as in its excitation of three-dimensional motion of the bridge. Support motions applied in any one of the three orthogonal directions (see Fig. I-1) will generally yield dynamic forces about the three axes of the bridge. For instance, the vertical component of ground motion is likely to excite vertical, torsional and coupled flexural-torsional vibrations and possibly longitudinal vibration, while the transverse component is likely to excite lateral, torsional and coupled bending-torsional motion, and finally the longitudinal component is likely to excite both vertical and longitudinal vibrations of the bridge. Factors such as coupled vibration, multiple-support excitations, and long natural periods of vibration all tend to increase the participation of a large number of modes in the total response of the structure. An important question to be answered in this proposed study is: how many modes are needed for a representative response of these flexible structures? Another question: is the current response spectrum method of dynamic analysis applicable in any sense to this problem and what is its range of applicability? Also, the interaction of superstructure components with each other and with the substructure will be studied.

The dynamic response analysis methodology is developed and refined taking into account the different seismic inputs at the support points of the bridge (anchorages and tower-piers). Appropriate ground motion inputs are taken from existing ground motion records recorded at time-synchronized closely-spaced stations, such as the 1979 Imperial Valley El Centro Arrays. The El Centro 1979 earthquake records were chosen because the recording stations (or arrays) were closely spaced to each other in the vicinity of the causative fault and were aligned approximately

along and transverse to the fault. The 1979 earthquake, which is considered to be the largest in California in the last quarter century, generated the most comprehensive set of data on ground shaking yet recorded from a damaging earthquake anywhere in the world (and can be appropriately used for studies of multiple-supported and extended structures). An equivalent seismic study of suspension bridges by Stringfellow [85] investigated the effect of propagating ground motions upon bridge response. In the present study, different ground motions are simultaneously applied at the bridge's support points, and the response of the bridge is calculated.

In the definition of the three-dimensional suspension bridge structure appearing in Fig. I-1, the main structural elements of the bridge are the tower-piers, anchorages, cables, and stiffening structure. The motion of a horizontal suspension bridge may be classified as vertical, torsional, and lateral, as shown in Fig. I-5 [1]. In the vertical motion, all points on a given cross section of the bridge move the same amount in the vertical direction, and they remain in phase (Fig. I-5a). In the torsional motion, each cross section of the bridge rotates about an axis which is parallel to the longitudinal axis of the bridge and which is in the same vertical plane as the centerline of the bridge. Points on opposite sides of the roadway move with equal displacements, but with opposite phase (Fig. I-5b). Finally, lateral motion involves the pendular swinging of each cross section in its own vertical plane, with an upward movement of the cables and suspended structure associated with their lateral movements (Fig. I-5c).

As shown in Fig. I-1, the seismic inputs to the bridge are the three orthogonal components of ground motion (vertical, transverse, or lateral,

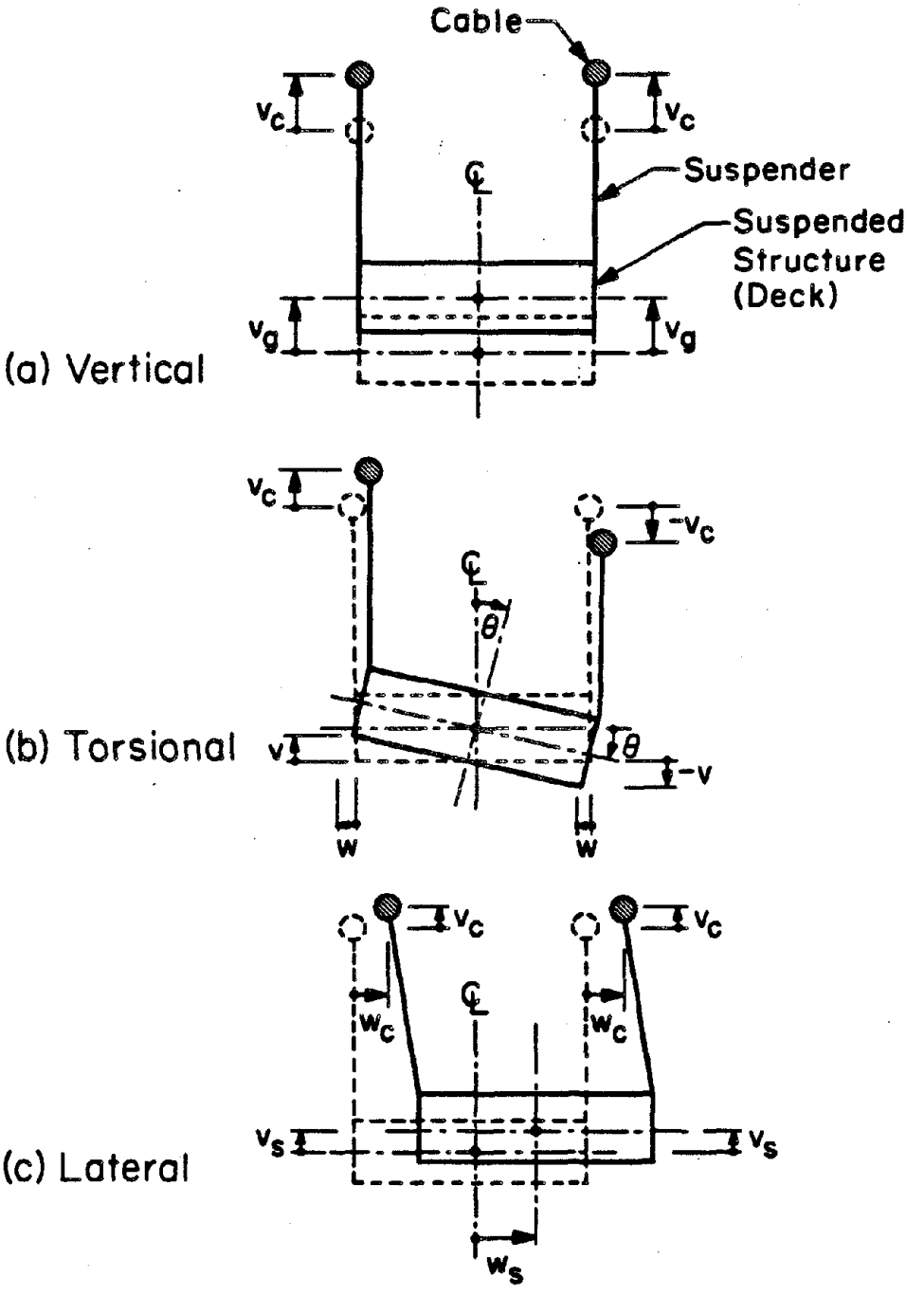

TYPES OF VIBRATIONAL MOTION IN SUSPENSION BRIDGES

Fig. I-5.

and longitudinal) occurring at each support point of the bridge (anchorages and tower-piers). It is very important to note that the motions at each support point are different from each other because of different foundation conditions, subject to seismic waves with different angles of incidence and different travel paths. Therefore, differences in amplitude as well as phase could occur for any long-span structure, such as a suspension bridge. Figure I-3 [19] shows, in a qualitative manner, the phase differences which could arise from a shear wave traveling along the longitudinal axis of the bridge or at an oblique angle to this axis. It is seen that because the seismic wavelengths are of the same order of length as the bridge span lengths, marked differences in phase occur at the bridge's support points. In addition to these phase differences, one would also anticipate amplitude attenuation as well as differences in frequency content due to faster attenuation of the high frequency components of ground motion. Because of all these inherent complications, it was decided that the utilization of real ground motions recorded at separation distances consistent with the dimensions of a suspension bridge would be most valuable for this type of extended structure. It should be mentioned that although the analysis in this report deals most directly with suspension bridges, the proposed methodology, when cast in its most general sense, can be applied to any extended-in-plane lifeline structure. For example, Iliescu [38] utilized some of these methodologies in analyzing the Melloland Bridge, a fairly short-span highway bridge. In this analysis the traveling wave effect was found to be significant upon the response of this bridge, even with its relatively short-span length.

The study which follows develops methods to analyze the dynamic response of suspension bridges to multiple-support seismic excitations.

These methods are utilized to analyze the response characteristics of three different suspension bridges: The Golden Gate Bridge in San Francisco, California, a relatively long-span bridge; The Tacoma Narrows Bridge in Tacoma, Washington, an intermediate-span bridge; and the Vincent Thomas Bridge in Los Angeles, California, a relatively short-span suspension bridge. The input ground motions utilized are mostly taken from the 1979 Imperial Valley earthquake, from the El Centro Arrays which are closely-spaced recording stations. In addition, selected responses are calculated using 1971 San Fernando ground motion records, as well as artificially-generated ground motions, for the sake of comparison.

As indicated previously, investigation of the earthquake response of different members of a suspension bridge may be made in separate parts. Accordingly, the earthquake response analysis of suspension bridges may be separated into the following sections:

i. Analysis of the Towers: An equivalent finite element model of the towers, subjected to longitudinal ground motion at the base will be developed and studied. The idealization of the tower and its various components will take into account the effects of substructures (pier systems), foundations and surrounding soils to obtain an adequate description of the various types of vibrations that can occur and to produce realistic results consistent with the input ground motions.

ii. Analysis of Cables and Suspended Structures: The coupled vibrational response of the cables and suspended structures to multiple-support excitations is considered; both an analytical model of

continuous structure and a finite element model is analyzed. For the general inputs, symmetric (or in-phase) and antisymmetric (or out-of-phase) cases can be treated separately in the linear analysis of the cables and suspended structures as shown in Fig. I-6, and the response of the structure can be obtained by superposition of the response to each independent input. The analytical approach (as a first step) is a reasonable way to determine the importance of various parameters controlling the bridge performance, to explore the critical requirements of analysis and design, and to pave the way for a more economical and reliable use of the finite element technique.

The analysis developed here will provide a basis for establishing new earthquake-resistant design criteria and acceptable damage levels for a wide class of suspension bridges. Procedures for enhancing the seismic resistance of existing bridges will also be discussed.

From the earthquake engineering and structural dynamics points of view, the minimum number and proper location of permanent instruments to record strong ground motion, on and in the vicinity of suspension and cable-stayed bridges, is very important. Proper placement will yield information about the response of the bridge components, the nature of different modes of vibration and the coupling of these modes. Information indicating the effects of soil-bridge interaction and, possibly, the damping of the structure as well as the phase differences in the ground motions at the piers and anchorages may also be obtained. Suggestions regarding the type and location of strong-motion instruments best suited for measuring earthquake response will be made, assuming both an ideal set of circumstances and economic limitations.

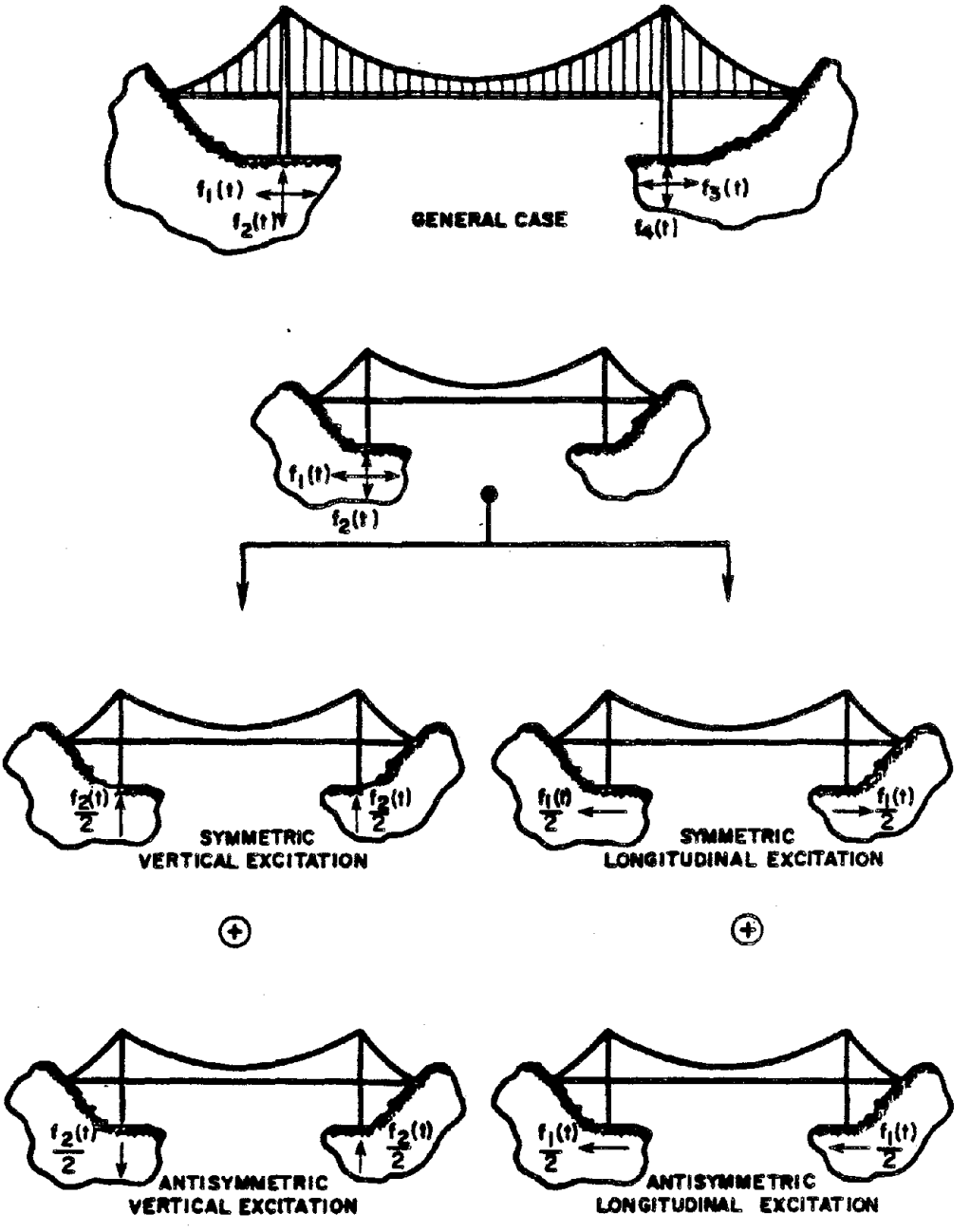

Fig. I-6. Symmetric and antisymmetric response studies. (Ref. 19)

The report is divided into six chapters, the first of which is this literature review and scope of work chapter. Some of the work appearing in the following chapters have appeared in published form in less detail than will be presented herein [see 12,15,16]. Chapter II deals with the vertical vibration of suspension bridges to multiple-support seismic excitations. The equations governing the response displacement, moments, stresses, and shear forces in the suspended structure, as well as the vibrationally induced cable tension are presented in the time domain and the frequency domain (using random vibration theory as well as convolution integrals). The vertical responses of the three previously mentioned suspension bridges are calculated in the time domain and are compared to the root mean square frequency domain results in order to estimate an appropriate peak factor for the vertical vibration problem. Chapter III investigates the torsional response of suspension bridges to the multiple-support rotational and torsional components of ground motion. A procedure is proposed for estimating maximum torsional and rotational components of ground motion from the corresponding three orthogonal recorded translation components. The torsional response of the suspended structure of the Golden Gate Bridge is calculated in the frequency domain as well as the torsionally induced vibrational cable tension, and an appropriate peak factor is utilized to estimate the peak torsional displacements, stresses, and cable tensions. Chapter IV investigates the lateral response methodology of suspension bridges to multiple-support excitations. Equations governing the lateral displacement of the cables and suspended structure, and laterally induced stresses, moments, and shear forces in the suspended structures, as well as cable tensions, are presented in the time and frequency domains. Peak responses for the Golden Gate

Bridge are calculated in the time domain and are compared to the root mean square results in order to estimate an appropriate peak factor for the lateral vibration problem. Chapter V concentrates on the longitudinal response of the Golden Gate's San Francisco tower-pier. The analysis methodology proposed is quite general, and includes the effect of surrounding water, and the flexibility of the soil underlying the foundation, and its associated geometric and hysteretic damping. The soil parameters are varied in order to observe the effect of soil flexibility upon the tower-pier response, which is again calculated in both the time and frequency domains.

REFERENCES OF CHAPTER I

1. Abdel-Ghaffar, Ahmed M., "Dynamic Analysis of Suspension Bridge Structures," Report No. EERL 76-01, Earthquake Engineering Research Laboratory, College of Engineering, California Institute of Technology, Pasadena, May 1976.

2. Abdel-Ghaffar, Ahmed M., "Studies on the Effect of Differential Motions of Two Foundations Upon the Response of the Superstructure of a Bridge," Report No. EERL 77-02, Earthquake Engineering Research Laboratory, College of Engineering, California Institute of Technology, Pasadena, January, 1977.

3. Abdel-Ghaffar, A. M., and Housner, G. W., "An Analysis of the Dynamic Characteristics of a Suspension Bridge by Ambient Vibration Measurements," Report No. EERL 77-01, Earthquake Engineering Research Laboratory, College of Engineering, California Institute of Technology, Pasadena, January 1977.

4. Abdel-Ghaffar, A. M., and Trifunac, M. D., "Antiplane Dynamic Soil-Bridge Interaction for Incident Plane SH-Waves (One Span Bridge)," Journal of Earthquake Engineering and Structural Dynamics, Vol. 5, No. 2, April-June 1978, p. 107.

5. Abdel-Ghaffar, A. M., "Free Lateral Vibrations of Suspension Bridges," Journal of the Structural Division, ASCE, Vol. 104, No. ST3, Proc. Paper 13609, March 1978, pp. 503-525.

6. Abdel-Ghaffar, A. M., "Free Torsional Vibrations of Suspension Bridges," Journal of the Structural Division, ASCE, Vol. 105, No. ST4, Proc. Paper 14535, April 1979, pp. 767-788.

7. Abdel-Ghaffar, A. M., "Vibration Studies and Tests of a Suspension Bridge," Journal of Earthquake Engineering and Structural Dynamics, Vol. 6, No. 5, Sep.-Oct., 1978, pp. 473-496.

8. Abdel-Ghaffar, A. M., and Housner, G. W., "Ambient Vibration Tests of a Suspension Bridge," Journal of Engineering Mechanics, ASCE, Vol. 104, No. EM5, Proc. Paper 14065, October 1978, pp. 983-999.

9. Abdel-Ghaffar, Ahmed M., "Vertical Vibration Analysis of Suspension Bridges," Journal of the Structural Engineering Division, ASCE, Vol. 106, No. ST10, Proc. Paper 15759, October 1980, pp. 2053-2075.

10. Abdel-Ghaffar, A. M., and Rubin, L. I., "Nonlinear Free Coupled Vibrations of Suspension Bridges: Theory," Journal of Engineering Mechanics, ASCE, Vol. 109, No. EM1, February 1983, pp. 319-329.

11. Abdel-Ghaffar, A. M., and Rubin, L. I., "Nonlinear Free Coupled Vibrations of Suspension Bridges: Application," Journal of Engineering Mechanics, ASCE, Vol. 109, No. EM1, February 1983, pp. 330-345.

12. Abdel-Ghaffar, A. M. and Rubin, L. I., "Vertical Seismic Behavior of Suspension Bridges," International Journal of Earthquake Engineering and Structural Dynamics, Vol. 11, 1-19 Jan-Feb. 1983, pp. 1-19.

13. Abdel-Ghaffar, Ahmed M., "Suspension Bridge Vibration: Continuum Formulation," Journal of Engineering Mechanics, ASCE, Vol. 108, No. EM6, December 1982, pp. 1215-1232.

14. Abdel-Ghaffar, Ahmed M., and Rood, Joel D., "Simplified Earthquake Analysis of Suspension Bridge Towers," Journal of the Engineering Mechanics Division, ASCE, Vol. 108, No. EM2, April 1982, pp. 291-308.

15. Abdel-Ghaffar, A. M., and Rubin, L. I., "Multiple-Support Excitations of Suspension Bridges," Journal of the Engineering Mechanics Division, ASCE, Vol. 108, No. EM2, April 1982, pp. 420-435.

16. Abdel-Ghaffar, A. M., and Rubin, L. I., "Lateral Earthquake Response of Suspension Bridges," Journal of the Structural Division, ASCE, Vol. 109, No. ST3, March 1983, pp. 664-675.

Abdel-Ghaffar, A. M., and Housner, G. W., "Vibrations in Suspension Bridges," Proceedings, Sixth World Conference on Earthquake Engineering, New Delhi, India, January 1977, Vol. 6, pp. 183.

17. Abdel-Ghaffar, A. M., and Trifunac, M. D., "Antiplane Dynamic Soil-Bridge Interaction for Incident Plane SH-Waves (Multi-Span Bridge)," Proceedings, Sixth World Conference on Earthquake Engineering, New Delhi, India, January 1977, pp. 4-145.

Abdel-Ghaffar, A. M., and Housner, G. W., "Analysis and Tests of Suspension Bridge Vibrations," Proceedings, Second Annual ASCE Engineering Mechanics Division Specialty Conference, North Carolina, May 23-25, 1977, pp. 502-506.

22. Abdel-Ghaffar, A. M., and Housner, G. W., "A Measuring Technique for Ambient Vibrations of Full-Scale Suspension Bridges," Proceedings of the Central American Conference on Earthquake Engineering, San Salvador, El Salvador, January 9-14, 1978, Vol. I, pp. 137-144.

18. Abdel-Ghaffar, Ahmed M., "Suspension Bridge Vibration: Continuum Formulation," Journal of Engineering Mechanics Division, ASCE, Vol. 108, No. EM6, December 1982, pp. 1215-1232.

19. Abdel-Ghaffar, A. M., and Scanlan, R. H., "Earthquake Response Analysis of Long- and Intermediate-Span Bridge Structures," A Research Proposal to the National Science Foundation, Civil Engineering Department, Princeton University, Princeton, NJ, March 1980.

20. Ammann, O. H., "Suspension Bridge Design as Governed by Dynamic Wind Action," Roads Engineering Construction, Vol. 91, October 1953, pp. 132-136, 156-174.

21. Ammann, O. H., von Karman, T., and Woodruff, G. B., The Failure of The Tacoma Narrows Bridge, A Report to the Honorable John M. Carmody, Administrator of the Federal Works Agency, Washington, D.C., March 28, 1941.

22. Baron, Frank, and Arioto, Anthony G., "Torsional Analysis of Suspension Bridge Towers," Journal of the Structural Division, ASCE, Vol. 86, No. ST1, January 1960, pp. 143-169.

23. Baron, Frank, and Arioto, Anthony G., "Torsional Behavior of Suspension Bridge Towers," Journal of the Structural Division, ASCE, Vol. 87, No. ST6, August 1961.

24. Baron, F., Arikan, M., and Hamati, E., "The Effects of Seismic Disturbances on the Golden Gate Bridge," Report No. EERC 76-31, Earthquake Engineering Research Center, College of Engineering, University of California, Berkeley, November 1976.

25. Baron, F., and Hamati, R. E., "Effects of Non-Uniform Seismic Excitations on the Dumbarton Bridge Replacement Structure," EERC Report No. 76-19, Earthquake Engineering Research Center, College of Engineering, University of California, Berkeley, July 1976.

26. Bleich, F., McCullough, C. B., Rosecrans, R., and Vincent, G. S., The Mathematical Theory of Vibration in Suspension Bridges, U.S. Bureau of Public Roads, Government Printing Office, Washington, D.C., 1950.

27. Bleich, F., "Dynamic Instability of Truss-Stiffened Suspension Bridges Under Wind Action," Transactions of the ASCE, Vol. 114, 1949, pp. 1177-1222.

28. Bleich, F. M., and Teller, L. W., "Structural Damping in Suspension Bridges," Transactions of the ASCE, Vol. 117, 1952, pp. 165-203.

29. Bogdanoff, J. L., Goldberg, J. E., and Schiff, A. J., "The Effect of Ground Transmission Time on the Response of Long Structures," Bulletin of the Seismological Society of America, Vol. 55, No. 3, June 1965, pp. 627-640.

30. Brady, A. G., Perez, V., and Mork, P. N., "The Imperial Valley Earthquake, October 15, 1979: Digitization and Processing of Accelerograph Records," U.S. Geological Survey, Seismic Engineering Branch, Open-File Report 80-703, April 1980, Menlo Park, CA.

31. Buckland, P. G., Hooley, R., Morgenstern, B. D., Rainer, J. H., and van Selst, A. M., "Suspension Bridge Vibrations: Computed and Measured," Journal of the Structural Division, ASCE, Vol. 105, No. ST5, May 1979, pp. 859-874.

32. Chen, M. C., and Penzien, J., "An Investigation of the Effectiveness of Existing Bridge Design Methodology in Providing Adequate Structural Resistance to Seismic Disturbances. Phase III: Analytical Investigations of Seismic Response of Short-, Single-, or Multiple-Span Highway Bridges," Report No. FHWA-RD-75-10, October 1974.

33. Farquharson, V., "Aerodynamic Stability of Suspension Bridges," Bulletin No. 116, Part I-V, University of Washington Engineering Experimental Station, 1949.

34. Fleming, J. F., and Egeseli, E. A., "Dynamic Response of Cable-Stayed Bridge Structures," Engineering Symposium on Cable-Stayed Bridges, Federal Highway Administration, Pasco, Washington, December 1977.

35. Godden, W. G., and Aslam, M., "Dynamic Model Studies of Ruck-A-Chuky Bridge," Journal of the Structural Division, ASCE, Proc. Paper 1420, Vol. 104, No. ST12, December 1978, pp. 1827-1844.

36. Hirai, Atsuhi, and Ito, Manabu, "Dynamic Effects Produced by Trains Upon Suspension Bridges," Proceedings of the International Symposium on Suspension Bridges, Lisbon, 1966.

37. Housner, G. W., Converse, F. J., and Clough, R. W., "Seismic Analysis of the Main Piers for the Tagus River Bridge," Lisbon, Portugal. Unpublished Report, Tudor Engineering Company, San Francisco, CA, June 1961.

38. Iliescu, Sanda D., "Dynamic Analysis of a Bridge," Senior Thesis, Civil Engineering Department, Princeton University, Princeton, NJ, April 1982.

39. Imbsen, R., Nutt, R. V., and Penzien, J., "Seismic Response of Bridges - Case Studies," Report No. UCB/EERC-78/14, Earthquake Engineering Research Center, University of California, Berkeley, November 1972.

40. Irvine, H. M., "The Estimation of Earthquake-Generated Additional Tension in a Suspension Bridge Cable," Journal of Earthquake Engineering and Structural Dynamics, Vol. 8, 1980, pp. 267-273.

41. Jennings, P. C., "Engineering Features of the San Fernando Earthquake of February 9, 1971," Earthquake Engineering Research Laboratory Report No. EERL 71-02, College of Engineering, California Institute of Technology, Pasadena, CA, June 1971.

42. Johnson, N. B., and Gallenty, R. D., "The Comparison of Response of a Highway Bridge to Uniform and Moving Ground Excitation," Shock and Vibration Bulletin, Vol. 42, No. 2, January 1972.

43. Konishi, Ichiro, and Yamada, Yoshikazu, "Earthquake Responses of a Long Span Suspension Bridge," Proceedings of the Second World Conference on Earthquake Engineering, Japan, July 1960, Vol. 2, pp. 863-878.

44. Konishi, Ichiro, and Yamada, Yoshikazu, "Earthquake Response and Earthquake Resistant Design of Long Span Suspension Bridges," Proceedings of the Third World Conference on Earthquake Engineering, New Zealand, Jan., Feb., 1965, Vol. III, pp. IV-312-323.

45. Konishi, Ichiro, and Yamada, Yoshikazu, "Studies on the Earthquake Resistant Design of Suspension Bridge Tower and Pier Systems," Proceedings of the Fourth World Conference on Earthquake Engineering, Santiago, Chile, January 1969, Vol. I-B4, pp. 107-118.

46. Konishi, Ichiro, Yamada, Yoshikazu, and Takaoka, Nobuyoshi, "Earthquake Resistant Design of Long Span Suspension Bridges," Proceedings of the JEES, November 1962, pp. 87-92.

47. Konishi, I., Yamada, Y., Takaoka, T., Idumi, H., and Isa, T., "Experimental Studies on Effects of Structural Damping and Foundation Conditions to Earthquake Responses of Suspension Bridge Tower Pier Systems," Proceedings of the JEES, October 1966, pp. 285-290.

48. Konishi, I., Yamada, Y., and Takaoka, N., "Response of Long Span Suspension Bridges Subjected to Ground Motion Due to Earthquake, Transactions of the JSCE, No. 159, November 1968, pp. 13-27.

49. Konishi, I., Yamada, Y., Takaoka, N., and Kunihiro, M., "Earthquake Resistant Design of Long Span Suspension Bridge Towers," Transactions of the JSCE, No. 104, April 1964, pp. 9-17.

50. Kubo, K., "Aseismicity of Suspension Bridges Forced to Vibrate Longitudinally," Proceedings of the Second World Conference on Earthquake Engineering, Japan, July 1960, Vol. 2, pp. 913-929.

51. Kuribayashi, E., "Application of Earthquake Forces Taking into Account Dynamic Structural Responses to Earthquake-Resistant Design of Long-Span and Deep-Foundation Suspension Bridges - Studies on Earthquake-Resistant Design of Bridges, Part II -," Report of PWRI, No. 136, July 1969, pp. 13-45.

52. Kuribayashi, E., and Yutaka, I., "An Application of Finite Element Method to Soil-Foundation Interaction Analyses," Bulletin of the New Zealand National Society for Earthquake Engineering, Vol. 7, No. 4, December 1974, pp. 188-199.

53. Kuribayashi, E., "Aseismic Design Method Taking into Account Dynamic Response for the Honshu-Shikoku Suspension Bridge," Proceedings of the JEES, October 1966, pp. 397-402.

54. Kuribayashi, E. Iwasaki, T., and Oyamada, Y., "Research on Earthquake-Resistant Design of the Honsu-Shikoku Suspension Bridges," Technical Memorandum of PWRI, October 1966, pp. 171-239.

55. Kuribayashi, E., Oyamada, Y., Iida, Y., "Earthquake Responses of the Honsu-Shikoku Suspension Bridge," Proceedings of the JEES, November 1970, pp. 629-634.

56. Kuribayashi, E., and Narita, N., "Vibration Test of the Wakato Suspension Bridge," 6th Symposium of Earthquake Engineering, 1963.

57. Kuribayashi, E., and Oyamada, Y., "Response Analysis of Suspension Bridge Including Substructures," 10th Symposium of Earthquake Engineering, 1969.

58. Masri, S. F., "Response of Beams to Propagating Boundary Excitation," Journal of Earthquake Engineering and Structural Dynamics, Vol. 4, 1976, pp. 497-509.

59. Masri, S. F., and Weingarten, V., "Transient Response of Cooling Towers to Propagating Boundary Excitation," Proceedings of the Sixth World Conference on Earthquake Engineering, New Delhi, India, Vol. 3, January 1977, pp. 257-262.

60. Moisseiff, L. S., and Leinhard, F., "Suspension Bridges Under the Action of Lateral Forces," Transactions of the ASCE, Vol. 98, 1933, pp. 1080-1109.

61. Moisseiff, L. S., "Provision for Seismic Forces in Design of the Golden Gate Bridge," Civil Engineering, Vol. 10, No. 1, January 1940.

62. Morgan, J. R., Hall, W. J., and Newmark, N. M., "Response of Simple Structural Systems to Traveling Seismic Waves," Report No. UILU-ENG-79-2015, Department of Civil Engineering, University of Illinois at Urbana-Champaign, September 1979.

63. Nojiri, Y., et al., "Earthquake Resistant Design of Prestressed Concrete Cable-Stayed Bridge," Proceedings of the Sixth World Conference on Earthquake Engineering, University of California, Berkeley, 1968.

64. Pugsley, A. G., "The Gravity Stiffness of a Suspension Bridge Cable," Quarterly Journal of Mechanics and Applied Mathematics, Vol. V, Part 4, 1952, pp. 385-394.

65. Pugsley, A. G., The Theory of Suspension Bridges, Edward Arnold, London, 1957.

66. Pugsley, A. G., "A Simple Theory of Suspension Bridges," Structural Engineering, March 1953.

67. Rainer, J. B. and Selst, V. A., "Dynamic Properties of Lions' Gate Suspension Bridge," ASCE/EMD Specialty Conference on Dynamic Response of Structures: Instrumentation, Testing Methods and System Identification, University of California, Los Angeles, March 30-31, 1976.

68. Rannie, W. D., The Failure of the Tacoma Narrows Bridge, Board of Engineers, Ammann, O. H., von Karman, T., Woodruff, G., Federal Works Agency, March 28, 1941.

69. Rohrs, J. H., "On the Oscillations of a Suspension Chain," Transactions of Cambridge Philosophical Society, Vol. IX, Part III, December 1851.

69. Rood, Joel, D., "Suspension Bridge Towers: Modeling for Seismic Design," Senior Thesis, Civil Engineering Department, Princeton University, Princeton, NJ, April 1980.

71. Scanlan, R. H., "Seismic Wave Effects on Soil-Structure Interaction," Journal of Earthquake Engineering and Structural Dynamics, Vol. 4, No. 4, April-June 1976, pp. 379-388.

72. Scanlan, R. H., and Tomko, J. J., "Airfoil and Bridge Deck Flutter Derivatives," Journal of the Engineering Mechanics Division, ASCE, Vol. 97, No. Em6, Proc. Paper 8609, December 1971.

73. Scanlan, R. H., and Sabzevari, A., "Aerodynamic Instability of Suspension Bridges," Journal of the Structural Division, ASCE, April 1968.

74. Scruton, C., "An Experimental Investigation of the Aerodynamic Stability of Suspension Bridges with Special Reference to the Proposed Severn Bridge," Proceedings of the Institute of Civil Engineering, March 1952.

75. Seed, H. B., Idriss, I. M., and Kiefer, F. W., "Characteristics of Rock Motions During Earthquakes," Earthquake Engineering Research Center Report No. EERC 68-5, College of Engineering, University of California, Berkeley, 1968.

76. Selberg, A., "Calculation of Lateral Truss in Suspension Bridges," International Association for Bridges and Structural Engineering, Zurich, 1943-1944, Vol. 7, pp. 311-325.

77. Selberg, A., Oscillation and Aerodynamic Stability of Suspension Bridges, ACTA Polytechnica Scandinavis, Civil Engineering and Building Construction Series, CI 13, 1961, pp. 308-377.

78. Selberg, A., "Damping Effect in Suspension Bridges," Proceedings, International Association for Bridge and Structural Engineering, Paper 10, Zurich, Switzerland, 1950.

79. Smith, F. C., and Vincent, G. S., The Aerodynamic Stability of Suspension Bridges with Special Reference to the Tacoma Narrows Bridge, Part II, "Mathematical Analysis," University of Washington, Engineering Experiment Station Bulletin No. 116, (1949-1954).

80. Steinman, D. B., A Practical Treatise on Suspension Bridges, John Wiley & Sons, Inc., New York, 1922.

81. Steinman, D. B., "Modes and Natural Frequencies of Suspension Bridge Oscillations, ASCE, September 1959, pp. 148-173.

82. Steinman, D. B., "Rigidity and Aerodynamic Stability of Suspension Bridges," Transactions of the American Society of Civil Engineers, Vol. 110, pp. 439-475.

83. Steinman, D. B., "Deflection Theory for Continuous Suspension Bridges," International Association for Bridge and Structural Engineering, Vol. 2, 1933-1934, pp. 400.

84. Steinman, D. B., "A Generalized Deflection Theory for Suspension Bridges," Transactions of the ASCE, Vol. 100, 1935, pp. 1133.

85. Stringfellow, Richard S., "Vertical and Lateral Response of Suspension Bridges to Travelling Earthquake Excitations," Senior Thesis, Civil Engineering Department, Princeton University, Princeton, NJ, April 1982.

86. Takaoka, Nobuyoshi, and Sato, Yuhji, "Influence of Rocking Motion of Tower Piers on the Earthquake Response of Long Span Suspension Bridge Towers," Transactions of the JSCE, Vol. 1, Part 2, 1969, pp. 435-444.

87. Tezcan, S. S., and Cherry, S., "Earthquake Analysis of Suspension Bridges," Proceedings of the Fourth World Conference on Earthquake Engineering, Santiago, Chile, January 1969, Vol. II-A3, pp. 125-140.

88. Tezcan, S. S., "Stiffness Analysis of Suspension Bridges by Iteration," Proceedings, Symposium on Suspension Bridges, Laboratorio Nacional de Engenharia Civil, Avenue Du Brasil, Lisbon, November 1966.

89. Toki, Kenzo, "Nonlinear Response of Continuous Bridge Subjected To Traveling Seismic Wave," Proceedings of the Seventh World Conference on Earthquake Engineering, Istanbul, September 1980.

90. Tseng, W. S., and Penzien, J., "Seismic Analysis of Long Multiple-Span Highway Bridges," Journal of Earthquake Engineering and Structural Dynamics, Vol. 4, 1975, pp. 3-24.

91. Tseng, W. S., and Penzien, J., "Seismic Response of Long Multiple-Span Highway Bridges," Journal of Earthquake Engineering and Structural Dynamics, Vol. 4, 1975, pp. 25-48.

92. Tseng, W. S., and Penzien, J., "Analytical Investigations of the Seismic Response of Long Multiple-Span Highway Bridges," Report No. EERC 73-12, Earthquake Engineering Research Center, University Of California, Berkeley, June 1973.

93. Vincent, G. S., "Golden Gate Bridge Vibration Studies," Transactions of the ASCE, Vol. 127, 1962, Part II, p. 667.

94. Vincent, G. S., "A Summary of Laboratory and Field Studies in the United States on Wind Effects on Suspension Bridges," Proceedings of Conference on Wind Effects on Buildings and Structures, Teddington, England, H.M.O.S., 1965, Vol. II, pp. 488-515.

95. Vincent, G. S., "Correlation of Predicted and Observed Suspension Bridge Behavior, Transactions of the ASCE, Vol. 127, Part II, Paper No. 3388, 1962, pp. 646-666.

96. Von Karman, T., and Biot, M. A., Mathematical Methods in Engineering, McGraw-Hill, 1940.

97. Werner, S. D., and Lee, L. C., "The Response of Structures to Traveling Body and Surface Waves," Proceedings of the Seventh World Conference on Earthquake Engineering, Istanbul, September 1980, Vol. 5, pp. 367-374.

98. Werner, S. D., Lee, L. C., Wong, H. L., and Trifunac, M. D., "Structural Response to Traveling Seismic Waves," Journal of the Structural Division, ASCE, Vol. 105, No. ST12, December 1979, pp. 2547-2564.

99. Werner, S. D., and Lee, L. C., "The Three-Dimensional Response of Structures Subjected to Traveling Rayleigh Wave Excitation," Proceedings of the Second United States National Conference on Earthquake Engineering, Earthquake Engineering Research Institute, Berkeley, CA, 1979, pp. 693-702.

100. Werner, S. D., et al., "An Evaluation of the Effects of Traveling Seismic Waves on the Three-Dimensional Response of Structures," Report No. 7720-4514, Agbabian Associates, El Segundo, CA, October 1977.

Werner, S. D., Lee, L. C., Wong, H. L., and Trifunac, M. D., "Effects of Traveling Seismic Waves on the Response of Bridges," Proceedings of a Workshop on Earthquake Resistant Design of Highway Bridges, Applied Technology Council, January 29-31, 1979.

101. Yamada, Yoshikazu, and Goto, Yozo, "Some Studies on the Vibration and Earthquake Response Analysis of the Tower-Pier System of Long Span Suspension Bridges," Transactions of the JSCE, Vol. 4, 1972.

102. Yamada, Y., Takemiya, H., and Kawano, K., "Random Response Analysis of a Non-Linear Soil-Suspension Bridge Pier," Journal of Earthquake Engineering and Structural Dynamics, Vol. 7, 1979, pp. 31-47.

103. Yamada, Y., Goto, Y., and Takemiya, H., "Studies on the Earthquake-Resistant Design of Suspension Bridge Tower and Pier System," Proceedings of the Fifth World Conference on Earthquake Engineering, Rome, 1973.

104. Yamada, Yoshikazu, and Takemiya, Hirokazu, "Studies on the Responses of Multi-Degree-of-Freedom Systems Subjected to Random Excitation with Applications to the Tower and Pier Systems of Long Span Suspension Bridges," Transactions of the JSCE, Vol. 1, Part 1, 1969.

105. Yamada, Yoshikazu, and Takemiya, Hirokazu, "Earthquake Response Analysis and Earthquake-Resistant Design of Multi-Degree-of-Freedom Systems," Proceedings of the JEES, November 1970, pp. 413-420.

106. Yamada, Yoshikazu, "Earthquake Resistant Design of Long-Span Bridges," Proceedings of the U.S.-Japan Seminar on Earthquake Engineering Research with Emphasis on Lifeline Systems, Japan Society for the Promotion of Earthquake Engineering, Tokyo, November 1976.

CHAPTER II

EARTHQUAKE-INDUCED VERTICAL VIBRATIONS OF LONG-SPAN SUSPENSION BRIDGES

II.1 INTRODUCTION

As mentioned previously in Chapter I, the design of a suspension bridge for a region where severe earthquakes may be expected is a problem which has received little study to date. The relatively flexible and extended-in-plane configuration of such a structure makes it susceptible to a unique class of vibration problems. The fundamental period of vibration of the suspension bridge may be quite long, and thus it may be necessary to include a relatively large number of modes of vibration in order to obtain a reasonable representation of the total response. In addition, several of the bridge's natural frequencies may be closely-spaced, hence the dynamic analysis must include the possibility of interaction among the various modes. The suspension bridge is excited by ground motion at each of its support points (anchorages and tower-piers). In addition, the vertical (or flexural) vibration of the cable-suspended structure turns out to be excited not only by vertical ground motions at each of the bridge's supports, but by longitudinal motions at its anchorages as well (as will be shown later).

The accuracy of calculated response characteristics for a long-span bridge depends upon a sound knowledge of the expected ground motions at its support points as well as a solid understanding of the mathematical

theory of suspension bridges. The bridge may be long with respect to the wavelengths of ground motion in the frequency range of importance to its earthquake response. Because of this fact, the support points of the bridge can be subjected to significantly different excitations. For such a complicated problem in which a number of excitations act together, the complication does not arise simply from the added number of excitations, but from the possibility that the different excitations are in some way related, so that their correlation (or interaction) must be taken into account. In general, the correlation of the motions at these support points is extremely complicated, particularly in the case of a long-span bridge, with different foundation conditions, subjected to seismic waves with different angles of incidence and different travel paths (reflections and refractions, etc.). However, such complications may be surpassed by utilizing existing strong motion records to define representative and appropriately-correlated multiple-support seismic inputs. Some of the ground motion records taken from the Imperial Valley (El Centro), California, earthquake (M_L = 6.6) of October 15, 1979 are utilized predominantly in this chapter to define the input support motions. However, for comparison purposes, some ground motions recorded during the 1971 San Fernando earthquake (M_L = 6.3) are used as inputs at one point in the chapter, and artificially generated earthquake ground motion records are used as inputs at another point in the chapter [12]. It should be noted that both the El Centro and San Fernando ground motion records were recorded at instrument locations whose horizontal separation distances are consistent with the suspension bridge's in-plane dimensions.

The usual methods of dynamic analysis involve response calculations in either the time or frequency domains. The analysis presented herein

includes both methodologies as well as a response spectra approach (which is based upon the summation of modal maxima obtained by time domain analysis). The frequency domain (random vibration) approach is seen to have the following advantages over the time domain:

1. The frequency domain has a computational advantage, since it is based upon product terms instead of convolution integrals as required in time-history analysis.
2. The frequency domain provides a clear picture of the contribution of each mode to the total response.
3. The effects of input correlation are more easily isolated in the frequency domain.
4. The effects of modal interaction (due to closely-spaced modes) are more easily handled in the frequency domain.
5. The state of the art in utilizing ground motion records is moving toward emphasis upon frequency content, in terms of Fourier amplitude spectra, power spectral density functions, etc.

Along with its advantages pointed out above, the frequency domain does have a disadvantage in that it results in the prediction of root mean square (RMS) response values rather than the peak responses which are vital parameters for the designer. However, peak responses may be related statistically to the root mean square values by a peak factor which is obtained through an approximate solution of the so-called "first passage problem." So it seems that the frequency domain provides for a clearer understanding of the various factors affecting the response.

As was mentioned previously in Chapter I, it was found (1,5) that suspension bridge vibration can be separated into two parts. In one part, the vibration of the tower-pier system is dominant, while in the

other part, the suspended structure vibration dominates. The vibration of the suspended structure may be further decomposed into its vertical (or flexural) motions, torsional motions, longitudinal motions and lateral motions. In this chapter, the dynamic analysis methodology for the vertical vibration of suspension bridges subjected to multiple-support excitations is outlined. Calculation of vertical response displacements, stresses, shear forces, and dynamically induced additional cable tensions are examined in both the time and frequency domains. Available methods for estimating the expected peak response values from the frequency domain root mean square results are reviewed, and finally the method for estimating vertical response using a response spectra approach is presented.

II.2. COORDINATE SYSTEMS OF THE BRIDGE MODEL

The coordinate systems used for the typical three-span suspension bridge is shown in Fig. II-1. For the purpose of studying the vertical vibration, the following is considered [1]:

1. For the cable, the x_i-axis of the i^{th} span is defined as the horizontal line passing through the left support of each span shown in Figure II-1, while the cable ordinate y_i, of the i^{th} span is measured downward from the closing chord of each span (the closing chords are shown dotted in Fig. II-1).
2. For the stiffening structure (girders or trusses), the x_i-axis of the i^{th} span is defined along the centerline of the span with the origin located at the left support of that span.
3. The vertical vibration $v_i(x_i,t)$ of each span is measured downward from the centerline of the stiffening structure.

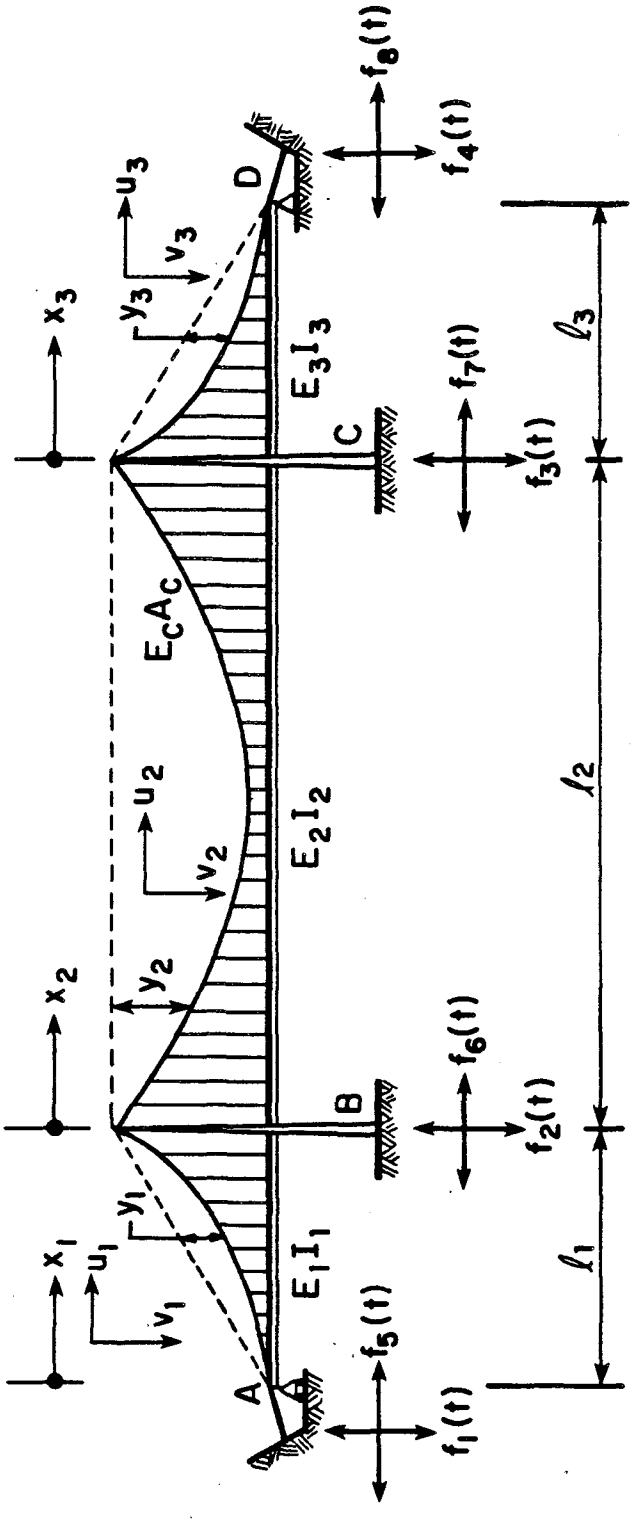

Fig. II-1 General definition diagram.

4. As will be shown at a later point, the vertical vibration is excited not only by vertical ground motion at the bridge's support points, but by longitudinal motion as well. In Fig. II-1, the vertical ground motions at supports A, B, C, and D (anchorages and tower-piers) are denoted $f_1(t)$, $f_2(t)$, $f_3(t)$, and $f_4(t)$ while the corresponding longitudinal motions are denoted $f_5(t)$, $f_6(t)$, $f_7(t)$, and $f_8(t)$.

II.3. FUNDAMENTAL ASSUMPTIONS

The following assumptions and approximations are made for the purpose of simplifying the vertical vibration analysis [1]:

1. All stresses in the bridge remain within the elastic limit and therefore obey Hooke's law.
2. The initial dead load is carried by the cable without causing stress in the stiffening girders (or trusses).
3. The stiffening structure in the i^{th} span is hinged at both ends, while the cable is continuous over all three spans.
4. The cables are of uniform cross section and of parabolic profile under dead load, and are roller supported at the tower tops.
5. The cables are assumed to be perfectly flexible, that is the flexural stiffness of the cables can be neglected.
6. The suspenders (or hangers) are considered inextensible and are assumed to remain vertical during vertical vibration. Therefore the vertical displacement of the cable and the stiffening structure are identical.
7. The vibrational suspender forces are considered as distributed loads as if the distance between the suspenders are very small.

Thus the suspenders form a continuous sheet or wall without shearing resistance.

8. To stay within the linear theory, small vibrational displacements are assumed.

9. The tower-piers move as rigid bodies under ground motion excitation. This is a reasonable first assumption to investigate vertical vibration because the tower-pier is much stiffer than the suspended structure.

10. The initial curvature of the stiffening structure is considered small in comparison with the cable curvature, and is therefore neglected.

11. The mass and elastic properties of the bridge can be taken as uniform along each span.

II.4. EQUATIONS OF MOTION GOVERNING EARTHQUAKE-INDUCED VERTICAL VIBRATION

Under the previous assumptions, the linearized equation of motion governing the vertical vibration of the i^{th} span of a suspension bridge is given by [1,2]:

$$\frac{\overset{*}{w}_i}{g}\frac{\partial^2 v_i}{\partial t^2} + c_i\frac{\partial v_i}{\partial t} + E_i I_i\frac{\partial^4 v_i}{\partial x_i^4} - H_w\frac{\partial^2 v_i}{\partial x_i^2} + \frac{\overset{*}{w}_i}{H_w}H(t) = 0, \quad i = 1,2,3 \qquad (2.1)$$

where $v_i = v_i(x_i,t)$ is the vertical response of the i^{th} span; $\overset{*}{w}_i$ is the dead weight of the bridge per unit length of the i^{th} span; E_i and I_i are respectively, the modulus of elasticity and moment of inertia of the i^{th} stiffening structure; g is the gravitational acceleration constant; c_i is the vertical damping coefficient in the i^{th} span; H_w is the initial (dead-load) horizontal component of cable tension; and

$H(t)$ is the additional (vibrational) horizontal component of cable tension given by [1,2]

$$H(t) = \frac{E_c A_c}{L_E} \sum_{i=1}^{3} \left[u_c(x_i,t) \Big|_0^{\ell_i} + \frac{dy_i}{dx_i} v_i \Big|_0^{\ell_i} + \frac{\overset{*}{w}_i}{H_w} \int_0^{\ell_i} v_i dx_i \right] \tag{2.2}$$

in which E_c is the cable's modulus of elasticity; A_c is the cable's cross-sectional area; u_c is the longitudinal cable displacement at the tower tops and anchorages; ℓ_i is the length of the i^{th} span; L_E is the cable's virtual length defined as [1,2]

$$L_E = \sum_{i=1}^{3} \int_0^{\ell_i} \left(\frac{ds_i}{dx_i} \right)^3 dx_i \tag{2.3}$$

where s_i is the coordinate measured tangent to the cable in the i^{th} span; and $y_i = y_i(x_i)$ is the cable ordinate measured from the closing chord of the i^{th} span (Fig. II-1). This dead-load cable profile is expressed as [1,2]

$$y_i(x_i) = \frac{\overset{*}{w}_i \ell_i}{2H_w} \left[\left(\frac{x_i}{\ell_i} \right) - \left(\frac{x_i}{\ell_i} \right)^2 \right] \qquad i = 1,2,3, \tag{2.4}$$

It should be noted from Eqs. 2.1 that the vertical vibrations of each span of the suspension bridge are coupled together by the vibration of the cable through $H(t)$. Also, the boundary conditions at the tower-piers and anchorages are time-dependent and can be written as

$$\left.\begin{aligned} v_i(0,t) &= f_i(t) \\ v_i(\ell_i,t) &= f_{i+1}(t) \\ v_i''(0,t) &= 0 \\ v_i''(\ell_i,t) &= 0 \end{aligned}\right\} \quad i = 1,2,3 \tag{2.5}$$

where $f_i(t)$, $(i = 1,2,3,4,)$, are the vertical ground displacements at supports A, B, C, and D of Figure II-1. Note that the double prime denotes differentiation with respect to x_i. Also note, by using Eqs. 2.4 and 2.5, the first two terms of Eq. 2.2 can be written as

$$\sum_{i=1}^{3} u_c(x_i,t)\Big|_0^{\ell_i} = \sum_{i=1}^{3} [f_{i+5}(t) - f_{1+4}(t)]$$

$$= f_8(t) - f_5(t) \tag{2.6}$$

and

$$\sum_{i=1}^{3} \frac{dy_i}{dx_i} v_i(x_i,t)\Big|_0^{\ell_i} = - \sum_{i=1}^{3} \frac{\overset{*}{w}_i \ell_i}{2H_w}[f_{i+1}(t) + f_i(t)] \tag{2.7}$$

where $f_i(t)$, $(i = 5,6,7,8)$ are the longitudinal components of ground motion at supports A, B, C, and D of Fig. II-1. Therefore, the additional horizontal component of cable tension (Eq. 2.2) becomes:

$$H(t) = \frac{E_c A_c}{L_E}\left\{\sum_{i=1}^{3}\left[\frac{\overset{*}{w}_i}{H_w}\int_0^{\ell_i} v_i dx_i - \frac{\overset{*}{w}_i \ell_i}{2H_w}(f_{i+1}(t) + f_i(t))\right]\right.$$

$$\left. + (f_8(t) - f_5(t))\right\} \tag{2.8}$$

From Eqs. 2.1 and 2.8 it can be seen that the bridge's vertical motion is excited not only by the vertical ground input motions $f_1(t)$, $f_2(t)$, $f_3(t)$, $f_4(t)$, but also by the two longitudinal ground displacements at the end anchorages, $f_5(t)$ and $f_8(t)$. Furthermore, the additional horizontal cable tension is not only a function of the response $v_i(x_i,t)$ but it is also a function of the input ground displacements at the supports of the bridge.

II.5. GENERAL SOLUTIONS

In order to conveniently satisfy the time-dependent boundary conditions (Eqs. 2.5) the Mindlin-Goodman solution is adopted [14], that is, the vertical displacement is separated into two parts

$$v_i(x_i,t) = \eta_i(x_i,t) + \sum_{j=1}^{4} g_{ji}(x_i) f_j(t), \quad i = 1,2,3, \tag{2.9}$$

where η_i is the relative or vibrational vertical displacement of the i^{th} span and $g_{ji}(x_i)$ are the quasi-static (or influence) functions which give the vertical displacement at x_i due to a unit vertical displacement of the suspended structure at the j^{th} support.

Substituting Eqs. 2.9 into Eqs. 2.1 and 2.8 gives the following equation governing the vibrational response:

$$\frac{\overset{*}{w}_i}{g}\frac{\partial^2\eta_i}{\partial t^2} + c_i\frac{\partial\eta_i}{\partial t} + E_iI_i\frac{\partial^4\eta_i}{\partial x_i^4} - H_w\frac{\partial^2\eta_i}{\partial x_i^2}$$

$$+ \frac{\overset{*}{w}_i}{H_w}\left[\frac{E_cA_c}{L_E}\sum_{m=1}^{3}\frac{\overset{*}{w}_m}{H_w}\int_0^{\ell_m}\eta_m(x_m,t)dx_m\right] =$$

$$- c_i\sum_{j=1}^{4} g_{ji}(x_i)\dot{f}_j(t) - \frac{\overset{*}{w}_i}{g}\sum_{j=1}^{4} g_{ji}(x_i)\ddot{f}_j(t)$$

$$- \frac{\overset{*}{w}_i}{H_w}\frac{E_cA_c}{L_E}[f_8(t) - f_5(t)] + \frac{E_cA_c}{L_E}\frac{\overset{*}{w}_i}{H_w}\left[\sum_{m=1}^{3}\frac{\overset{*}{w}_m\ell_m}{2H_w}\{f_{m+1}(t) + f_m(t)\}\right]$$

$$- \sum_{j=1}^{4} f_j(t) \left\{ E_i I_i \frac{d^4 g_{ji}(x_i)}{dx_i^4} - H_w \frac{d^2 g_{ji}(x_i)}{dx_i^2} \right.$$

$$\left. + \frac{\overset{*}{w}_i}{H_w} \left(\frac{E_c A_c}{L_E} \right) \sum_{n=1}^{3} \frac{\overset{*}{w}_n}{H_w} \int_0^{\ell_n} g_{jn}(x_n) dx_n \right\} \qquad i=1,2,3, \qquad (2.10)$$

Substituting Eq. 2.9 into Eq. 2.5, the boundary conditions upon the vibrational response become

$$\left.\begin{aligned} \eta_i(0,t) &= f_i(t) - \sum_{j=1}^{4} g_{ji}(0) f_j(t) \\ \eta_i(\ell_i,t) &= f_{i+1}(t) - \sum_{j=1}^{4} g_{ji}(\ell_i) f_j(t) \\ \eta_i''(0,t) &= - \sum_{j=1}^{4} g_{ji}''(0) f_j(t) \\ \eta_i''(\ell_i,t) &= - \sum_{j=1}^{4} g_{ji}''(\ell_i) f_j(t) \end{aligned}\right\} \quad i=1,2,3 \qquad (2.11)$$

The above boundary conditions can be made homogeneous by choosing

$$\left.\begin{aligned} g_{ji}(0) &= 1 \quad j = i \\ &= 0 \quad j \neq i \\ g_{ji}(\ell_i) &= 1 \quad j = (i+1) \\ &= 0 \quad j \neq (i+1) \\ g_{ji}''(0) &= g_{ji}''(\ell_i) = 0 \quad \text{for all } i,j \end{aligned}\right\} \quad \begin{aligned} &j=1,2,3,4, \\ &i=1,2,3, \end{aligned} \qquad (2.12)$$

Now the quasi-static functions are the solutions of the twelve differential equations represented by setting the last bracketed term in Eq. 2.10 to zero (for i=1,2,3 and j=1,2,3,4) subject to the boundary conditions of Eq. 2.12. These functions have the following form

$$g_{ji}(x_i) = A_{ji} \sinh(\lambda_i x_i) + B_{ji} \cosh(\lambda_i x_i) + C_{ji} x_i^2 + D_{ji} x_i + E_{ji}$$

$$i=1,2,3, \qquad j=1,2,3,4, \tag{2.13}$$

where $$\lambda_i = \sqrt{H_w / E_i I_i} \qquad i=1,2,3, \tag{2.14}$$

and the coefficients A_{ji}, B_{ji}, C_{ji}, D_{ji}, and E_{ji} are constants involving the bridge's structural properties. (Solution details are found in Appendix II-a.)

With the quasi-static functions uniquely defined, Eq. 2.10 reduces to

$$\frac{\overset{*}{w}_i}{g} \frac{\partial^2 \eta_i}{\partial t^2} + c_i \frac{\partial \eta_i}{\partial t} + E_i I_i \frac{\partial^4 \eta_i}{\partial x_i^4} - H_w \frac{\partial^2 \eta_i}{\partial x_i^2}$$

$$+ \frac{\overset{*}{w}_i}{H_w} \left[\frac{E_c A_c}{L_E} \sum_{m=1}^{3} \frac{\overset{*}{w}_m}{H_w} \int_0^{\ell_n} \eta_m(x_m, t)\, dx_m \right] =$$

$$- c_i \sum_{j=1}^{4} g_{ji}(x_i) \dot{f}_j(t) - \frac{\overset{*}{w}_i}{g} \sum_{j=1}^{4} g_{ji}(x_i) \ddot{f}_j(t)$$

$$- \frac{\overset{*}{w}_i}{H_w} \left(\frac{E_c A_c}{L_E} \right) [f_8(t) - f_5(t)]$$

$$+ \frac{\overset{*}{w}_i}{H_w} \left(\frac{E_c A_c}{L_E} \right) \sum_{m=1}^{3} \frac{\overset{*}{w}_m \ell_m}{2H_w} [f_{m+1}(t) + f_m(t)] \qquad i=1,2,3 \tag{2.15}$$

and the boundary conditions upon the vibrational response $\eta_i(x_i, t)$ become homogeneous, that is

$$\left.\begin{aligned} \eta_i(0,t) &= \eta_i(\ell_i, t) = 0 \\ \eta_i''(0,t) &= \eta_i''(\ell_i, t) = 0 \end{aligned}\right\} \qquad i=1,2,3 \tag{2.16}$$

Note that the equation governing the vertical vibrational response (Eq. 2.15) is excited by vertical ground accelerations, velocities and displacements at the anchorages. Although, as indicated by Baron, et al [5], the contribution to the total response from velocity (damping) terms is often small when compared to that of the acceleration and displacement terms, the velocity terms are included in this analysis for completeness.

II.6. EIGENVALUE PROBLEM - FREE VIBRATIONS

The solution to Eq. 2.15 is obtained by modal superposition, that is the vibrational displacement is taken to be

$$\eta_i(x_i,t) = \sum_{n=1}^{\infty} \phi_{ni}(x_i) q_n(t) \qquad , \qquad i=1,2,3 \tag{2.17}$$

where $\phi_{ni}(x_i)$ is the n^{th} vertical vibration mode shape in the i^{th} span of the bridge and $q_n(t)$ is the n^{th} generalized coordinate. The mode shapes and their associated natural frequencies are derived from Eqs. 2.15. With damping and forcing terms set to zero, Eqs. 2.15 become:

$$\frac{\overset{*}{w}_i}{g} \frac{\partial^2 \eta_i}{\partial t^2} + E_i I_i \frac{\partial^4 \eta_i}{\partial x_i^4} - H_w \frac{\partial^2 \eta_i}{\partial x_i^2}$$

$$+ \frac{\overset{*}{w}_i}{H_w} \left[\frac{E_c A_c}{L_E} \sum_{m=1}^{3} \frac{\overset{*}{w}_m}{H_w} \int_0^{\ell_m} \eta_m(x_m,t)\, dx_m \right] = 0 \qquad i=1,2,3, \tag{2.18}$$

The n^{th} mode shape and natural frequency, ω_n, is obtained by assuming the vibration to be sinusoidal, that is

$$\eta_j(x_j,t) = \phi_{nj}(x_j) e^{i\omega_n t} \qquad \begin{matrix} j=1,2,3, \\ n=1,2,3,\ldots \end{matrix} \tag{2.19}$$

in which $i = \sqrt{-1}$.

Substituting Eqs. 2.19 into Eqs. 2.18 results in

$$\frac{d^4\phi_{ni}}{dx_i^4} - \frac{H_w}{E_i I_i}\frac{d^2\phi_{ni}}{dx_i^2} - \frac{\overset{*}{w}_i \omega_n^2}{E_i I_i g}\phi_{ni} + \frac{\overset{*}{w}_i}{E_i I_i H_w}\tilde{H}_n = 0 \qquad \begin{matrix} i=1,2,3, \\ n=1,2,3,\ldots \end{matrix} \tag{2.20}$$

where the additional horizontal component of cable tension associated with the n^{th} mode shape, $\tilde{H}_n$, is given by:

$$\tilde{H}_n = \frac{E_c A_c}{L_E}\sum_{j=1}^{3}\frac{\overset{*}{w}_j}{H_w}\int_0^{\ell_j}\phi_{nj}(x_j)dx_j \qquad n=1,2,3,\ldots \tag{2.21}$$

The boundary conditions for each mode shape are similar to Eqs. 2.16, that is

$$\left.\begin{aligned} \phi_{ni}(0) &= \phi_{ni}(\ell_i) = 0 \\ \phi''_{ni}(0) &= \phi''_{ni}(\ell_i) = 0 \end{aligned}\right\} \qquad \begin{matrix} i=1,2,3 \\ n=1,2,3,\ldots \end{matrix} \tag{2.22}$$

Because $\tilde{H}_n$ is independent of x_j and may be treated as a constant, Eqs. 2.20 represent linear, ordinary differential equations of fourth order with constant coefficients. The general solution of Eqs. 2.20 can be expressed as

$$\phi_{ni}(x_i) = A_i \sin\left(\frac{\mu_i x_i}{\ell_i}\right) + B_i \cos\left(\frac{\mu_i x_i}{\ell_i}\right) + C_i \sinh\left(\frac{\nu_i x_i}{\ell_i}\right)$$

$$+ D_i \cosh\left(\frac{\nu_i x_i}{\ell_i}\right) + \frac{\overset{*}{w}_i \tilde{H}_n}{m_i H_w \omega_n^2} \qquad \begin{matrix} i=1,2,3, \\ n=1,2,3,\ldots \end{matrix} \tag{2.23}$$

where $m_i = \overset{*}{w}_i/g$

$$\mu_i = \sqrt{1/2\ \theta_i(z_i - 1)}$$

$$\nu_i = \sqrt{1/2\ \theta_i(z_i + 1)}$$

$$\left.\begin{aligned} z_i &= \sqrt{1 + \left(\frac{4E_i I_i m_i}{H_w^2}\right)\omega_n^2} \\ \theta_i &= \frac{H_w \ell_i^2}{E_i I_i} \end{aligned}\right\} \qquad \begin{aligned} &n=1,2,3,\ldots \\ &i=1,2,3, \end{aligned} \qquad (2.24)$$

and A_i, B_i, C_i, and D_i are arbitrary constants which are determined in conformity with the boundary conditions (Eqs. 2.22).

At this point, it is convenient to separate the investigation of the symmetric vertical modes from that of the antisymmetric vertical modes, that is, the problem can be divided into two parts:

1. The symmetric vertical modes of vibration in which there are an even number of internal nodes along the center span. Here the additional cable tension, $\tilde{H}_n$, is nonzero, that is, the center and side span vibrations are coupled through the vibration of the cable.
2. The antisymmetric vertical modes of vibration which result in an odd number of internal nodes along the center span. Here the additional cable tension, $\tilde{H}_n$, is zero, that is, there is no interaction between the center span and side spans.

The symmetric vertical modes are of the form (see Appendix II-b for details):

$$\phi_{ni}(x_i) = \frac{\overset{*}{w}_i \tilde{H}_n}{2m_i H_w z_i \omega_n^2}\left\{2z_i - \frac{z_i + 1}{\cos(\mu_i/2)}\cos\left[\mu_i\left(1/2 - \frac{x_i}{\ell_i}\right)\right] - \frac{z_i - 1}{\cosh(\nu_i/2)}\cosh\left[\nu_i\left(1/2 - \frac{x_i}{\ell_i}\right)\right]\right\} \qquad \begin{aligned} &i=1,2,3, \\ &n=1,2,3,\ldots \end{aligned} \qquad (2.25)$$

where the natural circular frequencies, ω_n, are determined by satisfying the transcendental equation

$$\frac{L_E}{E_c A_c} = \sum_{i=1}^{3} \left\{ \left(\frac{w_i^*}{H_w}\right)^2 \frac{\ell_i}{m_i z_i \omega_n^2} \left[z_i - \left(\frac{z_i + 1}{\mu_i}\right) \tan\left(\frac{\mu_i}{2}\right) - \left(\frac{z_i - 1}{\nu_i}\right) \tanh\left(\frac{\nu_i}{2}\right) \right] \right\} \tag{2.27}$$

In this report, the modes are normalized so that their highest ordinate has a unit magnitude.

The antisymmetric vertical modes of vibration involving the center span are (Appendix II-b)

$$\phi_{m2}(x_2) = \sin \frac{m\pi x_2}{\ell_2} \qquad m=2,4,6... \tag{2.27}$$

having associated natural circular frequencies

$$\omega_{2m} = \left(\frac{m\pi}{\ell_2}\right)^2 \sqrt{\frac{E_2 I_2}{m_2} + \frac{H_w \ell_2^2}{m_2 m^2 \pi^2}} \qquad m=2,4,6... \tag{2.28}$$

The antisymmetric vertical modes of vibration for the side spans are (Appendix II-b)

$$\phi_{mj}(x_j) = \sin\left(\frac{m\pi x_j}{\ell_j}\right) \qquad \begin{matrix} m=1,2,3,... \\ j=1,3, \end{matrix} \tag{2.29}$$

having associated natural circular frequencies

$$\omega_{jm} = \left(\frac{m\pi}{\ell_j}\right)^2 \sqrt{\frac{E_j I_j}{m_j} + \frac{H_w \ell_j^2}{m_j m^2 \pi^2}} \qquad \begin{matrix} m=1,2,3,... \\ j=1,3 \end{matrix} \tag{2.30}$$

II.7. MODAL SOLUTION - FORCED VIBRATIONS

Substituting Eq. 2.17 into Eq. 2.15 results in

$$\frac{\overset{*}{w}_i}{g} \sum_{n=1}^{\infty} \phi_{ni}(x_i)\ddot{q}_n(t) + c_i \sum_{n=1}^{\infty} \phi_{ni}(x_i)\dot{q}_n(t)$$

$$+ E_i I_i \sum_{n=1}^{\infty} \phi_{ni}^{IV}(x_i)q_n(t) - H_w \sum_{n=1}^{\infty} \phi_{ni}''(x_i)q_n(t)$$

$$+ \frac{\overset{*}{w}_i}{H_w}\left(\frac{E_c A_c}{L_E}\right) \sum_{j=1}^{3} \left\{ \frac{\overset{*}{w}_j}{H_w} \int_0^{\ell_j} \left[\sum_{n=1}^{\infty} \phi_{nj}(x_j)q_n(t) \right] dx_j \right\} =$$

$$- c_i \sum_{j=1}^{4} g_{ji}(x_i)\dot{f}_j(t) - \frac{\overset{*}{w}_i}{g} \sum_{j=1}^{4} g_{ji}(x_i)\ddot{f}_j(t)$$

$$- \frac{\overset{*}{w}_i}{H_w}\left(\frac{E_c A_c}{L_E}\right)[f_8(t) - f_5(t)]$$

$$+ \frac{\overset{*}{w}_i}{H_w}\left(\frac{E_c A_c}{L_E}\right) \sum_{m=1}^{3} \frac{\overset{*}{w}_m \ell_m}{2H_w} [f_{m+1}(t) + f_m(t)] \qquad i=1,2,3 \qquad (2.31)$$

Using Eqs. 2.20 and 2.21, the previous equation can be simplified to

$$\frac{\overset{*}{w}_i}{g} \sum_{n=1}^{\infty} \phi_{ni}(x_i)\ddot{q}_n(t) + c_i \sum_{n=1}^{\infty} \phi_{ni}(x_i)\dot{q}_n(t)$$

$$+ \frac{\overset{*}{w}_i}{g} \sum_{n=1}^{\infty} \omega_n^2 \phi_{ni}(x_i)q_n(t) =$$

$$- c_i \sum_{j=1}^{4} g_{ji}(x_i)\dot{f}_j(t) - \frac{\overset{*}{w}_i}{g} \sum_{j=1}^{4} g_{ji}(x_i)\ddot{f}_j(t)$$

$$- \frac{\overset{*}{w}_i}{H_w}\left(\frac{E_c A_c}{L_E}\right)[f_8(t) - f_5(t)] + \frac{\overset{*}{w}_i}{H_w}\left(\frac{E_c A_c}{L_E}\right) \sum_{m=1}^{3} \frac{\overset{*}{w}_m \ell_m}{2H_w}[f_{m+1}(t) + f_m(t)]$$

$$i=1,2,3 \qquad (2.32)$$

Now, multiplying Eqs. 2.32 by $\phi_{mi}(x_i)$, integrating over the i^{th} span (from zero to ℓ_i) and summing over all three spans (i=1,2,3) gives the equation governing the response of the n^{th} generalized coordinate

$$\ddot{q}_n(t) + 2\xi_n\omega_n\dot{q}_n(t) + \omega_n^2 q_n(t) = -\sum_{j=1}^{4} R_{jn}[2\xi_n\omega_n\dot{f}_j(t) + \ddot{f}_j(t)]$$

$$+ P_n\alpha\left\{\sum_{i=1}^{3}\beta_i\left[f_{i+1}(t) + f_i(t)\right] - \left[f_8(t) - f_5(t)\right]\right\} \quad n=1,2,3,... \tag{2.33}$$

where ξ_n is the damping ratio of the n^{th} vertical mode;

$$\alpha = \frac{E_c A_c g}{L_E H_w} \tag{2.34}$$

$$\beta_i = \frac{\overset{*}{w}_i \ell_i}{2H_w} \qquad i=1,2,3 \tag{2.35}$$

and R_{jn} and P_n are modal participation coefficients given by

$$R_{jn} = \left[\sum_{i=1}^{3}\overset{*}{w}_i\int_0^{\ell_i} g_{ji}(x_i)\phi_{ni}(x_i)dx_i\right] \Big/ \left[\sum_{i=1}^{3}\overset{*}{w}_i\int_0^{\ell_i}\phi_{ni}^2(x_i)dx_i\right]$$

$$j=1,2,3,4, \quad n=1,2,3,... \tag{2.36}$$

$$P_n = \left[\sum_{i=1}^{3}\overset{*}{w}_i\int_0^{\ell_i}\phi_{ni}(x_i)dx_i\right] \Big/ \left[\sum_{i=1}^{3}\overset{*}{w}_i\int_0^{\ell_i}\phi_{ni}^2(x_i)dx_i\right]$$

$$n=1,2,3... \tag{2.37}$$

Note that in the derivation of Equation 2.33, modal orthogonality was utilized (the details appear in Appendix II-c), that is

$$\sum_{i=1}^{3} \frac{\overset{*}{w}_i}{g} \int_0^{\ell_i} \phi_{ni}(x_i)\phi_{mi}(x_i)dx_i = 0 \qquad \text{for} \quad m \neq n \tag{2.38}$$

The solution to Eq. 2.33, assuming quiescent initial conditions, is given by the convolution integral

$$q_n(t) = \frac{1}{\omega_{nd}} \int_0^t \left\{ \left[-2\xi_n\omega_n \sum_{j=1}^{4} R_{jn}\dot{f}_j(\tau) \right] - \left[\sum_{j=1}^{4} R_{jn}\ddot{f}_j(\tau) \right] \right.$$

$$\left. + \left[P_n\alpha \sum_{i=1}^{3} \beta_i [f_{i+1}(\tau) + f_i(\tau)] \right] - P_n\alpha[f_8(\tau) - f_5(\tau)] \right\}$$

$$\left\{ e^{-\xi_n\omega_n(t-\tau)} \sin \omega_{nd}(t - \tau) \right\} d\tau \qquad n=1,2,3,... \tag{2.39}$$

where ω_{nd} is the damped natural circular frequency of the n^{th} vertical vibration mode, given by:

$$\omega_{nd} = \omega_n\sqrt{1 - \xi_n^2} \qquad n=1,2,3... \tag{2.40}$$

The total vertical displacement response is obtained as the sum of quasi-static and relative responses, that is:

$$v_i(x_i,t) = \sum_{j=1}^{4} g_{ji}(x_i)f_j(t) + \sum_{n=1}^{\infty} \phi_{ni}(x_i)q_n(t) \qquad i=1,2,3, \tag{2.41}$$

The total dynamic bending moment in the i^{th} stiffening structure may be calculated as

$$M_i(x_i,t) = E_iI_i\left[\sum_{j=1}^{4} g''_{ji}(x_i)f_j(t) + \sum_{n=1}^{\infty} \phi''_{ni}(x_i)q_n(t) \right] \quad i=1,2,3 \tag{2.42}$$

where $g''_{ji}(x_i)$ and $\phi''_{ni}(x_i)$ are the second spanwise derivatives of the quasi-static functions and mode shapes, respectively.

Similarly, the total dynamic shearing force in the i^{th} stiffening structure may be calculated as

$$V_i(x_i,t) = E_iI_i\left[\sum_{j=1}^{4} g'''_{ji}(x_i)f_j(t) + \sum_{n=1}^{\infty} \phi'''_{ni}(x_i)q_n(t)\right] \qquad i=1,2,3, \quad (2.43)$$

where $g'''_{ji}(x_i)$ and $\phi'''_{ni}(x_i)$ are the third spanwise derivatives of the quasi-static functions and mode shapes, respectively.

Furthermore, the dynamically-induced stresses in the chords of the i^{th} stiffening structure $\sigma_i(x_i,t)$ may be calculated using the flexural stress relation

$$\sigma_i(x_i,t) = \frac{d_i}{2I_i} M_i(x_i,t) \qquad i=1,2,3, \quad (2.44)$$

where d_i is the depth of the stiffening structure in the i^{th} span of the bridge.

II.8. FREQUENCY DOMAIN RANDOM VIBRATION APPROACH

Because of the advantages of frequency domain analysis pointed out in Section II.1, a random vibration frequency-domain approach is used to study the dynamic behavior of long-span suspension bridges when subjected to multiple-support earthquake excitations. For the six displacement inputs, there are six complex frequency response functions. To determine these functions, each $f_j(t)$, $(j=1,2,3,4,5,8)$, is taken equal to $\exp(i\omega t)$, where $i=\sqrt{-1}$, and the response of the n^{th} generalized coordinate excited by the j^{th} input motion is assumed to be of the form:

$$q_{nj}(t) = H_{nj}(\omega)\exp(i\omega t) \qquad \begin{matrix} n=1,2,3,\ldots \\ j=1,2,3,4,5,8. \end{matrix} \quad (2.45)$$

where H_{nj} is the n^{th} complex frequency response due to input displacement $f_j(t)$ at the support (see Fig. II-1). Now substituting Eq. 2.45 into Eq. 2.33 yields

$$H_{nj}(\omega) = \frac{[(R_{jn}\omega^2 + \gamma_j P_n \alpha) - i(2\xi_n \omega_n \omega R_{jn})]}{[(\omega_n^2 - \omega^2) + i(2\xi_n \omega_n \omega)]} \qquad \begin{matrix} j=1,2,3,4. \\ n=1,2,3,... \end{matrix} \tag{2.46}$$

$$H_{nj}(\omega) = \frac{\pm P_n \alpha}{[(\omega_n^2 - \omega^2) + i(2\xi_n \omega_n \omega)]} \qquad \begin{matrix} j=5(+) \\ j=8(-) \\ n=1,2,3,... \end{matrix} \tag{2.47}$$

where

$$\gamma_1 = \beta_1 = \frac{\overset{*}{w}_1 \ell_1}{2H_w}$$

$$\gamma_2 = \beta_1 + \beta_2 = \frac{\overset{*}{w}_1 \ell_1}{2H_w} + \frac{\overset{*}{w}_2 \ell_2}{2H_w} \tag{2.48}$$

$$\gamma_3 = \beta_2 + \beta_3 = \frac{\overset{*}{w}_2 \ell_2}{2H_w} + \frac{\overset{*}{w}_3 \ell_3}{2H_w}$$

$$\gamma_4 = \beta_3 = \frac{\overset{*}{w}_3 \ell_3}{2H_w}$$

Taking the finite Fourier transform of Eqs. 2.17 over the duration of the ground displacement, T_1, yields the Fourier transform of the vibrational response:

$$\Gamma(x_i,\omega) = \int_0^{T_1} \eta(x_i,t) e^{-i\omega t}\, dt$$

$$= \sum_{n=1}^{\infty} \phi_{ni}(x_i) \underline{Q}_n(\omega) \qquad i=1,2,3, \tag{2.49}$$

where $Q_n(\omega)$ is the finite Fourier transform of the generalized coordinate $q_n(t)$ given by:

$$Q_n(\omega) = \int_0^{T_1} q_n(t) e^{-i\omega t}\, dt \qquad n=1,2,3,... \tag{2.50}$$

A similar Fourier transformation of Eq. 2.33 yields

$$-\omega^2 Q_n(\omega) + 2i\xi_n\omega_n\omega Q_n(\omega) + \omega_n^2 Q_n(\omega) = \sum_{j=1,2,3,}^{4,5,8} \tilde{F}_{jn}(\omega) \quad n=1,2,3,... \tag{2.51}$$

where $\tilde{F}_{jn}(\omega)$ is given by:

$$\tilde{F}_{jn}(\omega) = [(R_{jn}\omega^2 + \gamma_j P_n \alpha) - i(2\xi_n\omega_n\omega R_{jn})]F_j(\omega) \qquad \begin{matrix} j=1,2,3,4 \\ n=1,2,3... \end{matrix} \tag{2.52}$$

$$\tilde{F}_{jn}(\omega) = \pm(P_n\alpha)F_j(\omega) \qquad \begin{matrix} j=5(+) \\ j=8(-) \\ n=1,2,3,... \end{matrix} \tag{2.53}$$

in which $F_j(\omega)$ is the finite Fourier transform of the input ground displacements $f_j(t)$, $(j=1,2,3,4,5,8)$, given by:

$$F_j(\omega) = \int_0^{T_1} f_j(t) e^{-i\omega t}\, dt \qquad j=1,2,3,4,5,8. \tag{2.54}$$

It follows from equations 2.46, 2.47, 2.51, 2.52 and 2.53 that the Fourier transform of the generalized coordinate can be expressed as:

$$Q_n(\omega) = \{H_n(\omega)\}^T\{F(\omega)\} \qquad n=1,2,3,... \tag{2.55}$$

where $\{H_n(\omega)\}^T$ denotes the transposed complex frequency response vector given by:

$$\{H_n(\omega)\}^T = \{H_{n1}(\omega)\ H_{n2}(\omega)\ H_{n3}(\omega)\ H_{n4}(\omega)\ H_{n5}(\omega)\ H_{n8}(\omega)\} \quad n=1,2,3... \tag{2.56}$$

and $\{F(\omega)\}$ is the Fourier transform vector of the ground-displacement inputs given by:

$$\{F(\omega)\} = \begin{Bmatrix} F_1(\omega) \\ F_2(\omega) \\ F_3(\omega) \\ F_4(\omega) \\ F_5(\omega) \\ F_8(\omega) \end{Bmatrix} \tag{2.57}$$

Now substituting Eq. 2.55 into Eq. 2.49 enables the Fourier transform of the vibrational response to be expressed as:

$$\Gamma(x_i,\omega) = \sum_{n=1}^{\infty} \phi_{ni}(x_i)\{H_n(\omega)\}^T\{F(\omega)\} \qquad i=1,2,3, \tag{2.58}$$

The power spectral density of the relative (or vibrational) response is given by:

$$G_\eta(x_i,\omega) = \lim_{T_1\to\infty} \frac{2}{T_1} E[\overset{*}{\Gamma}(x_i,\omega)\Gamma(x_i,\omega)] \qquad i=1,2,3, \tag{2.59}$$

where $E[\cdot]$ represents the expected value of the term inside the brackets, and the superposed asterisk denotes complex conjugate. An estimate of G_η can be obtained by simply omitting the limiting and expectation operations in Eq. 2.59, hence:

$$G_\eta(x_i,\omega) \simeq \frac{2}{T_1} \overset{*}{\Gamma}(x_i,\omega)\Gamma(x_i,\omega) \qquad i=1,2,3 \tag{2.60}$$

Substituting Eq. 2.58 into Eq. 2.60 yields

$$G_\eta(x_i,\omega) = \sum_{n=1}^{\infty}\sum_{m=1}^{\infty} \phi_{ni}(x_i)\phi_{mi}(x_i)\{\overset{*}{H}_n(\omega)\}^T[G_{ff}(\omega)]\{H_m(\omega)\} \quad i=1,2,3. \tag{2.61}$$

where any element of the 6x6 spectral matrix of correlated ground-displacement inputs, $[G_{ff}(\omega)]$, is defined by

$$G_{ij}(\omega) = \lim_{T_1 \to \infty} \frac{2}{T_1} E\left[\overset{*}{F}_i(\omega) F_j(\omega)\right] \simeq \frac{2}{T_1} \overset{*}{F}_i(\omega) F_j(\omega) \qquad i,j=1,2,3,4,5,8 \quad (2.62)$$

The diagonal elements of the matrix $[G_{ff}(\omega)]$, i=j in Eq. 2.62, correspond to the power spectral density of the j^{th} displacement input, $f_j(t)$, (j=1,2,3,4,5,8), while the off-diagonal elements of the matrix $[G_{ff}(\omega)]$ correspond to cross-spectral densities between the various input displacements. These cross-spectral terms are present because the various ground motions originate from the same source and are therefore related in some way, so that their correlation (or interaction) must be taken into account. The effect of input correlation upon the vertical response may be examined quite easily using Eq. 2.61. If the inputs are assumed to be uncorrelated, that is, independently applied and unrelated, Eq. 2.61 reduces to

$$G_\eta(x_i,\omega) = \sum_{n=1}^{\infty} \sum_{m=1}^{\infty} \phi_{ni}(x_i)\phi_{mi}(x_i) \left[\sum_{j=1,2,3,}^{4,5,8} (\overset{*}{H}_{nj}(\omega))(H_{mj}(\omega))G_j(\omega) \right]$$

$$i=1,2,3 \qquad (2.63)$$

in which $G_j(\omega)$ is the power-spectral density of the input displacement, $f_j(t)$, which is estimated as

$$G_j(\omega) \simeq \frac{2}{T_1} |F_j(\omega)|^2 \qquad j=1,2,3,4,5,8 \qquad (2.64)$$

In this uncorrelated case all the off-diagonal of the input matrix are equal to zero. The results of Eq. 2.61 can be compared to those of Eq. 2.63 in order to gain a better understanding of the effects of input correlation upon the response calculations. An alternate interpretation

of the correlated and uncorrelated ground motion inputs will be presented in the next section (II.9).

The second characteristic feature of Eq. 2.61 involves the double summation over the vertical modes and their associated complex frequency response functions. It should be noted that the complex frequency-response functions $H_{nj}(\omega)$ peak in amplitude at their associated natural frequencies ω_n and have much lower amplitudes elsewhere along the frequency band. Therefore, when the natural frequencies of vertical vibration are well separated and damping ratios are small, the effect of the cross-terms ($n \neq m$) in Eq. 2.61 becomes much less significant than the diagonal terms ($n = m$) [9]. Under these circumstances, the double summation may be replaced by a single sum, that is:

$$G_\eta(x_i,\omega) = \sum_{n=1}^{\infty} \phi_{ni}^2(x_i)\{H_n^*(\omega)\}[G_{ff}(\omega)]\{H_n(\omega)\} \qquad i=1,2,3. \tag{2.65}$$

However, due to the flexible nature of the suspension bridge, closely spaced modes are quite likely to occur. Under such circumstances the effect of the cross terms ($n \neq m$) are no longer negligible and an accurate representation of the response would have to include these modal interaction cross-terms. For the purpose of this report, Eq. 2.61 is utilized, that is, the effects of modal interaction are incorporated through a double summation.

The mean square value of the relative vertical displacement response, $\psi_\eta^2(x_i)$, is given by the integration of G_η over the entire frequency range.

$$\psi_\eta^2(x_i) = \frac{1}{2\pi}\int_0^\infty G_\eta(x_i,\omega)\,d\omega \qquad i=1,2,3. \tag{2.66}$$

and the square root of Eq. 2.66 is the root mean square (R.M.S.) vibrational displacement response.

The power spectral density of the total vertical response, $v_i(x_i,t)$, can be obtained by multiplying the Fourier transform of Eq. 2.9 by its complex conjugate and by $(2/T_1)$, which leads to

$$G_v(x_i,\omega) = G_\eta(x_i,\omega) + \sum_{j=1}^{4}\left[G_{\eta j}(x_i,\omega) + G_{j\eta}(x_i,\omega)\right]g_{ji}(x_i)$$

$$+ \sum_{j=1}^{4}\sum_{k=1}^{4} g_{ji}(x_i)g_{ki}(x_i)\left[G_{jk}(\omega)\right] \qquad i=1,2,3. \tag{2.67}$$

where

$$G_{\eta j}(x_i,\omega) = \frac{2}{T_1}\overset{*}{\Gamma}(x_i,\omega)F_j(\omega)$$

$$= \frac{2}{T_1}\sum_{n=1}^{\infty}\phi_{ni}(x_i)\{\overset{*}{H}_n(\omega)\}^T\{\overset{*}{F}(\omega)\}F_j(\omega) \qquad i=1,2,3 \quad j=1,2,3,4 \tag{2.68}$$

and

$$G_{j\eta}(x_i,\omega) = \frac{2}{T_1}\overset{*}{F}_j(\omega)\Gamma(x_i,\omega)$$

$$= \frac{2}{T_1}\sum_{n=1}^{\infty}\phi_{ni}(x_i)\overset{*}{F}_j(\omega)\{H_n(\omega)\}^T\{F(\omega)\} \qquad i=1,2,3 \quad j=1,2,3,4 \tag{2.69}$$

For the uncorrelated case, $G_{\eta j}$ and $G_{j\eta}$ reduce to

$$G_{\eta j}(x_i,\omega) = \sum_{n=1}^{\infty}\phi_{ni}(x_i)[\overset{*}{H}_{\eta j}(\omega)][G_j(\omega)] \qquad i=1,2,3 \quad j=1,2,3,4 \tag{2.70}$$

$$G_{j\eta}(x_i,\omega) = \sum_{n=1}^{\infty}\phi_{ni}(x_i)[H_{\eta j}(\omega)][G_j(\omega)] \qquad i=1,2,3, \quad j=1,2,3,4 \tag{2.71}$$

where $H_{nj}(\omega)$ is given by Eq. 2.46 and $G_j(\omega)$ is given by Eq. 2.64. In addition, the cross spectral terms, $G_{jk}(\omega)$ $(j \neq k)$, are equal to zero in Eq. 2.67 for the uncorrelated case.

The integration of G_v over the frequency domain provides the mean square value of the total displacement response, $\psi_v^2(x_i)$, whose square root is the root mean square (R.M.S.) total displacement response

$$\psi_v^2(x_i) = \frac{1}{2\pi}\int_0^\infty G_v(x_i,\omega)\,d\omega$$

$$= \psi_\eta^2(x_i) + \sum_{j=1}^{4} g_{ji}(x_i)[\psi_{\eta j}^2(x_i)]$$

$$+ \sum_{j=1}^{4}\sum_{k=1}^{4} g_{ji}(x_i)g_{ki}(x_i)[\psi_{jk}^2(x_i)] \quad i=1,2,3 \qquad (2.72)$$

where $\psi_\eta^2(x_i)$ is given by Eq. 2.66, and

$$\psi_{\eta j}^2(x_i) = \frac{1}{2\pi}\int_0^\infty [G_{\eta j}(x_i,\omega) + G_{j\eta}(x_i,\omega)]\,d\omega \quad i=1,2,3 \quad j=1,2,3,4 \qquad (2.73)$$

$$\psi_{jk}^2(x_i) = \frac{1}{2\pi}\int_0^\infty [G_{jk}(\omega)]\,d\omega \quad i=1,2,3 \quad j,k=1,2,3,4 \qquad (2.74)$$

The procedure outlined in the above section may be used to evaluate the power spectral density of the vibrationally-induced bending moment in the i^{th} stiffening structure by simply replacing the mode shapes, $\phi_{ni}(x_i)$ and quasi-static functions, $g_{ji}(x_i)$, by their second spanwise derivatives multiplied by the flexural rigidity of the i^{th} stiffening structure, that is, $E_iI_i\phi''_{ni}(x_i)$ and $E_iI_ig''_{ji}(x_i)$, respectively. Similarly, the power spectral density of the vibrationally-induced shearing force in the i^{th} stiffening structure may be obtained by replacing the mode

shapes, $\phi_{ni}(x_i)$ and quasi-static functions, $g_{ji}(x_i)$, by their third spanwise derivatives multiplied by the flexural rigidity of the i^{th} stiffening structure, that is, $E_iI_i\phi'''_{ni}(x_i)$ and $E_iI_ig'''_{ji}(x_i)$, respectively.

Mean square bending moments and shearing forces are obtained by Eq. 2.72 with the mode shapes and quasi-static functions replaced as above. Additionally, the mean square stresses in the chords of the i^{th} suspended structure can be related to the mean square bending moments using the following flexural stress relation:

$$\psi_\sigma^2(x_i) = \left(\frac{d_i}{2I_i}\right)^2 \psi_M^2(x_i) \qquad i=1,2,3 \tag{2.75}$$

where ψ_M^2 is the mean square bending moment in the i^{th} span, ψ_σ^2 is the mean square stress in the i^{th} span, d_i is the depth of the i^{th} stiffening structure, and I_i is the moment of inertia of the i^{th} stiffening structure.

II.9 AN ALTERNATE INTERPRETATION OF CORRELATED AND UNCORRELATED GROUND MOTION INPUTS

At this point it is important to define the concept of correlated and uncorrelated ground motion inputs. Let $v_1(x,t)$ be the vibrational displacement at point x as shown in Fig. II-2, due to the ground input $f_1(t)$ at the first support. Let $v_2(x,t)$ be the displacement at the same point, due to $f_2(t)$ at the second support (a different support than the first). The vibrational displacement due to both excitations is then $v(x,t) = v_1(x,t) + v_2(x,t)$ and the autocorrelation of $v(x,t)$ as a result of the two inputs is

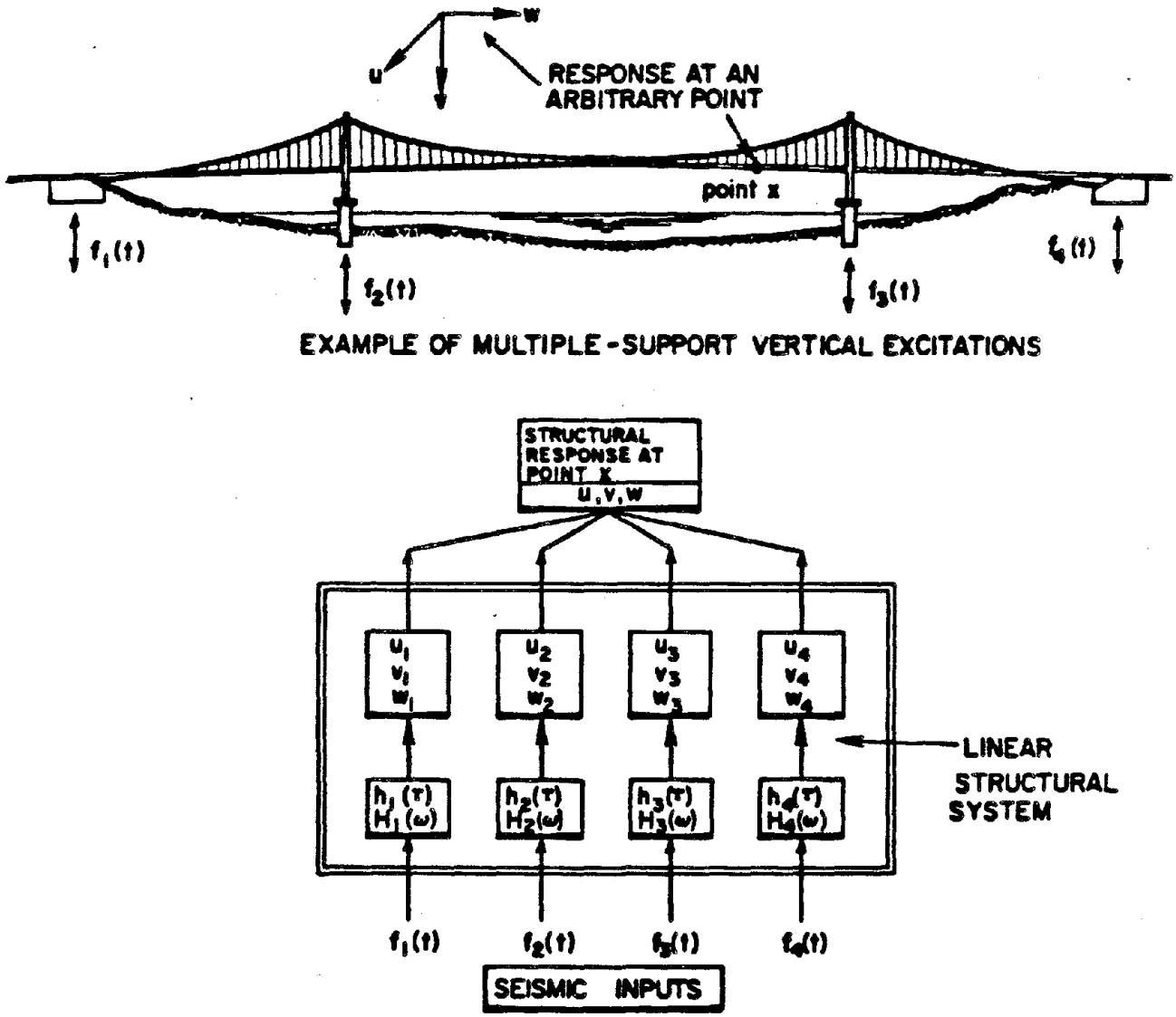

Fig. II-2 Multiple-support vertical seismic inputs.

$$R_v(\tau) = E[v(x,t)v(x,t+\tau)] = E[(v_1(x,t) + v_2(x,t))(v_1(x,t+\tau) + v_2(x,t+\tau))]$$

$$= E[v_1(x,t)v_1(x,t+\tau)] + E[v_1(x,t)v_2(x,t+\tau)]$$

$$+ E[v_2(x,t)v_1(x,t+\tau)] + E[v_2(x,t)v_2(x,t+\tau)]$$

$$= R_{v_1}(\tau) + R_{v_1v_2}(\tau) + R_{v_2v_1}(\tau) + R_{v_2}(\tau) \qquad (2.76)$$

and the Fourier transform of the last result is

$$G_v(f) = G_{v_1}(f) + G_{v_1v_2}(f) + G_{v_2v_1}(f) + G_{v_2}(f) \qquad (2.77)$$

Thus, the autocorrelation or the autospectral function of the vibrational displacement at the given point x on the bridge due to separate support excitations $f_1(t)$ and $f_2(t)$ cannot be determined simply by adding the autocorrelations (in time domain) or the autospectral functions (in frequency domain) resulting from each support excitation acting separately; $R_{v_1v_2}$, $R_{v_2v_1}$ or $G_{v_1v_2}$, $G_{v_2v_1}$ are here referred to as cross-correlation functions and cross spectral functions and in general are not equal. Thus the sum autospectral density function requires knowledge of the input cross-spectral functions as well as their autspectral functions.

Thus for the correlated multiple support excitations

$$R_{v_iv_j}(\tau) \quad \text{or} \quad G_{v_iv_j}(f) \neq 0, \quad i \neq j,\ i,j=1,2,\ldots,N \qquad (2.78)$$

and for the uncorrelated multiple support excitations

$$R_{v_iv_j}(\tau) \quad \text{or} \quad G_{v_iv_j}(f) = 0, \quad i \neq j,\ i,j=1,2,\ldots,N \qquad (2.79)$$

In the above equations $E[\cdot]$ represents the expected value of the term inside the brackets; f is the frequency; and N is the number of input support motions.

II.10. ADDITIONAL HORIZONTAL COMPONENT OF CABLE TENSION H(t)

The additional (vibrational) horizontal component of cable tension due to multiple-support excitations is given by (Eq. 2.8):

$$H(t) = \frac{E_c A_c}{L_E} \left\{ \sum_{i=1}^{3} \left[\frac{\overset{*}{w}_i}{H_w} \int_0^{\ell_i} v_i \, dx_i - \frac{\overset{*}{w}_i \ell_i}{2H_w} \{ f_{i+1}(t) + f_i(t) \} \right] + [f_8(t) - f_5(t)] \right\} \tag{2.80}$$

Substituting Eq. 2.41 into Eq. 2.80 results in:

$$H(t) = \frac{E_c A_c}{L_E} \left\{ \sum_{i=1}^{3} \left[\frac{\overset{*}{w}_i}{H_w} \left[\int_0^{\ell_i} \sum_{n=1}^{\infty} \phi_{ni}(x_i) dx_i \right] q_n(t) + \frac{\overset{*}{w}_i}{H_w} \sum_{j=1}^{4} \left[\int_0^{\ell_i} g_{ji}(x_i) dx_i \right] f_j(t) - \frac{\overset{*}{w}_i \ell_i}{2H_w} [f_{i+1}(t) + f_i(t)] \right] + [f_8(t) - f_5(t)] \right\} \tag{2.81}$$

where the generalized coordinates $q_n(t)$ are obtained by the convolution integral of Eq. 2.39.

In order to analyze the cable tension in the frequency domain, the finite Fourier transform of Eq. 2.81 becomes:

$$H(\omega) = \frac{E_c A_c}{L_E} \left\{ \sum_{i=1}^{3} \left[\frac{\overset{*}{w}_i}{H_w} \left[\int_0^{\ell_i} \sum_{n=1}^{\infty} \phi_{ni}(x_i) dx_i \right] Q_n(\omega) + \frac{\overset{*}{w}_i}{H_w} \sum_{j=1}^{4} \left[\int_0^{\ell_i} g_{ji}(x_i) dx_i \right] F_j(\omega) \right. \right.$$

$$- \frac{w_i^* \ell_i}{2H_w}[F_{i+1}(\omega) + F_i(\omega)]\Bigg] + [F_8(\omega) - F_5(\omega)]\Bigg\} \qquad (2.82)$$

where $F_j(\omega)$ $(j=1,2,3,4,5,8)$ is the finite Fourier transform of the input ground displacement (Eq. 2.54) and $Q_n(\omega)$ is the Fourier transform of the n^{th} generalized coordinate, calculated as

$$Q_n(\omega) = \{H_n(\omega)\}^T\{F(\omega)\} \qquad n=1,2,3,... \qquad (2.83)$$

where $\{H_n(\omega)\}^T$ is the transposed frequency-response vector corresponding to the n^{th} vertical vibration mode, and $\{F(\omega)\}$ is the Fourier transform vector of the ground-displacement inputs (see Eqs. 2.56, 2.57). Note that for antisymmetric vertical vibration, the first term in Eq. 2.82 vanishes since the additional cable tension associated with an antisymmetric vertical vibration mode is equal to zero (see Appendix II-b).

The power spectrum of $H(t)$ may be approximated as

$$G_H(\omega) \approx \frac{2}{T_1} H^*(\omega)H(\omega) \qquad (2.84)$$

where T_1 is the duration of the ground motion and the superposed asterisk denotes complex conjugate. Substituting Eqs. 2.82 and 2.83 into Eq. 2.84 results in an explicit expression for $G_H(\omega)$ (the details are found in Appendix II-d). For the uncorrelated calculation, only the terms which involve the input power-spectra are retained, since the supports motions are assumed to be unrelated, in this case, while the correlated case retains all of its terms (including the cross-spectra).

Mean square dynamically-induced cable tensions are obtained by integrating $G_H(\omega)$ over the entire frequency range, that is

$$\psi_H^2 = \frac{1}{2\pi} \int_0^\infty G_H(\omega)\, d\omega \tag{2.85}$$

and the square root of Eq. 2.85 is the root mean square (R.M.S.) dynamically-induced horizontal component of cable tension due to vertical vibration.

II.11. DISCUSSION OF PEAK RESPONSE FACTORS

The frequency-domain analysis results in mean square response values. For example, Eq. 2.72 gives the mean square vertical displacement response. The square root of the mean square response is defined as the root mean square (R.M.S.) response or the standard deviation of the response. From a practical point of view, the parameter of most interest in the analysis and design processes is the expected peak value of the response, which is to be compared with the allowable yield stress limit. The statistical distribution of the maximum response of a single-degree-of-freedom system is shown by Vanmarcke [17] to depend importantly upon the first three response spectral moments. In terms of response displacements, for example, these moments become:

$$\lambda_m(x_i) = \frac{1}{2\pi} \int_0^\infty \omega^m G_v(x_i,\omega)\, d\omega \qquad \begin{matrix} i=1,2,3 \\ m=0,1,2 \end{matrix} \tag{2.86}$$

When $m = 0$, Eq. 2.86 corresponds to the mean square displacement response (Eq. 2.72). In addition, when $m = 2$ Eq. 2.86 defines the mean square velocity response.

The relationship between peak response and root mean square values may be written as

$$v_{max}(x_i) = r_{T_1;p}\, \psi_v(x_i) = r_{T_1;p} \sqrt{\lambda_0} \qquad i=1,2,3, \tag{2.87}$$

where $v_{max}(x_i)$ is the expected peak displacement response in the i^{th} span, $\Psi_v(x_i) = \sqrt{\lambda_0}$ is the root mean square (R.M.S.) displacement in the i^{th} span and $r_{T_1;p}$ is the peak factor corresponding to a ground motion duration T_1 and a statistical confidence level p.

Several methods for determining the maximum response (or peak factor) have been proposed in the literature. Davenport [8] bases the maximum response behavior on a Poisson "threshhold crossing" model, which gives the mean, μ, and the standard deviation, σ, of the maximum response as

$$\mu = \left[\sqrt{2 \ln(\nu T_1)} + \frac{0.5772}{\sqrt{2 \ln(\nu T_1)}}\right]\sqrt{\lambda_0} \tag{2.88}$$

$$\sigma = \left[\frac{\pi}{\sqrt{6}} \frac{1}{\sqrt{2 \ln(\nu T_1)}}\right] \sqrt{\lambda_0} \tag{2.89}$$

where ν is the zero-crossing rate of the response, given by

$$\nu = \frac{1}{\pi} \sqrt{\lambda_2/\lambda_0} \tag{2.90}$$

Equations 2.88 and 2.89 imply that the peak factor has a mean and standard deviation corresponding to the bracketed terms in these equations.

Der Kiureghian [9,10] has shown that Davenport's result tends to overestimate the mean and underestimate the standard deviation, since threshold crossings are considered independent in the Poisson model. Der Kiureghian suggests that in order to account for the dependence between threshold crossings, a reduced zero-crossing rate, ν_e, should be used in Eq. 2.88, which represents an equivalent rate of statistically independent crossings, in which case

$$\nu_e = (1.63\delta^{0.45} - 0.38)\,\nu \qquad \delta \leq 0.69$$
$$\nu_e = \nu \qquad \delta \geq 0.69 \tag{2.91}$$

In addition, Eq. 2.89 is replaced by [9,10]

$$\sigma = \left[\frac{1.2}{\sqrt{2\ \ln(\nu_e T_1)}} - \frac{5.4}{13 + [2\ \ln(\nu_e T_1)]^{3.2}}\right]\sqrt{\lambda_0} \tag{2.92}$$

The parameter δ in Eq. 2.91 is a measure of the spread in the frequency content of the response power spectral density function about its center frequency Ω, where

$$\delta = \sqrt{1 - \frac{\lambda_1^2}{\lambda_0 \lambda_2}} \tag{2.93}$$

$$\Omega = \sqrt{\frac{\lambda_2}{\lambda_0}} \tag{2.94}$$

Vanmarcke [17] calculates the peak factor based upon an approximate solution of the so-called first passage problem, using the assumption of suddenly applied time-limited steady-state Gaussian excitations. The peak factor for this case becomes

$$r_{T_1;p} = \left[2\ \ln\left\{2n\left[1 - \exp\left(-\delta_e\sqrt{\pi\ \ln(2n)}\right)\right]\right\}\right]^{1/2} \tag{2.95}$$

where

$$n = (\Omega T_1/2\pi)(-\ln p)^{-1} \tag{2.96}$$

and δ_e is an empirical constant, given by

$$\delta_e \simeq \delta^{1.2} \tag{2.97}$$

For large values of δ_e, Eq. 2.95 approaches

$$r_{T_1;p} = \sqrt{2 \ln(2n)} \tag{2.98}$$

Equation 2.95 has the advantage that the peak factor is directly predicted rather than its mean and standard deviations. Also, the effect of dependent threshold crossings were included in Vanmarcke's analysis from the beginning, rather than being adjusted for at the end of the analysis.

Using the above relations, peak displacements, stresses, moments, and vibrational cable tensions can be estimated from the corresponding root mean square frequency-domain results.

II.12. RESPONSE SPECTRUM APPROACH (UNCORRELATED CASE)

A quick (first hand) estimate for the peak response may be calculated using response spectra methods. This estimate is unfortunately valid only for the uncorrelated ground-inputs case. Assuming the damping ratios, ξ_n, to be equal to zero for simplicity, Eq. 2.33 becomes

$$\ddot{q}_n(t) + \omega_n^2 q_n(t) = - \sum_{j=1}^{4} R_{jn} \ddot{f}_j(t)$$

$$+ P_n \alpha \sum_{i=1}^{3} \beta_i [f_{i+1}(t) + f_i(t)]$$

$$- P_n \alpha [f_8(t) - f_5(t)] \qquad n=1,2,3,... \tag{2.99}$$

The solution to the previous equation assuming quiescent initial conditions, is given by the convolution integral

$$q_n(t) = \frac{1}{\omega_n}\int_0^t \left\{ -\sum_{j=1}^{4} R_{jn}\ddot{f}_j(\tau) + P_n\alpha \sum_{i=1}^{3} \beta_i [f_{i+1}(\tau) + f_i(\tau)] \right.$$

$$\left. - P_n\alpha[f_8(\tau) - f_5(\tau)] \right\} \{\sin \omega_n(t - \tau)\}d\tau \qquad n=1,2,3... \qquad (2.100)$$

The contribution of a typical acceleration input in Eq. 2.100 to the response of the n^{th} generalized coordinate may be written

$$q_{nj}^{(a)}(t) = \frac{R_{jn}}{\omega_n}\int_0^t \ddot{f}_j(\tau)\sin \omega_n(t - \tau)d\tau \qquad \begin{matrix} j=1,2,3,4. \\ n=1,2,3,... \end{matrix} \qquad (2.101)$$

The maximum value of the previous equation is given by

$$\left|q_{nj}^{(a)}(t)\right|_{max} = \left|\frac{R_{jn}}{\omega_n}\int_0^t \ddot{f}_j(\tau)\sin \omega_n(t - \tau)d\tau\right| = |R_{jn}|SD_j^{(n)}$$

$$\begin{matrix} j=1,2,3,4 \\ n=1,2,3... \end{matrix} \qquad (2.102)$$

Where $SD_j^{(n)}$ is the spectral displacement of the j^{th} vertical support motion of the n^{th} natural period of the structure and $\left|q_{nj}^{(a)}(t)\right|_{max}$ represents the contribution of the j^{th} vertical support acceleration to the maximum response of the n^{th} generalized coordinate.

Similarly, the contribution of a typical vertical displacement input in Eq. 2.100 to the response of the n^{th} generalized coordinate may be written

$$q_{nj}^{(d_1)}(t) = \frac{P_n\alpha\beta_i}{\omega_n}\int_0^t f_j(\tau)\sin \omega_n(t - \tau)d\tau \qquad \begin{matrix} i=1,2,3 \\ j=1,2,3,4 \\ n=1,2,3,... \end{matrix} \qquad (2.103)$$

Integrating the previous equation by parts, assuming quiescent initial conditions, results in

$$q_{nj}^{(d_1)}(t) = \frac{P_n \alpha \beta_i}{\omega_n^2}\left[- f_j(t) + \frac{1}{\omega_n}\int_0^t \ddot{f}_j(\tau)\sin \omega_n(t-\tau)d\tau\right]\begin{matrix} i=1,2,3 \\ j=1,2,3,4 \\ n=1,2,3... \end{matrix} \quad (2.104)$$

The maximum value of the previous equation may be estimated by combining its two terms using the square root of sum of squares (SRSS) approach usually used in response spectra methods. This results in

$$\left|q_{nj}^{(d_1)}(t)\right|_{max} = \left|\frac{P_n \alpha \beta_i}{\omega_n^2}\right|\left\{\left(SD_j^{(n)}\right)^2 + \left(\left|f_j(t)\right|_{max}\right)^2\right\}^{1/2} \quad (2.105)$$

$$i=1,2,3 \qquad j=1,2,3,4 \qquad n=1,2,3,...$$

where $\left|f_j(t)\right|_{max}$ is the maximum amplitude of the j^{th} vertical support motion, and $\left|q_{nj}^{(d_1)}(t)\right|_{max}$ represents the contribution of the j^{th} vertical support displacement to the maximum response of the n^{th} generalized coordinate.

The contribution of a typical longitudinal displacement input in Eq. 2.100 to the response of the n^{th} generalized coordinate may be written

$$q_{nj}^{(d_2)}(t) = \pm \frac{P_n \alpha}{\omega_n}\int_0^t f_j(\tau)\sin \omega_n(t-\tau)d\tau \quad (2.106)$$

$$\begin{matrix} i=1,2,3, \\ j=5(+) \\ j=8(-) \\ n=1,2,3... \end{matrix}$$

Integrating the previous equation by parts, assuming quiescent initial conditions, results in

$$q_{nj}^{(d_2)}(t) = \pm \frac{P_n \alpha}{\omega_n^2}\left[- f_j(t) + \frac{1}{\omega_n}\int_0^t \ddot{f}_j(\tau)\sin \omega_n(t-\tau)d\tau\right]\begin{matrix} i=1,2,3 \\ j=5(+) \\ j=5(-) \\ n=1,2,3... \end{matrix} \quad (2.107)$$

The maximum value of the previous equation may be estimated by combining its two terms using the square root of sum of squares (SRSS) approach. This results in

$$\left|q_{nj}^{(d_2)}(t)\right|_{max} = \left|\frac{P_n \alpha \beta_i}{\omega_n^2}\right| \left\{\left(SD_j^{(n)}\right)^2 + \left(\left|f_j(t)\right|_{max}\right)^2\right\}^{1/2}$$

$$i=1,2,3$$

$$j=5,8$$

$$n=1,2,3... \qquad (2.108)$$

where $\left|f_j(t)\right|_{max}$ is the maximum amplitude of the j^{th} longitudinal support motion, and $\left|q_{nj}^{(d_1)}(t)\right|_{max}$ represents the contribution of the j^{th} longitudinal support displacement to the maximum response of the n^{th} generalized coordinate.

The various contributions to the maximum response of the generalized coordinate, $\left|q_n(t)\right|_{max}$, may be added by a square root of the sum of squares approach (SRSS), which essentially neglects the effects of input correlation and modal interaction in combining the modal contributions. This results in

$$\left|q_n(t)\right|_{max} \leq \left\{\sum_{j=1}^{4} (R_{jn})^2 \left(SD_j^{(n)}\right)^2 \right.$$

$$+ P_n^2 \frac{\alpha^2}{\omega_n^4} \sum_{i=1}^{3} (\beta_i)^2 \left[\left(SD_{i+1}^{(n)}\right)^2 + \left(SD_i^{(n)}\right)^2\right.$$

$$\left. + \left(\left|f_{i+1}(t)\right|_{max}\right)^2 + \left(\left|f_i(t)\right|_{max}\right)^2\right]$$

$$+ P_n^2 \frac{\alpha^2}{\omega_n^4} \left[\left(SD_5^{(n)}\right)^2 + \left(SD_8^{(n)}\right)^2\right.$$

$$\left.\left. + \left(\left|f_5(t)\right|_{max}\right)^2 + \left(\left|f_8(t)\right|_{max}\right)^2\right]\right\}^{1/2} \qquad n=1,2,3... \quad (2.109)$$

The peak displacement response may be estimated using Eqs. 2.41 and 2.109 and is given by

$$|v_i(x_i,t)|_{max} \leq \left\{ \sum_{j=1}^{4} [g_{ji}(x_i)]^2 \left(|f_j(t)|_{max} \right)^2 + \sum_{n=1}^{\infty} [\phi_{ni}(x_i)]^2 \left(|q_n(t)|_{max} \right)^2 \right\}^{1/2} \qquad i=1,2,3, \qquad (2.110)$$

Peak moments and shearing forces occurring in the i^{th} stiffening truss may be obtained by replacing $g_{ji}(x_i)$ and $\phi_{ni}(x_i)$ in Eq. 2.110 by their second and third spanwise derivatives multiplied by the flexural rigidity E_iI_i of the i^{th} suspended structure, that is $E_iI_i g''_{ji}(x_i)$, $E_iI_i \phi''_{ni}(x_i)$, and $E_iI_i g'''_{ji}(x_i)$, $E_iI_i \phi'''_{ni}(x_i)$, respectively.

The response spectra approach may be used to estimate the peak value of the additional horizontal component of cable tension, H(t). Equation 2.80 is used for this purpose, which after introducing the expression for $v_i(x_i,t)$ in terms of its quasi-static and modal contributions (Eq. 2.41) becomes

$$H(t) = \left(\frac{E_c A_c}{L_E} \right) \left\{ \sum_{n=1}^{\infty} \Gamma_n q_n(t) + \sum_{j=1}^{4} \gamma_j f_j(t) - \sum_{i=1}^{3} \left(\frac{w_i^* \ell_i}{2H_w} \right) [f_{i+1}(t) + f_i(t)] + [f_8(t) - f_5(t)] \right\} \qquad (2.111)$$

where the factors Γ_n and γ_j are given by

$$\Gamma_n = \sum_{i=1}^{3} \frac{w_i^*}{H_w} \int_0^{\ell_i} \phi_{ni}(x_i)\,dx_i \qquad n=1,2,3... \qquad (2.112)$$

$$\gamma_j = \sum_{i=1}^{3} \frac{w_i^*}{H_w} \int_0^{\ell_i} g_{ji}(x_i)\,dx_i \qquad j=1,2,3,4 \qquad (2.113)$$

In order to estimate $|H(t)|_{max}$, the maximum expected horizontal vibrational component of cable tension (for the uncorrelated case), the square root of sum of squares rule can be used to combine the various contributions in Eq. 2.111. This results in

$$|H(t)|_{max} \leq \left(\frac{E_c A_c}{L_E}\right) \left\{ \sum_{n=1}^{\infty} \Gamma_n^2 \left(|q_n(t)|_{max} \right)^2 + \sum_{j=1}^{4} \gamma_j^2 \left(|f_j(t)|_{max} \right)^2 \right.$$

$$- \sum_{i=1}^{3} \left(\frac{w_i^* \ell_i}{2H_w}\right)^2 \left[\left(|f_{i+1}(t)|_{max} \right)^2 + \left(|f_i(t)|_{max} \right)^2 \right]$$

$$\left. + \left[\left(|f_8(t)|_{max} \right)^2 + \left(|f_5(t)|_{max} \right)^2 \right] \right\}^{1/2} \qquad (2.114)$$

where $|q_n(t)|_{max}$ is calculated from Eq. 2.109.

II.13. APPLICATIONS

II.13.1 Vertical Seismic Behavior of the Vincent Thomas Bridge

In this section, the analysis outlined in this chapter is applied to the Vincent Thomas Suspension Bridge in Los Angeles, California [3] in order to estimate its vertical response characteristics. Frequency domain random vibration methods and time domain convolution integrals

are to be compared. The structural properties of the bridge are summarized in Table II-1. The vertical quasi-static functions are shown in Fig. II-3 for unit vertical ground motion displacement at each anchorage and tower base. The first ten symmetric and antisymmetric vertical mode shapes are shown in Fig. II-4, while their associated participation coefficients appear in Table II-2. These computed modes (obtained via Eqs. 2.25, 2.27 and 2.29) compare very well with those computed and measured in Refs. 1, 2, and 3.

It will be seen in a later section (II.13.3) that the antisymmetric vertical vibration response turns out to be much smaller than the symmetric vertical vibration response. This is due to the modal factor P_n being zero for the antisymmetric modes (because the net area underneath an antisymmetric mode is identically zero); and therefore the longitudinal ground motions, which excite the symmetric modes very strongly, do not excite the antisymmetric modes at all. It should also be noted that the additional horizontal component of cable tension (Eq. 2.80) essentially contains four contributions:

1. Contribution from pure ground motion displacement inputs (both vertical and longitudinal).
2. Contribution from symmetric vertical vibration.
3. Contribution from antisymmetric vertical vibration which turns out to be identically zero.
4. Contribution from the quasi-static motions.

The contribution from antisymmetric vertical vibration to the additional cable tension is zero because again the net area underneath an antisymmetric mode is identically zero. In this section, therefore, because of the higher order nature of the antisymmetric response, and because the

Table II-1

VERTICAL PROPERTIES OF THE VINCENT THOMAS BRIDGE

Parameter	Center Span	Side Spans
Span Length	$\ell_2 = 1500$ ft.	$\ell_1 = \ell_3 = 506.5$ ft.
$\overset{*}{w}_i$	$\overset{*}{w}_2 = 3.589$ k/ft	$\overset{*}{w}_1 = \overset{*}{w}_3 = 3.589$ k/ft
E_i	$E_2 = 29000$ ksi	$E_1 = E_3 = 29000$ ksi
I_i	$I_2 = 6050$ ft^2 in^2	$I_1 = I_3 = 6250$ ft^2 in^2
truss depth	d = 15 ft	d = 15 ft
Cable Properties		
	$E_c = 27000$ ksi	
	$A_c = 121.5$ in^2	
	$L_E = 3460$ ft	
	$H_w = 6750$ kip	

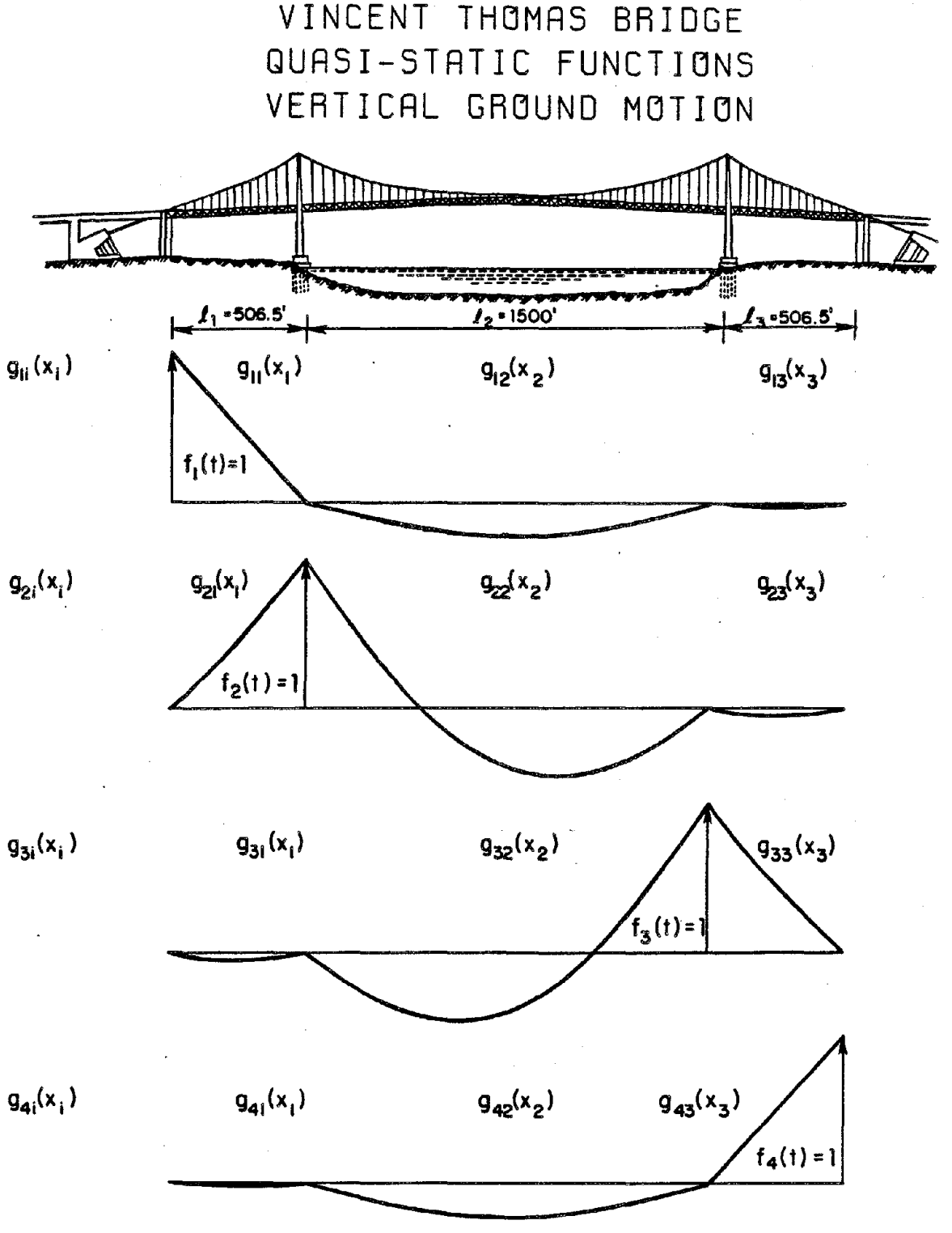

Fig. II-3 Vertical quasi-static functions of the Vincent Thomas Bridge.

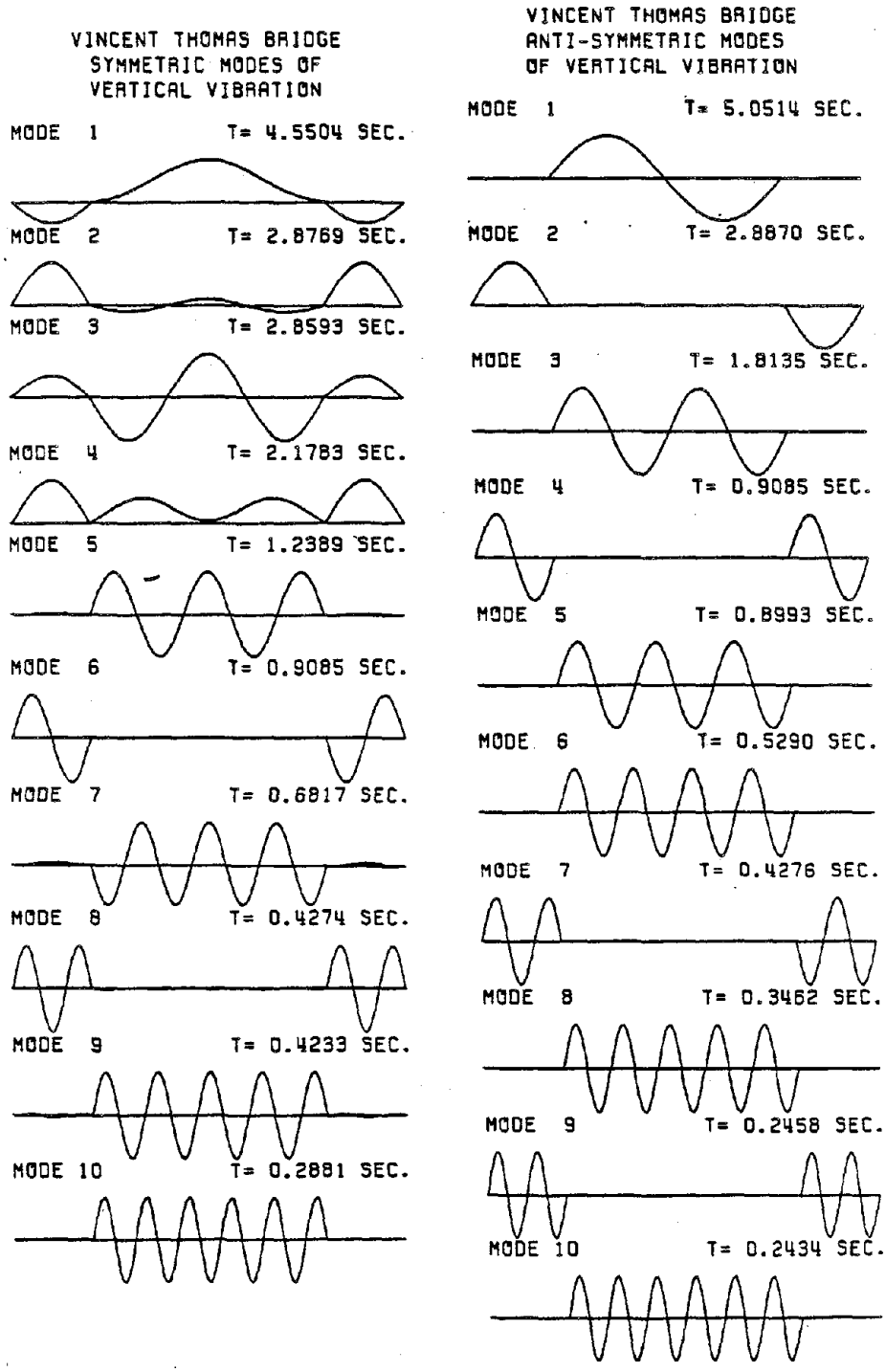

Fig. II-4 Mode shapes of vertical vibration of the Vincent Thomas Bridge (Eqs. 2.25, 2.27 and 2.29).

Table II-2

PARTICIPATION COEFFICIENTS OF VERTICAL EARTHQUAKE RESPONSE OF THE VINCENT THOMAS SUSPENSION BRIDGE

Mode Order n	Symmetric Vibration			Antisymmetric Vibration		
	$R_{1n} = R_{4n}$	$R_{2n} = R_{3n}$	P_n	$R_{1n} = -R_{4n}$	$R_{2n} = -R_{3n}$	P_n
1	-0.324	-0.387	0.647	0.00	0.318	0.0
2	0.293	0.209	1.158	0.318	0.318	0.0
3	0.092	-0.091	0.023	0.00	0.159	0.0
4	0.104	1.116	0.581	0.159	-0.159	0.0
5	0.001	0.127	0.333	0.00	0.106	0.0
6	0.159	-0.159	0.00	0.00	0.079	0.0
7	-0.002	-0.095	-0.032	0.106	0.106	0.0
8	0.106	0.104	0.431	0.00	0.063	0.0
9	0.002	0.072	0.152	0.079	-0.079	0.0
10	0.0	0.057	0.116	0.00	0.052	0.0

additional horizontal component of cable tension can be constructed from knowledge of the symmetric vertical vibration response as well as knowledge of the ground motion displacement inputs, only the symmetric vertical response will be investigated for the Vincent Thomas Bridge.

The complex frequency response functions $H_n(\omega)$ for the first four symmetric vertical modes of the bridge are shown in Fig. II-5 for 2% damping (for all modes) and corresponding to anchorage vertical input, tower vertical input, and anchorage longitudinal input. These functions measure the magnification (or gain) factor corresponding to a unit harmonic displacement upon the response of the generalized coordinate $q_n(t)$. It can be seen from these figures that the longitudinal anchorage motions contribute greatly to the symmetric vertical response, while contributing nothing to the antisymmetric vertical vibration. For higher modes, similar functions are obtained.

Three symmetric vertical response cases are studied for the Vincent Thomas Bridge. In the first case, the vertical motions at the left anchorage and left tower, $f_1(t)$ and $f_2(t)$, respectively, correspond to the vertical component of Array No. 5 of the El Centro Arrays; the vertical motions at the right tower and right anchorage, $f_3(t)$ and $f_4(t)$, respectively, correspond to the vertical component of Array No. 6; and the longitudinal motions $f_5(t)$ and $f_8(t)$ at the anchorages are taken as the associated SSOW components (of Arrays No. 5 and 6) (see Appendix II-e). It should be mentioned that for the Vincent Thomas Bridge, the distance between the towers and anchorages is only 506.5 feet, which is fairly short. Therefore, the left tower and left anchorage are assumed to move uniformly and are thus exposed to the same ground motion inputs; similarly the right anchorage and tower are assumed to move

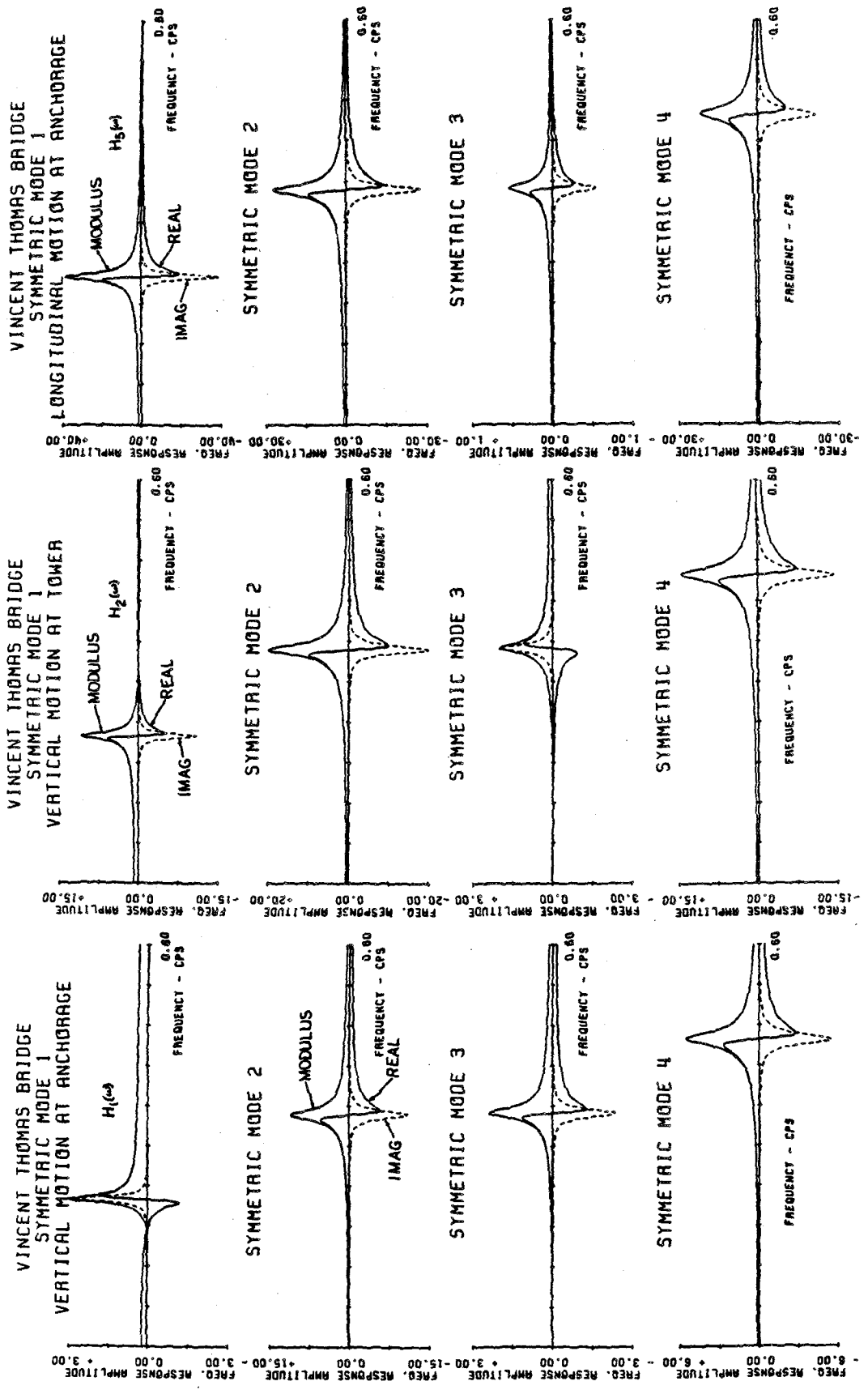

Fig. II-5 Frequency response functions for the first four symmetric modes of vertical vibration of the Vincent Thomas Bridge.

uniformly and are thus exposed to the same ground motion inputs. The second response case involves similar correspondences with Array Nos. 6 and 7. The third response case utilizes ground motions recorded during the San Fernando 1971 earthquake as inputs. In this case, the vertical motions $f_1(t)$ and $f_2(t)$ correspond to the vertical component recorded at the Athenium Building. The vertical motions $f_3(t)$ and $f_4(t)$ correspond to the vertical component recorded at the Millikan Library, and the longitudinal motions $f_5(t)$ and $f_8(t)$ are taken as the associated N90E components [11].

The autospectra of midspan displacement for both side and center spans are shown in Fig. II-6 for input arrays 5 and 6, and in Fig. II-7 for input arrays 6 and 7. It is seen that the bridge is responding mostly in its first two symmetric modes, most likely because their modal participation factors P_n are large and their natural frequencies lie within the region of the input spectra where the ground excitation energy is strong (see the input power and cross spectra - Appendix II-e). Also, the quasi-static contribution to the total response is small compared with the vibrational response for this case. For this reason, the displacements are quite similar in the left and right side spans, and thus only the results for the left side span are shown. It appears that the uncorrelated case has a conservative effect, i.e., the inclusion of the off-diagonal correlated terms in the spectral input matrix $[G_{ff}(\omega)]$ tends to reduce the symmetric vertical response for this specific case as shown in Figs. II-6 and II-7.

The autospectra of midspan second derivative (or curvature) responses for side and center spans, which are related to response bending moments and flexural stresses in the top and bottom chords of the bridge's

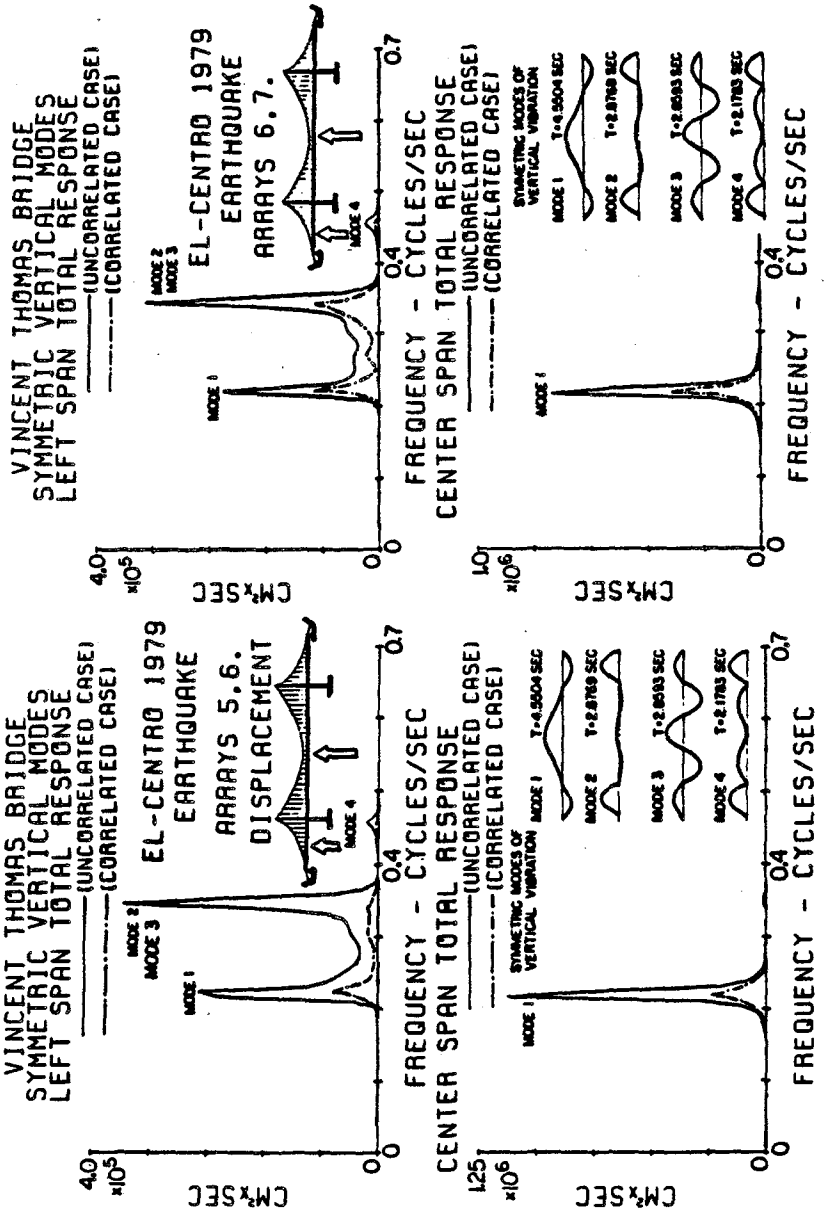

Fig. II-6 Autospectra of midspan displacements. Input arrays 5 and 6.

Fig. II-7 Autospectra of midspan displacements. Input arrays 6 and 7.

stiffening structure, are shown in Fig. II-8 for input arrays 5 and 6 and in Fig. II-9 for input arrays 6 and 7. Figures II-10 and II-11 show similar spectra for the third derivative response evaluated at the ends of each span, which is related to the dynamic shearing force. The arrows on the superimposed bridge in Figs. II-6, 7, 8, 9, 10, and 11 indicate the points at which the response is calculated. Again, the uncorrelated case is seen to be more conservative than the correlated case (for this specific bridge and these specific inputs).

Similar autospectra for the San Fernando 1971 input case are shown in Figs. II-12, 13, and 14, and the autospectra of the additional (vibrational) horizontal component of cable tension for all three response cases are shown in Fig. II-15. It appears that, in general, the first and second symmetric modes respond most strongly in all cases because of their sensitivity to longitudinal input motion at the anchorages (P_n is large -- see Table II-2) as well as their natural frequencies being within the spectral region of strong energy input. A graphical summary of the three response cases appears in Fig. II-16.

In Table II-3, the root mean square values of response are summarized and are compared with the computed maximum responses obtained from the time domain (Duhamel integral) analysis shown in Figs. II-17 through II-23. It seems that the expected value for the peak factor is about 2.2 from Table II-3. It is also seen from this table that the 1979 El Centro ground motions excite the bridge more strongly than the 1971 San Fernando ground motions. The reason for this lies in the closeness of the El Centro Arrays to the causative fault. In particular, input arrays No. 6 and 7 provide for the largest response. The conservative nature of input correlation can be seen from this table. Also, the values of

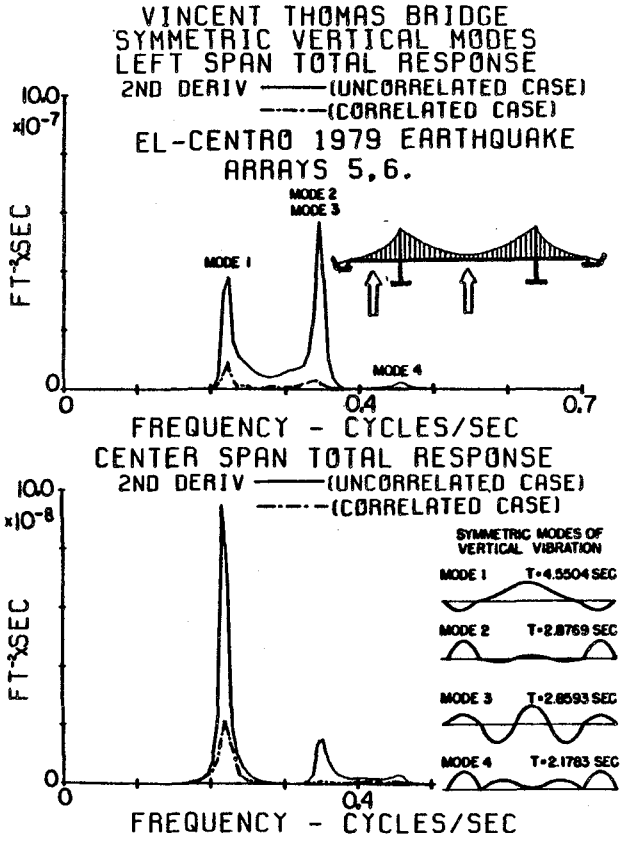

Fig. II-8 Autospectra of second derivative response at midspan. Input arrays 5 and 6.

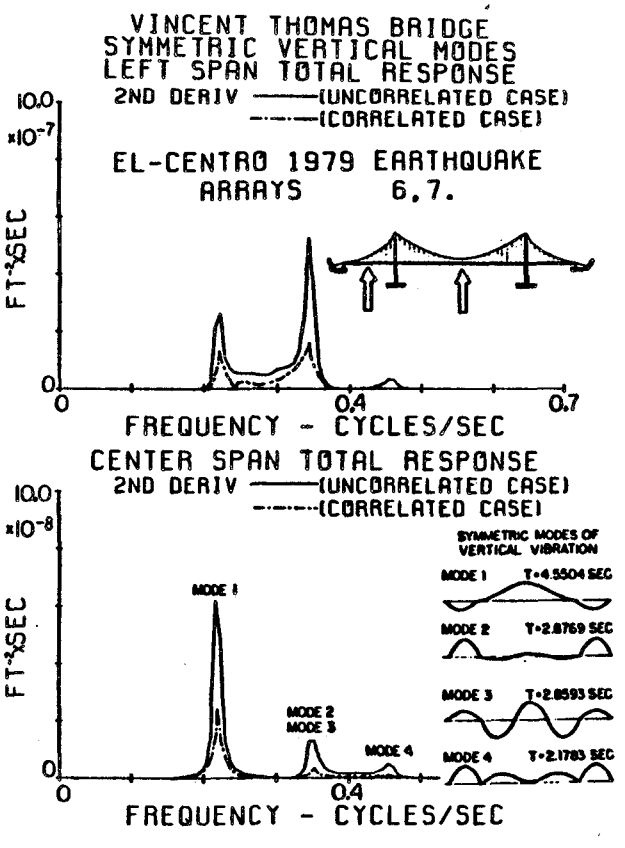

Fig. II-9 Autospectra of second derivative response at midspan. Input arrays 6 and 7.

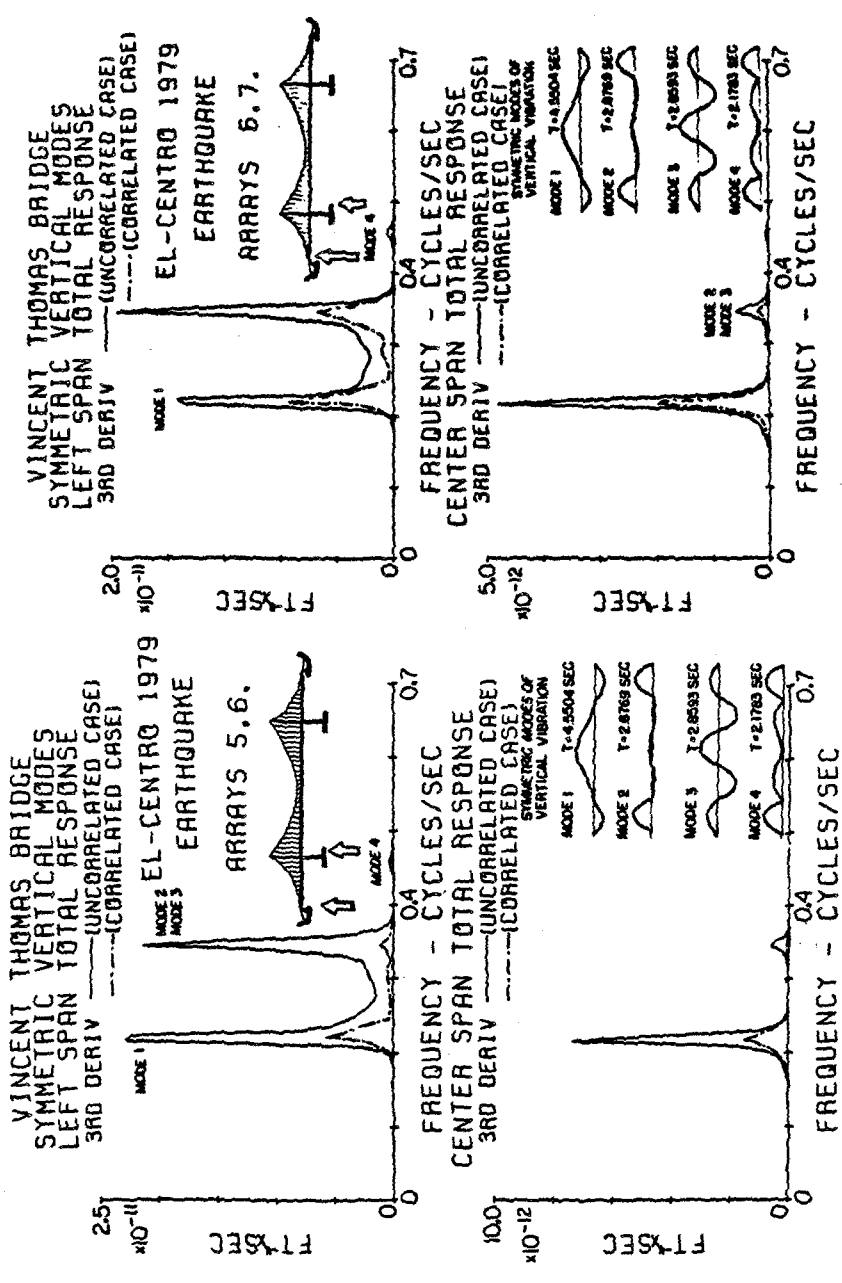

Fig. II-10 Autospectra of third derivative response at endspan. Input arrays 5 and 6.

Fig. II-11 Autospectra of third derivative response at endspan. Input arrays 6 and 7.

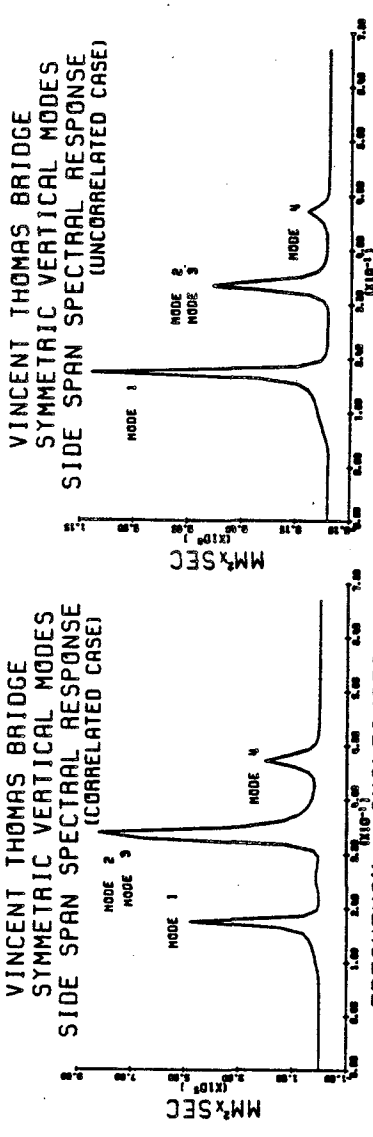

Fig. II-12a Autospectra of midspan displacements (correlated case). 1971 San Fernando earthquake inputs.

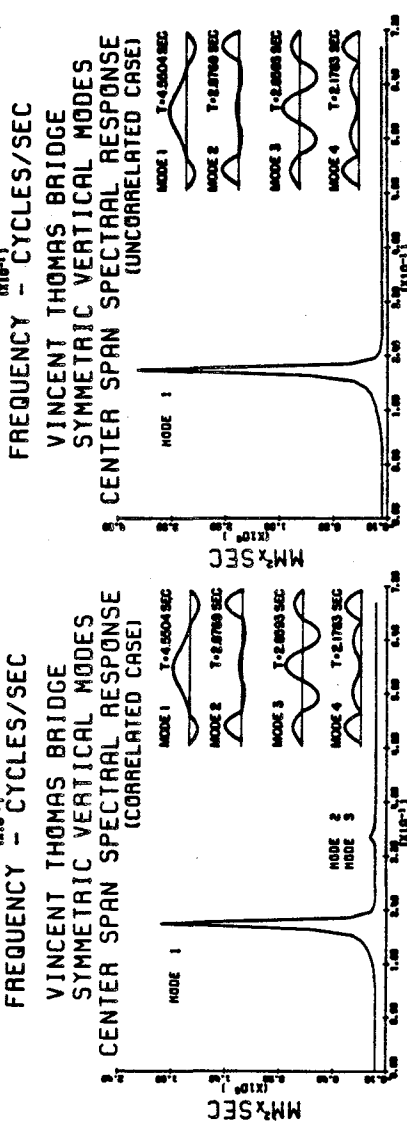

Fig. II-12b Autospectra of midspan displacements (uncorrelated case). 1971 San Fernando earthquake inputs.

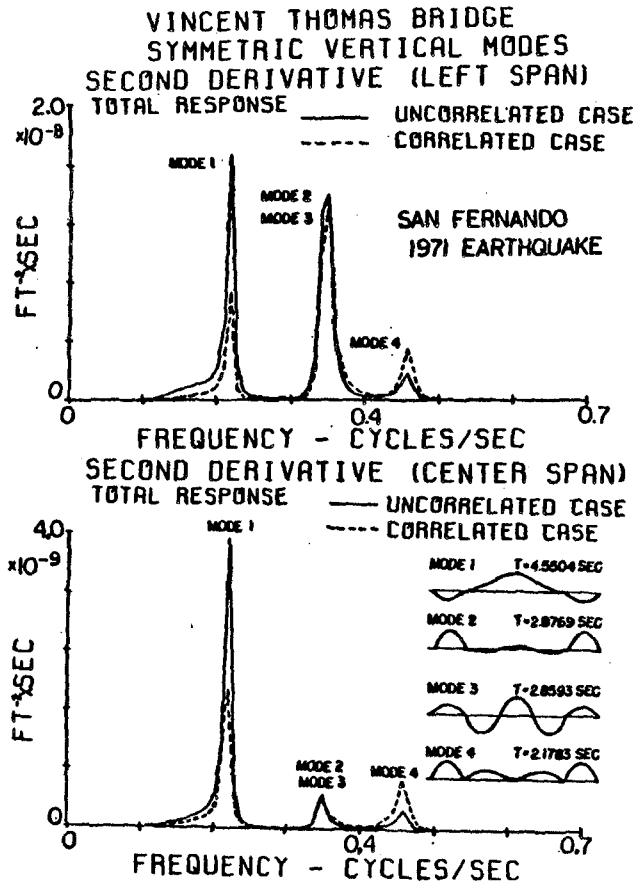

Fig. II-13 Autospectra of second derivative response at midspan. San Fernando Earthquake inputs.

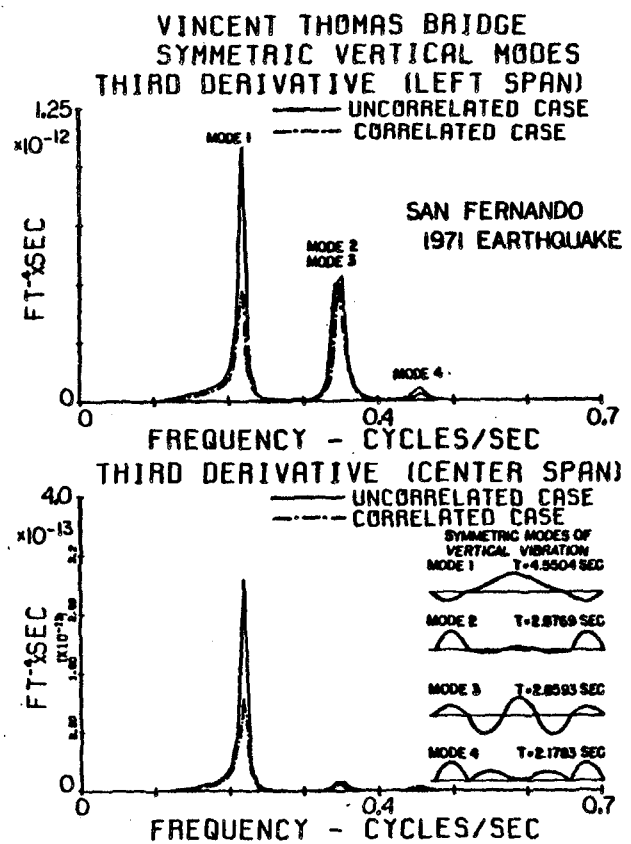

Fig. II-14 Autospectra of third derivative response at endspan. San Fernando earthquake inputs.

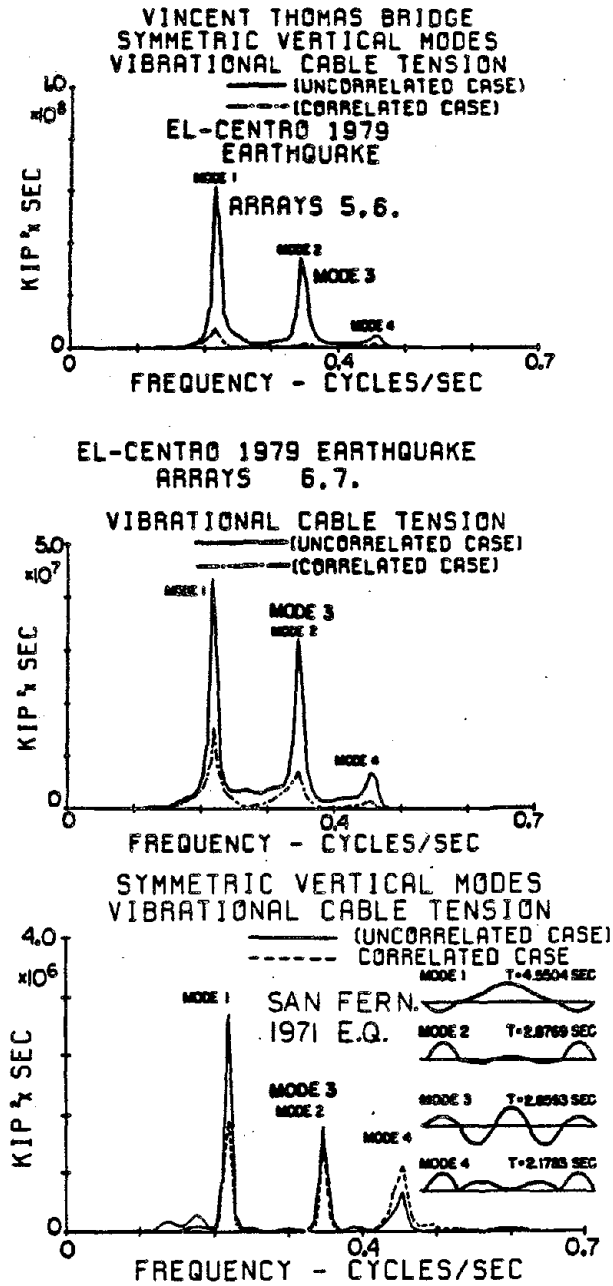

Fig. II-15 Autospectra of additional (vibrational) cable tension.

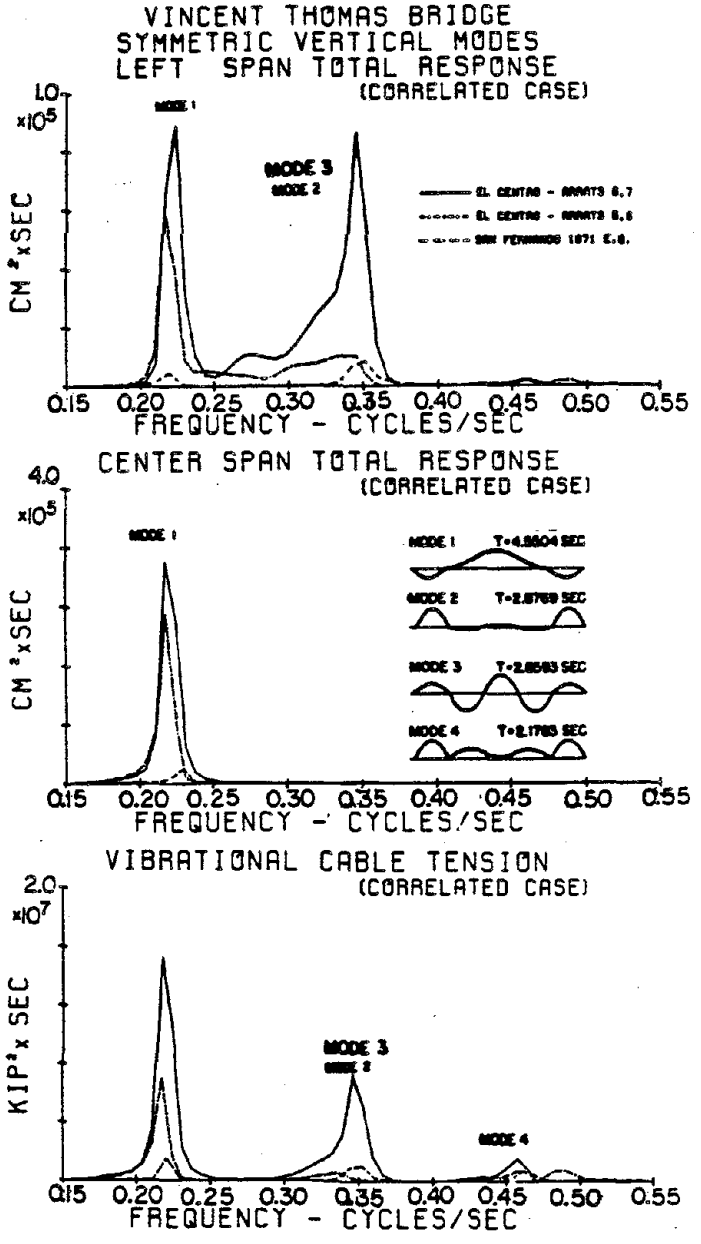

Fig. II-16 Comparison of autospectra for El Centro vs. San Fernando earthquake inputs.

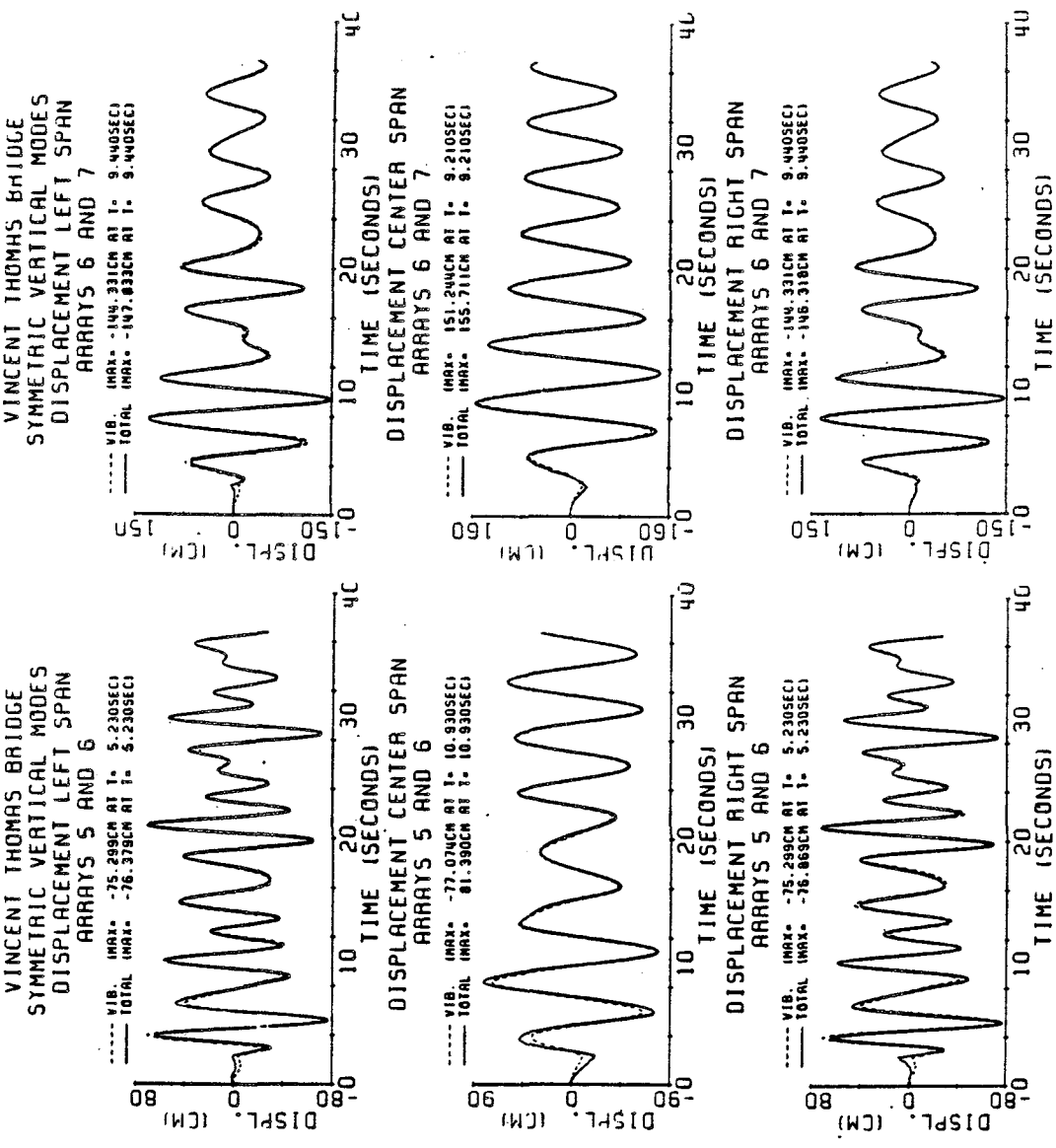

Fig. II-17 Time history of midspan displacement. Arrays 5 and 6.

Fig. II-18 Time history of midspan displacement. Arrays 6 and 7.

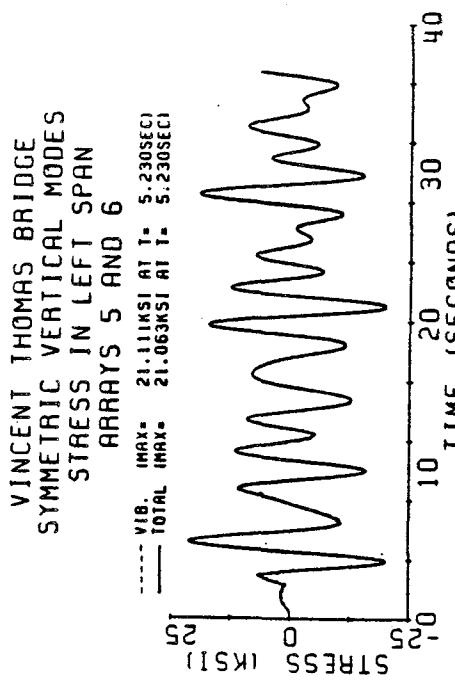

Fig. II-19 Time history of midspan stresses. Arrays 5 and 6.

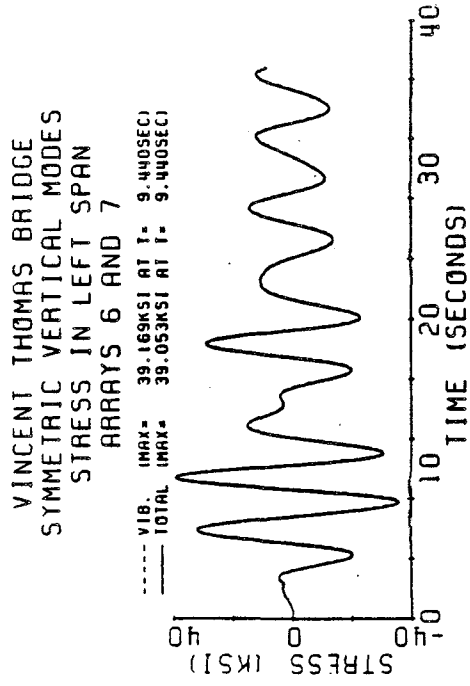

Fig. II-20 Time history of midspan stresses. Arrays 6 and 7.

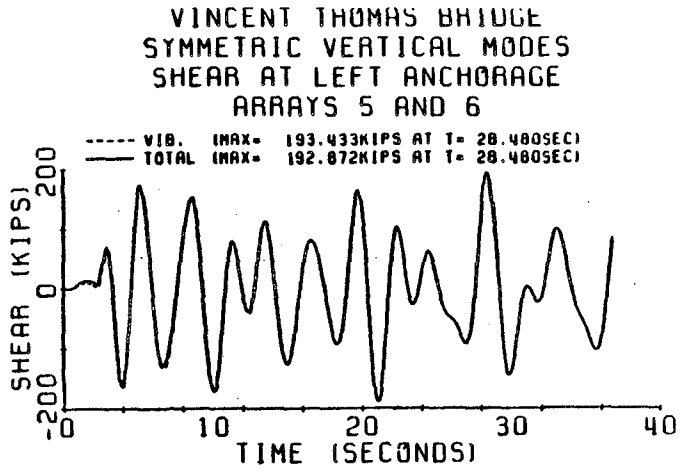

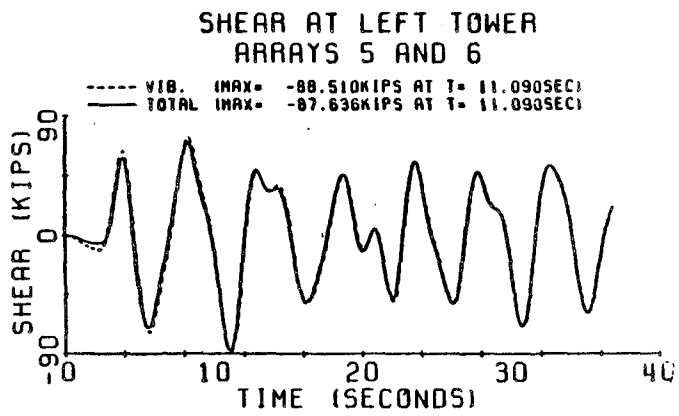

Fig. II-21 Time history of endspan shear force. Arrays 5 and 6.

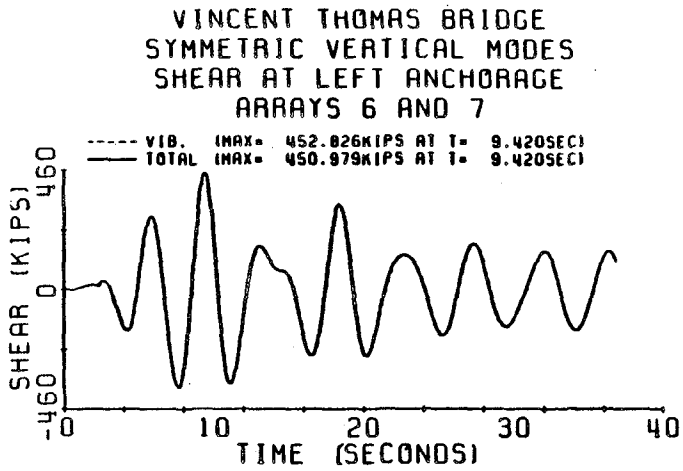

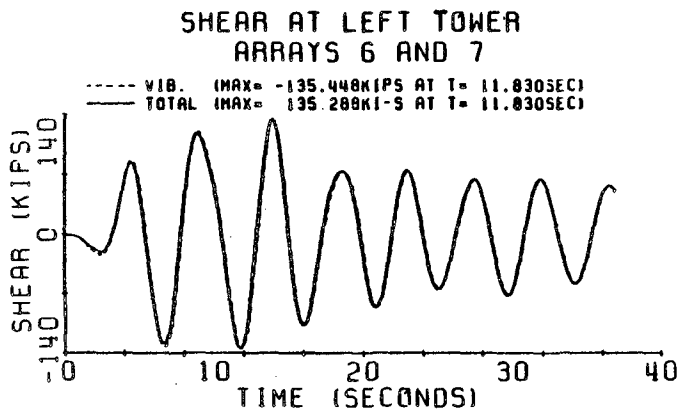

Fig. II-22 Time history of endspan shear force. Arrays 6 and 7.

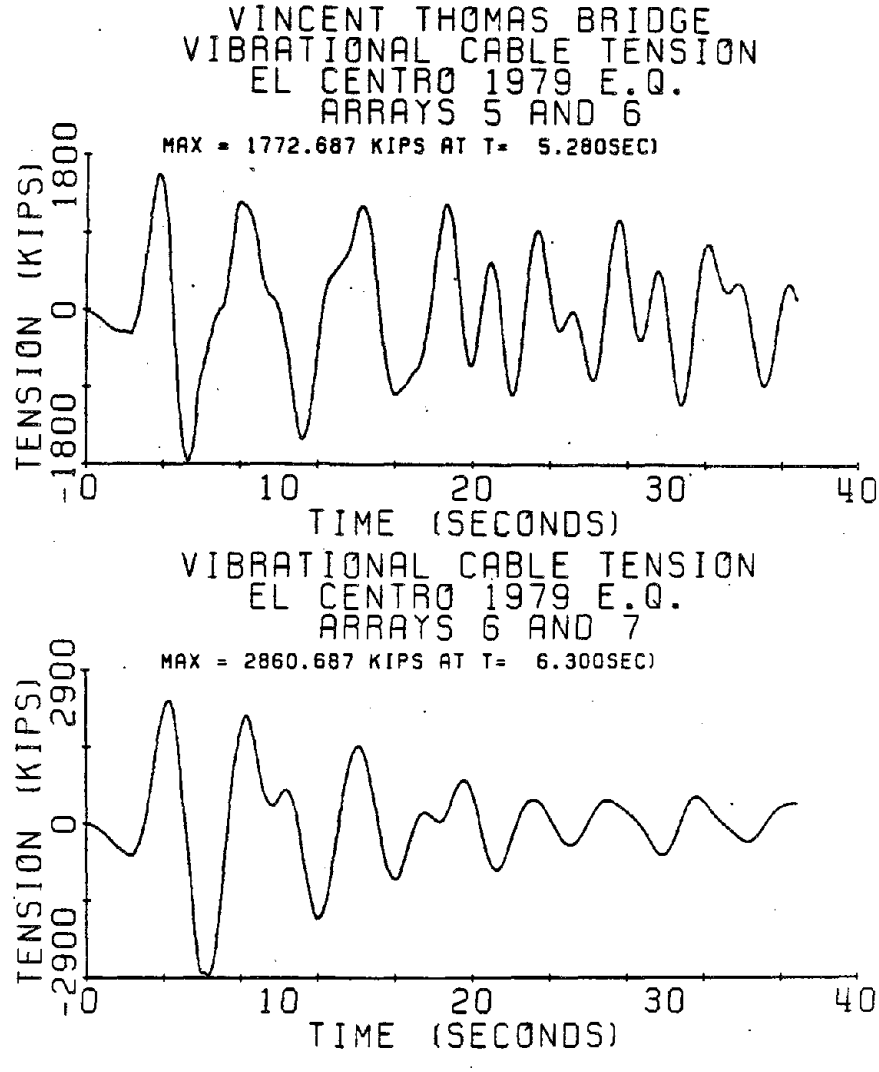

Fig. II-23 Time history of additional horizontal component of cable tension.

Table II-3

VERTICAL RESPONSE SUMMARY OF THE VINCENT THOMAS BRIDGE

Response Case			RMS Response (freq. domain)						Peak Response (Time Domain)			Peak/RMS		
			Correlated			Uncorrelated								
			LEFT	CENTER	RIGHT	LEFT	CENTER	RIGHT	LEFT	CENTER	RIGHT	LEFT	CENTER	RIGHT
MIDSPAN DISPLACEMENT (CM)	El Centro Arrays 5,6	VIB.	42.4	59.4	42.4	120.7	138.9	120.7	-75.3	-77.1	-75.3	1.8	1.3	1.8
		TOT.	45.8	57.9	45.6	122.0	137.8	121.9	-76.4	-81.4	-76.9	1.7	1.4	1.7
	El Centro Arrays 5,6	VIB.	62.7	69.8	62.7	112.4	114.8	112.4	-144.3	151.2	-144.3	2.3	2.2	2.3
		TOT.	64.4	70.0	62.3	113.3	114.9	112.2	-147.8	155.7	-146.3	2.3	2.2	2.3
	San Fernando	VIB.	18.3	17.8	18.3	18.2	27.1	18.2	--	--	--	--	--	--
		TOT.	18.5	17.9	18.5	21.2	27.5	21.2	--	--	--	--	--	--
MIDSPAN STRESS (KSI)	El Centro Arrays 5,6	VIB.	11.6	3.82	11.6	10.4	10.2	10.4	21.1	7.74	21.1	1.8	2.0	1.8
		TOT.	11.5	3.82	11.5	10.4	10.2	10.4	21.1	8.24	21.1	1.8	2.2	1.8
	El Centro Arrays 6,7	VIB.	17.1	4.85	17.1	30.8	8.80	30.8	39.2	-11.0	39.2	2.3	2.3	2.3
		TOT.	17.1	4.88	17.1	30.7	8.81	30.7	39.1	-11.0	39.1	2.3	2.3	2.3
	San Fernando	VIB.	5.05	1.53	5.05	5.79	1.97	5.79	--	--	--	--	--	--
		TOT.	5.05	1.53	5.05	5.79	1.97	5.79	--	--	--	--	--	--
SHEAR FORCE AT LEFT SIDE OF SPAN (KIPS)	El Centro Arrays 5,6	VIB.	125.6	57.5	125.6	366.1	128.6	366.1	193.4	-88.5	193.4	1.5	1.5	1.5
		TOT.	124.4	59.3	124.4	365.4	129.4	365.4	192.9	-87.6	192.9	1.6	1.5	1.6
	El Centro Arrays 6,7	VIB.	189.4	64.5	189.4	333.4	108.1	333.4	452.8	-135.4	452.8	2.4	2.1	2.4
		TOT.	189.1	64.6	189.1	333.2	108.1	333.2	451.0	-135.3	451.0	2.4	2.1	2.4
	San Fernando	VIB.	52.8	17.2	52.8	65.4	23.9	65.4	--	--	--	--	--	--
		TOT.	52.8	17.2	52.8	65.4	25.0	65.4	--	--	--	--	--	--
CABLE TENSION (KIPS)	El Centro Arrays 5,6		410.6			1493			1772			4.3		
	El Centro Arrays 6,7		644.4			1411			2861			4.4		
	San Fernando		236.2			280.6								

earthquake-induced flexural stresses and cable tensions represent a significant live-load condition for this bridge. For example, the peak stress of 39 ksi occurring in the side spans is quite high as a live load when compared to the yield stress of 52.0 ksi.

II.13.2 Vertical Seismic Behavior of the Tacoma Narrows Bridge

In this section, the analysis outlined in this chapter is applied to the Tacoma Narrows Suspension Bridge, in Washington, in order to estimate its vertical response characteristics. Frequency and time domain methods are to be compared. The structural properties of the bridge are summarized in Table II-4. The vertical quasi-static functions are shown in Fig. II-24 for unit vertical ground motion displacement at each anchorage and tower base. The first eight symmetric and antisymmetric vertical mode shapes are shown in Fig. II-25, while their associated participation coefficients appear in Table II-5. As in the previous section and for the same reasons, the symmetric vertical response only will be investigated herein.

The complex frequency response functions $H_n(\omega)$ for the first four symmetric vertical modes of the bridge are shown in Fig. II-26 for 2% damping (for all modes), and corresponding to anchorage vertical input, tower vertical input, and anchorage longitudinal input. The same two symmetric vertical response cases are studied for the Tacoma Narrows Bridge as for the Vincent Thomas Bridge (the first involving Arrays 5 and 6 as input and the second involving Arrays 6 and 7 as input). The autospectra of midspan displacement for both side and center spans are shown in Fig. II-27 for input arrays 5 and 6, and in Fig. II-28 for input arrays 6 and 7. It is seen that the side span response is

Table II-4

VERTICAL PROPERTIES OF THE TACOMA NARROWS BRIDGE

Parameter	Center Span	Side Span
Span Length	ℓ_2 = 2800 ft.	$\ell_1 = \ell_3$ = 1100 ft.
w_i^*	w_2^* = 4.33 k/ft.	$w_1^* = w_3^*$ = 4.33 k/ft.
E_i	E_2 = 29600 ksi	$E_1 = E_3$ = 29600 ksi
I_i	I_2 = 47520 ft^2 in^2	$I_1 = I_3$ = 47520 ft^2 in^2
truss depth	d = 33 ft.	d = 33 ft.

Cable Properties:

E_c = 26500 ksi

A_c = 252 in^2

L_E = 6080 ft.

H_w = 15155 kip

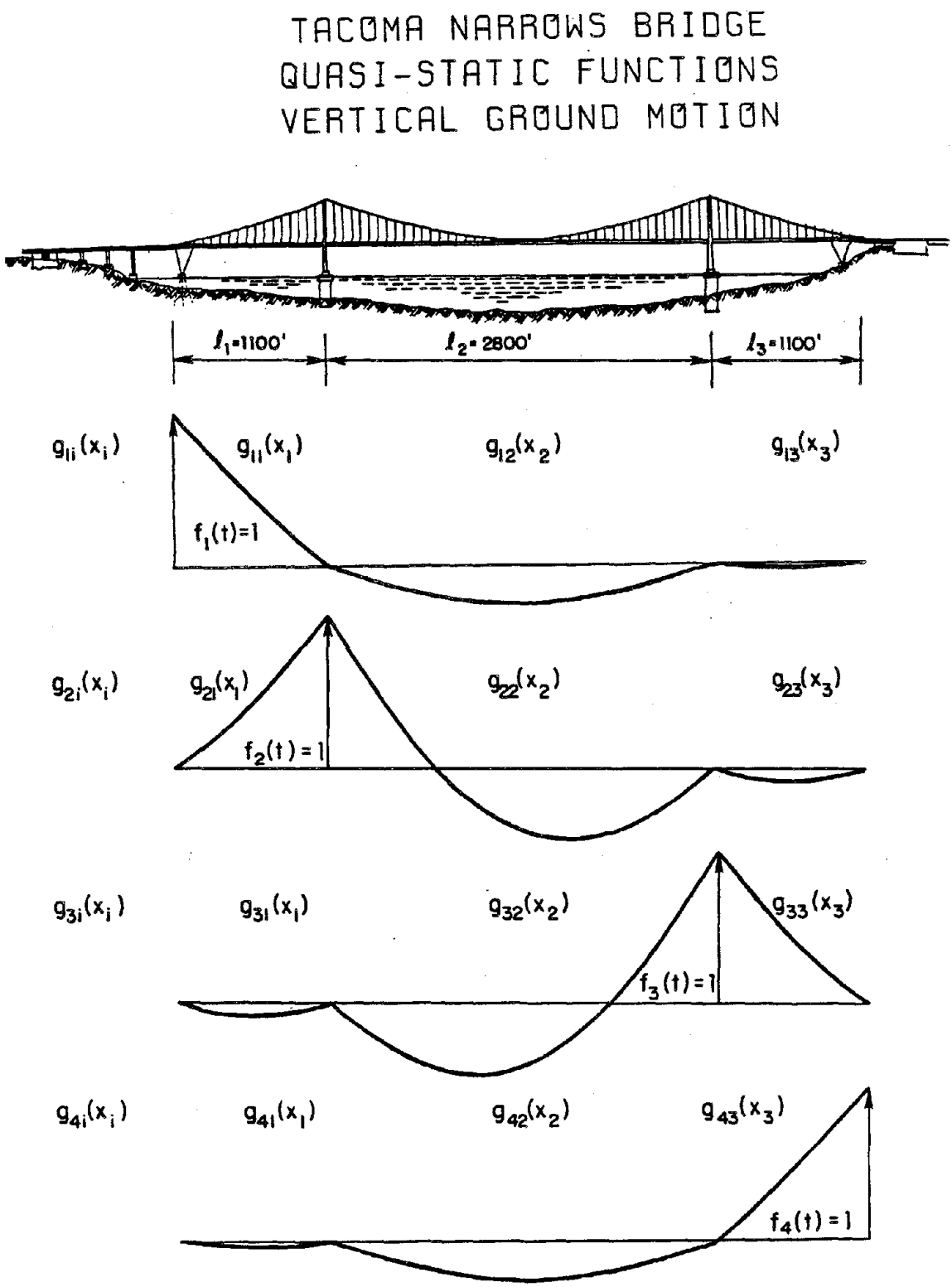

Fig. II-24 Vertical quasi-static functions of the Tacoma Narrows Bridge.

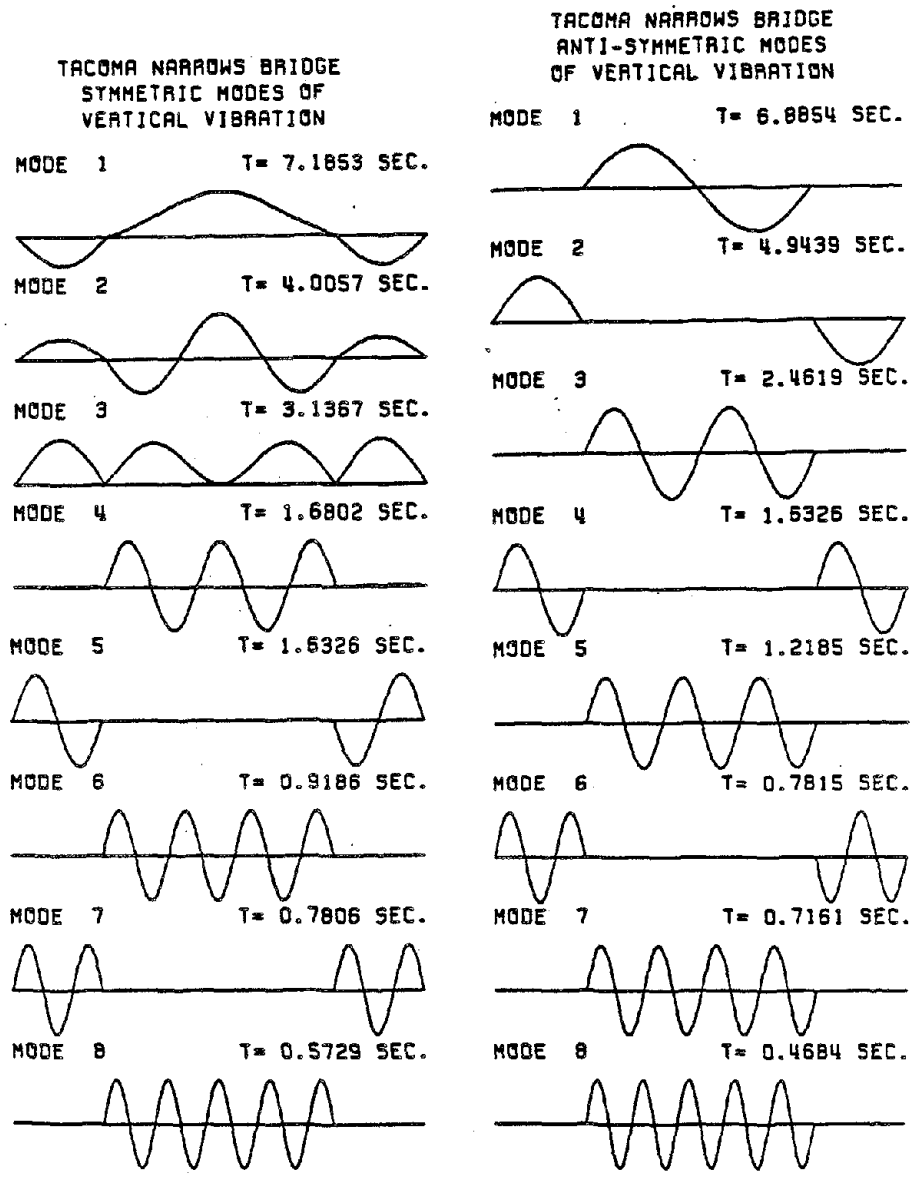

Fig. II-25 Mode shapes of vertical vibration of the Tacoma Narrows Bridge.

Table II-5

PARTICIPATION COEFFICIENTS OF VERTICAL EARTHQUAKE RESPONSE OF THE TACOMA NARROWS SUSPENSION BRIDGE

Mode Order n	Symmetric Vibration			Antisymmetric Vibration		
	$R_{1n} = R_{4n}$	$R_{2n} = R_{3n}$	P_n	$R_{1n} = -R_{4n}$	$R_{2n} = -R_{3n}$	P_n
1	-0.330	-0.339	0.398	0.0	0.318	0.0
2	0.075	-0.141	0.373	0.318	0.318	0.0
3	0.043	0.071	1.357	0.0	0.159	0.0
4	-0.001	0.126	0.330	0.159	-0.159	0.0
5	0.159	-0.159	0.0	0.0	0.106	0.0
6	-0.001	0.090	0.193	0.106	0.106	0.0
7	0.106	0.106	0.446	0.0	0.079	0.0
8	0.0	0.070	0.145	0.0	0.063	0.0

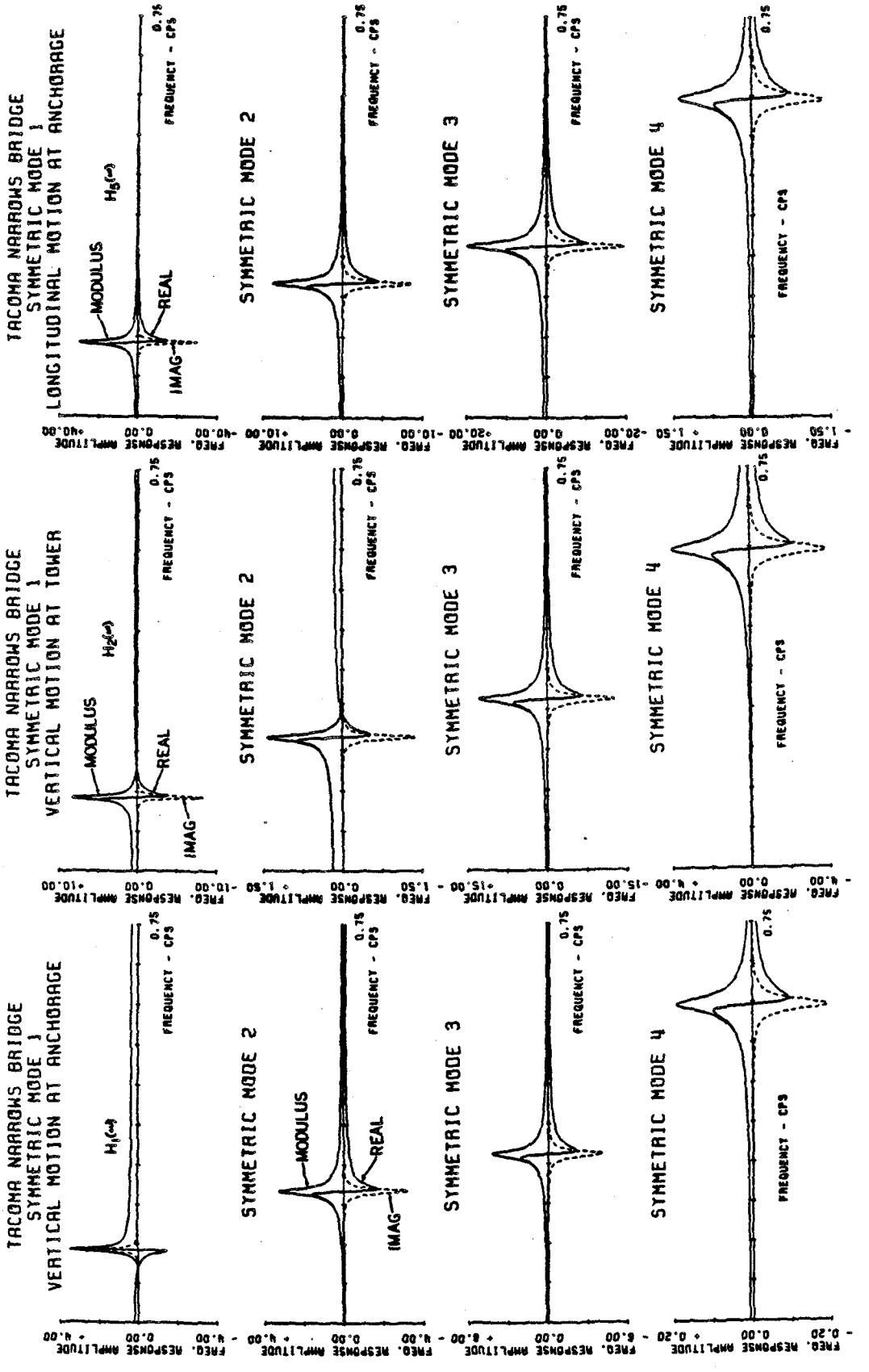

Fig. II-26 Frequency response functions for the first four symmetric modes of vertical vibration of the Tacoma Narrows Bridge.

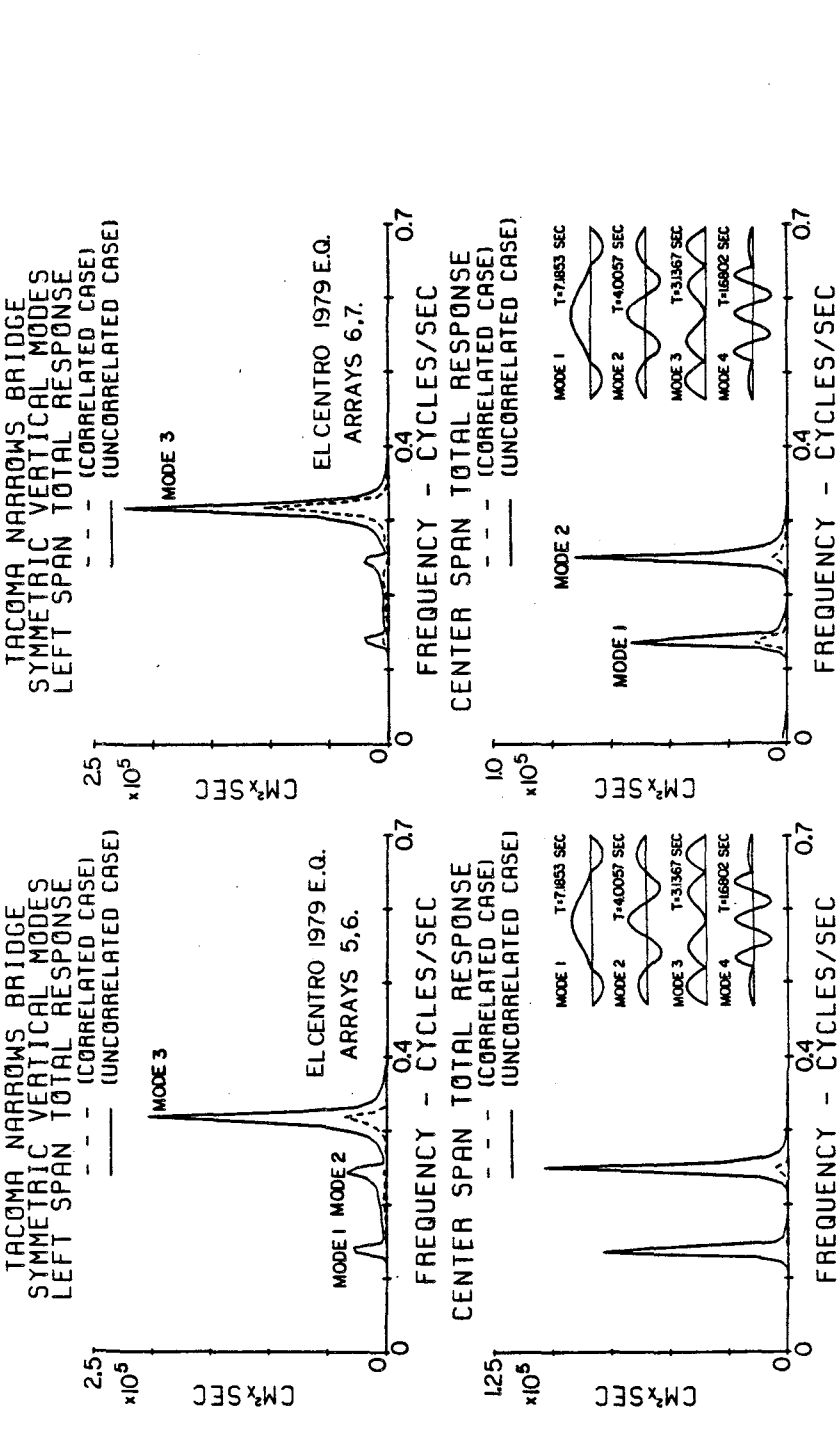

Fig. II-27 Autospectra of midspan displacements. Input Arrays 5 and 6.

Fig. II-28 Autospectra of midspan displacements. Input arrays 6 and 7.

dominated by the third symmetric mode, most likely because of its high modal participation factor P_n, and its natural frequency lies within the range of the input spectra where the ground excitation energy is strong. The center span response is dominated by the first two symmetric modes, the third symmetric mode being absent because of its zero ordinate at midspan. Similar characteristics, as before, are found as to the conservative nature of the uncorrelated case, and the similarity of left and right side span response.

The autospectra of midspan second derivative (or curvature) responses for side and center spans, which are related to response bending moments and flexural stresses in the top and bottom chords of the bridge's stiffening structure, are shown in Fig. II-29 for input arrays 5 and 6 and in Fig. II-30 for input arrays 6 and 7. Figures II-31 and II-32 show similar spectra for the third derivative response, evaluated at the ends of each span, which is related to the dynamic shear force. The autospectra of the additional (vibrational) horizontal component of the cable tension for both response cases are shown in Fig. II-33. The large contribution to the cable tension from the third symmetric mode arises from the modal factor P_n being large, i.e., its sensitivity to longitudinal input at the anchorages, and the area under this mode shape being large, and the associated cable tension being directly proportional to this area, and its natural frequency being in the frequency range of strong input excitation.

In Table II-6, the root mean square values of response are summarized and are compared with the computed maximum responses obtained from the time domain (Duhamel integral) analysis shown in Figs. II-34 through II-40. It seems that the expected value for the peak factor is about 2.5 from

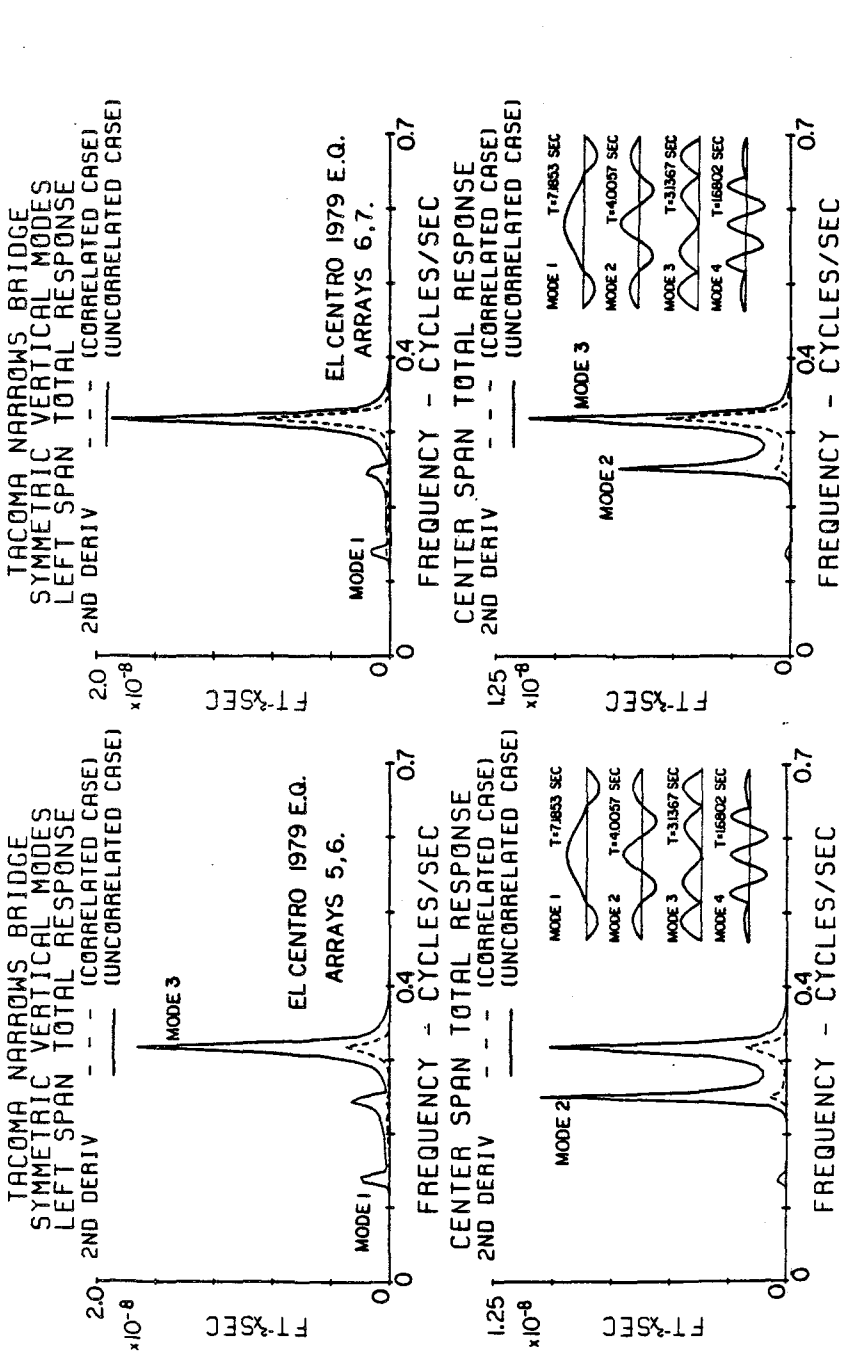

Fig. II-29 Autospectra of second derivative response at midspan.
Input arrays 5 and 6.

Fig. II-30 Autospectra of second derivative response at midspan.
Input arrays 6 and 7.

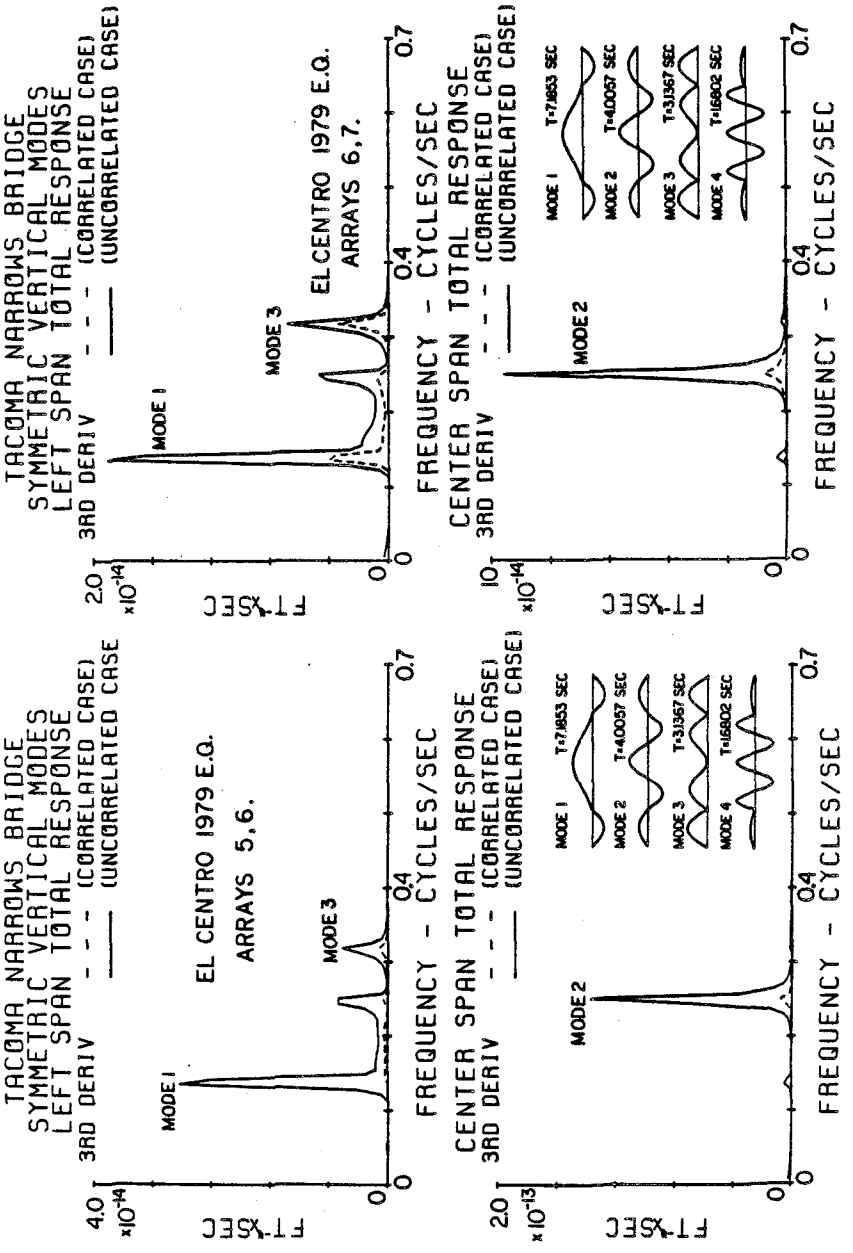

Fig. II-31 Autospectra of third derivative response at endspan.
Input arrays 5 and 6.

Fig. II-32 Autospectra of third derivative response at endspan.
Input arrays 6 and 7.

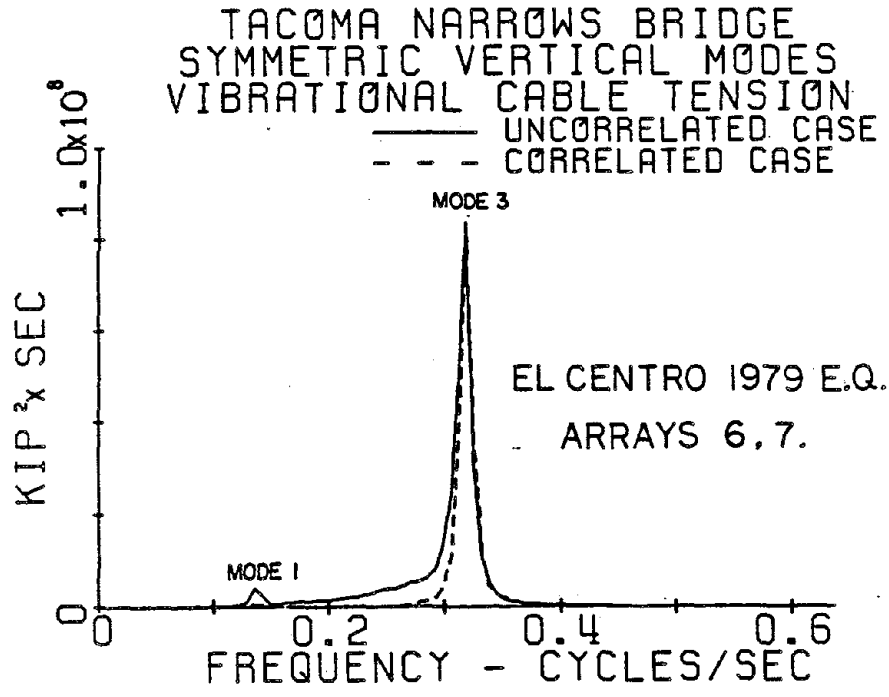

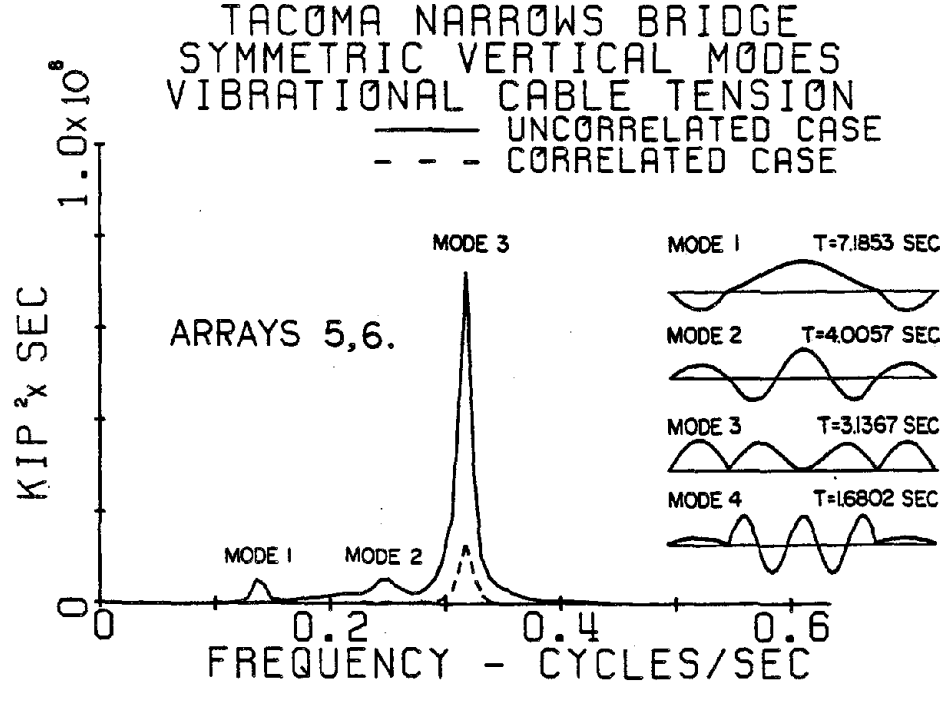

Fig. II-33 Autospectra of additional (vibrational) cable tension.

Table II-6

VERTICAL RESPONSE SUMMARY OF THE TACOMA NARROWS BRIDGE

Response Case			RMS Response (freq. domain)						Peak Response (Time Domain)			Peak/RMS		
			Correlated			Uncorrelated								
			LEFT	CENTER	RIGHT	LEFT	CENTER	RIGHT	LEFT	CENTER	RIGHT	LEFT	CENTER	RIGHT
MIDSPAN DISPLACEMENT (CM)	El Centro Arrays 5,6	VIB.	27.7	11.1	27.7	73.6	52.0	73.6	51.4	54.8	51.4	1.9	4.9	1.9
		TOT.	28.8	13.4	28.2	73.9	48.4	73.8	54.9	-66.3	54.1	1.9	4.9	1.9
	El Centro Arrays 6,7	VIB.	44.4	16.8	44.4	73.4	44.0	73.4	110.3	-66.4	110.3	2.5	4.0	2.5
		TOT.	45.6	16.8	44.1	74.0	44.0	73.1	104.4	-74.3	104.4	2.3	4.4	2.4
MIDSPAN STRESS (KSI)	El Centro Arrays 5,6	VIB.	7.80	6.62	7.80	20.6	18.8	20.6	-7.06	-7.17	-7.06	0.9	1.1	0.9
		TOT.	7.77	6.56	7.77	20.6	18.8	20.6	-6.95	-7.45	-6.95	0.9	1.1	0.9
	El Centro Arrays 6,7	VIB.	12.5	10.1	12.5	20.6	18.5	20.6	-15.2	12.4	-15.2	1.2	1.2	1.2
		TOT.	12.5	10.2	12.5	20.6	18.5	20.6	-15.2	12.3	15.2	1.2	1.2	1.2
SHEAR FORCE AT LEFT SIDE OF SPAN (KIPS)	El Centro Arrays 5,6	VIB.	20.5	40.2	20.5	78.3	132.6	78.3	81.9	119.3	81.9	4.0	3.0	4.0
		TOT.	26.2	43.1	26.2	79.9	133.4	79.9	82.0	114.7	82.0	3.1	2.7	3.1
	El Centro Arrays 6,7	VIB.	35.0	41.4	35.0	218.0	116.4	218.0	-120.8	-139.3	-120.8	3.5	3.4	3.5
		TOT.	35.3	41.2	35.3	218.4	116.3	218.4	-121.2	-134.5	-121.2	3.4	3.3	3.4
CABLE TENSION (KIPS)	El Centro Arrays 5,6			503.3			1354			1034.7			2.1	
	El Centro Arrays 6,7			1165			1412			1377.1			1.2	

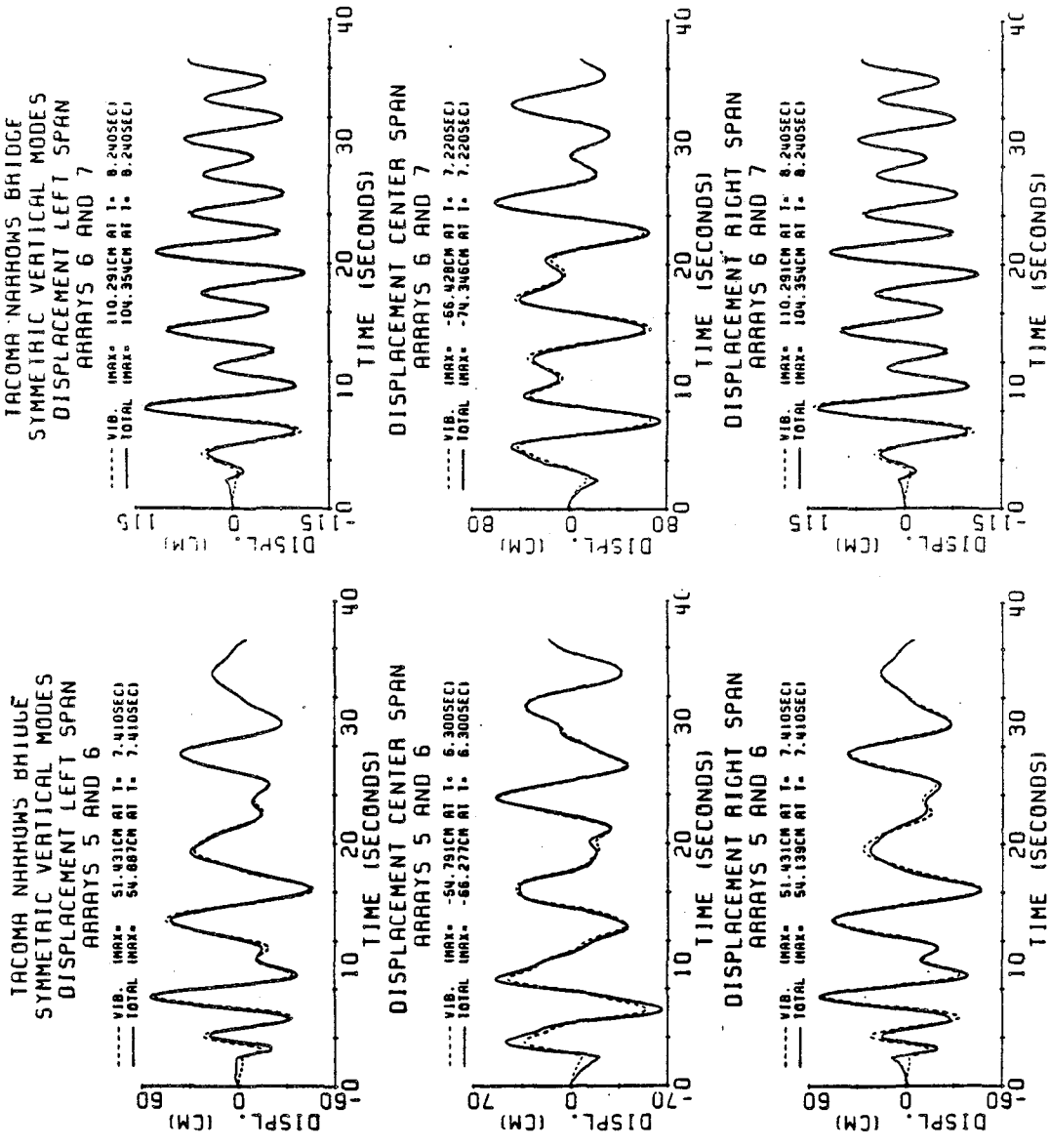

Fig. II-34 Time history of midspan displacements. Arrays 5 and 6.

Fig. II-35 Time history of midspan displacement. Arrays 6 and 7.

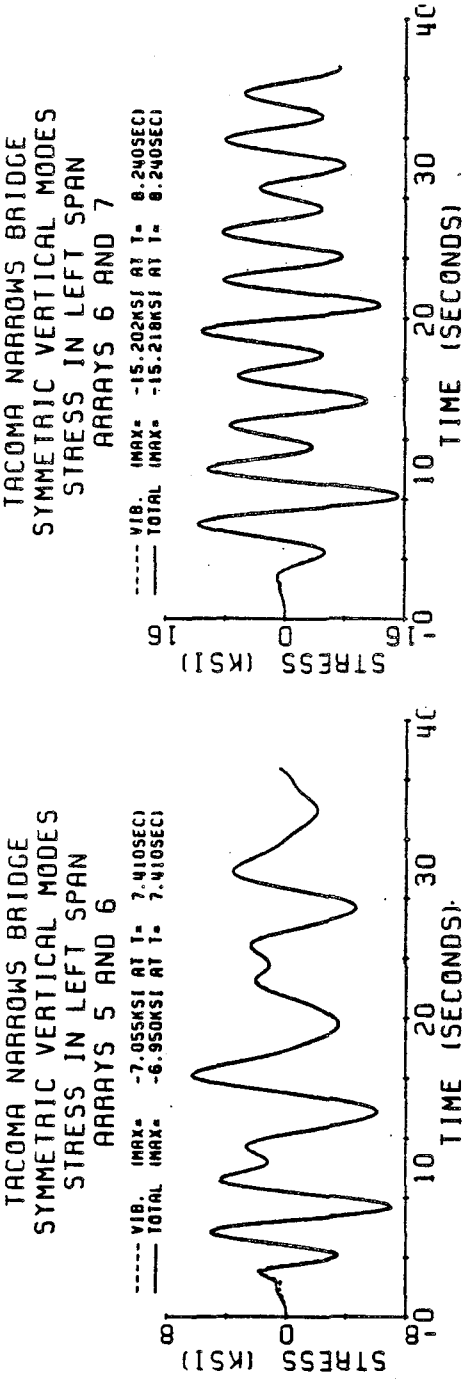

Fig. II-36 Time history of midspan stresses. Arrays 5 and 6.

Fig. II-37 Time history of midspan stresses. Arrays 6 and 7.

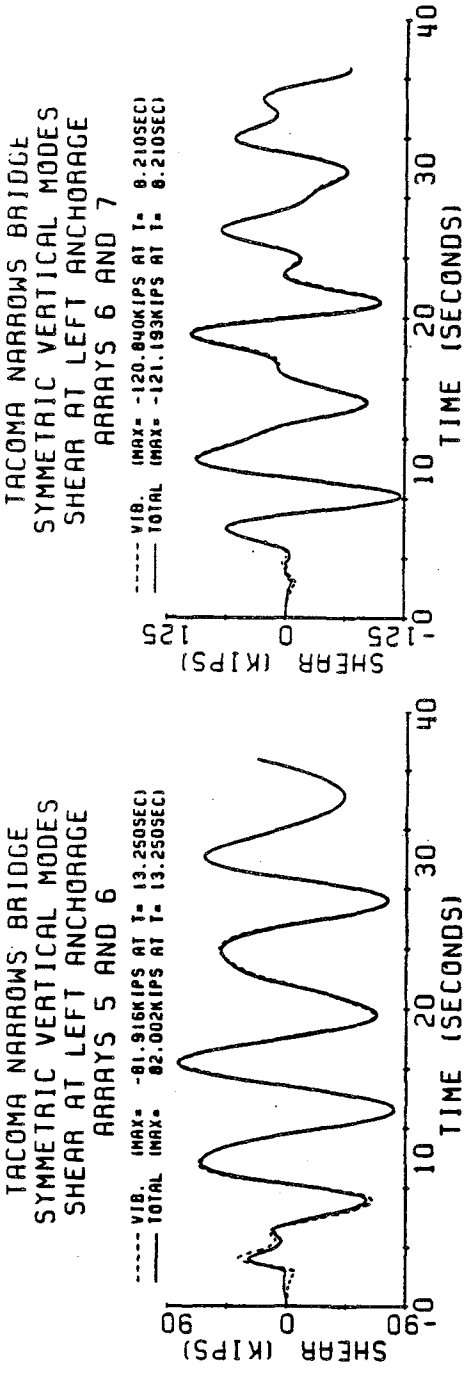

Fig. II-38 Time history of endspan shear force. Arrays 5 and 6.

Fig. II-39 Time history of endspan shear force. Arrays 6 and 7.

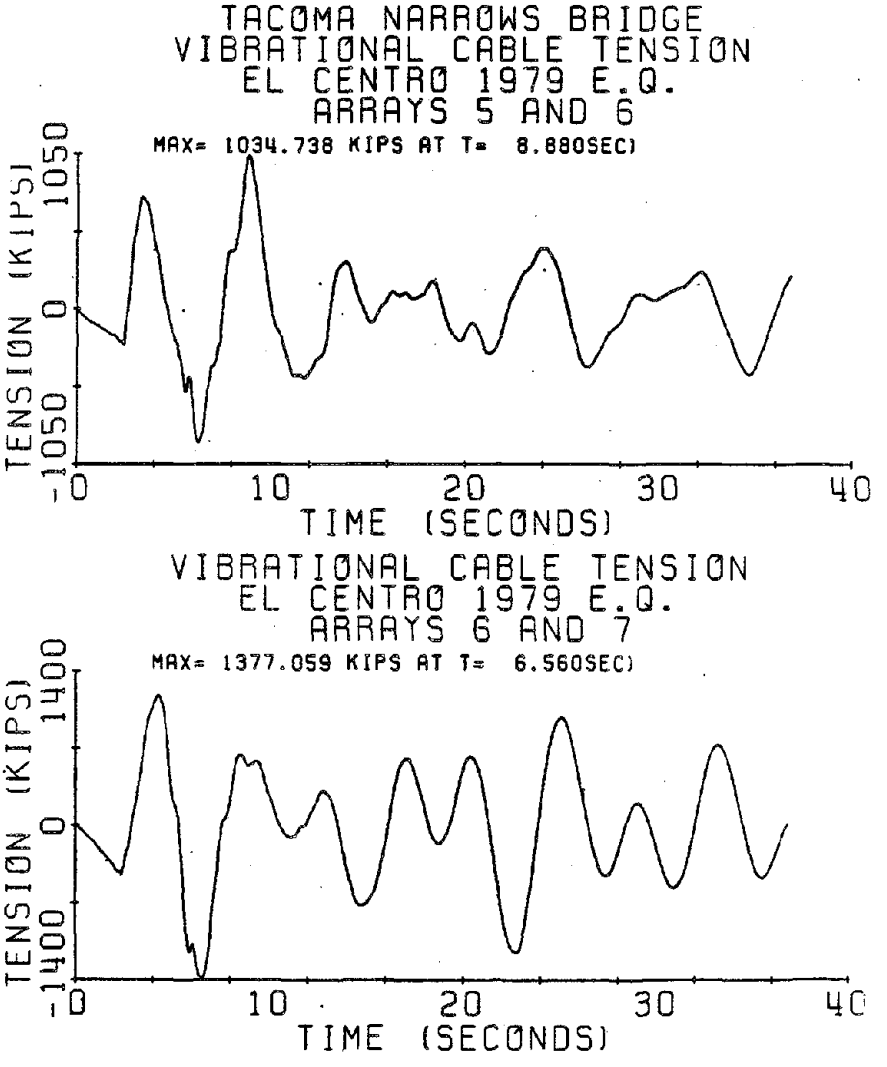

Fig. II-40 Time history of additional horizontal component of cable tension.

Table II-6, however there is considerable scattering about this value. It is seen that Arrays 6 and 7 excite the bridge more strongly than arrays 5 and 6. Also, the values of earthquake-induced flexural stresses and cable tensions represent a significant live-load condition for this bridge. The uncorrelated RMS value of 20.6 ksi live load stress is quite large when compared to the yield stress of 46.0 ksi.

II.13.3 Vertical Seismic Behavior of the Golden Gate Bridge

In this section, the analysis outlined in this chapter is applied to the Golden Gate Suspension Bridge, in San Francisco, California, in order to estimate its vertical response characteristics. Frequency domain, time domain (convolution integral), and response spectral methods are compared in this section, and the determination of appropriate peak factors are studied in detail. The structural properties of the bridge [5] are summarized in Table II-7. The vertical quasi-static functions are shown in Fig. II-41 for unit vertical ground motion displacement at each anchorage and tower base. The first ten symmetric and antisymmetric vertical mode shapes are shown in Fig. II-42, while their associated participation coefficients appear in Table II-8. Because the modal factor P_n is zero for the antisymmetric modes, the effect of antisymmetric vertical vibration is suspected to be of a higher order nature. This assumption will be examined in this section as well. The frequency response functions $H_n(\omega)$ for the first four symmetric and antisymmetric vertical modes of the bridge are shown in Figs. II-43 and II-44 for 2% damping, and corresponding to anchorage vertical input, tower vertical input, and anchorage longitudinal input. These functions measure the magnification (or gain) factor corresponding to a unit harmonic

Table II-7

VERTICAL PROPERTIES OF THE GOLDEN GATE BRIDGE

Parameter	Center Span	Side Spans
Span Length	ℓ_2 = 4200 ft.	$\ell_1 = \ell_3$ = 1125 ft.
w_i^*	w_2^* = 11.45 k/ft.	$w_1^* = w_3^*$ = 11.55 k/ft.
E_i	E_2 = 29000 ksi	$E_1 = E_3$ = 29000 ksi
I_i	I_2 = 43200 $ft^2 in^2$	$I_i = I_3$ = 28000 $ft^2 in^2$
truss depth	d = 25 ft.	d = 25 ft.

Cable Properties:

E_c = 29000 ksi

A_c = 831.9 in^2

L_E = 7698 ft.

H_w = 53467 kip

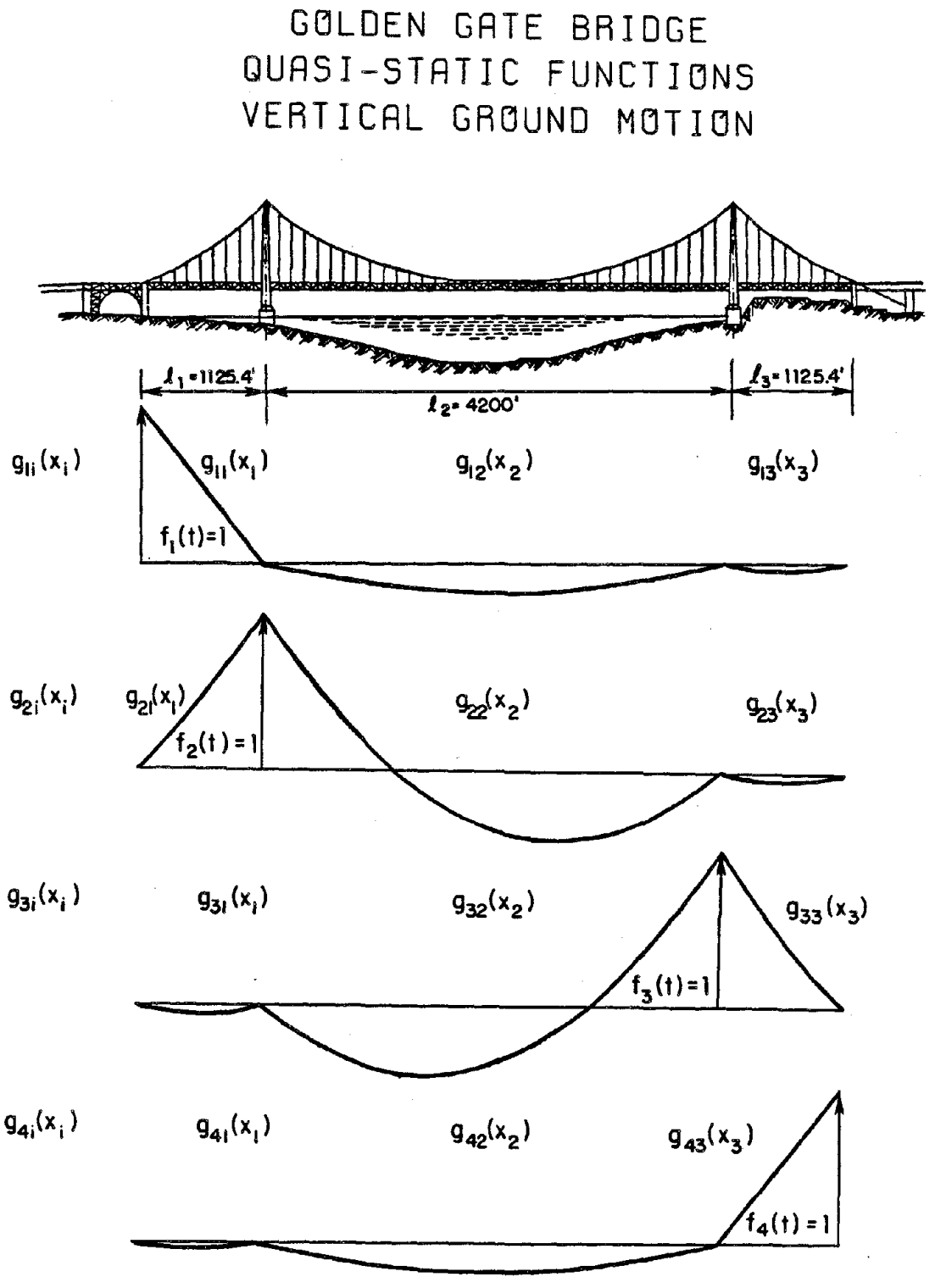

Fig. II-41 Quasi-static functions of the Golden Gate Bridge.

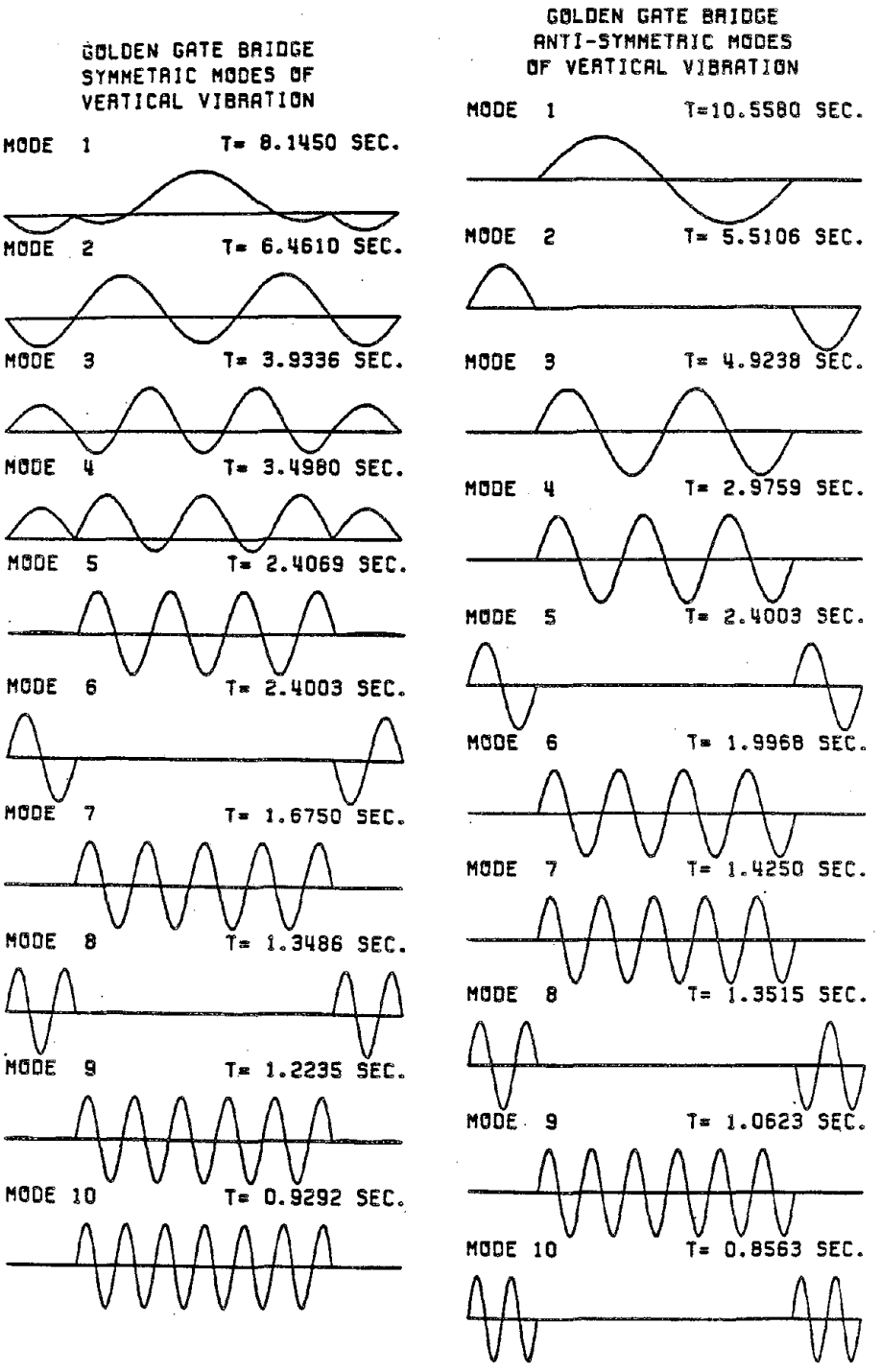

Fig. II-42 Mode shapes of vertical vibration of the Golden Gate Bridge.

Table II-8

PARTICIPATION COEFFICIENTS OF VERTICAL EARTHQUAKE RESPONSE OF THE GOLDEN GATE SUSPENSION BRIDGE

Mode Order n	Symmetric Vibration			Antisymmetric Vibration		
	$R_{1n} = R_{4n}$	$R_{2n} = R_{3n}$	P_n	$R_{1n} = -R_{4n}$	$R_{2n} = -R_{3n}$	P_n
1	-0.287	-0.467	0.478	0.0	0.318	0.0
2	-0.163	-0.018	0.258	0.318	0.318	0.0
3	0.039	-0.081	0.894	0.0	0.159	0.0
4	0.017	0.084	0.323	0.0	0.105	0.0
5	-0.002	0.090	0.289	0.159	-0.159	0.0
6	0.159	-0.159	0.0	0.0	0.079	0.0
7	-0.001	0.070	0.168	0.0	0.063	0.0
8	0.105	0.104	0.488	0.106	0.106	0.0
9	0.001	0.059	0.165	0.0	0.052	0.0
10	0.0	0.049	0.102	0.079	-0.079	0.0

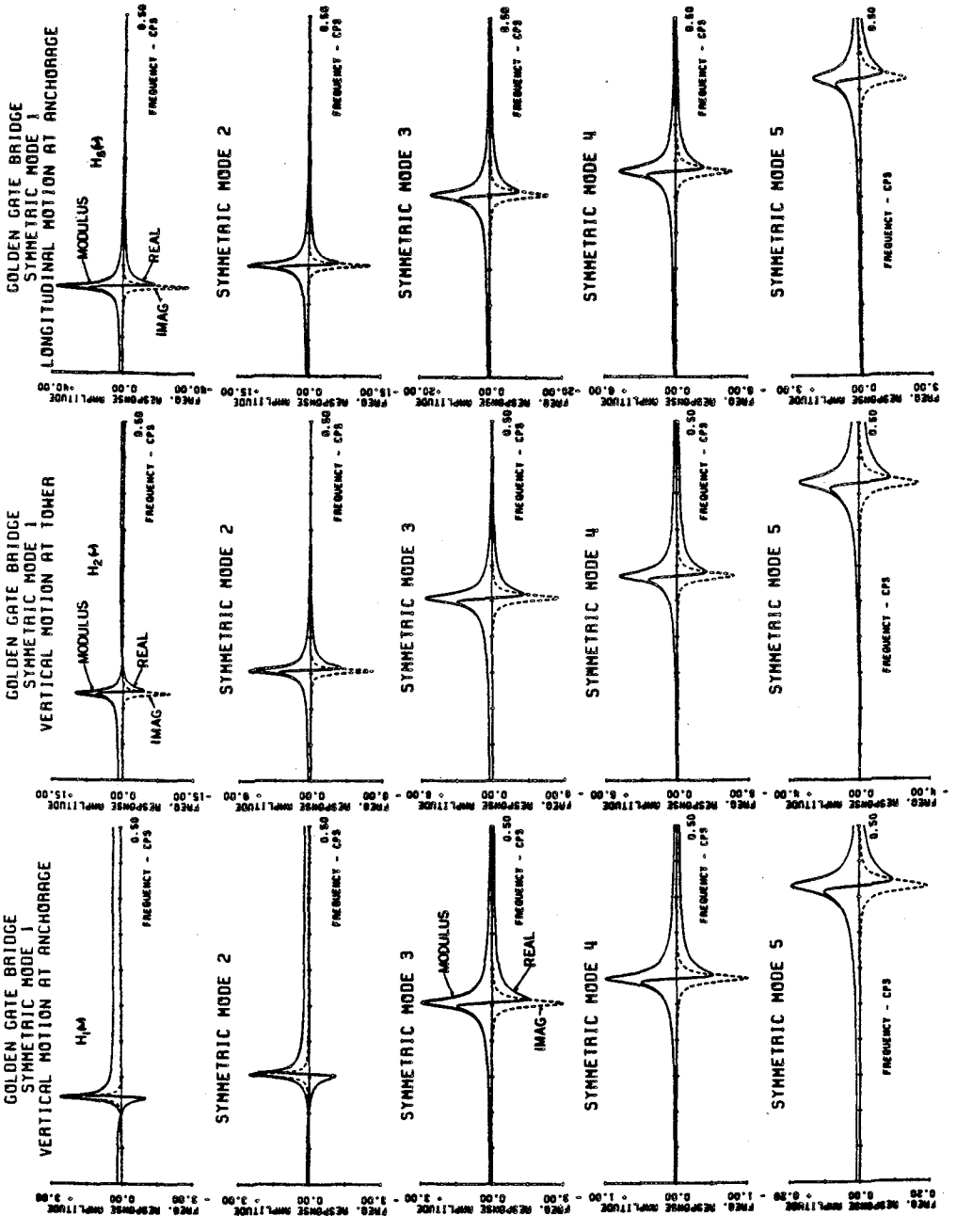

Fig. II-43 Frequency response functions for the first five symmetric modes of vertical vibration of the Golden Gate Bridge.

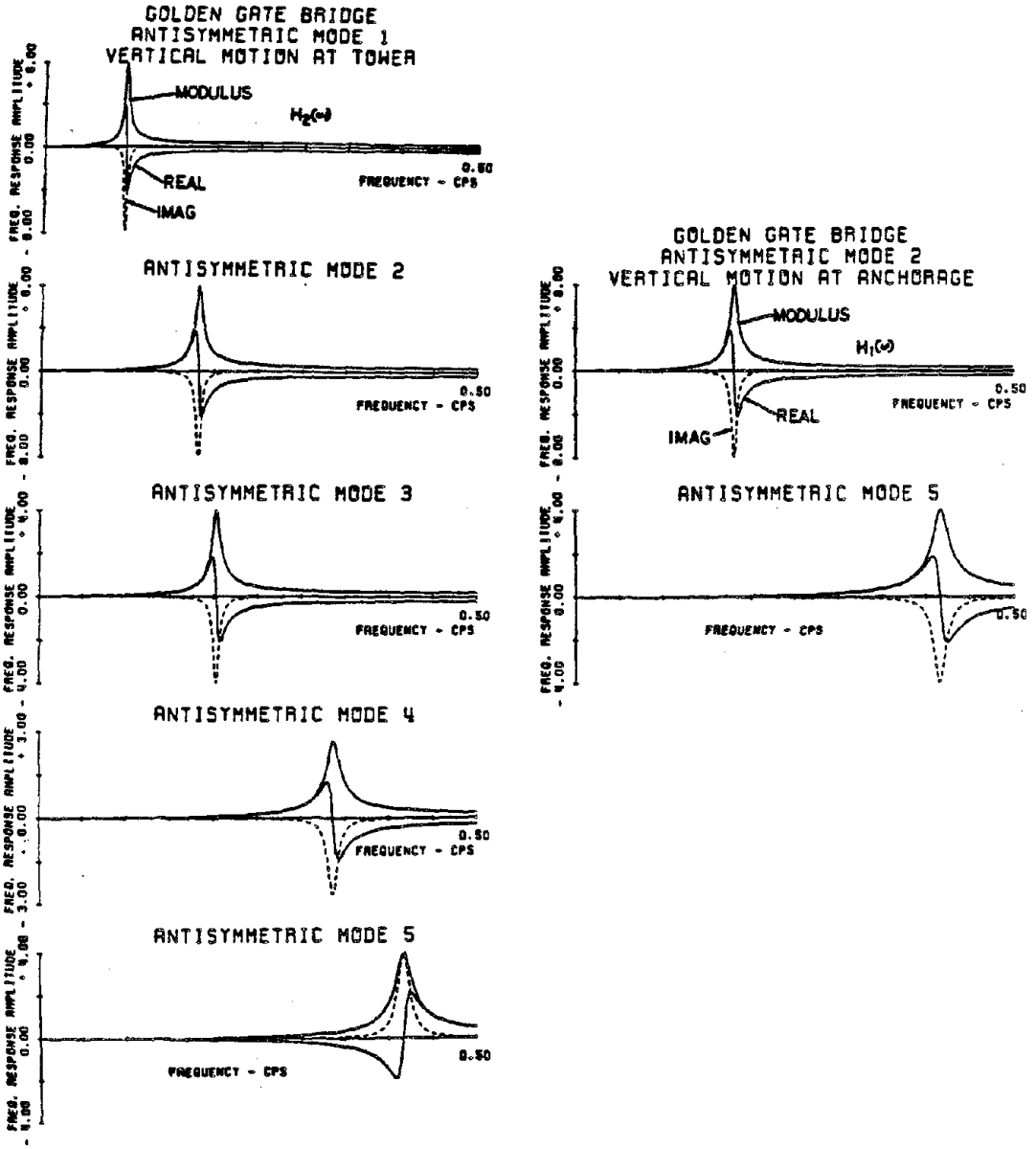

Fig. II-44 Frequency response functions for the first five antisymmetric modes of vertical vibration of the Golden Gate Bridge.

displacement upon the response of the generalized coordinate $q_n(t)$. It can be seen as before from these figures that the longitudinal anchorage motions contribute greatly to the symmetric vertical response, especially in the first three symmetric modes. For higher modes, similar functions are obtained.

Several symmetric vertical response cases are studied for the Golden gate Bridge. Because of the long center and side spans the vertical motions are taken to be different. In the first case, the vertical motions $f_1(t)$, $f_2(t)$, $f_3(t)$, and $f_4(t)$ correspond to the vertical components recorded at arrays Nos. 4, 5, 6, and 7 (1979 El Centro earthquake), respectively, while the longitudinal motions $f_5(t)$ and $f_8(t)$ are taken as the associated S50W components (of arrays No. 4 and 7). The second response case involved similar correspondences with arrays No. 5, 6, 7, and 8 (vertical and longitudinal motions).

In addition to the above symmetric response cases, three reference cases are studied in order to investigate the effects of the longitudinal displacement inputs upon the bridge response as follows:

1. Reference case 1 involves a uniform vertical excitation; $f_1(t)$, $f_2(t)$, $f_3(t)$, and $f_4(t)$ are all taken as the vertical uniform component at array No. 8, with no longitudinal excitation, i.e., $f_5(t) = f_8(t) = 0$.
2. Reference case 2 involves the same vertical motion as in Reference case 1, with $f_5(t)$ taken as the S50W component at array No. 5 and with $f_8(t) = 0$.
3. Reference case 3 is similar to reference case 2, but having $f_5(t)$ being taken from the S50W component of array No. 6 instead of array No. 5.

In addition to the above symmetric response cases, the antisymmetric response is studied for input arrays No. 4, 5, 6, and 7 as well as input arrays No. 5, 6, 7, and 8. Also, the symmetric response is studied using a set of artificially generated earthquakes as inputs [12].

The autospectra of midspan symmetric displacement for both the center and side spans are shown in Figs. II-45 for input arrays No. 4, 5, 6, and 7, and in Fig. II-46 for input arrays No. 5, 6, 7, and 8. It is observed that the quasi-static contribution to the total response is small, and therefore the displacements are quite similar in the left and right side spans. The first and third symmetric modes appear to dominate the response of the center span, most likely because their modal participation factors, P_n are large (Table II-8) and their natural frequencies lie within the spectral region of strong ground motion input. The first three symmetric modes dominate the response of the side spans, with the third mode having the largest contribution. It appears that the uncorrelated case is conservative, i.e., the inclusion of the off-diagonal correlated terms in the spectral matrix $[G_{ff}(\omega)]$ tends to reduce the symmetric spectral response (root mean square response) as shown in Figs. II-45 and II-46.

The autospectra of midspan second derivative responses for side and center spans, which are related to response bending moments and flexural stresses in the top and bottom chords of the bridge stiffening structure, are shown in Fig. II-47 for input arrays No. 4, 5, 6, and 7 and in Fig. II-48 for input arrays Nos. 5, 6, 7, and 8. Figures II-49 and II-50 show similar spectra for third derivative response, evaluated at the ends of each span, which is related to the dynamic shear force. The arrows on the superimposed bridge in Figs. II-45 through II-50 indicate

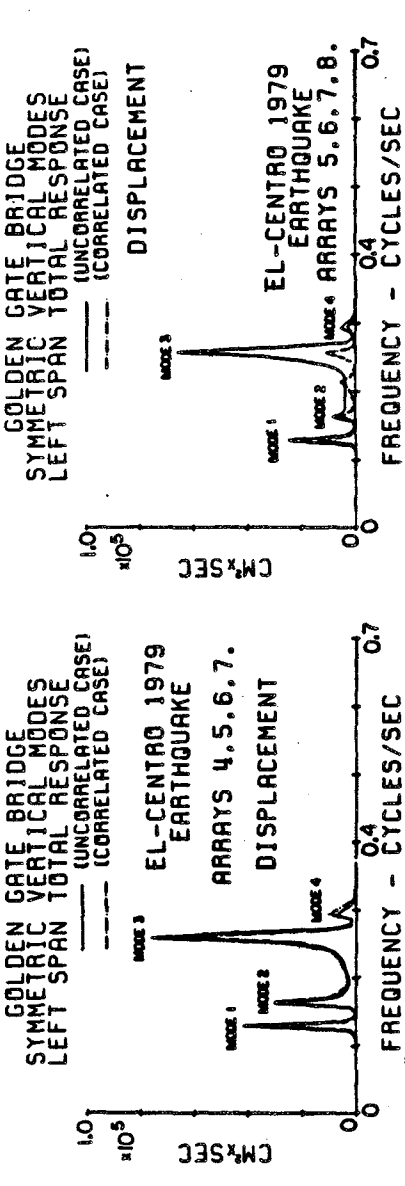

Fig. II-45 Autospectra of midspan displacement. Input arrays 4, 5, 6, 7.

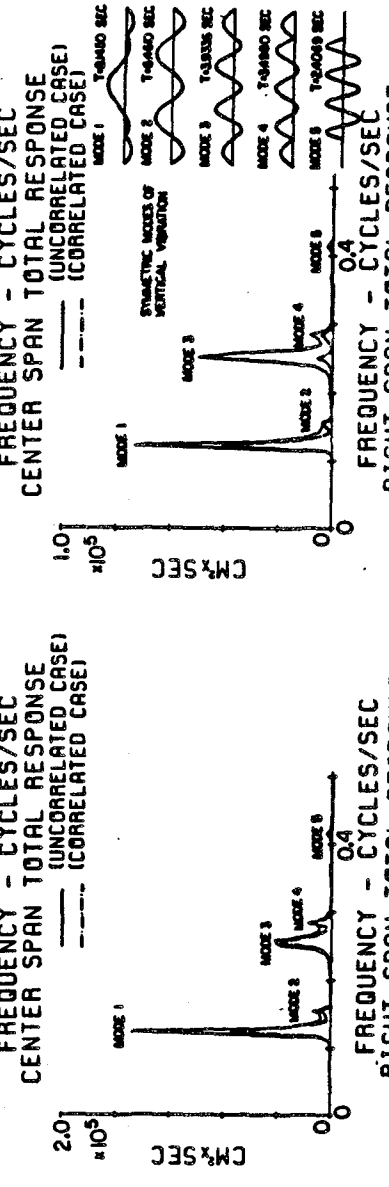

Fig. II-46 Autospectra of midspan displacement. Input arrays 5, 6, 7, 8.

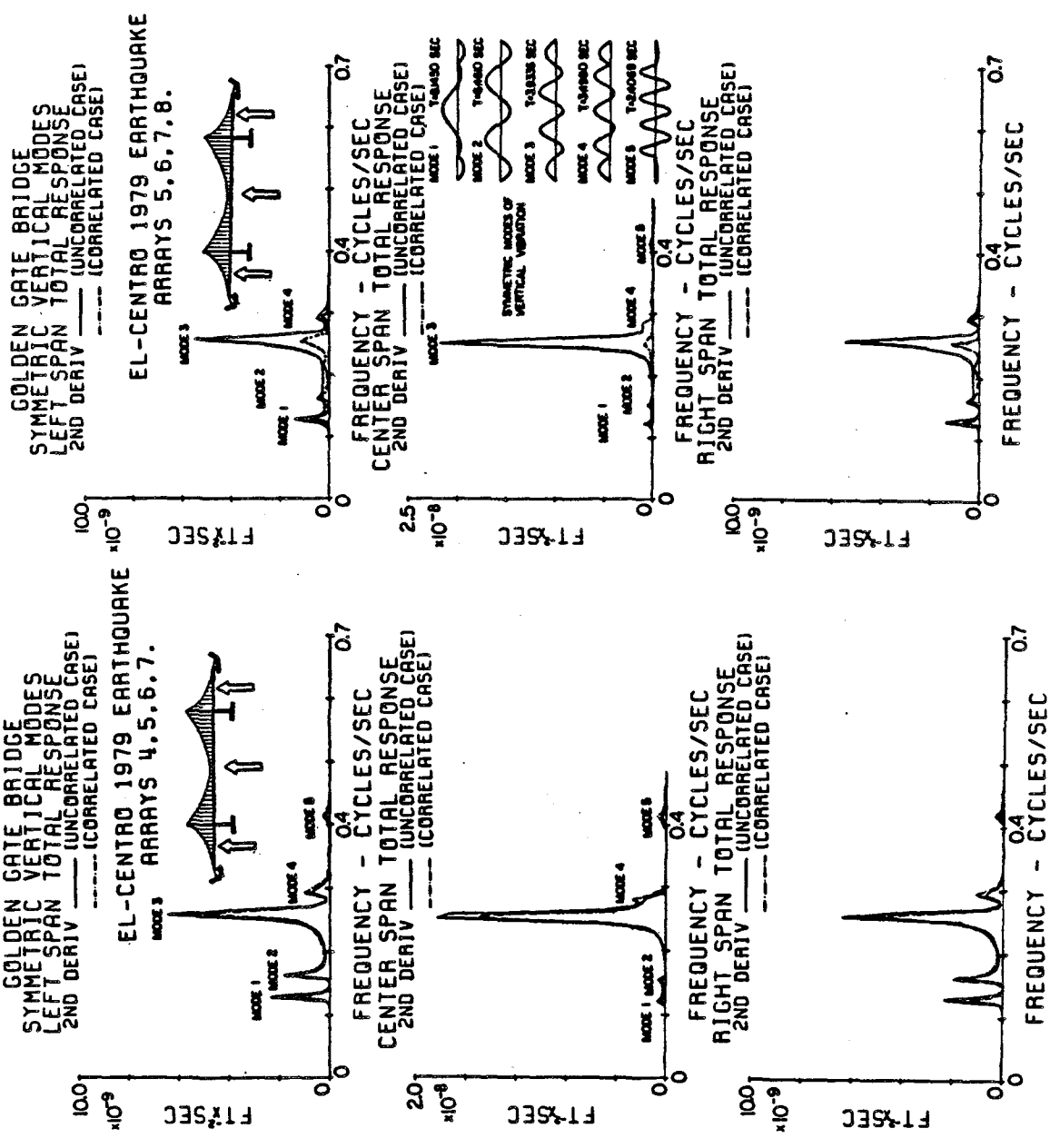

Fig. II-47 Autospectra of second derivative response at midspan. Input arrays 4, 5, 6, 7.

Fig. II-48 Autospectra of second derivative at midspan. Input arrays 5, 6, 7. 8.

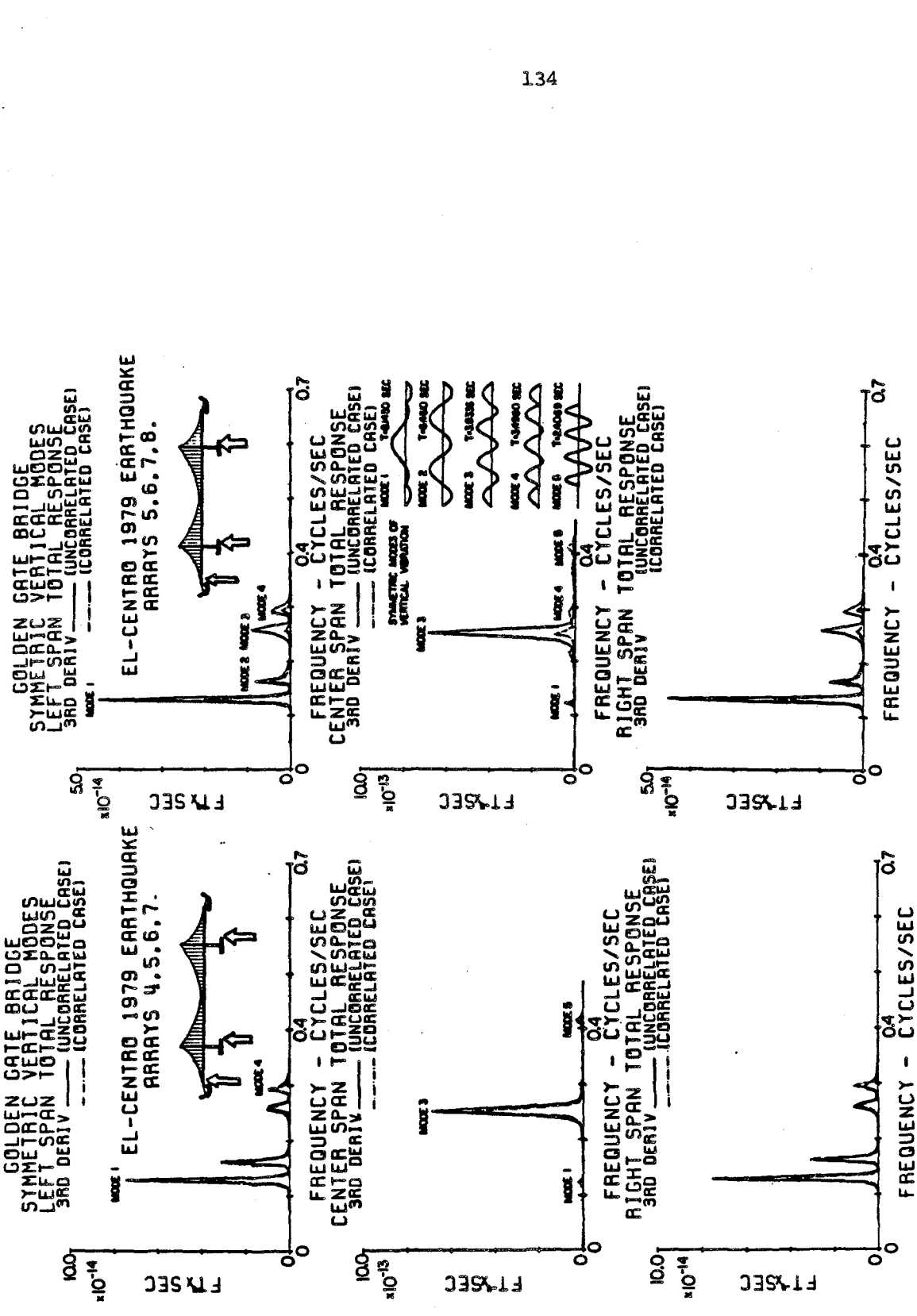

Fig. II-49 Autospectra of third derivative response at endspan. Input arrays 4, 5, 6, 7.

Fig. II-50 Autospectra of third derivative at endspan. Input arrays 5, 6, 7, 8.

the points at which the response is calculated. Again, the uncorrelated case is more conservative than the correlated case. The autospectra of the additional (vibrational) horizontal component of cable tension for both response cases are shown in Fig. II-51. It appears that, in general, the third mode responds most strongly in all cases because of its sensitivity to longitudinal input motion at the anchorages (P_n is large - See Table II-8).

In Table II-9, the expected peak values of the symmetric response predicted by Vanmarcke's and Der Keureghian's methods [9,10,17] are compared with the computed maximum response obtained from the time domain (Duhamel integral) analysis shown in Figs. II-52, 53, and 54. It appears that a peak factor of approximately 3.5 can be used to convert root mean square response values to expected peak values for this multimode multi-input problem. Peak displacements, stresses, shear forces, and dynamic cable tensions are shown for the Golden Gate Bridge in Table II-10 (based upon a peak factor of 3.50) and are compared to results obtained by the response spectral method. It should be mentioned that the response spectral method deals with the input excitations as being uncorrelated (independently applied). Therefore, the response spectral method should be compared to the uncorrelated frequency domain cases, which gives reasonable agreement.

For the correlated case the expected peak value of additional cable tension (expressed as a fraction of the static tension due to dead load, H_w = 53467 kips) is 6.4% for input arrays 5, 6, 7, and 8 and 15.7% for arrays 4, 5, 6, and 7. Baron, et al, [5] have predicted the same range of cable tension in a study of the response of the Golden Gate Bridge subjected to the propagating ground motion of the Taft, 1952, earthquake

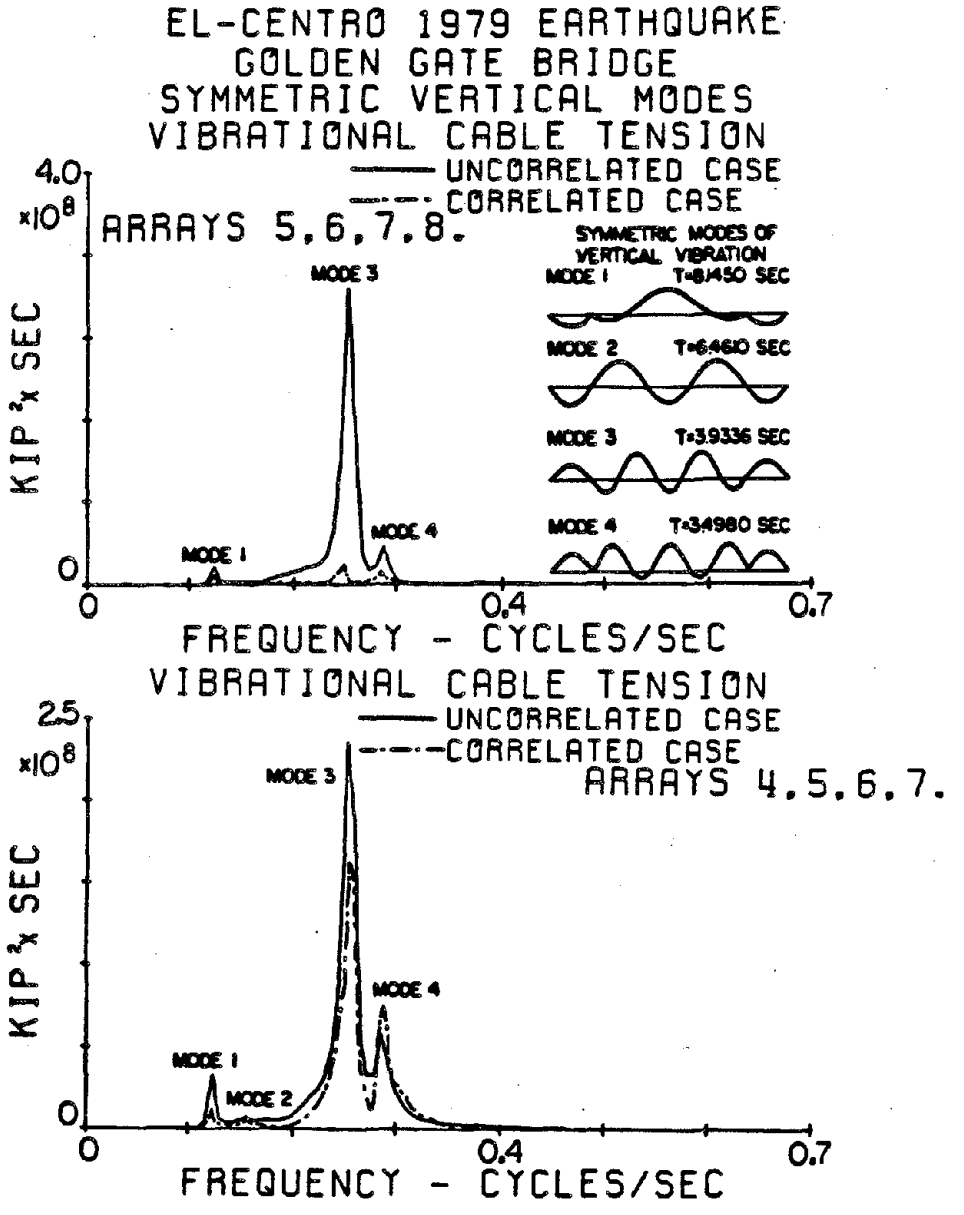

Fig. II-51 Autospectra of additional (vibrational) cable tension.

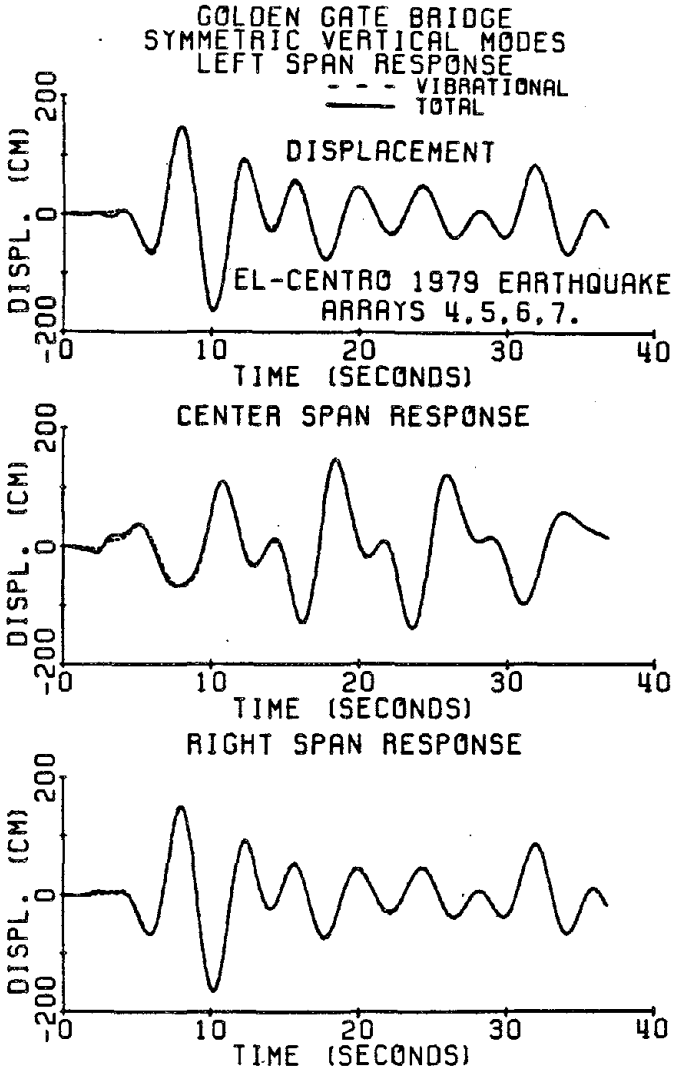

Fig. II-52 Time history of midspan displacements. Input arrays 4, 5, 6, 7.

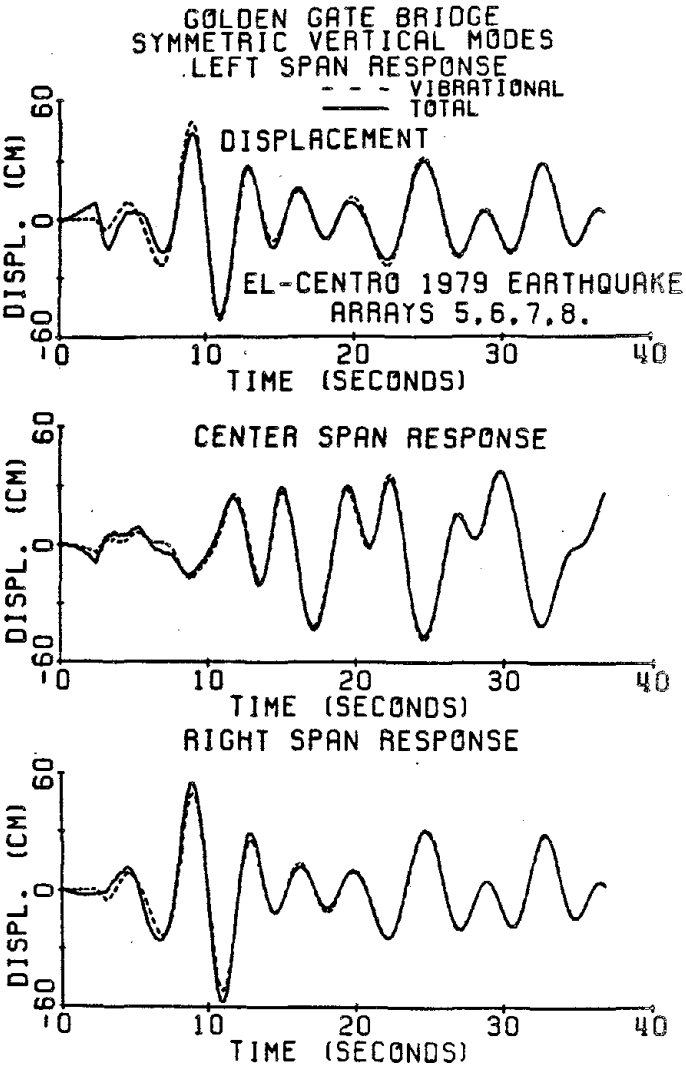

Fig. II-53 Time history of midspan displacements. Input arrays 5, 6, 7, 8.

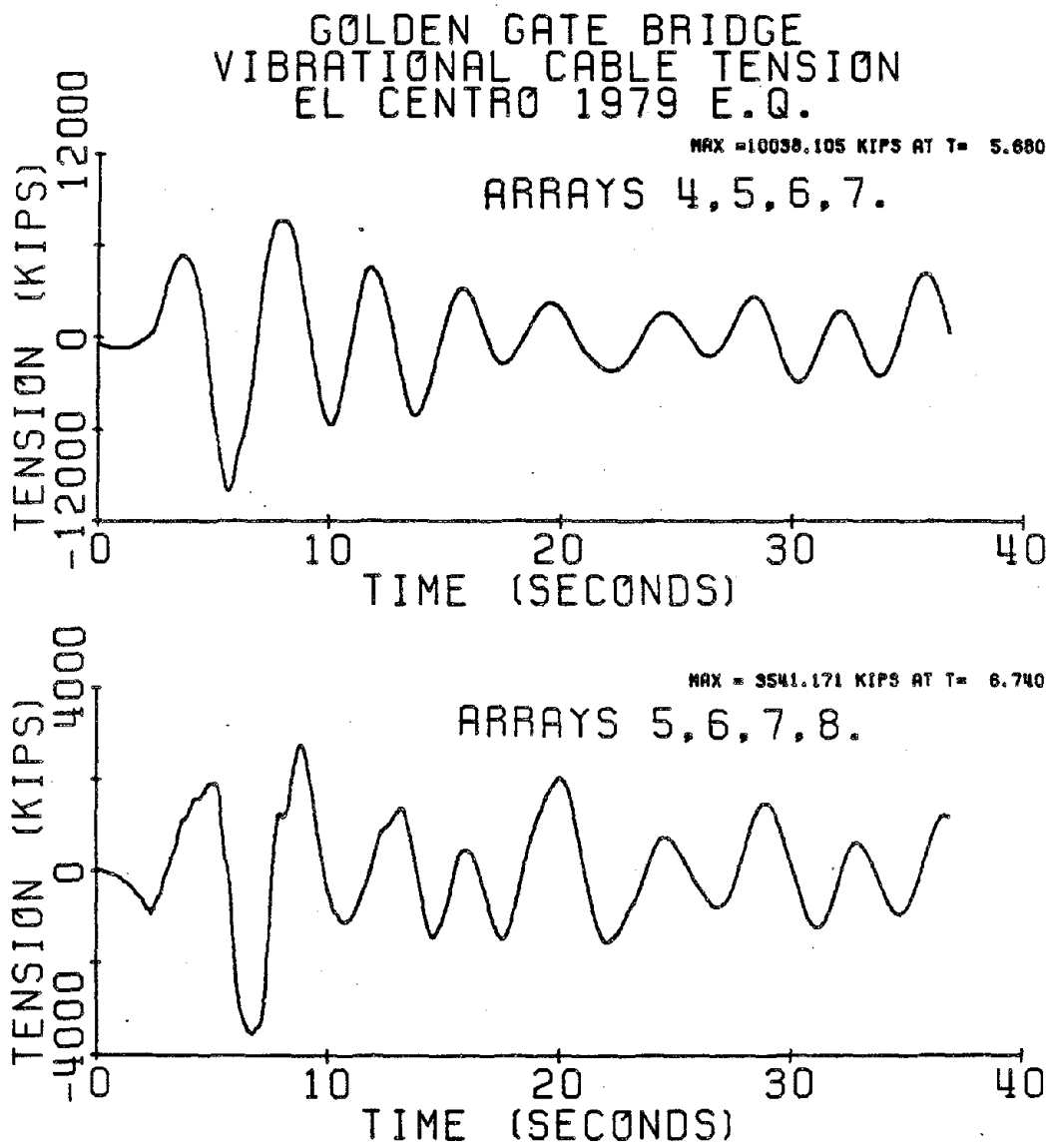

Fig. II-54 Time history of additional (vibrational) cable tension.

Table II-9

EXPECTED PEAK RESPONSE
GOLDEN GATE BRIDGE

RESPONSE CASE (CORRELATED CASES)	R.M.S.Response (Frequency Domain Analysis)	Peak Response (Time Domain Analysis)	Peak/ R.M.S.	Vanmarcke Peak Factor	Der Kiureghian		
					$\mu/\sqrt{\lambda_0}$	$\sigma/\sqrt{\lambda_0}$	$1/\sqrt{\lambda_0}(\mu + 2\sigma)$
Array Nos. 4, 5, 6, 7							
Left Span Displacement	45.25 cm	164.80 cm	3.64	3.35	2.54	0.50	3.54
Center Span Displacement	44.68 cm	146.89 cm	3.29	3.26	2.39	0.53	3.45
Right Span Displacement	44.01 cm	164.27 cm	3.73	3.35	2.54	0.50	3.54
Vibrational Cable Tension	2,405.1 kips	10,038.1 kips	4.17	3.09	2.14	0.57	3.28
Array Nos. 5, 6, 7, 8							
Left Span Displacement	17.13 cm	50.63 cm	2.96	3.23	2.35	0.53	3.41
Center Span Displacement	20.93 cm	46.00 cm	2.20	3.21	2.33	0.54	3.41
Right Span Displacement	14.89 cm	57.73 cm	3.88	3.23	2.35	0.53	3.41
Vibrational Cable Tension	977.6 kips	3.541.2 kips	3.62	3.20	2.30	0.54	3.38

(*)It appears that the mean plus two standard deviations will be a good peak factor.

Table II-10

EXPECTED PEAK VALUES(*) OF DISPLACEMENTS,

BENDING STRESSES, SHEAR FORCES AND CABLE TENSIONS

TOTAL RESPONSE	Correlated			Uncorrelated			Response Spectra Method(***)			ARRAY NUMBERS
	Left	Center	Right	Left	Center	Right	Left	Center	Right	
Displacement at midspan (cm)	158.4	156.4	154.0	167.2	184.4	163.9	143.8	227.2	144.0	4,5,6,7
	60.0	73.3	52.1	147.2	151.7	144.7	122.4	193.4	122.0	5,6,7,8
	53.9	55.0	53.9	--	--	--	--	--	--	Ref. 1
	73.9	131.3	73.9	--	--	--	--	--	--	Ref. 2
	90.0	139.0	90.0	--	--	--	--	--	--	Ref. 3
Bending stress(**) at midspan (ksi)	15.8	24.1	16.0	17.3	25.8	17.3	14.0	21.4	14.0	4,5,6,7
	5.1	6.4	5.1	14.8	25.0	14.8	11.8	17.4	11.8	5,6,7,8
Shear force at left side of each span (kips	172.3	884.8	172.0	211.9	948.9	211.9	217.5	776.7	217.5	4,5,6,7
	81.1	223.7	80.9	164.0	326.9	174.9	190.1	623.8	190.1	5,6,7,8
Cable tension (kips)	8417.9 kips			10403.8 kips			9527.40 kips			4,5,6,7
	3421.6 kips			8798.7 kips			8357.0 kips			5,6,7,8

(*)Based on peak factor value of 3.5.

(**)For the carbon steel of the Golden Gate Bridge the yield stress is: σ_y = 36 ksi.

(***)Using the square root of sum of squares approach.

(M_L = 7.7). This additional cable tension is a significant live load condition in a suspension bridge. Furthermore, the values of earthquake-induced flexural stresses in the stiffening structure are high for a live load as shown in Table II-10 when compared to the yield stress of 50.5 ksi.

Figure II-55 shows the side and center span midspan displacement response for the three reference cases. By comparing these reference cases, as well as their peak responses shown in Table II-10, it is seen that uniform vertical ground motion (Ref. case 1) is not a good assumption in calculating the vertical vibration of a suspension bridge, since longitudinal motions contribute greatly to the vertical bridge response (Ref. cases 2 and 3). The same conclusion may be reached by comparing response spectral calculations under the uniform ground motion assumption (Table II-11) against those calculations which involve longitudinal inputs (Table II-10). Figure II-56 serves as a graphical summary of the Golden Gate symmetric response cases. This figure shows that the vibrational spectral response is fairly similar to the total spectral response; i.e., the effect of the quasi-static displacements is of a higher order nature; however, this effect is incorporated in the participation factors R_{jn}. This trend shows itself again in the comparison of left span versus right span displacements; since the modes considered are symmetric, the only difference in these midspan displacements arise from quasi-static motions. The figure also emphasizes the importance of the longitudinal inputs upon the vertical response.

To check that the effect of antisymmetric vibration is of a higher order nature because the longitudinal anchorage ground motions do not excite the antisymmetric modes (since $P_n = 0$ for antisymmetric nodes), two antisymmetric vertical response cases are studied. In the first case,

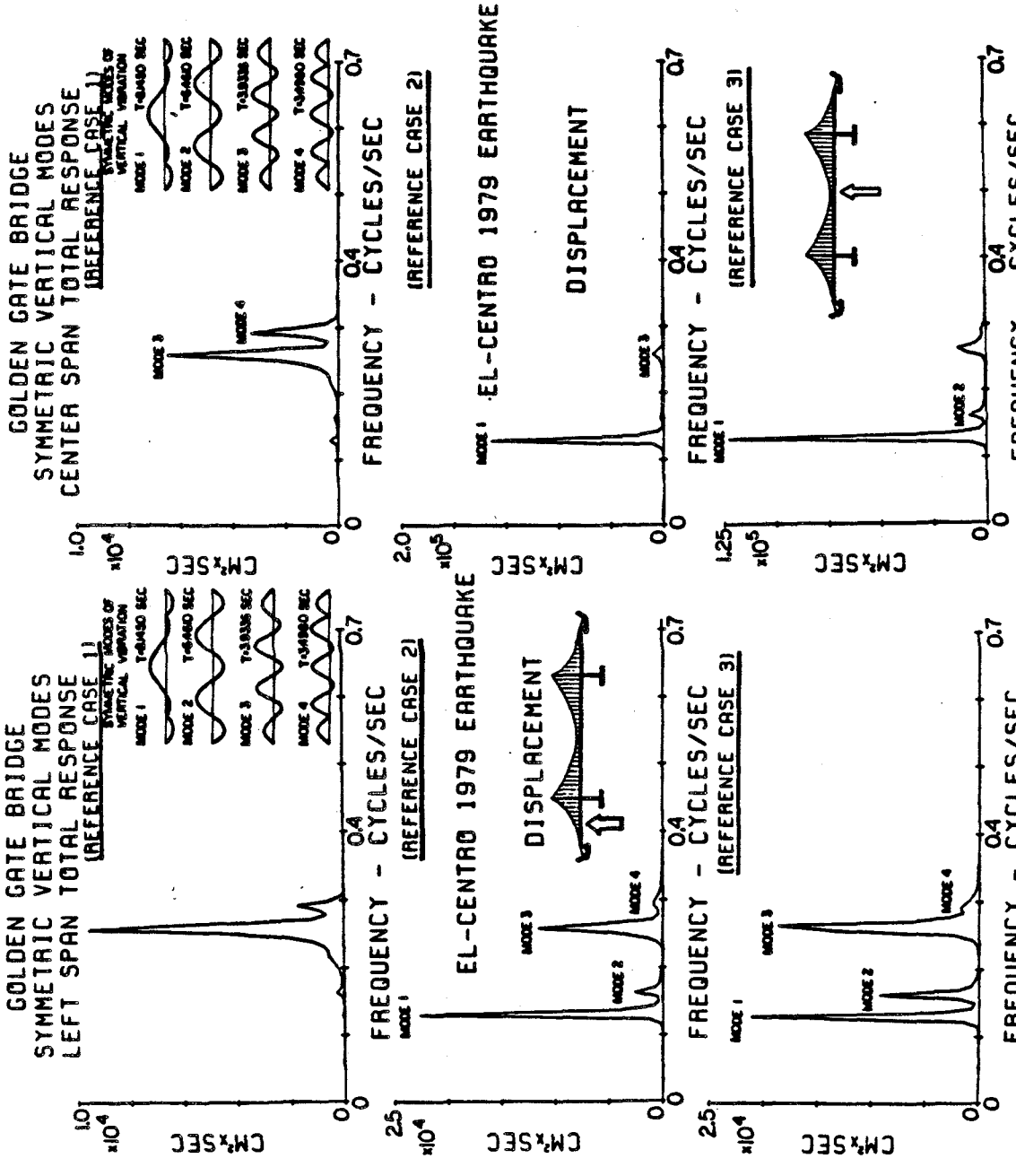

Fig. II-55 Autospectra of midspan displacements. Reference cases. Effect of longitudinal motion.

Table II-11

UNIFORM VERTICAL MOTION [ARRAY #6]
[$f_5(t) = f_8(t) = 0$; Response spectral approach]

TOTAL RESPONSE	Left Span	Center Span	Right Span
Displacement at midspan (cm)	37.2	51.9	37.2
Bending stress at midspan (ksi)	3.44	5.73	3.44
Shear force at left side of each span (kips)	48.2	206.2	48.2
Cable tension (kips)	2318.1 kips		

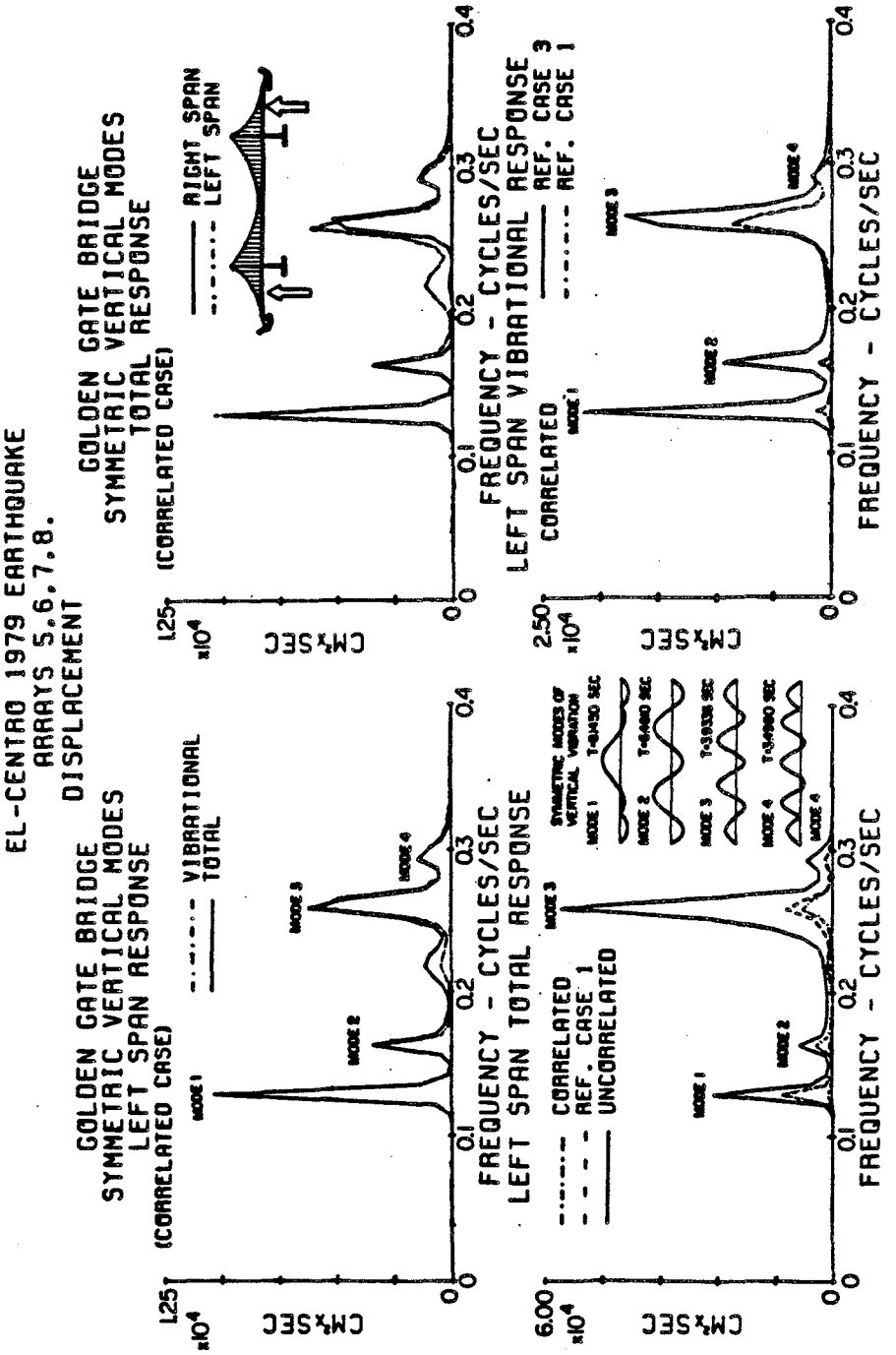

Fig. II-56 Autospectra of midspan displacements. Summary diagram.

the inputs are taken as El Centro Arrays No. 4, 5, 6, and 7, while the second case involves input arrays No. 5, 6, 7, and 8. The autospectra of displacement at three points on the bridge are shown in Fig. II-57 for the first input case and in Fig. II-58 for the second input case. Figures II-59 and II-60, show similar autospectra of response stresses. In these figures, Point 1 corresponds to the displacement (or stress) at the midspan of the left side span, Point 2 corresponds to the displacement (or stress) at quarter span of the center span ($\ell_2/4$) and Point 3 corresponds to displacement (or stress) at the 4/10 span of the center span ($0.4 \cdot \ell_2$). Figures II-61 and II-62 show the autospectra of shear force at the left side of each span. For these figures, Point 1 corresponds to the left end of the left side span and Point 2 corresponds to the left end of the center span. The root mean square (R.M.S.) response values due to antisymmetric vertical vibration are summarized in Table II-12, and clearly, when compared to Table II-10, show that the antisymmetric vibration is of a higher order nature.

In order to further investigate the symmetric vertical response of the Golden Gate Bridge, as well as gain more confidence in the statistical peak factors, the vertical seismic response of the Golden Gate Bridge is investigated using artificially generated earthquake ground motions as inputs. These inputs are described in detail in Ref. 12 and appear in Appendix II-e. The Type A and Type B models, which intend to represent the acceleration in a magnitude 8 shock and magnitude 7 shock, respectively, are utilized in this study. The acceleration, velocity, and displacement ground motion histories for the various inputs are shown along with their associated power spectral density of displacement functions. The artificial earthquake ground motion A-3 is

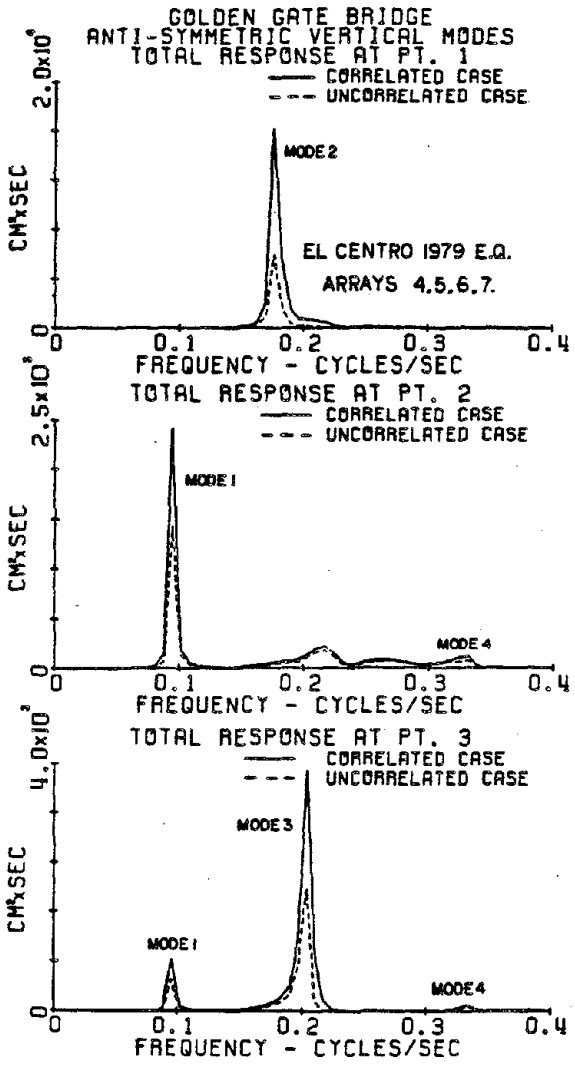

Fig. II-57 Autospectra of antisymmetric displacement response. Input arrays 4, 5, 6. 7.

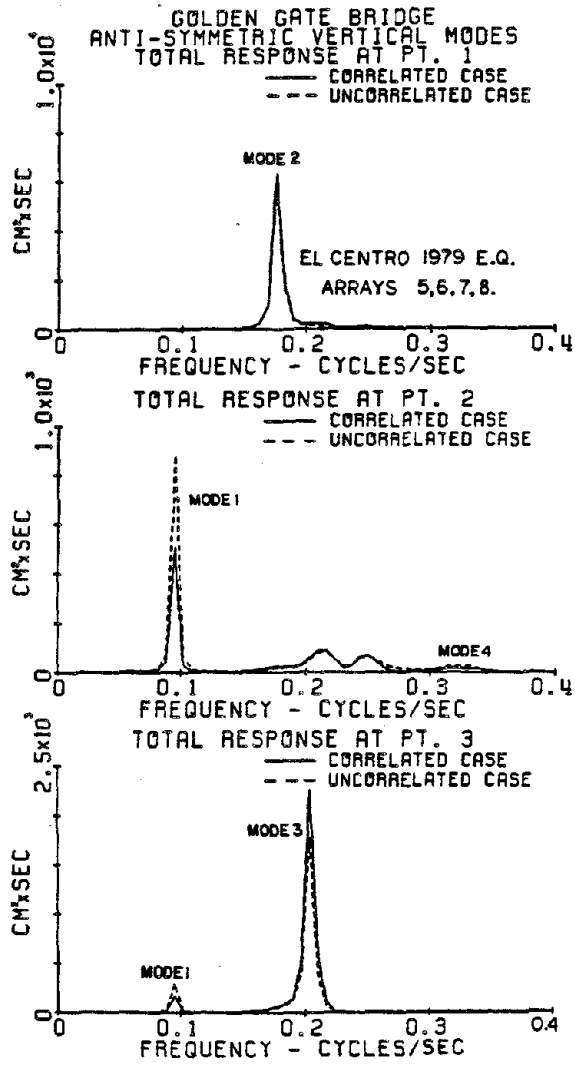

Fig. II-58 Autospectra of antisymmetric displacement response. Input arrays 5, 6, 7, 8.

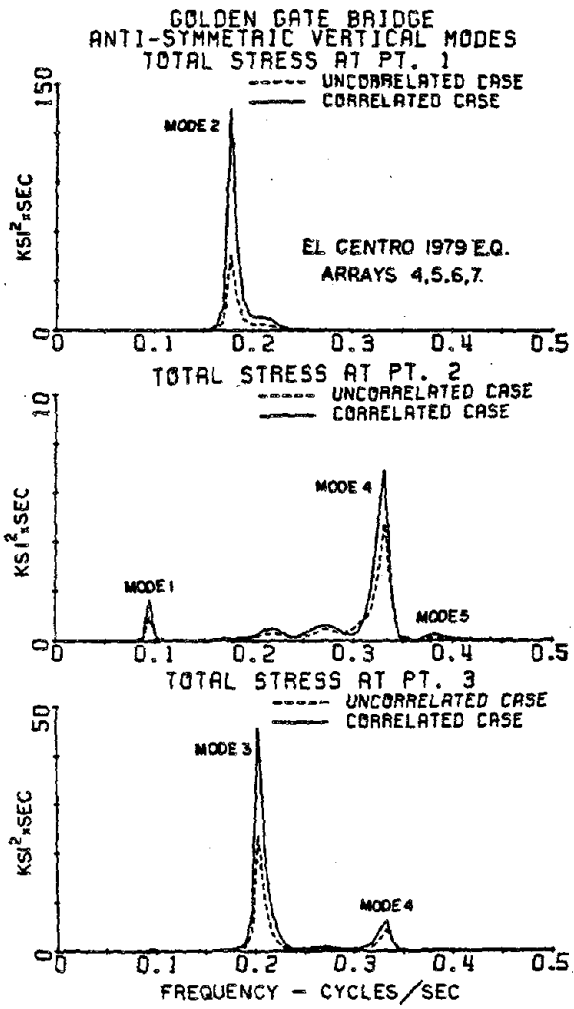

Fig. II-59 Autospectra of antisymmetric response stresses. Input arrays 4, 5, 6, 7.

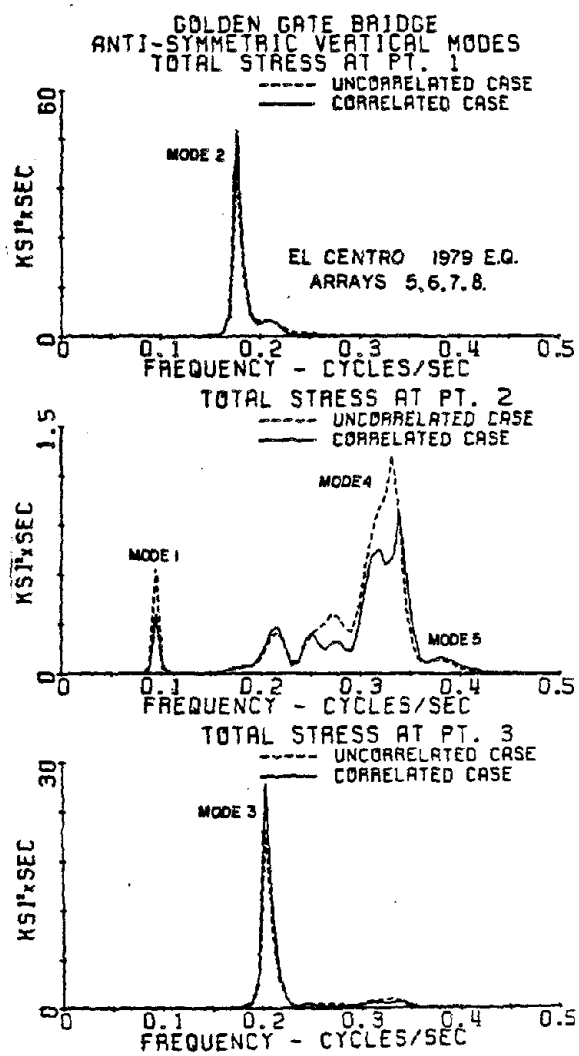

Fig. II-60 Autospectra of antisymmetric response stresses. Input arrays 5, 6, 7, 8.

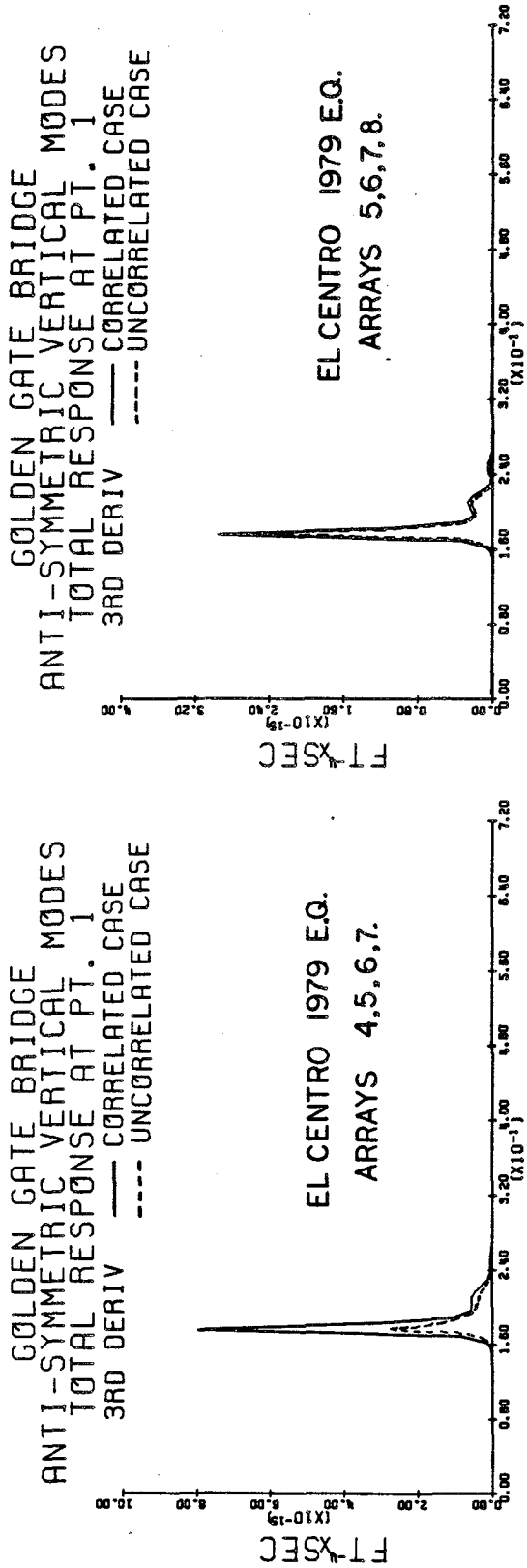

Fig. II-61 Autospectra of antisymmetric third derivative response at endspan.
Input arrays 4, 5, 6, 7.

Fig. II-62 Autospectra of antisymmetric third derivative response at endspan.
Input arrays 5, 6, 7, 8.

Table II-12

EXPECTED ROOT MEAN SQUARE
VALUES OF DISPLACEMENTS, BENDING STRESSES,
AND SHEAR FORCES
DUE TO ANTISYMMETRIC VERTICAL VIBRATION

TOTAL RESPONSE	Correlated			Uncorrelated			Array Numbers
	PT 1	PT 2	PT 3	PT 1	PT 2	PT 3	
Displacement (cm)	15.0	6.25	8.97	9.17	5.52	6.24	4,5,6,7
	10.8	3.30	5.40	9.39	3.94	5.44	5,6,7,8
Bending Stress (ksi)	1.36	0.43	0.87	0.83	0.36	0.64	4,5,6,7
	0.82	0.25	0.63	0.79	0.28	0.59	5,6,7,8
Shear Force at Left Side of Span (kips)	17.2	19.9	17.2	10.9	15.2	10.9	4,5,6,7
	10.4	13.9	10.4	10.2	13.2	10.2	5,6,7,8

taken as the vertical input motion $f_1(t)$, A-4 is taken as $f_2(t)$, B-1 is taken as $f_3(t)$, B-2 is taken as $f_4(t)$, and the longitudinal inputs $f_5(t)$ and $f_8(t)$ are taken as the artificial motions A-1 and A-2, respectively.

The autospectra of midspan symmetric displacement response to the artificially-generated inputs are shown in Fig. II-63 while the autospectra of midspan stresses are shown in Fig. II-64. The autospectra of shear force at the endspans are shown in Fig. II-65, while the autospectra of the additional (vibrational) component of the cable tension is shown in Fig. II-66. In Table II-13, the expected peak values of the symmetric response predicted by Vanmarcke's and Der Kiureghian's methods are compared with the computed maximum response obtained from the time domain (Duhmael integral) analysis shown in Figs. II-67 and II-68. It again appears that a peak factor of approximately 3.5 is appropriate to convert root mean square values to expected peak values, with the possible exception of the cable tension response, whose calculated peak factor is quite high (6.64).

It should be remembered that both Vanmarcke's and Der Kiureghian's analyses deal with a single, Gaussian, suddenly applied, steady-state input. It would seem that the multiple-support excitation problem may be quite more complicated, and additional studies may be necessary to completely comprehend the complex nature of the peak factors. Figure II-69 shows the peak factor distribution for one of the displacement response cases. It is seen that Vanmarcke's and Der Kiureghian's peak factor distributions are fairly similar. Also, it is seen that for 95% confidence, one should take the peak factor to be about 3.5, and the expected value (or mean) of the peak factor should be about 2.1.

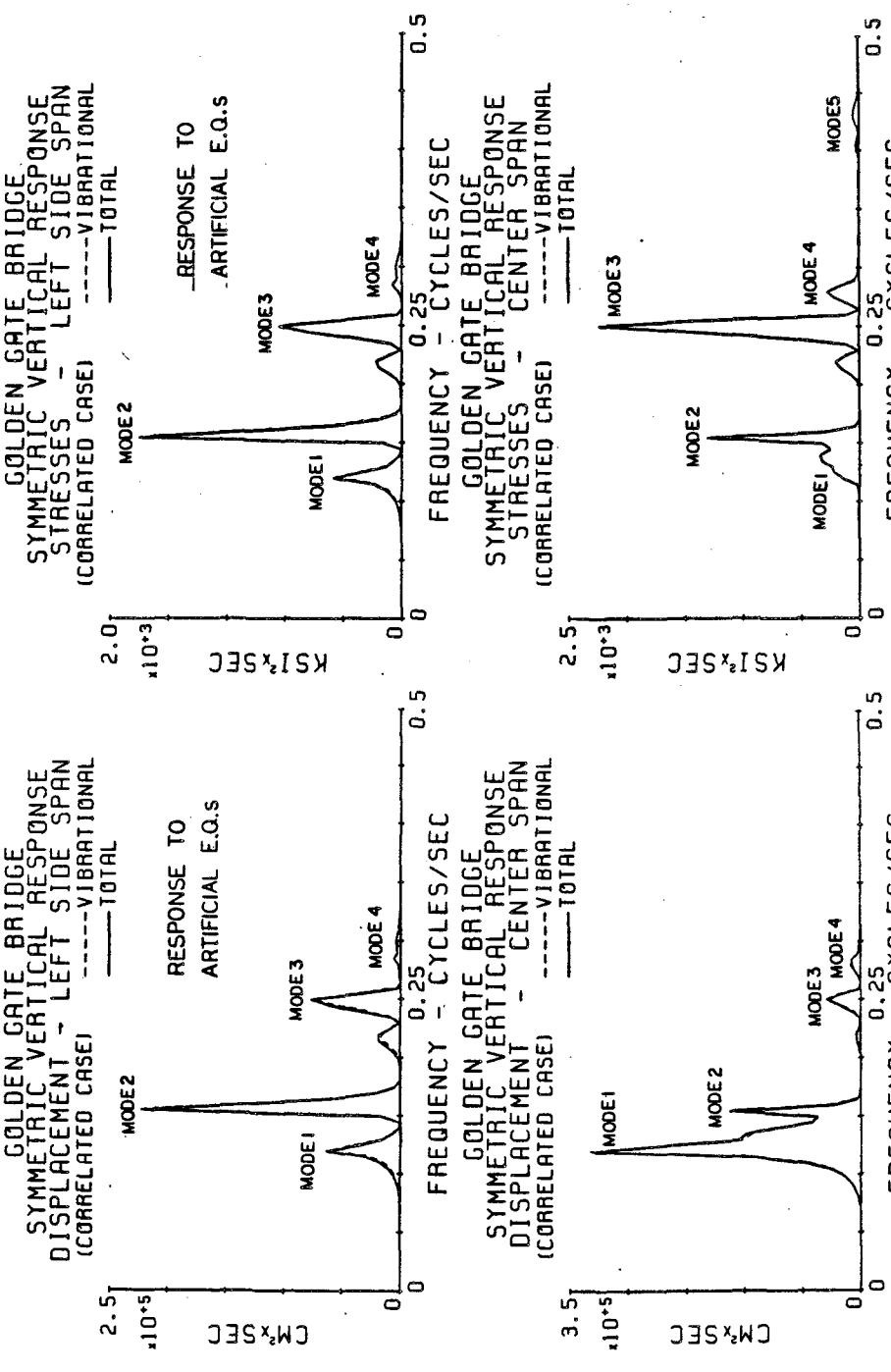

Fig. II-63 Autospectra of midspan displacement response to artificial earthquake inputs.

Fig. II-64 Autospectra of midspan response stresses to artificial earthquake inputs.

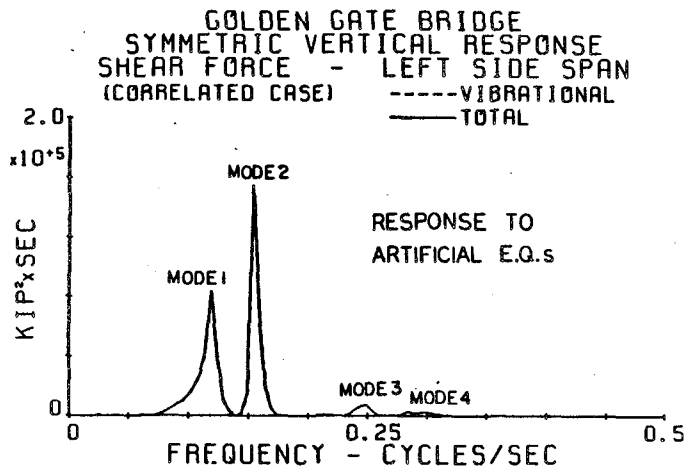

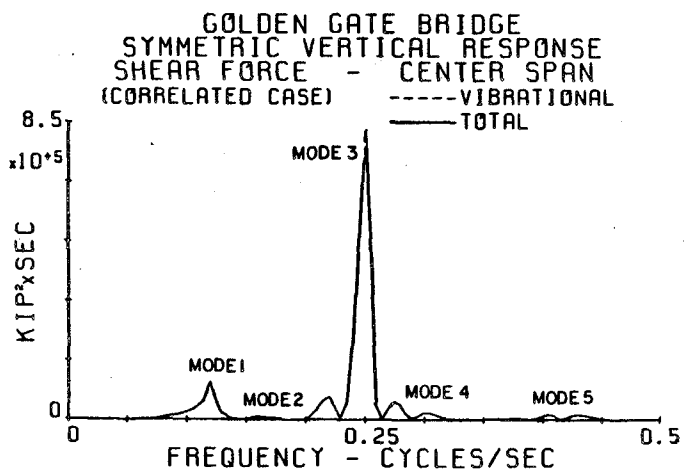

Fig. II-65 Autospectra of endspan shear force response to artificial earthquake inputs.

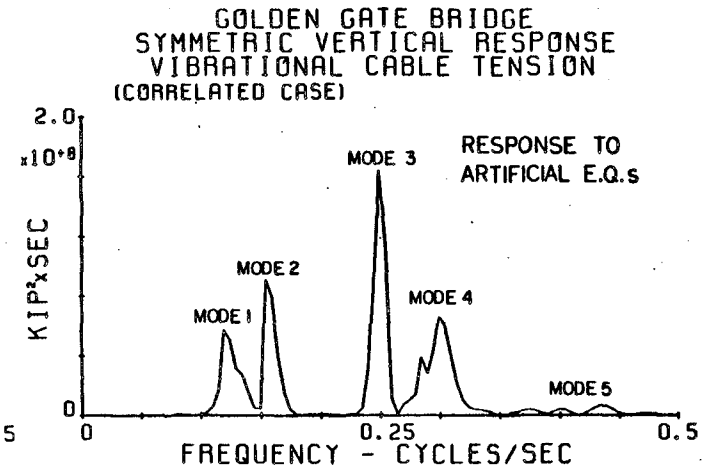

Fig. II-66 Autospectra of additional (vibrational) cable tension response to artificial earthquake inputs.

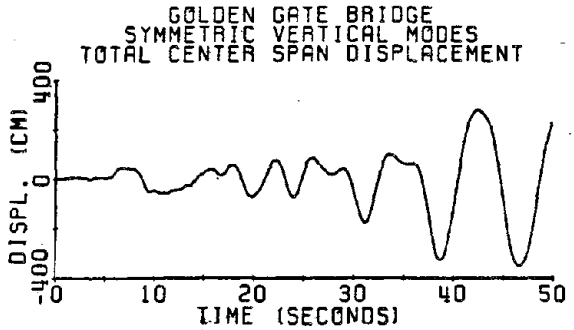

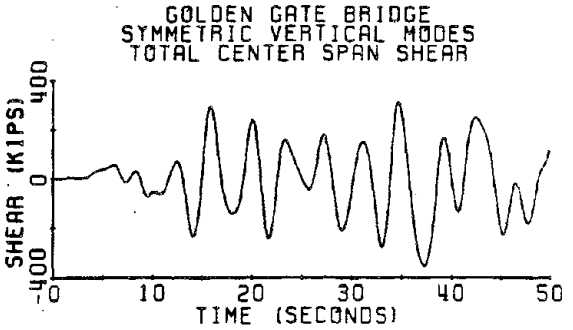

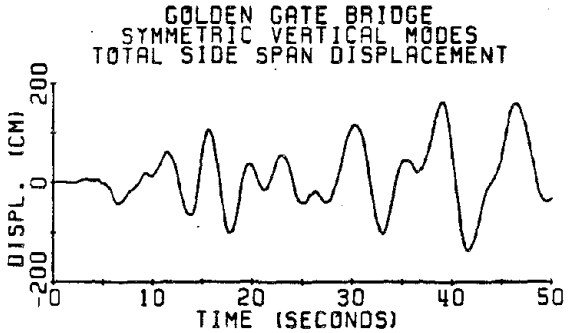

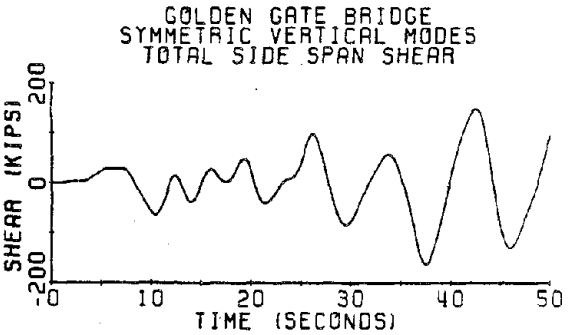

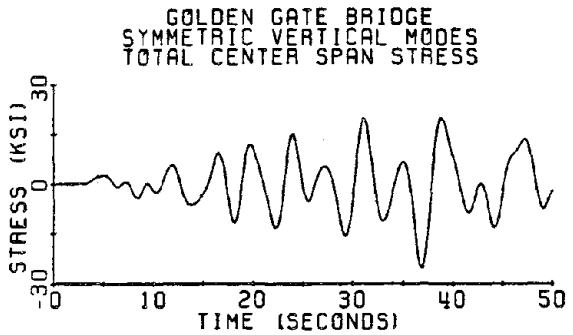

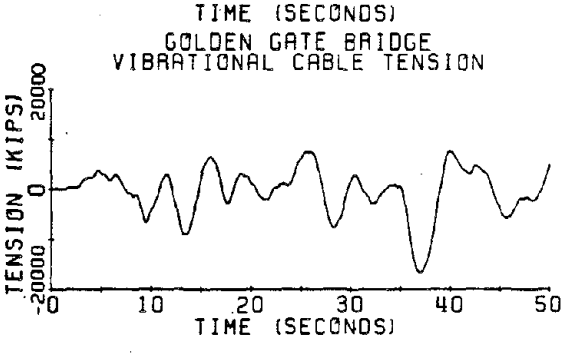

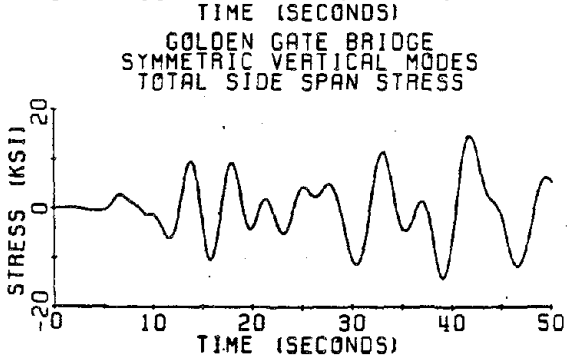

RESPONSE TO
ARTIFICIAL E.Q.S

Fig. II-67 Time history of midspan displacement and stress response to artificial earthquake inputs.

Fig. II-68 Time history of endspan shear force and additional (vibrational) cable tension. response to artificial earthquake inputs.

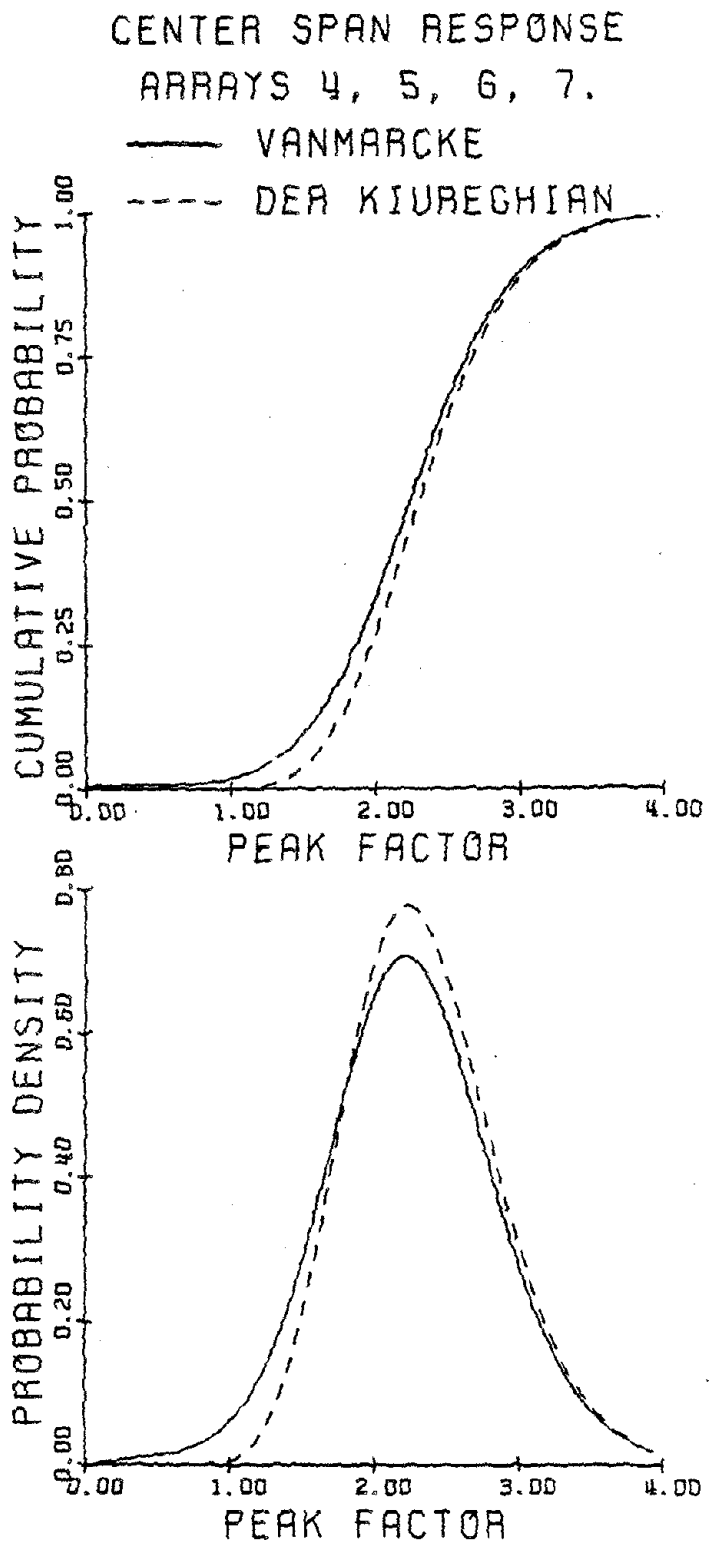

Fig. II-69 Peak factor probability distribution and probability density functions.

From Tables II-9 and II-13, it can be seen that the actual peak factors, obtained by dividing the time domain results by the associated root mean square frequency domain results, are all fairly high, that is, they do not appear to have an expected value of 2.1, but rather an expected value close to 3.5. This indicates that for the multiple-support excitation problem, additional analysis may be necessary in order to accurately predict peak factors.

Table II-13

EXPECTED PEAK RESPONSE
TO ARTIFICIAL EARTHQUAKES

(Golden Gate Bridge)

RESPONSE CASE (Correlated Cases)	R.M.S. Response (Frequency Domain Analysis)	Peak Response (Time Domain Analysis)	Peak/ R.M.S.	Vanmarcke Peak Factor	Der Kiureghian		
					$\mu/\sqrt{\lambda_0}$	$\sigma/\sqrt{\lambda_0}$	$1/\sqrt{\lambda_0}$ $(\mu+2\sigma)$
Left Span Displacement (cm)	69.2	161	2.33	3.28	2.41	0.52	3.45
Center Span Displacement (cm)	92.3	351	3.80	3.21	2.32	0.54	3.40
Right Span Displacement (cm)	67.9	161	2.37	3.27	2.40	0.52	3.44
Left Span Stress (ksi)	6.43	14.8	2.30	3.29	2.42	0.52	3.46
Center Span Stress (ksi)	7.46	25.4	3.40	3.34	2.48	0.51	3.50
Right Span Stress (ksi)	6.43	14.8	2.30	3.29	2.42	0.52	3.46
Left Span Shear (kips)	53.2	163	3.06	3.20	2.31	0.54	3.39
Center Span Shear (kips)	124	355	2.86	3.33	2.47	0.51	3.49
Right Span Shear (kips)	53.3	163	3.06	3.20	2.31	0.54	3.39
Cable Tension (kips)	2530	16800	6.64	3.40	2.56	0.50	3.56

APPENDIX II-a

Solution for the Vertical Quasi-Static Functions

A. Unit displacement at Left Anchorage:

The solution for the quasi-static function corresponding to unit displacement at support A of figure II-1 is obtained by satisfying the following three equations:

$$E_i I_i \frac{d^4 g_{1i}(x_i)}{dx_i^4} - H_w \frac{d^2 g_{1i}(x_i)}{dx_i^2} + \frac{\overset{*}{w}_i}{H_w} \left(\frac{E_c A_c}{L_E}\right) \left[\sum_{n=i}^{3} \frac{\overset{*}{w}_n}{H_w} \int_0^{\ell_n} g_{1n}(x_n)\, dx_n \right] = 0$$

$$i = 1,2,3 \qquad \text{(II-a-1)}$$

subject to the boundary conditions

$$\begin{aligned} &g_{11}(0) = 1 \qquad g_{12}(0) = 0 \qquad g_{13}(0) = 0 \\ &g_{11}(\ell_1) = 0 \qquad g_{12}(\ell_2) = 0 \qquad g_{13}(\ell_3) = 0 \\ &g_{11}''(0) = g_{12}''(0) = g_{13}''(0) = 0 \\ &g_{11}''(\ell_1) = g_{12}''(\ell_2) = g_{13}''(\ell_3) = 0 \end{aligned} \qquad \text{(II-a-2)}$$

The form of the solution can be taken as

$$g_{1i}(x_i) = A_{1i} \sinh(\lambda_i x_i) + B_{1i} \cosh(\lambda_i x_i) + C_{1i} x_i^2 + D_{1i} x_i + E_{1i} \qquad i = 1,2,3 \qquad \text{(II-a-3)}$$

where $\lambda_i = \sqrt{\frac{H_w}{E_i I_i}}$ $\quad i = 1,2,3$ (II-a-4)

Substituting Eqs. II-a-3 into Eqs. II-a-1 results in the following three equations:

$$2H_w C_{1i} = \frac{\overset{*}{w}_i}{H_w} \left(\frac{E_c A_c}{L_E}\right) \left\{ \sum_{n=1}^{3} \frac{\overset{*}{w}_n}{H_w} \left[\frac{A_{1n}}{\lambda_n} [\cosh(\lambda_n \ell_n) - 1] + \frac{B_{1n}}{\lambda_n} \sinh(\lambda_n \ell_n) + \frac{C_{1n} \ell_n^3}{3} + \frac{D_{1n} \ell_n^2}{2} + E_{1n} \ell_n \right] \right\}$$

$$i = 1,2,3 \qquad \text{(II-a-5)}$$

Equations II-a-3 and II-a-5 can be used in conjunction with the boundary conditions (II-a-2) in order to solve for the 15 unknown coefficients present in Eq. II-a-3, hence uniquely defining the first quasi-static function $g_{1i}(x_i)$.

Introducing $g_{11}(x_1)$ from Eq. II-a-3 into the boundary conditions results in the equations

$$\begin{aligned}
&B_{11} + E_{11} = 1 \\
&B_{11}\lambda_1^2 + 2C_{11} = 0 \\
&A_{11} \sinh(\lambda_1 \ell_1) + B_{11} \cosh(\lambda_1 \ell_1) + C_{11} \ell_1^2 + D_{11} \ell_1 + E_{11} = 0 \\
&A_{11}\lambda_1^2 \sinh(\lambda_1 \ell_1) + B_{11}\lambda_1^2 \cosh(\lambda_1 \ell_1) + 2C_{11} = 0
\end{aligned} \qquad \text{(II-a-6)}$$

From the previous equations, the coefficients A_{11}, C_{11}, D_{11}, and E_{11} can be written in terms of B_{11} as

$$E_{11} = 1 - B_{11}$$

$$C_{11} = \frac{-B_{11}\lambda_1^2}{2}$$

$$A_{11} = -\frac{B_{11}[\cosh(\lambda_1\ell_1)-1]}{\sinh(\lambda_1\ell_1)} = -B_{11}\tanh\left(\frac{\lambda_1\ell_1}{2}\right) \qquad \text{(II-a-7)}$$

$$D_{11} = \frac{B_{11}\lambda_1^2\ell_1}{2} - \frac{1}{\ell_1}$$

Similarly, introducing $g_{12}(x_2)$ into the boundary conditions gives

$$B_{12} + E_{12} = 0$$

$$B_{12}\lambda_2^2 + 2C_{12} = 0$$

$$A_{12}\sinh(\lambda_2\ell_2) + B_{12}\cosh(\lambda_2\ell_2) + C_{12}\ell_2^2 + D_{12}\ell_2 + E_{12} = 0$$

$$A_{12}\lambda_2^2\sinh(\lambda_2\ell_2) + B_{12}\lambda_2^2\cos(\lambda_2\ell_2) + 2C_{12} = 0 \qquad \text{(II-a-8)}$$

Again, the coefficients A_{12}, C_{12}, D_{12}, and E_{12} can be written in terms of B_{12} as

$$E_{12} = -B_{12}$$

$$C_{12} = -\frac{B_{12}\lambda_2^2}{2}$$

$$A_{12} = \frac{-B_{12}[\cosh(\lambda_2\ell_2)-1]}{\sinh(\lambda_2\ell_2)} = -B_{12}\tanh(\frac{\lambda_2\ell_2}{2}) \qquad \text{(II-a-9)}$$

$$D_{12} = \frac{B_{12}\lambda_2^2\ell_2}{2}$$

Introducing $g_{13}(x_3)$ into the boundary conditions gives

$$B_{13} + E_{13} = 0$$

$$B_{13}\lambda_3^2 + 2C_{13} = 0$$

$$A_{13}\sinh(\lambda_3\ell_3) + B_{13}\cosh(\lambda_3\ell_3) + C_{13}\ell_3^2 + D_{13}\ell_3 + E_{13} = 0 \qquad \text{(II-a-10)}$$

$$A_{13}\lambda_3^2\sinh(\lambda_3\ell_3) + B_{13}\lambda_3^2\cosh(\lambda_3\ell_3) + 2C_{13} = 0$$

which results in

$$E_{13} = -B_{13}$$

$$C_{13} = -\frac{B_{13}\lambda_3^2}{2}$$

$$A_{13} = -\frac{B_{13}[\cosh(\lambda_3\ell_3)-1]}{\sinh(\lambda_3\ell_3)} = -B_{13}\tanh(\frac{\lambda_3\ell_3}{2}) \qquad \text{(II-a-11)}$$

$$D_{13} = \frac{B_{13}\lambda_3^2\ell_3}{2}$$

From Eqs. II-a-5, the following relationship is apparent:

$$\frac{C_{11}}{\overset{*}{w}_1} = \frac{C_{12}}{\overset{*}{w}_2} = \frac{C_{13}}{\overset{*}{w}_3} \tag{II-a-12}$$

Using Eqs. II-a-7, 9, 11 the previous equation can be written

$$\frac{B_{11}\lambda_1^2}{\overset{*}{w}_1} = \frac{B_{12}\lambda_2^2}{\overset{*}{w}_2} = \frac{B_{13}\lambda_3^3}{\overset{*}{w}_3} \tag{II-a-13}$$

Therefore,

$$B_{12} = B_{11} \left(\frac{\overset{*}{w}_2}{\overset{*}{w}_1}\right) \left(\frac{\lambda_1}{\lambda_2}\right)^2$$
$$B_{13} = B_{11} \left(\frac{\overset{*}{w}_3}{\overset{*}{w}_1}\right) \left(\frac{\lambda_1}{\lambda_3}\right)^2 \tag{II-a-14}$$

Substituting Eqs. II-a-7, 9, 11, and 14 into Eq. II-a-5, and solving for B_{11}

$$B_{11} = \frac{-\left(\frac{\overset{*}{w}_1}{H_w}\right)\left(\frac{E_c A_c}{L_E}\right)\left(\frac{\overset{*}{w}_1 \ell_1}{2H_w}\right)}{\left(\frac{E_c A_c}{L_E}\right)\left[\sum_{i=1}^{3}\left(\frac{\overset{*}{w}_i}{H_w}\right)^2\left(\frac{\lambda_1}{\lambda_i}\right)^2\left(\frac{2}{\lambda_i}\tanh\frac{\lambda_i \ell_i}{2} + \frac{\lambda_i^2 \ell_i^3}{12} - \ell_i\right)\right] + \lambda_1^2 H_w} \tag{II-a-15}$$

Once B_{11} is known, the quasi-static function $g_{1i}(x_i)$ is completely determined since the coefficients A_{1i}, B_{1i}, C_{1i}, D_{1i}, and E_{1i} appearing in Eq. II-a-3 can all be defined in terms of the coefficient B_{11} using Eqs. II-a-7, 9, 11, 14.

B. Unit Displacement at Left Tower-Pier

The solution for the quasi-static function corresponding to unit displacement at support B of figure II-1 is obtained by satisfying the following three equations:

$$E_i I_i \frac{d^4 g_{2i}(x_i)}{dx_i^4} - H_w \frac{d^2 g_{2i}(x_i)}{dx_i^2} + \frac{\overset{*}{w}_i}{H_w} \left(\frac{E_c A_c}{L_E}\right) \left[\sum_{n=1}^{3} \frac{\overset{*}{w}_n}{H_w} \int_0^{\ell_n} g_{2n}(x_n)\, dx_n \right] = 0$$

$$i = 1,2,3 \qquad \text{(II-a-16)}$$

subject to the boundary conditions

$$\begin{aligned} &g_{21}(0) = 0 \qquad g_{22}(0) = 1 \qquad g_{23}(0) = 0 \\ &g_{21}(\ell_1) = 1 \qquad g_{22}(\ell_2) = 0 \qquad g_{23}(\ell_3) = 0 \\ &g_{21}''(0) = g_{22}''(0) = g_{23}''(0) = 0 \\ &g_{21}''(\ell_1) = g_{22}''(\ell_2) = g_{23}''(\ell_3) = 0 \end{aligned} \qquad \text{(II-a-17)}$$

The form of the solution can be taken as

$$g_{2i}(x_i) = A_{2i} \sinh(\lambda_i x_i) + B_{2i} \cosh(\lambda_i x_i) + C_{2i} x_i^2 + D_{2i} x_i + E_{2i} \qquad \text{(II-a-18)}$$

$$i = 1,2,3$$

where λ_i is defined by Eq. II-a-4. Substituting Eqs. II-a-18 into Eqs. II-a-16 results in the following three equations:

$$2H_w C_{2i} = \frac{\overset{*}{w}_i}{H_w} \left(\frac{E_c A_c}{L_E}\right) \left\{ \sum_{n=1}^{3} \frac{\overset{*}{w}_n}{H_w} \left[\frac{A_{2n}}{\lambda_n} [\cosh(\lambda_n \ell_n) - 1] + \frac{B_{2n}}{\lambda_n} \sinh(\lambda_n \ell_n) + \frac{C_{2n} \ell_n^3}{3} + \frac{D_{2n} \ell_n^2}{2} + E_{2n} \ell_n \right] \right\}$$

$$i = 1,2,3 \qquad \text{(II-a-19)}$$

Introducing $g_{21}(x_1)$ from Eq. II-a-18 into the boundary conditions results in the equations

$$B_{21} + E_{21} = 0$$

$$B_{21}\lambda_1^2 + 2C_{21} = 0$$

$$A_{21} \sinh(\lambda_1 \ell_1) + B_{21} \cosh(\lambda_1 \ell_1) + C_{21} \ell_1^2 + D_{21} \ell_1 + E_{21} = 1$$

$$A_{21}\lambda_1^2 \sinh(\lambda_1 \ell_1) + B_{21}\lambda_1^2 \cosh(\lambda_1 \ell_1) + 2C_{21} = 0 \qquad \text{(II-a-20)}$$

From the previous equations, the coefficients A_{21}, C_{21}, D_{21} and E_{21} can be written in terms of B_{21} as

$$E_{21} = - B_{21}$$

$$C_{21} = - \frac{B_{21}\lambda_1^2}{2}$$

$$A_{21} = - \frac{B_{21}[\cosh(\lambda_1 \ell_1)-1]}{\sinh(\lambda_1 \ell_1)} = - B_{21} \tanh(\frac{\lambda_1 \ell_1}{2}) \qquad \text{(II-a-21)}$$

$$D_{21} = \frac{B_{21}\lambda_1^2 \ell_1}{2} + \frac{1}{\ell_1}$$

Similarly, introducing $g_{22}(x_2)$ into the boundary conditions gives

$$B_{22} + E_{22} = 1$$

$$B_{22}\lambda_2^2 + 2C_{22} = 0$$

$$A_{22} \sinh(\lambda_2 \ell_2) + B_{22} \cosh(\lambda_2 \ell_2) + C_{22}\ell_2^2 + D_{22}\ell_2 + E_{22} = 0$$

$$A_{22}\lambda_2^2 \sinh(\lambda_2 \ell_2) + B_{22}\lambda_2^2 \cosh(\lambda_2 \ell_2) + 2C_{22} = 0 \qquad \text{(II-a-22)}$$

From the previous equations, the coefficients A_{22}, C_{22}, D_{22} and E_{22} can be written in terms of B_{22} as

$$E_{22} = 1 - B_{22}$$

$$C_{22} = - \frac{B_{22}\lambda_2^2}{2}$$

$$A_{22} = - \frac{B_{22}[\cosh(\lambda_2 \ell_2) - 1]}{\sinh(\lambda_2 \ell_2)} = - B_{22} \tanh(\frac{\lambda_2 \ell_2}{2}) \qquad \text{(II-a-23)}$$

$$D_{22} = \frac{B_{22}\lambda_2^2 \ell_2}{2} - \frac{1}{\ell_2}$$

Introducing $g_{23}(x_3)$ into the boundary conditions gives

$$B_{23} + E_{23} = 0$$

$$B_{23}\lambda_3^2 + 2C_{23} = 0$$

$$A_{23} \sinh(\lambda_3 \ell_3) + B_{23} \cosh(\lambda_3 \ell_3) + C_{23}\ell_3^2 + D_{23}\ell_3 + E_{23} = 0$$

$$A_{23}\lambda_3^2 \sinh(\lambda_3 \ell_3) + B_{23}\lambda_3^2 \cosh(\lambda_3 \ell_3) + 2C_{23} = 0 \qquad \text{(II-a-24)}$$

which results in

$$E_{23} = - B_{23}$$

$$C_{23} = - \frac{B_{23}\lambda_3^2}{2}$$

$$A_{23} = - \frac{B_{23}[\cosh(\lambda_3 \ell_3) - 1]}{\sinh(\lambda_3 \ell_3)} = - B_{23} \tanh\left(\frac{\lambda_3 \ell_3}{2}\right)$$

$$D_{23} = \frac{B_{23}\lambda_3^2 \ell_3}{2} \qquad \text{(II-a-25)}$$

From Eqs. II-a-19 the following relationship is apparent:

$$\frac{C_{21}}{w_i^*} = \frac{C_{22}}{w_2^*} = \frac{C_{23}}{w_3^*} \qquad \text{(II-a-26)}$$

Using Eqs. II-a-21, 23, 25, the previous equation can be written

$$\frac{B_{21}\lambda_1^2}{w_1^*} = \frac{B_{22}\lambda_2^2}{w_2^*} = \frac{B_{23}\lambda_3^2}{w_3^*} \qquad \text{(II-a-27)}$$

Therefore,

$$B_{22} = B_{21}\left(\frac{\overset{*}{w}_2}{\overset{*}{w}_1}\right)\left(\frac{\lambda_1}{\lambda_2}\right)^2$$

$$B_{23} = B_{21}\left(\frac{\overset{*}{w}_3}{\overset{*}{w}_1}\right)\left(\frac{\lambda_1}{\lambda_3}\right)^2 \qquad \text{(II-a-28)}$$

Substituting Eqs. II-a-21, 23, 25, 28 into Eqs. II-a-19, and solving for B_{21}

$$B_{21} = \frac{-\left(\frac{\overset{*}{w}_1}{H_w}\right)\left(\frac{E_c A_c}{L_E}\right)\left(\frac{\overset{*}{w}_1 \ell_1}{2H_w} + \frac{\overset{*}{w}_2 \ell_2}{2H_w}\right)}{\frac{E_c A_c}{L_E}\left[\sum_{i=1}^{3}\left(\frac{\overset{*}{w}_i}{H_w}\right)^2\left(\frac{\lambda_1}{\lambda_i}\right)^2\left(\frac{2}{\lambda_i}\tanh\frac{\lambda_i \ell_i}{2} + \frac{\lambda_i^2 \ell_i^3}{12} - \ell_i\right)\right] + \lambda_1^2 H_w} \qquad \text{(II-a-29)}$$

Once B_{21} is known, the quasi-static function $g_{2i}(x_i)$ is completely determined since the coefficients A_{2i}, B_{2i}, C_{2i}, D_{2i}, and E_{2i} appearing in Eq. II-a-18 can all be defined in terms of the coefficient B_{21} using Eqs. II-a-21, 23, 25, 28.

C. Unit Displacement at Right Tower-Pier

The solution for the quasi-static function corresponding to unit displacement at support C of figure II-1 is obtained by satisfying the following three equations

$$E_i I_i \frac{d^4 g_{3i}(x_i)}{dx_i^4} - H_w \frac{d^2 g_{3i}(x_i)}{dx_i^2} + \frac{\overset{*}{w}_i}{H_w} \left(\frac{E_c A_c}{L_E}\right) \left[\sum_{n=1}^{3} \frac{\overset{*}{w}_n}{H_w} \int_0^{\ell_n} g_{3n}(x_n)\, dx_n\right] = 0$$

$$i = 1,2,3 \qquad \text{(II-a-30)}$$

subject to the boundary conditions

$$g_{31}(0) = 0 \qquad g_{32}(0) = 0 \qquad g_{33}(0) = 1$$

$$g_{31}(\ell_1) = 0 \qquad g_{32}(\ell_2) = 0 \qquad g_{33}(\ell_3) = 0$$

$$g_{31}''(0) = g_{32}''(0) = g_{33}''(0) = 0 \qquad \text{(II-a-31)}$$

$$g_{31}''(\ell_1) = g_{32}''(\ell_2) = g_{33}''(\ell_3) = 0$$

The form of the solution can be taken as

$$g_{3i}(x_i) = A_{3i} \sinh(\lambda_i x_i) + B_{3i} \cosh(\lambda_i x_i) + C_{3i} x_i^2 + D_{3i} x_i + E_{3i}$$

$$i = 1,2,3 \qquad \text{(II-a-32)}$$

where λ_i is defined by Eq. II-a-4. Substituting Eqs. II-a-32 into Eqs. II-a-30 results in the following three equations

$$2H_w C_{3i} = \frac{w_i^*}{H_w} \left(\frac{E_c A_c}{L_E}\right) \left\{ \sum_{n=1}^{3} \frac{w_n^*}{H_w} \left[\frac{A_{3n}}{\lambda_n} \left[\cosh (\lambda_n \ell_n) - 1 \right] \right.\right.$$

$$\left.\left. + \frac{B_{3n}}{\lambda_n} \sinh (\lambda_n \ell_n) + \frac{C_{3n} \ell_n^3}{3} + \frac{D_{3n} \ell_n}{2} + E_{3n} \ell_n \right] \right\}$$

$$i = 1,2,3 \qquad \text{(II-a-33)}$$

Introducing $g_{31}(x_1)$ from Eq. II-a-32 into the boundary conditions results in the equations

$$B_{31} + E_{31} = 0$$

$$B_{31} \lambda_1^2 + 2C_{31} = 0$$

$$A_{31} \sinh (\lambda_1 \ell_1) + B_{31} \cosh (\lambda_1 \ell_1) + C_{31} \ell_1^2 + D_{31} \ell_1 + E_{31} = 0$$

$$A_{31} \lambda_1^2 \sinh (\lambda_1 \ell_1) + B_{31} \lambda_1^2 \cosh (\lambda_1 \ell_1) + 2C_{31} = 0 \qquad \text{(II-a-34)}$$

From the previous equations, the coefficients A_{31}, C_{31}, D_{31}, and E_{31} can be written in terms of B_{31} as

$$E_{31} = -B_{31}$$

$$C_{31} = -\frac{B_{31} \lambda_1^2}{2}$$

$$A_{31} = -\frac{B_{31} \left[\cosh (\lambda_1 \ell_1) - 1 \right]}{\sinh (\lambda_1 \ell_1)} = -B_{31} \tanh \left(\frac{\lambda_1 \ell_1}{2}\right) \qquad \text{(II-a-35)}$$

$$D_{31} = \frac{B_{31} \lambda_1^2 \ell_1}{2}$$

Similarly, introducing $g_{32}(x_2)$ into the boundary conditions gives:

$$B_{32} + E_{32} = 0$$

$$B_{32}\lambda_2^2 + 2C_{32} = 0$$

$$A_{32} \sinh(\lambda_2\ell_2) + B_{32} \cosh(\lambda_2\ell_2) + C_{32}\ell_2^2 + D_{32}\ell_2 + E_{32} = 1$$

$$A_{32}\lambda_2^2 \sinh(\lambda_2\ell_2) + B_{32}\lambda_2^2 \cosh(\lambda_2\ell_2) + 2C_{32} = 0 \qquad \text{(II-a-36)}$$

Again, the coefficients A_{32}, C_{32}, D_{32}, and E_{32} can be written in terms of B_{32} as

$$E_{32} = - B_{32}$$

$$C_{32} = - \frac{B_{32}\lambda_2^2}{2}$$

$$A_{32} = - \frac{B_{32}\,[\cosh(\lambda_2\ell_2) - 1]}{\sinh(\lambda_2\ell_2)} = - B_{32} \tanh\left(\frac{\lambda_2\ell_2}{2}\right) \qquad \text{(II-a-37)}$$

$$D_{32} = \frac{B_{32}\lambda_2^2\ell_2}{2} + \frac{1}{\ell_2}$$

Introducing $g_{33}(x_3)$ into the boundary conditions gives:

$$B_{33} + E_{33} = 1$$

$$B_{33}\lambda_3^2 + 2C_{33} = 0$$

$$A_{33}\sinh(\lambda_3\ell_3) + B_{33} \cosh(\lambda_3\ell_3) + C_{33}\ell_3^2 + D_{33}\ell_3 + E_{33} = 0$$

$$A_{33}\lambda_3^2 \sinh(\lambda_3\ell_3) + B_{33}\lambda_3^2 \cosh(\lambda_3\ell_3) + 2C_{33} = 0 \qquad \text{(II-a-38)}$$

which results in

$$E_{33} = 1 - B_{33}$$

$$C_{33} = -\frac{B_{33}\lambda_3^2}{2}$$

$$A_{33} = -\frac{B_{33}\,[\cosh(\lambda_3\ell_3) - 1]}{\sinh(\lambda_3\ell_3)} = -B_{33}\tanh\left(\frac{\lambda_3\ell_3}{2}\right) \qquad \text{(II-a-39)}$$

$$C_{33} = \frac{B_{33}\lambda_3^2\ell_3}{2} - \frac{1}{\ell_3}$$

From Eqs. II-a-33 the following relationship is apparent

$$\frac{C_{31}}{\overset{*}{w}_1} = \frac{C_{32}}{\overset{*}{w}_2} = \frac{C_{33}}{\overset{*}{w}_3} \qquad \text{(II-a-40)}$$

Using Eqs. II-a-35, 37, 39, the previous equation can be written

$$\frac{B_{31}\lambda_1^2}{\overset{*}{w}_1} = \frac{B_{32}\lambda_2^2}{\overset{*}{w}_2} = \frac{B_{33}\lambda_3^2}{\overset{*}{w}_3} \qquad \text{(II-a-41)}$$

Therefore,

$$B_{32} = B_{31}\left(\frac{\overset{*}{w}_2}{\overset{*}{w}_1}\right)\left(\frac{\lambda_1}{\lambda_2}\right)^2$$

$$B_{33} = B_{31}\left(\frac{\overset{*}{w}_3}{\overset{*}{w}_1}\right)\left(\frac{\lambda_1}{\lambda_3}\right)^2 \qquad \text{(II-a-42)}$$

Substituting Eqs. II-a-35, 37, 39, 42 into Eq. II-a-33 and solving for B_{31}

$$B_{31} = \frac{-\left(\frac{\overset{*}{w}_1}{H_w}\right)\left(\frac{E_c A_c}{L_E}\right)\left(\frac{\overset{*}{w}_2\ell_2}{2H_w} + \frac{\overset{*}{w}_3\ell_3}{2H_w}\right)}{\frac{E_c A_c}{L_E}\left[\sum_{i=1}^{3}\left(\frac{\overset{*}{w}_i}{H_w}\right)\left(\frac{\lambda_1}{\lambda_i}\right)^2\left(\frac{2}{\lambda_i}\tanh\frac{\lambda_i\ell_i}{2} + \frac{\lambda_i^2\ell_i^3}{12} - \ell_i\right)\right] + \lambda_1^2 H_w} \qquad \text{(II-a-43)}$$

Once B_{31} is known, the quasi-static function $g_{3i}(x_i)$ is completely determined since the coefficients A_{3i}, B_{3i}, C_{3i}, D_{3i}, and E_{3i} appearing in Eq. II-a-32 can all be defined in terms of the coefficient B_{31} using Eqs. II-a-35, 37, 39, 42.

D. Unit Displacement at Right Anchorage

The solution for the quasi-static function corresponding to unit displacement at support D of figure II-1 is obtained by satisfying the following three equations

$$E_i I_i \frac{d^4 g_{4i}(x_i)}{dx_i^4} - H_w \frac{d^2 g_{4i}(x_i)}{dx_i^2} + \frac{\overset{*}{w}_i}{H_w} \left(\frac{E_c A_c}{L_E}\right) \left[\sum_{n=1}^{3} \frac{\overset{*}{w}_n}{H_w} \int_0^{\ell_n} g_{4n}(x_n)\, dx_n \right] = 0$$

$$i = 1,2,3 \qquad \text{(II-a-44)}$$

subject to the boundary conditions

$$g_{41}(0) = 0 \qquad g_{42}(0) = 0 \qquad g_{43}(0) = 0$$

$$g_{41}(\ell_1) = 0 \qquad g_{42}(\ell_2) = 0 \qquad g_{43}(\ell_3) = 1$$

$$g_{41}''(0) = g_{42}''(0) = g_{43}''(0) = 0 \qquad \text{(II-a-45)}$$

$$g_{41}''(\ell_1) = g_{42}''(\ell_2) = g_{43}''(\ell_3) = 0$$

The form of the solution can be taken as

$$g_{4i}(x_i) = A_{4i} \sinh(\lambda_i x_i) + B_{4i} \cosh(\lambda_i x_i) + C_{4i} x_i^2 + D_{4i} x_i + E_{4i} \qquad i=1,2,3 \qquad \text{(II-a-46)}$$

where λ_i is defined by Eq. II-a-4. Substituting Eqs. II-a-46 into Eqs. II-a-44 results in the following three equations

$$2H_w C_{4i} = \frac{\overset{*}{w}_i}{H_w} \left(\frac{E_c A_c}{L_E}\right) \left\{ \sum_{n=1}^{3} \frac{\overset{*}{w}_n}{H_w} \left[\frac{A_{4n}}{\lambda_n} [\cosh(\lambda_n \ell_n) - 1] + \frac{B_{4n}}{\lambda_n} \sinh(\lambda_n \ell_n) + \frac{C_{4n} \ell_n^3}{3} + \frac{D_{4n} \ell_n^2}{2} + E_{4n} \ell_n \right] \right\}$$

$$i=1,2,3 \qquad \text{(II-a-47)}$$

Introducing $g_{41}(x_1)$ from Eq. II-a-46 into the boundary conditions results in the equations

$$B_{41} + E_{41} = 0$$

$$B_{41} \lambda_1^2 + 2C_{41} = 0$$

$$A_{41} \sinh(\lambda_1 \ell_1) + B_{41} \cosh(\lambda_1 \ell_1) + C_{41} \ell_1^2 + D_{41} \ell_1 + E_{41} = 0$$

$$A_{41} \lambda_1^2 \sinh(\lambda_1 \ell_1) + B_{41} \lambda_1^2 \cosh(\lambda_1 \ell_1) + 2C_{41} = 0 \qquad \text{(II-a-48)}$$

From the previous equations, the coefficients A_{41}, C_{41}, D_{41}, and E_{41} can be written in terms of B_{41} as

$$E_{41} = - B_{41}$$

$$C_{41} = - \frac{B_{41}\lambda_1^2}{2}$$

$$A_{41} = - \frac{B_{41}\,[\cosh\,(\lambda_1\ell_1) - 1]}{\sinh\,(\lambda_1\ell_1)} = - B_{41}\,\tanh\,(\frac{\lambda_1\ell_1}{2}) \qquad \text{(II-a-49)}$$

$$D_{41} = \frac{B_{41}\lambda_1^2\ell_1}{2}$$

Similarly, introducing $g_{42}(x_2)$ into the boundary conditions gives

$$B_{42} + E_{42} = 0$$

$$B_{42}\lambda_2^2 + 2C_{42} = 0$$

$$A_{42}\,\sinh\,(\lambda_2\ell_2) + B_{42}\,\cosh\,(\lambda_2\ell_2) + C_{42}\ell_2^2 + D_{42}\ell_2 + E_{42} = 0$$

$$A_{42}\lambda_2^2\,\sinh\,(\lambda_2\ell_2) + B_{42}\lambda_2^2\,\cosh\,(\lambda_2\ell_2) + 2C_{42} = 0 \qquad \text{(II-a-50)}$$

Again, the coefficients A_{42}, C_{42}, D_{42}, and E_{42} can be written in terms of B_{42} as

$$E_{42} = -B_{42}$$

$$C_{42} = - \frac{B_{42}\lambda_2^2}{2}$$

$$A_{42} = - \frac{B_{42}\,[\cosh\,(\lambda_2\ell_2) - 1]}{\sinh\,(\lambda_2\ell_2)} = - B_{42}\,\tanh\,(\frac{\lambda_2\ell_2}{2})$$

$$D_{42} = \frac{B_{42}\lambda_2^2\ell_2}{2} \qquad \text{(II-a-51)}$$

Introducing $g_{43}(x_3)$ into the boundary conditions gives

$$B_{43} + E_{43} = 0$$

$$B_{43}\lambda_3^2 + 2C_{43} = 0$$

$$A_{43} \sinh(\lambda_3\ell_3) + B_{43} \cosh(\lambda_3\ell_3) + C_{43}\ell_3^2 + D_{43}\ell_3 + E_{43} = 1$$

$$A_{43}\lambda_3^2 \sinh(\lambda_3\ell_3) + B_{43}\lambda_3^2 \cosh(\lambda_3\ell_3) + 2C_{43} = 0 \qquad \text{(II-a-52)}$$

which results in

$$E_{43} = -B_{43}$$

$$C_{43} = -\frac{B_{43}\lambda_3^2}{2}$$

$$A_{43} = -\frac{B_{43}\,[\cosh(\lambda_3\ell_3) - 1]}{\sinh(\lambda_3\ell_3)} = -B_{43} \tanh\left(\frac{\lambda_3\ell_3}{2}\right)$$

$$D_{43} = \frac{B_{43}\lambda_3^2\ell_3}{2} + \frac{1}{\ell_3} \qquad \text{(II-a-53)}$$

From Eqs. II-a-47 the following relationship is apparent

$$\frac{C_{41}}{{}^{*}w_1} = \frac{C_{42}}{{}^{*}w_2} = \frac{C_{43}}{{}^{*}w_3} \qquad \text{(II-a-54)}$$

Using Eqs. II-a-49, 51, 53 the previous equation can be written

$$\frac{B_{41}\lambda_1^2}{{}^{*}w_1} = \frac{B_{42}\lambda_2^2}{{}^{*}w_2} = \frac{B_{43}\lambda_3^2}{{}^{*}w_3} \qquad \text{(II-a-55)}$$

Therefore,

$$B_{42} = B_{41} \left(\frac{\overset{*}{w}_2}{\overset{*}{w}_1}\right) \left(\frac{\lambda_1}{\lambda_2}\right)^2$$

$$B_{43} = B_{41} \left(\frac{\overset{*}{w}_3}{\overset{*}{w}_1}\right) \left(\frac{\lambda_1}{\lambda_3}\right)^2 \qquad \text{(II-a-56)}$$

Substituting Eqs. II-a-49, 51, 53, 56 into Eq. II-a-47 and solving for B_{41}

$$B_{41} = \frac{-\left(\frac{\overset{*}{w}_1}{H_w}\right)\left(\frac{E_c A_c}{L_E}\right)\left(\frac{\overset{*}{w}_3 \ell_3}{2H_w}\right)}{\frac{E_c A_c}{L_E}\left[\sum_{i=1}^{3}\left(\frac{\overset{*}{w}_i}{H_w}\right)^2\left(\frac{\lambda_1}{\lambda_i}\right)^2\left(\frac{2}{\lambda_i}\tanh\frac{\lambda_i \ell_i}{2} + \frac{\lambda_i^2 \ell_i^3}{12} - \ell_i\right)\right] + \lambda_1^2 H_w} \qquad \text{(II-a-57)}$$

Once B_{41} is known, the quasi-static function $g_{4i}(x_i)$ is completely determined since the coefficients A_{4i}, B_{4i}, C_{4i}, D_{4i}, and E_{4i} appearing in Eq. II-a-46 can all be defined in terms of the coefficient B_{41} using Eqs. II-a-49, 51, 53, 56.

APPENDIX II-b

Solution for the Vertical Mode Shapes and Natural Frequencies

If it is assumed that the mass of the bridge as well as its elastic properties are uniform along the i^{th} span, the eigenvalue problem assumes the form

$$\frac{\overset{*}{w}_i}{g}\frac{\partial^2\eta_i}{\partial t^2} + E_iI_i\frac{\partial^4\eta_i}{\partial x_i^4} - H_w\frac{\partial^2\eta_i}{\partial x_i^2} + \frac{\overset{*}{w}_i}{H_w}\left[\frac{E_cA_c}{L_E}\sum_{m=1}^{3}\int_0^{\ell_m}\eta_m(x_m,t)\,dx_m\right] = 0$$

$$i = 1, 2, 3 \qquad \text{(II-b-1)}$$

where the bracketed term in Eq. II-b-1 represents the additional horizontal component of cable tension H(t). The n^{th} vertical mode shape and natural frequency is obtained by assuming the vibration to be sinusoidal, that is

$$\eta_i(x_i,t) = \phi_{ni}(x_i)e^{i\omega_n t}$$

$$i = 1, 2, 3 \qquad n = 1, 2, 3 \ldots \qquad \text{(II-b-2)}$$

in which $i = \sqrt{-1}$ and ω_n is the n^{th} natural circular frequency of vertical vibration. Substituting Eq. II-b-2 into Eqs. II-b-1 yields the equations of motion in the form

$$\frac{d^4\phi_{ni}}{dx_i^4} - \frac{H_w}{E_iI_i}\frac{d^2\phi_{ni}}{dx_i^2} - \frac{m_i\omega_n^2}{E_iI_i}\phi_{ni} + \frac{\overset{*}{w}_i}{E_iI_iH_w}\tilde{H}_n = 0$$

$$i = 1, 2, 3 \qquad n = 1, 2, 3 \ldots \qquad \text{(II-b-3)}$$

where

$$m_i = \frac{\overset{*}{w}_i}{g} \qquad i = 1, 2, 3 \qquad \text{(II-b-4)}$$

and the additional horizontal component of cable tension associated with the n^{th} vertical mode shape, $\tilde{H}_n$, is given by

$$\tilde{H}_n = \frac{E_c A_c}{L_E} \sum_{j=1}^{3} \frac{\overset{*}{w}_j}{H_w} \int_0^{\ell_j} \phi_{nj}(x_j)\,dx_j$$

$$n = 1, 2, 3... \qquad \text{(II-b-5)}$$

Because $\tilde{H}_n$ is independent of x_j and may be treated as a constant, Eqs.II-b-3 represent linear, ordinary differential equations of fourth order with constant coefficients. The general solutions of Eqs.II-b-3 are expressed as

$$\phi_{ni}(x_i) = A_i \sin\left(\frac{\mu_i x_i}{\ell_i}\right) + B_i \cos\left(\frac{\mu_i x_i}{\ell_i}\right) + C_i \sinh\left(\frac{\nu_i x_i}{\ell_i}\right) + D_i \cosh\left(\frac{\nu_i x_i}{\ell_i}\right) + \frac{\overset{*}{w}_i \tilde{H}_n}{m_i H_w \omega_n^2}$$

$$i = 1, 2, 3 \qquad n = 1, 2, 3 \ldots \qquad \text{(II-b-6)}$$

where

$$\left.\begin{aligned} \mu_i &= \sqrt{\tfrac{1}{2}\,\theta_i (Z_i - 1)} \\ \nu_i &= \sqrt{\tfrac{1}{2}\,\theta_i (Z_i + 1)} \\ Z_i &= \sqrt{1 + \left(\frac{4E_i I_i m_i}{H_w^2}\right)\omega_n^2} \\ \theta_i &= \frac{H_w \ell_i^2}{E_i I_i} \end{aligned}\right\} \qquad \begin{aligned} &i = 1, 2, 3 \\ &n = 1, 2, 3 \ldots \end{aligned} \qquad \text{(II-b-7)}$$

and A_i, B_i, C_i, and D_i are arbitrary constants and are determined in conformity with the boundary conditions at the supports of the i^{th} stiffening girder (or truss). The first four terms in Eq. II-b-6 represent the general solutions of the homogeneous equations ($\tilde{H}_n = 0$), while the last term of the same equation represents the particular solutions of the complete differential equations.

It is convenient to separate the investigation of the symmetric vertical modes from that of the antisymmetric vertical modes; that is, the problem can be divided into two parts:

1. The symmetric vertical modes of vibration in which there are an even number of internal nodes along the center span. Here $\tilde{H}_n$ is not zero.
2. The antisymmetric vertical modes of vibration which result in an odd number of internal nodes along the center span. Here $\tilde{H}_n$ is zero.

Symmetric Modes of Vertical Vibration

Assuming the stiffening structures to be simply supported at the towers and anchorages, the boundary conditions become

$$\left.\begin{aligned} &\text{for } x_i = 0 \qquad \phi_{ni} = 0, \qquad E_i I_i \frac{d^2\phi_{ni}}{dx_i^2} = 0 \\ &\text{for } x_i = \ell_i \qquad \phi_{ni} = 0, \qquad E_i I_i \frac{d^2\phi_{ni}}{dx_i^2} = 0 \end{aligned}\right\} \quad \begin{aligned} &n = 1, 2, 3 \ldots \\ &i = 1, 2, 3 \end{aligned} \qquad \text{(II-b-8)}$$

expressing the fact that the displacement and moment are zero at the supports of each span. Introducing Eq. II-b-6 into the above boundary conditions establishes the symmetric vertical modes as

$$\phi_{ni}(x_i) = \frac{\overset{*}{w}_i \tilde{H}_n}{2m_i H_w Z_i \omega_n^2} \left[2Z_i - \frac{Z_i + 1}{\cos(\mu_i/2)} \cos\left[\mu_i \left(\frac{1}{2} - \frac{x_i}{\ell_i}\right)\right] \right.$$

$$\left. - \frac{Z_i - 1}{\cosh(\nu_i/2)} \cosh\left[\nu_i \left(\frac{1}{2} - \frac{x_i}{\ell_i}\right)\right] \right]$$

$$i = 1, 2, 3 \qquad n = 1, 2, 3 \ldots \qquad \text{(II-b-9)}$$

Finally, substituting Eqs. II-b-9 into Eq. II-b-5 in order to obtain the frequency equation, the following transcendental equation upon the natural circular frequency, ω_n, is obtained:

$$\frac{L_E}{E_c A_c} = \sum_{i=1}^{3} \left| \left(\frac{\overset{*}{w}_i}{H_w}\right)^2 \frac{\ell_i}{m_i Z_i \omega_n^2} \left[Z_i - \left(\frac{Z_i + 1}{\mu_i}\right) \tan\left(\frac{\mu_i}{2}\right) \right.\right.$$

$$\left.\left. - \left(\frac{Z_i - 1}{\nu_i}\right) \tanh\left(\frac{\nu_i}{2}\right) \right] \right|$$

$$n = 1, 2, 3 \ldots \qquad \text{(II-b-10)}$$

Antisymmetric Modes of Vertical Vibration

An antisymmetric vibrational deflection of the cable and stiffening girder causes no additional cable tension $\tilde{H}_n$. Therefore, there is no interaction between the center span and side spans. For this reason, two types of independent vibration in a three-span bridge are possible. Setting $\tilde{H}_n = 0$ in Eq. II-b-6 yields:

$$\phi_{ni}(x_i) = A_i \sin\left(\frac{\mu_i x_i}{\ell_i}\right) + B_i \cos\left(\frac{\mu_i x_i}{\ell_i}\right) + C_i \sinh\frac{\nu_i x_i}{\ell_i} + D_i \cosh\left(\frac{\nu_i x_i}{\ell_i}\right)$$

$$n = 1, 2, 3 \ldots \qquad i = 1, 2, 3 \qquad \text{(II-b-11)}$$

The boundary conditions for the center span are:

$$\left.\begin{array}{lll} \text{for } x_2 = 0 & \phi_{n2} = 0 & E_2 I_2 \dfrac{d^2\phi_{n2}}{dx_2^2} = 0 \\ \text{for } x_2 = \dfrac{\ell_2}{2} & \phi_{n2} = 0 & E_2 I_2 \dfrac{d^2\phi_{n2}}{dx_2^2} = 0 \end{array}\right\} \quad n = 1, 2, 3 \ldots \qquad \text{(II-b-12)}$$

The second part of Eq. II-b-12 indicates that the center of the span remains at rest and is also an inflection point.

Substituting Eq. II-b-11 into the boundary conditions (II-b-12), the frequency equation is derived in the form:

$$\sin\frac{\mu_2}{2} = 0 \qquad \text{(II-b-13)}$$

from which may be seen

$$\mu_2 = 2\pi, 4\pi, 6\pi \ldots \qquad \text{(II-b-14)}$$

The antisymmetric vertical modes of vibration for the center span then become:

$$\phi_{m2}(x_2) = A_2 \sin\frac{m\pi x_2}{\ell_2} \qquad m = 2, 4, 6 \ldots \qquad \text{(II-b-15)}$$

Substituting this last expression into equation II-b-3 (with $\bar{H}_n = 0$), the natural circular frequencies for the center span are determined:

$$\omega_{2m} = \left(\frac{m\pi}{\ell_2}\right)^2 \sqrt{\frac{E_2 I_2}{m_2} + \frac{H_w \ell_2^2}{m_2 m^2 \pi^2}}$$

$$m = 2, 4, 6 \ldots \qquad \text{(II-b-16)}$$

The boundary conditions for the side spans are:

$$\left.\begin{array}{lll} \text{for } x_j = 0 & \phi_{nj} = 0 & E_j I_j \dfrac{d^2\phi_{nj}}{dx_j^2} = 0 \\ \text{for } x_j = \ell_j & \phi_{nj} = 0 & E_j I_j \dfrac{d^2\phi_{nj}}{dx_j^2} = 0 \end{array}\right\} \quad \begin{array}{l} n = 1, 2, 3 \ldots \\ j = 1, 3 \end{array}$$

(II-b-17)

Substituting Eq. II-b-11 into the above boundary conditions, the frequency equation is derived in the form:

$$\sin \mu_j = 0 \qquad j = 1, 3 \qquad \text{(II-b-18)}$$

from which may be seen

$$\mu_j = \pi, 2\pi, 3\pi \ldots \qquad j = 1, 3 \qquad \text{(II-b-19)}$$

The antisymmetric vertical modes of vibration for the side spans then become

$$\phi_{mj}(x_j) = A_j \sin\left(\frac{m\pi x_j}{\ell_j}\right)$$

$$m = 1, 2, 3 \ldots \qquad j = 1, 3 \qquad \text{(II-b-20)}$$

Substituting this last expression into Eq. II-b-3 (with $\tilde{H}_n = 0$), the natural circular frequencies for the side span vibration are determined:

$$\omega_{jm} = \left(\frac{m\pi}{\ell_j}\right)^2 \sqrt{\frac{E_j I_j}{m_j} + \frac{H_w \ell_j^2}{m_j m^2 \pi^2}}$$

$$m = 1, 2, 3 \ldots \qquad j = 1, 3 \qquad \text{(II-b-21)}$$

APPENDIX II-c

Orthogonality of Vertical Mode Shapes

The n^{th} vertical mode shape $\phi_{ni}(x_i)$ satisfies the equation

$$-\omega_n^2 \frac{\overset{*}{w}_i}{g} \phi_{ni}(x_i) + E_i I_i \phi_{ni}^{IV}(x_i) - H_w \phi_{ni}''(x_i)$$

$$+ \frac{\overset{*}{w}_i}{H_w} \left[\frac{E_c A_c}{L_E} \sum_{j=1}^{3} \frac{\overset{*}{w}_j}{H_w} \int_0^{\ell_j} \phi_{nj}(x_j)\, dx_j \right] = 0$$

$$n = 1,2,3,... \quad i = 1,2,3 \qquad \text{(II-c-1)}$$

where ω_n is the n^{th} natural circular frequency of vertical vibration.

The m^{th} vertical mode shape, $\phi_{mi}(x_i)$, satisfies a similar equation, that is:

$$-\omega_m^2 \frac{\overset{*}{w}_i}{g} \phi_{mi}(x_i) + E_i I_i \phi_{mi}^{IV}(x_i) - H_w \phi_{mi}''(x_i)$$

$$+ \frac{\overset{*}{w}_i}{H_w} \left[\frac{E_c A_c}{L_E} \sum_{j=1}^{3} \frac{\overset{*}{w}_j}{H_w} \int_0^{\ell_j} \phi_{mj}(x_j)\, dx_j \right] = 0$$

$$m = 1,2,3... \quad i = 1,2,3 \qquad \text{(II-c-2)}$$

Multiplying Eq. II-c-1 by $\phi_{mi}(x_i)$, integrating from zero to ℓ_i, and summing over all three spans (i=1,2,3), results in

$$-\omega_n^2\left[\sum_{i=1}^{3}\frac{\overset{*}{w}_i}{g}\int_0^{\ell_i}\phi_{ni}(x_i)\,\phi_{mi}(x_i)\,dx_i\right]+\left[\sum_{i=1}^{3}E_iI_i\int_0^{\ell_i}\phi_{ni}^{IV}(x_i)\,\phi_{mi}(x_i)\,dx_i\right]$$

$$-H_w\left[\sum_{i=1}^{3}\int_0^{\ell_i}\phi_{ni}''(x_i)\,\phi_{mi}(x_i)\,dx_i\right]$$

$$+\frac{E_cA_c}{L_E}\left[\sum_{i=1}^{3}\frac{\overset{*}{w}_i}{H_w}\int_0^{\ell_i}\phi_{mi}(x_i)\,dx_i\right]\left[\sum_{j=1}^{3}\frac{\overset{*}{w}_j}{H_w}\int_0^{\ell_j}\phi_{nj}(x_j)\,dx_j\right]=0$$

$$n = 1,2,3\ldots \qquad \text{(II-c-3)}$$

Multiplying Eq. II-c-2 by $\phi_{ni}(x_i)$, integrating from zero to ℓ_i, and summing over all three spans (i=1,2,3), results in

$$-\omega_m^2\left[\sum_{i=1}^{3}\frac{\overset{*}{w}_i}{g}\int_0^{\ell_i}\phi_{ni}(x_i)\,\phi_{mi}(x_i)\,dx_i\right]+\left[\sum_{i=1}^{3}E_iI_i\int_0^{\ell_i}\phi_{mi}^{IV}(x_i)\,\phi_{ni}(x_i)\,dx_i\right]$$

$$-H_w\left[\sum_{i=1}^{3}\int_0^{\ell_i}\phi_{mi}''(x_i)\,\phi_{ni}(x_i)\,dx_i\right]$$

$$+\frac{E_cA_c}{L_E}\left[\sum_{i=1}^{3}\frac{\overset{*}{w}_i}{H_w}\int_0^{\ell_i}\phi_{ni}(x_i)\,dx_i\right]\left[\sum_{j=1}^{3}\frac{\overset{*}{w}_j}{H_w}\int_0^{\ell_j}\phi_{mj}(x_j)\,dx_j\right]=0$$

$$m = 1,2,3\ldots \qquad \text{(II-c-4)}$$

Subtracting Eq. II-c-3 from Eq. II-c-4 yields

$$(\omega_n^2 - \omega_m^2) \sum_{i=1}^{3} \frac{\overset{*}{w}_i}{g} \int_0^{\ell_i} \phi_{ni}(x_i)\phi_{mi}(x_i)dx_i$$

$$+ \sum_{i=1}^{3} E_i I_i \int_0^{\ell_i} [\phi_{mi}^{IV}(x_i)\phi_{ni}(x_i) - \phi_{ni}^{IV}(x_i)\phi_{mi}(x_i)]dx_i$$

$$- H_w \sum_{i=1}^{3} \int_0^{\ell_i} [\phi_{mi}''(x_i)\phi_{ni}(x_i) - \phi_{ni}''(x_i)\phi_{mi}(x_i)]dx_i = 0$$

$$n = 1,2,3,... \quad m = 1,2,3,... \qquad \text{(II-c-5)}$$

Now the last two bracketed terms in Eq. II-c-5 can be shown to vanish by integrating by parts. For example

$$\int_0^{\ell_i} \phi_{mi}''(x_i)\phi_{ni}(x_i)dx_i = \phi_{ni}(x_i)\phi_{mi}'(x_i)\Big|_0^{\ell_i} - \int_0^{\ell_i} \phi_{mi}'(x_i)\phi_{ni}'(x_i)dx_i$$

$$= - \int_0^{\ell_i} \phi_{mi}'(x_i)\phi_{ni}'(x_i)dx_i$$

$$n=1,2,3,... \quad m=1,2,3,... \qquad \text{(II-c-6)}$$

since $\phi_{ni}(0) = \phi_{ni}(\ell_i) = 0$ from the boundary conditions.

Similarly,

$$\int_0^{\ell_i} \phi_{ni}'''(x_i)\phi_{mi}(x_i)dx_i = \phi_{mi}(x_i)\phi_{ni}''(x_i)\Big|_0^{\ell_i}$$

$$- \int_0^{\ell_i} \phi_{mi}'(x_i)\phi_{ni}''(x_i)dx_i$$

$$= - \int_0^{\ell_i} \phi_{mi}'(x_i)\phi_{ni}''(x_i)dx_i$$

$$n = 1,2,3,\ldots \quad m = 1,2,3,\ldots \qquad \text{(II-c-7)}$$

Also it can be seen that

$$\int_0^{\ell_i} \phi_{mi}^{IV}(x_i)\phi_{ni}(x_i)dx_i = \phi_{ni}(x_i)\phi_{mi}'''(x_i)\Big|_0^{\ell_i} - \int_0^{\ell_i} \phi_{mi}'''(x_i)\phi_{ni}'(x_i)dx_i$$

$$= - \phi_{ni}'(x_i)\phi_{mi}''(x_i)\Big|_0^{\ell_i} + \int_0^{\ell_i} \phi_{mi}''(x_i)\phi_{ni}''(x_i)dx_i$$

$$= \int_0^{\ell_i} \phi_{mi}''(x_i)\phi_{ni}''(x_i)dx_i \qquad \begin{matrix} n=1,2,3\ldots \\ m=1,2,3\ldots \end{matrix} \qquad \text{(II-c-8)}$$

since $\phi_{ni}(0) = \phi_{ni}(\ell_i) = 0$ and $\phi_{ni}''(0) = \phi_{ni}''(\ell_i) = 0$ from the boundary conditions.

Similarly,

$$\int_0^{\ell_i} \phi_{ni}^{IV}(x_i)\phi_{mi}(x_i)dx_i = \phi_{mi}(x_i)\phi_{ni}'''(x_i)\Big|_0^{\ell_i} - \int_0^{\ell_i} \phi_{ni}'''(x_i)\phi_{mi}'(x_i)dx_i$$

$$= -\phi_{mi}'(x_i)\phi_{ni}''(x_i)\Big|_0^{\ell_i} + \int_0^{\ell_i} \phi_{mi}''(x_i)\phi_{ni}''(x_i)dx_i$$

$$= \int_0^{\ell_i} \phi_{mi}''(x_i)\phi_{ni}''(x_i)dx_i$$

$$n = 1,2,3,\ldots \qquad m = 1,2,3\ldots \qquad \text{(II-c-9)}$$

Substituting Eqs. II-c-6, 7, 8, 9 into Eq. II-c-5 yields modal orthogonality of the form

$$(\omega_n^2 - \omega_m^2)\left[\sum_{i=1}^{3} \frac{w_i^*}{g}\int_0^{\ell_i} \phi_{ni}(x_i)\phi_{mi}(x_i)dx_i\right] = 0$$

$$n = 1,2,3,\ldots \qquad m = 1,2,3,\ldots \qquad \text{(II-c-10)}$$

That is

$$\sum_{i=1}^{3} \frac{w_i}{g}\int_0^{\ell_i} \phi_{ni}(x_i)\phi_{mi}(x_i)dx_i = 0$$

$$\text{for } n \neq m \qquad \text{(II-c-11)}$$

APPENDIX II-d

Cable Tension Response in Frequency Domain (Calculational Details)

The finite Fourier transform of the vibrational horizontal component of cable tension is given by

$$H(\omega) = \frac{E_c A_c}{L_E} \left\{ \sum_{i=1}^{3} \left[\frac{w_i^*}{H_w} \left[\int_0^{\ell_i} \sum_{n=1}^{\infty} \phi_{ni}(x_i)\, dx_i \right] Q_n(\omega) \right. \right.$$

$$+ \frac{w_i}{H_w} \sum_{j=1}^{4} \left[\int_0^{\ell_i} g_{ji}(x_i)\, dx_i \right] F_j(\omega)$$

$$\left. - \frac{w_i^* \ell_i}{2H_w} [f_{i+1}(\omega) + F_i(\omega)] \right]$$

$$\left. + [F_8(\omega) - F_5(\omega)] \right\} \qquad \text{(II-d-1)}$$

where $F_j(\omega)$ (j=1,2,3,4,5,8), is the finite Fourier transform of the j^{th} input ground displacement over the duration of the ground motion, T_1, and $Q_n(\omega)$ is the finite Fourier transform of the n^{th} generalized coordinate given by

$$F_j(\omega) = \int_0^{T_1} f_j(t) e^{-i\omega t}\, dt \qquad j=1,2,3,4,5,8. \qquad \text{(II-d-2)}$$

$$Q_n(\omega) = \{H_n(\omega)\}^T \{F(\omega)\} \qquad n=1,2,3... \qquad \text{(II-d-3)}$$

where $\{H_n(\omega)\}^T$ is the transposed complex frequency-response vector corresponding to the n^{th} vertical vibration mode, and $\{F(\omega)\}$ is the Fourier transform vector of the ground-displacement inputs.

The power spectrum of H(t) may be approximated as

$$G_H(\omega) \cong \frac{2}{T_1} \overset{*}{H}(\omega)\, H(\omega) \qquad \text{(II-d-4)}$$

where T_1 is the duration of the ground motion and the superposed asterisk denotes complex conjugate.

Substituting Eqs. II-d-1 and II-d-3 into the previous equation results in an expression involving sixteen different terms. These will be taken one at a time in order to isolate the effects of input correlation.

A) Pure relative response

In performing the multiplication of Eq. II-d-4, one of the terms encountered involves the first term of Eq. II-d-1 multiplied by its complex conjugate, that is

$$G_A(\omega) = \left(\frac{E_c A_c}{L_E}\right)^2 \frac{2}{T_1} \left(\sum_{i=1}^{3} \left(\frac{\overset{*}{w}_i}{H_w}\right) \left\{ \left[\int_0^{\ell_i} \sum_{n=1}^{\infty} \phi_{ni}(x_i)\, dx_i \right] \overset{*}{Q}_n(\omega) \right\} \right)$$

$$\cdot \left(\sum_{j=1}^{3} \left(\frac{\overset{*}{w}_j}{H_w}\right) \left\{ \left[\int_0^{\ell_j} \sum_{m=1}^{\infty} \phi_{mi}(x_i)\, dx_i \right] Q_m(\omega) \right\} \right) \qquad \text{(II-d-5)}$$

which can be written:

$$G_A(\omega) = \frac{2}{T_1}\left(\frac{E_c A_c}{L_E}\right)^2 \sum_{n=1}^{\infty}\sum_{m=1}^{\infty} \Gamma_n \Gamma_m \overset{*}{Q}_n(\omega)\, Q_m(\omega)$$

$$= \left(\frac{E_c A_c}{L_E}\right)^2 \sum_{n=1}^{\infty}\sum_{m=1}^{\infty} \Gamma_n \Gamma_m \{\overset{*}{H}_n(\omega)\}^T [G_{ff}(\omega)]\, \{H_m(\omega)\} \qquad \text{(II-d-6)}$$

where the modal factors Γ_n are given by

$$\Gamma_n = \sum_{i=1}^{3} \frac{\overset{*}{w}_i}{H_w} \int_0^{\ell_i} \phi_{ni}(x_i)\, dx_i \qquad n=1,2,3... \qquad \text{(II-d-7)}$$

and $[G_{ff}(\omega)]$ is the 6×6 spectral matrix whose terms are defined by

$$G_{ij}(\omega) = \frac{2}{T_1} \overset{*}{F}_i(\omega)\; F_j(\omega) \qquad i,j = 1,2,3,4,5,8 \qquad \text{(II-d-8)}$$

Now for the correlated case, the spectral matrix is full, while for the uncorrelated case, only the diagonal terms (i=j in Eq. II-d-8) are retained.

B. Pure Quasi-Static Response

This involves the second term in Eq. II-d-1 multipled by its complex conjugate, that is

$$G_B(\omega) = \frac{2}{T_1}\left(\frac{E_c A_c}{L_E}\right)^2 \sum_{j=1}^{4}\sum_{k=1}^{4} \gamma_j \gamma_k \overset{*}{F}_j(\omega)\, F_k(\omega)$$

$$= \left(\frac{E_c A_c}{L_E}\right)^2 \sum_{j=1}^{4}\sum_{k=1}^{4} \gamma_j \gamma_k [G_{jk}(\omega)] \qquad \text{(II-d-9)}$$

where $$\gamma_j = \sum_{i=1}^{3} \frac{w_i^*}{H_w} \int_0^{\ell_i} g_{ji}(x_i)\,dx_i \qquad j=1,2,3,4. \tag{II-d-10}$$

and $G_{jk}(\omega)$ is defined by Eq. II-d-8.

For the correlated case, all power and cross-spectral terms are included in Eq. II-d-9, while for the uncorrelated case, only the diagonal terms remain, that is Eq. II-d-9 reduces to

$$G_B(\omega) = \left(\frac{E_c A_c}{L_E}\right)^2 \sum_{j=1}^{4} \gamma_j^2 \; |G_j(\omega)|^2 \tag{II-d-11}$$

where $G_j(\omega)$ is the power-spectra of the j^{th} input support displacement (j=1,2,3,4) given by:

$$G_j(\omega) \approx \frac{2}{T_1} \; |F_j(\omega)|^2 \tag{II-d-12}$$

C. Response Due to Vertical Support Displacements

This involves the third term in Eq. II-d-1 multiplied by its complex conjugate, that is

$$G_C(\omega) = \frac{2}{T_1} \left(\frac{E_c A_c}{L_E}\right)^2 \sum_{i=1}^{3} \sum_{j=1}^{3} \beta_i \beta_j \{F_{i+1}^*(\omega) + F_i^*(\omega)\} \cdot \{F_{j+1}(\omega) + F_j(\omega)\}$$

$$= \left(\frac{E_c A_c}{L_E}\right)^2 \sum_{i=1}^{3} \sum_{j=1}^{3} \beta_i \beta_j \{G_{i+1,j+1}(\omega) + G_{i,j+1}(\omega) + G_{i+1,j}(\omega) + G_{i,j}(\omega)\} \tag{II-d-13}$$

which, for the uncorrelated case reduces to:

$$G_C(\omega) = \left(\frac{E_c A_c}{L_E}\right)^2 \{ \beta_1^2 [G_1(\omega) + G_2(\omega)] + 2\beta_1\beta_2 G_2(\omega) + \beta_2^2 [G_2(\omega) + G_3(\omega)] + 2\beta_2\beta_3 G_3(\omega) + \beta_3^2 [G_3(\omega) + G_4(\omega)] \} \quad \text{(II-d-14)}$$

D. Response Due to Longitudinal Support Displacements

This involves the fourth term in Eq. II-d-1 multiplied by its complex conjugate, that is

$$G_D(\omega) = \frac{2}{T_1} \left(\frac{E_c A_c}{L_E}\right)^2 [\overset{*}{F}_8(\omega) - \overset{*}{F}_5(\omega)][F_8(\omega) - F_5(\omega)]$$

$$= \left(\frac{E_c A_c}{L_E}\right)^2 [G_8(\omega) + G_5(\omega) - G_{58}(\omega) - \overset{*}{G}_{58}(\omega)] \quad \text{(II-d-15)}$$

which for the uncorrelated case reduces to:

$$G_D(\omega) = \left(\frac{E_c A_c}{L_E}\right)^2 [G_8(\omega) + G_5(\omega)] \quad \text{(II-d-16)}$$

E. Cross term: relative and quasi-static responses

This involves the complex conjugate of the first term in Eq. II-d-1 multiplied by the second term in this equation, that is

$$G_{AB}(\omega) = \frac{2}{T_1}\left(\frac{E_c A_c}{L_E}\right)^2 \sum_{n=1}^{\infty} \sum_{j=1}^{4} \Gamma_n \gamma_j \overset{*}{Q}_n(\omega) F_j(\omega) \qquad \text{(II-d-17)}$$

where Γ_n was defined in Eq. II-d-7, and γ_j was defined in Eq. II-d-10. Using Eq. II-d-3, the previous equation may be written:

$$G_{AB}(\omega) = \frac{2}{T_1}\left(\frac{E_c A_c}{L_E}\right)^2 \sum_{n=1}^{\infty} \sum_{j=1}^{4} \Gamma_n \gamma_j \{\overset{*}{H}_n(\omega)\}^T \{\overset{*}{F}(\omega)\} F_j(\omega) \qquad \text{(II-d-18)}$$

which, for the uncorrelated case reduces to

$$G_{AB}(\omega) = \left(\frac{E_c A_c}{L_E}\right)^2 \sum_{n=1}^{\infty} \sum_{j=1}^{4} \Gamma_n \gamma_j H_{nj}(\omega) [G_j(\omega)] \qquad \text{(II-d-19)}$$

where $H_{nj}(\omega)$ is the complex frequency-response function corresponding to the n^{th} vertical vibration mode and the j^{th} vertical input motion.

F. Cross-term: Relative response and response due to vertical support displacements

This involves the complex conjugate of the first term in Eq. II-d-1 multiplied by the third term in this equation, that is

$$G_{AC}(\omega) = -\frac{2}{T_1}\left(\frac{E_c A_c}{L_E}\right)^2 \sum_{n=1}^{\infty} \sum_{i=1}^{3} \Gamma_n \beta_i \overset{*}{Q}_n(\omega) (F_{i+1}(\omega) + F_i(\omega))$$

$$= -\frac{2}{T_1}\left(\frac{E_c A_c}{L_E}\right)^2 \sum_{n=1}^{\infty} \sum_{i=1}^{3} \Gamma_n \beta_i \{\overset{*}{H}_n(\omega)\}^T \{\overset{*}{F}(\omega)\} (F_{i+1}(\omega) + F_i(\omega)) \qquad \text{(II-d-20)}$$

which, for the uncorrelated case, reduces to

$$G_{AC}(\omega) = -\left(\frac{E_c A_c}{L_E}\right)^2 \sum_{n=1}^{\infty} \sum_{i=1}^{3} \Gamma_n \beta_i [\overset{*}{H}_{ni}(\omega) G_i(\omega) + \overset{*}{H}_{n,i+1}(\omega) G_{i+1}(\omega)] \qquad \text{(II-d-21)}$$

G. Cross-term: Relative Response and Response Due to Longitudinal Support Displacements

This involves the complex conjugate of the first term in Eq. II-d-1 multiplied by the fourth term in this equation, that is

$$G_{AD}(\omega) = \frac{2}{T_1}\left(\frac{E_c A_c}{L_E}\right)^2 \sum_{n=1}^{\infty} \Gamma_n \overset{*}{Q}_n(\omega)\ [F_8(\omega) - F_5(\omega)]$$

$$= \frac{2}{T_1}\left(\frac{E_c A_c}{L_E}\right)^2 \sum_{n=1}^{\infty} \Gamma_n \{\overset{*}{H}_n(\omega)\}^T \{\overset{*}{F}(\omega)\}\ [F_8(\omega) - F_5(\omega)] \qquad \text{(II-d-22)}$$

which, for the uncorrelated case, reduces to

$$G_{AD}(\omega) = \left(\frac{E_c A_c}{L_E}\right)^2 \sum_{n=1}^{\infty} \Gamma_n [\overset{*}{H}_{n8}(\omega) G_8(\omega) - \overset{*}{H}_{n5}(\omega) G_5(\omega)] \qquad \text{(II-d-23)}$$

H. Cross-term: Quasi-Static Response and Response Due to Vertical Support Displacements

This involves the complex conjugate of the second term in Eq. II-d-1 multiplied by the third term in this equation, that is

$$G_{BC}(\omega) = -\frac{2}{T_1}\left(\frac{E_c A_c}{L_E}\right)^2 \sum_{j=1}^{4} \sum_{i=1}^{3} \gamma_j \beta_i \overset{*}{F}_j(\omega)\ [F_{i+1}(\omega) + F_i(\omega)] \qquad \text{(II-d-24)}$$

which, for the uncorrelated case, reduces to

$$G_{BC}(\omega) = -\left(\frac{E_c A_c}{L_E}\right)^2 [\gamma_1 \beta_1 G_1(\omega) + \gamma_2(\beta_1 + \beta_2) G_2(\omega)$$

$$+ \gamma_3(\beta_2 + \beta_3) G_3(\omega) + \gamma_4 \beta_3 G_4(\omega)] \qquad \text{(II-d-25)}$$

I. Cross-term: Quasi-Static Response and Response Due to Longitudinal Support Displacements

This involves the complex conjugate of the second term in Eq. II-d-1 multiplied by the fourth term in this equation, that is

$$G_{BD}(\omega) = \frac{2}{T_1}\left(\frac{E_c A_c}{L_E}\right)^2 \sum_{j=1}^{4} \gamma_j \overset{*}{F}_j(\omega)\left[F_8(\omega) - F_5(\omega)\right] \qquad \text{(II-d-26)}$$

which reduces to zero for the uncorrelated case.

J. Cross-term: Response Due to Vertical Support Displacements and Response Due to Longitudinal Support Displacements

This involves the complex conjugate of the third term in Eq. II-d-1 multiplied by the fourth term in this equation, that is

$$G_{CD}(\omega) = \frac{2}{T_1}\left(\frac{E_c A_c}{L_E}\right)^2 \sum_{i=1}^{3} \beta_i\left[\overset{*}{F}_{i+1}(\omega) + \overset{*}{F}_i(\omega)\right]\left[F_8(\omega) - F_5(\omega)\right] \qquad \text{(II-d-27)}$$

which reduces to zero for the uncorrelated case.

Power Spectrum of $H(t)$

The power spectrum of H(t) is given by Eq. II-d-4, which can be written as

$$\begin{aligned} G_H(\omega) &= G_A(\omega) + G_B(\omega) + G_C(\omega) + G_D(\omega) \\ &+ \left[G_{AB}(\omega) + \overset{*}{G}_{AB}(\omega)\right] \\ &+ \left[G_{AC}(\omega) + \overset{*}{G}_{AC}(\omega)\right] \\ &+ \left[G_{AD}(\omega) + \overset{*}{G}_{AD}(\omega)\right] \\ &+ \left[G_{BC}(\omega) + \overset{*}{G}_{BC}(\omega)\right] \\ &+ \left[G_{BD}(\omega) + \overset{*}{G}_{BD}(\omega)\right] \\ &+ \left[G_{CD}(\omega) + \overset{*}{G}_{CD}(\omega)\right] \end{aligned} \qquad \text{(II-d-28)}$$

where the terms on the right hand side of Eq. II-d-28 have been previously defined, and the superposed asterisk denotes complex conjugate.

APPENDIX II-e

MULTIPLE SUPPORT SEISMIC INPUTS

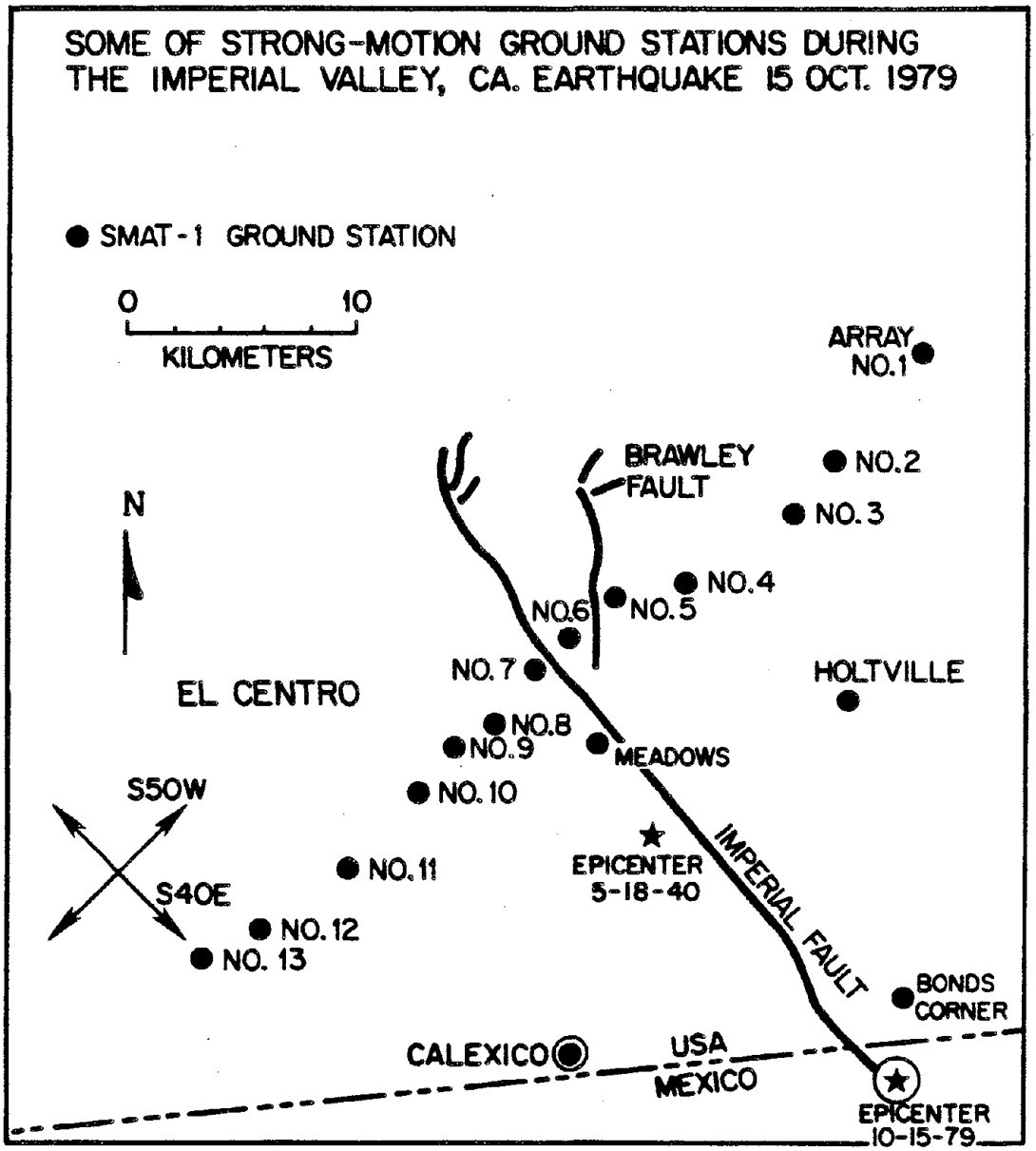

Fig. II-e-1 Strong motion recording stations of the El Centro Array.

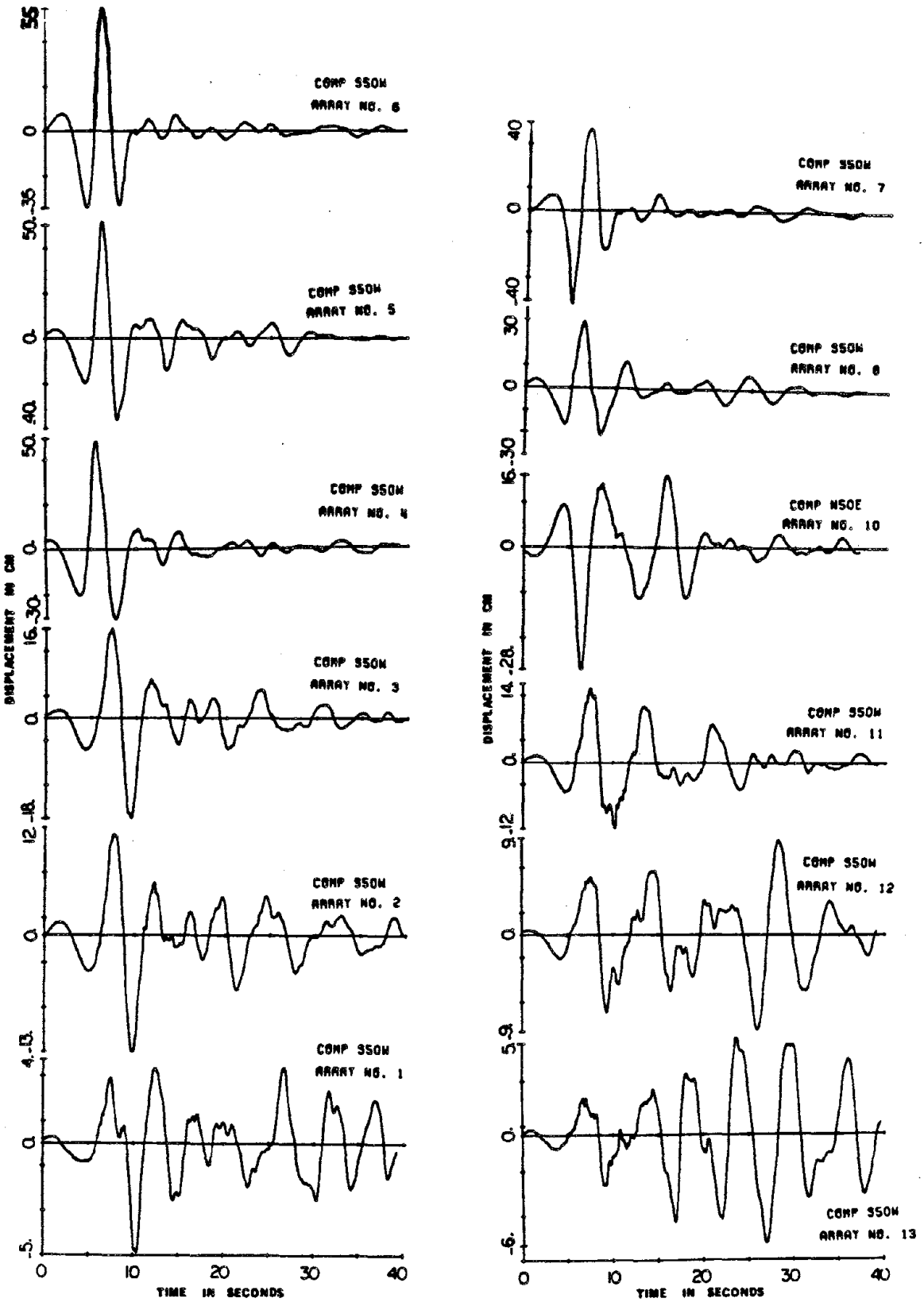

Fig. II-e-2 Displacement time histories of S50°W components of El Centro Array.

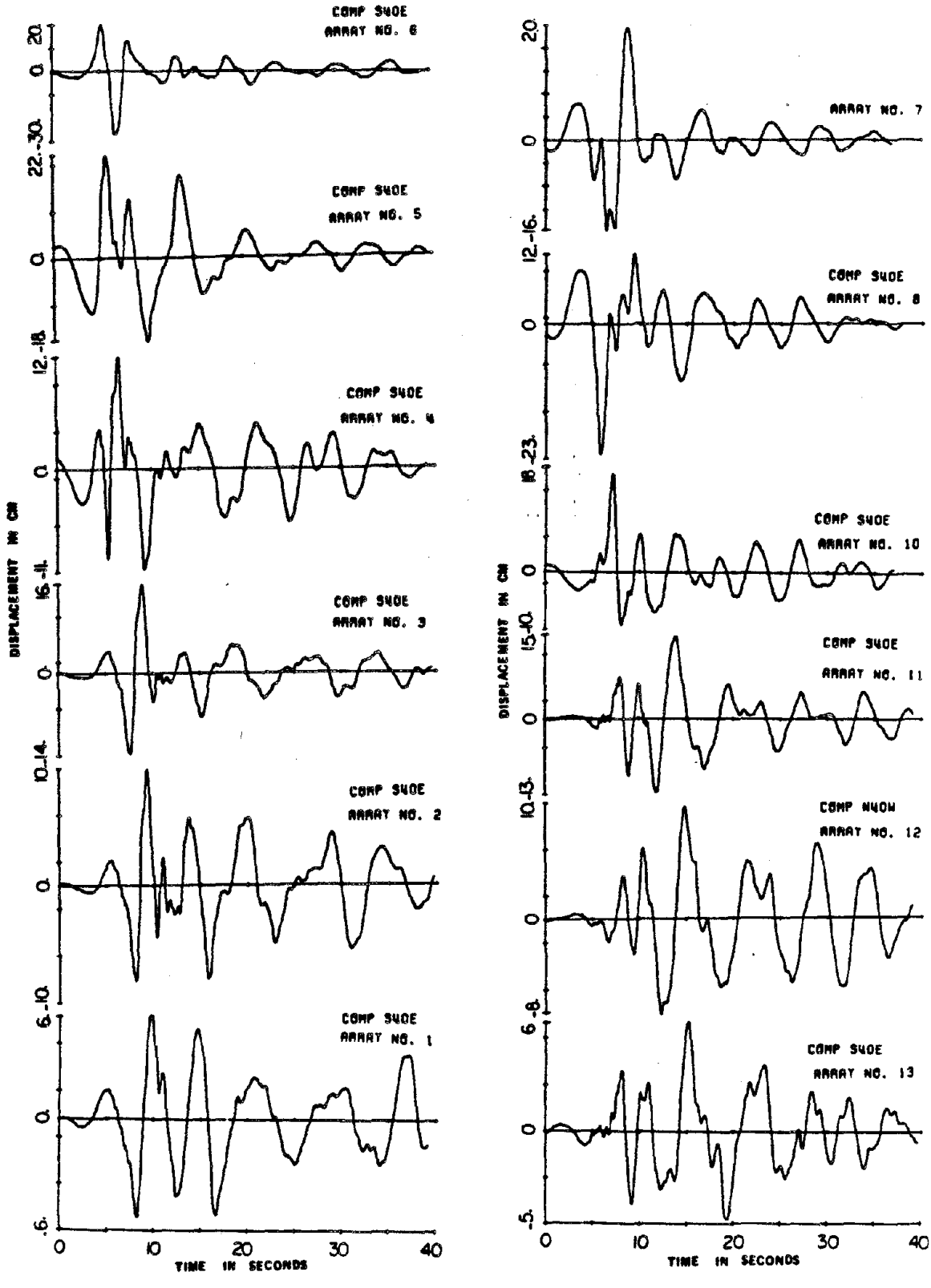

Fig. II-e-3 Displacement time histories of S40°E components of El Centro Array.

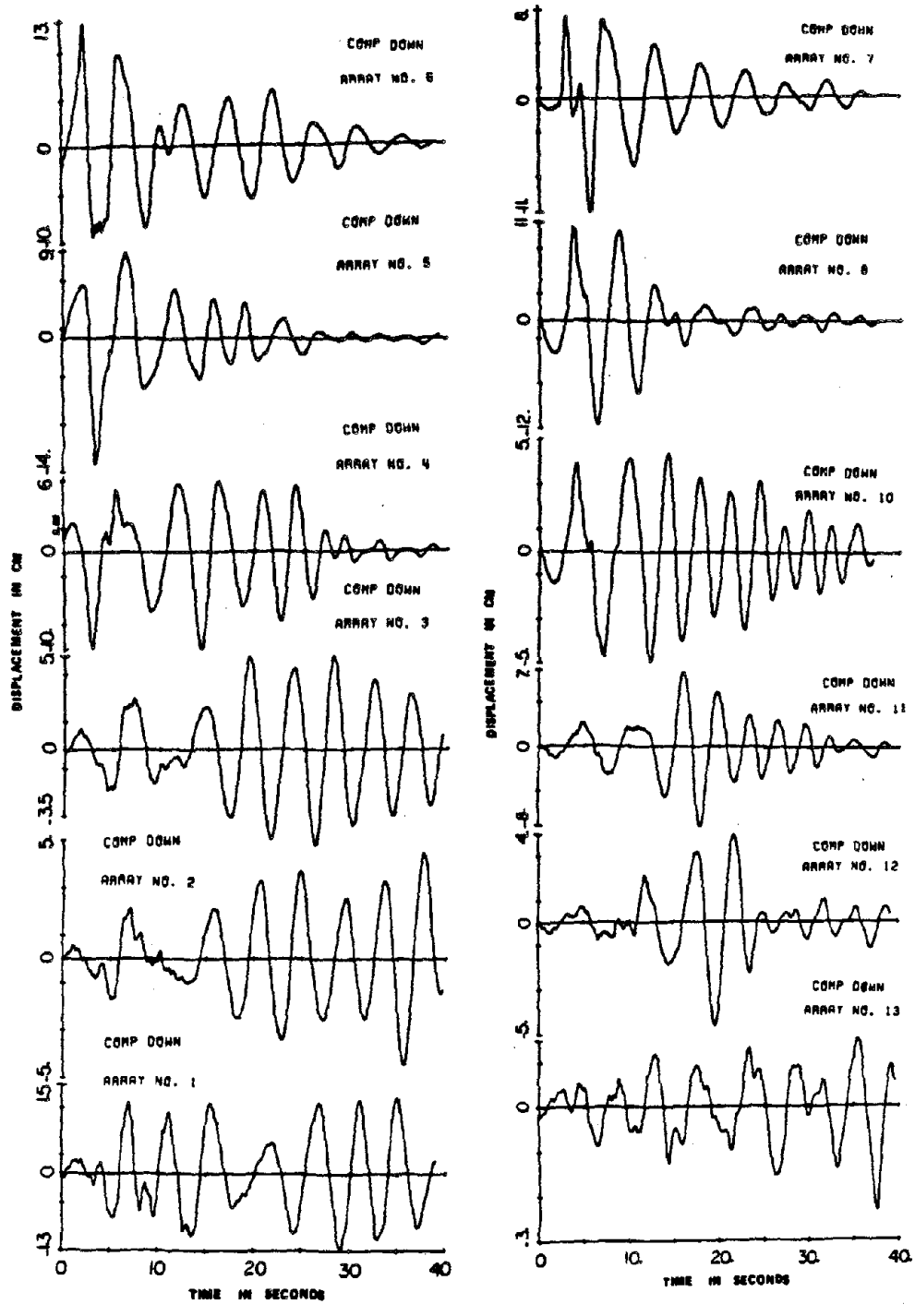

Fig. II-e-4 Displacement time histories of vertical components of El Centro Array.

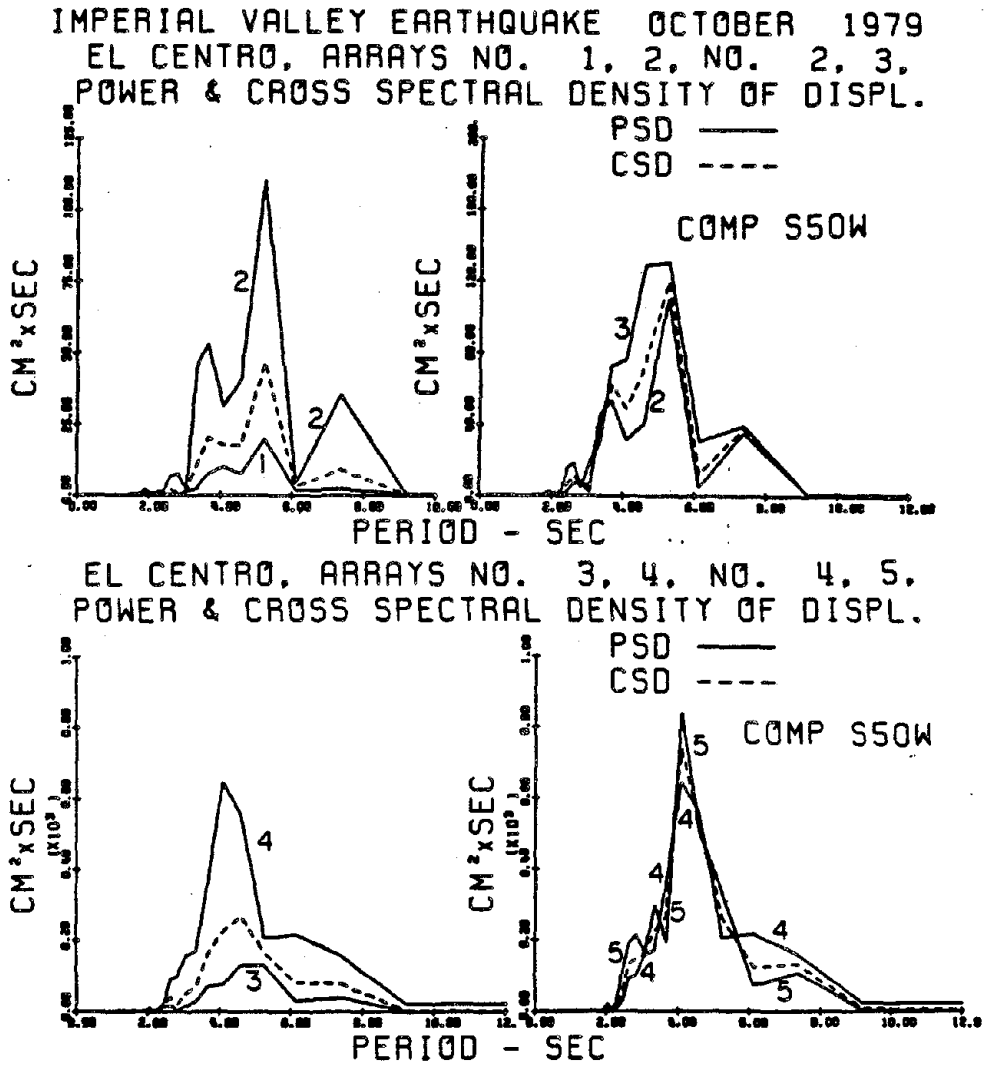

Fig. II-e-5a Power and cross-spectral densities of displacement of El Centro Array (component S50°W).

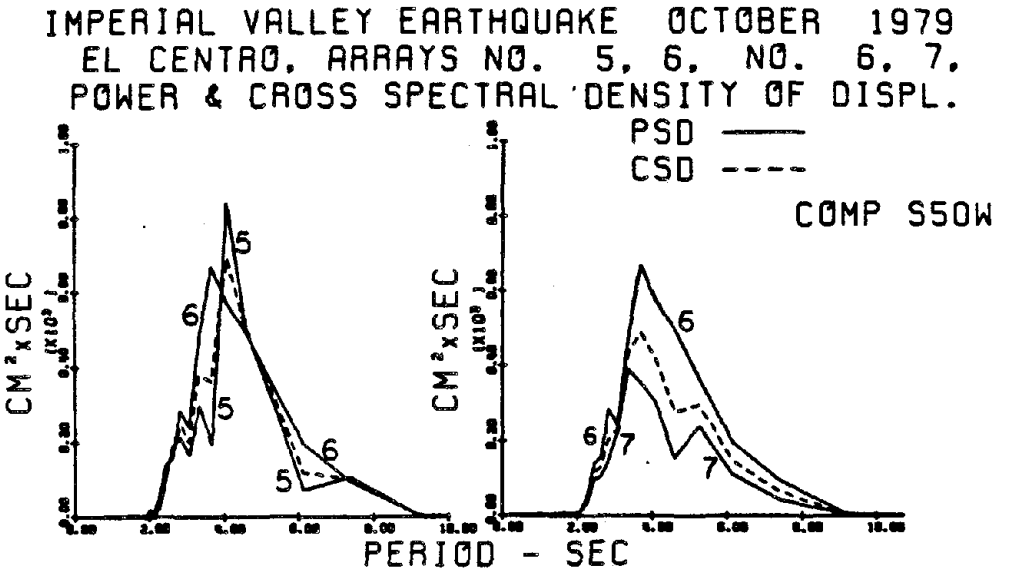

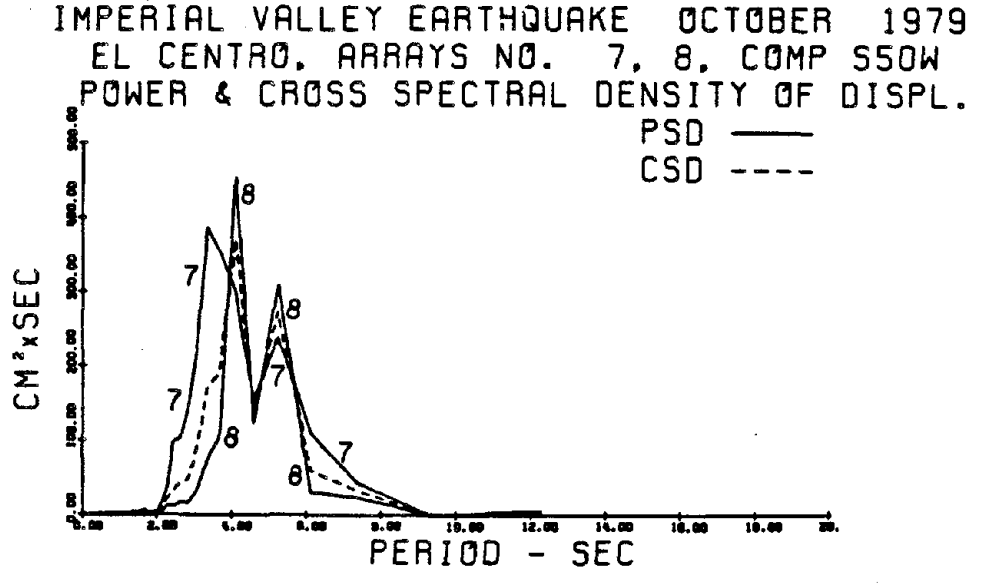

Fig. II-e-5b Power and cross-spectral densities of displacement of El Centro Array (Component S50°W).

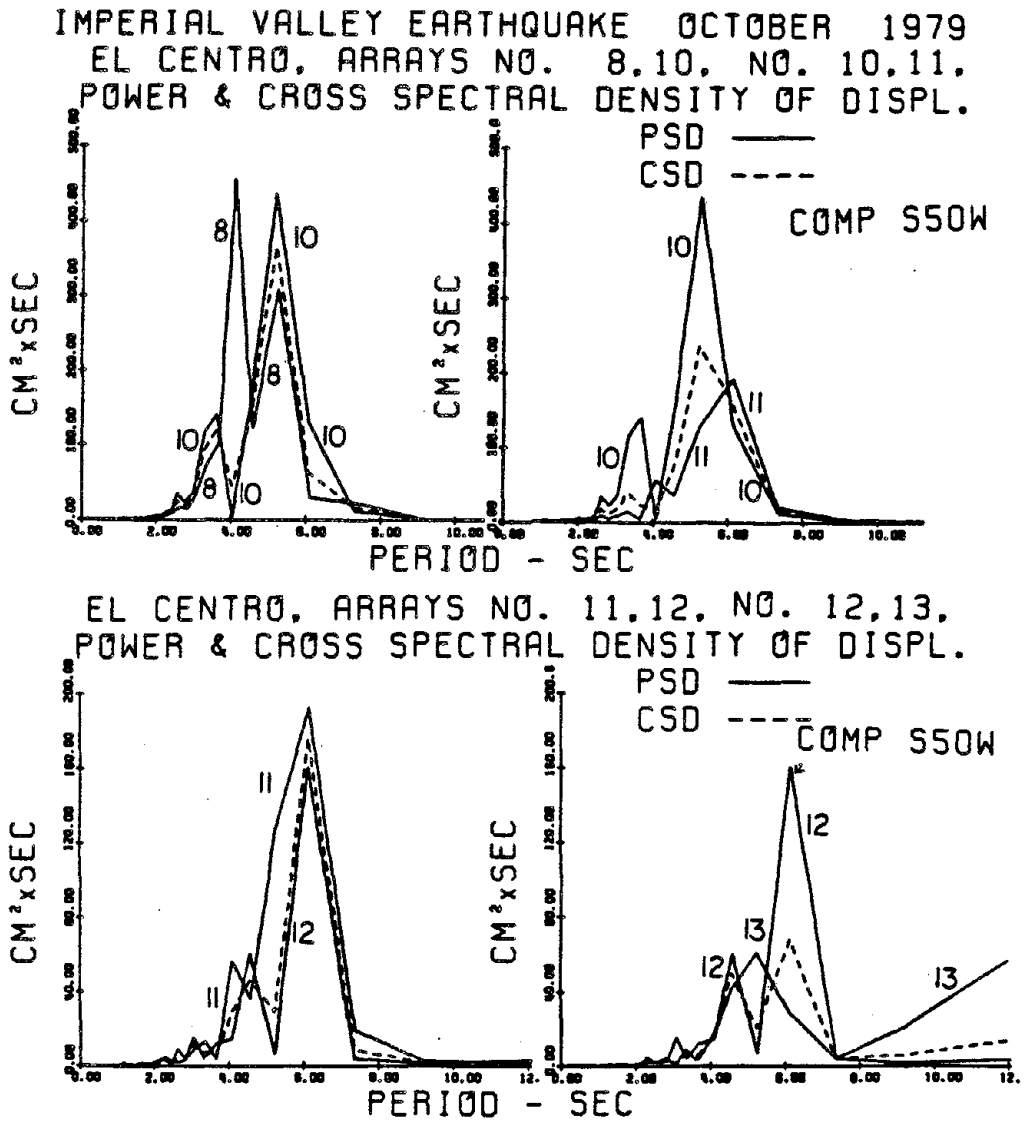

Fig. II-e-5c Power and cross-spectral densities of displacement of El Centro Array (Component S50°W).

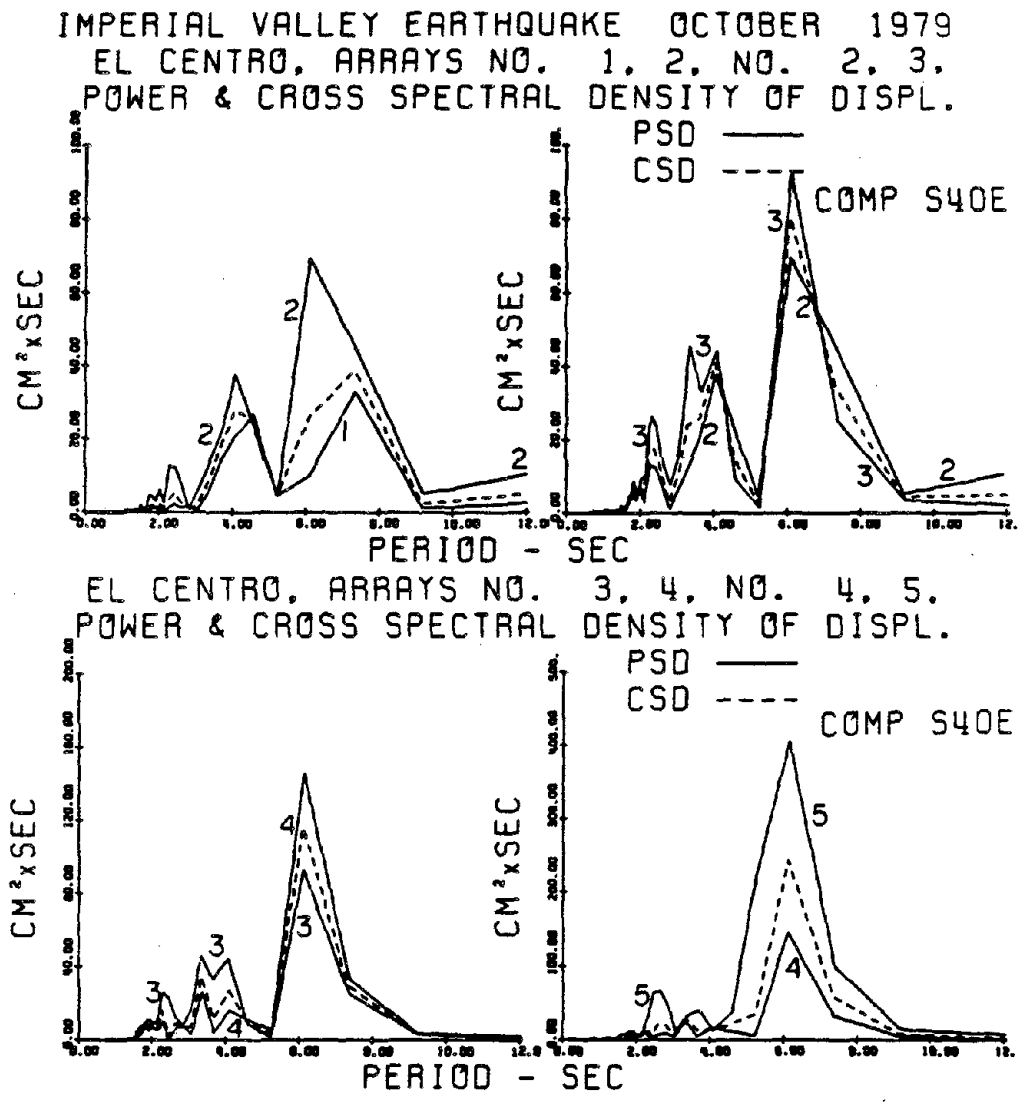

Fig. II-e-6a Power and cross-spectral densities of displacement of El Centro Array (Component S40°E).

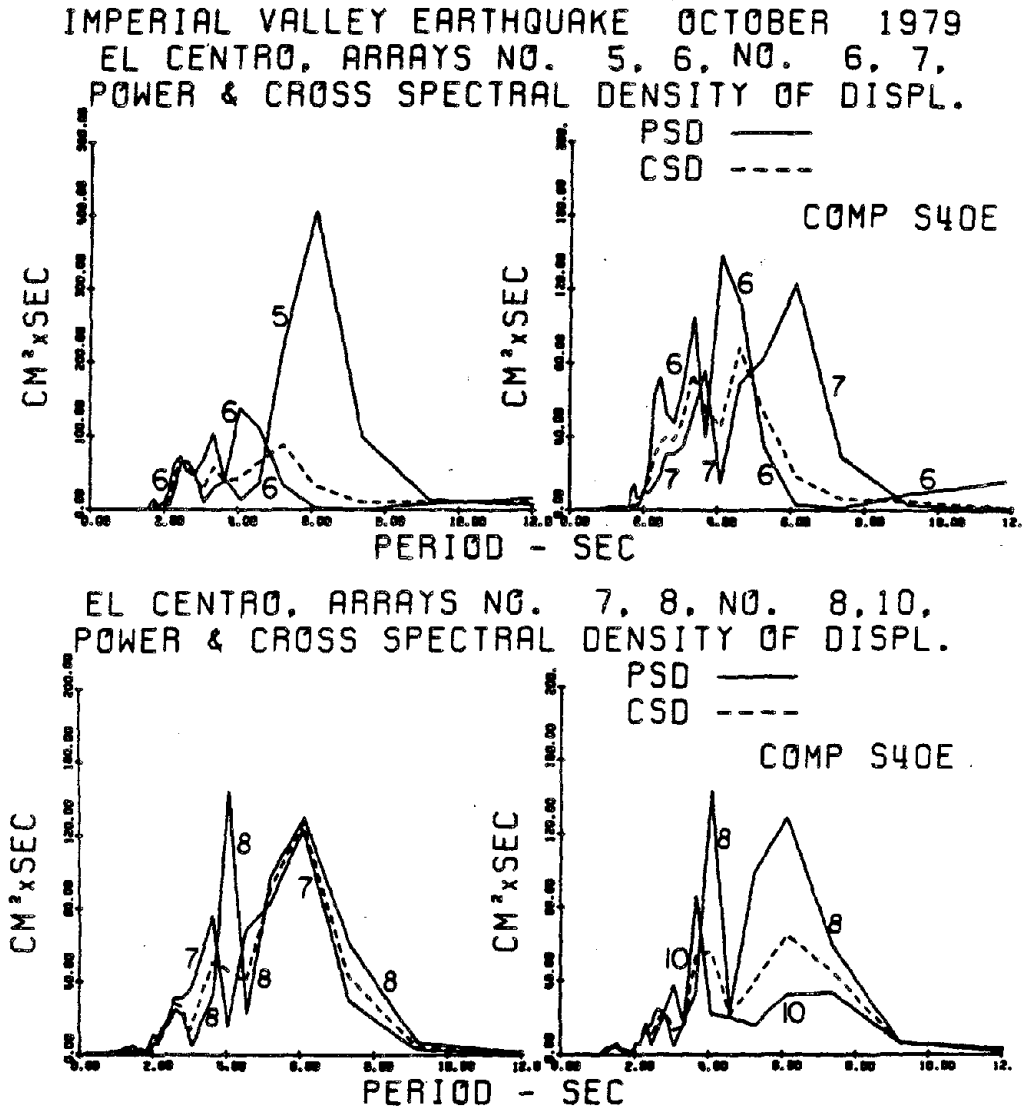

Fig. II-e-6b Power and cross-spectral densities of displacement of El Centro Array (Component S40°E).

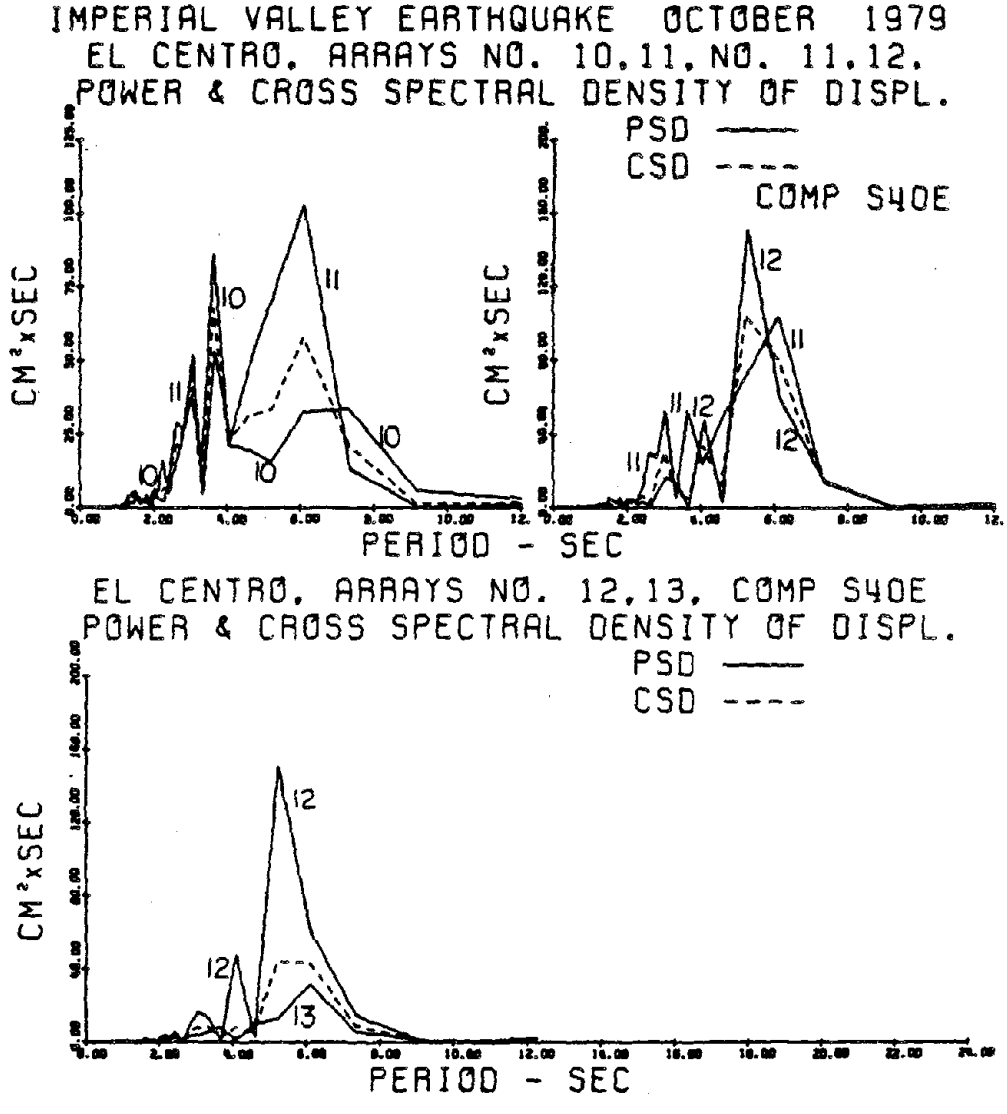

Fig. II-e-6c Power and cross-spectral densities of displacement of El Centro Array (Component S40°E).

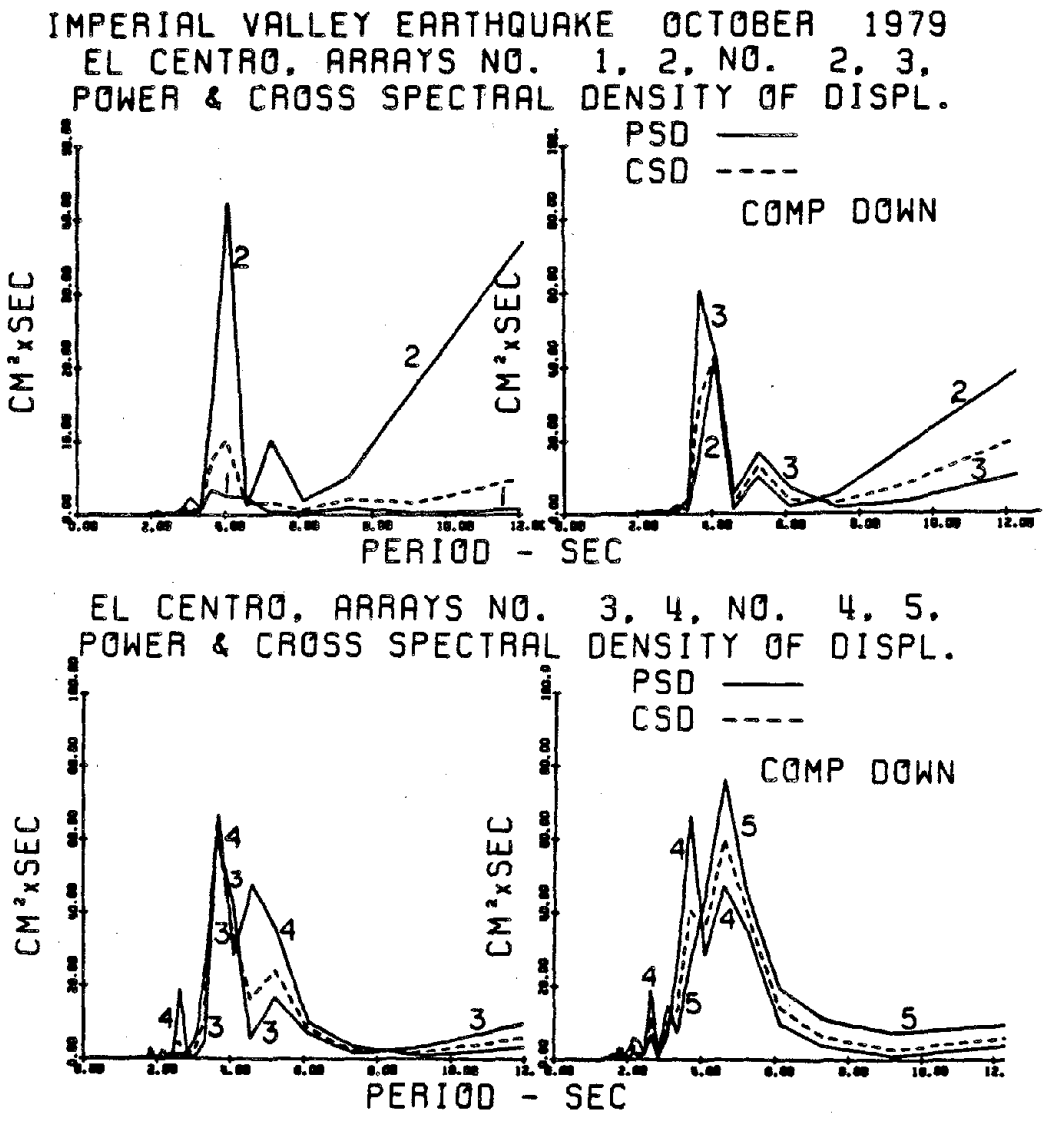

Fig. II-e-7a Power and cross-spectral densities of displacement of El Centro Array (vertical component).

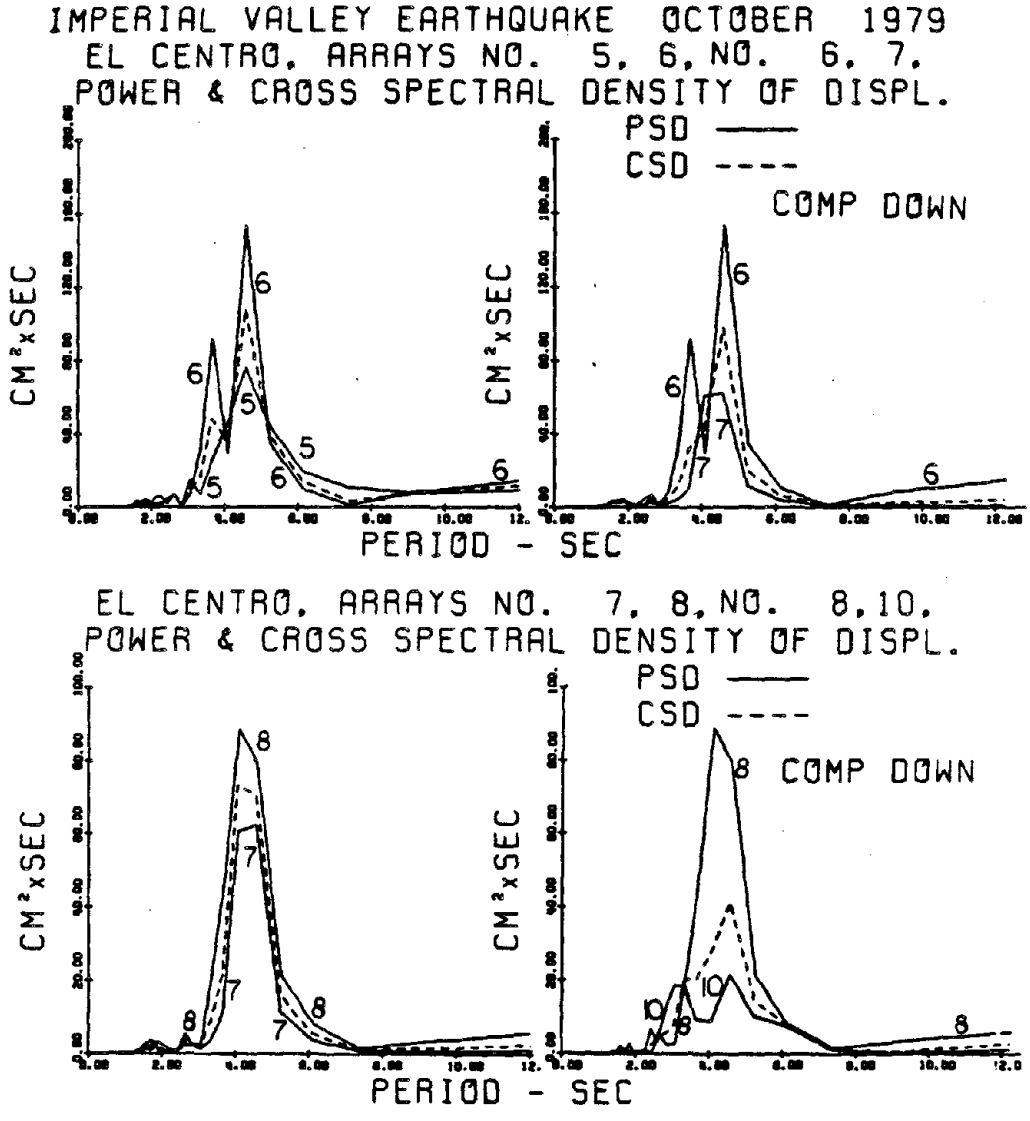

Fig. II-e-7b Power and cross-spectral densities of displacement of El Centro Array (vertical component).

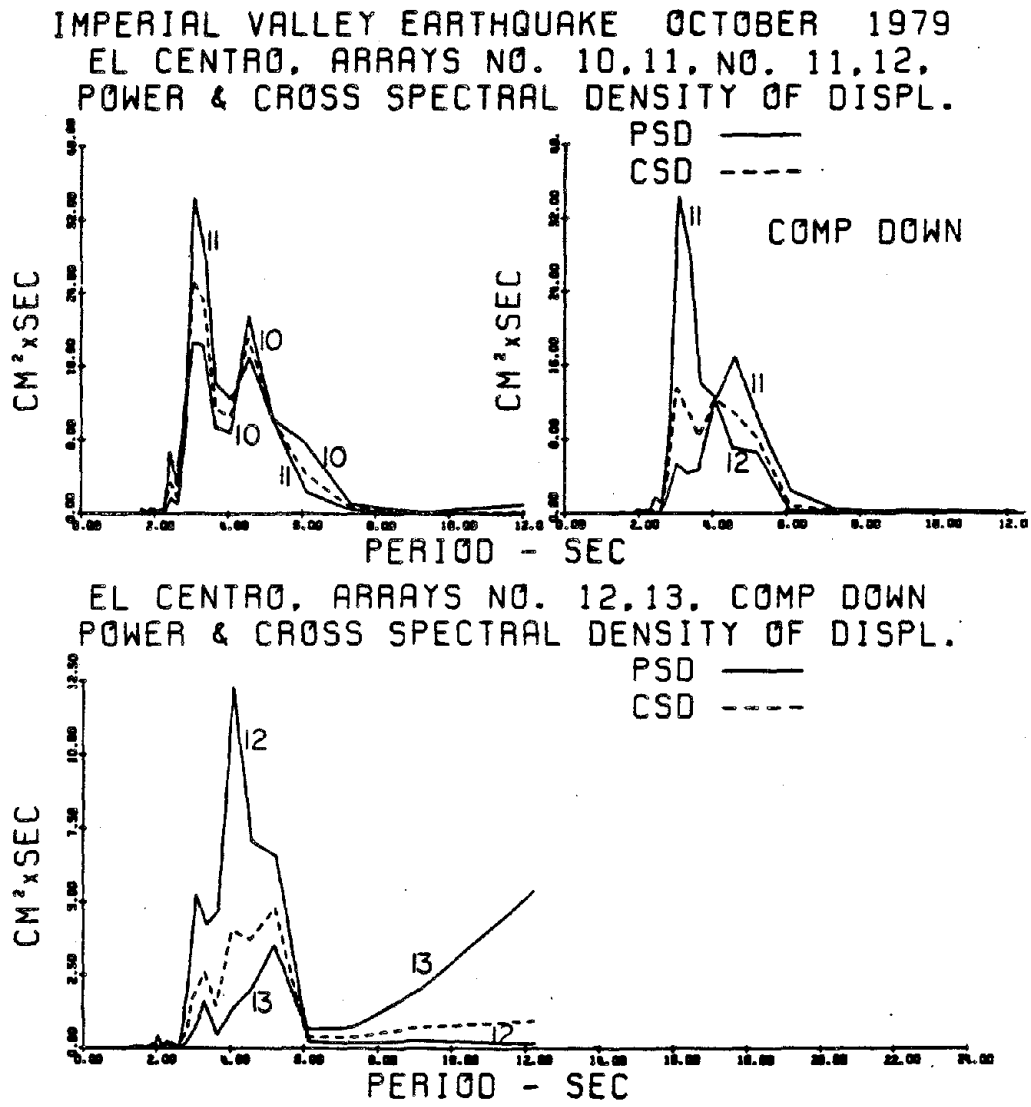

Fig. II-e-7c Power and cross-spectral densities of displacement of El Centro Array (vertical component).

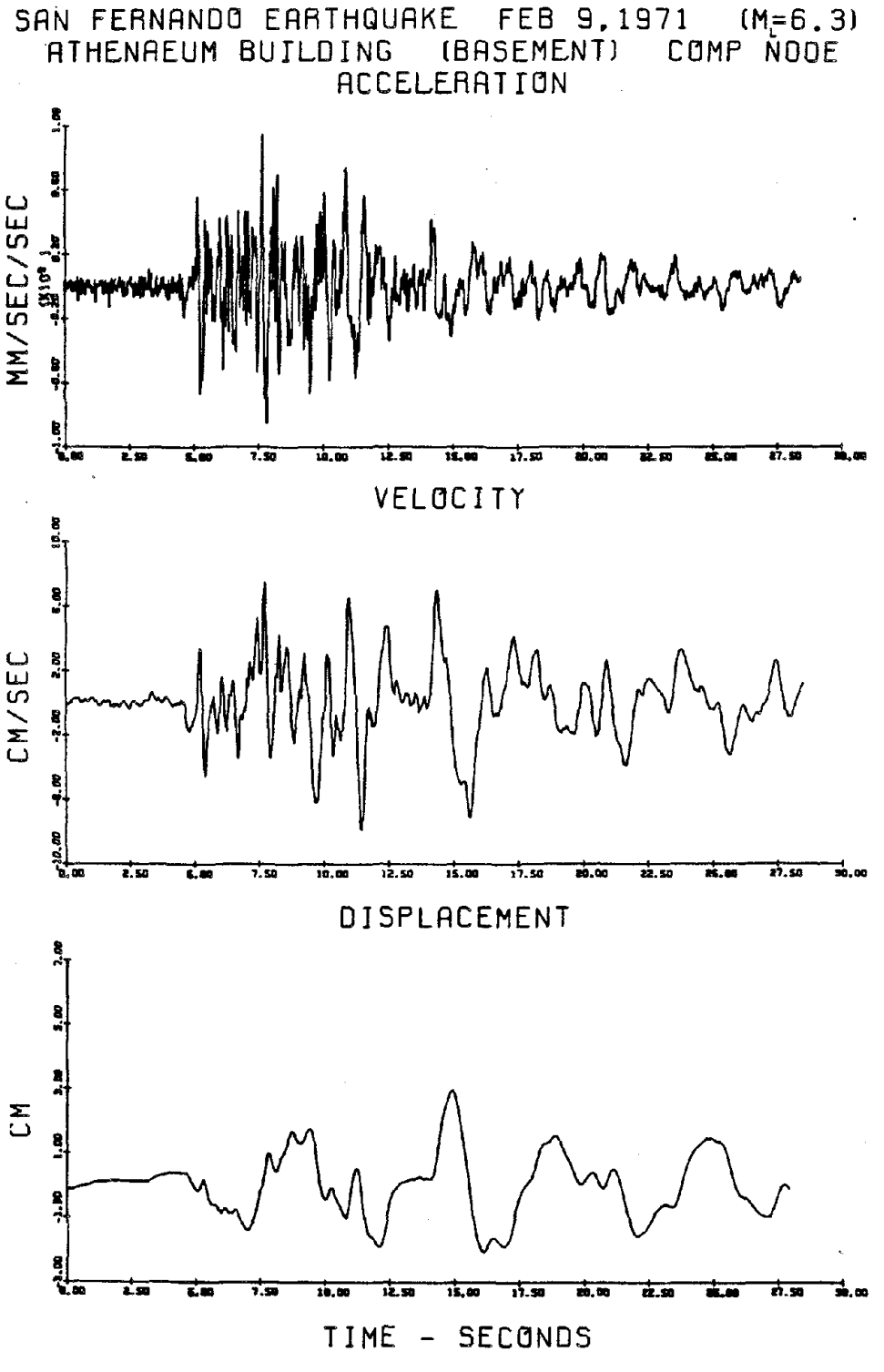

Fig. II-e-8 Acceleration, velocity and displacement time histories of Athenaeum Building record, component N00°E (San Fernando 1971 Earthquake).

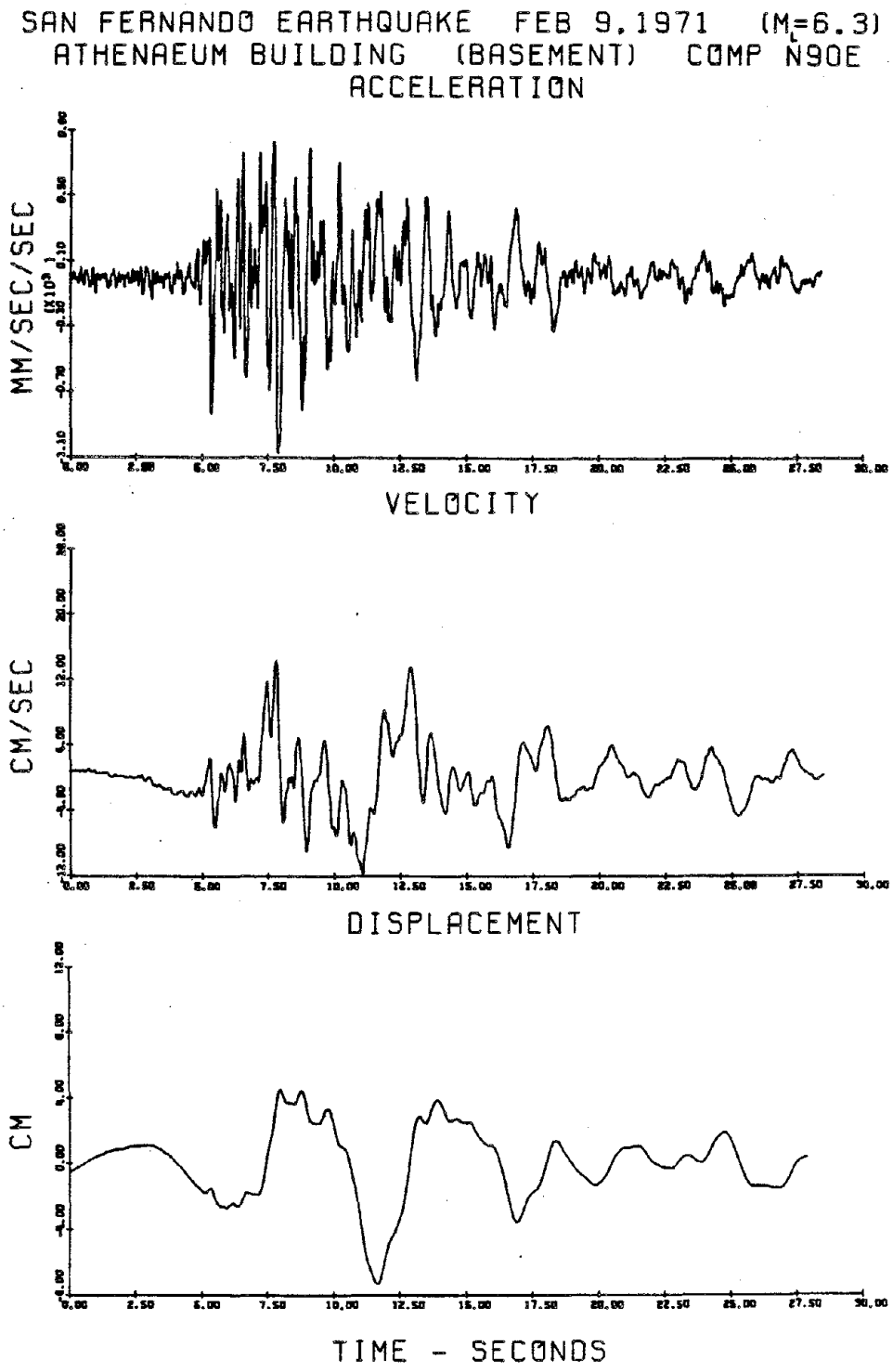

Fig. II-e-9 Acceleration, velocity and displacement time histories of Athenaeum Building record, Component N90°E (San Fernando 1971 Earthquake).

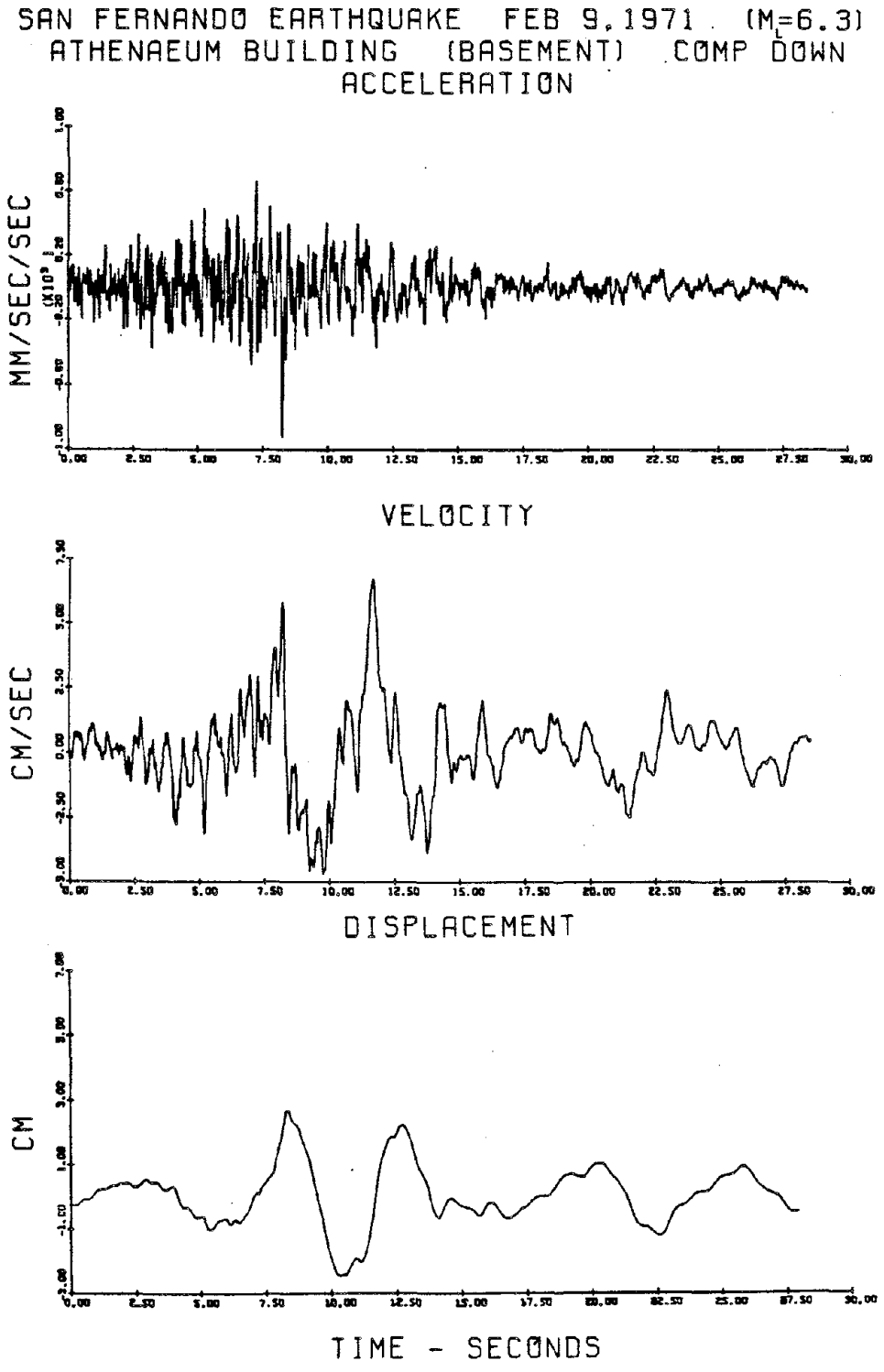

Fig. II-e-10 Acceleration, velocity and displacement time histories of Athenaeum Building record, vertical component (San Fernando 1971 Earthquake).

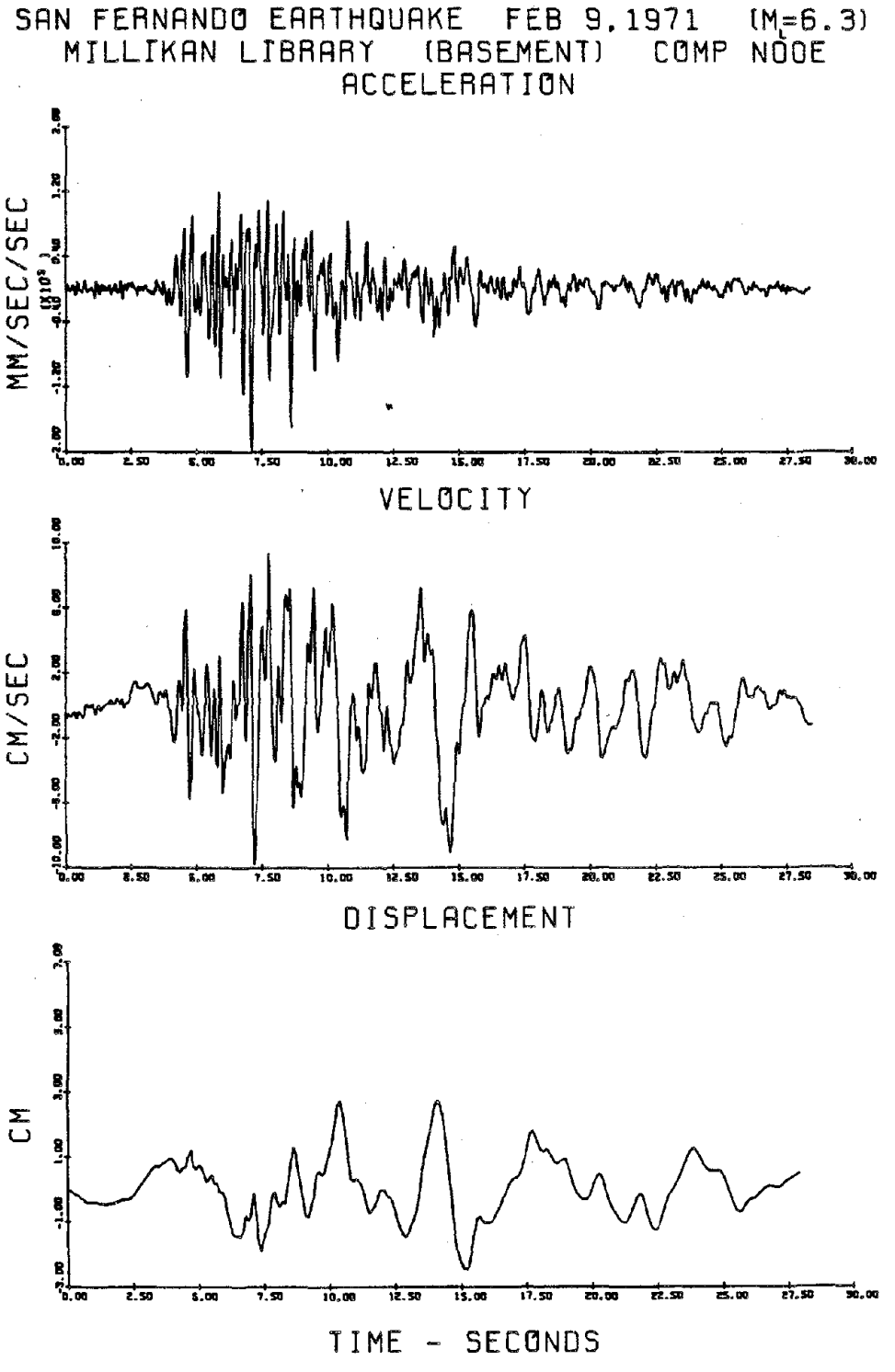

Fig. II-e-11 Acceleration, velocity and displacement time histories of Millikan Library Record, Component N00°E (San Fernando 1971 Earthquake).

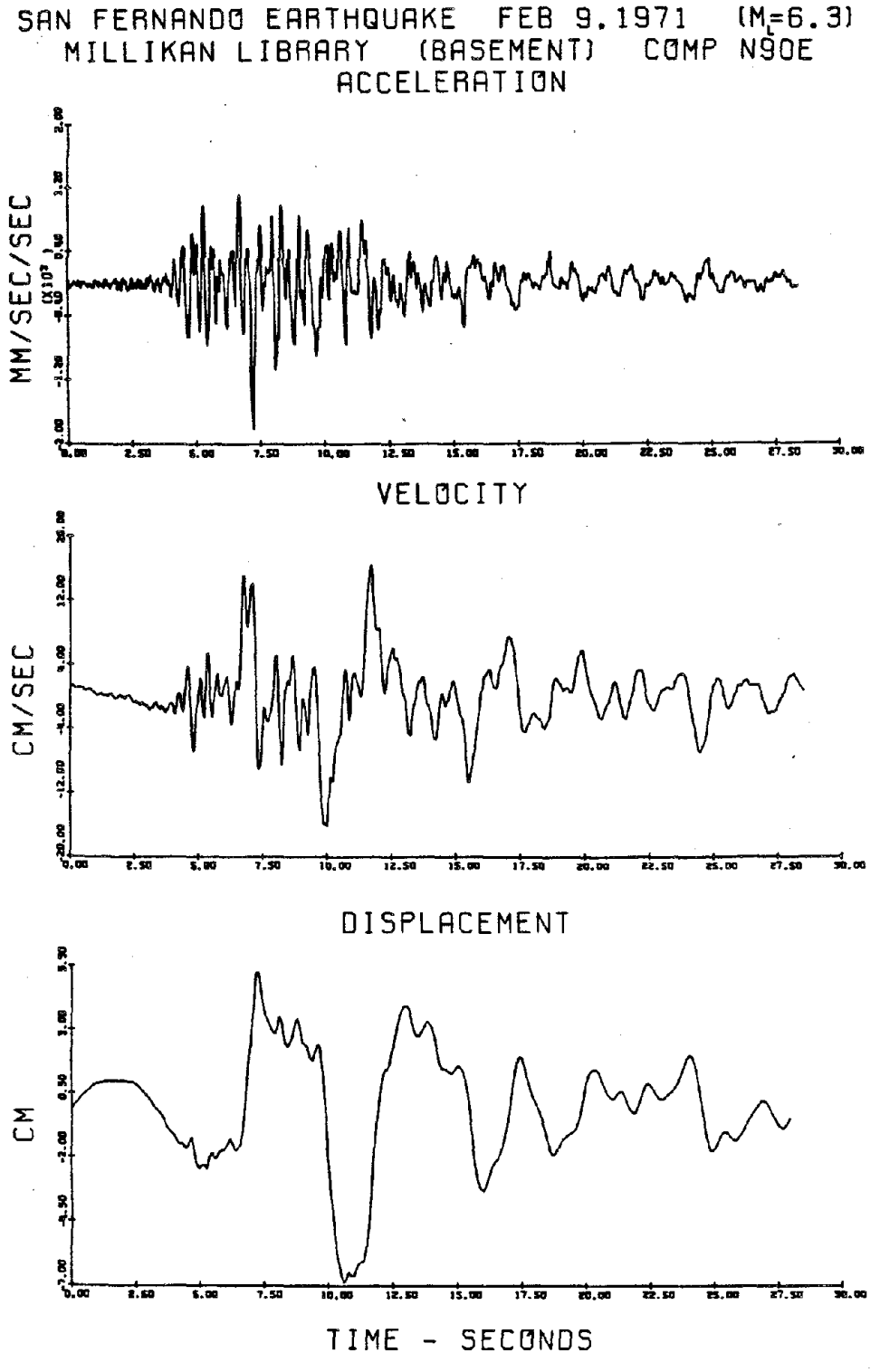

Fig. II-e-12 Acceleration, velocity and displacement time histories of Millikan Library Record, Component N90°E (San Fernando 1971 Earthquake).

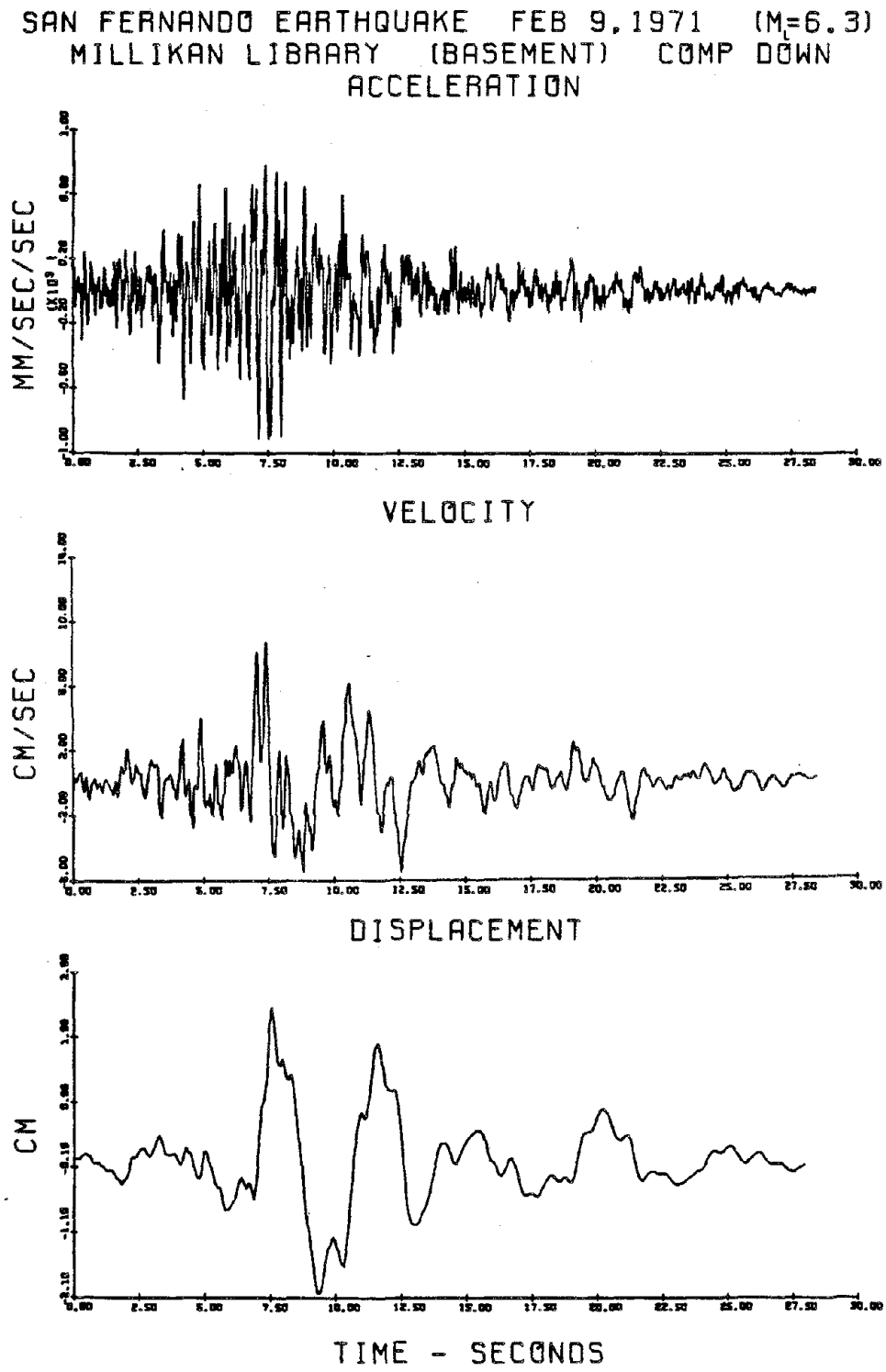

Fig. II-e-13 Acceleration, velocity and displacement time histories of Millikan Library Record, vertical component (San Fernando 1971 Earthquake).

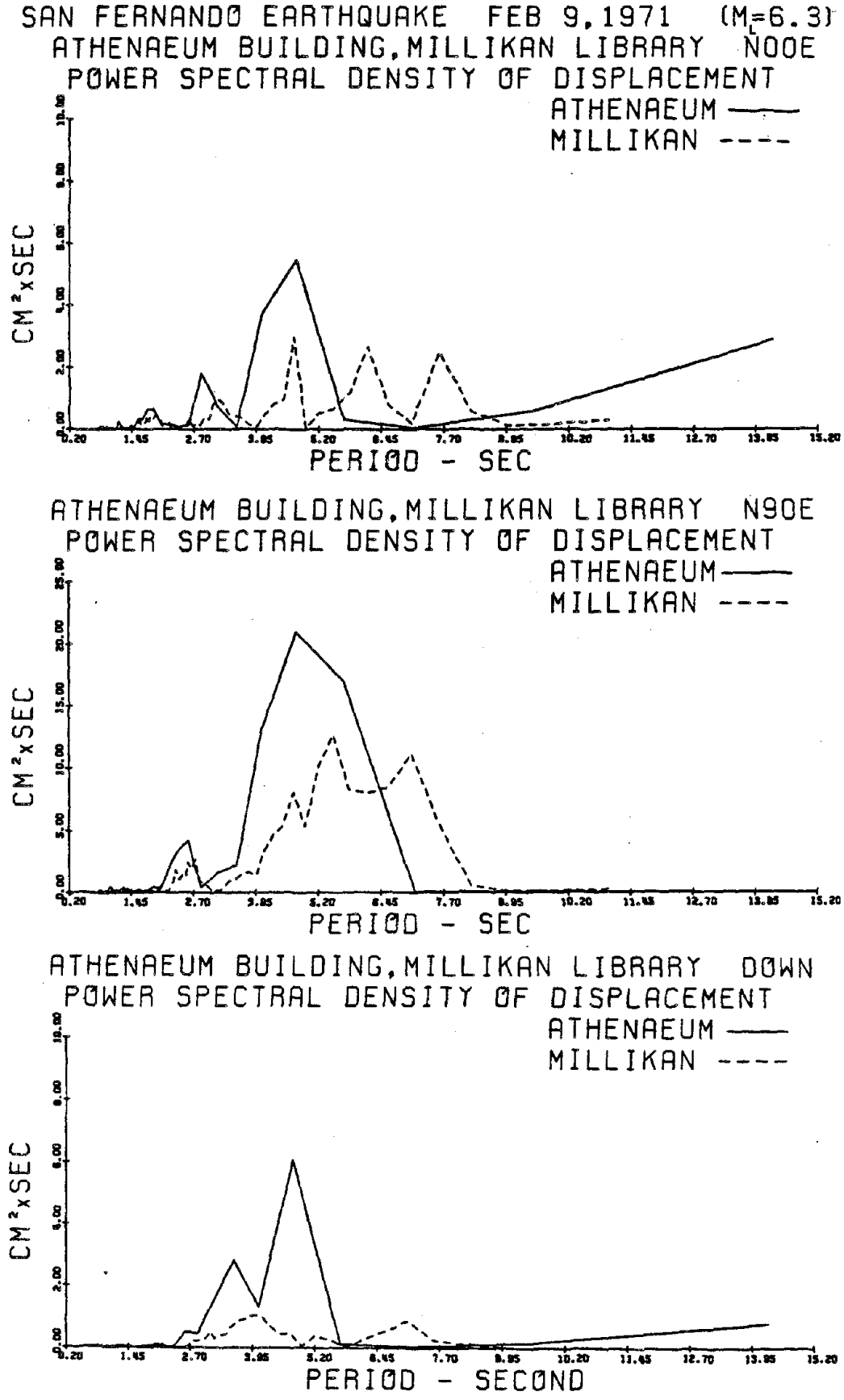

Fig. II-e-14 Power and cross-spectra of displacement of Athenaeum Building and Millikan Library Records (San Fernando 1971 Earthquake).

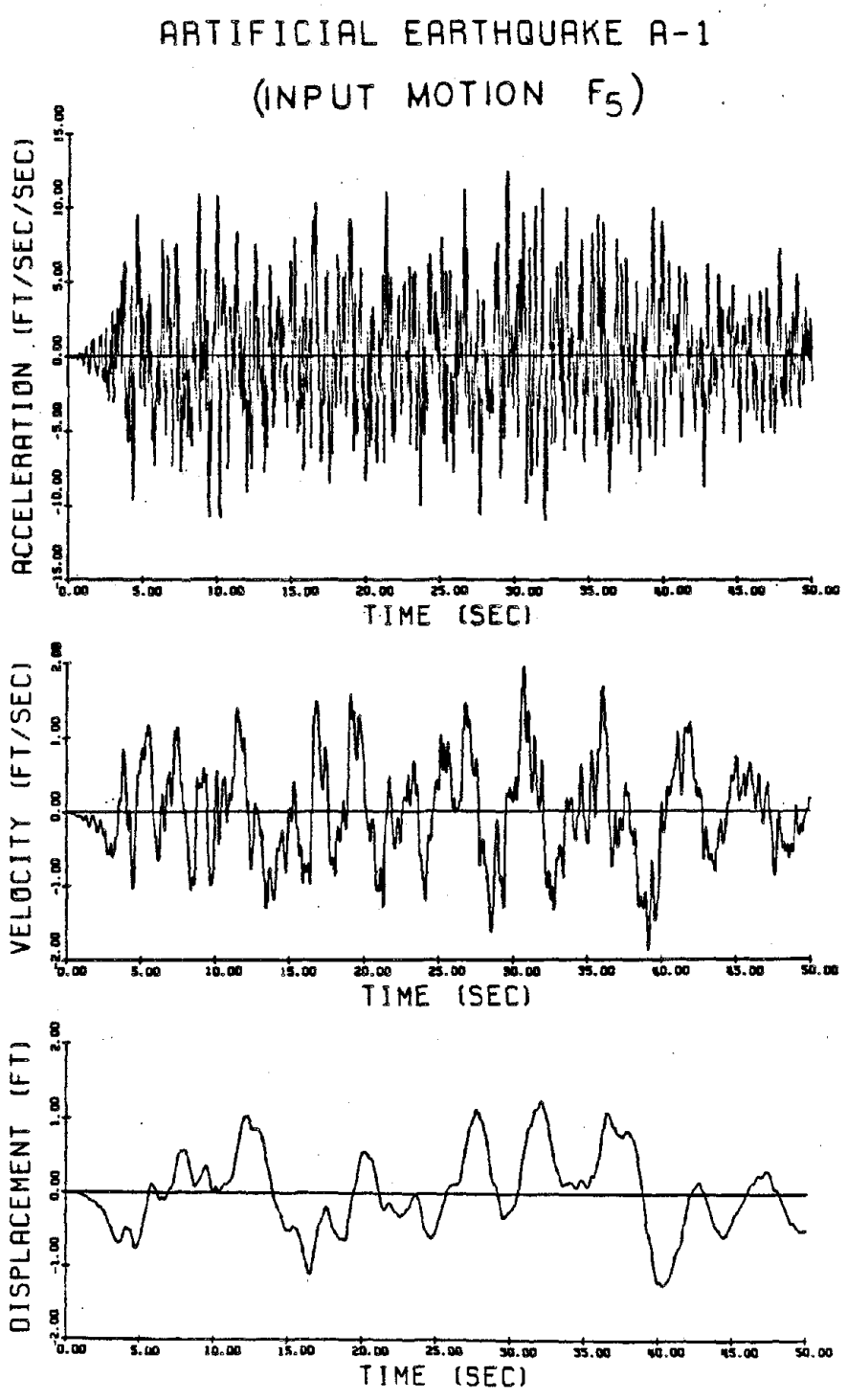

Fig. II-e-15 Acceleration, velocity and displacement time histories of artificial earthquake motion A-1.

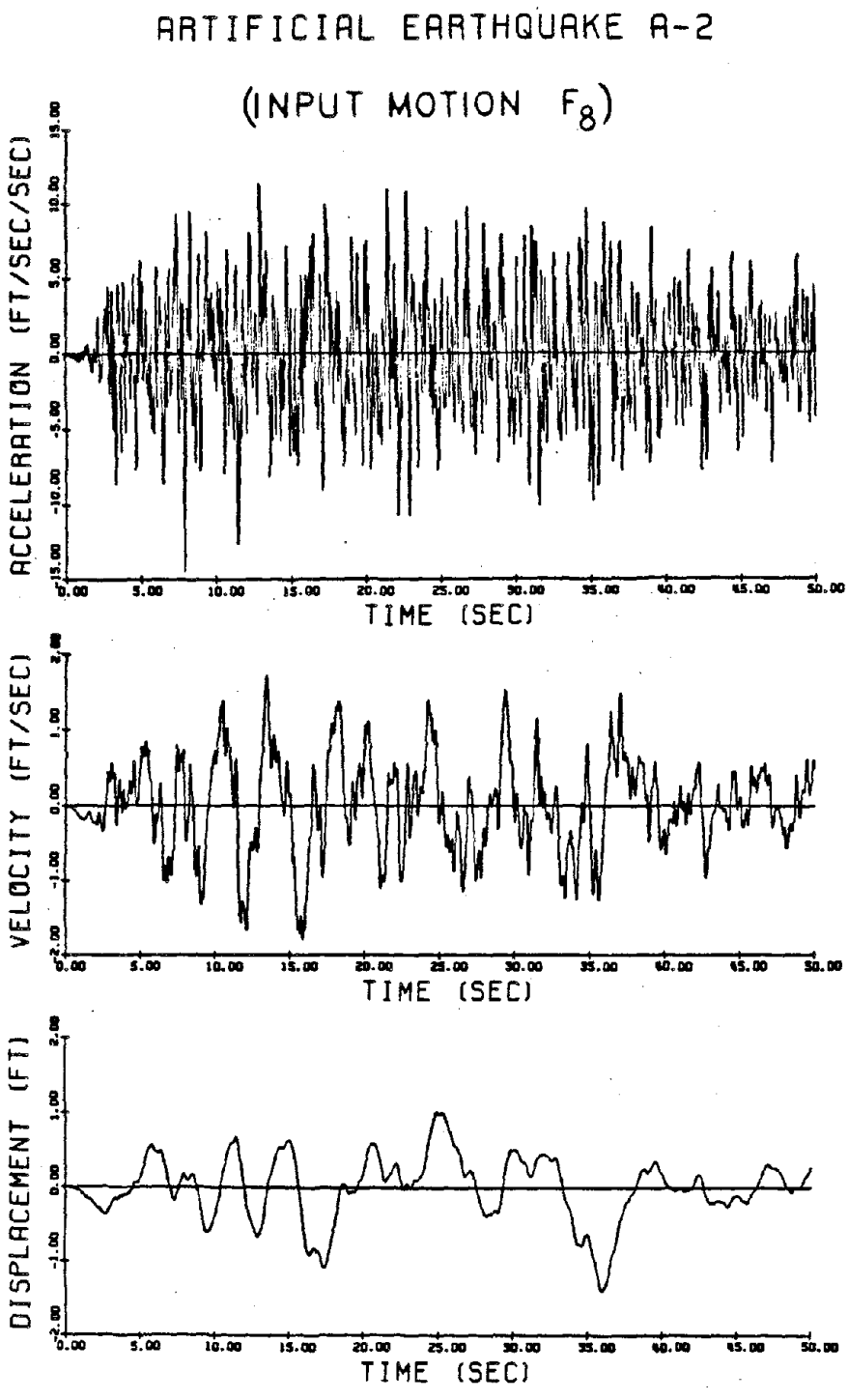

Fig. II-e-16 Acceleration, velocity and displacement time histories of artificial earthquake motion A-2.

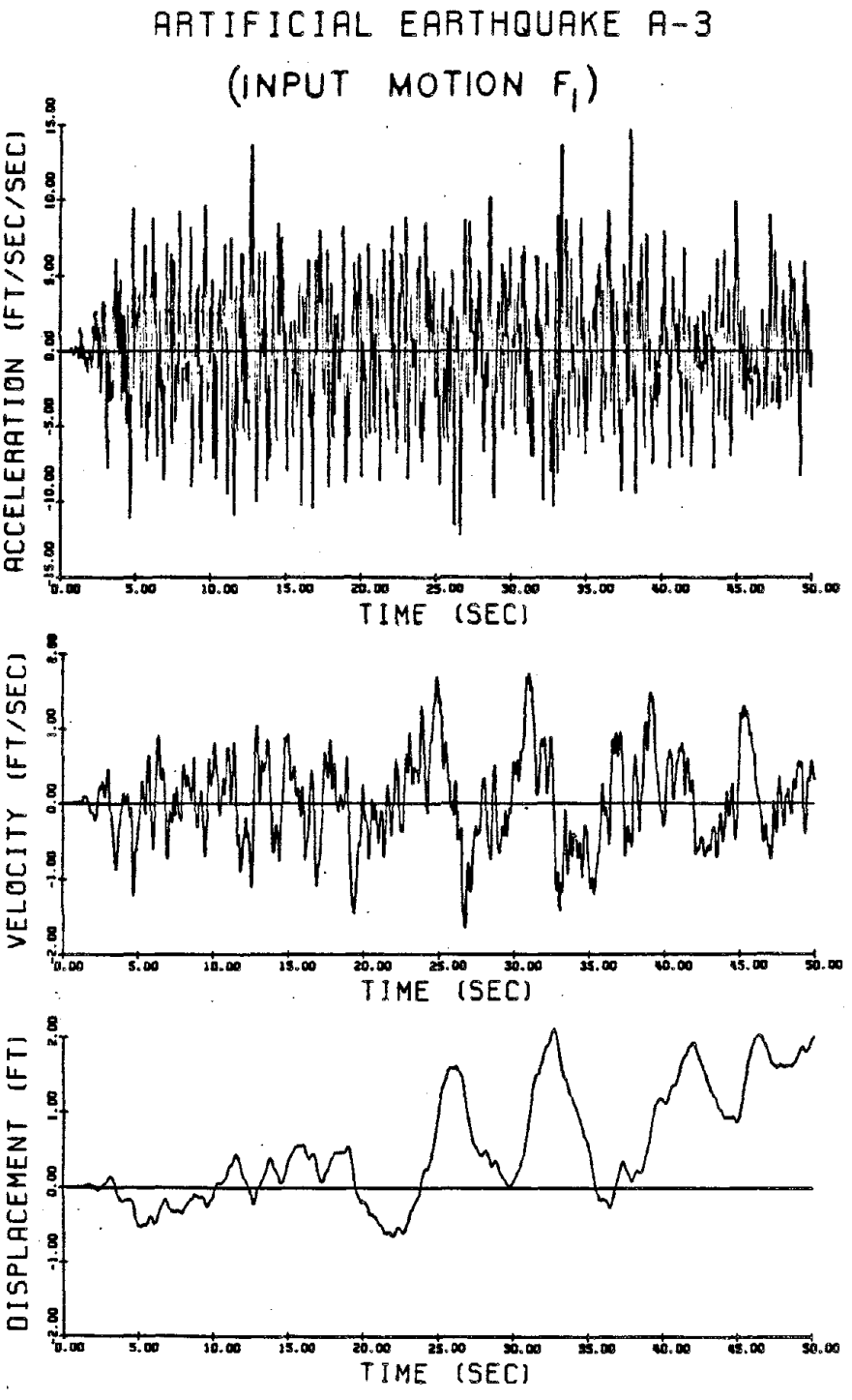

Fig. II-e-17 Acceleration, velocity and displacement time histories of artificial earthquake motion A-3.

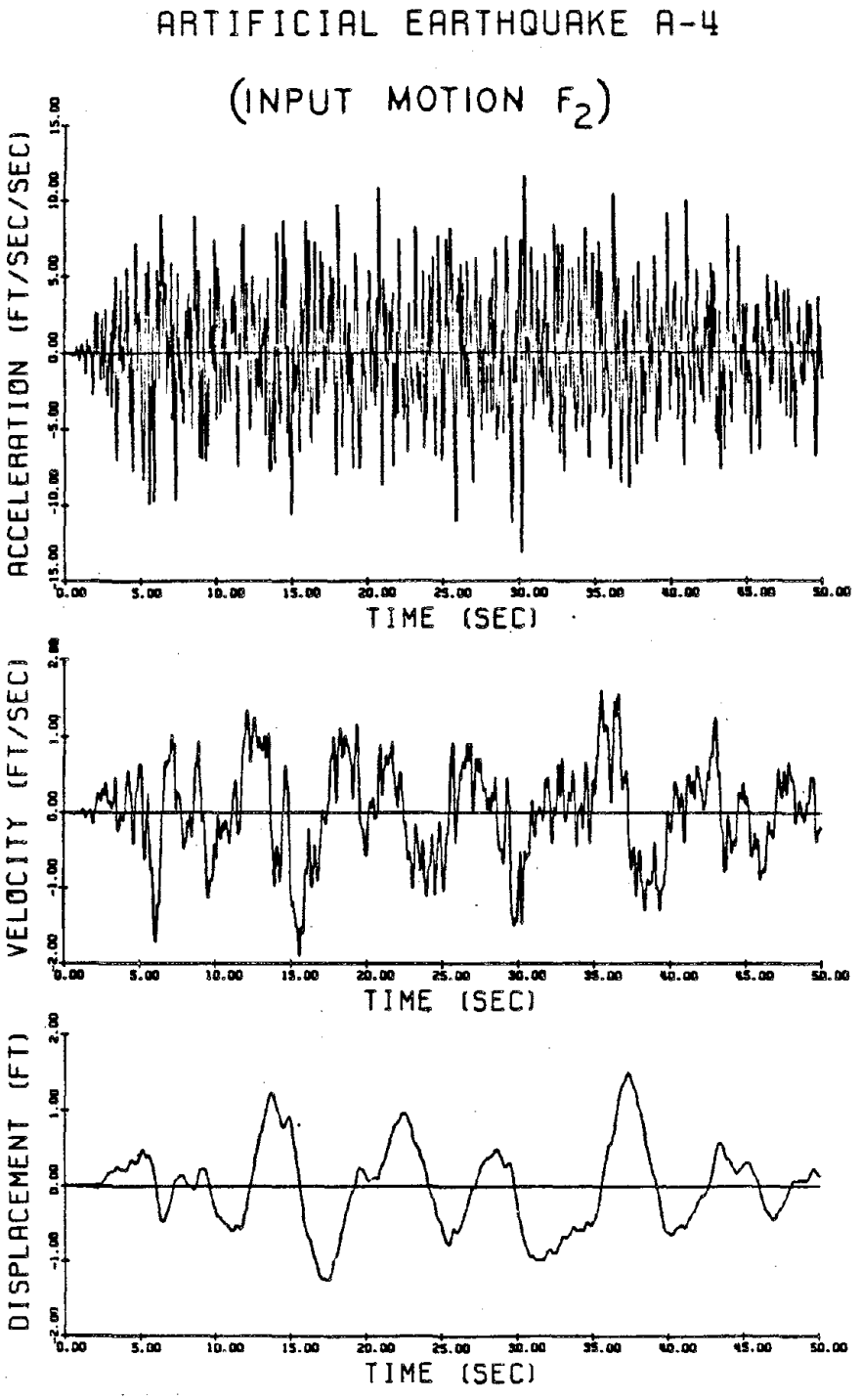

Fig. II-e-18 Acceleration, velocity and displacement time histories of artificial earthquake motion A-4.

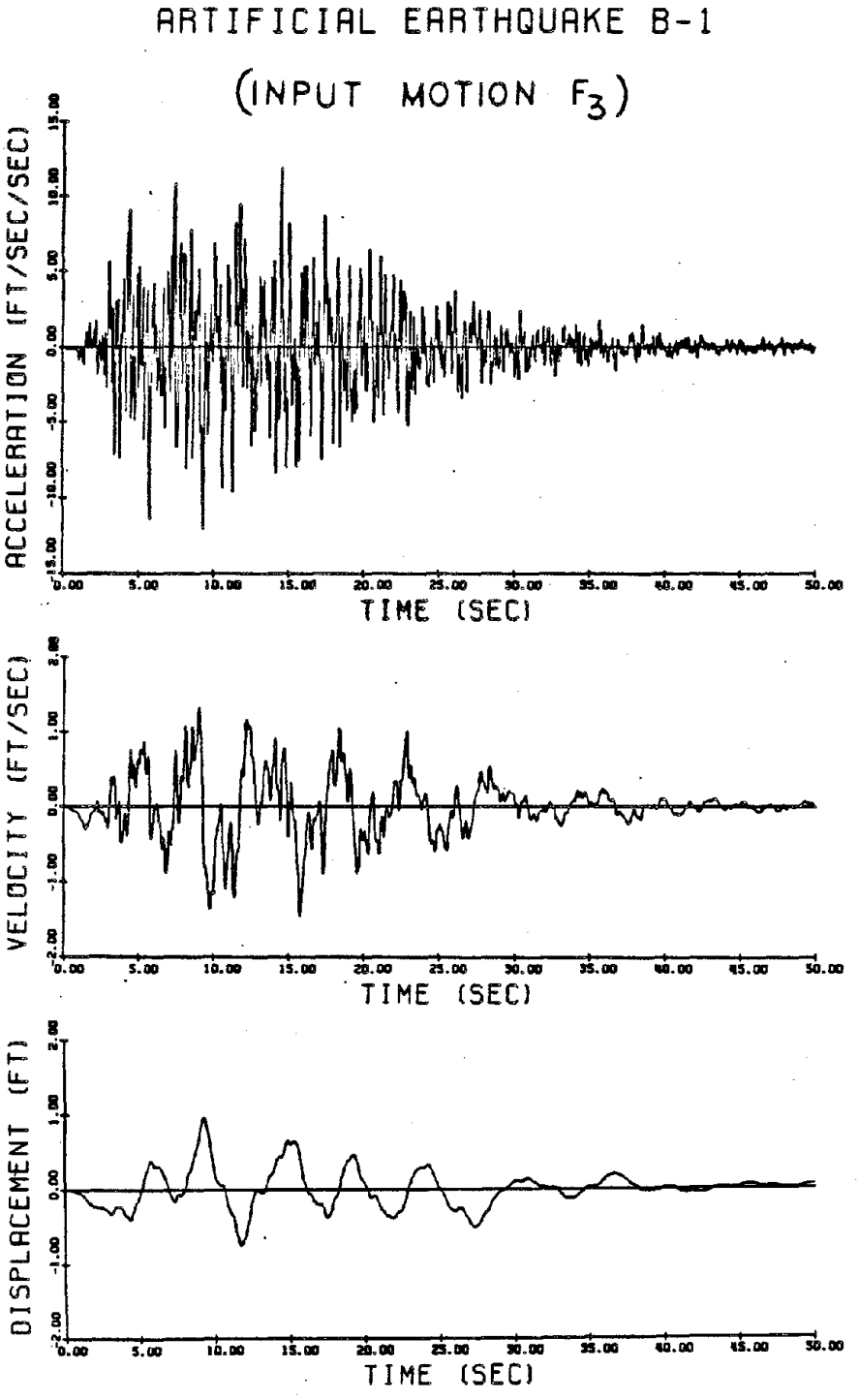

Fig. II-e-19 Acceleration, velocity and displacement time histories of artificial earthquake motion B-1.

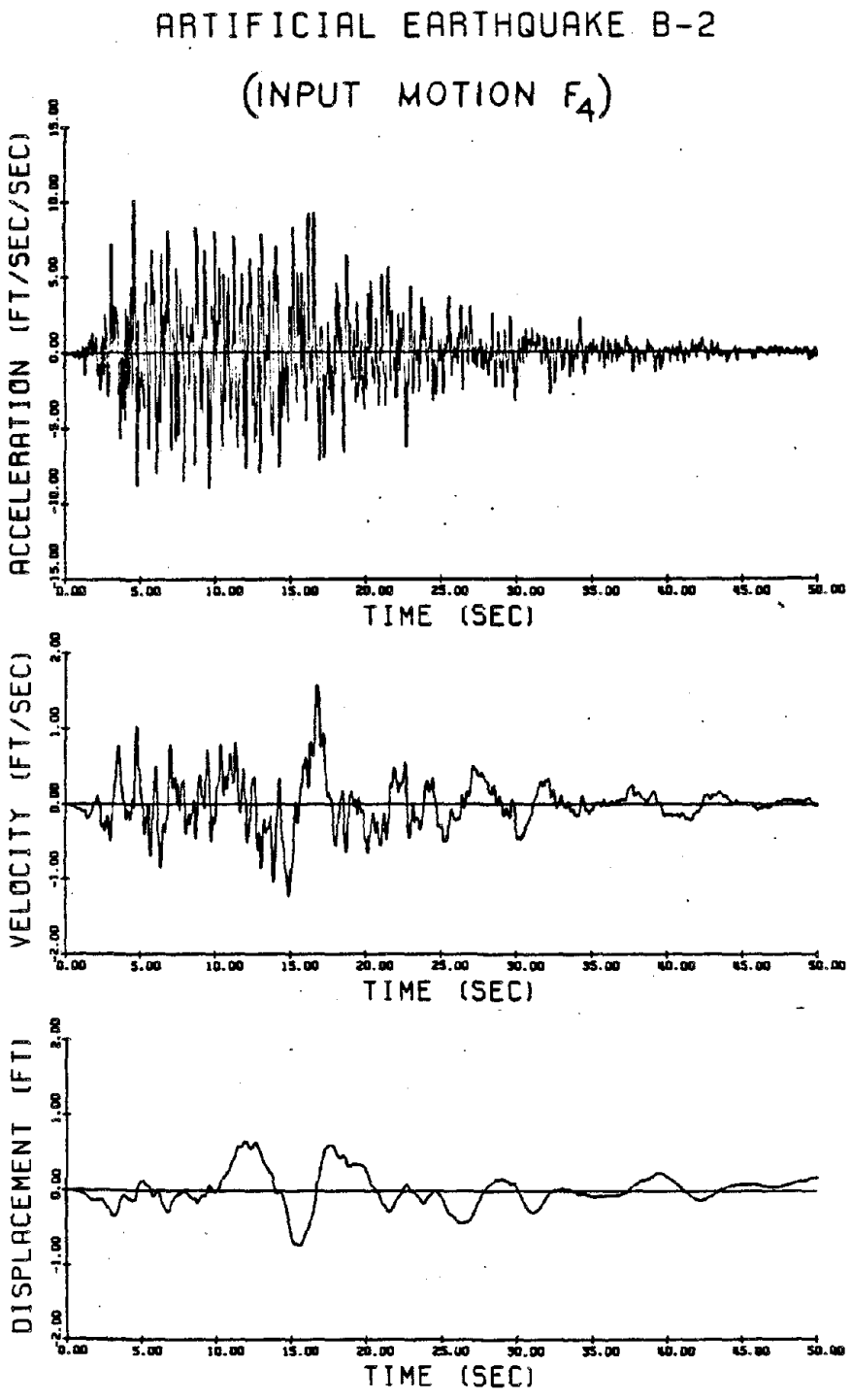

Fig. II-e-20 Acceleration, velocity and displacement time histories of artificial earthquake motion B-2.

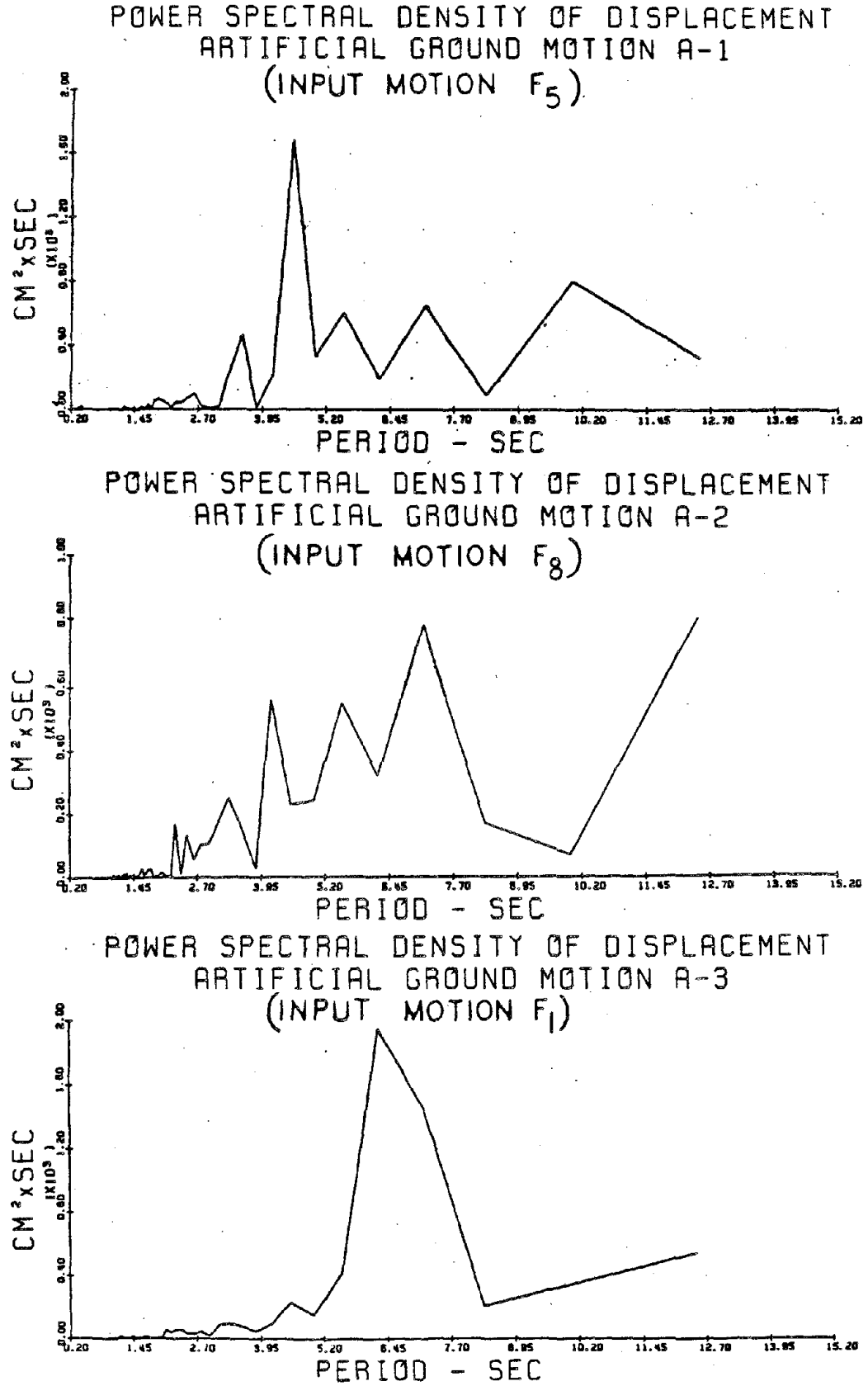

Fig. II-e-21 Power spectra of displacement of artificial earthquake motions A-1, A-2, and A-3.

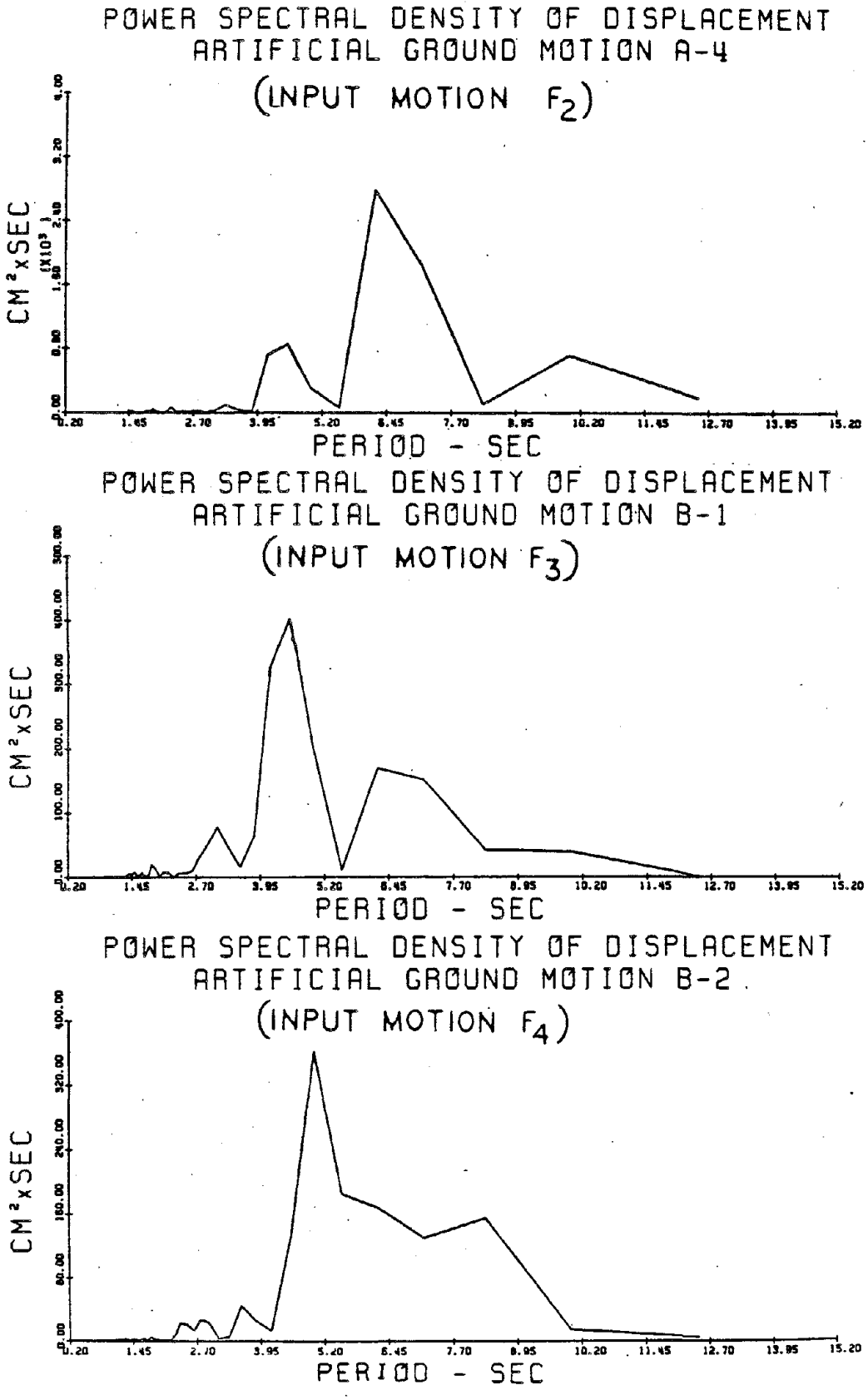

Fig. II-e-22 Power spectra of displacement of artificial earthquake motions A-4, B-1, and B-2.

REFERENCES OF CHAPTER II

1. Abdel-Ghaffar, Ahmed M., "Dynamic Analysis of Suspension Bridge Structures," Report No. EERL 76-01, Earthquake Engineering Research Laboratory, College of Engineering, California Institite of Technology, Pasadena, California, May 1976.

2. Abdel-Ghaffar, Ahmed M., "Vertical Vibration Analysis of Suspension Bridges," Journal of Structural Engineering Division, ASCE, Vol. 106, No. ST10, Proc. Paper 15759, October 1980, pp. 2053-2075.

3. Abdel-Ghaffar, A.M., and Housner, G.W., "An Analysis of a Suspension Bridge by Ambient Vibration Measurements," Earthquake Engineering Research Laboratory Report No. EERL 77-01, California Institute of Technology, Pasadena, California, January 1977.

4. Abdel-Ghaffar, Ahmed M., and Rubin, Lawrence I., "Suspension Bridge Response to Multiple-Support Excitations," ASCE International Convention, New York, Preprint 81-071, May 11-15, 1981. Also in the Journal of Engineering Mechanics Division, ASCE, Vol. 108, No. EM2, Proc. Paper 15982, April 1982, pp. 419-435.

5. Baron, F., Arikan, M., and Hamati, E., "The Effects of Seismic Disturbances on the Golden Gate Bridge," Report No. EERC 76-31, Earthquake Engineering Research Center, College of Engineering, University of California, Berkeley, November 1976.

6. Bendat, Julius S., and Piersol, Allan G., Engineering Applications of Correlation and Spectral Analysis, John Wiley & Sons, Inc., New York, 1980.

7. Bleich, F., McCullough, C.B., Rosecrans, R., and Vincent, G.S., The Mathematical Theory of Vibration in Suspension Bridges, U.S. Bureau of Public Roads, Government Printing Office, Washington 25, DC, 1950.

8. Davenport, A.G., "The Distribution of Largest Values of a Random Function with Application to Gust Loading," Proceedings of the Institute of Civil Engineering, London, England, Vol. 28, 1964, pp. 187-196.

9. Der Kiureghian, Armen, Sackman, Jerome L., and Nour-Omid, Bahram, "Dynamic Response of Light Equipment in Structures," Report No. UCB/EERC-81/05, Earthquake Engineering Research Center, University of California, Berkeley, California, April 1981.

10. Der Kiureghian, Armen, "Structural Response to Stationary Excitation," Journal of the Engineering Mechanics Division, ASCE, Vol. 106, No. EM6, Proc. Paper 15898, December 1980, pp. 1195-1213.

11. Jennings, P.C., "Engineering Features of the San Fernando Earthquake of February 9, 1971," Earthquake Engineering Research Laboratory Report No. EERL 71-02, College of Engineering, California Institute of Technology, Pasadena, California, June 1971.

12. Jennings, P.C., Housner, G.W., and Tsai, N.C., "Simulated Earthquake Motions," Earthquake Engineering Research Laboratory, College of Engineering, California Institute of Technology, Pasadena, California, April 1968.

13. Kelly, James M., and Sackman, Jerome L., "Conservatism in Summation Rules for Closely Spaced Modes," Report No. UCB/EERC-79/11, Earthquake Engineering Research Center, College of Engineering, University of California, Berkeley, May 1979.

14. Mindlin, R.D., and Goodman, L.E., "Beam Vibrations with Time-Dependent Boundary Conditions," Journal of Applied Mechanics, ASME, Vol. 17, 1950, pp. 377-380.

15. Pugsley, A.G., The Theory of Suspension Bridges, Edward Arnold, London, 1957.

16. Steinman, D.B., "Modes and Natural Frequencies of Suspension Bridge Oscillations," ASCE, pp. 148-173, September 1959.

17. Vanmarcke, Erik H., "Structural Response to Earthquakes," Chapter 8, from Seismic Risk and Engineering Decisions, Edited by C. Lomnitz and E. Rosenblueth, Elsevier Publishing Company, Amsterdam, London, New York, 1976.

18. Vanmarcke, Erik H., "Properties of Spectral Moments with Applications to Random Vibration," Journal of the Engineering Mechanics Division, ASCE, Vol. 98, No. EM2, April 1972, pp. 425-446.

CHAPTER III

TORSIONAL RESPONSE OF SUSPENSION BRIDGES TO MULTIPLE-SUPPORT EXCITATIONS

III.1. INTRODUCTION

This chapter presents the dynamic analysis methodology for earthquake-induced torsional vibrations of suspension bridges. The interesting feature in this problem arises from the torsional vibration being excited by the torsional (or horizontal ground rotation about a vertical axis) and rocking (or vertical motion about a horizontal axis that is parallel to the longitudinal axis of the bridge) components of ground motions occurring at the bridge's support points (anchorages and tower-piers) as illustrated in Figs. III-1 through III-4. Because the current state of the art involves recording only the three perpendicular translational components of earthquake ground motion (two horizontal in addition to vertical), the rocking and torsional ground input components can at best be estimated from these recorded translational components using wave propagation theory.

As in the analysis of Chapter II, a frequency-domain random vibration approach is used in this chapter to take into account the differences in ground motion inputs as well as the correlation among the various input motions. In general, the correlation of the motions at these support points is extremely complicated, particularly in the case of a long-span bridge, with different foundation conditions, subjected to seismic waves

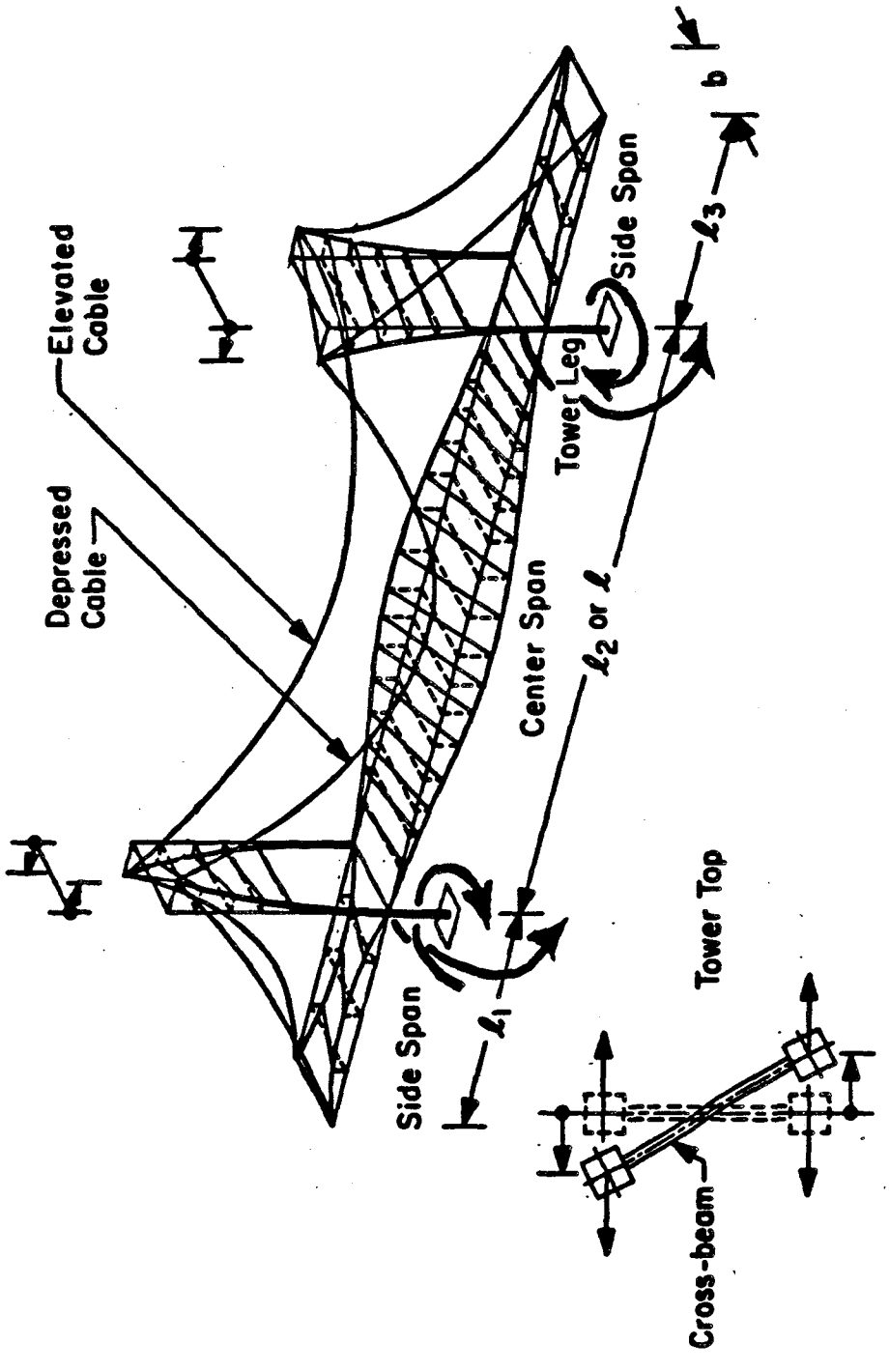

Fig. III-1 TORSIONAL VIBRATIONS OF SUSPENSION BRIDGES

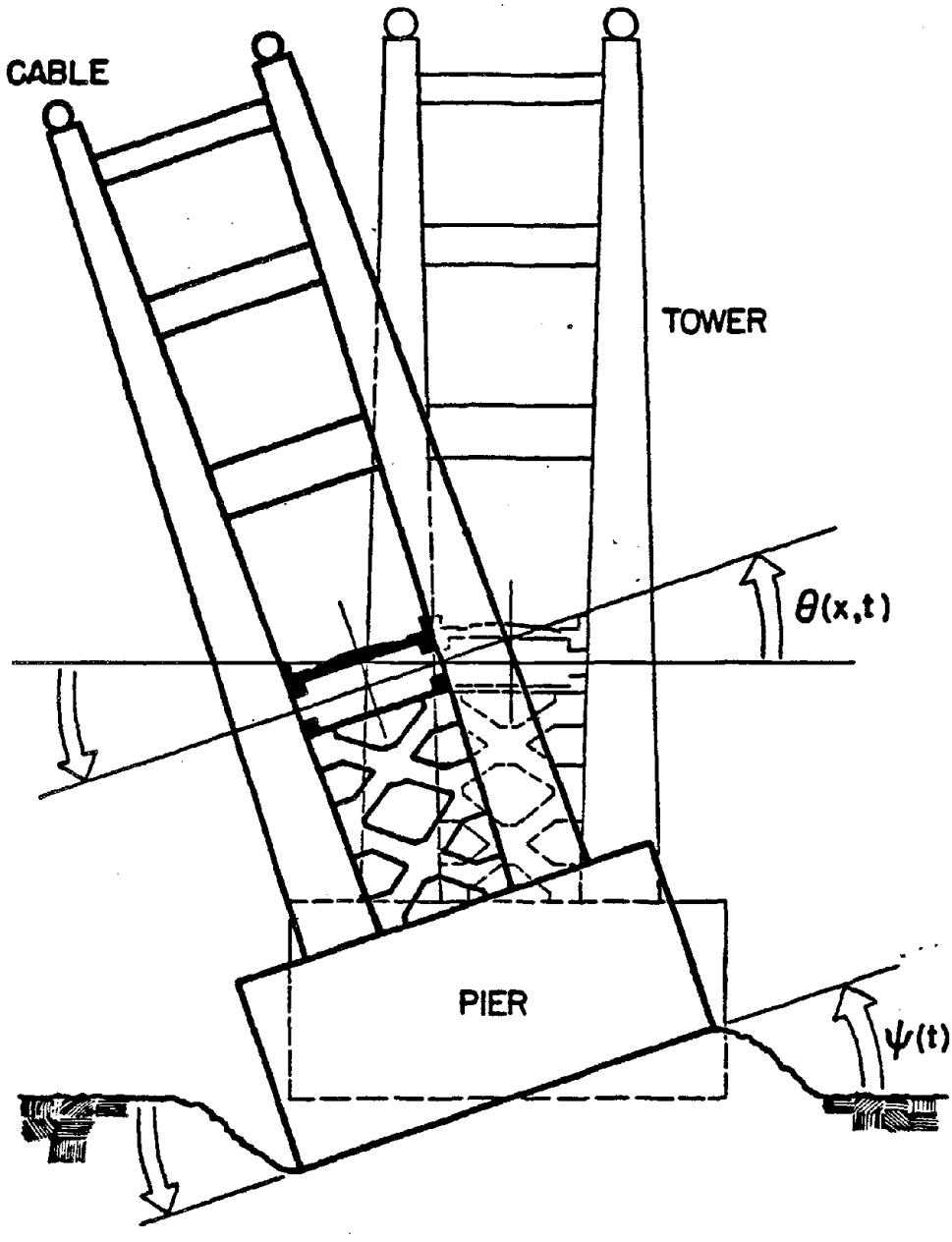

Fig. III-2 TORSIONAL VIBRATION OF THE BRIDGE INDUCED BY TOWER PIER ROCKING MOTION

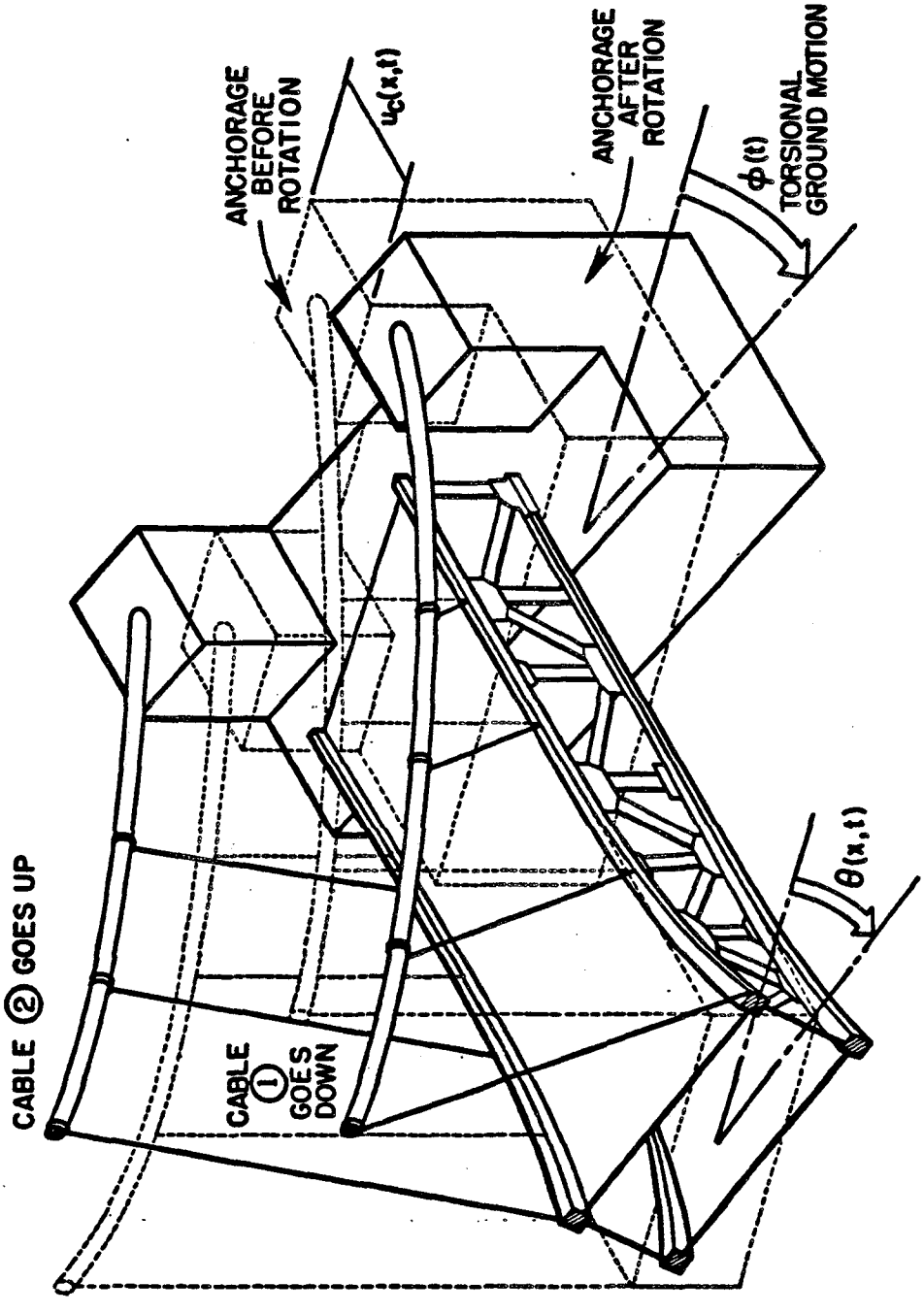

Fig. III-3 SCHEMATIC DIAGRAM SHOWING THE TORSIONAL VIBRATION OF THE BRIDGE INDUCED BY THE HORIZONTAL ROTATION OF THE ANCHORAGES

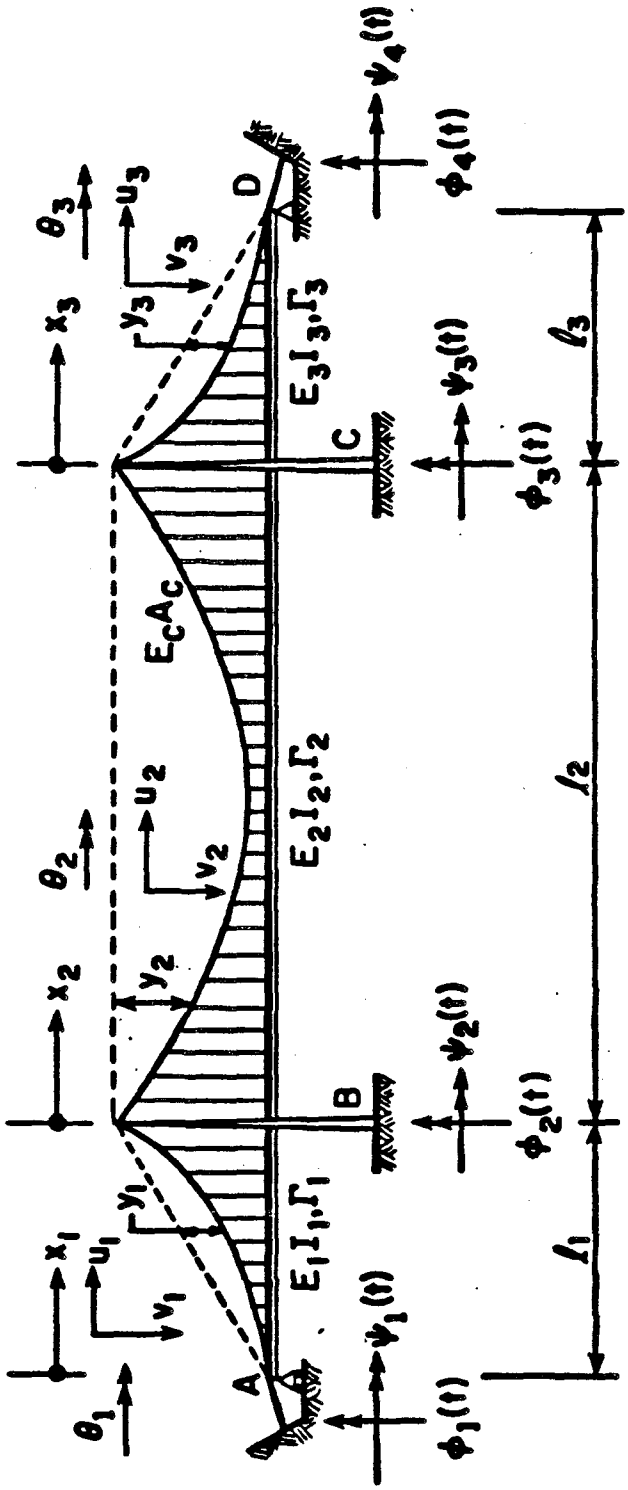

Fig. III-4 Torsional vibration definition diagram.

with different angles of incidence and different travel paths (reflections and refractions, etc.). However, as mentioned previously, such complications can be surpassed by utilizing existing strong motion translation records along with simplified propagation assumptions to define representative and appropriately correlated multiple-support rotational seismic inputs. Ground motion records taken from the Imperial Valley (El Centro), California, earthquake (M_L = 6.6) of October 15, 1979 are used in defining the input support motions (see Appendix II-e). These ground motion records were recorded at several instrument locations whose separation distances are consistent with the suspension bridge's dimensions.

Finally, the torsional response of the Golden Gate Suspension Bridge, in California, is investigated in order to estimate its earthquake response characteristics. Two cases of torsional response are considered. In the first case, the ground motions recorded at Arrays No. 4, 5, 6, and 7 (of the 13 El Centro Arrays; see Appendix II-e) are utilized to define the rotational input motions at support points (anchorages and tower-piers), while the second response case uses the records at Arrays No. 5, 6, 7, and 8 to define the rotational inputs. Mean square torsional response, as well as mean square horizontal components of cable tension due to torsional vibration, are obtained and peak responses are estimated by using a peak factor of about 3.5 (obtained from Chapter II).

III.2. COORDINATE SYSTEMS

The coordinate systems used for the typical three-span suspension bridge are the same as the ones used in Chapter II for vertical vibration (see Fig. III-4). In addition, for the purpose of studying the torsional vibration, the following is considered [1,2]:

1. The principal vibrational torsional modes are identical to the corresponding vertical modes, except that the two sides of the deck and the two cables each move in opposite directions, i.e., 180° out of phase as shown in Fig. III-3. Certain differences between the frequencies of these two comparable modes -- flexural and torsional - arise, however, from the different stiffness and inertial conditions involved. In the flexural modes, the vertical motion of the deck is uniform across any one cross-section; in the torsional modes, one side is rising when the other is going down, and the midpoint of the deck remains stationary.
2. The torsional vibration $\theta(x_i,t)$ of each span is measured as a clockwise rotation of the stiffening structure from its originally horizontal orientation.
3. As will be shown at a later point, the torsional vibration is excited by rocking ground motion (about a horizontal line parallel to a longitudinal axis of the bridge) at the bridge's support points as well as torsional (horizontal rotation) ground motion. In Fig. III-4, the rocking ground motions at supports A, B, C, and D (anchorages and tower-piers) are denoted $\psi_1(t)$, $\psi_2(t)$, $\psi_3(t)$, and $\psi_4(t)$ while the corresponding torsional ground motions are denoted $\phi_1(t)$, $\phi_2(t)$ $\phi_3(t)$, and $\phi_4(t)$.

III.3. SIMPLIFYING ASSUMPTIONS

Certain simplifying assumptions are introduced here in addition to the fundamental assumptions adopted in the earthquake analysis of vertical vibration (Chapter II). Not only is it assumed that the hangers are vertical and inextensible, the cables parabolic, and only small deformations allowed, but also the following simplifying assumptions are introduced [1,2]:

1. The cross section of the bridge deck is assumed to be symmetric about the center of the section. This cross section consists of four horizontal chords (or flanges) and four shear web systems (either diagonal and vertical truss members or web plates).
2. The suspenders (or hangers) are considered inextensible and are assumed to remain vertical during torsional vibration.
3. The tower-piers undergo rocking and torsional motions as rigid bodies under ground motion excitation. This is a reasonable first approximation to investigate torsional vibration since the tower-pier is much stiffer than the suspended structure.

III.4. EQUATION OF MOTION GOVERNING TORSIONAL VIBRATION

Under the previous assumptions, the linearized equation of motion governing the torsional vibration of the i^{th} span of a suspension bridge is given by [1,2]:

$$I_{mi}\frac{\partial^2\theta_i}{\partial t^2} + E_i\Gamma_i\frac{\partial^4\theta_i}{\partial x_i^4} - \left(G_iJ_i + H_w\frac{b^2}{2}\right)\frac{\partial^2\theta_i}{\partial x_i^2} + c_i\frac{\partial\theta_i}{\partial t} + \frac{\overset{*}{w}_i b}{H_w}H(t) = 0, \qquad i=1,2,3. \tag{3.1}$$

where $\theta = \theta_i(x_i,t)$ is the torsional response of the i^{th} span; $\overset{*}{w}_i$ is the dead weight of the bridge per unit length of the i^{th} span; I_{mi} is the equivalent mass polar moment of inertia of the bridge cross section in the i^{th} span (including the contribution of the two cables) per unit length; E_i is the modulus of elasticity of the suspended structure in the i^{th} span; Γ_i is the warping constant of the cross section (see Ref. 1) in the i^{th} span; $E_i\Gamma_i$ is the warping rigidity of the cross section in the i^{th} span; G_i is the shear modulus of the i^{th} span; J_i is the torsion constant of the i^{th} span; G_iJ_i is the torsional rigidity of the i^{th} span; b is the deck width of the bridge; c_i is the torsional damping coefficient for the i^{th} span; H_w is the initial (dead-load) horizontal component of cable tension; and $H(t)$ is the additional (vibrational) horizontal component of cable tension given by [1,2]:

$$H(t) = \frac{E_c A_c}{L_E} \sum_{j=1}^{3} \left[\frac{b}{2} \int_0^{\ell_j} \left(\frac{dy_j}{dx_j}\right)\left(\frac{\partial\theta_j}{\partial x_j}\right) dx_j + u_c(x_j,t) \Big|_0^{\ell_j} \right] \tag{3.2}$$

in which E_c is the cable's modulus of elasticity; A_c is the cable's cross sectional area; u_c is the longitudinal cable displacement at the tower tops and anchorages; ℓ_j is the length of the j^{th} span; L_E is the cable's virtual length defined as [1];

$$L_E = \sum_{i=1}^{3} \int_0^{\ell_i} \left(\frac{ds_i}{dx_i}\right)^3 dx_i \tag{3.3}$$

where s_i is the coordinate measured tangent to the cable in the i^{th} span; and $y_j = y_j(x_j)$ is the cable ordinate measured from the closing chord of the j^{th} span (Fig. III-4). This dead load cable profile is expressed as [1,2]:

$$y_i(x_i) = \frac{\overset{*}{w}_i \ell_i}{2H_w}\left[\left(\frac{x_i}{\ell_i}\right) - \left(\frac{x_i}{\ell_i}\right)^2\right] \qquad i=1,2,3. \tag{3.4}$$

It should be recognized from Eqs. 3.1 that the torsional vibrations of each span of the suspension bridge are coupled together by the vibration of the cable through H(t). In torsional vibration, the two cables vibrate in their vertical planes in opposite phase. The downward movement of the cable tends to increase its length and thus increase the horizontal component of cable tension, while the upward movement of the cable tends to reduce its length and thus reduce the horizontal component of cable tension. The boundary conditions at the tower-piers and anchorages are time dependent and can be written as

$$\begin{aligned} &\theta_i(0,t) = \psi_i(t) \\ &\theta_i(\ell_i,t) = \psi_{i+1}(t) \\ &\theta_i''(0,t) = 0 \\ &\theta_i''(\ell_i,t) = 0 \end{aligned} \qquad i=1,2,3. \tag{3.5}$$

where $\psi_i(t)$, (i=1,2,3,4), are the rocking components of ground motion displacement at supports A, B, C, and D of Fig. III-4. Also note that by integrating Eq. 3.2 by parts and utilizing Eq. 3.4 the additional horizontal component of cable tension can be given by

$$H(t) = \frac{E_c A_c}{L_E}\sum_{j=1}^{3}\left[\frac{\overset{*}{w}_j b}{2H_w}\int_0^{\ell_j}\theta_j dx_j + \frac{b}{2}\left(\frac{dy_j}{dx_j}\right)\theta_j\Big|_0^{\ell_j} + u_c(x_j,t)\Big|_0^{\ell_j}\right] \tag{3.6}$$

The last two terms in Eq. 3.6 may be written as

$$\sum_{j=1}^{3}\frac{b}{2}\left(\frac{dy_j}{dx_j}\right)\theta_j\Big|_0^{\ell_j} = -\frac{b}{2}\sum_{j=1}^{3}\frac{\overset{*}{w}_j \ell_j}{2H_w}\left[\psi_{j+1}(t) + \psi_j(t)\right] \tag{3.7}$$

and

$$\sum_{j=1}^{3} u_c(x_j,t)\Big|_0^{\ell_j} = \sum_{j=1}^{3} \frac{b}{2}[\phi_{j+1}(t) - \phi_j(t)]$$

$$= \frac{b}{2}[\phi_4(t) - \phi_1(t)] \qquad (3.8)$$

where $\phi_j(t)$, (j=1,2,3,4), are the torsional components of ground motion displacement at supports A, B, C, and D of Fig. III-4.

Therefore, the additional horizontal component of cable tension (Eq. 3.6) becomes

$$H(t) = \left(\frac{E_c A_c}{L_E}\right)\left(\frac{b}{2}\right)\left\{\sum_{j=1}^{3}\left\{\frac{\overset{*}{w}_j}{H_w}\int_0^{\ell_j}\theta_j dx_j - \frac{\overset{*}{w}_j \ell_j}{2H_w}[\psi_{j+1}(t) + \psi_j(t)]\right\}\right.$$

$$\left. + [\phi_4(t) - \phi_1(t)]\right\} \qquad (3.9)$$

From Eqs. 3.1 and 3.9, it can be seen that the bridge's torsional motion is excited not only by rocking ground motion inputs $\psi_1(t)$, $\psi_2(t)$, $\psi_3(t)$, and $\psi_4(t)$ (that is, by the vertical rotation of the ground about a horizontal axis parallel to the longitudinal axis of the bridge), but also by the two torsional ground motion inputs (that is, the horizontal ground motion rotation about a vertical axis) at the end anchorages, $\phi_1(t)$ and $\phi_4(t)$.

III.5. GENERAL SOLUTION

In order to conveniently satisfy the time-dependent boundary conditions (Eq. 3.5), again the Mindlin-Goodman solution is adopted [7], that is, the torsional displacement is separated into two parts

$$\theta_i(x_i,t) = \eta_i(x_i,t) + \sum_{j=1}^{4} g_{ji}(x_i)\psi_j(t) \qquad i=1,2,3. \qquad (3.10)$$

where η_i is the relative or vibrational rotation of the i^{th} suspended span and $g_{ji}(x_i)$ is the quasi-static (or influence) function which gives the rotation at x_i due to a unit rotation of the suspended structure at the j^{th} support.

Substituting Eqs. 3.10 into Eqs. 3.1 and 3.9 gives the following equation governing the vibrational response:

$$
\begin{aligned}
&I_{mi}\frac{\partial^2\eta_i}{\partial t^2} + E_i\Gamma_i\frac{\partial^4\eta_i}{\partial x_i^4} - \left(G_iJ_i + H_w\frac{b^2}{2}\right)\frac{\partial^2\eta_i}{\partial x_i^2} \\
&\quad + c_i\frac{\partial\eta_i}{\partial t} + \frac{\overset{*}{w}_i b}{H_w}\left[\left(\frac{E_cA_c}{L_E}\right)\left(\frac{b}{2}\right)\sum_{n=1}^{3}\frac{\overset{*}{w}_n}{H_w}\int_0^{\ell_n}\eta_n dx_n\right] = \\
&\quad - I_{mi}\sum_{j=1}^{4} g_{ji}(x_i)\ddot{\psi}_j(t) - c_i\sum_{j=1}^{4} g_{ji}(x_i)\dot{\psi}_j(t) \\
&\quad + \left(\frac{\overset{*}{w}_i b}{H_w}\right)\left(\frac{E_cA_c}{L_E}\right)\left(\frac{b}{2}\right)\sum_{n=1}^{3}\frac{\overset{*}{w}_n\ell_n}{2H_w}\left[\psi_{n+1}(t) + \psi_n(t)\right] \\
&\quad - \left(\frac{\overset{*}{w}_i b}{H_w}\right)\left(\frac{E_cA_c}{L_E}\right)\left(\frac{b}{2}\right)\left[\phi_4(t) - \phi_1(t)\right] \\
&\quad - \sum_{j=1}^{4}\psi_j(t)\left\{E_i\Gamma_i g_{ji}^{IV}(x_i) - \left(G_iJ_i + H_w\frac{b^2}{2}\right)g_{ji}''(x_i)\right. \\
&\quad \left. + \left(\frac{\overset{*}{w}_i b}{H_w}\right)\left(\frac{E_cA_c}{L_E}\right)\left(\frac{b}{2}\right)\sum_{n=1}^{3}\frac{\overset{*}{w}_n}{H_w}\int_0^{\ell_n} g_{jn}(x_n)dx_n\right\}, \qquad i=1,2,3. \qquad (3.11)
\end{aligned}
$$

Substituting Eqs. 3.10 into Eq. 3.5, the boundary conditions upon the vibrational response become

$$\eta_i(0,t) = \psi_i(t) - \sum_{j=1}^{4} g_{ji}(0)\psi_j(t)$$

$$\eta_i(\ell_i,t) = \psi_{i+1}(t) - \sum_{j=1}^{4} g_{ji}(\ell_i)\psi_j(t)$$

$$i=1,2,3 \qquad (3.12)$$

$$\eta_i''(0,t) = 0 - \sum_{j=1}^{4} g_{ji}''(0)\psi_j(t)$$

$$\eta_i''(\ell_i,t) = 0 - \sum_{j=1}^{4} g_{ji}''(\ell_i)\psi_j(t)$$

The above boundary conditions can be made homogeneous by choosing

$$\left.\begin{matrix} g_{ji}(0) \\ g_{ji}(\ell_i) \end{matrix}\right\} \begin{cases} = 1 & j = i \\ = 0 & j \neq i \end{cases} \qquad \begin{matrix} i=1,2,3. \\ j=1,2,3,4. \end{matrix} \qquad (3.13)$$

$$g_{ji}''(0) = g_{ji}''(\ell_i) = 0 \quad \text{for all } i,j$$

Now the quasi-static functions are the solutions of the twelve equations represented by setting the last bracketed term in Eq. 3.11 to zero (for i = 1,2,3, and j = 1,2,3,4) subject to the boundary conditions of Eq. 3.13. These functions have the form

$$g_{ji}(x_i) = A_{ji}\sinh(\lambda_i x_i) + B_{ji}\cosh(\lambda_i x_i) + C_{ji}x_i^2 + D_{ji}x_i + E_{ji}$$

$$\begin{matrix} i=1,2,3. \\ j=1,2,3,4. \end{matrix} \qquad (3.14)$$

where

$$\lambda_i = \sqrt{\frac{\left(G_i J_i + H_w \frac{b^2}{2}\right)}{E_i \Gamma_i}} \quad , \; i=1,2,3 \tag{3.15}$$

and the coefficients A_{ji}, B_{ji}, C_{ji}, D_{ji}, and E_{ji} are constants involving the bridge's structural properties (solution details are found in Appendix III-a).

With the quasi-static functions uniquely defined, Eq. 3.11 reduces to

$$I_{mi} \frac{\partial^2 \eta_i}{\partial t^2} + E_i \Gamma_i \frac{\partial^4 \eta_i}{\partial x_i^4} - \left(G_i J_i + H_w \frac{b^2}{2}\right) \frac{\partial^2 \eta_i}{\partial x_i^2} + c_i \frac{\partial \eta_i}{\partial t}$$

$$+ \frac{\overset{*}{w}_i b}{H_w}\left[\left(\frac{E_c A_c}{L_E}\right)\left(\frac{b}{2}\right) \sum_{n=1}^{3} \frac{\overset{*}{w}_n}{H_w} \int_0^{\ell_n} \eta_n dx_n\right] = - I_{mi} \sum_{j=1}^{4} g_{ji}(x_i) \ddot{\psi}_j(t)$$

$$- c_i \sum_{j=1}^{4} g_{ji}(x_i) \dot{\psi}_j(t) + \frac{\overset{*}{w}_i b}{H_w}\left(\frac{E_c A_c}{L_E}\right)\left(\frac{b}{2}\right) \sum_{n=1}^{3} \frac{\overset{*}{w}_n \ell_n}{2H_w}[\psi_{n+1}(t) + \psi_n(t)]$$

$$- \frac{\overset{*}{w}_i b}{H_w}\left(\frac{E_c A_c}{L_E}\right)\left(\frac{b}{2}\right)[\phi_4(t) - \phi_1(t)] \quad , \qquad i=1,2,3 \tag{3.16}$$

and the boundary conditions upon the vibrational response $\eta_i(x_i,t)$ become homogeneous, that is

$$\eta_i(0,t) = \eta_i(\ell_i,t) = 0$$

$$\eta_i''(0,t) = \eta_i''(\ell_i,t) = 0 \quad , \qquad i=1,2,3. \tag{3.17}$$

Note that the equation governing the torsional vibrational response (Eq. 3.16) is excited by rocking ground motion acceleration, velocity, and displacement terms at each support point, as well as torsional ground motion displacements at the anchorages. Although, as indicated by Baron,

et al [3], the contribution from velocity terms is often small when compared to the displacement and acceleration terms, the velocity terms are included in this analysis for completeness.

III.6. EIGENVALUE PROBLEM - FREE VIBRATIONS

The solution to Eq. 3.16 is obtained by modal superposition, that is the vibrational displacement is taken to be

$$\eta_i(x_i,t) = \sum_{n=1}^{\infty} \Theta_{ni}(x_i) q_n(t) \quad , \qquad i=1,2,3. \tag{3.18}$$

where $\Theta_{ni}(x_i)$ is the n^{th} torsional vibration mode shape in the i^{th} span of the bridge and $q_n(t)$ is the n^{th} generalized coordinate. The mode shapes and their associated natural frequencies are derived from Eqs. 3.16. With damping and forcing terms set to zero, Eqs. 3.16 become

$$I_{mi} \frac{\partial^2 \eta_i}{\partial t^2} + E_i \Gamma_i \frac{\partial^4 \eta_i}{\partial x_i^4} - \left(G_i J_i + H_w \frac{b^2}{2}\right) \frac{\partial^2 \eta_i}{\partial x_i^2}$$

$$+ \frac{\overset{*}{w}_i b}{H_w} \left[\left(\frac{E_c A_c}{L_E} \right) \left(\frac{b}{2} \right) \sum_{n=1}^{3} \frac{\overset{*}{w}_n}{H_w} \int_0^{\ell_n} \eta_n(x_n,t)\, dx_n \right] = 0 \qquad i=1,2,3. \tag{3.19}$$

The n^{th} torsional mode shape and natural frequency, ω_n, is obtained by assuming the vibration to be sinusoidal, that is

$$\eta_j(x_j,t) = \Theta_{nj}(x_j) \exp(i\omega_n t) \qquad \begin{matrix} j=1,2,3. \\ n=1,2,3... \end{matrix} \tag{3.20}$$

in which $i = \sqrt{-1}$.

Substituting Eqs. 3.20 into Eq. 3.19 results in

$$E_i \Gamma_i \frac{d^4 \Theta_{ni}}{dx_i^4} - \left(G_i J_i + H_w \frac{b^2}{2}\right) \frac{d^2 \Theta_{ni}}{dx_i^2} - I_{mi} \omega_n^2 \Theta_{ni} + \frac{\overset{*}{w}_i b}{H_w} \tilde{H}_n = 0 \tag{3.21}$$

$$\begin{matrix} i=1,2,3 \\ n=1,2,3... \end{matrix}$$

where the additional horizontal cable tension associated with the n^{th} torsional mode shape, $\tilde{H}_n$, is given by

$$\tilde{H}_n = \frac{E_c A_c}{L_E}\left(\frac{b}{2}\right) \sum_{j=1}^{3} \frac{\overset{*}{w}_j}{H_w} \int_0^{\ell_j} \Theta_{nj}(x_j)\,dx_j \qquad n=1,2,3... \tag{3.22}$$

The boundary conditions for each torsional mode shape become similar to Eqs. 3.17, that is

$$\left.\begin{aligned} \Theta_{ni}(0) &= \Theta_{ni}(\ell_i) = 0 \\ \Theta''_{ni}(0) &= \Theta''_{ni}(\ell_i) = 0 \end{aligned}\right\} \qquad \begin{matrix} i=1,2,3. \\ n=1,2,3... \end{matrix} \tag{3.23}$$

Because $\tilde{H}_n$ is independent of x_j and may be treated as a constant, Eqs. 3.21 represent linear, ordinary differential equations of fourth order with constant coefficients. The general solution of Eqs. 3.21 can be expressed as

$$\Theta_{ni}(x_i) = A_i \sin\left(\frac{\mu_i x_i}{\ell_i}\right) + B_i \cos\left(\frac{\mu_i x_i}{\ell_i}\right) + C_i \sinh\left(\frac{\nu_i x_i}{\ell_i}\right)$$

$$+ D_i \cosh\left(\frac{\nu_i x_i}{\ell_i}\right) + \frac{\overset{*}{w}_i b \tilde{H}_n}{I_{mi} H_w \omega_n^2} \qquad \begin{matrix} i=1,2,3. \\ n=1,2,3... \end{matrix} \tag{3.24}$$

where

$$\mu_i = \delta_i \sqrt{\frac{Z_i - 1}{2}}$$

$$\nu_i = \delta_i \sqrt{\frac{Z_i + 1}{2}}$$

$$Z_i = \sqrt{1 + \frac{4I_{mi}\ell_i^2\omega_n^2}{\delta_i^2\left(G_iJ_i + H_w\frac{b^2}{2}\right)}}$$

$$\delta_i = \ell_i\sqrt{\frac{G_iJ_i + H_w\frac{b^2}{2}}{E_i\Gamma_i}} \qquad \begin{matrix} i=1,2,3 \\ n=1,2,3... \end{matrix} \qquad (3.25)$$

and A_i, B_i, C_i, and D_i are arbitrary constants which are determined in conformity with the boundary conditions (Eqs. 3.23).

At this point, it is convenient to separate the investigation of the symmetric torsional modes from that of the antisymmetric torsional modes, that is, the problem can be divided into two parts:

1. The symmetric torsional modes of vibration in which there are an even number of internal nodes along the center span. Here the additional cable tension, $\tilde{H}_n$, is nonzero, that is, the center and side spans are coupled through the vibration of the cable.
2. The antisymmetric torsional modes of vibration which result in an odd number of internal nodes along the center span. Here the additional cable tension, $\tilde{H}_n$, is zero, that is, there is no interaction between the center span and side spans.

The symmetric torsional modes are of the form (see Appendix III-b for details):

$$\Theta_{ni}(x_i) = \frac{\overset{*}{w}_i b\tilde{H}_n}{2I_{mi}H_wZ_i\omega_n^2}\left\{2Z_i - \frac{Z_i + 1}{\cos(\mu_i/2)}\cos\left[\mu_i\left(\frac{1}{2} - \frac{x_i}{\ell_i}\right)\right]\right.$$

$$\left. - \frac{Z_i - 1}{\cosh(\nu_i/2)}\cosh\left[\nu_i\left(\frac{1}{2} - \frac{x_i}{\ell_i}\right)\right]\right\} \qquad \begin{matrix} i=1,2,3 \\ n=1,2,3... \end{matrix} \qquad (3.26)$$

where the natural circular frequencies, ω_n, are determined by satisfying the transcendental equation

$$\frac{L_E}{E_c A_c} = \sum_{i=1}^{3} \left\{ \left(\frac{\overset{*}{w}_i}{H_w}\right)^2 \left(\frac{b^2}{2}\right) \left(\frac{\ell_i}{I_{mi} Z_i \omega_n^2}\right) \left[Z_i - \frac{Z_i + 1}{\mu_i} \tan\left(\frac{\mu_i}{2}\right) \right.\right.$$

$$\left.\left. - \frac{Z_i - 1}{\nu_i} \tanh\left(\frac{\nu_i}{2}\right) \right] \right\} \tag{3.27}$$

It should be noted that the amplitudes of the symmetric torsional modes in Eq. 3.26 are arbitrary. In this report, the modes are normalized so that their highest ordinate has a unit magnitude.

The antisymmetric torsional modes of vibration involving the center span are (Appendix III-b):

$$\Theta_{m2}(x_2) = \sin\left(\frac{m\pi x_2}{\ell_2}\right) \qquad m=2,4,6... \tag{3.28}$$

having associated natural circular frequencies

$$\omega_{2m} = \left(\frac{m\pi}{\ell_2}\right)^2 \sqrt{\frac{E_2 \Gamma_2}{I_{m2}} + \frac{\left(G_2 J_2 + H_w \frac{b^2}{2}\right) \ell_2^2}{I_{m2} m^2 \pi^2}} \qquad m=2,4,6... \tag{3.29}$$

The antisymmetric torsional modes of vibration involving the side spans are (Appendix III-b):

$$\Theta_{mj}(x_j) = \sin\left(\frac{m\pi x_j}{\ell_j}\right) \qquad \begin{matrix} j=1,3. \\ m=1,2,3... \end{matrix} \tag{3.30}$$

having associated natural circular frequencies

$$\omega_{jm} = \left(\frac{m\pi}{\ell_j}\right)^2 \sqrt{\frac{E_j\Gamma_j}{I_{mj}} + \frac{\left(G_jJ_j + H_w\frac{b^2}{2}\right)\ell_j^2}{I_{mj}m^2\pi^2}} \qquad \begin{matrix} j=1,3 \\ m=1,2,3... \end{matrix} \qquad (3.31)$$

III.7. MODAL SOLUTIONS - FORCED VIBRATIONS

Substituting Eqs. 3.18 into Eqs. 3.16 results in

$$I_{mi}\sum_{n=1}^{\infty}\Theta_{ni}(x_i)\ddot{q}_n(t) + c_i\sum_{n=1}^{\infty}\Theta_{ni}(x_i)\dot{q}_n(t) + E_i\Gamma_i\sum_{n=1}^{\infty}\Theta_{ni}^{IV}(x_i)q_n(t)$$

$$- \left(G_iJ_i + H_w\frac{b^2}{2}\right)\sum_{n=1}^{\infty}\Theta_{ni}''(x_i)q_n(t)$$

$$+ \frac{\overset{*}{w}_i b}{H_w}\left(\frac{E_cA_c}{L_E}\right)\left(\frac{b}{2}\right)\sum_{j=1}^{3}\left\{\frac{\overset{*}{w}_j}{H_w}\int_0^{\ell_j}\left[\sum_{n=1}^{\infty}\Theta_{nj}(x_j)q_n(t)\right]dx_j\right\}$$

$$= -I_{mi}\sum_{j=1}^{4}g_{ji}(x_i)\ddot{\psi}_j(t) - c_i\sum_{j=1}^{4}g_{ji}(x_i)\dot{\psi}_j(t)$$

$$+ \frac{\overset{*}{w}_i b}{H_w}\left(\frac{E_cA_c}{L_E}\right)\left(\frac{b}{2}\right)\sum_{n=1}^{3}\frac{\overset{*}{w}_n\ell_n}{2H_w}[\psi_{n+1}(t) + \psi_n(t)]$$

$$- \frac{\overset{*}{w}_i b}{H_w}\left(\frac{E_cA_c}{L_E}\right)\left(\frac{b}{2}\right)[\phi_4(t) - \phi_1(t)] \qquad i=1,2,3 \qquad (3.32)$$

Using Eqs. 3.21 and 3.22, the previous equation can be simplified to

$$I_{mi}\sum_{n=1}^{\infty}\Theta_{ni}(x_i)\ddot{q}_n(t) + c_i\sum_{n=1}^{\infty}\Theta_{ni}(x_i)\dot{q}_n(t)$$

$$+ I_{mi}\sum_{n=1}^{\infty}\omega_n^2\Theta_{ni}(x_i)q_n(t) = -I_{mi}\sum_{j=1}^{4}g_{ji}(x_i)\ddot{\psi}_j(t)$$

$$- c_i \sum_{j=1}^{4} g_{ji}(x_i)\dot{\psi}_j(t) + \frac{\overset{*}{w}_i b}{H_w}\left(\frac{E_c A_c}{L_E}\right)\left(\frac{b}{2}\right) \sum_{n=1}^{3} \frac{\overset{*}{w}_n \ell_n}{2H_w}[\psi_{n+1}(t) + \psi_n(t)]$$

$$- \frac{\overset{*}{w}_i b}{H_w}\left(\frac{E_c A_c}{L_E}\right)\left(\frac{b}{2}\right)[\phi_4(t) - \phi_1(t)] \qquad i=1,2,3. \qquad (3.33)$$

Now, multiplying Eqs. 3.33 by $\Theta_{mi}(x_i)$, integrating over the i^{th} span (from zero to ℓ_i) and summing over all three spans (i = 1,2,3) gives the equation governing the response of the n^{th} generalized coordinate

$$\ddot{q}_n(t) + 2\zeta_n\omega_n\dot{q}_n(t) + \omega_n^2 q_n(t) = - \sum_{j=1}^{4} R_{jn}\ddot{\psi}_j(t)$$

$$- 2\zeta_n\omega_n \sum_{j=1}^{4} R_{jn}\dot{\psi}_j(t) + P_n\alpha \sum_{i=1}^{3} \beta_i[\psi_{i+1}(t) + \psi_i(t)]$$

$$- P_n\alpha[\phi_4(t) - \phi_1(t)] \qquad n=1,2,3... \qquad (3.34)$$

where ζ_n is the damping ratio of the n^{th} torsional mode:

$$\alpha = \frac{E_c A_c g}{L_E H_w} \qquad (3.35)$$

$$\beta_i = \frac{\overset{*}{w}_i \ell_i}{2H_w} \qquad i=1,2,3 \qquad (3.36)$$

and R_{jn} and P_n are modal participation coefficients given by

$$R_{jn} = \frac{\left[\sum_{i=1}^{3} I_{mi} \int_0^{\ell_i} g_{ji}(x_i)\Theta_{ni}(x_i)\,dx_i\right]}{\left[\sum_{i=1}^{3} I_{mi} \int_0^{\ell_i} \Theta_{ni}^2(x_i)\,dx_i\right]} \qquad \begin{matrix} j=1,2,3,4. \\ n=1,2,3... \end{matrix} \qquad (3.37)$$

$$P_n = \frac{\frac{b^2}{2}\left[\sum_{i=1}^{3} \frac{\overset{*}{w}_i}{g} \int_0^{\ell_i} \Theta_{ni}(x_i)\,dx_i\right]}{\left[\sum_{i=1}^{3} I_{mi} \int_0^{\ell_i} \Theta_{ni}^2(x_i)\,dx_i\right]} \qquad n=1,2,3... \qquad (3.38)$$

where g is the gravitational acceleration constant. Note that in the derivation of Eq. 3.34, modal orthogonality was utilized (the details appear in Appendix III-c), that is

$$\sum_{i=1}^{3} I_{mi} \int_0^{\ell_i} \Theta_{ni}(x_i)\Theta_{mi}(x_i)\,dx_i = 0 \qquad \text{for } m \neq n \qquad (3.39)$$

The solution to Eq. 3.34, assuming quiescent initial conditions, is given by the convolution integral

$$q_n(t) = \frac{1}{\omega_{nd}} \int_0^t \left\{\left[-2\zeta_n\omega_n \sum_{j=1}^{4} R_{jn}\dot{\psi}_j(\tau)\right] - \left[\sum_{j=1}^{4} R_{jn}\ddot{\psi}_j(\tau)\right]\right.$$

$$\left. + \left[P_n\alpha \sum_{i=1}^{3} \beta_i\{\psi_{i+1}(\tau) + \psi_i(\tau)\}\right] - P_n\alpha[\phi_4(\tau) - \phi_1(\tau)\right\} \cdot$$

$$\cdot \left\{e^{-\zeta_n\omega_n(t-\tau)} \sin \omega_{nd}(t-\tau)\right\} \qquad n=1,2,3... \qquad (3.40)$$

where ω_{nd} is the damped natural circular frequency of the n^{th} torsional vibration mode given by

$$\omega_{nd} = \omega_n \sqrt{1 - \zeta_n^2} \quad , \qquad n=1,2,3... \qquad (3.41)$$

The total torsional response is obtained as the sum of quasi-static and relative responses, that is

$$\Theta_i(x_i,t) = \sum_{j=1}^{4} g_{ji}(x_i)\psi_j(t) + \sum_{n=1}^{\infty} \Theta_{ni}(x_i)q_n(t) \quad , \quad i=1,2,3. \qquad (3.42)$$

III.8. FREQUENCY-DOMAIN - RANDOM VIBRATION APPROACH

The frequency domain is utilized to study the torsional vibration. For the six rotational ground motion inputs, there are six complex frequency response functions. To determine these functions, each $\psi_j(t)$, $(j = 1,2,3,4)$, and each $\phi_k(t)$, $(k = 1,4)$ is taken equal to $\exp(i\omega t)$, where $i = \sqrt{-1}$, and the response of the n^{th} generalized coordinate excited by the j^{th} and k^{th} input motions are assumed to be of the form

$$q_{nj}(t) = H_{nj}(\omega)\exp(i\omega t) \qquad j=1,2,3,4,$$
$$q_{nk}(t) = H_{nk}(\omega)\exp(i\omega t) \qquad k=1,4 \qquad n=1,2,3... \tag{3.43}$$

Where H_{nj} is the n^{th} complex frequency response due to input rocking rotation $\psi_j(t)$ at the support (see Fig. III-4) and H_{nk} is the n^{th} complex frequency response due to input torsional rotation $\phi_k(t)$ at the support (see Fig. III-4). Now substituting Eq. 3.43 into Eq. 3.34 yields

$$H_{nj}(\omega) = \frac{\left[(R_{jn}\omega^2 + \gamma_j P_n \alpha) - i(2\zeta_n \omega_n \omega R_{jn})\right]}{\left[(\omega_n^2 - \omega^2) + i(2\zeta_n \omega_n \omega)\right]} \qquad j=1,2,3,4 \quad n=1,2,3... \tag{3.44}$$

$$H_{nk}(\omega) = \frac{\pm P_n \alpha}{\left[(\omega_n^2 - \omega^2) + i(2\zeta_n \omega_n \omega)\right]} \qquad k=1(+),\ k=4(-) \quad n=1,2,3... \tag{3.45}$$

where

$$\gamma_1 = \beta_1 = \frac{\overset{*}{w}_1 \ell_1}{2H_w}$$

$$\gamma_2 = \beta_1 + \beta_2 = \frac{\overset{*}{w}_1 \ell_1}{2H_w} + \frac{\overset{*}{w}_2 \ell_2}{2H_w}$$

$$\gamma_3 = \beta_2 + \beta_3 = \frac{\overset{*}{w}_2 \ell_2}{2H_w} + \frac{\overset{*}{w}_3 \ell_3}{2H_w}$$

$$\gamma_4 = \beta_3 = \frac{\overset{*}{w}_3 \ell_3}{2H_w} \tag{3.46}$$

Taking the finite Fourier transform of Eqs. 3.18 over the duration of the ground displacement, T_1, yields the Fourier transform of the vibrational response

$$\Lambda(x_i,\omega) = \int_0^{T_1} \eta_i(x_i,t) e^{-i\omega t}\, dt$$

$$= \sum_{n=1}^{\infty} \Theta_{ni}(x_i) Q_n(\omega) \quad , \qquad i=1,2,3 \tag{3.47}$$

where $Q_n(\omega)$ is the finite Fourier transform of the generalized coordinate $q_n(t)$ given by

$$Q_n(\omega) = \int_0^{T_1} q_n(t) e^{-i\omega t}\, dt \quad , \qquad n=1,2,3... \tag{3.48}$$

A similar Fourier transformation of Eq. 3.34 yields

$$-\omega^2 Q_n(\omega) + 2i\zeta_n \omega_n \omega Q_n(\omega) + \omega_n^2 Q_n(\omega) = \sum_{j=1}^{6} \tilde{\Psi}_{jn}(\omega) \quad , \quad n=1,2,3... \tag{3.49}$$

where $\tilde{\Psi}_{jn}(\omega)$ is given by

$$\tilde{\Psi}_{jn}(\omega) = [(R_{jn}\omega^2 + \gamma_j P_n \alpha) - i(2\zeta_n \omega_n \omega R_{jn})]\Psi_j(\omega) \qquad \begin{matrix} j=1,2,3,4. \\ n=1,2,3... \end{matrix} \tag{3.50}$$

$$\begin{aligned} \tilde{\Psi}_{5n}(\omega) &= + P_n \alpha \Phi_1(\omega) \\ \tilde{\Psi}_{6n}(\omega) &= - P_n \alpha \Phi_4(\omega) \end{aligned} \qquad n=1,2,3... \tag{3.51}$$

in which $\Psi_j(\omega)$ is the finite Fourier transform of the ground motion rocking inputs $\psi_j(t)$, $(j = 1,2,3,4)$, and $\Phi_j(\omega)$ is the finite Fourier transform of the ground motion torsion inputs $\phi_j(t)$, $(j = 1,4)$, given by

$$\Psi_j(\omega) = \int_0^{T_1} \psi_j(t) e^{-i\omega t}\, dt \quad , \quad j=1,2,3,4$$

$$\Phi_j(\omega) = \int_0^{T_1} \phi_j(t) e^{-i\omega t}\, dt \quad , \quad j=1,4 \tag{3.52}$$

It follows from Eqs. 3.44, 3.45, 3.49, 3.50, and 3.51 that the Fourier transform of the generalized coordinate can be expressed as

$$Q_n(\omega) = \{H_n(\omega)\}^T \{\Psi(\omega)\} \quad , \quad n=1,2,3... \tag{3.53}$$

where $\{H_n(\omega)\}^T$ denotes the transposed complex frequency response vector given by

$$\{H_n(\omega)\}^T = \{H_{n1}(\omega)\ H_{n2}(\omega)\ H_{n3}(\omega)\ H_{n4}(\omega)\ H_{n5}(\omega)\ H_{n6}(\omega)\} \quad , \quad n=1,2,3... \tag{3.54}$$

and $\{\Psi(\omega)\}$ is the Fourier transform vector of rotational ground motion inputs given by

$$\{\Psi(\omega)\} = \begin{Bmatrix} \Psi_1(\omega) \\ \Psi_2(\omega) \\ \Psi_3(\omega) \\ \Psi_4(\omega) \\ \Phi_1(\omega) \\ \Phi_4(\omega) \end{Bmatrix} \tag{3.55}$$

Now substituting Eq. 3.53 into Eq. 3.47 enables the Fourier transform of the vibrational response to be expressed as

$$\Lambda(x_i,\omega) = \sum_{n=1}^{\infty} \Theta_{ni}(x_i)\{H_n(\omega)\}^T\{\Psi(\omega)\} \qquad , \quad i=1,2,3. \tag{3.56}$$

The power spectral density of the relative (or vibrational) response is given by

$$G_\eta(x_i,\omega) = \lim_{T_1\to\infty} \frac{2}{T_1} E[\overset{*}{\Lambda}(x_i,\omega)\,\Lambda(x_i,\omega)] \qquad i=1,2,3 \tag{3.57}$$

where $E[\cdot]$ represents the expected value of the term inside the brackets, and the superposed asterisk denotes complex conjugate. An estimate of G_η can be obtained by simply omitting the limiting and expectation operations in Eq. 3.57, hence

$$G_\eta(x_i,\omega) \simeq \frac{2}{T_1} \overset{*}{\Lambda}(x_i,\omega)\Lambda(x_i,\omega), \qquad i=1,2,3, \tag{3.58}$$

Substituting Eq. 3.56 into Eq. 3.58 yields

$$G_\eta(x_i,\omega) = \sum_{n=1}^{\infty}\sum_{m=1}^{\infty} \Theta_{ni}(x_i)\Theta_{mi}(x_i)\{\overset{*}{H}_n(\omega)\}^T[G_{ff}(\omega)]\{H_m(\omega)\} \qquad i=1,2,3 \tag{3.59}$$

where any element of the 6x6 spectral matrix of correlated rotational ground motion displacement inputs $[G_{ff}(\omega)]$ is defined by

$$[G_{ff}(\omega)] = \lim_{T_1\to\infty} \frac{2}{T_1} E[\{\overset{*}{\Psi}(\omega)\}^T\{\Psi(\omega)\}]$$

$$\simeq \frac{2}{T_1} \{\overset{*}{\Psi}(\omega)\}^T\{\Psi(\omega)\} \tag{3.60}$$

The diagonal elements of the matrix $[G_{ff}(\omega)]$, $i = j$ in Eq. 3.60, correspond to the power spectral density of the j^{th} rotational displacement inputs $\psi_j(t)$, $(j = 1,2,3,4)$, and $\phi_1(t)$, $\phi_4(t)$, while the off-diagonal elements of the matrix $[G_{ff}(\omega)]$ correspond to cross-spectral densities between the various rotational ground motion displacement inputs. These cross-spectral terms are present because the various ground motions originate from the same source and are therefore related in some way, so that their correlation (or interaction) must be taken into account. The effect of input correlation upon the torsional response may be examined quite easily using Eq. 3.59. If the inputs are assumed to be uncorrelated, that is, independently applied and unrelated, Eq. 3.59 reduces to

$$G_\eta(x_i,\omega) = \sum_{n=1}^{\infty} \sum_{m=1}^{\infty} \Theta_{ni}(x_i)\Theta_{mi}(x_i)\left[\sum_{j=1}^{6} \left(H^*_{nj}(\omega)\right)\left(H_{mj}(\omega)\right)G_j(\omega)\right] \qquad i=1,2,3 \tag{3.61}$$

in which $G_j(\omega)$ is the power spectral density of the rotational ground motion input $\psi_j(t)$ which is estimated as

$$G_j(\omega) \simeq \frac{2}{T_1}\left|\Psi_j(\omega)\right|^2 \qquad j=1,2,3,4$$

$$G_j(\omega) \simeq \frac{2}{T_1}\left|\Phi_1(\omega)\right|^2 \qquad j=5$$

$$G_j(\omega) \simeq \frac{2}{T_1}\left|\Phi_4(\omega)\right|^2 \qquad j=6 \tag{3.62}$$

The results of Eq. 3.59 can be compared to those of Eq. 3.61 in order to gain a better understanding of the effects of input correlation upon the response calculations.

The second characteristic feature of Eq. 3.59 involves the double summation over the torsional modes and their associated complex frequency response functions. It should be noted that the complex frequency response functions $H_{nj}(\omega)$ peak in amplitude at their associated natural frequencies ω_n, and have much lower amplitudes elsewhere along the frequency band. Therefore, when the natural frequencies of torsional vibration are well separated and damping ratios are small, the effect of the cross-terms $(n \neq m)$ in Eq. 3.59 becomes much less significant than the diagonal terms $(n = m)$ [6]. Under these circumstances, the double summation may be replaced by a single sum, that is

$$G_\eta(x_i,\omega) = \sum_{n=1}^{\infty} \theta_{ni}^2(x_i)\{\overset{*}{H}_n(\omega)\}[G_{ff}(\omega)]\{H_n(\omega)\} \quad , \qquad i=1,2,3. \tag{3.63}$$

However, due to the flexible nature of the suspension bridge, closely-spaced modes are quite likely to occur. Under such circumstances, the effect of the cross terms are no longer negligible, and an accurate representation of the response would have to include these modal interaction terms. For the purpose of this report, Eq. 3.59 is utilized, that is, the effects of modal interaction are incorporated through a double summation.

The mean square value of the relative torsional response, $\psi_\eta^2(x_i)$ is given by the integration of G_η over the entire frequency range

$$\psi_\eta^2(x_i) = \frac{1}{2\pi}\int_0^\infty G_\eta(x_i,\omega)\,d\omega \qquad\qquad i=1,2,3 \tag{3.64}$$

and the square root of Eq. 3.64 is the root mean square (R.M.S.) vibrational response.

The power spectral density of the total torsional displacement response can be obtained by multiplying the Fourier transform of Eq. 3.10 by its complex conjugate and by $(2/T_1)$, which leads to

$$G_\theta(x_i,\omega) = G_\eta(x_i,\omega) + \sum_{j=1}^{4} [G_{\eta j}(x_i,\omega) + G_{j\eta}(x_i,\omega)]\, g_{ji}(x_i) + \sum_{j=1}^{4}\sum_{k=1}^{4} g_{ji}(x_i)\, g_{ki}(x_i)\, [G_{jk}(\omega)] \quad , \quad i=1,2,3 \tag{3.65}$$

where

$$G_{\eta j}(x_i,\omega) = \frac{2}{T_1} \overset{*}{\Lambda}(x_i,\omega)\, \Psi_j(\omega)$$

$$= \frac{2}{T_1} \sum_{n=1}^{\infty} \Theta_{ni}(x_i) \{\overset{*}{H}_n(\omega)\}^T \{\overset{*}{\Psi}(\omega)\} \Psi_j(\omega), \qquad \begin{matrix} i=1,2,3 \\ j=1,2,3,4. \end{matrix} \tag{3.66}$$

and

$$G_{j\eta}(x_i,\omega) = \frac{2}{T_1} \overset{*}{\Psi}_j(\omega)\, \Lambda(x_i,\omega)$$

$$= \frac{2}{T_1} \sum_{n=1}^{\infty} \Theta_{ni}(x_i) \overset{*}{\Psi}_j(\omega) \{H_n(\omega)\}^T \{\Psi(\omega)\} \quad , \quad \begin{matrix} i=1,2,3 \\ j=1,2,3,4 \end{matrix} \tag{3.67}$$

For the uncorrelated case, $G_{\eta j}$ and $G_{j\eta}$ reduce to

$$G_{\eta j}(x_i,\omega) = \sum_{n=1}^{\infty} \Theta_{ni}(x_i) [\overset{*}{H}_{nj}(\omega)]\, [G_j(\omega)] \quad , \quad \begin{matrix} i=1,2,3 \\ j=1,2,3,4 \end{matrix} \tag{3.68}$$

$$G_{j\eta}(x_i,\omega) = \sum_{n=1}^{\infty} \Theta_{ni}(x_i) [H_{nj}(\omega)]\, [G_j(\omega)] \quad , \quad \begin{matrix} i=1,2,3 \\ j=1,2,3,4 \end{matrix} \tag{3.69}$$

where $H_{nj}(\omega)$ is given by Eq. 3.44 and $G_j(\omega)$ is given by Eq. 3.63. In addition, the cross-spectral terms $G_{jk}(\omega)$, $(j \neq k)$, are equal to zero in Eq. 3.65 for the uncorrelated case.

The integration of G_θ over the frequency domain provides the mean square torsional response, $\psi^2_\theta(x_i)$, whose square root defines the root mean square (R.M.S.) torsional response

$$\psi^2_\theta(x_i) = \frac{1}{2\pi}\int_0^\infty G_\theta(x_i,\omega)\,d\omega$$

$$= \psi^2_\eta(x_i) + \sum_{j=1}^{4} g_{ji}(x_i)\left[\psi^2_{\eta j}(x_i)\right]$$

$$+ \sum_{j=1}^{4}\sum_{k=1}^{4} g_{ji}(x_i)\,g_{ki}(x_i)\left[\psi^2_{jk}(x_i)\right] \quad , \quad i=1,2,3 \qquad (3.70)$$

where $\psi^2_\eta(x_i)$ is given by Eq. 3.64, and

$$\psi^2_{\eta j}(x_i) = \frac{1}{2\pi}\int_0^\infty [G_{\eta j}(x_i,\omega) + G_{j\eta}(x_i,\omega)]\,d\omega \quad , \quad \begin{matrix} i=1,2,3 \\ j=1,2,3,4 \end{matrix} \qquad (3.71)$$

$$\psi^2_{jk}(x_i) = \frac{1}{2\pi}\int_0^\infty [G_{jk}(\omega)]\,d\omega \quad , \quad \begin{matrix} i=1,2,3 \\ j,k=1,2,3,4 \end{matrix} \qquad (3.72)$$

III.9. ADDITIONAL HORIZONTAL COMPONENT OF CABLE TENSION H(t)

The additional horizontal component of cable tension due to multiple support torsional excitations is given by (Eq. 3.9)

$$H(t) = \left(\frac{E_c A_c}{L_E}\right)\left(\frac{b}{2}\right)\left\{\sum_{i=1}^{3}\left[\frac{\overset{*}{w}_i}{H_w}\int_0^{\ell_i}\theta_i\,dx_i - \frac{\overset{*}{w}_i \ell_i}{2H_w}\left\{\psi_{i+1}(t) + \psi_i(t)\right\}\right]\right.$$

$$\left. + \left[\phi_4(t) - \phi_1(t)\right]\right\} \qquad (3.73)$$

Substituting Eq. 3.42 into Eq. 3.73 results in

$$H(t) = \left(\frac{E_c A_c}{L_E}\right)\left(\frac{b}{2}\right)\left\{\sum_{i=1}^{3}\left[\frac{w_i^*}{H_w}\left\{\int_0^{\ell_i}\sum_{n=1}^{\infty}\Theta_{ni}(x_i)\,dx_i\right\}q_n(t)\right.\right.$$

$$+\frac{w_i^*}{H_w}\sum_{j=1}^{4}\left\{\int_0^{\ell_i} g_{ji}(x_i)\,dx_i\right\}\psi_j(t)$$

$$\left.\left.-\frac{w_i^*\ell_i}{2H_w}\left\{\psi_{i+1}(t)+\psi_i(t)\right\}\right]+\left[\phi_4(t)-\phi_1(t)\right]\right\} \qquad (3.74)$$

where the generalized coordinates $q_n(t)$ are obtained by the convolution integral of Eq. 3.40.

In order to analyze the cable tension in the frequency domain, the finite Fourier transform of Eq. 3.74 becomes

$$H(\omega) = \left(\frac{E_c A_c}{L_E}\right)\left(\frac{b}{2}\right)\left\{\sum_{i=1}^{3}\left[\frac{w_i^*}{H_w}\left\{\int_0^{\ell_i}\sum_{n=1}^{\infty}\Theta_{ni}(x_i)\,dx_i\right\}Q_n(\omega)\right.\right.$$

$$+\frac{w_i^*}{H_w}\sum_{j=1}^{4}\left\{\int_0^{\ell_i} g_{ji}(x_i)\,dx_i\right\}\Psi_j(\omega)$$

$$\left.\left.-\frac{w_i^*\ell_i}{2H_w}\left\{\Psi_{i+1}(\omega)+\Psi_i(\omega)\right\}\right]+\left[\Phi_4(\omega)-\Phi_1(\omega)\right]\right\} \qquad (3.75)$$

where $\Psi_j(\omega)$, $(j = 1,2,3,4)$ is the finite Fourier transform of the rocking input ground motions (Eq. 3.52), $\Phi_j(\omega)$, $(j = 1,4)$ is the finite Fourier transform of the torsional input ground motions (Eq. 3.52), and $Q_n(\omega)$ is the Fourier transform of the n^{th} generalized coordinate, calculated as

$$Q_n(\omega) = \{H_n(\omega)\}^T\{\Psi(\omega)\} \quad , \qquad n=1,2,3... \tag{3.76}$$

where $\{H_n(\omega)\}^T$ is the transposed frequency response vector corresponding to the n^{th} torsional vibration mode, and $\{\Psi(\omega)\}$ is the Fourier transform vector of the rotational ground motion inputs (see Eqs. 3.54, 3.55). Note that for antisymmetric torsional vibration, the first term in Eq. 3.75 vanishes, since the additional cable tension associated with an antisymmetric torsional vibration mode is equal to zero (see Appendix III-b).

The power spectrum of $H(t)$ may be approximated as

$$G_H(\omega) \simeq \frac{2}{T_1} \overset{*}{H}(\omega) H(\omega) \tag{3.77}$$

where T_1 is the duration of the ground motion and the superposed asterisk denotes complex conjugate. Substituting Eqs. 3.75 and 3.76 into Eq. 3.77 results in an explicit expression for $G_H(\omega)$, (the details are found in Appendix III-d). For the uncorrelated calculation, only the terms which involve the input power spectra are retained, since the rotational support motions are assumed to be unrelated in this case, while the correlated case retains all of its terms (including cross-spectra).

Mean square dynamically-induced cable tensions are obtained by integrating $G_H(\omega)$ over the entire frequency range, that is

$$\psi_H^2 = \frac{1}{2\pi} \int_0^\infty G_H(\omega)\, d\omega \tag{3.78}$$

and the square root of Eq. 3.78 is the root mean square (R.M.S.) additional horizontal component of cable tension due to torsional vibration.

II.10 DEFINITION OF TORSIONAL AND ROCKING GROUND MOTION INPUTS

In order to implement the analysis presented in this chapter, appropriate rotational (rocking and torsional) seismic inputs are required at the bridge's support points (Figs. III-1 to III-4). Because currently available strong motion accelerographs only record the three orthogonal translational components of ground motion, the rotational inputs can at best be only estimated. This section presents a simplified approach, based upon wave propagation theory, toward defining reasonable rotational ground motion inputs from recorded translational ground motion records. The method developed in this section is applied to the 1979 El Centro translational records of Arrays No. 4, 5, 6, 7, and 8 (see Appendix II-e) in order to develop rotational inputs to the bridge. The main assumptions are as follows [10,11]:

1. The vertical component of ground motion is assumed to be the result of an SV wave approaching from the epicenter and striking the ground surface at an incidence angle $\theta_0 = 45°$. This wave motion results in the rocking (vertical rotation about a horizontal axis parallel to the longitudinal axis of the bridge) input.
2. The horizontal components of ground motion are assumed to be the result of the superposition of two independent SH waves propagating along two perpendicular directions. The total torsional (horizontal rotation about a vertical axis) input is the sum of the torsional effect due to each wave.
3. The wavelengths of the seismic waves are long compared to the in-plane dimensions of the anchorages and piers. Thus each foundation can be assumed to rotate as a point.

Consider an SV wave propagating from the earthquake's epicenter toward the recording site and striking the ground surface at an incidence angle $\theta_0 = 45°$ as shown in Fig. III-5(a). Under these conditions, the incident SV wave reflects as an in-phase SV wave (a Lame reflection mode), and the resulting horizontal and vertical soil particle motions become

$$u_x = A_0 \cos\theta_0 \left\{\exp[i\kappa_0(x \sin\theta_0 - z \cos\theta_0 - c_s t)] - \exp[i\kappa_0(x \sin\theta_0 + z \cos\theta_0 - c_s t)]\right\} \tag{3.79}$$

and

$$u_z = A_0 \sin\theta_0 \left\{\exp[i\kappa_0(x \sin\theta_0 - z \cos\theta_0 - c_s t)] + \exp[i\kappa_0(x \sin\theta_0 + z \cos\theta_0 - c_s t)]\right\} \tag{3.80}$$

where c_s is the shear wave velocity, $i = \sqrt{-1}$, θ_0 is the incidence angle ($\theta_0 = 45°$), and κ_0 is the wave number defined by

$$\kappa_0 = \frac{\omega}{c_s} \tag{3.81}$$

where ω is the circular frequency of the incident waves.

From Eqs. 3.79 and 3.80, the horizontal and vertical displacement components at the ground surface ($z = 0$) become

$$u_x\Big|_{z=0} = 0 \tag{3.81}$$

$$u_z\Big|_{z=0} = 2A_0 \sin\theta_0 \left\{\exp[i\kappa_0(x \sin\theta_0 - c_s t)]\right\} \tag{3.82}$$

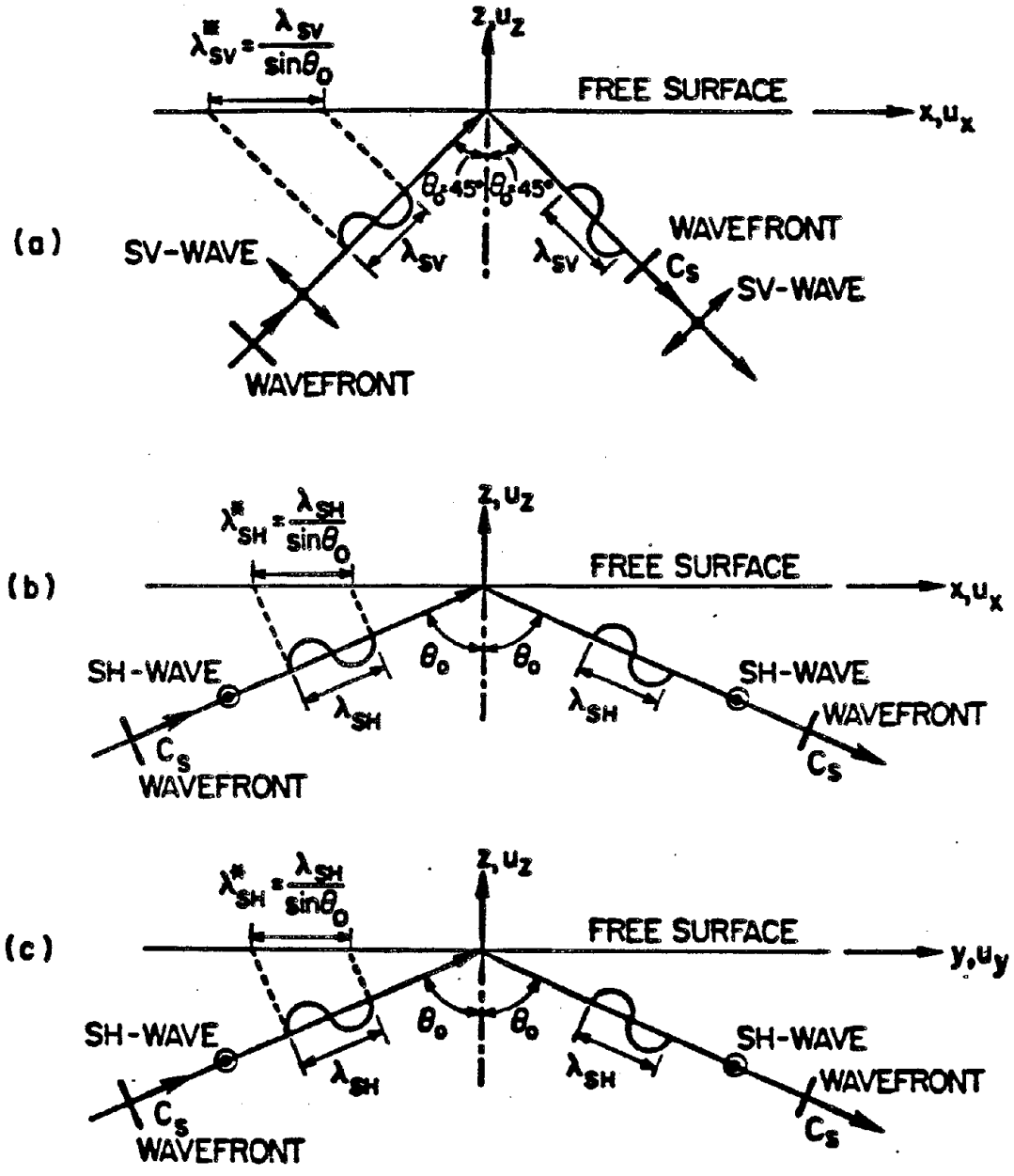

Fig. III-5 Definition diagram for rotational ground motion inputs (a) SV wave propagating in x direction, (b) SH wave propagating in x direction, (c) SH wave propagating in y direction.

The rotational motion about the y-axis (rocking input) is given by

$$\psi_y = \frac{1}{2}\left[\frac{\partial u_x}{\partial z} - \frac{\partial u_z}{\partial x}\right]$$

$$= -\frac{1}{2} A_0(i\kappa_0) \left\{\exp[i\kappa_0(x \sin\theta_0 - z \cos\theta_0 - c_s t)]\right.$$

$$\left. + \exp[i\kappa_0(x \sin\theta_0 + z \cos\theta_0 - c_s t)]\right\} \qquad (3.83)$$

At the ground surface $(z = 0)$ this becomes

$$\psi_y\Big|_{z=0} = - A_0(i\kappa_0) \left\{\exp[i\kappa_0(x \sin\theta_0 - c_s t)]\right\} \qquad (3.84)$$

From Eqs. 3.82 and 3.84, along with the conservative assumption that $\theta_0 = 45°$

$$\psi_y\Big|_{z=0} = \left(\frac{-i\omega}{2c_s}\sqrt{2}\right) u_z\Big|_{z=0} \qquad (3.85)$$

Taking the Fourier transform of Eq. 3.85 gives

$$\psi_y(\omega) = -\frac{i\omega}{2c_s}\sqrt{2}\ U_z(\omega) \qquad (3.86)$$

where $U_z(\omega)$ is the Fourier transform of the recorded vertical ground motion displacement and $\psi_y(\omega)$ is the Fourier transform of rocking displacement ground motion (at the ground surface). From the previous equation, one can estimate the Fourier transform of the rocking displacement inputs as being proportional to $i\omega U_z(\omega)$, the Fourier transform of the recorded vertical velocity components.

For the purpose of computing the torsional (horizontal rotation about a vertical axis) component of ground motion, it is proposed that the surface horizontal ground motion can be considered as the superposition of two independent SH waves propagating along two perpendicular

directions as shown in Fig. III-5(b) and (c). The total rotational effect is equal to the sum of the rotational effect due to each wave [11]. One possible interpretation for the above would involve one SH wave originating from the earthquake's epicenter and the other SH wave arriving from the nearest fault location.

The horizontal soil particle motion resulting from an SH wave propagating in the x-direction and reflecting from the free surface as an in-phase SH wave is

$$u_y = A_0 \left\{ \exp[i\kappa_0(x \sin\theta_0 - z \cos\theta_0 - c_s t)] + \exp[i\kappa_0(x \sin\theta_0 + z \cos\theta_0 - c_s t)] \right\} \tag{3.87}$$

which at the ground surface $(z = 0)$ becomes

$$u_y\Big|_{z=0} = 2A_0 \left\{ \exp[i\kappa_0(x \sin\theta_0 - c_s t)] \right\} \tag{3.88}$$

The horizontal rotation about the z-axis (torsion) is given by

$$\phi_z = \frac{1}{2}\left[\frac{\partial u_y}{\partial x} - \frac{\partial u_x}{\partial y}\right]$$

$$= \frac{1}{2} A_0 (i\kappa_0)\sin\theta_0 \left\{ \exp[i\kappa_0(x \sin\theta_0 - z \cos\theta_0 - c_s t)] + \exp[i\kappa_0(x \sin\theta_0 + z \cos\theta_0 - c_s t)] \right\} \tag{3.89}$$

which at the ground surface $(z = 0)$ becomes

$$\phi_z\Big|_{z=0} = A_0 (i\kappa_0)\sin\theta_0 \left\{ \exp[i\kappa_0(x \sin\theta_0 - c_s t)] \right\} \tag{3.90}$$

From Eq. 3.88 and Eq. 3.90, the torsion caused by the SH wave propagating in the x direction becomes

$$\phi_z\Big|_{z=0} = \frac{i\kappa_0}{2}(\sin\theta_0)\ u_y\Big|_{z=0} = \frac{i\omega}{2c_s}(\sin\theta_0)\ u_y\Big|_{z=0} \tag{3.91}$$

It can be seen from Eq. 3.91 that the worst torsional input results when the horizontal motion in the y direction is caused by an SH wave incident at $\theta_0 = 90°$ (the grazing angle). For this case

$$\phi_z\Big|_{z=0} = \frac{i\omega}{2c_s}\ u_y\Big|_{z=0} \tag{3.92}$$

The horizontal soil particle motion resulting from an SH wave propagating in the y direction and reflecting from the free surface as an in-phase SH wave is

$$u_x = A_0\left\{\exp[i\kappa_0(y\sin\theta_0 - z\cos\theta_0 - c_s t)] + \exp[i\kappa_0(y\sin\theta_0 + z\cos\theta_0 - c_s t)]\right\} \tag{3.93}$$

which at the ground surface $(z = 0)$ becomes

$$u_x\Big|_{z=0} = 2A_0\left\{\exp[i\kappa_0(y\sin\theta_0 - c_s t)]\right\} \tag{3.94}$$

The horizontal rotation about the z-axis (torsion) is given by

$$\phi_z = \frac{1}{2}\left[\frac{\partial u_y}{\partial x} - \frac{\partial u_x}{\partial y}\right]$$

$$= -\frac{1}{2}A_0(i\kappa_0)\sin\theta_0\left\{\exp[i\kappa_0(y\sin\theta_0 - z\cos\theta_0 - c_s t)] + \exp[i\kappa_0(y\sin\theta_0 + z\cos\theta_0 - c_s t)]\right\} \tag{3.95}$$

which at the ground surface $(z = 0)$ becomes

$$\phi_z\Big|_{z=0} = -A_0(i\kappa_0)\sin\theta_0\left\{\exp[i\kappa_0(y\sin\theta_0 - c_s t)]\right\} \tag{3.96}$$

From Eq. 3.94 and Eq. 3.96, the torsion caused by the SH wave propagating in the y direction becomes

$$\phi_z\Big|_{z=0} = -\frac{i\kappa_0}{2}(\sin\theta_0)u_x\Big|_{z=0} = -\frac{i\omega}{2c_s}(\sin\theta_0)\ u_x\Big|_{z=0} \tag{3.97}$$

Again, the worst case of torsional input occurs when the incidence angle $\theta_0 = 90°$ (the grazing angle). For this case

$$\phi_z\Big|_{z=0} = -\frac{i\omega}{2c_s}u_x\Big|_{z=0} \tag{3.98}$$

Adding the results of Eqs. 3.92 and 3.98 gives

$$\phi_z\Big|_{z=0} = \frac{i\omega}{2c_s}\left[u_y\Big|_{z=0} - u_x\Big|_{z=0}\right] \tag{3.99}$$

Taking the Fourier transform of Eq. 3.99 results in

$$\Phi_z(\omega) = \frac{i\omega}{2c_s}\left[U_y(\omega) - U_x(\omega)\right] \tag{3.100}$$

where $U_y(\omega)$ and $U_x(\omega)$ are the Fourier transforms of the recorded horizontal ground motion displacements and $\Psi_z(\omega)$ is the Fourier transform of horizontal torsional displacement ground motion (at the ground surface). From the previous equation, one can estimate the Fourier transform of the torsional displacement inputs as being proportional to the difference between $i\omega U_y(\omega)$ and $i\omega U_x(\omega)$, that is, the difference between the Fourier transforms of the recorded horizontal velocity components.

The ground motion records utilized to define the rotational inputs are those of the 1979 Imperial Valley (El Centro) earthquake, ($M_L = 6.6$). Among the valuable records recovered from this earthquake were the translational components of arrays no. 4, 5, 6, 7, and 8 from the 13

arrays comprising the El Centro Array (see Appendix II-e). After assuming the propagation direction (from the epicenter) to be predominantly in the N40°W direction, the power spectra of rocking and torsional inputs can be computed for various shear wave velocities and are shown in Fig. III-6. A comparison of these figures shows that for rocking motion, Array No. 6 is the most intense location. Also, the torsional motions are seen to be stronger in Arrays No. 4, 5, and 6 (arrays west of the Imperial Fault). At each site, the torsional component of ground motion is stronger than the rocking motion component, and also, the slower the shear wave velocity, the more intense are the input rotational spectra. Because of this last comment, as well as the fact that the stiffness of the soil (and hence the shear wave velocity) may decrease considerably under high amplitude vibration, a very conservative shear wave velocity estimate of 500 ft/sec is used in the following analysis.

III.11. APPLICATION: TORSIONAL SEISMIC BEHAVIOR OF THE GOLDEN GATE BRIDGE

The analysis outlined in this chapter is applied to the Golden Gate Suspension Bridge in San Francisco, California in order to estimate its earthquake-induced torsional response characteristics. The structural properties of the bridge are summarized in Table III-1. The torsional quasi-static functions are shown in Fig. III-7 for unit rocking ground motion displacement at each anchorage and tower base. The first eight symmetric and antisymmetric torsional mode shapes are shown in Fig. III-8, while their associated participation coefficients appear in Table III-2. It is noted at this point that the symmetric torsional vibration of the cable-suspended structure is excited very strongly by the torsional (horizontal rotational) ground motion inputs occurring

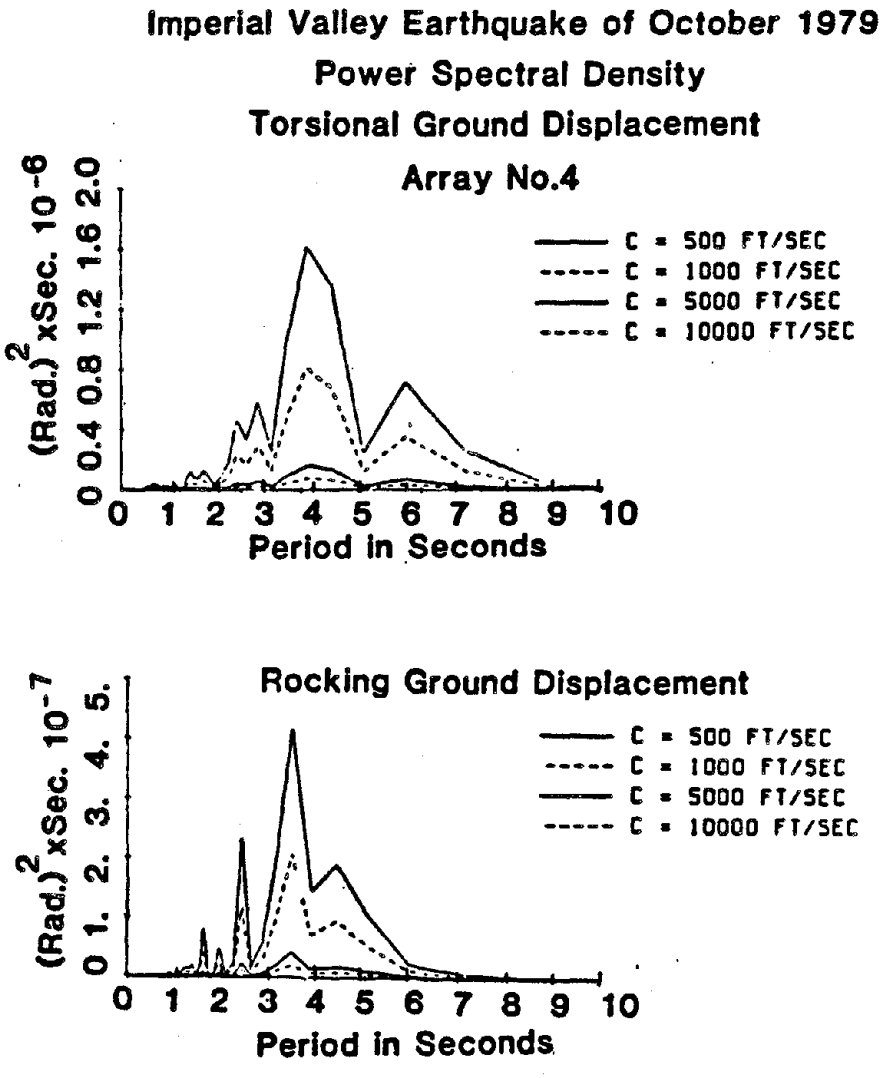

Fig. III-6a Power spectra of the torsional and rocking ground input motions.

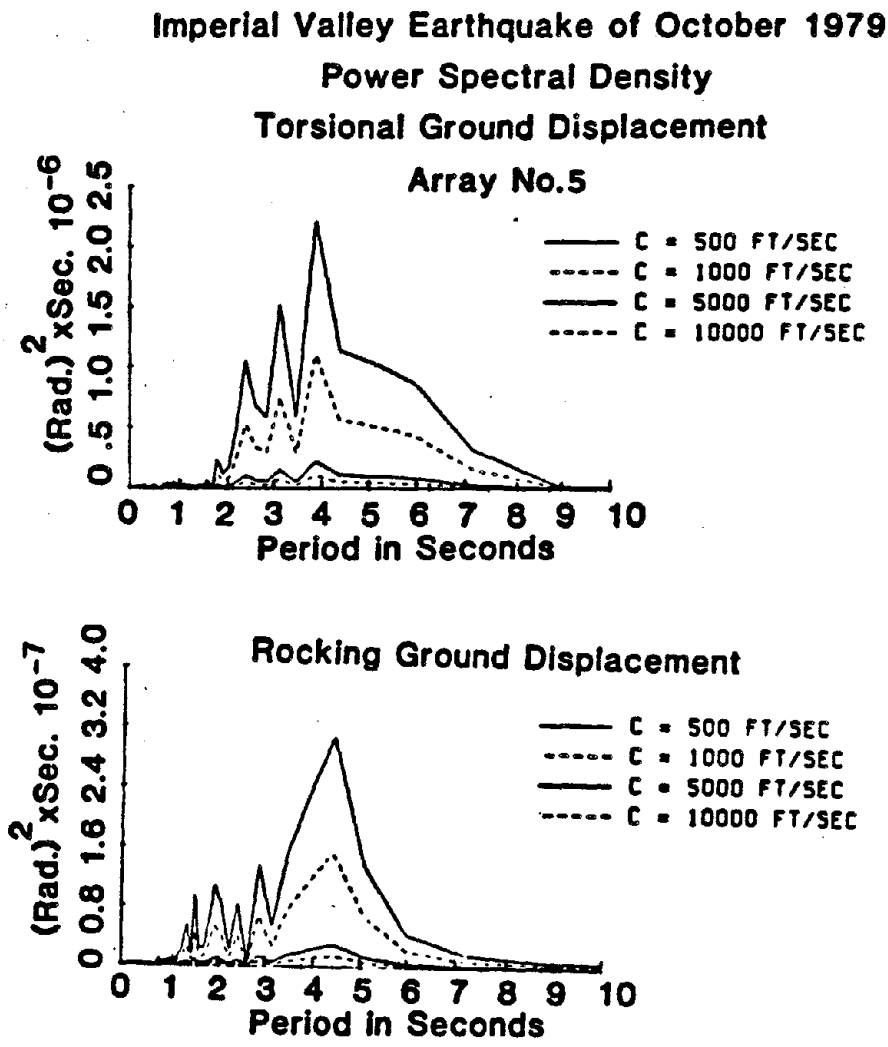

Fig. III-6b Power spectra of the torsional and rocking ground input motions.

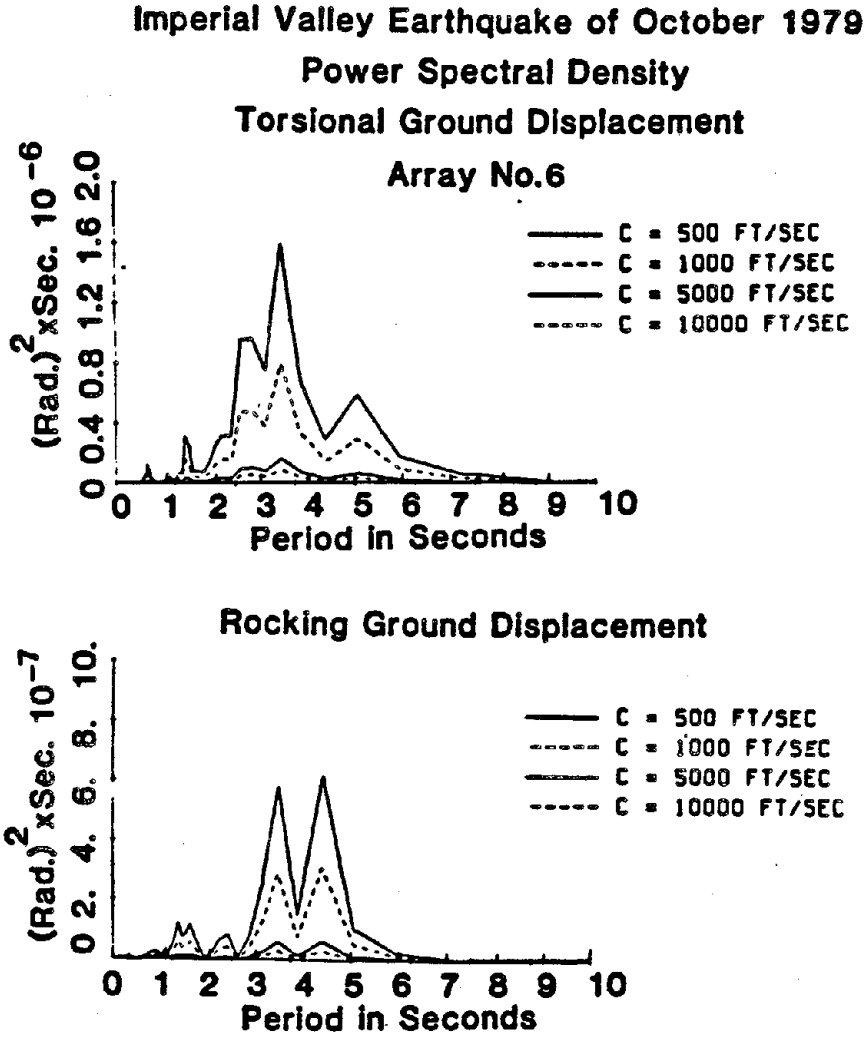

Fig. III-6c Power spectra of the torsional and rocking ground input motions.

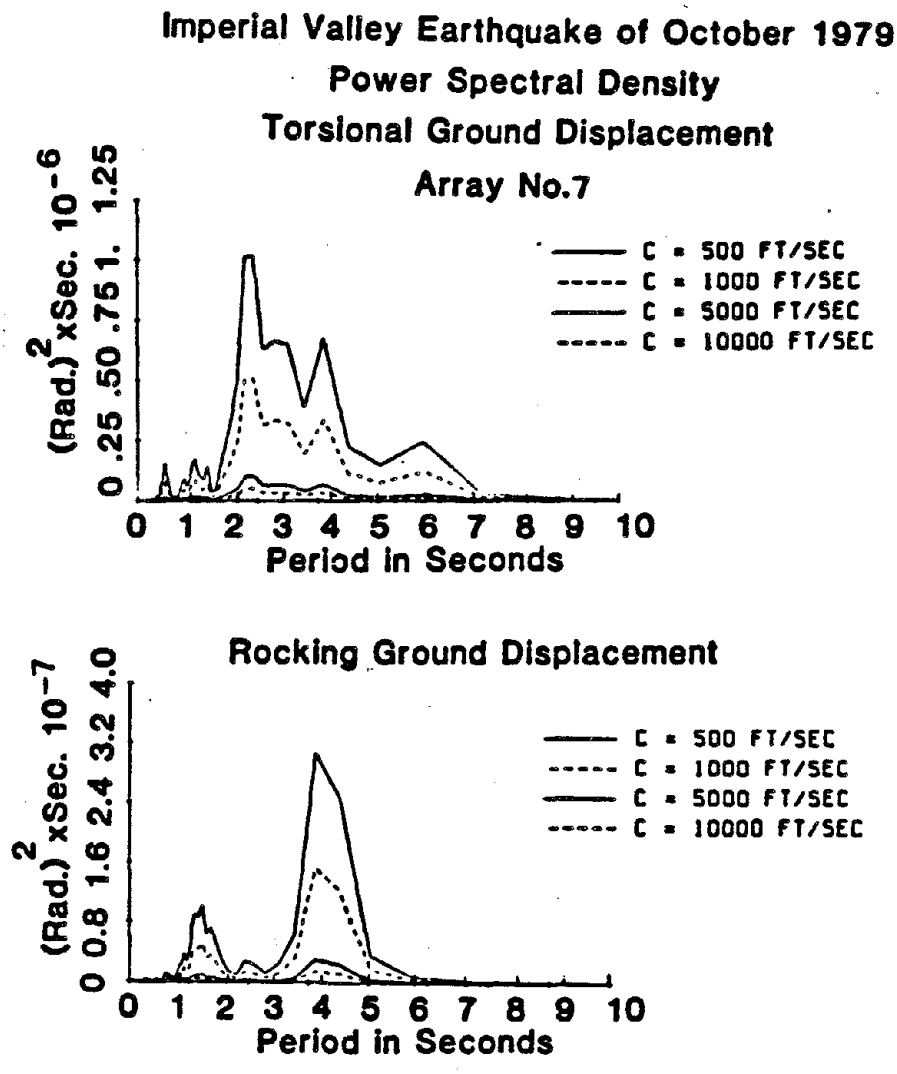

Fig. III-6d Power spectra of the torsional and rocking ground input motions.

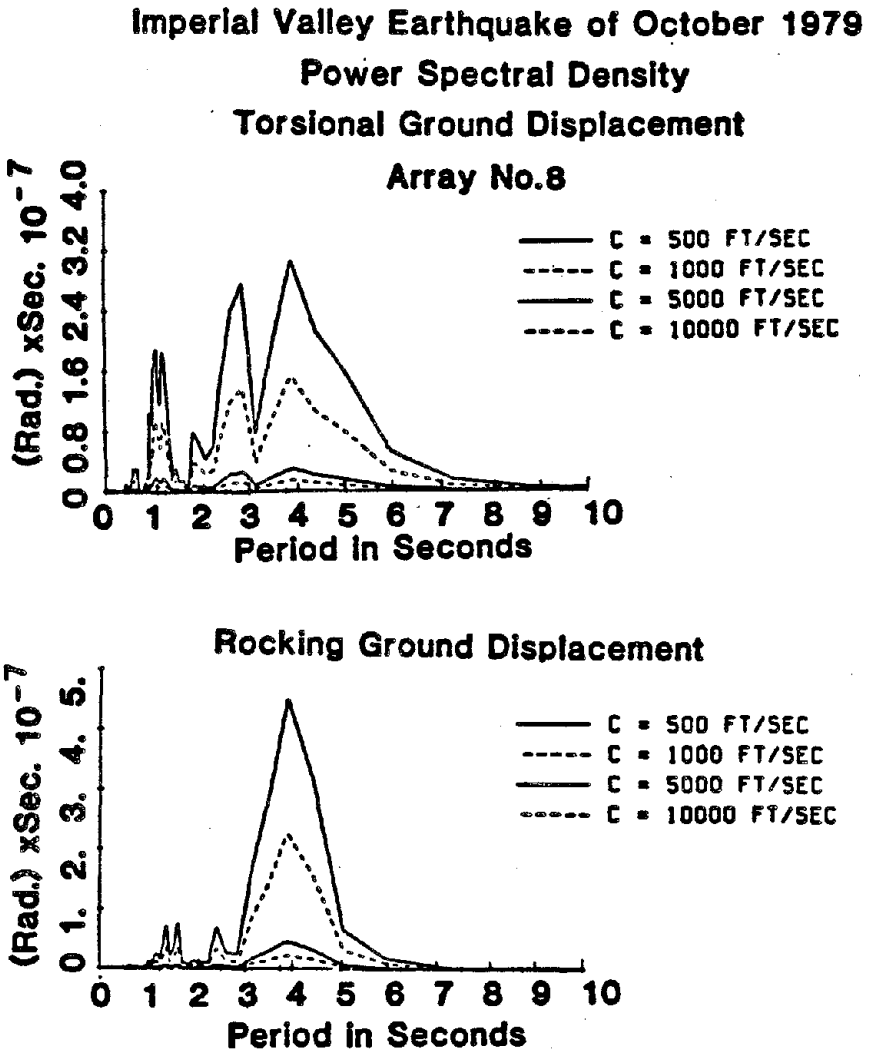

Fig. III-6e Power spectra of the torsional and rocking ground input motions.

Table III-1

Torsional Properties of the Golden Gate Bridge

Parameter	Center Span	Side Spans
Span Length	ℓ_2 = 4200 ft	$\ell_1=\ell_3$ = 1125 ft
$\overset{*}{w}_i$	$\overset{*}{w}_2$ = 11.45 k/ft	$\overset{*}{w}_1 = \overset{*}{w}_2$ = 11.55 k/ft
E_i	E_2 = 29,000 ksi	$E_1=E_3$ = 29,000 ksi
I_{mi}	I_{m2} = 859.9 k·sec^2	$I_{m1}=I_{m3}$ = 869.9 k·sec^2
Γ_i	Γ_2 = 1.357x10^{8}ft^{4}in^2	$\Gamma_1=\Gamma_3$ = 8.751x10^{7}ft^{4}in^2
G_i	G_2 = 11,600 ksi	$G_1=G_3$ = 11,600 ksi
J_i	J_2 = 25,815 ft^{2}in^2	$J_1=J_3$ = 25,815 ft^{2}in^2
Truss Depth	d_2 = 25 ft	$d_1=d_2$ = 25 ft
Span Width	b = 90 ft	b = 90 ft
Cable Properties	E_c = 29,000 ksi A_c = 831.9 in^2 L_E = 7,698 ft H_w = 53,467 kips	

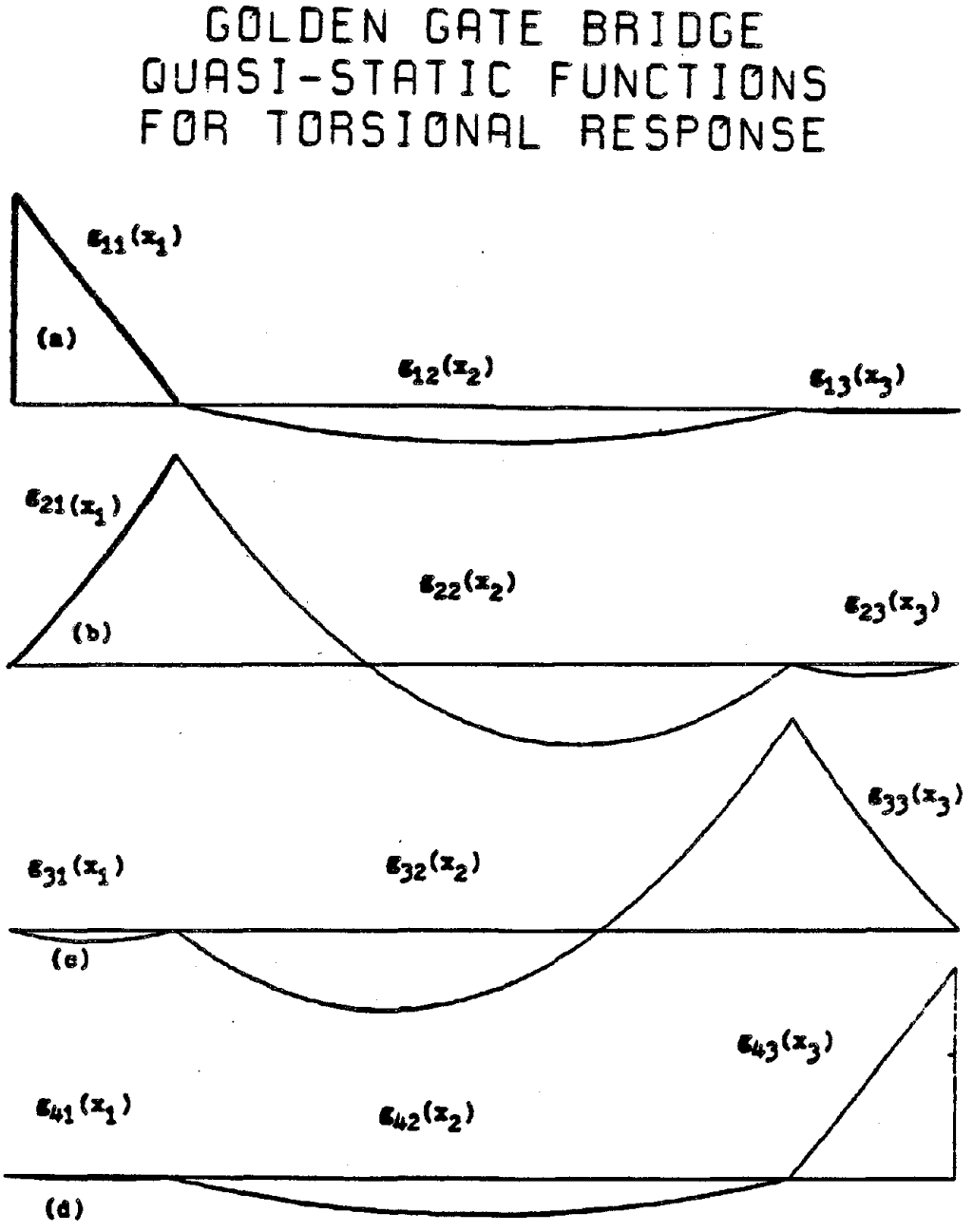

Fig. III-7 Golden Gate Bridge, torsional quasi-static functions. (a) Unit rocking at left anchorage, (b) unit rocking at left tower-pier, (c) unit rocking at right tower-pier, (d) unit rocking at right anchorage.

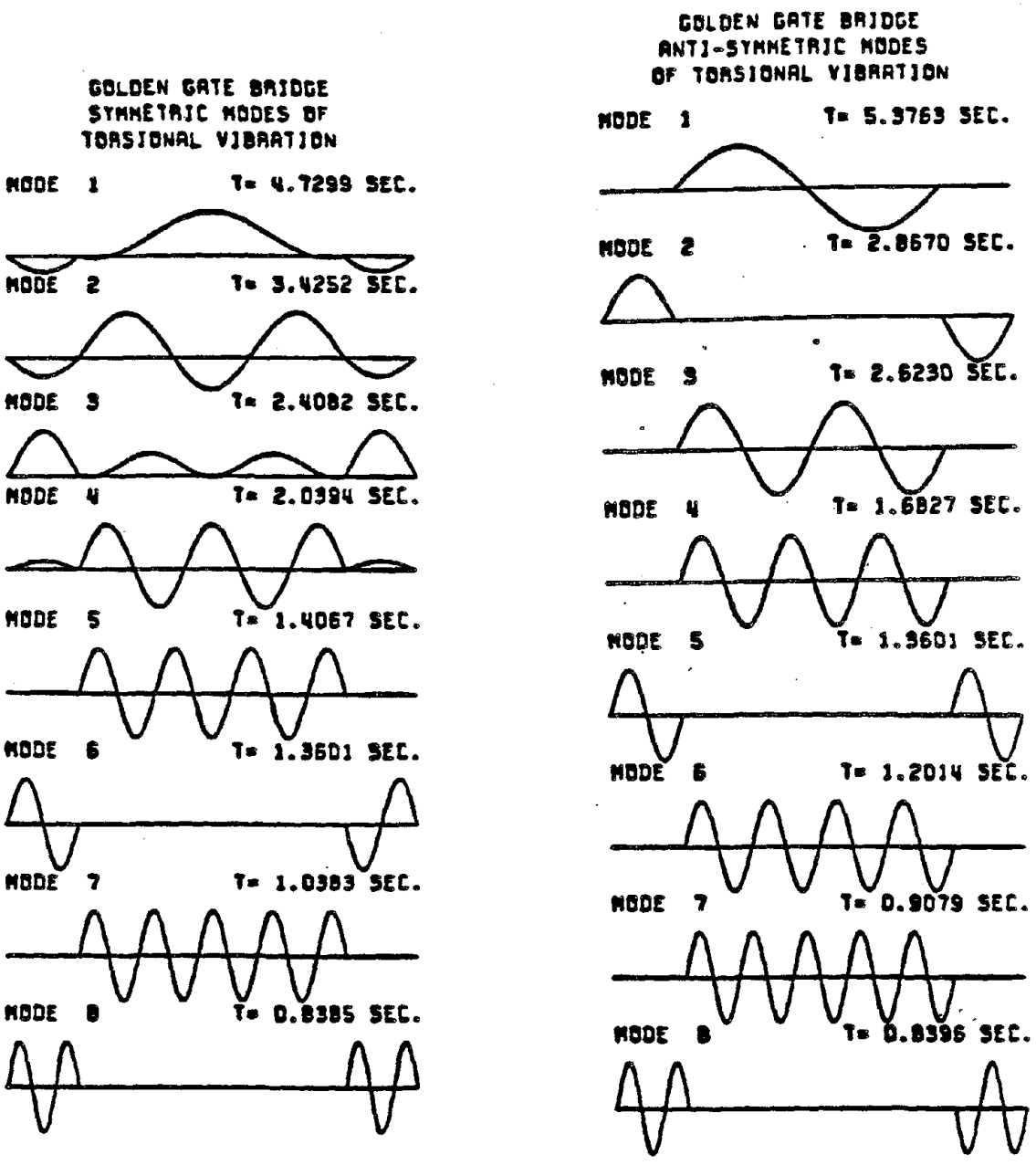

Fig. III-8 Torsional mode shapes of the Golden Gate Bridge.

Table III-2

Participation Coefficients of Torsional Earthquake Response for the Golden Gate Bridge

Mode Order n	Symmetric Vibration			Antisymmetric Vibration		
	$R_{1n} = R_{4n}$	$R_{2n} = R_{3n}$	P_n	$R_{1n} = -R_{4n}$	$R_{2n} = -R_{3n}$	P_n
1	-0.268	-0.352	1.413	0.0	0.318	0.0
2	-0.117	0.657	0.657	0.318	0.318	0.0
3	0.151	0.125	2.686	0.0	0.159	0.0
4	0.013	0.140	0.955	0.0	0.106	0.0
5	-0.0003	0.091	0.390	0.159	-0.159	0.0
6	0.159	-0.159	0.0	0.0	0.079	0.0
7	-0.0005	0.070	0.265	0.0	0.063	0.0
8	0.106	0.105	0.770	0.106	0.106	0.0

at the tower-piers and anchorages. The antisymmetric torsional vibration, on the other hand, is not excited at all by the torsional (horizontal rotational) ground motion inputs, but only by the rocking (vertical rotational) inputs (because of the modal participation factors P_n being identically zero for antisymmetric modes). Therefore, analogous to the vertical vibration findings, the antisymmetric torsional vibration response turns out to be much smaller than the symmetric torsional vibration response. It should also be noted that the additional (vibrational) horizontal component of cable tension as in the vertical vibration case (Eq. 3.75) essentially contains four contributions

1. Contribution from pure ground motion rotational inputs (both torsion (horizontal rotation) and rocking (vertical rotation)), as seen in the second through fifth terms of Eq. 3.75.
2. Contribution from symmetric torsional vibrational deflection θ as seen in the first term of Eq. 3.75.
3. Contribution from antisymmetric torsional vibration which turns out to be identically zero.
4. Contribution from the quasi-static motions as in the second term of Eq. 3.75.

The contribution from antisymmetric vibrational torsional displacement to the additional cable tension is zero because the net area underneath an antisymmetric mode is identically zero. In this section, therefore, because of the higher order nature of the antisymmetric response, and because the additional horizontal component of cable tension can be constructed from knowledge of the symmetric torsional vibration response as well as knowledge of the ground motion inputs, only the symmetric torsional response will be investigated herein.

The frequency response functions $H_n(\omega)$ for the first through fourth symmetric torsional modes of the bridge are shown in Fig. III-9 for 2% damping, and corresponding to anchorage rocking input, tower rocking input, and anchorage torsional input. These functions measure the magnification (or gain) factor corresponding to a unit harmonic input upon the generalized coordinate $q_n(t)$. It can be seen as was stated previously that the torsional inputs contribute more significantly than the rocking inputs to the torsional response by examining these magnification factors.

Two symmetric torsional response cases are studied for the Golden Gate Bridge. In the first case, the rocking motions ψ_1, ψ_2, ψ_3, and ψ_4 correspond to the calculated rocking motions at arrays No. 4, 5, 6, and 7, respectively, while the torsional motions ϕ_1 and ϕ_4 correspond to the associated torsional components (of Arrays No. 4 and 7). The second response case involves similar correspondences with Arrays No. 5, 6, 7, and 8 of the 1979 El Centro earthquake.

The autospectra of mid-span torsional displacement for both the center and side spans are shown in Fig. III-10 for input Arrays 4, 5, 6, and 7. It is observed that the quasi-static contribution to the total torsional response is small, and therefore the response is quite similar in the left and right side spans. The quasi-static contribution is inherent in the participation coefficient R_{jn} (Eq. 3.37). Thus, it is erroneous to conclude that the quasi-static functions have no influence upon the response and consequently should be ignored. Without their presence, the participation factors would be altered, and different response values would result. The first and third symmetric torsional modes appear to dominate the response, most likely because of their modal

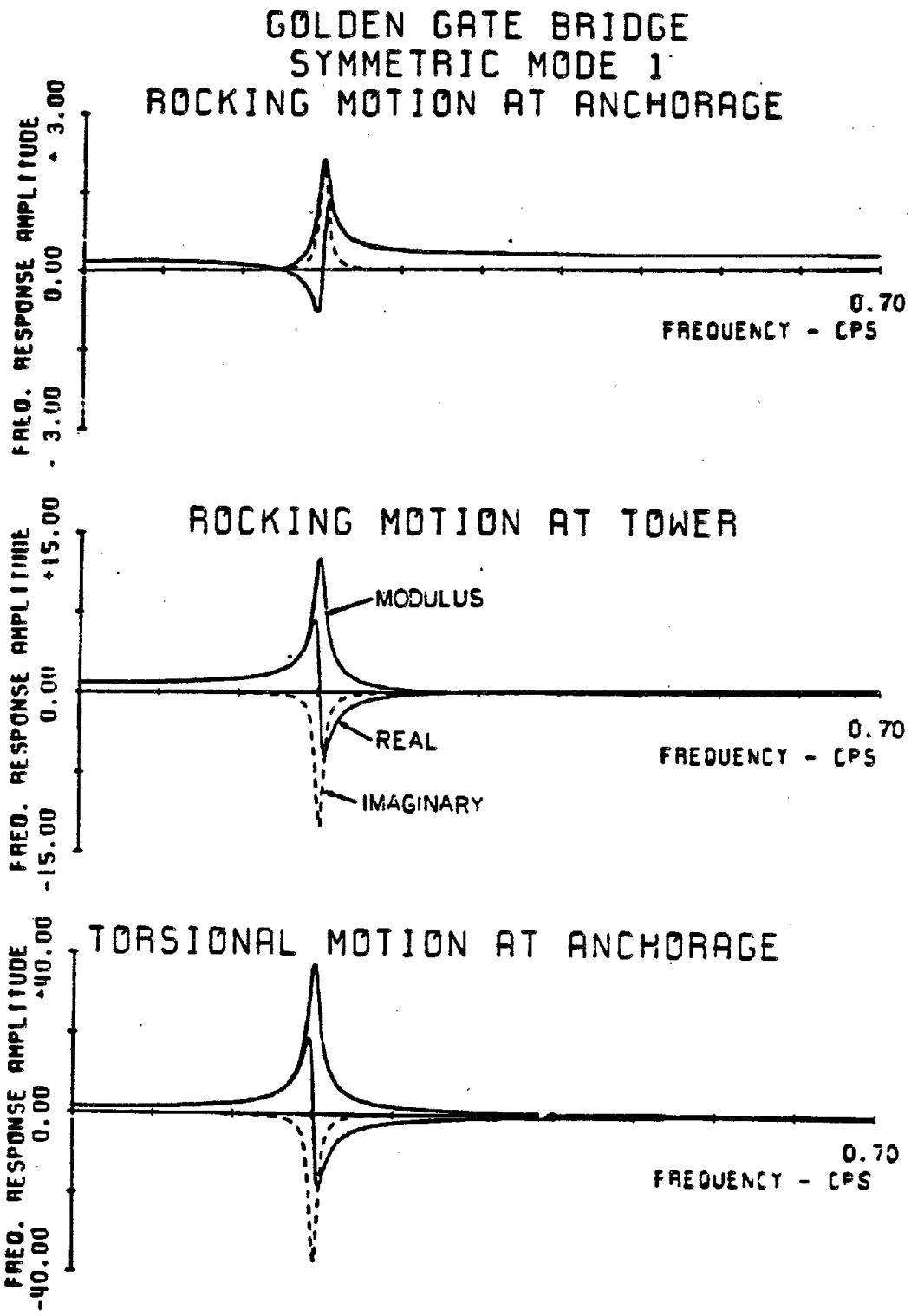

Fig. III-9a Complex frequency response functions.

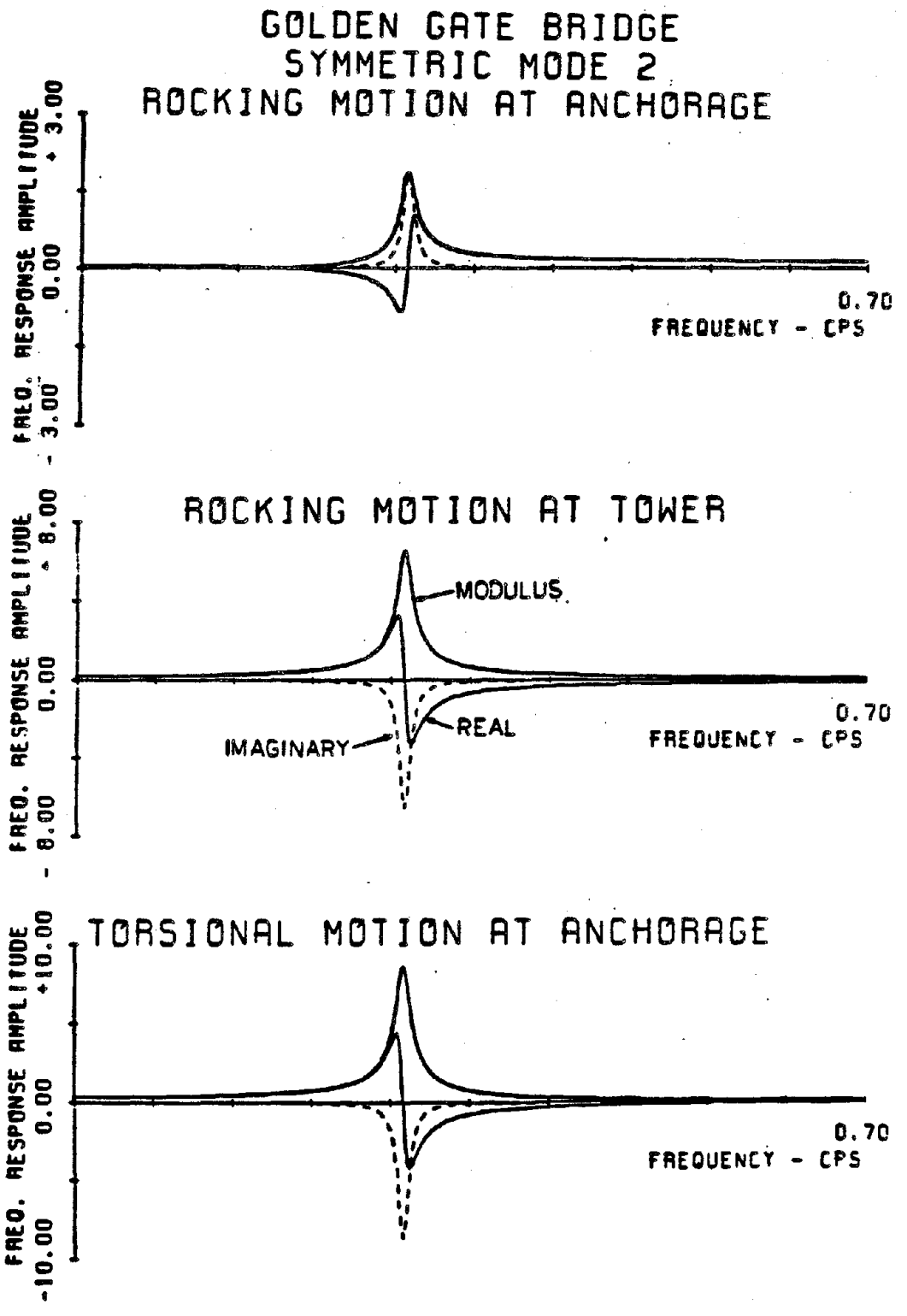

Fig. III-9b Complex frequency response functions.

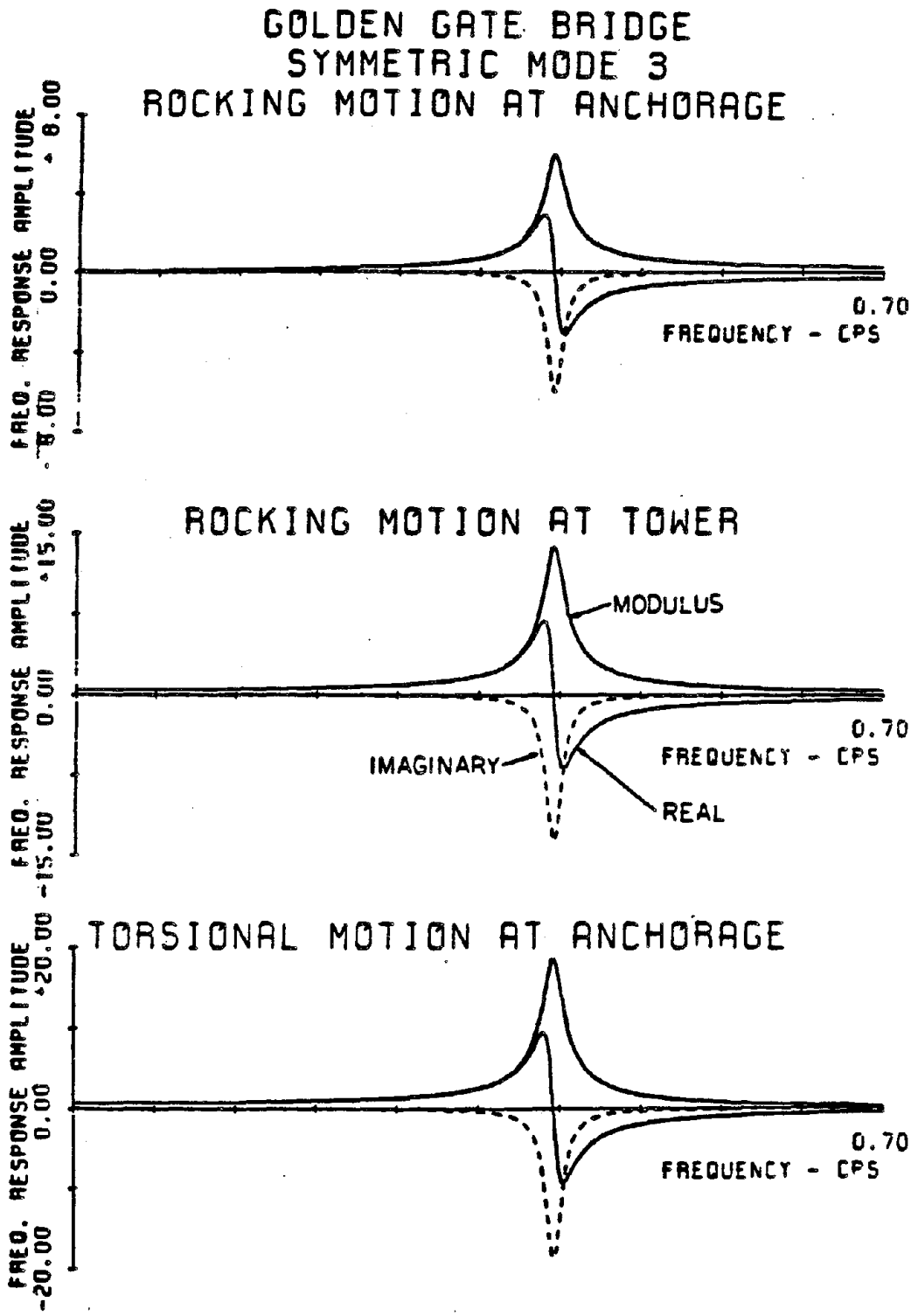

Fig. III-9c Complex frequency response functions.

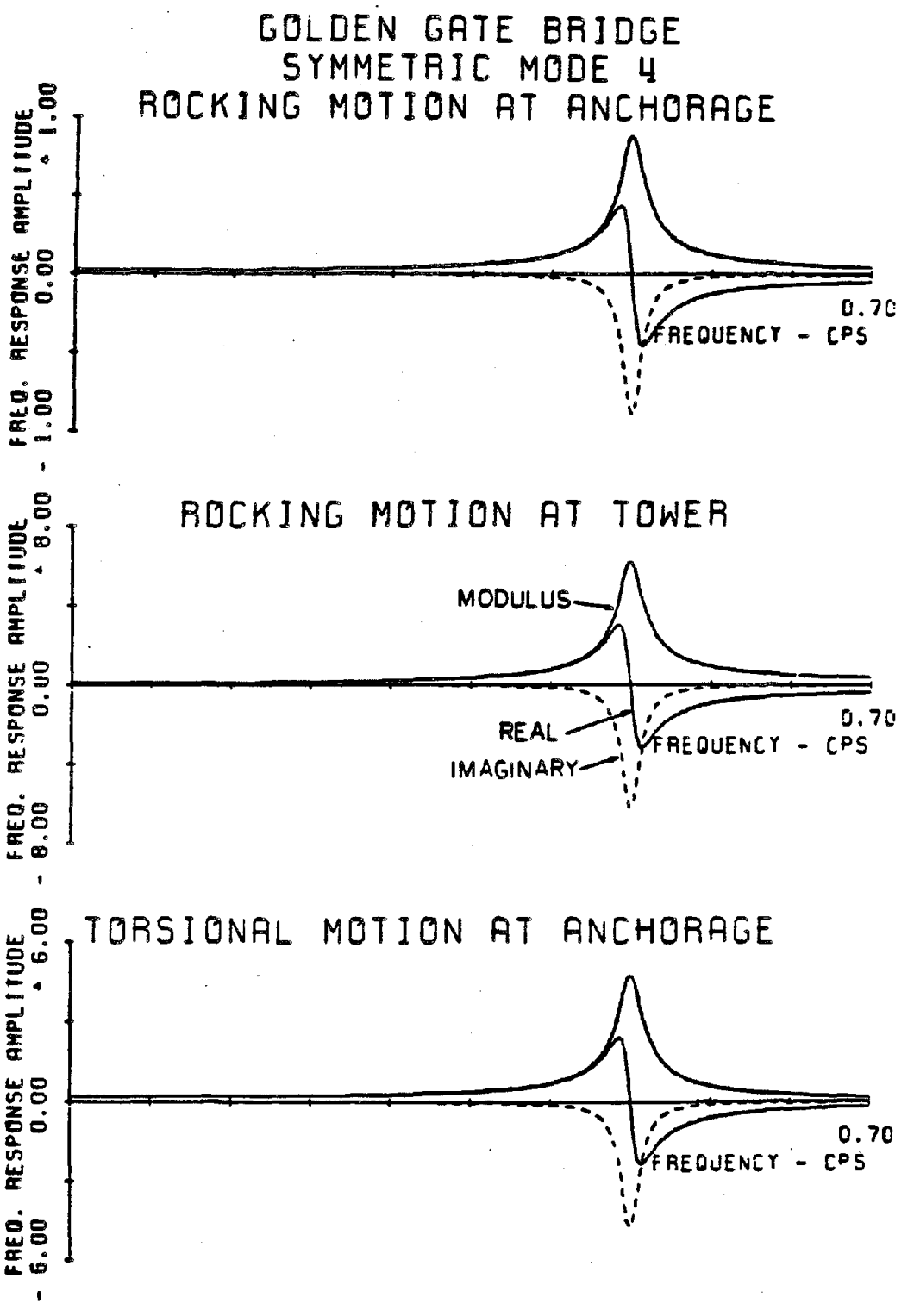

Fig. III-9d Complex frequency response functions.

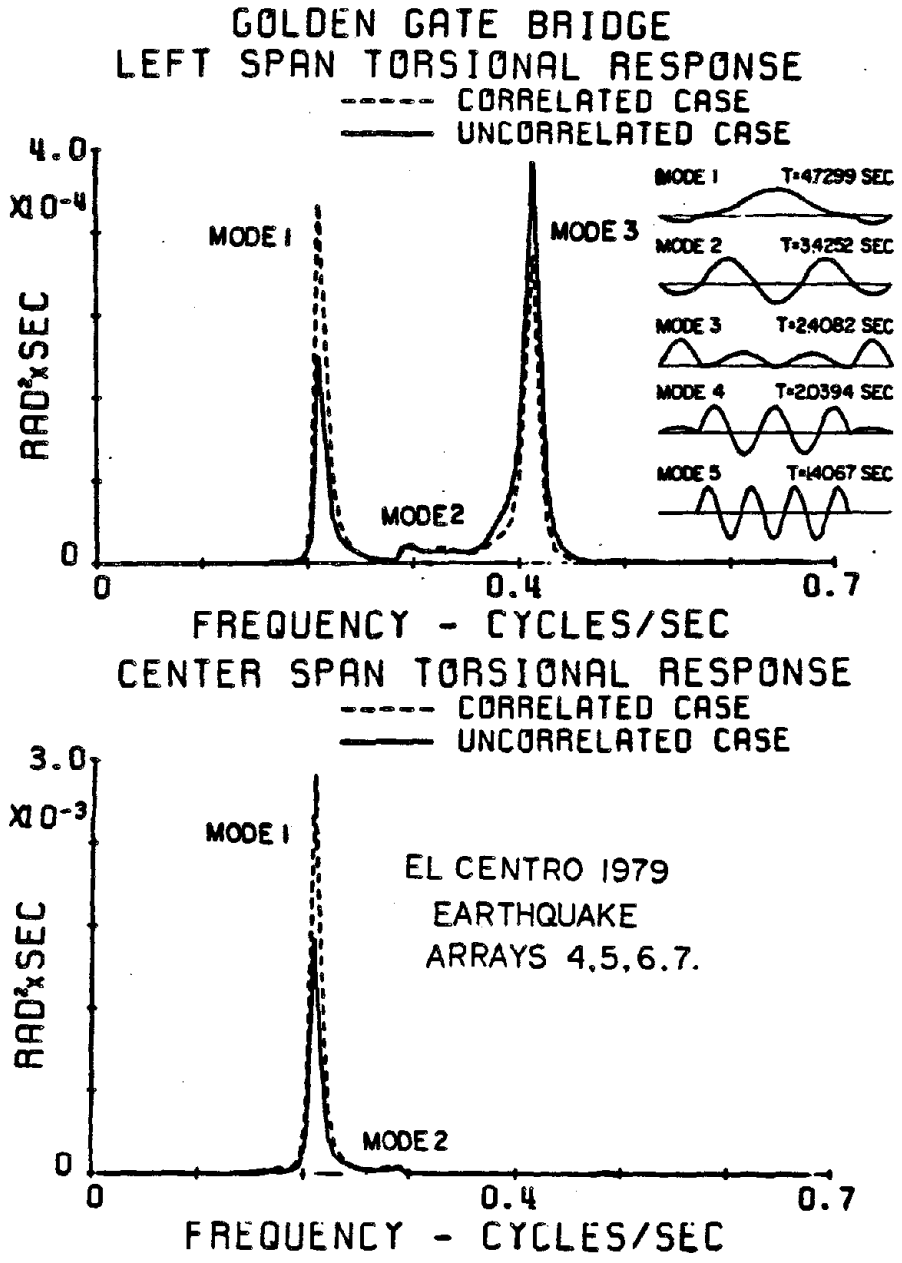

Fig. III-10 Autospectra of midspan torsional displacement response of Golden Gate Bridge.

participation factors P_n being large (Table III-2). Similar torsional response spectra for input Arrays No. 5, 6, 7, and 8 are shown in Fig. III-11.

It should be noted that flexural stresses induced by torsional vibration in the chord members of the suspended structure may be calculated by replacing the mode shapes, $\Theta_{ni}(x_i)$, and quasi-static functions $g_{ji}(x_i)$, by $E_i(b/2)(d/2)\Theta''_{ni}(x_i)$ and $E_i(b/2)(d/2)\, g''_{ji}(x_i)$ respectively, where E_i is the modulus of elasticity of the i^{th} suspended structure; b is the deck width; and d is the depth of the suspended structure. Thus, Eq. 4.42 becomes

$$\sigma_i(x_i,t) = E_i(b/2)(d/2)\left[\sum_{j=1}^{4} g''_{ji}(x_i)\psi_j(t) + \sum_{n=1}^{\infty} \Theta''_{ni}(x_i)q_n(t)\right]$$

$$i=1,2,3 \qquad (4.101)$$

where $\sigma_i(x_i,t)$ is the stress in the chords of the i^{th} suspended structure; and $g''_{ji}(x_i)$ and $\Theta''_{ni}(x_i)$ are the second spanwise derivatives of the quasi-static functions and mode shapes, respectively.

It should be noted that with reference to the vertical vibration problem (Chapter II) it was found that the uncorrelated calculation is usually conservative in nature. However, from Figs. III-10, 11, 12, and 13 it can be seen that this is not necessarily the case in torsional vibration. The power spectral density of the flexural stresses induced by torsional vibration can be calculated by Eq. 3.65 with the mode shapes and quasi-static functions replaced as above. The autspectra of torsional response stresses appear in Figs. III-12 for both input cases, while the autospectra of the additional (vibrational) horizontal component of cable tension appears in Fig. III-13. As a final note, mean square responses can be determined by integrating under the spectra of Figs.

III-10, 11, 12, and 13. The square root of the mean square responses are known as the root mean square responses (R.M.S.) and are shown in Table III-3. Estimated peak responses can be determined by multiplying the root mean square values by a peak factor taken as 3.5 (see Chapter II). The peak responses are shown in Table III-3, along with the peak vertical deflections at the edge of the suspended structure, equal to (b/2) multiplied by the peak rotational values (where b is the width of the suspended structure). The maximum torsionally-induced stress of 34.55 ksi occurring at center span for the uncorrelated case (Arrays 4, 5, 6, 7) is a high value of live load when compared to the yield stress of 50.5 ksi.

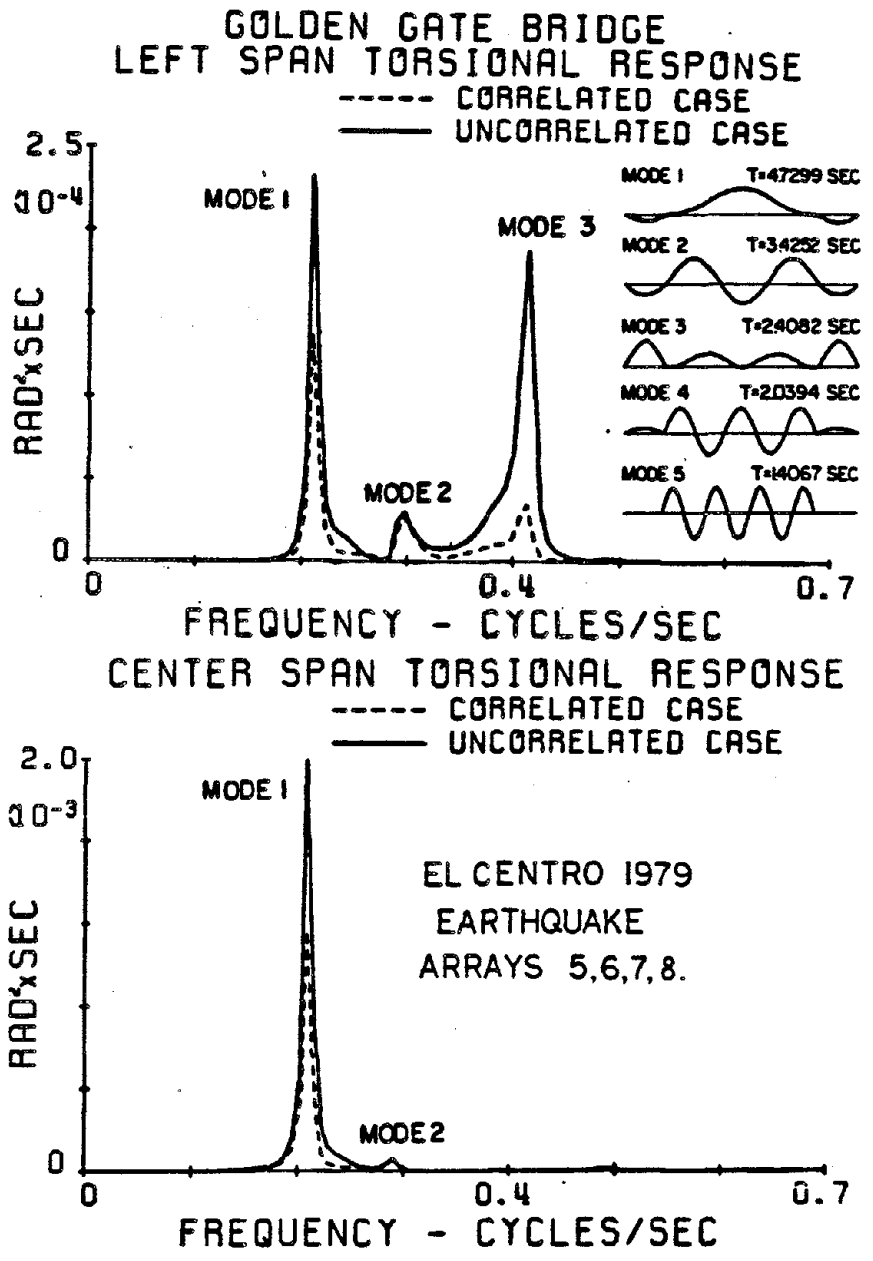

Fig. III-11 Autospectra of midspan torsional displacement response of Golden Gate Bridge.

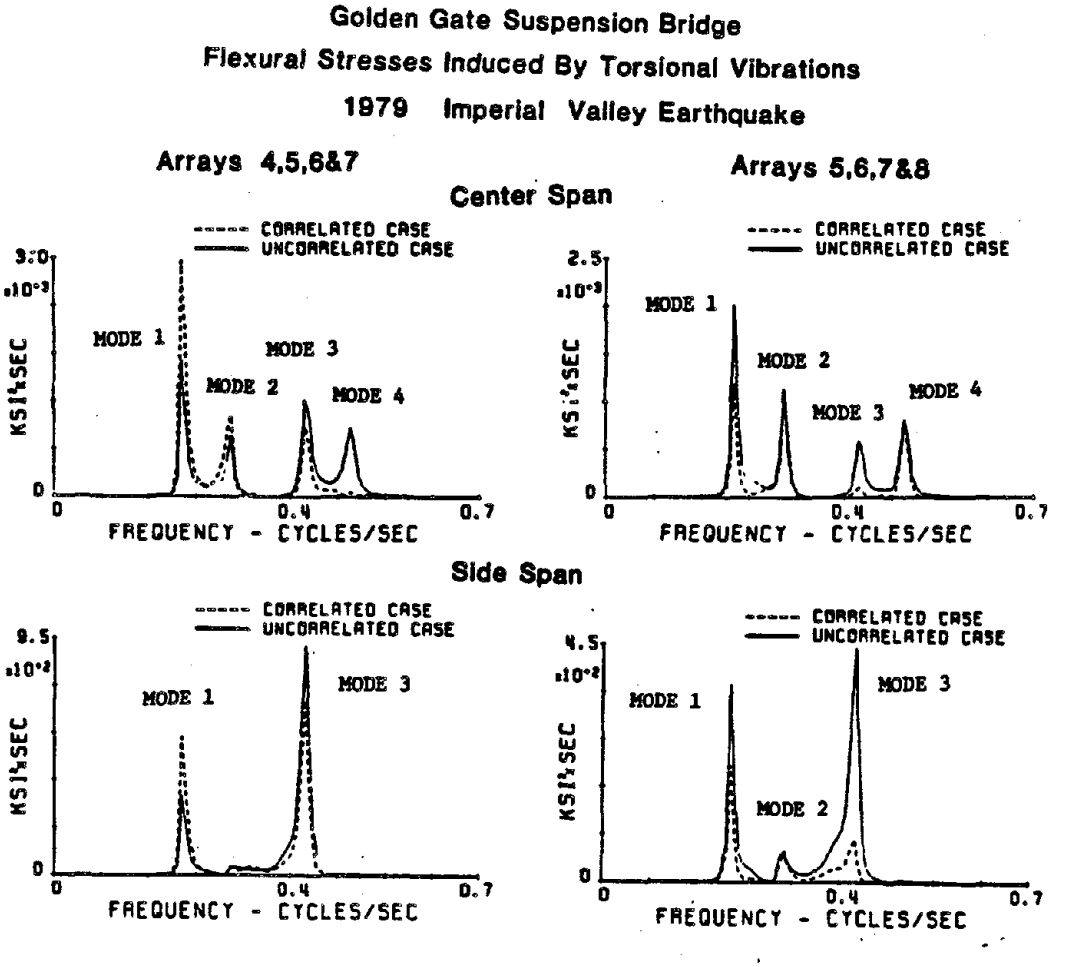

Fig. III-12 Autospectra of midspan torsional stress response of Golden Gate Bridge.

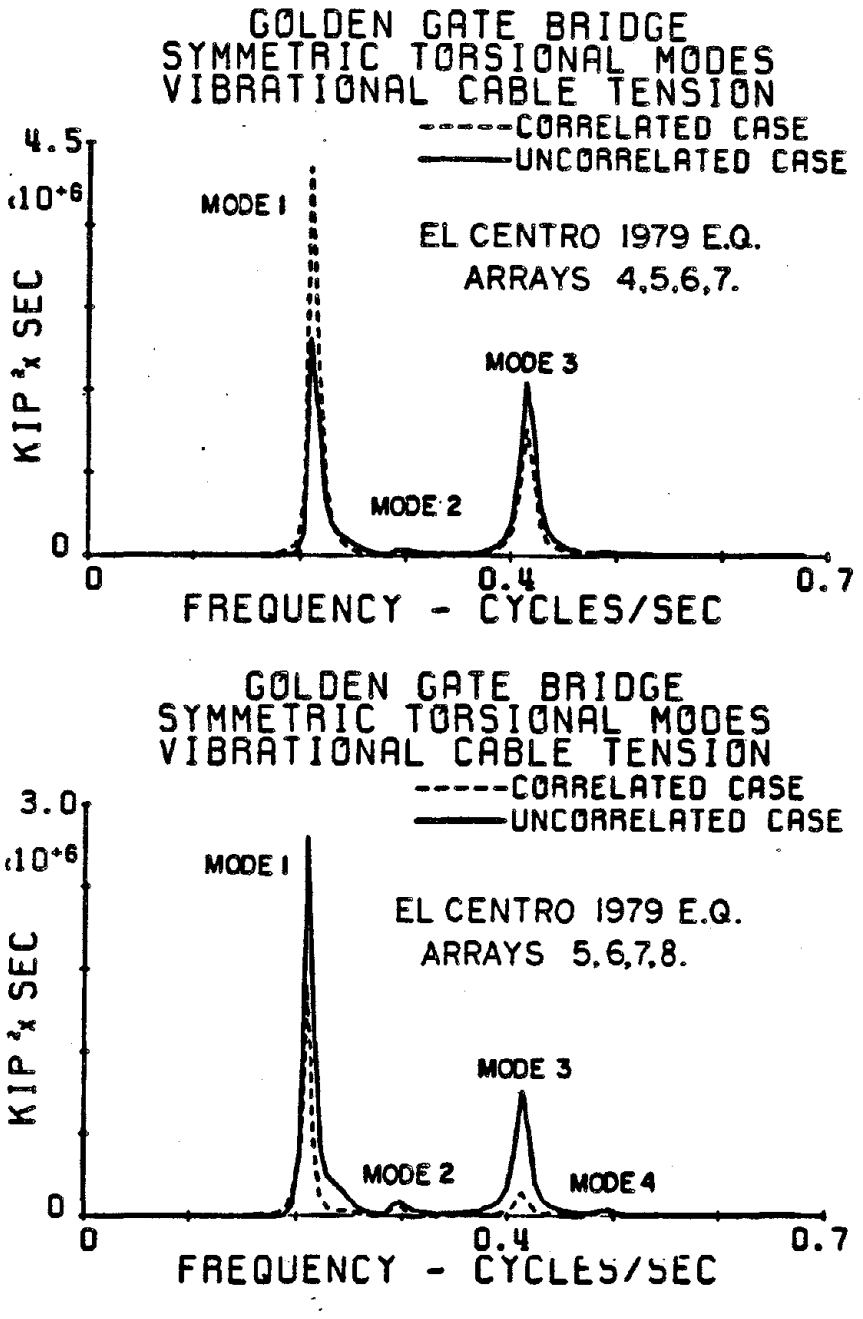

Fig. III-13 Autospectra of additional (vibrational) cable tension due to torsional vibration of Golden Gate Bridge.

Table III-3

ROOT MEAN SQUARE RESPONSES & EXPECTED PEAK RESPONSES - GOLDEN GATE BRIDGE

RESPONSE CASE	R.M.S. Response		Peak Response*		(b/2)·Peak Response**	
	Correl.	Uncorr.	Correl.	Uncorr.	Correl. (cm.)	Uncorr. (cm.)
Arrays 4,5,6,7						
Left Span Displ.(rad.)	0.003549	0.003616	0.0124	0.0127	17.0	17.4
Center Span Displ. (rad.)	0.006545	0.005082	0.0229	0.0178	31.4	24.4
Right Span Displ (rad.)	0.003544	0.003618	0.0124	0.0127	17.0	17.4
Left Span Stress (ksi)	5.04	5.35	17.64	18.73	--	--
Center Span Stress (ksi)	9.53	9.87	33.36	34.55	--	--
Right Span Stress (ksi)	5.04	5.35	17.64	18.73	--	--
Cable Tension (kip)	299.7 kip	293.5	1049	1027	--	--
Arrays 5,6,7,8						
Left Span Displ. (rad.)	0.001909	0.003032	0.00668	0.0106	9.2	14.6
Center Span Displ.(rad.)	0.004105	0.005393	0.0144	0.0189	19.7	25.9
Right Span Displ. (rad.)	0.001878	0.003028	0.00657	0.0106	9.0	14.5
Left Span Stress (ksi)	2.62	4.36	9.17	15.26	--	--
Center Span Stress (ksi)	7.10	9.03	24.85	31.61	--	--
Right Span Stress (ksi)	2.62	4.36	9.17	15.26	--	--
Cable Tension (kip)	169.0	256.7	592	898	--	--

*Based upon a peak factor of 3.5 (Chapter II0.
**Equal to peak deflection at edge of roadway.

Appendix III-a

Solution for the Torsional Quasi-Static Functions

A. Unit Rotation at Left Anchorage

The solution for the quasi-static function corresponding to unit rotation at support A of Fig. III-4 is obtained by satisfying the following three equations:

$$E_i\Gamma_i \frac{d^4 g_{1i}(x_i)}{dx_i^4} - \left(G_iJ_i + H_w \frac{b^2}{2}\right) \frac{d^2 g_{1i}(x_i)}{dx_i^2}$$

$$+ \frac{\overset{*}{w}_i b}{H_w} \left(\frac{E_c A_c}{L_E}\right)\left(\frac{b}{2}\right) \left[\sum_{n=1}^{3} \frac{\overset{*}{w}_n}{H_w} \int_0^{\ell_n} g_{1n}(x_n)\,dx_n\right] = 0$$

$$i = 1, 2, 3 \qquad \text{(III-a-1)}$$

subject to the boundary conditions

$$g_{11}(0) = 1 \qquad g_{12}(0) = 0 \qquad g_{13}(0) = 0$$

$$g_{11}(\ell_1) = 0 \qquad g_{12}(\ell_2) = 0 \qquad g_{13}(\ell_3) = 0$$

$$g_{11}''(0) = g_{12}''(0) = g_{13}''(0) = 0$$

$$g_{11}''(\ell_1) = g_{12}''(\ell_2) = g_{13}''(\ell_3) = 0 \qquad \text{(III-a-2)}$$

The form of the solution can be taken as

$$g_{1i}(x_i) = A_{1i} \sinh(\lambda_i x_i) + B_{1i} \cosh(\lambda_i x_i) + C_{1i} x_i^2$$

$$+ D_{1i} x_i + E_{1i} \quad , \qquad i = 1, 2, 3 \qquad \text{(III-a-3)}$$

where

$$\lambda_i = \sqrt{\frac{\left(G_i J_i + H_w \frac{b^2}{2}\right)}{E_i \Gamma_i}} \qquad i = 1, 2, 3 \qquad \text{(III-a-4)}$$

Substituting Eq. III-a-3 into Eq. III-a-1 results in the following three equations:

$$2\left[G_i J_i + H_w \frac{b^2}{2}\right] C_{1i} = \frac{\overset{*}{w}_i b}{H_w}\left(\frac{E_c A_c}{L_E}\right)\left(\frac{b}{2}\right)\left\{\sum_{n=1}^{3} \frac{\overset{*}{w}_n}{H_w}\left[\frac{A_{1n}}{\lambda_n}\{\cosh(\lambda_n \ell_n) - 1\}\right.\right.$$

$$\left.\left. + \frac{B_{1n}}{\lambda_n}\sinh(\lambda_n \ell_n) + \frac{C_{1n}\ell_n^3}{3} + \frac{D_{1n}\ell_n^2}{2} + E_{1n}\ell_n\right]\right\}$$

$$i = 1, 2, 3 \qquad \text{(III-a-5)}$$

Equations III-a-3 and III-a-5 can be used in conjunction with the boundary conditions (Eq. III-a-2) in order to solve for the 15 unknown coefficients present in Eq. III-a-3, hence uniquely defining the first quasi-static function $g_{1i}(x_i)$.

Introducing $g_{11}(x_1)$ from Eq. III-a-3 into the boundary conditions results in the equations

$$B_{11} + E_{11} = 1$$

$$B_{11}\lambda_1^2 + 2C_{11} = 0$$

$$A_{11}\sinh(\lambda_1 \ell_1) + B_{11}\cosh(\lambda_1 \ell_1) + C_{11}\ell_1^2 + D_{11}\ell_1 + E_{11} = 0$$

$$A_{11}\lambda_1^2\sinh(\lambda_1 \ell_1) + B_{11}\lambda_1^2\cosh(\lambda_1 \ell_1) + 2C_{11} = 0$$

(III-a-6)

From the previous equations, the coefficients A_{11}, C_{11}, D_{11}, and E_{11} can be written in terms of B_{11} as

$$E_{11} = 1 - B_{11}$$

$$C_{11} = -\frac{1}{2} B_{11}\lambda_1^2$$

$$A_{11} = \frac{-B_{11}(\cosh(\lambda_1\ell_1) - 1)}{\sinh(\lambda_1\ell_1)} = -B_{11}\tanh\left(\frac{\lambda_1\ell_1}{2}\right)$$

$$D_{11} = \frac{1}{2} B_{11}\lambda_1^2\ell_1 - (1/\ell_1) \qquad \text{(III-a-7)}$$

Similarly, introducing $g_{12}(x_2)$ into the boundary conditions gives

$$B_{12} + E_{12} = 0$$

$$B_{12}\lambda_2^2 + 2C_{12} = 0$$

$$A_{12}\sinh(\lambda_2\ell_2) + B_{12}\cosh(\lambda_2\ell_2) + C_{12}\ell_2^2 + D_{12}\ell_2 + E_{12} = 0$$

$$A_{12}\lambda_2^2\sinh(\lambda_2\ell_2) + B_{12}\lambda_2^2\cosh(\lambda_2\ell_2) + 2C_{12} = 0 \qquad \text{(III-a-8)}$$

Again, the coefficients A_{12}, C_{12}, D_{12}, and E_{12} can be written in terms of B_{12} as

$$E_{12} = -B_{12}$$

$$C_{12} = -\frac{1}{2} B_{12}\lambda_2^2$$

$$A_{12} = -\frac{B_{12}(\cosh(\lambda_2\ell_2) - 1)}{\sinh(\lambda_2\ell_2)} = -B_{12}\tanh\left(\frac{\lambda_2\ell_2}{2}\right)$$

$$D_{12} = \frac{1}{2} B_{12}\lambda_2^2\ell_2 \qquad \text{(III-a-9)}$$

Introducing $g_{13}(x_3)$ into the boundary conditions gives

$$B_{13} + E_{13} = 0$$

$$B_{13}\lambda_3^3 + 2C_{13} = 0$$

$$A_{13}\sinh(\lambda_3\ell_3) + B_{13}\cosh(\lambda_3\ell_3) + C_{13}\ell_3^2 + D_{13}\ell_3 + E_{13} = 0$$

$$A_{13}\lambda_3^2\sinh(\lambda_3\ell_3) + B_{13}\lambda_3^2\cosh(\lambda_3\ell_3) + 2C_{13} = 0$$

(III-a-10)

which results in

$$E_{13} = - B_{13}$$

$$C_{13} = - \frac{1}{2} B_{13}\lambda_3^2$$

$$A_{13} = \frac{- B_{13}(\cosh(\lambda_3\ell_3) - 1)}{\sinh(\lambda_3\ell_3)} = - B_{13}\tanh\left(\frac{\lambda_3\ell_3}{2}\right)$$

$$D_{13} = \frac{1}{2} B_{13}\lambda_3^2\ell_3 \qquad \text{(III-a-11)}$$

From Eq. III-a-5, the following relationship is apparent:

$$\frac{C_{11}(G_1J_1 + H_w\frac{b^2}{2})}{\overset{*}{w}_1} = \frac{C_{12}(G_2J_2 + H_w\frac{b^2}{2})}{\overset{*}{w}_2} = \frac{C_{13}(G_3J_3 + H_2\frac{b^2}{2})}{\overset{*}{w}_3}$$

(III-a-12)

Using Eqs. III-a-7, 9, and 11, the previous equation can be written

$$\frac{B_{11}\lambda_1^2(G_1J_1 + H_w\frac{b^2}{2})}{\overset{*}{w}_1} = \frac{B_{12}\lambda_2^2(G_2J_2 + H_w\frac{b^2}{2})}{\overset{*}{w}_2} = \frac{B_{13}\lambda_3^2(G_3J_3 + H_w\frac{b^2}{2})}{\overset{*}{w}_3}$$

(III-a-13)

Therefore:

$$B_{12} = B_{11}(\overset{*}{w}_2/\overset{*}{w}_1)(\lambda_1/\lambda_2)^2 \frac{(G_1J_1 + H_w\frac{b^2}{2})}{(G_2J_2 + H_w\frac{b^2}{2})}$$

$$B_{13} = B_{11}(\overset{*}{w}_3/\overset{*}{w}_1)(\lambda_1/\lambda_3)^2 \frac{(G_1J_1 + H_w\frac{b^2}{2})}{(G_3J_3 + H_w\frac{b^2}{2})} \qquad \text{(III-a-14)}$$

Substituting Eqs. III-a-7, 9,11, and 14 into Eq. III-a-5 and solving for B_{11}

$$B_{11} = -\left(\frac{E_cA_c}{L_E}\right)\left(\frac{\overset{*}{w}_1b^2}{2H_w}\right)\left(\frac{\overset{*}{w}_1\ell_1}{2H_w}\right)\Big/\left\{\left(\frac{E_cA_c}{L_E}\right)\left(\frac{b^2}{2}\right)\left[\sum_{i=1}^{3}\left(\frac{w_i}{H_w}\right)^2\left(\frac{\lambda_1}{\lambda_i}\right)^2 \cdot \left(\frac{G_1J_1 + H_w\frac{b^2}{2}}{G_iJ_i + H_w\frac{b^2}{2}}\right)\left(\frac{2}{\lambda_i}\tanh\frac{\lambda_i\ell_i}{2} + \frac{\lambda_i^2\ell_i^3}{12} - \ell_i\right)\right] + \lambda_1^2\left[G_1J_1 + H_w\frac{b^2}{2}\right]\right\}$$

(III-a-15)

Once B_{11} is known, the quasi-static function $g_{1i}(x_i)$ is completely determined since the coefficients A_{1i}, B_{1i}, C_{1i}, D_{1i}, and E_{1i} appearing in Eq. III-a-3 can all be defined in terms of the coefficient B_{11} using Eqs. III-a-7, 9, 11, and 14.

B. Unit Rotation at Left Tower-Pier

The solution for the quasi-static function corresponding to unit rotation at support B of Fig. III-1 is obtained by satisfying the following three equations:

$$E_i\Gamma_i \frac{d^4 g_{2i}(x_i)}{dx_i^4} - (G_iJ_i + H_w \frac{b^2}{2}) \frac{d^2 g_{2i}(x_i)}{dx_i^2}$$

$$+ \frac{\overset{*}{w}_i b}{H_w}\left(\frac{E_c A_c}{L_E}\right)\left(\frac{b}{2}\right)\left[\sum_{n=1}^{3} \frac{\overset{*}{w}_n}{H_w} \int_0^{\ell_n} g_{2n}(x_n)dx_n\right] = 0$$

$$i = 1, 2, 3 \qquad \text{(III-a-16)}$$

subject to the boundary conditions

$$g_{21}(0) = 0 \qquad g_{22}(0) = 1 \qquad g_{23}(0) = 0$$

$$g_{21}(\ell_1) = 1 \qquad g_{22}(\ell_2) = 0 \qquad g_{23}(\ell_3) = 0$$

$$g_{21}''(0) = g_{22}''(0) = g_{23}''(0) = 0$$

$$g_{21}''(\ell_1) = g_{22}''(\ell_2) = g_{23}''(\ell_3) = 0 \qquad \text{(III-a-17)}$$

The form of the solution can be taken as

$$g_{2i}(x_i) = A_{2i}\sinh(\lambda_i x_i) + B_{2i}\cosh(\lambda_i x_i) + C_{2i}x_i^2$$

$$+ D_{2i}x_i + E_{2i} \qquad i = 1, 2, 3 \qquad \text{(III-a-18)}$$

where λ_i is defined by Eq. III-a-4.

Substituting Eq. III-a-18 into Eq. III-a-16 results in the following three equations:

$$2\left[G_i J_i + H_w \frac{b^2}{2}\right] C_{2i} = \frac{\overset{*}{w}_i b}{H_w} \left(\frac{E_c A_c}{L_E}\right)\left(\frac{b}{2}\right)\left\{ \sum_{n=1}^{3} \frac{\overset{*}{w}_n}{H_w}\left[\frac{A_{2n}}{\lambda_n}\{\cosh(\lambda_n \ell_n) - 1\}\right.\right.$$

$$\left.\left. + \frac{B_{2n}}{\lambda_n}\sinh(\lambda_n \ell_n) + \frac{C_{2n}\ell_n^3}{3} + \frac{D_{2n}\ell_n^2}{2} + E_{2n}\ell_n\right]\right\}$$

$$i = 1, 2, 3 \qquad \text{(III-a-19)}$$

Introducing $g_{21}(x_1)$ from Eq. III-a-18 into the boundary conditions results in the equations

$$B_{21} + E_{21} = 0$$

$$B_{21}\lambda_1^2 + 2C_{21} = 0$$

$$A_{21}\sinh(\lambda_1 \ell_1) + B_{21}\cosh(\lambda_1 \ell_1) + C_{21}\ell_1^2 + D_{21}\ell_1 + E_{21} = 1$$

$$A_{21}\lambda_1^2\sinh(\lambda_1 \ell_1) + B_{21}\lambda_1^2\cosh(\lambda_1 \ell_1) + 2C_{21} = 0 \qquad \text{(III-a-20)}$$

From the previous equations, the coefficients A_{21}, C_{21}, D_{21}, and E_{21} can be written in terms of B_{21} as

$$E_{21} = - B_{21}$$

$$C_{21} = - \frac{1}{2} B_{21}\lambda_1^2$$

$$A_{21} = \frac{- B_{21}(\cosh(\lambda_1 \ell_1) - 1)}{\sinh(\lambda_1 \ell_1)} = - B_{21} \tanh\left(\frac{\lambda_1 \ell_1}{2}\right)$$

$$D_{21} = \frac{1}{2} B_{21}\lambda_1^2 \ell_1 + (1/\ell_1) \qquad \text{(III-a-21)}$$

Similarly, introducing $g_{22}(x_2)$ into the boundary conditions gives

$$B_{22} + E_{22} = 1$$

$$B_{22}\lambda_2^2 + 2C_{22} = 0$$

$$A_{22}\sinh(\lambda_2\ell_2) + B_{22}\cosh(\lambda_2\ell_2) + C_{22}\ell_2^2 + D_{22}\ell_2 + E_{22} = 0$$

$$A_{22}\lambda_2^2\sinh(\lambda_2\ell_2) + B_{22}\lambda_2^2\cosh(\lambda_2\ell_2) + 2C_{22} = 0 \qquad \text{(III-a-22)}$$

From the previous equations, the coefficients A_{22}, C_{22}, D_{22}, and E_{22} can be written in terms of B_{22} as

$$E_{22} = 1 - B_{22}$$

$$C_{22} = -\frac{1}{2} B_{22}\lambda_2^2$$

$$A_{22} = \frac{-B_{22}(\cosh(\lambda_2\ell_2) - 1)}{\sinh(\lambda_2\ell_2)} = -B_{22}\tanh\left(\frac{\lambda_2\ell_2}{2}\right)$$

$$D_{22} = \frac{1}{2} B_{22}\lambda_2^2\ell_2 - (1/\ell_2) \qquad \text{(III-a-23)}$$

Introducing $g_{23}(x_3)$ into the boundary conditions gives

$$B_{23} + E_{23} = 0$$

$$B_{23}\lambda_3^2 + 2C_{23} = 0$$

$$A_{23}\sinh(\lambda_3\ell_3) + B_{23}\cosh(\lambda_3\ell_3) + C_{23}\ell_3^2 + D_{23}\ell_3 + E_{23} = 0$$

$$A_{23}\lambda_3^2\sinh(\lambda_3\ell_3) + B_{23}\lambda_3^2\cosh(\lambda_3\ell_3) + 2C_{23} = 0 \qquad \text{(III-a-24)}$$

which results in

$$E_{23} = - B_{23}$$

$$C_{23} = - \frac{1}{2} B_{23}\lambda_3^2$$

$$A_{23} = \frac{- B_{23}(\cosh(\lambda_3 \ell_3) - 1)}{\sinh(\lambda_3 \ell_3)} = - B_{23}\tanh\left(\frac{\lambda_3 \ell_3}{2}\right)$$

$$D_{23} = \frac{1}{2} B_{23}\lambda_3^2 \ell_3 \qquad \text{(III-a-25)}$$

From Eq. III-a-19, the following relationship is apparent:

$$\frac{C_{21}(G_1J_1 + H_w \frac{b^2}{2})}{\overset{*}{w}_1} = \frac{C_{22}(G_2J_2 + H_w \frac{b^2}{2})}{\overset{*}{w}_2} = \frac{C_{23}(G_3J_3 + H_w \frac{b^2}{2})}{\overset{*}{w}_3}$$

(III-a-26)

Using Eqs. III-a-21, 23, and 25, the previous equation can be written

$$\frac{B_{21}\lambda_1^2(G_1J_1 + H_w \frac{b^2}{2})}{\overset{*}{w}_1} = \frac{B_{22}\lambda_2^2(G_2J_2 + H_w \frac{b^2}{2})}{\overset{*}{w}_2} = \frac{B_{23}\lambda_3^2(G_3J_3 + H_w \frac{b^2}{2})}{\overset{*}{w}_3}$$

(III-a-27)

Therefore:

$$B_{22} = B_{21}(\overset{*}{w}_2/\overset{*}{w}_1)(\lambda_1/\lambda_2)^2 \frac{(G_1J_1 + H_w \frac{b^2}{2})}{(G_2J_2 + H_w \frac{b^2}{2})}$$

$$B_{23} = B_{21}(\overset{*}{w}_3/\overset{*}{w}_1)(\lambda_1/\lambda_3)^2 \frac{(G_1J_1 + H_w \frac{b^2}{2})}{(G_3J_3 + H_w \frac{b^2}{2})} \qquad \text{(III-a-28)}$$

Substituting Eqs. III-a-21, 23, 25, and 28 into Eqs. III-a-19 and solving for B_{21}

$$B_{21} = -\left(\frac{E_c A_c}{L_E}\right)\left(\frac{\overset{*}{w}_1 b^2}{2H_w}\right)\left(\frac{\overset{*}{w}_1 \ell_1}{2H_w} + \frac{\overset{*}{w}_2 \ell_2}{2H_w}\right) \Bigg/ \Bigg\{\left(\frac{E_c A_c}{L_E}\right)\left(\frac{b^2}{2}\right)\Bigg[\sum_{i=1}^{3}\left(\frac{\overset{*}{w}_i}{H_w}\right)^2$$

$$\cdot \left(\frac{\lambda_1}{\lambda_i}\right)^2 \left(\frac{G_1 J_1 + H_w \frac{b^2}{2}}{G_i J_i + H_w \frac{b^2}{2}}\right)\left(\frac{2}{\lambda_i}\tanh\frac{\lambda_i \ell_i}{2} + \frac{\lambda_i^2 \ell_i^3}{12} - \ell_i\right)\Bigg]$$

$$+ \lambda_1^2\left[G_1 J_1 + H_w \frac{b^2}{2}\right]\Bigg\} \qquad \text{(III-a-29)}$$

Once B_{21} is known, the quasi-static function $g_{2i}(x_i)$ is completely determined since the coefficients A_{2i}, B_{2i}, C_{2i}, D_{2i}, and E_{2i} appearing in Eq. III-a-18 can all be defined in terms of the coefficient B_{21} using Eqs. III-a-21, 23, 25 and 28.

C. Unit Rotation at Right Tower-Pier

The solution for the quasi-static function corresponding to unit rotation at support C of Fig. III-4 is obtained by satisfying the following three equations:

$$E_i \Gamma_i \frac{d^4 g_{3i}(x_i)}{dx_i^4} - \left(G_i J_i + H_w \frac{b^2}{2}\right)\frac{d^2 g_{3i}(x_i)}{dx_i^2}$$

$$+ \frac{\overset{*}{w}_i b}{H_w}\left(\frac{E_c A_c}{L_E}\right)\left(\frac{b}{2}\right)\left[\sum_{n=1}^{3}\frac{\overset{*}{w}_n}{H_w}\int_0^{\ell_n} g_{3n}(x_n)dx_n\right] = 0$$

$$i = 1, 2, 3 \qquad \text{(III-a-30)}$$

subject to the boundary conditions

$$g_{31}(0) = 0 \qquad g_{32}(0) = 0 \qquad g_{33}(0) = 1$$

$$g_{31}(\ell_1) = 0 \qquad g_{32}(\ell_2) = 1 \qquad g_{33}(\ell_3) = 0$$

$$g_{31}''(0) = g_{32}''(0) = g_{33}''(0) = 0$$

$$g_{31}''(\ell_1) = g_{32}''(\ell_2) = g_{33}''(\ell_3) = 0 \qquad \text{(III-a-31)}$$

The form of the solution can be taken as

$$g_{3i}(x_i) = A_{3i}\sinh(\lambda_i x_i) + B_{3i}\cosh(\lambda_i x_i) + C_{3i}x_i^2$$

$$+ D_{3i}x_i + E_{3i} \qquad i = 1, 2, 3 \qquad \text{(III-a-32)}$$

where λ_i is defined by Eq. III-a-4.

Substituting Eq. III-a-32 into Eq. III-a-30 results in the following three equations:

$$2\left[G_i J_i + H_w \frac{b^2}{2}\right] C_{3i} = \frac{\overset{*}{w}_i b}{H_w}\left(\frac{E_c A_c}{L_E}\right)\left(\frac{b}{2}\right)\left\{\sum_{n=1}^{3}\frac{\overset{*}{w}_n}{H_w}\left[\frac{A_{3n}}{\lambda_n}\{\cosh(\lambda_n \ell_n) - 1\}\right.\right.$$

$$\left.\left. + \frac{B_{3n}}{\lambda_n}\sinh(\lambda_n \ell_n) + \frac{C_{3n}\ell_n^3}{3} + \frac{D_{3n}\ell_n^2}{2} + E_{3n}\ell_n\right]\right\}$$

$$i = 1, 2, 3 \qquad \text{(III-a-33)}$$

Introducing $g_{31}(x_1)$ from Eq. III-a-32 into the boundary conditions results in the equations

$$B_{31} + E_{31} = 0$$

$$B_{31}\lambda_1^2 + 2C_{31} = 0$$

$$A_{31}\sinh(\lambda_1 \ell_1) + B_{31}\cosh(\lambda_1 \ell_1) + C_{31}\ell_1^2 + D_{31}\ell_1 + E_{31} = 0$$

$$A_{31}\lambda_1^2\sinh(\lambda_1 \ell_1) + B_{31}\lambda_1^2\cosh(\lambda_1 \ell_1) + 2C_{31} = 0 \qquad \text{(III-a-34)}$$

From the previous equations, the coefficients A_{31}, C_{31}, D_{31}, and E_{31} can be written in terms of B_{31} as

$$E_{31} = - B_{31}$$

$$C_{31} = - \frac{1}{2} B_{31}\lambda_1^2$$

$$A_{31} = \frac{- B_{31}(\cosh(\lambda_1 \ell_1) - 1)}{\sinh(\lambda_1 \ell_1)} = - B_{31} \tanh\left(\frac{\lambda_1 \ell_1}{2}\right)$$

$$D_{31} = \frac{1}{2} B_{31}\lambda_1^2 \ell_1 \qquad \text{(III-a-35)}$$

Similarly, introducing $g_{32}(x_2)$ into the boundary conditions gives

$$B_{32} + E_{32} = 0$$

$$B_{32}\lambda_2^2 + 2C_{32} = 0$$

$$A_{32}\sinh(\lambda_2 \ell_2) + B_{23}\cosh(\lambda_2 \ell_2) + C_{32}\ell_2^2 + D_{32}\ell_2 + E_{32} = 1$$

$$A_{32}\lambda_2^2\sinh(\lambda_2 \ell_2) + B_{32}\lambda_2^2\cosh(\lambda_2 \ell_2) + 2C_{32} = 0 \qquad \text{(III-a-36)}$$

Again, the coefficients A_{32}, C_{32}, D_{32}, and E_{32} can be written in terms of B_{32} as

$$E_{32} = - B_{32}$$

$$C_{32} = - \frac{1}{2} B_{32}\lambda_2^2$$

$$A_{32} = \frac{- B_{32}(\cosh(\lambda_2\ell_2) - 1)}{\sinh(\lambda_2\ell_2)} = - B_{32} \tanh\left(\frac{\lambda_2\ell_2}{2}\right)$$

$$D_{32} = \frac{1}{2} B_{32}\lambda_2^2\ell_2 + (1/\ell_2) \qquad \text{(III-a-37)}$$

Introducing $g_{33}(x_3)$ into the boundary conditions gives

$$B_{33} + E_{33} = 1$$

$$B_{33}\lambda_3^2 + 2C_{33} = 0$$

$$A_{33}\sinh(\lambda_3\ell_3) + B_{33}\cosh(\lambda_3\ell_3) + C_{33}\ell_3^2 + D_{33}\ell_3 + E_{33} = 0$$

$$A_{33}\lambda_3^2\sinh(\lambda_3\ell_3) + B_{33}\lambda_3^2\cosh(\lambda_3\ell_3) + 2C_{33} = 0 \qquad \text{(III-a-38)}$$

which results in

$$E_{33} = 1 - B_{33}$$

$$C_{33} = - \frac{1}{2} B_{33}\lambda_3^2$$

$$A_{33} = \frac{- B_{33}(\cosh(\lambda_3\ell_3) - 1)}{\sinh(\lambda_3\ell_3)} = - B_{33} \tanh\left(\frac{\lambda_3\ell_3}{2}\right)$$

$$D_{33} = \frac{1}{2} B_{33}\lambda_3^2\ell_3 - (1/\ell_3) \qquad \text{(III-a-39)}$$

From Eq. III-a-33, the following relationship is apparent:

$$\frac{C_{31}(G_1J_1 + H_w\frac{b^2}{2})}{\overset{*}{w}_1} = \frac{C_{32}(G_2J_2 + H_w\frac{b^2}{2})}{\overset{*}{w}_2} = \frac{C_{33}(G_3J_3 + H_w\frac{b^2}{2})}{\overset{*}{w}_3}$$

(III-a-40)

Using Eqs. III-a-35, 37, and 39, the previous equation can be written

$$\frac{B_{31}\lambda_1^2(G_1J_1 + H_w\frac{b^2}{2})}{\overset{*}{w}_1} = \frac{B_{32}\lambda_2^2(G_2J_2 + H_w\frac{b^2}{2})}{\overset{*}{w}_2} = \frac{B_{33}\lambda_3^2(G_3J_3 + H_2\frac{b^2}{2})}{\overset{*}{w}_3}$$

(III-a-41)

Therefore:

$$B_{32} = B_{31}(\overset{*}{w}_2/\overset{*}{w}_1)(\lambda_1/\lambda_2)^2\frac{(G_1J_1 + H_w\frac{b^2}{2})}{(G_2J_2 + H_w\frac{b^2}{2})}$$

$$B_{33} = B_{31}(\overset{*}{w}_3/\overset{*}{w}_1)(\lambda_1/\lambda_3)^2\frac{(G_1J_1 + H_w\frac{b^2}{2})}{(G_3J_3 + H_w\frac{b^2}{2})}$$

(III-a-42)

Substituting Eqs. III-a-35, 37, 39, and 42 into Eq. III-a-33 and solving for B_{31}

$$B_{31} = -\left(\frac{E_cA_c}{L_E}\right)\left(\frac{\overset{*}{w}_1b^2}{2H_w}\right)\left(\frac{\overset{*}{w}_2\ell_2}{2H_w} + \frac{\overset{*}{w}_3\ell_3}{2H_w}\right)\Bigg/\left\{\left(\frac{E_cA_c}{L_E}\right)\left(\frac{b^2}{2}\right)\left[\sum_{i=1}^{3}\left(\frac{\overset{*}{w}_i}{H_w}\right)^2\left(\frac{\lambda_1}{\lambda_i}\right)^2\right.\right.$$

$$\left.\left.\cdot\left(\frac{G_1J_1 + H_w\frac{b^2}{2}}{G_iJ_i + H_w\frac{b^2}{2}}\right)\left(\frac{2}{\lambda_i}\tanh\frac{\lambda_i\ell_i}{2} + \frac{\lambda_i^2\ell_i^3}{12} - \ell_i\right)\right] + \lambda_1^2\left[G_1J_1 + H_w\frac{b^2}{2}\right]\right\}$$

(III-a-43)

Once B_{31} is known, the quasi-static function $g_{3i}(x_i)$ is completely determined since the coefficients A_{3i}, B_{3i}, C_{3i}, D_{3i}, and E_{3i}

appearing in Eq. III-a-32 can all be defined in terms of the coefficient B_{31} using Eqs. III-a-35, 37, 39, and 42.

D. Unit Rotation at Right Anchorage

The solution for the quasi-static function corresponding to unit rotation at support D of Fig. III-4 is obtained by satisfying the following three equations:

$$E_i\Gamma_i \frac{d^4 g_{4i}(x_i)}{dx_i^4} - \left(G_iJ_i + H_w \frac{b^2}{2}\right) \frac{d^2 g_{4i}(x_i)}{dx_i^2}$$

$$+ \frac{\overset{*}{w}_i b}{H_w} \left(\frac{E_c A_c}{L_E}\right) \left(\frac{b}{2}\right) \left[\sum_{n=1}^{3} \frac{\overset{*}{w}_n}{H_w} \int_0^{\ell_n} g_{4n}(x_n)dx_n\right] = 0$$

$$i = 1, 2, 3 \qquad \text{(III-a-44)}$$

subject to the boundary conditions

$$g_{41}(0) = 0 \qquad g_{42}(0) = 0 \qquad g_{43}(0) = 0$$

$$g_{41}(\ell_1) = 0 \qquad g_{42}(\ell_2) = 0 \qquad g_{43}(\ell_3) = 1$$

$$g_{41}''(0) = g_{42}''(0) = g_{43}''(0) = 0$$

$$g_{41}''(\ell_1) = g_{42}''(\ell_2) = g_{43}''(\ell_3) = 0 \qquad \text{(III-a-45)}$$

The form of the solution can be taken as

$$g_{4i}(x_i) = A_{4i}\sinh(\lambda_i x_i) + B_{4i}\cosh(\lambda_i x_i) + C_{4i}x_i^2$$

$$+ D_{4i}x_i + E_{4i} \qquad i = 1, 2, 3 \qquad \text{(III-a-46)}$$

where λ_i is defined by Eq. III-a-4.

Substituting Eq. III-a-46 into Eq. III-a-44 results in the following three equations:

$$2\left[G_i J_i + H_w \frac{b^2}{2}\right] C_{4i} = \frac{\overset{*}{w}_i b}{H_w}\left(\frac{E_c A_c}{L_E}\right)\left(\frac{b}{2}\right)\left\{\sum_{n=1}^{3} \frac{\overset{*}{w}_n}{H_w}\left[\frac{A_{4n}}{\lambda_n}\{\cosh(\lambda_n \ell_n) - 1\}\right.\right.$$

$$\left.\left. + \frac{B_{4n}}{\lambda_n}\sinh(\lambda_n \ell_n) + \frac{C_{4n}\ell_n^3}{3} + \frac{D_{4n}\ell_n^2}{2} + E_{4n}\ell_n\right]\right\}$$

$$i = 1, 2, 3 \qquad \text{(III-a-47)}$$

Introducing $g_{41}(x_1)$ from Eq. III-a-46 into the boundary conditions results in the equations

$$B_{41} + E_{41} = 0$$

$$B_{41}\lambda_1^2 + 2C_{41} = 0$$

$$A_{41}\sinh(\lambda_1 \ell_1) + B_{41}\cosh(\lambda_1 \ell_1) + C_{41}\ell_1^2 + D_{41}\ell_1 + E_{41} = 0$$

$$A_{41}\lambda_1^2\sinh(\lambda_1 \ell_1) + B_{41}\lambda_1^2\cosh(\lambda_1 \ell_1) + 2C_{41} = 0 \qquad \text{(III-a-48)}$$

From the previous equations, the coefficients A_{41}, C_{41}, D_{41}, and E_{41} can be written in terms of B_{41} as

$$E_{41} = - B_{41}$$

$$C_{41} = - \frac{1}{2} B_{41}\lambda_1^2$$

$$A_{41} = \frac{- B_{41}(\cosh(\lambda_1 \ell_1) - 1)}{\sinh(\lambda_1 \ell_1)} = - B_{41} \tanh\left(\frac{\lambda_1 \ell_1}{2}\right)$$

$$D_{41} = \frac{1}{2} B_{41}\lambda_1^2 \ell_1 \qquad \text{(III-a-49)}$$

Similarly, introducing $g_{42}(x_2)$ into the boundary conditions gives

$$B_{42} + E_{42} = 0$$

$$B_{42}\lambda_2^2 + 2C_{42} = 0$$

$$A_{42}\sinh(\lambda_2\ell_2) + B_{42}\cosh(\lambda_2\ell_2) + C_{42}\ell_2^2 + D_{42}\ell_2 + E_{42} = 0$$

$$A_{42}\lambda_2^2\sinh(\lambda_2\ell_2) + B_{42}\lambda_2^2\cosh(\lambda_2\ell_2) + 2C_{42} = 0 \qquad \text{(III-a-50)}$$

Again, the coefficients A_{42}, C_{42}, D_{42}, and E_{42} can be written in terms of B_{42} as

$$E_{42} = - B_{42}$$

$$C_{42} = - \frac{1}{2} B_{42}\lambda_2^2$$

$$A_{42} = \frac{- B_{42}(\cosh(\lambda_2\ell_2) - 1)}{\sinh(\lambda_2\ell_2)} = - B_{42} \tanh\left(\frac{\lambda_2\ell_2}{2}\right)$$

$$D_{42} = \frac{1}{2} B_{42}\lambda_2^2\ell_2 \qquad \text{(III-a-51)}$$

Introducing $g_{43}(x_3)$ into the boundary conditions gives

$$B_{43} + E_{43} = 0$$

$$B_{43}\lambda_3^2 + 2C_{43} = 0$$

$$A_{43}\sinh(\lambda_3\ell_3) + B_{43}\cosh(\lambda_3\ell_3) + C_{43}\ell_3^2 + D_{43}\ell_3 + E_{43} = 1$$

$$A_{43}\lambda_3^2\sinh(\lambda_3\ell_3) + B_{43}\lambda_3^2\cosh(\lambda_3\ell_3) + 2C_{43} = 0 \qquad \text{(III-a-52)}$$

which results in

$$E_{43} = - B_{43}$$

$$C_{43} = - \frac{1}{2} B_{43} \lambda_3^2$$

$$A_{43} = \frac{- B_{43}(\cosh(\lambda_3 \ell_3) - 1)}{\sinh(\lambda_3 \ell_3)} = - B_{43} \tanh\left(\frac{\lambda_3 \ell_3}{2}\right)$$

$$D_{43} = \frac{1}{2} B_{43} \lambda_3^2 \ell_3 + (1/\ell_3) \qquad \text{(III-a-53)}$$

From Eq. III-a-47, the following relationship is apparent:

$$\frac{C_{41}(G_1 J_1 + H_w \frac{b^2}{2})}{\overset{*}{w}_1} = \frac{C_{42}(G_2 J_2 + H_w \frac{b^2}{2})}{\overset{*}{w}_2} = \frac{C_{43}(G_3 J_3 + H_w \frac{b^2}{2})}{\overset{*}{w}_3}$$

(III-a-54)

Using Eqs. III-a-49, 51, and 53, the previous equation can be written

$$\frac{B_{41}\lambda_1^2(G_1 J_1 + H_w \frac{b^2}{2})}{\overset{*}{w}_1} = \frac{B_{42}\lambda_2^2(G_2 J_2 + H_w \frac{b^2}{2})}{\overset{*}{w}_2} = \frac{B_{43}\lambda_3^2(G_3 J_3 + H_w \frac{b^2}{2})}{\overset{*}{w}_3}$$

(III-a-55)

Therefore:

$$B_{42} = B_{41}(\overset{*}{w}_2/\overset{*}{w}_1)(\lambda_1/\lambda_2)^2 \frac{(G_1 J_1 + H_w \frac{b^2}{2})}{(G_2 J_2 + H_w \frac{b^2}{2})}$$

$$B_{43} = B_{41}(\overset{*}{w}_3/\overset{*}{w}_1)(\lambda_1/\lambda_3)^2 \frac{(G_1 J_1 + H_w \frac{b^2}{2})}{(G_3 J_3 + H_w \frac{b^2}{2})} \qquad \text{(III-a-56)}$$

Substituting Eqs. III-a-49, 51, 53, and 56 into Eq. III-a-47 and solving for B_{41}

$$B_{41} = -\left(\frac{E_c A_c}{L_E}\right)\left(\frac{\overset{*}{w}_1 b^2}{2H_w}\right)\left(\frac{\overset{*}{w}_3 \ell_3}{2H_w}\right) \Bigg/ \left\{\left(\frac{E_c A_c}{L_E}\right)\left(\frac{b^2}{2}\right)\left[\sum_{i=1}^{3}\left(\frac{\overset{*}{w}_i}{H_w}\right)^2\left(\frac{\lambda_1}{\lambda_i}\right)^2 \cdot \left(\frac{G_1 J_1 + H_w \frac{b^2}{2}}{G_i J_i + H_w \frac{b^2}{2}}\right)\left(\frac{2}{\lambda_i}\tanh\frac{\lambda_i \ell_i}{2} - \frac{\lambda_i^2 \ell_i^3}{12} - \ell_i\right)\right] + \lambda_1^2\left[G_1 J_1 + H_w \frac{b^2}{2}\right]\right\}$$

(III-a-57)

Once B_{41} is known, the quasi-static function $g_{4i}(x_i)$ is completely determined since the coefficients A_{4i}, B_{4i}, C_{4i}, D_{4i}, and E_{4i} appearing in Eq. III-a-46 can all be defined in terms of the coefficient B_{41} using Eqs. III-a-49, 51, 53, and 56.

Appendix III-b

Solutions for the Torsional Mode Shapes

If it is assumed that the mass of the bridge as well as its elastic properties are uniform along the i^{th} span, the eigenvalue problem assumes the form

$$I_{mi}\frac{\partial^2\eta_i}{\partial t^2} + E_i\Gamma_i\frac{\partial^4\eta_i}{\partial x_i^4} - \left(G_iJ_i + H_w\frac{b^2}{2}\right)\frac{\partial^2\eta_i}{\partial x_i^2} + \frac{\overset{*}{w}_i b}{H_w}\left[\left(\frac{E_cA_c}{L_E}\right)\frac{b}{2}\sum_{n=1}^{3}\frac{\overset{*}{w}_n}{H_w}\int_0^{\ell_n}\eta_n(x_n,t)\,dx_n\right] = 0$$

$$i = 1, 2, 3 \qquad \text{(III-b-1)}$$

where the bracketed term in Eq. III-b-1 represents the additional horizontal component of cable tension H(t).

The n^{th} torsional mode shape and natural frequency is obtained by assuming the vibration to be sinusoidal, that is

$$\eta_j(x_j,t) = \Theta_{nj}(x_j)e^{i\omega_n t}$$

$$j = 1, 2, 3 \qquad n = 1, 2, 3 \ldots \qquad \text{(III-b-2)}$$

in which $i = \sqrt{-1}$ and ω_n is the n^{th} natural circular frequency of torsional vibration. Substituting Eq. III-b-2 into Eq. III-b-1 yields the equations of motion in the form

$$E_i\Gamma_i\frac{d^4\Theta_{ni}}{dx_i^4} - \left(G_iJ_i + H_w\frac{b^2}{2}\right)\frac{d^2\Theta_{ni}}{dx_i^2} - I_{mi}\omega_n^2\Theta_{ni} + \frac{\overset{*}{w}_i b}{H_w}\tilde{H}_n = 0$$

$$i = 1, 2, 3 \qquad n = 1, 2, 3 \ldots \qquad \text{(III-b-3)}$$

where the additional horizontal component of cable tension associated with the n^{th} torsional mode shape, $\tilde{H}_n$, is given by

$$\tilde{H}_n = \left(\frac{E_c A_c}{L_E}\right)\left(\frac{b}{2}\right) \sum_{j=1}^{3} \frac{\overset{*}{w}_j}{H_w} \int_0^{\ell_j} \Theta_{nj}(x_j)dx_j$$

$$n = 1, 2, 3 \ldots \qquad \text{(III-b-4)}$$

Because $\tilde{H}_n$ is independent of x_j and may be treated as a constant, Eq. III-b-3 represents linear, ordinary differential equations of fourth order with constant coefficients. The general solutions of Eq. III-b-3 are expressed as

$$\Theta_{ni}(x_i) = A_i \sin\left(\frac{\mu_i x_i}{\ell_i}\right) + B_i \cos\left(\frac{\mu_i x_i}{\ell_i}\right) + C_i \sinh\left(\frac{\nu_i x_i}{\ell_i}\right) + D_i \cosh\left(\frac{\nu_i x_i}{\ell_i}\right) + \frac{\overset{*}{w}_i b \tilde{H}_n}{I_{mi} H_w \omega_n^2}$$

$$i = 1, 2, 3 \qquad n = 1, 2, 3 \ldots \qquad \text{(III-b-5)}$$

where

$$\mu_i = \delta_i \sqrt{\frac{Z_i + 1}{2}}$$

$$\nu_i = \delta_i \sqrt{\frac{Z_i - 1}{2}}$$

$$Z_i = \sqrt{1 + \frac{4 I_{mi} \ell_i^2 \omega_n^2}{\delta_i^2 \left(G_i J_i + H_w \frac{b^2}{2}\right)}}$$

$$\delta_i = \ell_i \sqrt{\frac{G_i J_i + H_w \frac{b^2}{2}}{E_i \Gamma_i}}$$

$$i = 1, 2, 3 \qquad n = 1, 2, 3 \ldots \qquad \text{(III-b-6)}$$

and A_i, B_i, C_i, and D_i are arbitrary constants determined in conformity with the boundary conditions at the supports of the i^{th} stiffening structure. The first four terms in Eq. III-b-5 represent the general solutions of the homogeneous equations ($\tilde{H}_n = 0$), while the last term of the same equation represents the particular solutions of the complete differential equations.

It is convenient to separate the investigation of the symmetric torsional modes from that of the antisymmetric torsional modes; that is, the problem can be divided into two parts:

1. The symmetric torsional modes of vibration in which there are an even number of internal nodes along the center span. Here $\tilde{H}_n$ is not zero.
2. The antisymmetric torsional modes of vibration in which there are an odd number of internal nodes along the center span. Here $\tilde{H}_n$ is zero.

Symmetric Modes of Torsional Vibration

When the bridge is a three-span symmetric type in which the stiffening structure of each span are simply supported by cables held on top of the towers by roller supports, the boundary conditions become

$$\text{for} \quad x_i = 0 \qquad \Theta_{ni} = 0 \quad , \quad E_i\Gamma_i \frac{d^2\Theta_{ni}}{dx_i^2} = 0$$

$$\text{for} \quad x_i = \ell_i \qquad \Theta_{ni} = 0 \quad , \quad E_i\Gamma_i \frac{d^2\Theta_{ni}}{dx_i^2} = 0$$

$$i = 1, 2, 3 \qquad n = 1, 2, 3 \ldots \qquad \text{(III-b-7)}$$

expressing the fact that the angle of twist and the normal stresses are zero at the supports of each span. Introducing Eq. III-b-5 into the above boundary conditions establishes the symmetric torsional modes as

$$\Theta_{ni}(x_i) = \frac{\overset{*}{w}_i b \tilde{H}_n}{2 I_{mi} H_w Z_i \omega_n^2} \left[2Z_i - \frac{Z_i + 1}{\cos(\mu_i/2)} \cos\left[\mu_i\left(\frac{1}{2} - \frac{x_i}{\ell_i}\right)\right] \right.$$

$$\left. - \frac{Z_i - 1}{\cosh(\nu_i/2)} \cosh\left[\nu_i\left(\frac{1}{2} - \frac{x_i}{\ell_i}\right)\right] \right]$$

$$i = 1, 2, 3 \qquad n = 1, 2, 3 \ldots \qquad \text{(III-b-8)}$$

Finally, substituting Eq. III-b-8 into Eq. III-b-4 in order to obtain the frequency equation, the following transcendental equation upon the natural circular frequency ω_n is obtained

$$\frac{L_E}{E_c A_c} = \left(\frac{b^2}{2}\right) \left\{ \sum_{i=1}^{3} \left(\frac{\overset{*}{w}_i}{H_w}\right)^2 \left(\frac{\ell_i}{I_{mi} Z_i \omega_n^2}\right) \left[Z_i - \left(\frac{Z_i + 1}{\mu_i}\right) \tan\left(\frac{\mu_i}{2}\right) \right.\right.$$

$$\left.\left. - \left(\frac{Z_i - 1}{\nu_i}\right) \tanh\left(\frac{\nu_i}{2}\right) \right\}\right.$$

$$n = 1, 2, 3 \ldots \qquad \text{(III-b-9)}$$

Antisymmetric Modes of Torsional Vibration

An antisymmetric vibration deflection of the cable and stiffening structure causes no additional cable tension $\tilde{H}_n$. Therefore, there is no interaction between the center span and side spans. For

this reason, two types of independent vibration in a three-span bridge are possible. Setting $\tilde{H}_n = 0$ in Eq. III-b-5 yields

$$\Theta_{ni}(x_i) = A_i \sin\left(\frac{\mu_i x_i}{\ell_i}\right) + B_i \cos\left(\frac{\mu_i x_i}{\ell_i}\right)$$

$$+ C_i \sinh\left(\frac{\nu_i x_i}{\ell_i}\right) + D_i \cosh\left(\frac{\nu_i x_i}{\ell_i}\right)$$

$$i = 1, 2, 3 \qquad n = 1, 2, 3 \ldots \qquad \text{(III-b-10)}$$

The boundary conditions for the center span are

$$\text{for} \quad x_2 = 0 \qquad \Theta_{n2} = 0 \quad , \quad E_2\Gamma_2 \frac{d^2\Theta_{n2}}{dx_2^2} = 0$$

$$\text{for} \quad x_2 = \frac{\ell_2}{2} \qquad \Theta_{n2} = 0 \quad , \quad E_2\,{}_2 \frac{d^2\Theta_{n2}}{dx_2^2} = 0$$

$$n = 1, 2, 3 \ldots \qquad \text{(III-b-11)}$$

The second part of Eq. III-b-11 indicates that the center of the span remains at rest and is also an inflection point.

Substituting Eq. III-b-10 into the boundary conditions (Eq. III-b-11), the frequency equation is derived in the form

$$\sin\left(\frac{\mu_2}{2}\right) = 0 \qquad \text{(III-b-12)}$$

from which it may be seen

$$\mu_2 = 2\pi, 4\pi, 6\pi \ldots, \qquad \text{(III-b-13)}$$

The antisymmetric torsional modes of vibration for the center span then become

$$\Theta_{m2}(x_2) = A_2 \sin \frac{m\pi x_2}{\ell_2}$$

$$m = 2, 4, 6 \ldots \qquad \text{(III-b-14)}$$

Substituting this last expression into Eq. III-b-3 (with $\tilde{H}_n = 0$), the natural circular frequencies for the center span are determined

$$\omega_{2m} = \sqrt{\frac{E_2\Gamma_2}{I_{m2}} + \frac{\left(G_2J_2 + H_w\frac{b^2}{2}\right)\ell_2^2}{I_{m2}m^2\pi^2}}$$

$$m = 2, 4, 6 \ldots \qquad \text{(III-b-15)}$$

The boundary conditions for the side spans are

$$\text{for} \quad x_j = 0 \qquad \Theta_{nj} = 0 \quad , \quad E_j\Gamma_j \frac{d^2\Theta_{nj}}{dx_j^2} = 0$$

$$\text{for} \quad x_j = \ell_j \qquad \Theta_{nj} = 0 \quad , \quad E_j\Gamma_j \frac{d^2\Theta_{nj}}{dx_j^2} = 0$$

$$j = 1, 3 \qquad n = 1, 2, 3 \ldots \qquad \text{(III-b-16)}$$

Substituting Eq. III-b-10 into the above boundary conditions, the frequency equation is derived in the form

$$\sin \mu_j = 0 \qquad j = 1, 3 \qquad \text{(III-b-17)}$$

from which it may be seen

$$\mu_j = \pi,\ 2\pi,\ 3\pi \ldots \qquad j = 1,\ 3 \qquad \text{(III-b-18)}$$

The antisymmetric torsional modes of vibration for the side spans then become

$$\Theta_{mj}(x_j) = A_j \sin\left(\frac{m\pi x_j}{\ell_j}\right)$$

$$j = 1,\ 3 \qquad m = 1,\ 2,\ 3 \ldots \qquad \text{(III-b-19)}$$

Substituting this last expression into Eq. III-b-3 (with $\tilde{H}_n = 0$), the natural frequencies for the side span vibration are determined

$$\omega_{jm} = \left(\frac{m\pi}{\ell_j}\right)^2 \sqrt{\frac{E_j \Gamma_j}{I_{mj}} + \frac{\left(G_j J_j + H_w \frac{b^2}{2}\right)\ell_j^2}{I_{mj}\, m^2\pi^2}}$$

$$j = 1,\ 3 \qquad m = 1,\ 2,\ 3 \ldots \qquad \text{(III-b-20)}$$

Appendix III-c

Orthogonality of Torsional Mode Shapes

The n^{th} torsional mode shape, $\Theta_{ni}(x_i)$, satisfies the equation

$$- \omega_n^2 I_{mi} \Theta_{ni}(x_i) + E_i \Gamma_i \Theta_{ni}^{IV}(x_i) - \left(G_i J_i + H_w \frac{b^2}{2}\right) \Theta_{ni}''(x_i)$$

$$+ \left(\frac{w_i^* b}{H_w}\right)\left[\left(\frac{E_c A_c}{L_E}\right)\left(\frac{b}{2}\right) \sum_{j=1}^{3} \frac{w_j^*}{H_w} \int_0^{\ell_j} \Theta_{nj}(x_j)dx_j\right] = 0$$

$$i = 1, 2, 3 \qquad n = 1, 2, 3 \ldots \qquad \text{(III-c-1)}$$

where ω_n is the n^{th} natural circular frequency of torsional vibration.

The m^{th} torsional mode shape, $\Theta_{mi}(x_i)$, satisfies a similar equation, that is

$$- \omega_m^2 I_{mi} \Theta_{mi}(x_i) + E_i \Gamma_i \Theta_{mi}^{IV}(x_i) - \left(G_i J_i + H_w \frac{b^2}{2}\right) \Theta_{mi}''(x_i)$$

$$+ \left(\frac{w_i^* b}{H_w}\right)\left[\left(\frac{E_c A_c}{L_E}\right)\left(\frac{b}{2}\right) \sum_{j=1}^{3} \frac{w_j^*}{H_w} \int_0^{\ell_j} \Theta_{mj}(x_j)dx_j\right] = 0$$

$$i = 1, 2, 3 \qquad n = 1, 2, 3 \ldots \qquad \text{(III-c-2)}$$

Multiplying Eq. III-c-1 by $\Theta_{mi}(x_i)$, integrating from zero to ℓ_i and summing over all three spans, (i = 1, 2, 3), results in

$$- \omega_n^2 \left[\sum_{i=1}^{3} I_{mi} \int_0^{\ell_i} \Theta_{ni}(x_i)\Theta_{mi}(x_i)dx_i \right]$$

$$+ \left[\sum_{i=1}^{3} E_i\Gamma_i \int_0^{\ell_i} \Theta_{ni}^{IV}(x_i)\Theta_{mi}(x_i)dx_i \right]$$

$$- \left[\sum_{i=1}^{3} \left(G_iJ_i + H_w \frac{b^2}{2} \right) \int_0^{\ell_i} \Theta_{ni}''(x_i)\Theta_{mi}(x_i)dx_i \right]$$

$$+ \left(\frac{E_cA_c}{L_E} \right) \left(\frac{b^2}{2} \right) \left[\sum_{i=1}^{3} \frac{w_i^*}{H_w} \int_0^{\ell_i} \Theta_{mi}(x_i)dx_i \right] \cdot$$

$$\cdot \left[\sum_{j=1}^{3} \frac{w_j^*}{H_w} \int_0^{\ell_j} \Theta_{nj}(x_j)dx_j \right] = 0$$

$$n = 1, 2, 3 \ldots \qquad \text{(III-c-3)}$$

Multiplying Eq. III-c-2 by $\Theta_{ni}(x_i)$, integrating from zero to ℓ_i, and summing over all three spans, (i = 1, 2, 3), results in

$$- \omega_m^2 \left[\sum_{i=1}^{3} I_{mi} \int_0^{\ell_i} \Theta_{ni}(x_i)\Theta_{mi}(x_i)dx_i \right]$$

$$+ \left[\sum_{i=1}^{3} E_i\Gamma_i \int_0^{\ell_i} \Theta_{mi}^{IV}(x_i)\Theta_{ni}(x_i)dx_i \right]$$

$$- \left[\sum_{i=1}^{3} \left(G_iJ_i + H_w \frac{b^2}{2} \right) \int_0^{\ell_i} \Theta_{mi}''(x_i)\Theta_{ni}(x_i)dx_i \right]$$

$$+ \left(\frac{E_c A_c}{L_E}\right) \left(\frac{b^2}{2}\right) \left[\sum_{i=1}^{3} \frac{\overset{*}{w}_i}{H_w} \int_0^{\ell_i} \Theta_{ni}(x_i)dx_i\right]$$

$$\cdot \left[\sum_{j=1}^{3} \frac{\overset{*}{w}_j}{H_w} \int_0^{\ell_j} \Theta_{mj}(x_j)dx_j\right] = 0$$

$$m = 1, 2, 3 \ldots \qquad \text{(III-c-4)}$$

Subtracting Eq. III-c-3 from Eq. III-c-4 yields

$$(\omega_n^2 - \omega_m^2)\left[\sum_{i=1}^{3} I_{mi} \int_0^{\ell_i} \Theta_{ni}(x_i)\Theta_{mi}(x_i)dx_i\right]$$

$$+ \left[\sum_{i=1}^{3} E_i\Gamma_i \int_0^{\ell_i} \{\Theta_{mi}^{IV}(x_i)\Theta_{ni}(x_i) - \Theta_{ni}^{IV}(x_i)\Theta_{mi}(x_i)\ dx_i\right]$$

$$- \left[\sum_{i=1}^{3} \left(G_iJ_i + H_w\frac{b^2}{2}\right)\int_0^{\ell_i} \{\Theta''_{mi}(x_i)\Theta_{ni}(x_i)\right.$$

$$\left. - \Theta''_{ni}(x_i)\Theta_{mi}(x_i)\}dx_i\right] = 0$$

$$n = 1, 2, 3 \ldots \qquad m = 1, 2, 3 \ldots \qquad \text{(III-c-5)}$$

Now the last two bracketed terms in Eq. III-c-5 can be shown to vanish by integrating by parts. For example:

$$\int_0^{\ell_i} \Theta''_{mi}(x_i)\Theta_{ni}(x_i)dx_i = \Theta_{ni}(x_i)\Theta'_{mi}(x_i)\Big|_0^{\ell_i} - \int_0^{\ell_i} \Theta'_{mi}(x_i)\Theta'_{ni}(x_i)dx_i$$

$$= - \int_0^{\ell_i} \Theta'_{mi}(x_i)\Theta'_{ni}(x_i)dx_i$$

$$n = 1, 2, 3 \ldots \qquad m = 1, 2, 3 \ldots \qquad \text{(III-c-6)}$$

since $\Theta_{ni}(0) = \Theta_{ni}(\ell_i) = 0$ from the boundary conditions.

Similarly,

$$\int_0^{\ell_i} \Theta''_{ni}(x_i)\Theta_{mi}(x_i)dx_i = \Theta_{mi}(x_i)\Theta'_{ni}(x_i)\Big|_0^{\ell_i} - \int_0^{\ell_i} \Theta'_{mi}(x_i)\Theta'_{ni}(x_i)dx_i$$

$$= - \int_0^{\ell_i} \Theta'_{mi}(x_i)\Theta'_{ni}(x_i)dx_i$$

$$n = 1, 2, 3 \ldots \qquad m = 1, 2, 3 \ldots \qquad \text{(III-c-7)}$$

Also it can be seen that

$$\int_0^{\ell_i} \Theta_{mi}^{IV}(x_i)\Theta_{ni}(x_i)dx_i = \Theta_{ni}(x_i)\Theta_{mi}'''(x_i)\Big|_0^{\ell_i}$$

$$- \int_0^{\ell_i} \Theta_{mi}'''(x_i)\Theta_{ni}'(x_i)dx_i$$

$$= - \Theta_{ni}'(x_i)\Theta_{mi}''(x_i)\Big|_0^{\ell_i}$$

$$+ \int_0^{\ell_i} \Theta_{mi}''(x_i)\Theta_{ni}''(x_i)dx_i$$

$$= \int_0^{\ell_i} \Theta_{mi}''(x_i)\Theta_{ni}''(x_i)dx_i$$

$$n = 1, 2, 3 \ldots \qquad m = 1, 2, 3 \ldots \qquad \text{(III-c-8)}$$

since $\Theta_{ni}(0) = \Theta_{ni}(\ell_i) = 0$ and $\Theta_{mi}''(0) = \Theta_{mi}''(\ell_i) = 0$ from the boundary conditions.

Similarly,

$$\int_0^{\ell_i} \Theta_{ni}^{IV}(x_i)\Theta_{mi}(x_i)dx_i = \Theta_{mi}(x_i)\Theta_{ni}'''(x_i)\Big|_0^{\ell_i}$$

$$- \int_0^{\ell_i} \Theta_{ni}'''(x_i)\Theta_{mi}'(x_i)\,dx_i$$

$$= - \Theta'_{mi}(x_i)\Theta''_{ni}(x_i)\Big|_0^{\ell_i}$$

$$+ \int_0^{\ell_i} \Theta''_{mi}(x_i)\Theta''_{ni}(x_i)dx_i$$

$$= \int_0^{\ell_i} \Theta''_{mi}(x_i)\Theta''_{ni}(x_i)dx_i$$

$$n = 1, 2, 3 \ldots \qquad m = 1, 2, 3 \ldots \qquad \text{(III-c-9)}$$

Substituting Eqs. III-c-6, 7, 8 and 9 into Eq. III-c-5 yields modal orthogonality of the form

$$(\omega_n^2 - \omega_m^2)\left[\sum_{i=1}^{3} I_{mi} \int_0^{\ell_i} \Theta_{ni}(x_i)\Theta_{mi}(x_i)dx_i\right] = 0$$

$$n = 1, 2, 3 \ldots \qquad m = 1, 2, 3 \ldots \qquad \text{(III-c-10)}$$

That is

$$\sum_{i=1}^{3} I_{mi} \int_0^{\ell_i} \Theta_{ni}(x_i)\Theta_{mi}(x_i)dx_i = 0 \quad \text{for} \quad n \neq m$$

(III-c-11)

Appendix III-d

Cable Tension Response in Frequency Domain

The finite Fourier transform of the vibrational horizontal component of cable tension is given by

$$H(\omega) = \left(\frac{E_c A_c}{L_E}\right)\left(\frac{b}{2}\right)\left\{\sum_{i=1}^{3}\left[\frac{\overset{*}{w}_i}{H_w}\left\{\int_0^{\ell_i}\sum_{n=1}^{\infty}\Theta_{ni}(x_i)dx_i\right\}Q_n(\omega)\right.\right.$$

$$\left.+\frac{\overset{*}{w}_i}{H_w}\sum_{j=1}^{4}\left\{\int_0^{\ell_i} g_{ji}(x_i)dx_i\right\}\Psi_j(\omega) - \frac{\overset{*}{w}_i \ell_i}{2H_w}\{\Psi_{i+1}(\omega) + \Psi_i(\omega)\}\right]$$

$$\left.+\{\Phi_4(\omega) - \Phi_1(\omega)\}\right\} \qquad \text{(III-d-1)}$$

where $\Psi_j(\omega)$, (j = 1, 2, 3, 4), is the finite Fourier transform of the j^{th} ground motion rocking input and $\Phi_j(\omega)$, (j = 1, 4) is the finite Fourier transform of the j^{th} ground motion torsional input over the duration of the ground motion T_1, and $Q_n(\omega)$ is the finite Fourier transform of the n^{th} generalized coordinate given by

$$\Psi_j(\omega) = \int_0^{T_1}\Psi_j(t)e^{-i\omega t}\,dt \qquad j = 1, 2, 3, 4$$

$$\Phi_j(\omega) = \int_0^{T_1}\phi_j(t)e^{-i\omega t}\,dt \qquad j = 1, 4 \qquad \text{(III-d-2)}$$

$$Q_n(\omega) = \{H_n(\omega)\}^T\{\Psi(\omega)\} \qquad n = 1, 2, 3 \ldots \qquad \text{(III-d-3)}$$

where $\{H_n(\omega)\}^T$ is the transposed complex frequency response vector corresponding to the n^{th} torsional vibration mode, and $\{\Psi(\omega)\}$ is the Fourier transform vector of the rotational ground motion displacement inputs.

The power spectrum of H(t) may be approximated as

$$G_H(\omega) \simeq \frac{2}{T_1} \overset{*}{H}(\omega)\ H(\omega) \qquad \text{(III-d-4)}$$

where T_1 is the duration of the ground motion and the superposed asterisk denotes complex conjugate.

Substituting Eqs. III-d-1 and III-d-3 into the previous equation results in an expression involving sixteen different terms. These will be taken one at a time in this section in order to isolate the effects of input correlation.

A. Pure Relative Response

In performing the multiplication of Eq. III-d-4, one of the terms encountered involves the first term of Eq. III-d-1 multiplied by its complex conjugate, that is

$$G_A(\omega) = \left(\frac{E_c A_c}{L_E}\right)^2 \left(\frac{b}{2}\right)^2 \left(\frac{2}{T_1}\right) \left[\sum_{i=1}^{3} \left(\frac{\overset{*}{w}_i}{H_w}\right) \left\{ \left[\int_0^{\ell_i} \sum_{n=1}^{\infty} \Theta_{ni}(x_i)\,dx_i \right] \overset{*}{Q}_n(\omega) \right\} \right]$$

$$\cdot \left[\sum_{j=1}^{3} \left(\frac{\overset{*}{w}_j}{H_w}\right) \left\{ \left[\int_0^{\ell_i} \sum_{m=1}^{\infty} \Theta_{mi}(x_i)\,dx_i \right] Q_m(\omega) \right\} \right] \qquad \text{(III-d-5)}$$

which can be written

$$G_A(\omega) = \frac{2}{T_1}\left(\frac{E_c A_c}{L_E}\right)^2\left(\frac{b}{2}\right)^2 \sum_{n=1}^{\infty}\sum_{m=1}^{\infty} \Gamma_n \Gamma_m Q_n^*(\omega) Q_m(\omega)$$

$$= \left(\frac{E_c A_c}{L_E}\right)^2\left(\frac{b}{2}\right)^2 \sum_{n=1}^{\infty}\sum_{m=1}^{\infty} \Gamma_n \Gamma_m \{H_n^*(\omega)\}[G_{ff}(\omega)]\{H_m(\omega)\}$$

(III-d-6)

where the modal factors Γ_n are given by

$$\Gamma_n = \sum_{i=1}^{3} \frac{w_i^*}{H_w} \int_0^{\ell_i} \Theta_{ni}(x_i)dx_i \qquad n = 1, 2, 3 \ldots$$

(III-d-7)

and $[G_{ff}(\omega)]$ is the 6 x 6 spectral matrix whose terms are defined by

$$[G_{ff}(\omega)] = \frac{2}{T_1}\{\Psi^*(\omega)\}^T[\Psi(\omega)] \qquad \text{(III-d-8)}$$

Now for the correlated case, the spectral matrix is full, while for the uncorrelated case, only the diagonal terms (i = j in Eq. III-d-8) are retained.

B. Pure Quasi-Static Response

This involves the second term in Eq. III-d-1 multiplied by its complex conjugate, that is

$$G_B(\omega) = \frac{2}{T_1}\left(\frac{E_c A_c}{L_E}\right)^2\left(\frac{b}{2}\right)^2 \sum_{j=1}^{4}\sum_{k=1}^{4} \gamma_j \gamma_k \Psi_j^*(\omega)\Psi_k(\omega)$$

$$= \left(\frac{E_c A_c}{L_E}\right)^2\left(\frac{b}{2}\right)^2 \sum_{j=1}^{4}\sum_{k=1}^{4} \gamma_j \gamma_k G_{jk}(\omega) \qquad \text{(III-d-9)}$$

where

$$\gamma_j = \sum_{i=1}^{3} \frac{w_i^*}{H_w} \int_0^{\ell_i} g_{ji}(x_i)\,dx_i \qquad j = 1, 2, 3, 4 \qquad \text{(III-d-10)}$$

and $G_{jk}(\omega)$ is defined by Eq. III-d-8.

For the correlated case, all power and cross-spectral terms are included in Eq. III-d-9, while for the uncorrelated case, only the diagonal terms remain, that is Eq. III-d-9 reduces to

$$G_B(\omega) = \left(\frac{E_c A_c}{L_E}\right)^2 \left(\frac{b}{2}\right)^2 \sum_{j=1}^{4} \gamma_j^2\, G_j(\omega) \qquad \text{(III-d-11)}$$

where $G_j(\omega)$ is the power-spectra of the j^{th} rotational input support displacement, (j = 1, 2, 3, 4) given by

$$G_j(\omega) = \frac{2}{T_1} \left|\Psi_j(\omega)\right|^2 \qquad \text{(III-d-12)}$$

C. Response Excited by Rocking Ground Motion Inputs

This involves the third term in Eq. III-d-1 multiplied by its complex conjugate, that is

$$G_c(\omega) = \frac{2}{T_1} \left(\frac{E_c A_c}{L_E}\right)^2 \left(\frac{b}{2}\right)^2 \sum_{i=1}^{3} \sum_{j=1}^{3} \beta_i \beta_j \{\Psi_{i+1}^*(\omega)$$

$$+ \Psi_i^*(\omega)\}\{\Psi_{i+1}(\omega) + \Psi_i(\omega)\}$$

$$= \left(\frac{E_c A_c}{L_E}\right)^2 \left(\frac{b}{2}\right)^2 \sum_{i=1}^{3} \sum_{j=1}^{3} \beta_i \beta_j \left[G_{i+1,j+1}(\omega) + G_{i,j+1}(\omega)\right.$$

$$\left. + G_{i+1,j}(\omega) + G_{ij}(\omega)\right] \qquad \text{(III-d-13)}$$

which for the uncorrelated case reduces to

$$G_c(\omega) = \left(\frac{E_c A_c}{L_E}\right)^2 \left(\frac{b}{2}\right)^2 [\beta_1^2\{G_1(\omega) + G_2(\omega)\} + 2\beta_1\beta_2 G_2(\omega)$$

$$+ \beta_2^2\{G_2(\omega) + G_3(\omega)\} + 2\beta_2\beta_3 G_3(\omega)$$

$$+ \beta_3^2\{G_3(\omega) + G_4(\omega)\}] \qquad \text{(III-d-14)}$$

D. Response Excited by Torsional Ground Motion Inputs

This involves the fourth term in Eq. III-d-1 multiplied by its complex conjugate, that is

$$G_D(\omega) = \frac{2}{T_1}\left(\frac{E_c A_c}{L_E}\right)^2 \left(\frac{b}{2}\right)^2 \{\overset{*}{\Phi}_4(\omega) - \overset{*}{\Phi}_1(\omega)\}\{\Phi_4(\omega) - \Phi_1(\omega)\}$$

$$= \left(\frac{E_c A_c}{L_E}\right)^2 \left(\frac{b}{2}\right)^2 [G_6(\omega) + G_5(\omega) - G_{56}(\omega) - \overset{*}{G}_{56}(\omega)]$$

(III-d-15)

which for the uncorrelated case reduces to

$$G_D(\omega) = \left(\frac{E_c A_c}{L_E}\right)^2 \left(\frac{b}{2}\right)^2 [G_6(\omega) + G_5(\omega)] \qquad \text{(III-d-16)}$$

E. Cross-term: Relative and Quasi-Static Responses

This involves the complex conjugate of the first term in Eq. III-d-1 multiplied by the second term in this equation that is

$$G_{AB}(\omega) = \frac{2}{T_1}\left(\frac{E_c A_c}{L_E}\right)^2\left(\frac{b}{2}\right)^2 \sum_{n=1}^{\infty}\sum_{j=1}^{4} \Gamma_n \gamma_j \overset{*}{Q}_n(\omega)\Psi_j(\omega) \qquad \text{(III-d-17)}$$

where Γ_n was defined in Eq. III-d-7 and γ_j was defined in Eq. III-d-10. Using Eq. III-d-5, the previous equation may be written

$$G_{AB}(\omega) = \frac{2}{T_1}\left(\frac{E_c A_c}{L_E}\right)^2\left(\frac{b}{2}\right)^2 \sum_{n=1}^{\infty}\sum_{j=1}^{4} \Gamma_n \gamma_j \{\overset{*}{H}_n(\omega)\}^T\{\overset{*}{\Psi}(\omega)\}\Psi_j(\omega) \qquad \text{(III-d-18)}$$

which, for the uncorrelated case reduces to

$$G_{AB}(\omega) = \left(\frac{E_c A_c}{L_E}\right)^2\left(\frac{b}{2}\right)^2 \sum_{n=1}^{\infty}\sum_{j=1}^{4} \Gamma_n \gamma_j H_{nj}(\omega)\, G_j(\omega) \qquad \text{(III-d-19)}$$

where $H_{nj}(\omega)$ is the complex frequency response function corresponding to the n^{th} torsional vibration mode and the j^{th} rocking input motion.

F. Cross-term: Relative Response and Response Due to Rocking Ground Motion Inputs

This involves the complex conjugate of the first term in Eq. III-d-1 multiplied by the third term in this equation, that is

$$G_{AC}(\omega) = -\frac{2}{T_1}\left(\frac{E_c A_c}{L_E}\right)^2\left(\frac{b}{2}\right)^2 \sum_{n=1}^{\infty}\sum_{i=1}^{3} \Gamma_n \beta_i \overset{*}{Q}_n(\omega)\{\Psi_{i+1}(\omega) + \Psi_i(\omega)\}$$

$$= -\frac{2}{T_1}\left(\frac{E_c A_c}{L_E}\right)^2\left(\frac{b}{2}\right)^2 \sum_{n=1}^{\infty}\sum_{i=1}^{3} \Gamma_n \beta_i \{\overset{*}{H}_n(\omega)\}^T\{\overset{*}{\Psi}(\omega)\}(\Psi_{i+1}(\omega) + \Psi_i(\omega)\} \qquad \text{(III-d-20)}$$

which, for the uncorrelated case reduces to

$$G_{AC}(\omega) = - \left(\frac{E_c A_c}{L_E}\right)^2 \left(\frac{b}{2}\right)^2 \sum_{n=1}^{\infty} \sum_{i=1}^{3} \Gamma_n \beta_i [H^*_{ni}(\omega) G_i(\omega) + H^*_{n,i+1}(\omega)\ G_{i+1}(\omega)] \qquad \text{(III-d-21)}$$

G. Cross-term: Relative Response and Response Due to Torsional Ground Motion Inputs

This involves the complex conjugate of the first term in Eq. III-d-1 multiplied by the fourth term in this equation, that is

$$G_{AD}(\omega) = \frac{2}{T_1} \left(\frac{E_c A_c}{L_E}\right)^2 \left(\frac{b}{2}\right)^2 \sum_{n=1}^{\infty} \Gamma_n Q^*_n(\omega) [\Phi_4(\omega) - \Phi_1(\omega)]$$

$$= \frac{2}{T_1} \left(\frac{E_c A_c}{L_E}\right)^2 \left(\frac{b}{2}\right)^2 \sum_{n=1}^{\infty} \Gamma_n \{H^*_n(\omega)\}^T \{\Psi^*(\omega)\} [\Phi_4(\omega) - \Phi_1(\omega)] \qquad \text{(III-d-22)}$$

which for the uncorrelated case reduces to

$$G_{AD}(\omega) = \left(\frac{E_c A_c}{L_E}\right)^2 \left(\frac{b}{2}\right)^2 \sum_{n=1}^{\infty} \Gamma_n [H^*_{n6}(\omega) G_6(\omega) - H^*_{n5}(\omega) G_5(\omega)] \qquad \text{(III-d-23)}$$

H. Cross-term: Quasi-Static Response and Response Due to Rocking Ground Motion Inputs

This involves the complex conjugate of the second term in Eq. III-d-1 multiplied by the third term in this equation, that is

$$G_{BC}(\omega) = -\frac{2}{T_1}\left(\frac{E_c A_c}{L_E}\right)^2\left(\frac{b}{2}\right)^2 \sum_{j=1}^{4}\sum_{i=1}^{3} \gamma_j \beta_i \Psi_j^*(\omega)\,[\Psi_{i+1}(\omega) + \Psi_i(\omega)] \qquad \text{(III-d-24)}$$

which for the uncorrelated case reduces to

$$G_{BC}(\omega) = -\left(\frac{E_c A_c}{L_E}\right)^2\left(\frac{b}{2}\right)^2 [\gamma_1\beta_1 G_1(\omega) + \gamma_2(\beta_1 + \beta_2)G_2(\omega) + \gamma_3(\beta_2 + \beta_3)G_3(\omega) + \gamma_4\beta_3 G_4(\omega)] \qquad \text{(III-d-25)}$$

I. Cross-term: Quasi-Static Response and Response Due to Torsional Ground Motion Inputs

This involves the complex conjugate of the second term in Eq. III-d-1 multiplied by the fourth term in this equation, that is

$$G_{BD}(\omega) = \frac{2}{T_1}\left(\frac{E_c A_c}{L_E}\right)^2\left(\frac{b}{2}\right)^2 \sum_{j=1}^{4} \gamma_j \Psi_j^*(\omega)\,[\Phi_4(\omega) - \Phi_1(\omega)] \qquad \text{(III-d-26)}$$

which reduces to zero for the uncorrelated case.

J. Cross-term: Response due to Rocking Ground Motion Inputs and Response Due to Torsional Ground Motion Inputs

This involves the complex conjugate of the third term in Eq. III-d-1 multiplied by the fourth-term in this equation, that is

$$G_{CD}(\omega) = -\frac{2}{T_1}\left(\frac{E_c A_c}{L_E}\right)^2 \left(\frac{b}{2}\right)^2 \sum_{i=1}^{3} \beta_i [\overset{*}{\Psi}_{i+1}(\omega) + \overset{*}{\Psi}_i(\omega)][\Phi_4(\omega) - \Phi_1(\omega)] \qquad \text{(III-d-27)}$$

which reduces to zero for the uncorrelated case.

Power Spectrum of H(t)

The power spectrum of H(t) is given by Eq. III-d-4, and can be written as

$$\begin{aligned} G_H(\omega) = {} & G_A(\omega) + G_B(\omega) + G_C(\omega) + G_D(\omega) + [G_{AB}(\omega) + \overset{*}{G}_{AB}(\omega)] \\ & + [G_{AC}(\omega) + \overset{*}{G}_{AC}(\omega)] + [G_{AD}(\omega) + \overset{*}{G}_{AD}(\omega)] \\ & + [G_{BC}(\omega) + \overset{*}{G}_{BC}(\omega)] + [G_{BD}(\omega) + \overset{*}{G}_{BD}(\omega)] \\ & + [G_{CD}(\omega) + \overset{*}{G}_{CD}(\omega)] \end{aligned} \qquad \text{(III-d-28)}$$

where the terms on the right hand side of Eq. III-d-28 have been previously defined, and the superposed asterisk denotes complex conjugate.

REFERENCES OF CHAPTER III

1. Abdel-Ghaffar, Ahmed M., "Dynamic Analysis of Suspension Bridge Structures," Report No. EERL 76-01, Earthquake Engineering Research Laboratory, College of Engineering, California Institute of Technology, Pasadena, May 1976.

2. Abdel-Ghaffar, Ahmed M., "Free Torsional Vibrations of Suspension Bridges," Journal of the Structural Division, ASCE, Vol. 105, No. ST4, Proc. Paper 14535, April 1979, pp. 767-788.

3. Baron, F., Arikan, M., and Hamati, E., "The Effects of Seismic Disturbances on the Golden Gate Bridge," Report No. EERC 76-31, Earthquake Engineering Research Center, College of Engineering, University of California, Berkeley, November 1976.

4. Bendat, Julius S., and Piersol, Allan G., Engineering Applications of Correlation and Spectral Analysis, John Wiley & Sons, Inc., New York, 1980.

5. Bleich, F., McCullough, C.B., Rosecrans, R., and Vincent, G.S., The Mathematical Theory of Vibration in Suspension Bridges, U.S. Bureau of Public Roads, Government Printing Office, Washington 25, D.C., 1950.

6. Kelly, James M., and Sackman, Jerome L., "Conservatism in Summation Rules for Closely Spaced Modes," Report No. UCB/EERC-79/11, Earthquake Engineering Research Center, College of Engineering, University of California, Berkeley, May 1979.

7. Mindlin, R.D., and Goodman, L.E., "Beam Vibrations with Time-Dependent Boundary Conditions," Journal of Applied Mechanics, ASME, Vol. 17, 1950, pp. 377-380.

8. Pugsley, A.G., The Theory of Suspension Bridges, Edward Arnold, London, 1957.

9. Steinman, D.B., "Modes and Natural Frequencies of Suspension Bridge Oscillations," ASCE, pp. 148-173, September 1959.

10. Trifunac, M.D., "A Note on Rotational Components of Earthquake Motions on Ground Surface for Incident Body Waves," Soil Dynamics and Earthquake Engineering, Vol. 1, No. 1, 1982, pp. 11-19.

11. Tso, W.K., and Hsu, T.-I., "Torsional Spectrum for Earthquake Motions," Earthquake Engineering and Structural Dynamics, Vol. 6, 1978, pp. 375-382.

12. Vanmarcke, Erik H., "Structural Response to Earthquakes,"Chapter 8, from Seismic Risk and Engineering Decisions, Edited by C. Lomnitz and E. Rosenblueth, Elsevier Publishing Company, Amsterdam, London, New York, 1976.

CHAPTER IV

LATERAL EARTHQUAKE RESPONSE OF SUSPENSION BRIDGES TO MULTIPLE-SUPPORT EXCITATIONS

IV.1 INTRODUCTION

This chapter presents the dynamic analysis methodology for earthquake-induced lateral vibrations of suspension bridges. A suspension bridge is excited into lateral motion by lateral (or transverse) horizontal components of ground motion occurring at its support points (anchorages or tower-piers). As will be seen later, the lateral vibration of the suspended structure and cables within the center span are uncoupled from the other side spans under small vibrational (linear) amplitudes. However, within each span the lateral vibrational deflections of the cables and suspended structure are strongly coupled. The hangers (or suspenders) which connect the suspended structure to the cables cause the two systems to interact so that the deformation of one system exerts an influence on the other. The resulting coupled equations of motion are quite complicated, and as yet have not been solved in closed form. For this reason, the method chosen to analyze the lateral vibration in this chapter involves a matrix finite element approach, which was originally developed by Abdel-Ghaffar (1,2) for the analysis of free lateral vibrations of suspension bridges, and is utilized here to study the multiple-support seismic lateral excitation problem.

A frequency-domain random vibration approach is used in this chapter to take into account the differences in lateral ground motion inputs at each of the bridge's support points as well as the correlation among the various input motions. In general, the correlation of these motions is extremely complicated, particularly in the case of a long-span bridge, with different foundation conditions, subjected to seismic waves with different angles of incidence and different travel paths (reflections and refractions, etc.). However, such complications can be overcome by utilizing existing strong motion records, to define representative and appropriately correlated multiple-support lateral seismic inputs. Ground motion records taken from the Imperial Valley (El Centro), California, earthquake (M_L = 6.6) of October 15, 1979, are, again, used in defining the input support motions (Appendix II-e). As mentioned previously, these ground motion records were recorded at several instrument locations whose separation distances are consistent with a long-span suspension bridge's dimensions.

Finally, the lateral response of the Golden Gate Suspension Bridge, in California, is investigated in order to estimate its lateral earthquake response characteristics. Three cases of lateral response are compared. In the first case, the S40°E components of ground motions recorded at Arrays No. 4, 5, 6, and 7 (of the 13 El Centro Arrays; see Appendix II-e) are utilized to define the lateral input support motions (at anchorages and tower-piers), while the second case involves a similar correspondence with Arrays No. 5, 6, 7, and 8. The third case involves a uniform lateral ground motion assumption over all four supports with the records of Array No. 5 used as input. Root mean square lateral response displacements, stresses, shear forces, as well as

horizontal components of cable tension due to lateral vibration are obtained for each response case, and peak responses are estimated by using a peak factor of 3.5 originally obtained from Chapter II of this report (vertical vibrations), and found to be appropriate for lateral vibrations as well. Selected time domain (convolution integral) analysis cases also are shown in this chapter in an attempt to verify these peak factors.

IV.2 COORDINATE SYSTEMS

The coordinate system used for the typical three-span bridge is shown in Fig. IV-1. For the purpose of studying the lateral vibration, the following is considered (1,2)

1. For the suspended structure (girders or trusses), the x_i-axis of the i^{th} span is defined along the centerline of the span with the origin located at the left support of that span.
2. For the cables, the x_i-axis of the i^{th} span is defined as the horizontal line passing through the left support of each span, while the cable ordinate $y_c(x_i)$ of the i^{th} span is measured downward from the closing chord of each span. The cable ordinate $h(x_i)$ is measured upward from the centerline of the suspended structure.
3. The vibrational displacements of the suspended structure are measured from the $x_i - y_i$ plane and the $x_i - z_i$ plane. These displacements in the y_i and z_i directions are denoted as $v_s(x_i,t)$ and $w_s(x_i,t)$, respectively.

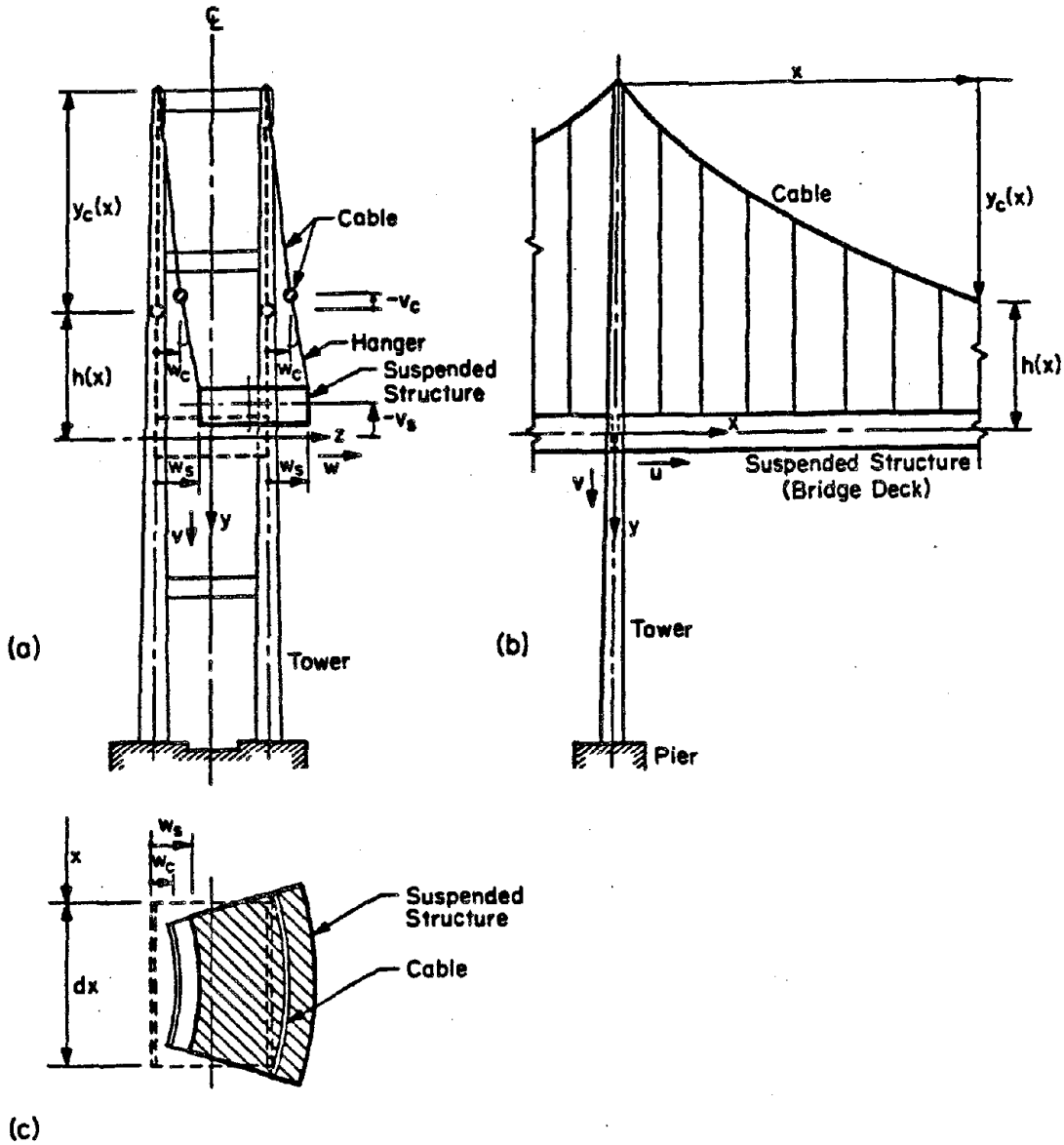

Fig. IV-1 Laterally vibrating suspension bridge definition diagrams (Ref. 1)

4. The vibrational displacements of the cables are measured vertically and horizontally from the static position of the cable. These displacements in the y_i and z_i directions are denoted as $v_c(x_i,t)$ and $w_c(x_i,t)$, respectively.

IV.3 FUNDAMENTAL ASSUMPTIONS

The following assumptions and approximations are made for the purpose of simplifying the lateral vibration analysis (1,2):

1. All stresses in the bridge remain within the elastic limit and therefore obey Hooke's law.
2. The cables are of uniform cross section and of parabolic profile under dead load.
3. The cables are assumed to be perfectly flexible, that is the flexural stiffness of the cables can be neglected.
4. The suspenders (or hangers) are considered inextensible during lateral vibration.
4. Small vibrations about the equilibrium position are assumed, that is, the vibration amplitudes are sufficiently small so that the stiffness of the structure may be taken to be constant during the motion.
6. The tower-piers move as rigid bodies under ground motion excitation. This is a reasonable first assumption to investigate lateral vibration because the tower-pier system is much stiffer than the suspended structure-cables system.
7. The initial curvature of the stiffening structure is considered small in comparison with the cable curvature and is therefore neglected.

8. The coupling between lateral, torsional, and vertical motions, which has significant influence only for large amplitude displacements, is neglected.

9. The upward vibrational-displacements of the cables and the suspended structure incidental to their lateral movements may be approximated by

$$- v_c(x_i,t) \simeq \frac{w_c^2(x_i,t)}{2y_c(x_i)} \qquad i=1,2,3 \qquad (4.1)$$

$$- v_s(x_i,t) \simeq \frac{w_c^2(x_i,t)}{2y_c(x_i)} + \frac{[w_s(x_i,t) - w_c(x_i,t)]^2}{2h(x_i)} \qquad i=1,2,3 \qquad (4.2)$$

IV.4 EQUATIONS OF MOTION GOVERNING LATERAL VIBRATIONS

Under the previous assumptions, the linearized equation of motion governing the lateral free vibration of the i^{th} span of a suspension bridge is given by (1,2):

$$\overset{*}{m}_c \frac{\partial^2 w_c}{\partial t^2} - 2H_w \frac{\partial^2 w_c}{\partial x_i^2} - \overset{*}{w}_{si}\left(\frac{w_s - w_c}{h}\right) + 2(\overset{*}{w}_c + \overset{*}{w}_{si})\frac{w_c}{y_c} = 0 \ , \quad i=1,2,3 \qquad (4.3)$$

for the cable; and

$$\overset{*}{m}_{si} \frac{\partial^2 w_s}{\partial t^2} + \frac{\partial^2}{\partial x_i^2}\left(E_{si}I_{si}\frac{\partial^2 w_s}{\partial x_i^2}\right) + \overset{*}{w}_{si}\left(\frac{w_s - w_c}{h}\right) = 0 \ , \qquad i=1,2,3 \qquad (4.4)$$

for the suspended structure; where $w_c = w_c(x_i,t)$ is the lateral vibrational response of the cables in the i^{th} span; $w_s = w_s(x_i,t)$ is the lateral vibrational response of the suspended structure in the i^{th} span;

$\overset{*}{w}_c$ and $\overset{*}{m}_c$ are respectively, the dead weight and mass of both cables per unit span length; $\overset{*}{w}_{si}$ and $\overset{*}{m}_{si}$ are respectively, the dead weight and mass of the suspended structure (both trusses) per unit length of the i^{th} span; E_{si} is the modulus of elasticity of the suspended structure in the i^{th} span; I_{si} is the area moment of inertia of the suspended structure about its vertical axis, y_i, in the i^{th} span (includes the contribution from the two stiffening trusses as well as the contribution from the lateral bracing systems); H_w is the initial (dead-load) horizontal component of cable tension; and $y_c(x_i)$ is the parabolic dead-load cable profile given by:

$$y_c(x_i) = \frac{\overset{*}{w}_c + \overset{*}{w}_{si}}{4H_w}\left[\left(\frac{x_i}{\ell_i}\right) - \left(\frac{x_i}{\ell_i}\right)^2\right] \quad , \qquad i=1,2,3, \tag{4.5}$$

where ℓ_i is the length of the i^{th} span, and $h(x_i)$ is the cable ordinate as measured from the centerline of the suspended structure (see Fig. IV-1).

It is seen from Eq. 4.3 and Eq. 4.4 that under linear assumptions, the lateral vibration of each span of the suspension bridge are uncoupled. This occurs because the additional (vibrational) horizontal component of cable tension $H(t)$ due to lateral vibration contains only nonlinear terms, as follows (1):

$$H(t) = \left(\frac{E_c A_c}{L_E}\right) \sum_{i=1}^{3}\left[\frac{1}{2}\int_0^{\ell_i}\left(\frac{\partial w_c}{\partial x_i}\right)^2 dx_i + \int_0^{\ell_i}\left(\frac{\partial v_c}{\partial x_i}\right)\left(\frac{dy_c}{dx_i}\right) dx_i + \frac{1}{2}\int_0^{\ell_i}\left(\frac{\partial v_c}{\partial x_i}\right)^2 dx_i\right] \quad , \tag{4.6}$$

where $v_c(x_i,t)$ is the upward deflection of the cables incidental to their lateral deflection (Eq. 4.1); E_c and A_c are respectively, the modulus of elasticity and cross-sectional area of each cable; and L_E is the cable's virtual length defined as (1):

$$L_E = \sum_{i=1}^{3} \int_0^{\ell_i} \left(\frac{ds_i}{dx_i}\right)^3 dx_i \tag{4.7}$$

where s_i is the coordinate measured tangent to the cable in the i^{th} span, and ℓ_i is the length of the i^{th} span.

Although the lateral vibrations of each span are uncoupled, within each span the lateral deflections of the cables and suspended structure are strongly coupled. The hangers (or suspenders) which connect the suspended structure to the cables cause the two systems to interact so that the deformation of one system exerts an influence on the other. The governing equations of motion (Eqs. 4.3 and 4.4) are thus coupled together, and are in addition of the variable coefficient type. To date, no closed form solutions of these equations are known. For this reason, an approximate finite element solution originally proposed by Abdel-Ghaffar (1,2) will be utilized here in order to analyze the earthquake-induced lateral vibrations.

IV.5 MATRIX EQUATIONS OF MOTION: A FINITE ELEMENT APPROACH

Because the lateral vibration of the center span can be treated separately from the side spans, the earthquake response analysis methodology is presented here for the center span; the side span analysis being quite similar. Furthermore, since the towers are relatively rigid in the lateral direction, it is assumed here that the ground motion

input to the support of the suspended structure is equal to the ground motion input to the cable saddle at the top of the tower; both inputs being identical to the lateral tower base input. Because of the long span of the structure, the ground motions are in general different at each of its support points.

The equations of motion of lateral vibration of the center span (with N degrees of freedom as shown in Fig. IV-2) when subjected to seismic excitations at the tower bases and cable supports in the lateral direction can be expressed in matrix form as:

$$[M]\{\ddot{u}\} + [C]\{\dot{u}\} + [K]\{u\} = \{0\} \tag{4.8}$$

where [M] is the mass matrix which includes the masses of the suspended structure and the cables; [K] is the stiffness matrix which includes the stiffness contribution from the elastic deformation of the cables and suspended structure, as well as the gravitational stiffness of the cables and suspended structure arising from their upward incidental motion; [C] is the damping matrix; and $\{u\}$ is the total vibrational displacement vector.

The formation of the stiffness and mass matrices is derived in Ref. 1, and is summarized in Appendix IV-a of this report. Basically, the finite element technique involves idealizing the cable by a set of pretensioned string or truss elements, while idealizing the suspended structure by a set of beam elements. These two sets of elements, connected by rigid hangers, form the bridge elements (Fig. IV-2). The total vibrational displacement vector, $\{u\}$, thus contains degrees of freedom corresponding to displacements of the cables and suspended structure as well as degrees of freedom corresponding to rotations of

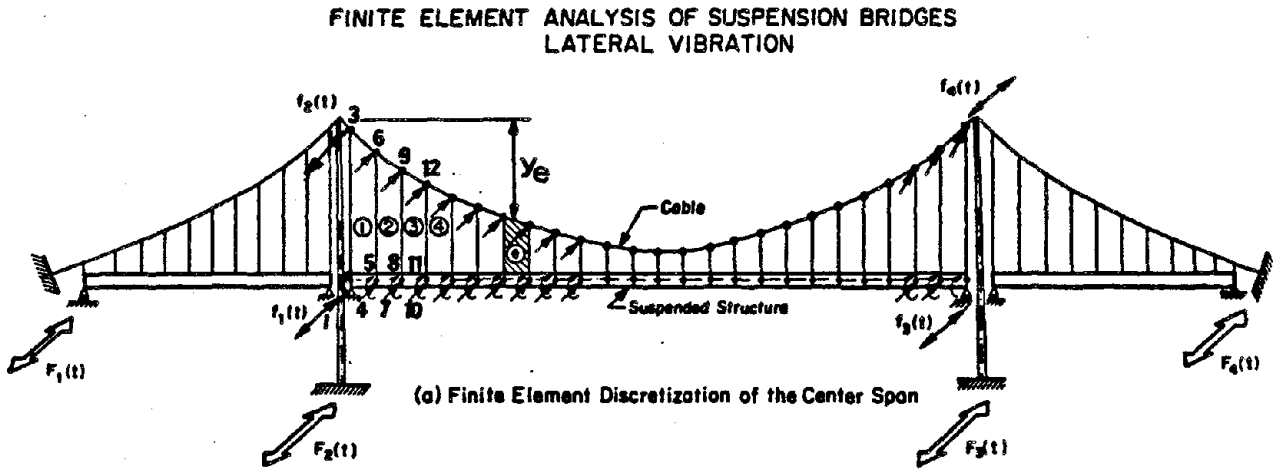

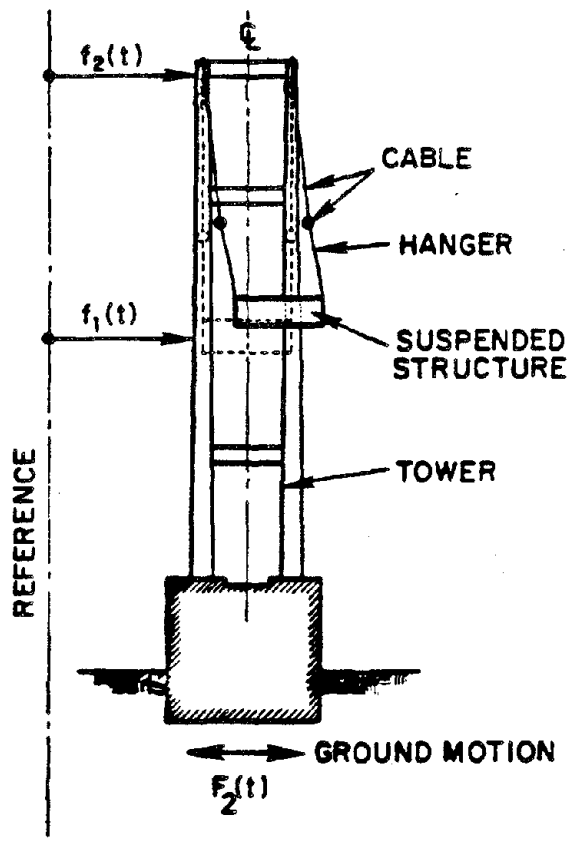

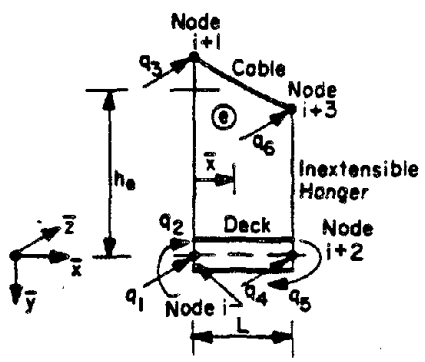

Bridge Element ⓔ with the Generalized Nodal Displacements

Fig. IV-2 Matrix formulation definition diagrams (Ref. 1).

the suspended structure, as shown in Fig. IV-2. The stiffness and inertia properties can be formed for each set of elements and then assembled to obtain the global stiffness and mass matrices.

Now Eq. 4.8 may be written in partitioned form as (3):

$$\begin{bmatrix} M_{ss} & M_{sg} \\ M_{gs} & M_{gg} \end{bmatrix} \begin{Bmatrix} \ddot{u}_s \\ \ddot{u}_g \end{Bmatrix} + \begin{bmatrix} C_{ss} & C_{sg} \\ C_{gs} & C_{gg} \end{bmatrix} \begin{Bmatrix} \dot{u}_s \\ \dot{u}_g \end{Bmatrix} + \begin{bmatrix} K_{ss} & K_{sg} \\ K_{gs} & K_{gg} \end{bmatrix} \begin{Bmatrix} u_s \\ u_g \end{Bmatrix} = \begin{Bmatrix} 0 \\ 0 \end{Bmatrix} \quad (4.9)$$

where the subscript "g" designates the degrees of freedom corresponding to the points of application of ground motions (i.e., the displacement degrees of freedom at the two tower connections; Fig. IV-2); and the subscript "s" corresponds to all other structural degrees of freedom of the bridge.

IV.6 GENERAL SOLUTION

The nodal displacements may be decomposed into quasi- (or pseudo-) static displacements and relative (or vibrational) displacements. Quasi-static displacements are those resulting from the static application of support displacements (degrees of freedom with subscript g) at any time t. Thus the displacement can be written as

$$\begin{Bmatrix} u_s \\ u_g \end{Bmatrix} = \begin{Bmatrix} u_{ps} \\ u_{pg} \end{Bmatrix} + \begin{Bmatrix} u_{vs} \\ 0 \end{Bmatrix} \quad (4.10)$$

where the subscript "p" denotes the pseudo-static displacements and the subscript "v" denotes the vibrational displacements.

The pseudo-static displacement vector can be expressed as

$$\begin{Bmatrix} u_{ps} \\ u_{pg} \end{Bmatrix} = \sum_{i=1}^{4} \begin{Bmatrix} g_{psi} \\ g_{pgi} \end{Bmatrix} f_i(t) \quad (4.11)$$

where g_{ps1} and g_{ps3} are the quasi-static functions that result from unit displacement at the left and right ends of the suspended structure, respectively; g_{ps2} and g_{ps4} are the quasi-static functions that result from unit displacement at the left and right ends of the cables, respectively; $f_1(t)$ and $f_3(t)$ are the input displacement motions to the left and right ends of the suspended structure, respectively; $f_2(t)$ and $f_4(t)$ are the input displacement motions to the left and right ends of the cables, respectively; and g_{pgi} is a 4 x 1 vector whose i^{th} element is equal to unity with all its other elements being zero.

Substituting Eqs. 4.11 and 4.10 into Eq. 4.9 gives:

$$[M_{ss}]\{\ddot{u}_{vs}\} + [C_{ss}]\{\dot{u}_{vs}\} + [K_{ss}]\{u_{vs}\} =$$

$$- \sum_{i=1}^{4} \left([M_{ss} M_{sg}] \ddot{f}_i(t) + [C_{ss} C_{sg}] \dot{f}_i(t) \right.$$

$$\left. + [K_{ss} K_{sg}] f_i(t) \right) \begin{Bmatrix} g_{psi} \\ g_{pgi} \end{Bmatrix} \tag{4.12}$$

The previous equation can be simplified by noting that for an unloaded bridge with a static condition of support displacements, one has

$$[K_{ss} \quad K_{sg}] \begin{Bmatrix} u_{ps} \\ u_{pg} \end{Bmatrix} = \{0\} \tag{4.13}$$

Substituting Eq. 4.11 into Eq. 4.13 yields

$$\sum_{i=1}^{4} [K_{ss} K_{sg}] \begin{Bmatrix} g_{psi} \\ g_{pgi} \end{Bmatrix} = 0 \tag{4.14}$$

Thus, the quasi-static vectors can be defined in the following manner:

$$\{g_{psi}\} = -[K_{ss}]^{-1}[K_{sg}]\{g_{pgi}\} \quad , \quad i=1,2,3,4 \tag{4.15}$$

and the equation governing the lateral vibrational response (Eq. 4.12) reduces to

$$[M_{ss}]\{\ddot{u}_{vs}\} + [C_{ss}]\{\dot{u}_{vs}\} + [K_{ss}]\{u_{vs}\} = -\sum_{i=1}^{4}([M_{ss} \quad M_{sg}]\ddot{f}_i(t) + [C_{ss} \quad C_{sg}]\dot{f}_i(t))\begin{Bmatrix} g_{psi} \\ g_{pgi} \end{Bmatrix} \tag{4.16}$$

Note that the previous equation is excited by lateral ground acceleration and velocity terms. Although, as indicated by Baron, et al (3), the contribution to the total response from velocity terms is often small, the velocity terms are included in this analysis for completeness.

III.7 EIGENVALUE PROBLEM - FREE VIBRATIONS

The solution to Eq. 4.16 is obtained by modal superposition, that is the vibrational displacement is taken to be

$$\{u_{vs}\} = \sum_{n=1}^{N}\{\phi_n\}q_n(t) \quad , \tag{4.17}$$

where $\{\phi_n\}$ is the n^{th} lateral vibration mode shape in the center span; $q_n(t)$ is the n^{th} generalized coordinate; and N corresponds to the total number of degrees of freedom in the finite element model. Usually, the number of modes necessary for an accurate response analysis will be significantly less than the number of degrees of freedom N,

which is an inherent advantage of using the modal superposition method. The lateral mode shapes and corresponding natural circular frequencies, ω_n are obtained from the solution of the matrix eigenvalue problem

$$(-\omega_n^2[M_{ss}] + [K_{ss}])\{\phi_n\} = \{0\} \quad , \quad n=1,2,3... \tag{4.18}$$

IV.8 MODAL SOLUTIONS - FORCED VIBRATIONS

Substituting Eqs. 4.17 into Eq. 4.16 results in

$$\sum_{n=1}^{N} \left([M_{ss}]\{\phi_n\}\ddot{q}_n(t) + [C_{ss}]\{\phi_n\}\dot{q}_n(t) + [K_{ss}]\{\phi_n\}q_n(t)\right) =$$

$$- \sum_{i=1}^{4} \left([M_{ss}M_{sg}]\ddot{f}_i(t) + [C_{ss}C_{sg}]\dot{f}_i(t)\right)\begin{Bmatrix} g_{psi} \\ g_{pgi} \end{Bmatrix} \tag{4.19}$$

Now, multiplying Eq. 4.19 by $\{\phi_m\}^T$ and using modal orthogonality (see Appendix IV-b), that is

$$\{\phi_m\}^T[M_{ss}]\{\phi_n\} = 0 \quad , \quad n \neq m \quad , \tag{4.20}$$

yields the governing equation for the n^{th} generalized coordinate

$$\ddot{q}_n(t) + 2\zeta_n \omega_n \dot{q}_n(t) + \omega_n^2 q_n(t) = \sum_{i=1}^{4} (\alpha_{ni}\ddot{f}_i(t) + \beta_{ni}\dot{f}_i(t)) \quad n=1,2,3... \tag{4.21}$$

where ζ_n is the damping ratio of the n^{th} lateral vibration mode, and the modal participation coefficients α_{ni} and β_{ni} are given by

$$\alpha_{ni} = \frac{-\{\phi_n\}^T [M_{ss} \quad M_{sg}]\{g_{psi} \quad g_{pgi}\}^T}{\{\phi_n\}^T [M_{ss}]\{\phi_n\}} \quad , \quad \begin{matrix} i=1,2,3,4, \\ n=1,2,3... \end{matrix} \tag{4.22}$$

and

$$\beta_{ni} = \frac{-\{\phi_n\}^T [C_{ss} \quad C_{sg}] \{g_{psi} \quad g_{pgi}\}^T}{\{\phi_n\}^T [M_{ss}] \{\phi_n\}} \quad , \qquad \begin{matrix} i=1,2,3,4 \\ n=1,2,3... \end{matrix} \qquad (4.23)$$

It is important to note that for the purpose of calculating the modal participation factors, β_{ni}, involving the damping matrix [C], the following approach is used. For each mode, the damping matrix is assumed diagonal. Those degrees of freedom corresponding to the translation of the suspended structure are entered as $[(2\zeta_n \omega_n m_s^*) \cdot L]$ where m_s^* is the mass of the suspended structure per unit length and L is the element length (Fig. IV-1). Those degrees of freedom corresponding to the translation of the cables are entered as $[(2\zeta_n \omega_n m_c^*) \cdot L]$ where m_c^* is the mass of the cables per unit length. The matrices $[C_{ss}]$ and $[C_{sg}]$ are isolated from the diagonal [C] matrix, and the modal participation coefficients β_{ni} can be calculated using Eq. 4.23.

The solution to Eq. 4.21, assuming quiescent initial conditions is given by the convolution integral

$$q_n(t) = \frac{1}{\omega_{nd}} \int_0^t \left\{ \sum_{i=1}^{4} \left(\alpha_{ni} \ddot{f}_i(\tau) + \beta_{ni} \dot{f}_i(\tau) \right) \right\} \cdot \left\{ e^{-\zeta_n \omega_n (t-\tau)} \sin \omega_{nd}(t-\tau) \right\} d\tau$$

$$n=1,2,3... \qquad (4.24)$$

where ω_{nd} is the damped natural circular frequency of the n^{th} lateral vibration mode, given by:

$$\omega_{nd} = \omega_n \sqrt{1 - \zeta_n^2} \qquad n=1,2,3... \qquad (4.25)$$

The total lateral displacement response is obtained as the sum of quasi-static and relative responses, that is

$$\begin{Bmatrix} u_s \\ u_g \end{Bmatrix} = \sum_{i=1}^{N} \begin{Bmatrix} g_{psi} \\ g_{pgi} \end{Bmatrix} f_i(t) + \sum_{n=1}^{N} \begin{Bmatrix} \phi_n \\ 0 \end{Bmatrix} q_n(t) \tag{4.26}$$

For the purpose of calculating dynamically-induced bending moments, flexural stresses, and shear forces in the suspended structure, it becomes necessary to define the vectors $\{\bar{g}_{psi}\}$ and $\{\bar{\phi}_n\}$ as quasi-static rotation and modal rotation vectors which are extracted from the original quasi-static and modal vectors in such a manner that only those degrees of freedom corresponding to the rotations of the suspended structure are entered in the overbarred vectors. Under such a definition, the dynamic bending moment about the suspended structure's vertical axis may be written as

$$\{M_s\} = E_{s2}I_{s2}\left(\sum_{i=1}^{N} \{\bar{g}'_{psi}\}f_i(t) + \sum_{n=1}^{N} \{\bar{\phi}'_n\}q_n(t)\right) \tag{4.27}$$

where $\{M_s\}$ is the vector of dynamic bending moments corresponding to the structural degrees of freedom; E_{s2} is the modulus of elasticity of the center span suspended structure; I_{s2} is the area moment of inertia of the center span suspended structure about its vertical axis; and the prime denotes the first spanwise derivatives (of the quasi-static and modal rotational degrees of freedom).

Similarly, the total dynamic lateral shearing force at any point in the suspended structure may be calculated as

$$\{V_s\} = E_{s2}I_{s2}\left(\sum_{i=1}^{4} \{\bar{g}''_{psi}\}f_i(t) + \sum_{n=1}^{N} \{\bar{\phi}''_n\}q_n(t)\right) \tag{4.28}$$

where $\{V_s\}$ is the vector of shearing forces corresponding to the structural degrees of freedom; and the double prime denotes the second

spanwise derivatives (of the quasi-static and modal rotational degrees of freedom).

Furthermore, the dynamically induced lateral flexural stresses may be related to the bending moments by the following relation

$$\{\sigma_s\} = \frac{b}{2I_{s2}} \{M_s\} \tag{4.29}$$

where $\{\sigma_s\}$ is the vector of laterally-induced flexural stresses in the suspended structure's chord members; and b is the deck width of the bridge.

IV.9 FREQUENCY-DOMAIN, RANDOM VIBRATION APPROACH

In order to study the lateral dynamic behavior of long-span suspension bridges when subjected to multiple-support earthquake excitations, a random vibration approach is utilized. For the four displacement inputs of the center span, there are four complex frequency response functions. To determine these functions, each input $f_j(t)$, $(j = 1, 2, 3, 4)$, is taken equal to $\exp(i\omega t)$, where $i = \sqrt{-1}$, and the response of the n^{th} generalized coordinate excited by the j^{th} input motion is assumed to be of the form

$$q_{nj}(t) = H_{nj}(\omega)\exp(i\omega t) \qquad \begin{matrix} j=1,2,3,4 \\ n=1,2,3... \end{matrix} \tag{4.30}$$

where H_{nj} is the n^{th} complex frequency response due to input displacement $f_j(t)$ at the support of the suspended structure or the cables. Now substituting Eq. 4.30 into Eq. 4.21 yields

$$H_{nj}(\omega) = \frac{-\omega^2\alpha_{nj} + i\omega\beta_{nj}}{(\omega_n^2 - \omega^2) + i(2\zeta_n\omega_n\omega)} \quad , \qquad \begin{matrix} j=1,2,3,4 \\ n=1,2,3,... \\ i = \sqrt{-1} \end{matrix} \tag{4.31}$$

Taking the finite Fourier transform of Eq. 4.17 over the time duration of the ground motion input displacement, T_1, yields the Fourier transform of the vibrational response

$$\{U_{vs}(\omega)\} = \int_0^{T_1} \{u_{vs}\}e^{-i\omega t}\,dt = \sum_{n=1}^{N} \{\phi_n\}Q_n(\omega) \tag{4.32}$$

where $Q_n(\omega)$ is the finite Fourier transform of the generalized coordinate $q_n(t)$, given by

$$Q_n(\omega) = \int_0^{T_1} q_n(t)e^{-i\omega t}\,dt \qquad n=1,2,3... \tag{4.33}$$

A similar Fourier transformation of Eq. 3.21 yields

$$[(\omega_n^2 - \omega^2) + i(2\zeta_n\omega_n\omega)]Q_n(\omega) = \sum_{j=1}^{4} [-\omega^2\alpha_{nj} + i\omega\beta_{nj}]F_j(\omega) \qquad n=1,2,3... \tag{4.34}$$

in which $F_j(\omega)$ is the finite Fourier transform of the j^{th} displacement input $f_j(t)$, given by

$$F_j(\omega) = \int_0^{T_1} f_j(t)e^{-i\omega t}\,dt \qquad j=1,2,3,4 \tag{4.35}$$

It follows from Eqs. 4.31 and 4.34 that the Fourier transform of the generalized coordinate can be expressed as

$$Q_n(\omega) = \{H_n(\omega)\}^T\{F(\omega)\} \qquad n=1,2,3... \tag{4.36}$$

where $\{H_n(\omega)\}^T$ denotes the transposed complex frequency response vector given by

$$\{H_n(\omega)\}^T = \{H_{n1}(\omega)\ H_{n2}(\omega)\ H_{n3}(\omega)\ H_{n4}(\omega)\} \qquad n=1,2,3... \tag{4.37}$$

and $\{F(\omega)\}$ is the Fourier transform vector of displacement inputs given by

$$\{F(\omega)\} = \begin{Bmatrix} F_1(\omega) \\ F_2(\omega) \\ F_3(\omega) \\ F_4(\omega) \end{Bmatrix} \tag{4.38}$$

Now substituting Eq. 4.36 into Eq. 4.32 enables the Fourier transform of the vibrational response to be expressed as

$$\{U_{vs}(\omega)\} = \sum_{n=1}^{N} \{\phi_n\}\{H_n(\omega)\}^T\{F(\omega)\} \tag{4.39}$$

The relative-displacement power-spectral density function is given by

$$\{G_{uvs}\} = \lim_{T_1 \to \infty} \frac{2}{T_1} E[\{\overset{*}{U}_{vs}(\omega)\}\{U_{vs}(\omega)\}^T] \tag{4.40}$$

where $E[\cdot]$ represents the expected value of the term inside the brackets and the superposed asterisk denotes complex conjugate. An estimate of $\{G_{uvs}\}$ can be obtained by simply omitting the limiting and expectation operations in Eq. 4.40, hence

$$\{G_{uvs}\} \simeq \frac{2}{T_1} [\{\overset{*}{U}_{vs}(\omega)\}\{U_{vs}(\omega)\}^T] \tag{4.41}$$

Substituting Eq. 4.39 into Eq. 4.41 yields

$$\{G_{uvs}\} = \sum_{n=1}^{N} \sum_{m=1}^{N} \{\phi_n\}\{\phi_m\}^T\{\overset{*}{H}_n(\omega)\}^T[G_{ff}(\omega)]\{H_m(\omega)\} \tag{4.42}$$

where any element of the 4x4 spectral matrix of correlated displacement inputs $[G_{ff}(\omega)]$ is defined by

$$G_{ij}(\omega) = \lim_{T_1 \to \infty} \frac{2}{T_1} E[F_i^*(\omega) F_j(\omega)] \simeq \frac{2}{T_1} F_i^*(\omega) F_j(\omega) \qquad \begin{matrix} i=1,2,3,4 \\ j=1,2,3,4 \end{matrix} \qquad (4.43)$$

The diagonal elements of the matrix $[G_{ff}(\omega)]$, $i=j$ in Eq. 4.43, correspond to the power spectral density of the j^{th} displacement input $f_j(t)$, while the off-diagonal elements of the matrix $[G_{ff}(\omega)]$ correspond to cross-spectral densities between the various displacement inputs. These cross-spectral terms are present because the various input motions originated from the same source, and are therefore related in some way so that their correlation (or interaction) must be taken into account. The effect of input correlation upon the lateral response may be examined quite easily using Eq. 4.42. If the inputs are assumed to be uncorrelated, that is, independently applied and unrelated, Eq. 4.42 reduces to

$$\{G_{uvs}\} = \sum_{n=1}^{N} \sum_{m=1}^{N} \{\phi_n\}\{\phi_m\}^T \sum_{j=1}^{4} \left(H_{nj}^*(\omega)\right)\left(H_{mj}(\omega)\right) G_j(\omega) \qquad (4.44)$$

in which $G_j(\omega)$ is the power spectral density of the j^{th} displacement input $f_j(t)$ which is estimated as

$$G_j(\omega) \simeq \frac{2}{T_1} |F_j(\omega)|^2 \qquad j=1,2,3,4. \qquad (4.45)$$

The results of Eq. 4.42 can be compared to those of Eq. 4.44 in order to gain a better understanding of the effects of input correlation upon the response calculations.

The second characteristic feature of Eq. 4.42 involves the double summation over the lateral modes and their associated complex frequency response functions. It should be noted that the complex frequency response functions $H_{nj}(\omega)$ peak in amplitude at their associated

natural frequencies ω_n, and have much lower amplitudes elsewhere along the frequency band. Therefore, when the natural frequencies of lateral vibration are well separated and damping ratios are small, the effect of cross-terms ($n \neq m$) in Eq. 4.42 becomes much less significant than the diagonal terms ($n = m$) (4). Under these circumstances, the double summation may be replaced by a single sum, that is

$$\{G_{uvs}\} = \sum_{n=1}^{N} \{\phi_n\}\{\phi_n\}^T \{H_n^*(\omega)\}^T [G_{ff}(\omega)] \{H_n(\omega)\} \tag{4.46}$$

However, due to the flexible nature of the suspension bridge, closely-spaced modes are quite likely to occur. Under such circumstances, the effect of the cross terms are no longer negligible, and an accurate representation of the response would have to include these modal interaction terms. For the purpose of this chapter, Eq. 4.42 is utilized, that is, the effects of modal interaction are incorporated through a double summation.

The mean square value of the relative lateral response $\{\Psi^2_{uvs}\}$ is given by the integration of $\{G_{uvs}\}$ over the entire frequency range, that is

$$\{\Psi^2_{uvs}\} = \frac{1}{2\pi} \int_0^\infty \{G_{uvs}\} d\omega \tag{4.47}$$

and the square root of Eq. 4.47 is the root mean square (R.M.S.) relative lateral response.

The power spectral density of the total lateral displacement response can be obtained by multiplying Eq. 4.26 by its complex conjugate and by $(2/T_1)$, which leads to

$$\begin{Bmatrix} G_{us} \\ G_{ug} \end{Bmatrix} = \sum_{j=1}^{4} \sum_{k=1}^{4} \begin{Bmatrix} g_{psk} \\ g_{pgk} \end{Bmatrix} \{ g_{psj} \quad g_{pgj} \} \cdot G_{jk}(\omega) + \sum_{j=1}^{4} \left(\begin{Bmatrix} G_{uvsj} \\ 0 \end{Bmatrix} + \begin{Bmatrix} G_{juvs} \\ 0 \end{Bmatrix} \right) \{ g_{psj} \quad g_{pgj} \} + \begin{Bmatrix} G_{uvs} \\ 0 \end{Bmatrix} \tag{4.48}$$

where

$$\{G_{uvsj}\} = \frac{2}{T_1} \{\overset{*}{U}_{vs}(\omega)\} F_j(\omega)$$

$$= \frac{2}{T_1} \sum_{n=1}^{N} \{\phi_n\} \{\overset{*}{H}_n(\omega)\}^T \{\overset{*}{F}(\omega)\} F_j(\omega) \qquad j=1,2,3,4 \tag{4.49}$$

and

$$\{G_{juvs}\} = \frac{2}{T_1} \overset{*}{F}_j(\omega) \{U_{vs}(\omega)\}$$

$$= \frac{2}{T_1} \sum_{n=1}^{N} \{\phi_n\} \overset{*}{F}_j(\omega) \{H_n(\omega)\}^T \{F(\omega)\} \qquad j=1,2,3,4 \tag{4.50}$$

For the uncorrelated case $\{G_{uvsj}\}$ and $\{G_{juvs}\}$ reduce to

$$\{G_{uvsj}\} = \sum_{n=1}^{N} \{\phi_n\} [\overset{*}{H}_{nj}(\omega)] G_j(\omega) \quad , \qquad j=1,2,3,4, \tag{4.51}$$

$$\{G_{juvs}\} = \sum_{n=1}^{N} \{\phi_n\} [H_{nj}(\omega)] G_j(\omega) \quad , \qquad j=1,2,3,4 \tag{4.52}$$

where $H_{nj}(\omega)$ is given by Eq. 4.31 and $G_j(\omega)$ is given by Eq. 4.45. In addition, the cross-spectral terms $G_{jk}(\omega)$, $(j \neq k)$, are equal to zero in Eq. 4.48 for the uncorrelated case.

The integration of $\{G_{us}\}$ and $\{G_{ug}\}$ over the frequency domain provides the mean square total lateral displacement response, $\{\Psi_u^2\}$,

$$\begin{Bmatrix} \Psi^2_{us} \\ \Psi^2_{us} \end{Bmatrix} = \frac{1}{2\pi} \int_0^\infty \begin{Bmatrix} G_{us} \\ G_{ug} \end{Bmatrix} d\omega$$

$$= \begin{Bmatrix} \Psi^2_{uvs} \\ 0 \end{Bmatrix} + \sum_{j=1}^{4} \begin{Bmatrix} \Psi^2_{uvsj} \\ 0 \end{Bmatrix} \begin{Bmatrix} g_{psj} \\ g_{pgj} \end{Bmatrix}^T + \sum_{j=1}^{4} \sum_{k=1}^{4} \begin{Bmatrix} g_{psk} \\ g_{pgk} \end{Bmatrix} \begin{Bmatrix} g_{psj} \\ g_{pgj} \end{Bmatrix}^T \Psi^2_{jk} \qquad (4.53)$$

where $\{\Psi^2_{uvs}\}$ is given by Eq. 4.47, and

$$\{\Psi^2_{uvsj}\} = \frac{1}{2\pi} \int_0^\infty (\{G_{uvsj}\} + \{G_{juvs}\}) d\omega \qquad j=1,2,3,4 \qquad (4.54)$$

$$\Psi^2_{jk} = \frac{1}{2\pi} \int_0^\infty G_{jk}(\omega)\ d\omega \qquad \begin{matrix} j=1,2,3,4 \\ k=1,2,3,4 \end{matrix} \qquad (4.55)$$

The procedure outlined in the above section may be used to evaluate the power spectral density of the vibrationally-induced bending moment in the center span suspended structure by simply replacing the mode shapes, $\{\phi_n\}$, and quasi-static functions $\{g_{psi}\}$ by $E_{s2}I_{s2}\{\bar{\phi}'_n\}$ and $E_{s2}I_{s2}\{\bar{g}'_{psi}\}$, respectively, where $E_{s2}I_{s2}$ is the lateral flexural rigidity of the center span; and the overbarred vectors are extracted from the original quasi-static and modal vectors in such a manner that only those degrees of freedom corresponding to the rotations of the suspended structure are entered in these vectors. Similarly, the power spectral density of the vibrationally-induced lateral shearing force in the suspended structure may be obtained by replacing the modes and quasi-static functions by $E_{s2}I_{s2}\{\bar{\phi}''_n\}$ and $E_{s2}I_{s2}\{\bar{g}''_{psi}\}$, respectively. In addition, the autospectra of laterally-induced flexural stresses in the suspended structure's chord members is given by the following flexural stress relation

$$\{G_\sigma\} = \left(\frac{b}{2I_{s2}}\right)^2 \{G_M\} \tag{4.56}$$

where $\{G_M\}$ is the autospectra of lateral response bending moments; $\{G_\sigma\}$ is the autospectra of lateral response stresses; b is the width of the suspended structure; and I_{s2} is the area moment of inertia of the center span suspended structure about its vertical axis.

Mean square lateral bending moments, shearing forces and bending stresses are obtained by using Eq. 4.53 with the mode shapes and quasi-static functions replaced as described above.

IV.10 ADDITIONAL HORIZONTAL COMPONENT OF CABLE TENSION H(t)

The additional horizontal component of cable tension due to multiple-support lateral excitation $H(t)$ is given by

$$H(t) = H_v(t) + H_p(t) \tag{4.57}$$

where $H_v(t)$ is the vibrational (relative) contribution to the cable tension and $H_p(t)$ is the quasi-static contribution to the cable tension. The vibrational contribution to the cable tension, $H_v(t)$, is given by (Eq 4.6)

$$H_v(t) = \left(\frac{E_c A_c}{L_E}\right) \sum_{i=1}^{3} \left[\frac{1}{2} \int_0^{\ell_i} \left(\frac{\partial w_c}{\partial x_i}\right)^2 dx_i + \int_0^{\ell_i} \left(\frac{\partial v_c}{\partial x_i}\right)\left(\frac{dy_c}{dx_i}\right) dx_i \right.$$

$$\left. + \frac{1}{2} \int_0^{\ell_i} \left(\frac{\partial v_c}{\partial x_i}\right)^2 dx_i \right] \tag{4.58}$$

where $w_c(x_i,t)$ is the relative lateral motion of the i^{th} suspended structure; $v_c(x_i,t)$ is the upward deflection of the cables incidental

to their lateral deflection (Eq. 4.1); $y_c(x_i)$ is the parabolic cable profile (Eq. 4.5); E_c and A_c are respectively, the modulus of elasticity and cross sectional area of each cable; and L_E is the virtual length (Eq. 4.7).

It should be noted that Eq. 4.58 contains only nonlinear terms. The procedure utilized in this section involves using the linear lateral displacement response solution obtained in the previous sections in order to provide an estimate for the vibrational cable tension $H(t)$, which is expected to be quite small in comparison with the dead load horizontal component of cable tension H_w. Now substituting Eqs. 4.1 and 4.5 into Eq. 4.58, and integrating the second term in Eq. 4.58 by parts results in

$$H_v(t) = \left(\frac{E_c A_c}{L_E}\right) \sum_{i=1}^{3} \left[\frac{1}{2} \int_0^{\ell_i} \left(\frac{\partial w_c}{\partial x_i}\right)^2 dx_i + \left(\frac{\overset{*}{w}_c + \overset{*}{w}_{si}}{2H_w}\right) \int_0^{\ell_i} \left(\frac{w_c^2}{2y_c}\right) dx_i \right.$$

$$\left. + \frac{1}{2} \int_0^{\ell_i} \left[\frac{\partial}{\partial x_i}\left(\frac{w_c^2}{2y_c}\right)\right]^2 dx_i \right] \tag{4.59}$$

where $\overset{*}{w}_c$ is the dead weight of both cables per unit span length; $\overset{*}{w}_{si}$ is the dead weight of the suspended structure per unit length of the i^{th} span; and H_w is the horizontal component of dead load cable tension.

In order to analyze the cable tension in the frequency domain, the finite Fourier transform of Eq. 4.59 becomes

$$\bar{H}_v(\omega) = \left(\frac{E_c A_c}{L_E}\right) \sum_{i=1}^{3} \left[\frac{1}{2} \int_0^{\ell_i} \left(\frac{\partial \bar{w}_c}{\partial x_i}\right)^2 dx_i + \left(\frac{\overset{*}{w}_c + \overset{*}{w}_{si}}{2H_w}\right) \int_0^{\ell_i} \left(\frac{\bar{w}_c^2}{2y_c}\right) dx_i \right.$$

$$\left. + \frac{1}{2} \int_0^{\ell_i} \left[\frac{\partial}{\partial x_i}\left(\frac{\bar{w}_c^2}{2y_c}\right)\right]^2 dx_i \right] \tag{4.60}$$

where $\bar{w}_c(x_i,\omega)$ is the finite Fourier transform of the cables' lateral vibrational response in the i^{th} span. This equation can be solved by considering the cables' response at its discrete degrees of freedom, which was obtained from the previous lateral displacement response analysis, that is

$$\bar{w}_c(x_i,\omega) = \sum_{n=1}^{N_i} \phi_n(x_i) Q_{ni}(\omega) \tag{4.61}$$

where $\phi_n(x_i)$ is the cables' configuration in the n^{th} lateral mode shape of the i^{th} suspended span; $Q_{ni}(\omega)$ is the Fourier transform of the n^{th} generalized coordinate of the i^{th} span (Eq. 4.36); x_i are the degrees of freedom corresponding to the cables in the i^{th} span; and N_i are the number of degrees of freedom utilized in the finite element modeling of the i^{th} suspended span. The procedure involves substituting the results of Eq. 4.61 into Eq. 4.60 and then integrating Eq. 4.60 numerically to obtain the vibrational displacement contribution to the Fourier transform of the additional horizontal component of cable tension.

The quasi-static contribution to the cable tension in the frequency domain can be evaluated similar to Eq. 4.60, that is

$$H_p(\omega) = \left(\frac{E_c A_c}{L_E}\right) \sum_{i=1}^{3} \left[\frac{1}{2} \int_0^{\ell_i} \left(\frac{\partial \bar{w}_g}{\partial x_i}\right)^2 dx_i + \left(\frac{w_c^* + w_{si}^*}{2H_w}\right) \int_0^{\ell_i} \bar{v}_g dx_i \right.$$

$$\left. + \frac{1}{2} \int_0^{\ell_i} \left(\frac{\partial \bar{v}_g}{\partial x_i}\right)^2 dx_i \right] \tag{4.62}$$

where $\bar{w}_g(x_i,\omega)$ is the finite Fourier transform of the cables' lateral quasi-static response in the i^{th} suspended span, given by

$$\bar{w}_g(x_i,\omega) = \sum_{j=1}^{4} g_{cj}(x_i)F_{ji}(\omega) \qquad i=1,2,3 \qquad (4.63)$$

in which $F_{ji}(\omega)$ is the finite Fourier transform of the j^{th} lateral input displacement in the i^{th} span; and $g_{cj}(x_i)$ is the j^{th} quasi-static cable configuration in the i^{th} span. The finite Fourier transform of the cables' incidental upward quasi-static motion in the i^{th} span, $\bar{v}_g(x_i,\omega)$, is given by

$$\bar{v}_g(x_i,\omega) = \sum_{j=1}^{2} \frac{\left[g_{cj}(x_i) - \left(1 - \frac{x_i}{\ell_i}\right)\right]^2}{2y_c(x_i)} F_{ji}(\omega)$$

$$+ \sum_{j=3}^{4} \frac{\left[\frac{x_i}{\ell_i} - g_{cj}(x_i)\right]^2}{2y_c(x_i)} F_{ji}(\omega) \qquad i=1,2,3, \qquad (4.64)$$

Again, by substituting the results of Eqs. 4.63 and 4.64 into Eq. 4.62 and integrating this equation numerically, the quasi-static contribution to the Fourier transform of the cable tension, $H_p(\omega)$ can be evaluated.

The power spectral density of the additional horizontal component of cable tension (for the correlated case) can be approximated as

$$G_H(\omega) \simeq \frac{2}{T_1} \overset{*}{H}(\omega)\, H(\omega) = \frac{2}{T_1}\left(\overset{*}{H}_v(\omega) + \overset{*}{H}_p(\omega)\right)\left(H_v(\omega) + H_p(\omega)\right) \qquad (4.65)$$

where T_1 is the time duration of the ground motion input and the superposed asterisk denotes complex conjugate. Finally, mean square dynamically-induced cable tensions are obtained by integrating $G_H(\omega)$ over the entire frequency range, that is

$$\Psi_H^2 = \frac{1}{2\pi} \int_0^\infty G_H(\omega)\, d\omega \tag{4.66}$$

and the square root of the previous equation is the root mean square (R.M.S.) dynamically-induced horizontal component of cable tension due to lateral vibration.

IV.11 APPLICATION: LATERAL SEISMIC BEHAVIOR OF THE GOLDEN GATE BRIDGE

IV.11.1 Correlated Case

The analysis outlined in this chapter is applied to the Golden Gate Suspension Bridge in San Francisco, California, in order to estimate its lateral response characteristics. The structural properties (needed in lateral dynamic analysis) of the bridge are summarized in Table IV-1. The lateral quasi-static functions are shown for the center span and left side spans in Fig. IV-3, corresponding to unit displacement of the cables or suspended structure at each of the bridge's support points (anchorages and tower piers). The quasi-static functions for the right side span are simply antisymmetric to those of the left side span, and therefore are not explicitly shown. The first six symmetric and six antisymmetric modes of both center and side span lateral vibration are shown in Fig. IV-4, while their associated participation coefficients appear in Table IV-2 and Table IV-3. It can be seen quite clearly from Fig. IV-4 that there is a strong coupled (double-pendulum type) motion between the cables and suspended structure in the center span of the bridge, while in the side span this coupled motion appears in the lower modes only. One should also note that for the center span symmetric lateral modes, the participation coefficients α_{n1} and α_{n3} are equal, as are α_{n2} and α_{n4}, β_{n1} and β_{n3}, and β_{n2} and β_{n4}.

Table IV-1

Lateral Structural Properties of the Golden Gate Bridge

Parameter	Center Span	Side Spans
Span Length	ℓ_2 = 4200 ft	$\ell_1 = \ell_3$ = 1125 ft
Span Width	b = 90 ft	b = 90 ft
$\overset{*}{w}_{Si}$	$\overset{*}{w}_{S2}$ = 16.02 k/ft	$\overset{*}{w}_{S1} = \overset{*}{w}_{S3}$ = 16.42 k/ft
E_{Si}	E_{S2} = 29000 ksi	$E_{S1} = E_{S3}$ = 29000 ksi
I_{Si}	I_{S2} = 1,100,100 in^2ft^2	$I_{S1} = I_{S3}$ = 1,100,100 in^2ft^2
Cable Properties	E_C = 29000 ksi A_C = 831.9 in^2 L_E = 7698 ft H_W = 53467 kips $\overset{*}{w}_C$ = 6.68 k/ft	

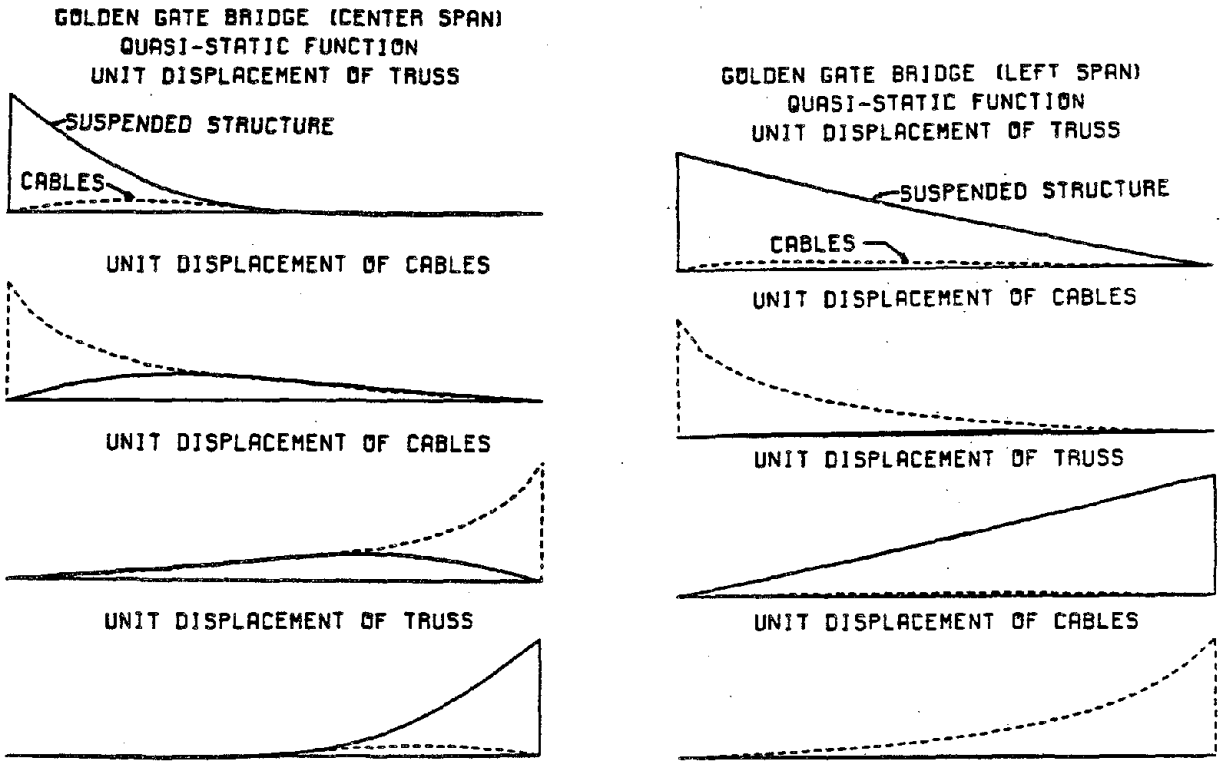

Fig. IV-3 Lateral quasi-static functions of the center and side spans of the Golden Gate Suspension Bridge.

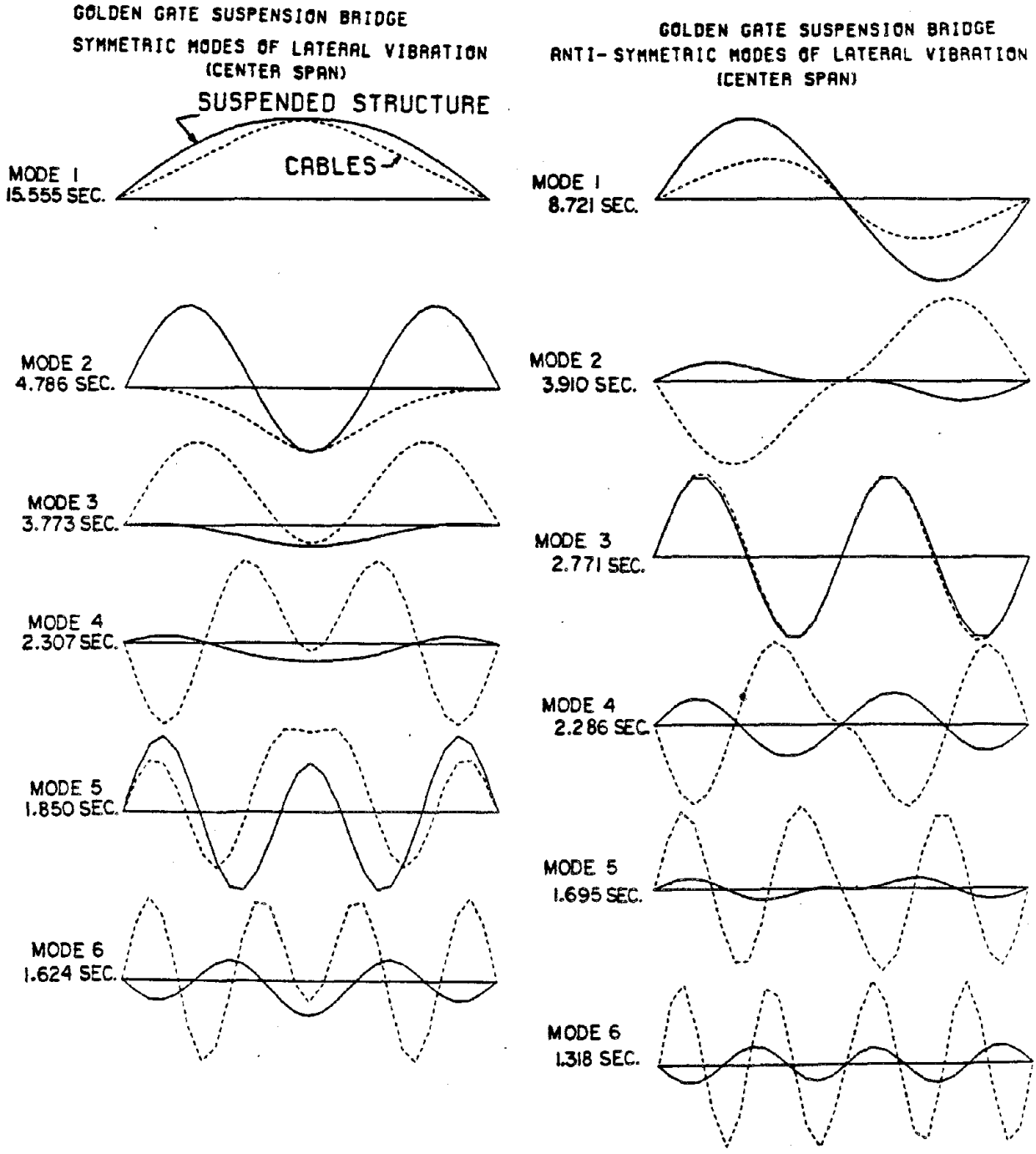

Fig. IV-4a Lateral modes of vibration of the Golden Gate Bridge (center span).

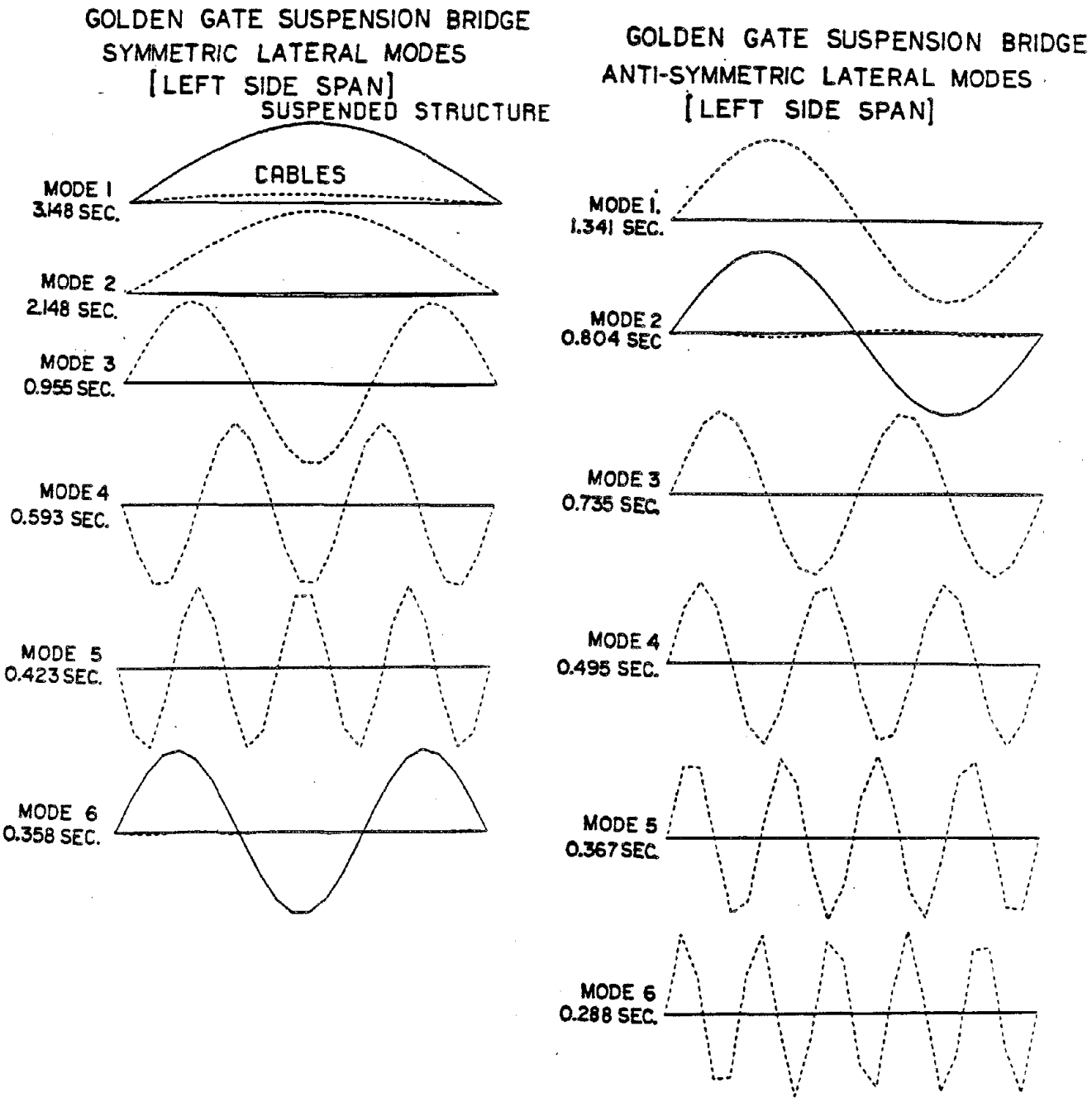

Fig. IV-4b Lateral modes of vibration of the Golden Gate Bridge (side spans).

Table IV-2

Participation Coefficients of Lateral Earthquake Response
for the Golden Gate Bridge; Center Span Vibration

Mode Order n	α_{n1}	α_{n2}	α_{n3}	α_{n4}	β_{n1}	β_{n2}	β_{n3}	β_{n4}
Sym 1	-0.110	-0.206	-0.110	-0.206	-0.00176	-0.00332	-0.00176	-0.00332
Sym 2	-0.193	0.0019	-0.193	0.0019	-0.0100	0.0	-0.0100	0.0
Sym 3	-0.0267	-0.177	-0.0267	-0.177	-0.00180	-0.0117	-0.00180	-0.0117
Sym 4	-0.0304	0.115	-0.0304	0.115	-0.00323	0.0124	-0.00323	0.0124
Sym 5	-0.110	-0.0223	-0.110	-0.0223	-0.0146	-0.00299	-0.0146	-0.00299
Sym 6	0.0681	-0.0761	0.0681	-0.0761	0.0102	-0.0116	0.0102	-0.0116
A.S.1	-0.210	-0.0884	0.210	0.0884	-0.00603	-0.00254	+0.00603	+0.00254
A.S.2	-0.0790	0.162	0.0790	-0.162	-0.00498	0.0104	0.00498	-0.0104
A.S.3	-0.115	-0.0404	0.115	0.0404	-0.0102	-0.00364	0.0102	0.00364
A.S.4	-0.0926	0.0908	0.0926	-0.0908	-0.00997	0.00988	0.00997	-0.00998
A.S.5	+0.0452	-0.0898	-0.0452	0.0898	-0.00654	-0.0131	0.00654	0.0131
A.S.6	0.0601	-0.0666	-0.0601	0.0666	0.0111	-0.0125	-0.0111	0.0125

Table IV-3

Participation Coefficients of Lateral Earthquake Response for the Golden Gate Bridge; Left Side Span Vibration

Mode Order n	α_{n1}	α_{n2}	α_{n3}	α_{n4}	β_{n1}	β_{n2}	β_{n3}	β_{n4}
Sym 1	-0.586	-0.0381	-0.610	-0.0186	-0.0467	-0.00304	-0.0486	-0.00148
Sym 2	0.00858	-0.230	0.0403	-0.260	0.000975	-0.0268	0.00470	-0.0303
Sym 3	-0.0203	0.158	0.00764	-0.165	-0.00543	-0.0411	0.00199	-0.0431
Sym 4	0.00474	0.112	0.00168	0.115	0.00219	0.0466	0.000714	0.0479
Sym 5	0.00355	0.0885	0.000899	0.0899	0.00238	0.0513	0.000537	0.0524
Sym 6	-0.211	0.000352	-0.212	-0.000410	-0.146	0.000235	-0.147	-0.000282
A.S.1	-0.0234	-0.194	0.0137	0.207	-0.00445	-0.0360	0.00256	0.0386
A.S.2	-0.315	-0.00108	0.317	0.00192	-0.0978	-0.000338	0.0985	0.000593
A.S.3	-0.000991	-0.1318	-0.00714	0.136	-0.000491	-0.0445	-0.00242	0.0461
A.S.4	-0.00412	-0.0996	-0.000701	0.102	-0.00232	-0.0495	-0.000353	0.0507
A.S.5	-0.00553	-0.0803	-0.00325	0.0813	-0.00408	-0.0535	-0.00219	0.0544
A.S.6	-0.00130	-0.0690	0.000300	0.0695	-0.00158	-0.0583	0.000255	0.0591

Similarly, for the center span antisymmetric lateral modes, $\alpha_{n1} = -\alpha_{n3}$, $\alpha_{n2} = -\alpha_{n4}$, and so on. The above equivalences among modal participation coefficients results from the structural symmetry of the center span. For the side spans, this symmetry does not exist, and therefore the modal participation coefficients are all individually different.

The center span lateral analysis incorporates six symmetric modes and five antisymmetric modes which lie within the frequency band of the earthquake inputs. The frequency response functions $H_{nj}(\omega)$ for the center span modes, corresponding to 2% damping, are shown in Fig. IV-5. These functions measure the magnification (or gain) factor corresponding to a unit harmonic input upon the response of the generalized coordinate, $q_n(t)$. Again, because of the inherent symmetry of the center span, the frequency response functions $H_{n3}(\omega)$ and $H_{n4}(\omega)$ are simply equal to $H_{n1}(\omega)$ and $H_{n2}(\omega)$, respectively for the symmetric modes, or $-H_{n1}(\omega)$ and $-H_{n2}(\omega)$ for the antisymmetric modes. The side span lateral analysis incorporates two symmetric modes and one antisymmetric mode which lie within the frequency band of the earthquake inputs. The frequency response functions $H_{nj}(\omega)$ for the side span modes, corresponding to 2% damping, are shown in Fig. IV-6. Because of the lack of structural symmetry in the side spans, the four complex frequency response functions are in general different. Therefore, all four complex frequency response functions are shown in this figure for the left side span, with the right side span being similar.

Three cases of lateral response are studied for the Golden Gate Bridge. In the first case, the lateral input motions at each support point, $F_1(t)$, $F_2(t)$, $F_3(t)$, and $F_4(t)$ respectively correspond to the S40°E components of horizontal ground motion recorded at Arrays

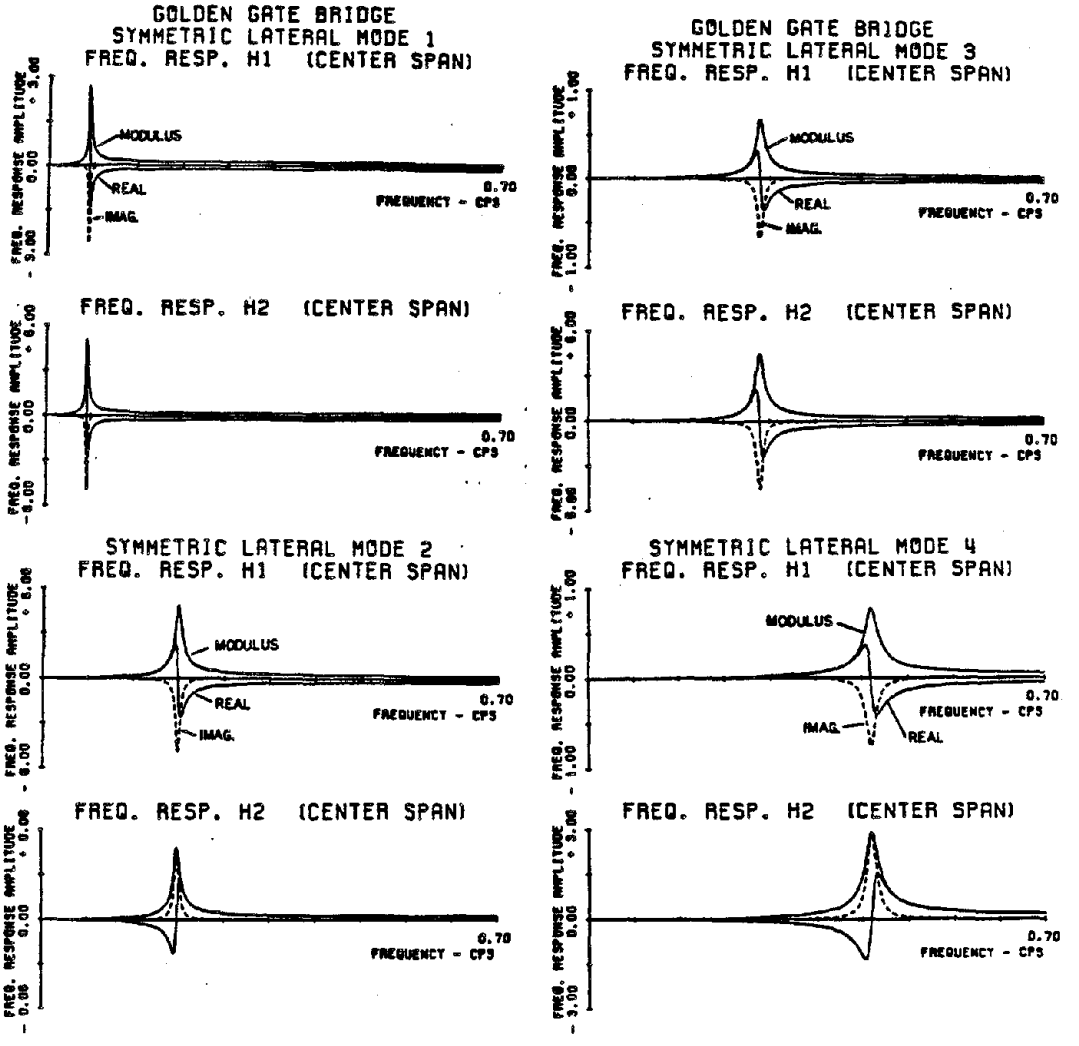

Fig. IV-5a Complex frequency response functions of center span lateral vibration.

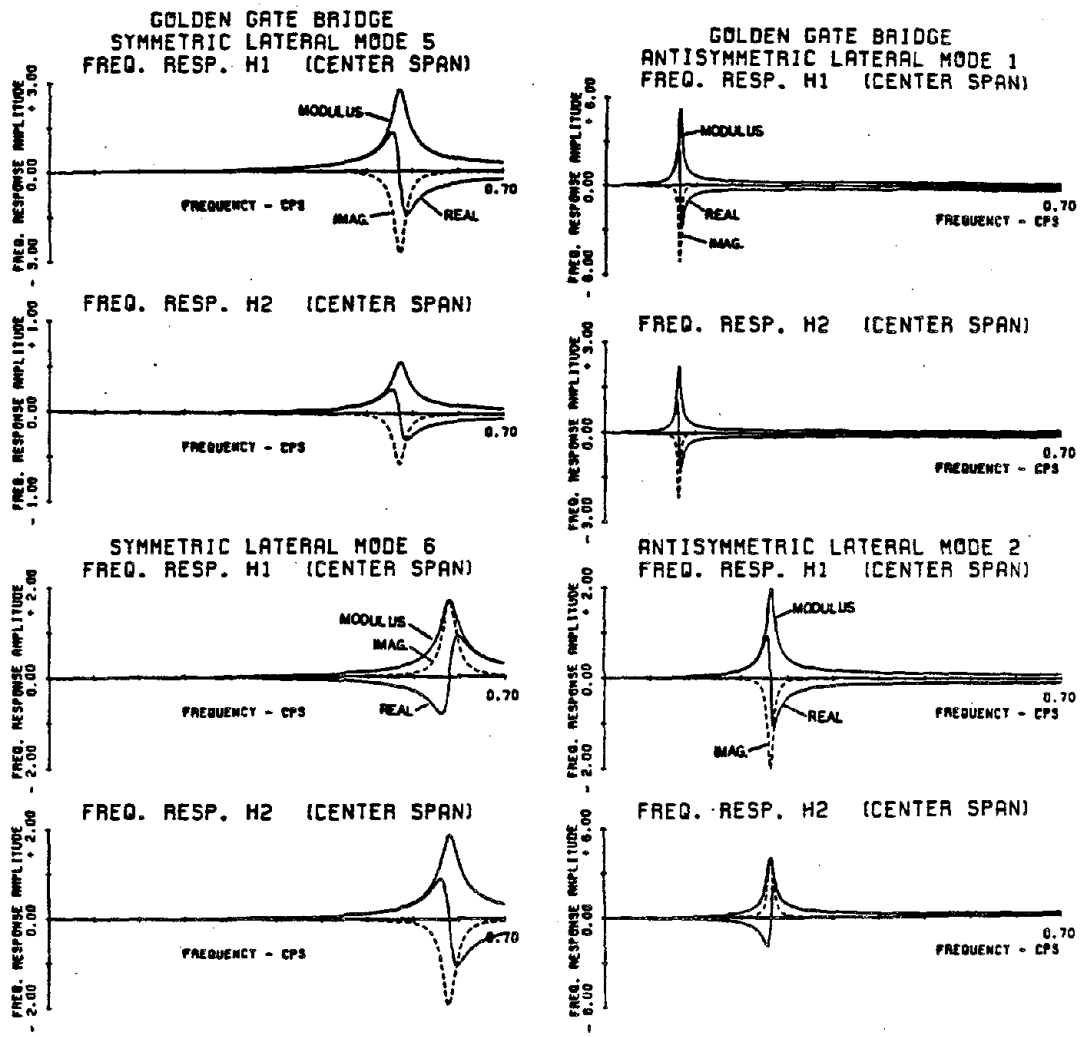

Fig. IV-5b Complex frequency response functions of center span lateral vibration.

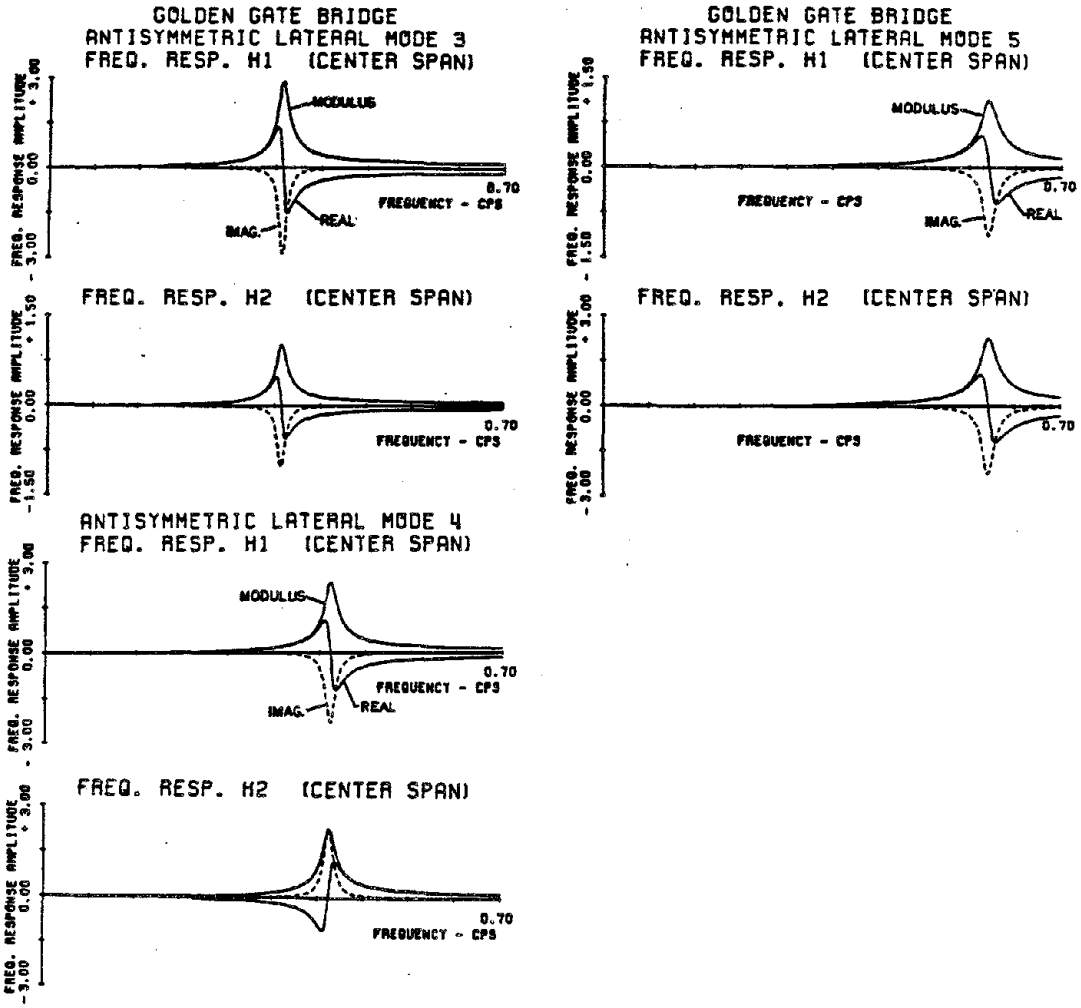

Fig. IV-5c Complex frequency response functions of center span lateral vibration.

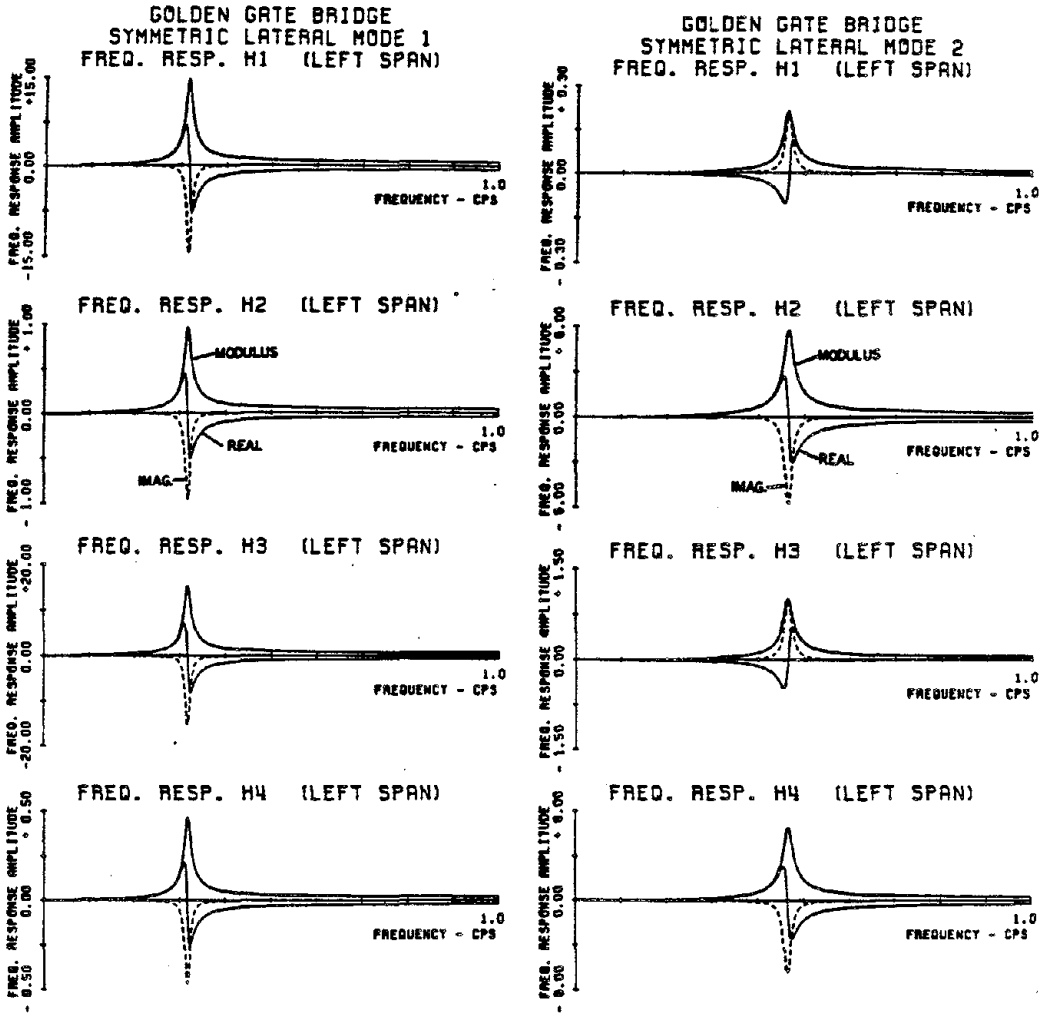

Fig. IV-6a Complex frequency response functions of left side span lateral vibration.

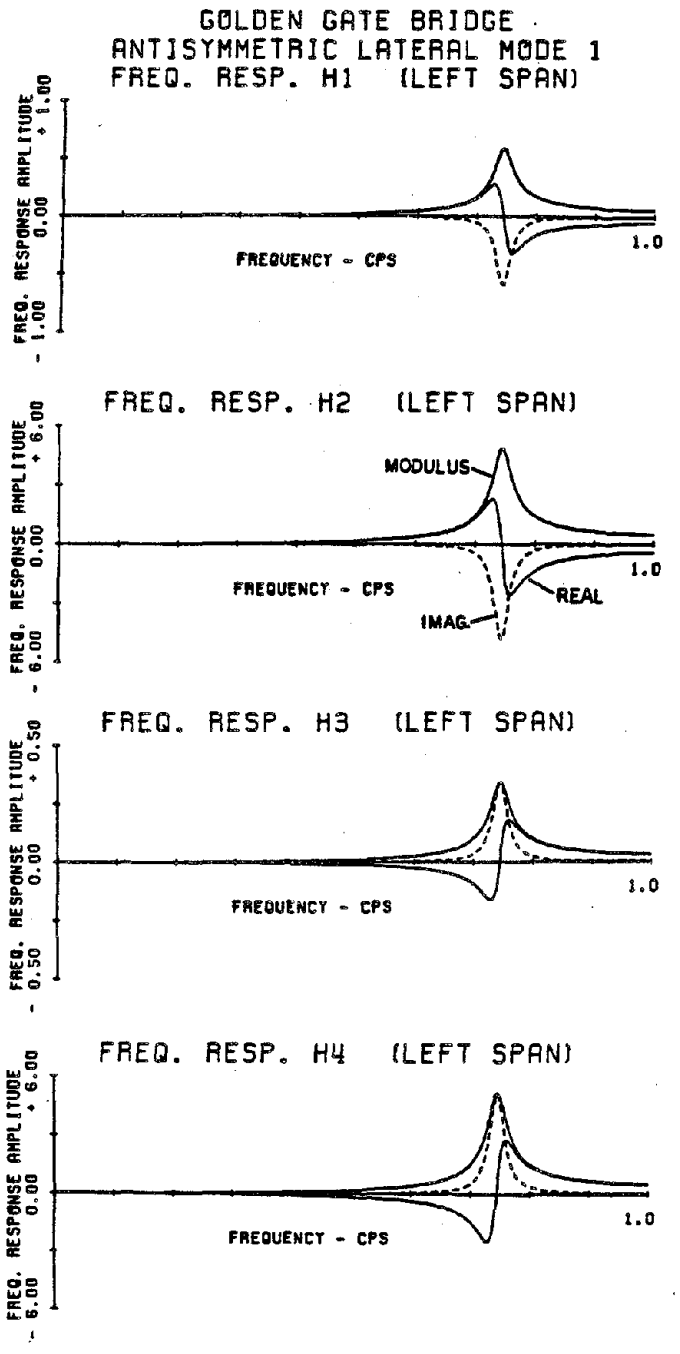

Fig. IV-6b Complex frequency response functions of left side span lateral vibration.

No. 4, 5, 6, and 7 of the 1979 El Centro Arrays (see Appendix II-e); while the second case involves similar correspondences among Arrays No. 5, 6, 7, and 8. The third lateral response case involves a uniform lateral ground motion applied to all supports. The S40E component recorded at Array No. 5 is utilized for this purpose. Time histories and power spectra corresponding to these inputs appear in Appendix II-e of Chapter II of this report.

The autospectra of lateral displacement of the cables and suspended structure (for the correlated case) at the quarter points of each span appear in Fig. IV-7 for input Arrays 4, 5, 7, and 7. The response is separated into vibrational (relative or modal) response, shown in dotted lines, and the total response which includes quasi-static contributions, shown in solid lines. It is fairly clear that a relatively large number of modes participate in the total lateral response. In contrast to the vertical response analysis, the antisymmetric vibrations are no longer of a higher order effect, that is, both symmetric and antisymmetric modes contribute to the lateral response. Also, the quasi-static contributions to the lateral response are seen to be more significant than in the vertical vibration problem. One notices this from the non-structural response peaks, corresponding to the predominant frequencies of strong input motion, which occur and which are of a purely quasi-static nature. Even in those response cases where the quasi-static contribution to the response is small or seemingly negligible, it should be remembered that the quasi-static contribution is inherent in the participation coefficients (Eqs. 4.22 and 4.23) and thus it is erroneous to conclude that the quasi-static functions have no impact upon the response.

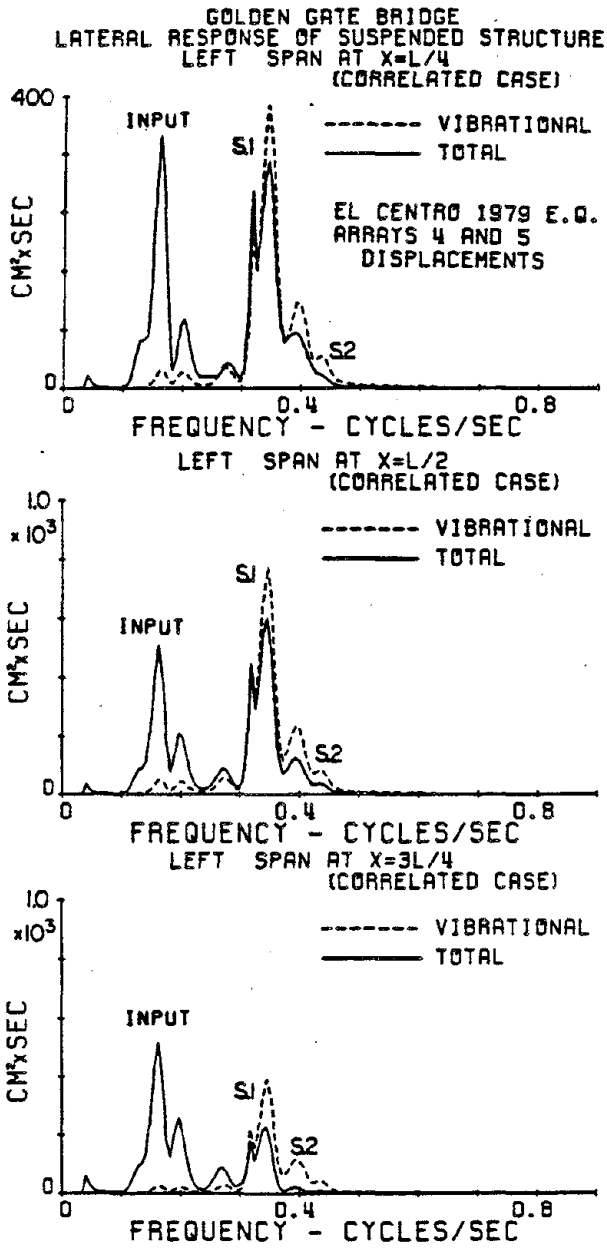

Fig. IV-7a Autospectra of the suspended structure displacement (left side span).

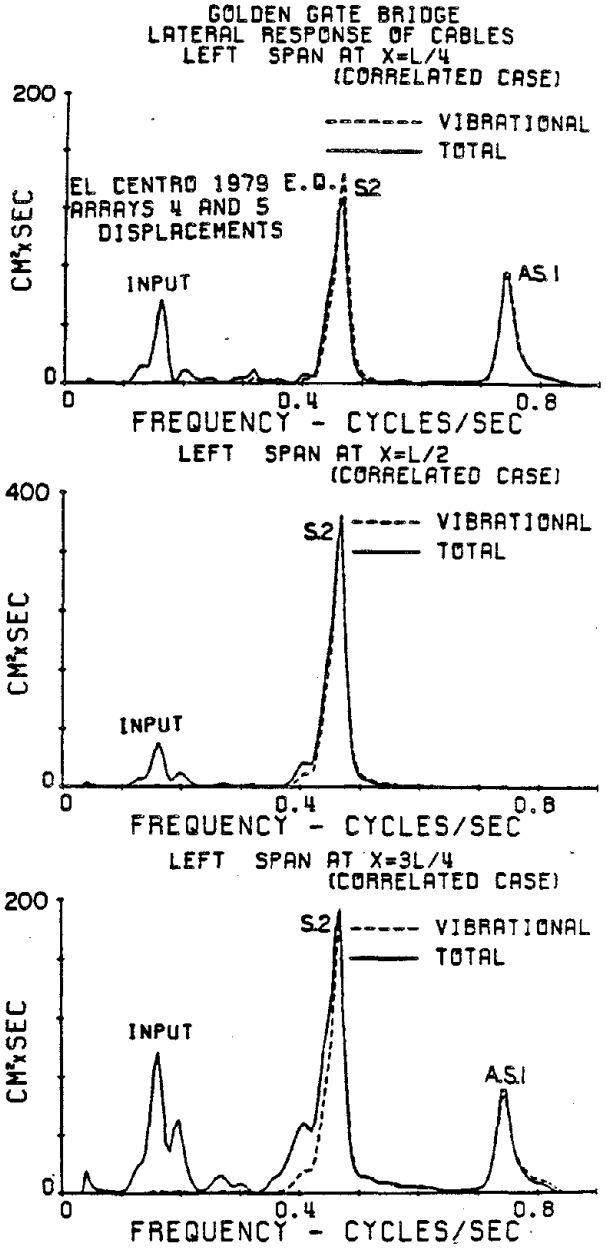

Fig. IV-7b Autospectra of the cables' displacement (left side span).

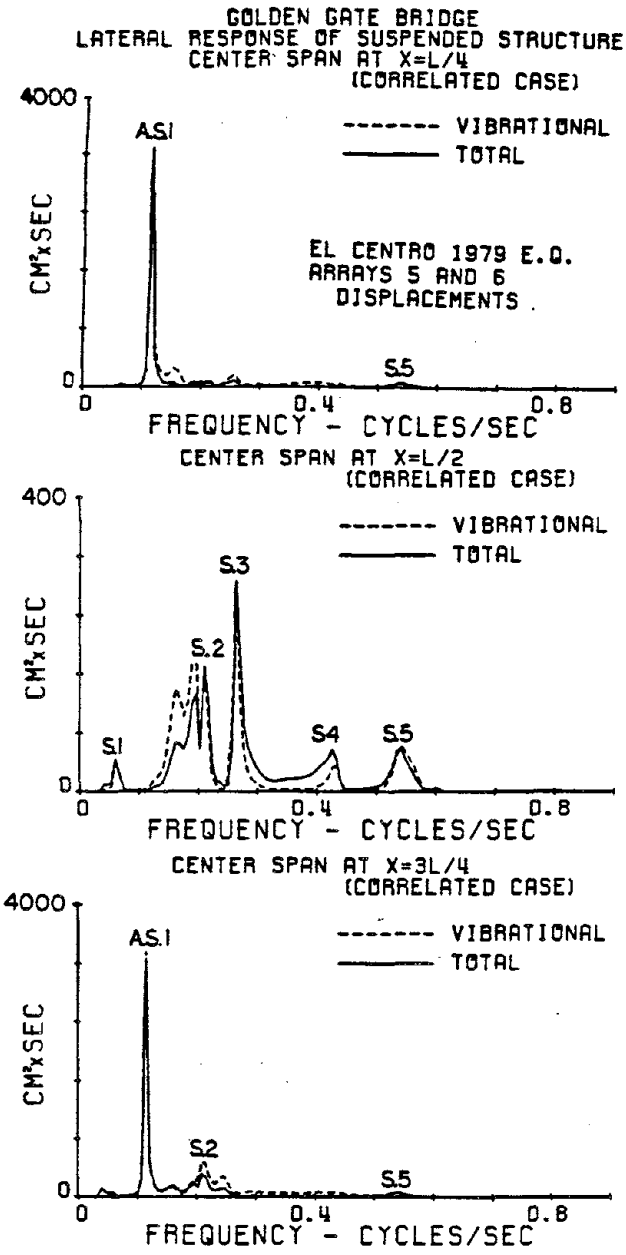

Fig. IV-7c Autospectra of the suspended structure displacement (center span).

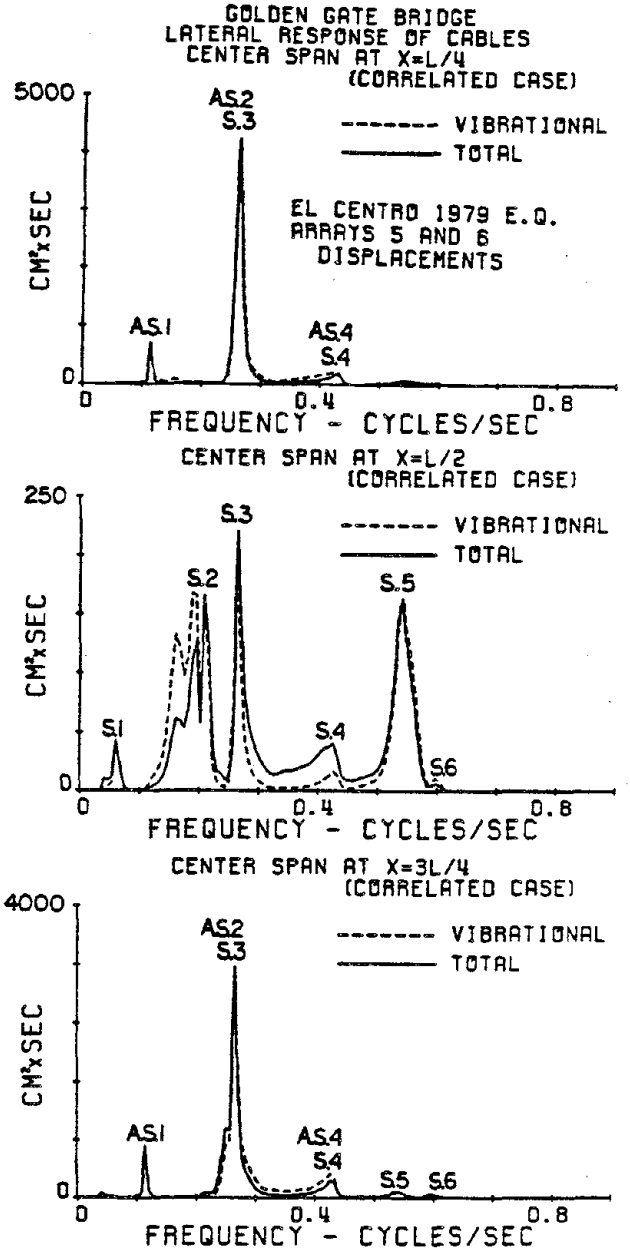

Fig. IV-7d Autospectra of the cables' displacement (center span).

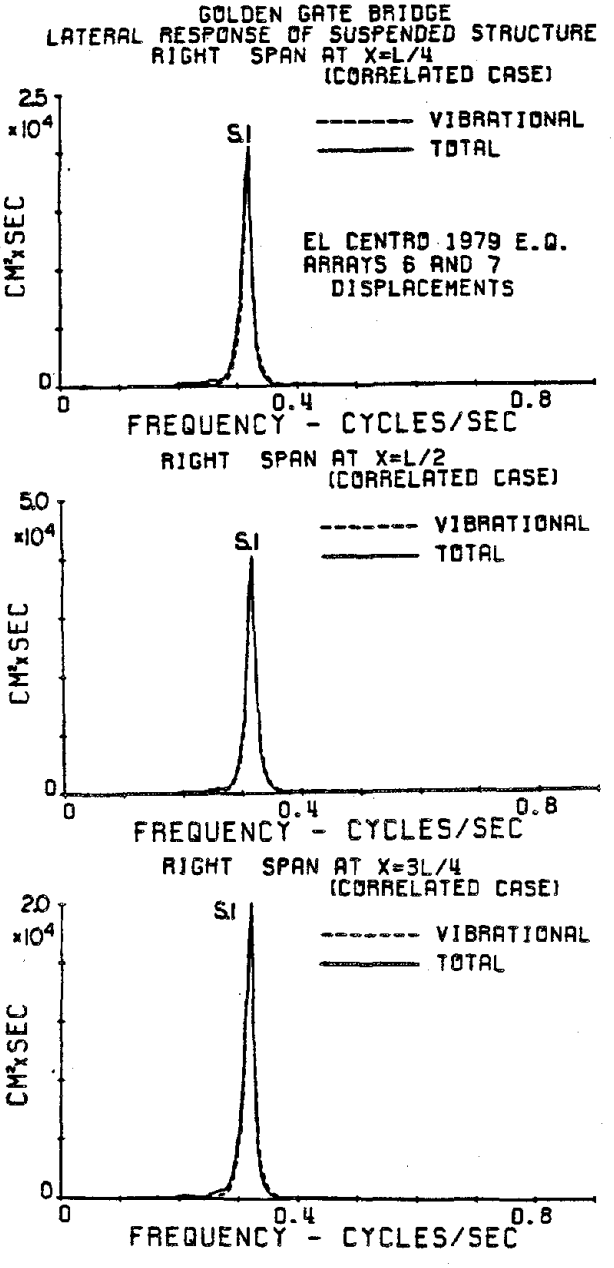

Fig. IV-7c Autospectra of the suspended structure displacement (right side span).

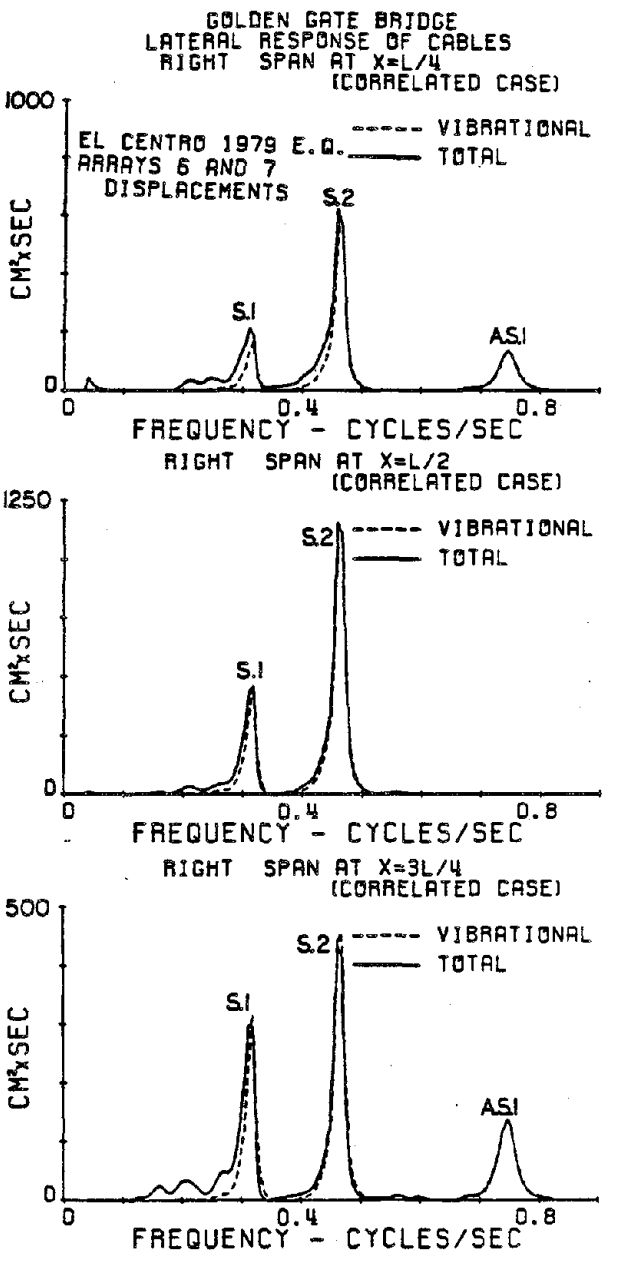

Fig. IV-7f Autospectra of the cables' displacement (right side span).

Similar autospectra of lateral displacement are shown in Fig. IV-8 for input Arrays 5, 6, 7, and 8, while the autospectra of response flexural stresses for both sets of arrays are shown in Fig. IV-9 (for the correlated case). The responses obtained for each set of input arrays are seen to be remarkably different in character due to the different frequency content of each input, as well as the phasing between the inputs. Figure IV-10 shows the autospectra of lateral displacement response under the uniform lateral motion assumption (correlated case), while Fig. IV-11 shows the corresponding autospectra of response stresses. Table IV-4 summarizes the root mean (R.M.S.) lateral displacement response values (for the correlated cases) obtained by integrating each autospectrum over the entire frequency range and taking the square root of the results of the integration. Figure IV-12 shows the autospectra of the additional horizontal component of cable tension, H(t), for all three lateral response cases. The root mean square (R.M.S.) cable tensions in these figures range from about 22 kips to 28 kips, which is very small in comparison with the cable tension due to dead loads, H_w = 53467 kips. Therefore, as was initially expected, the additional horizontal cable tension due to lateral vibration is very small and thus can be neglected.

Figure IV-13 shows the autospectra of the lateral shear force (for the correlated case) occurring at the left side of each span for both sets of multiple-support lateral inputs. Again, it is seen that the higher modes can contribute significantly to the response. Table IV-5 summarizes the root mean square (R.M.S.) stresses and shear forces for the correlated excitation cases.

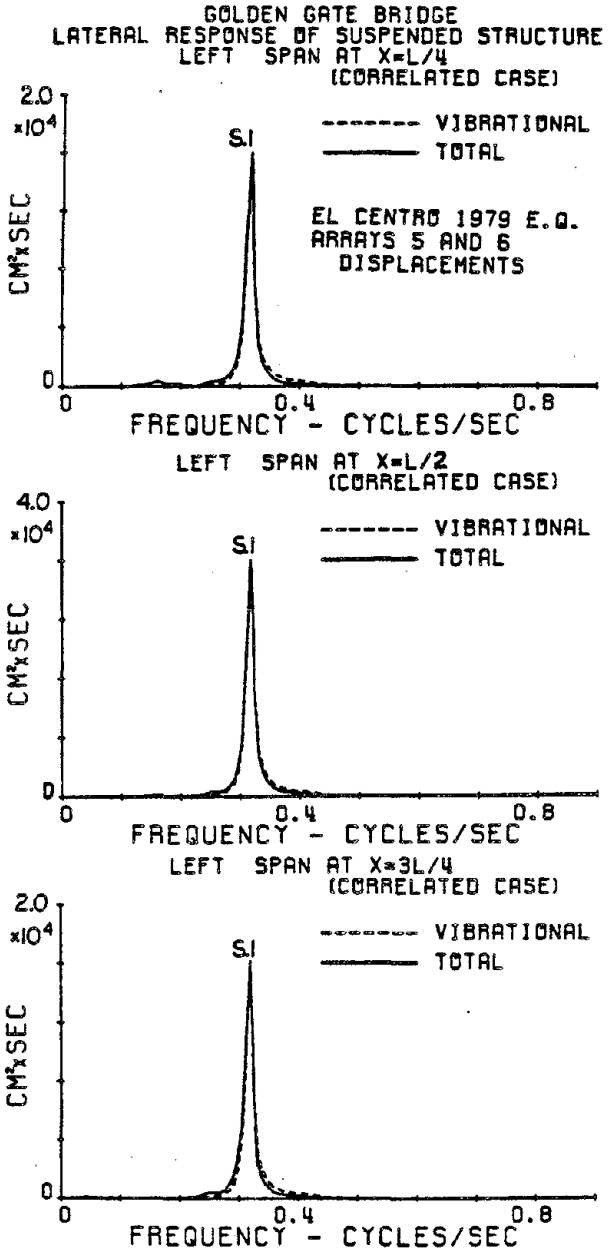

Fig. IV-8a Autospectra of the suspended structure displacement (left side span).

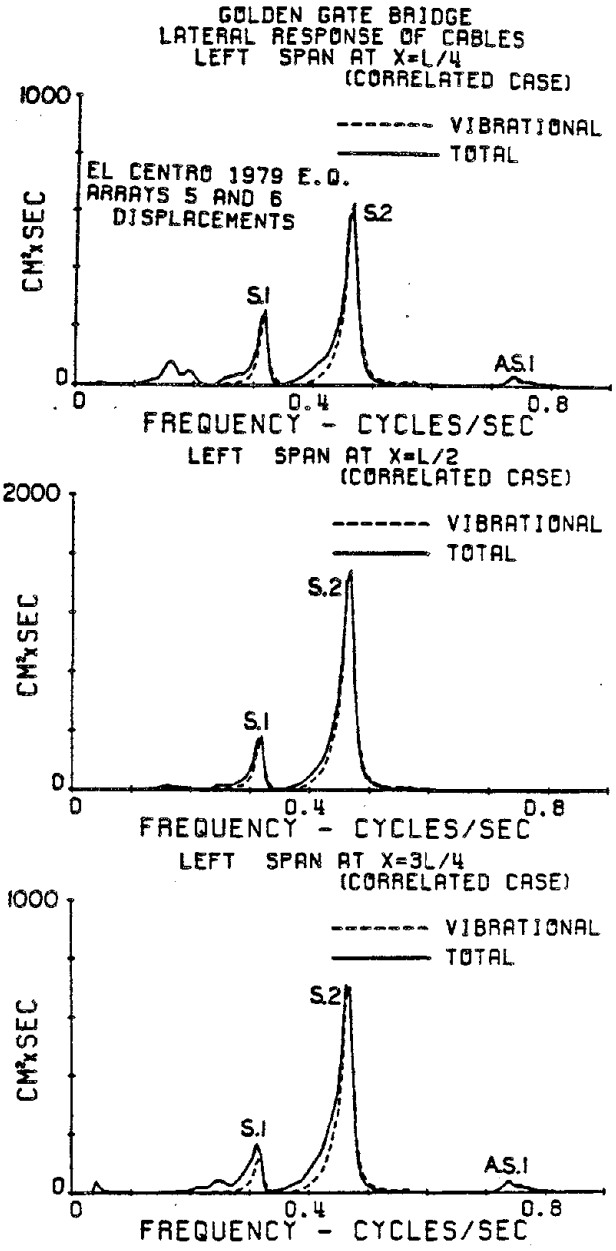

Fig. IV-8b Autospectra of the cables' displacement (left side span).

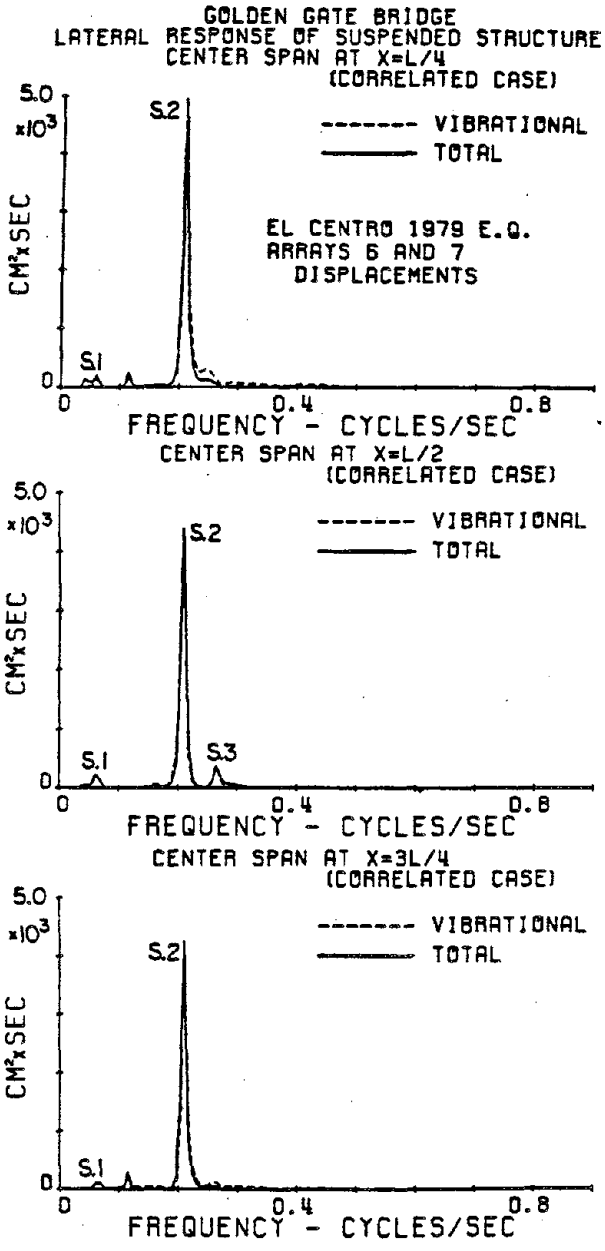

Fig. IV-8c Autospectra of the suspended structure displacement (center span).

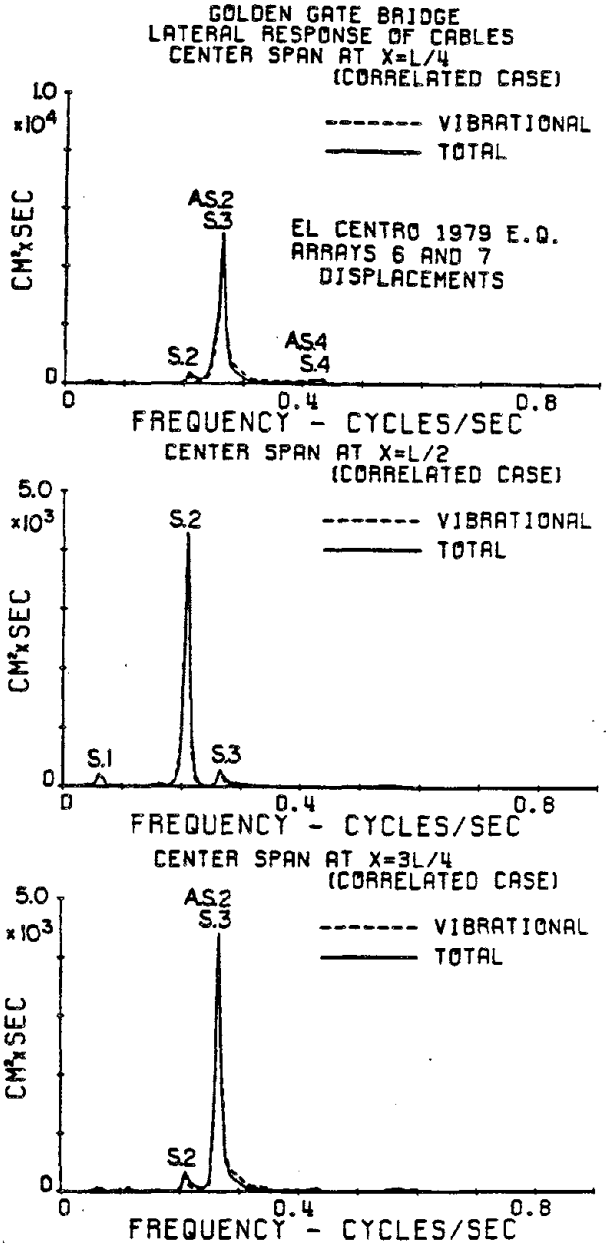

Fig. IV-8d Autospectra of the cables' displacement (center span).

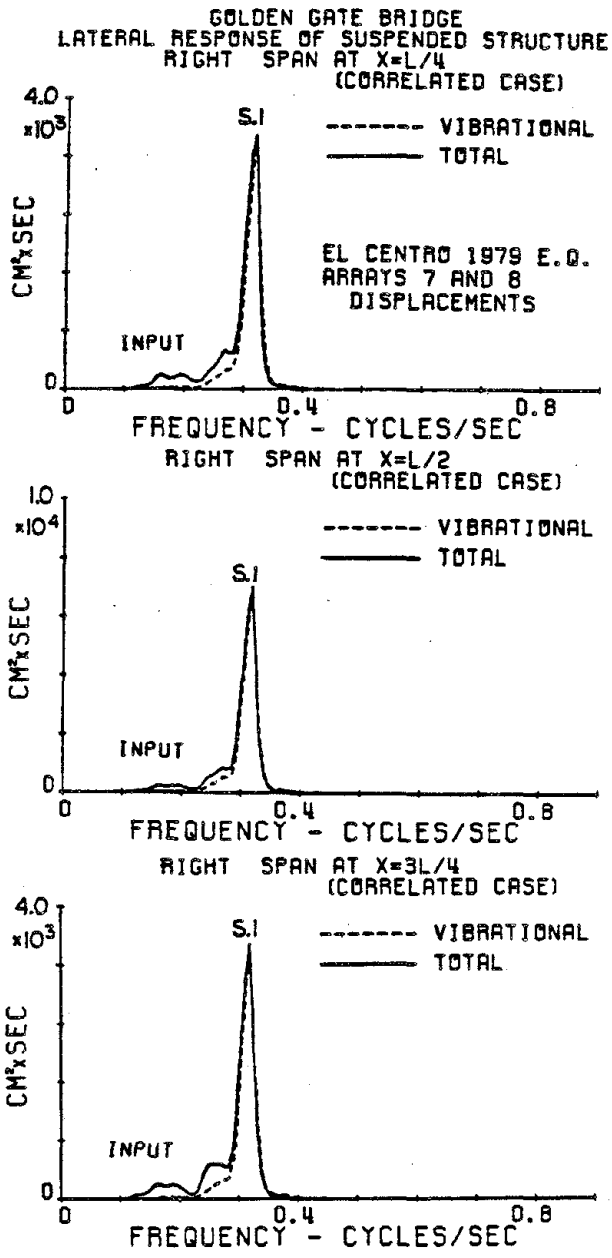

Fig. IV-8e Autospectra of the suspended structure displacement (right side span).

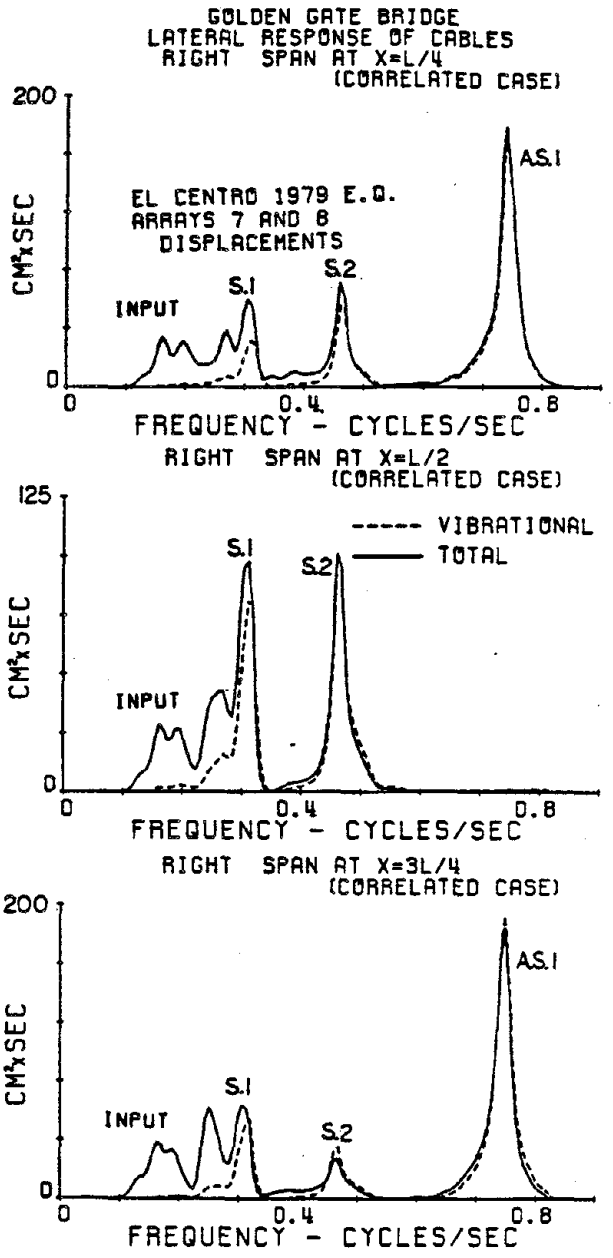

Fig. IV-8f Autospectra of the cables' displacement (right side span).

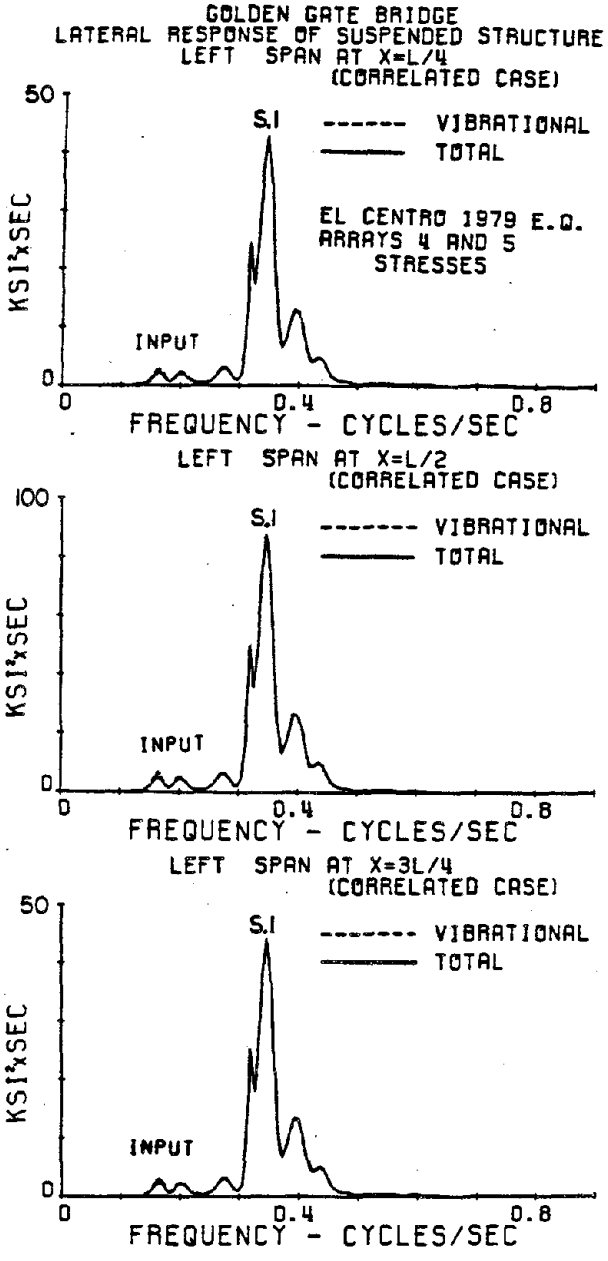

Fig. IV-9a Autospectra of the suspended structure stresses (left side span).

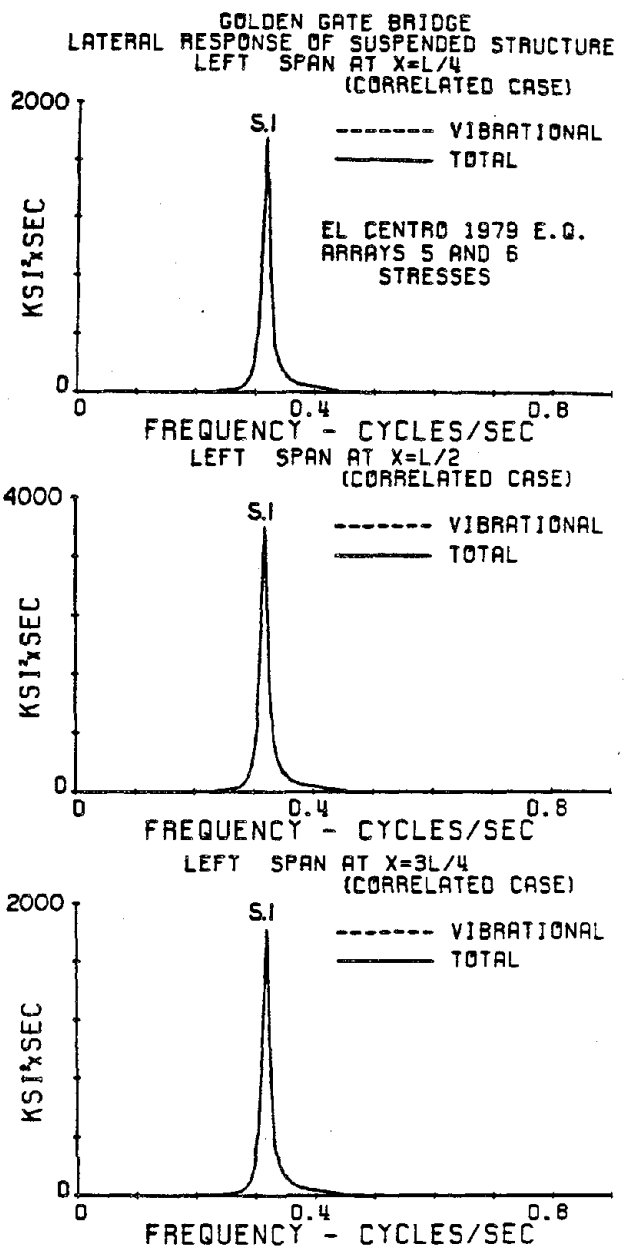

Fig. IV-9b Autospectra of the suspended structure stresses (left side span).

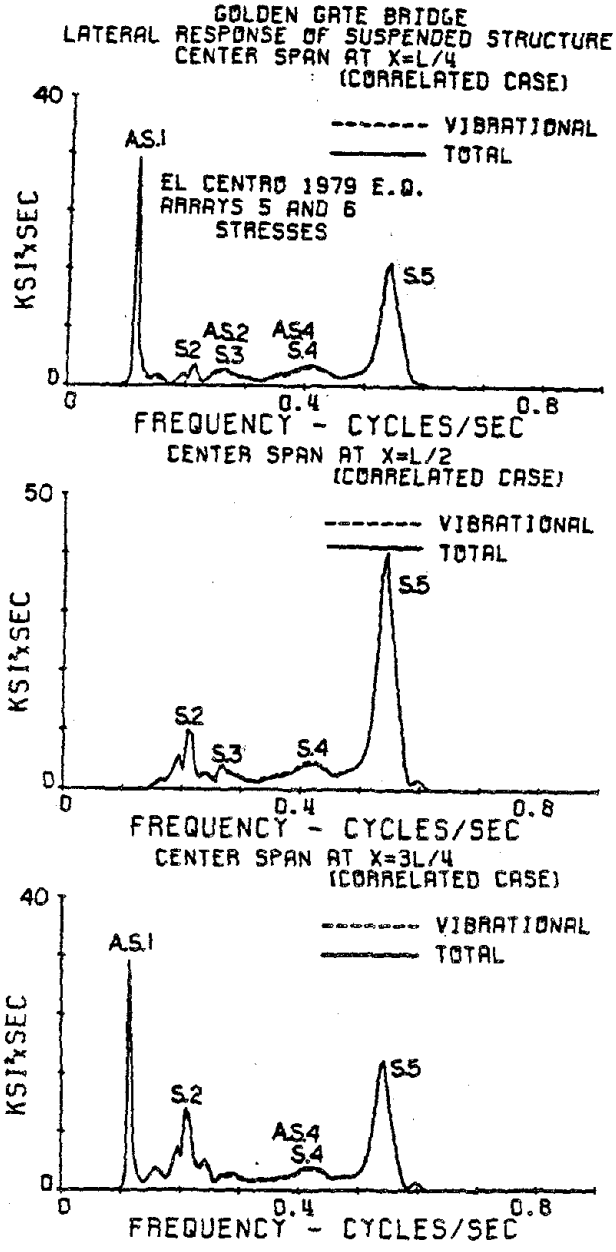

Fig. IV-9c Autospectra of the suspended structure stresses (center span).

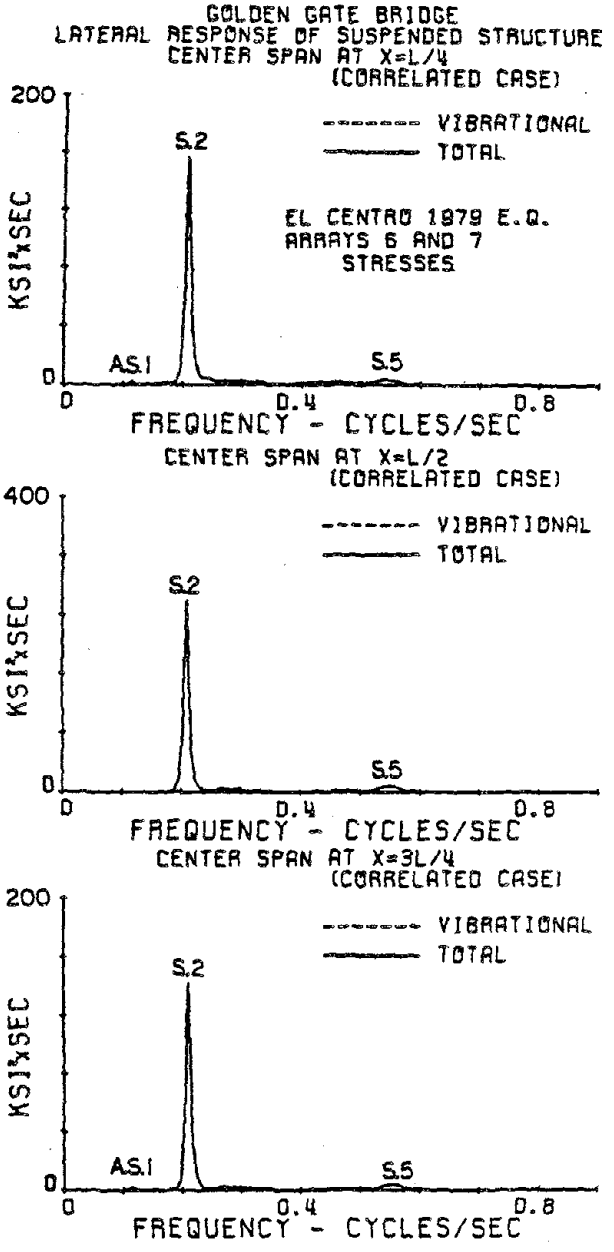

Fig. IV-9d Autospectra of the suspended structure stresses (center span).

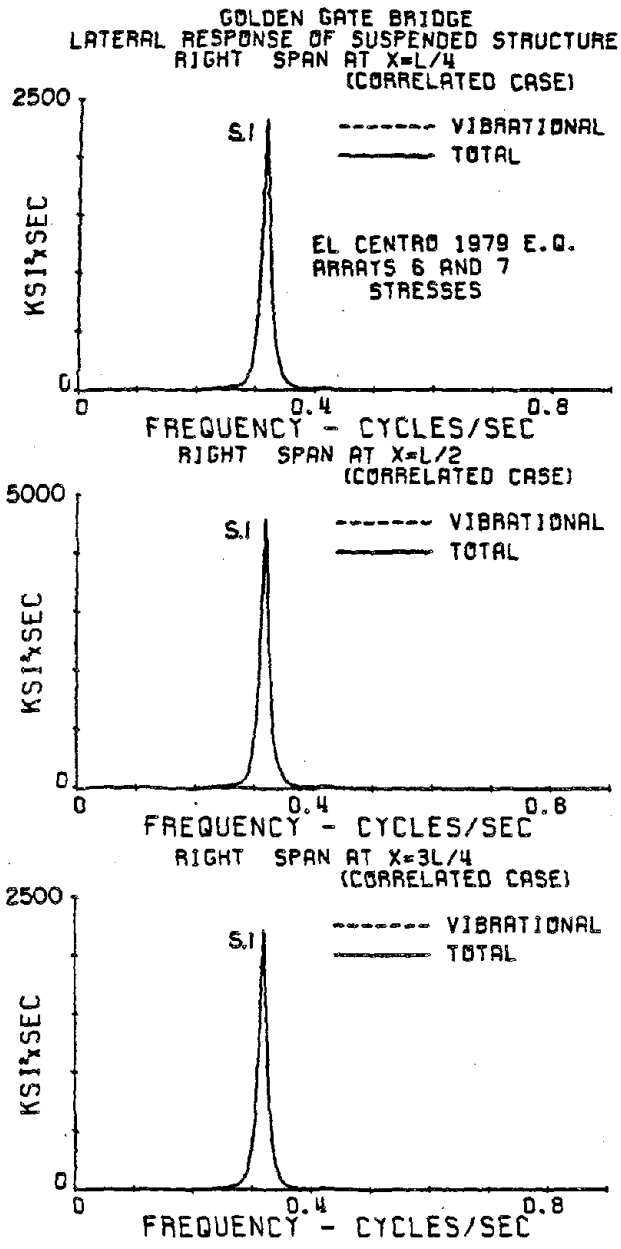

Fig. IV-9e Autospectra of the suspended structure stresses (right side span).

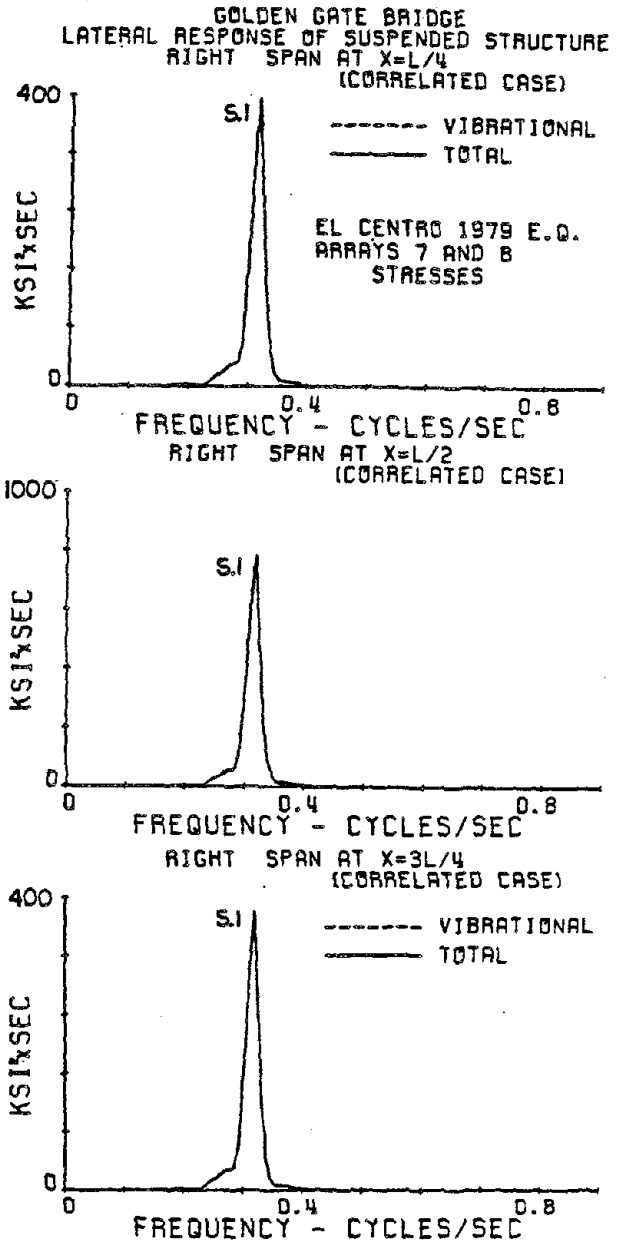

Fig. IV-9f Autospectra of the suspended structure stresses (right side span).

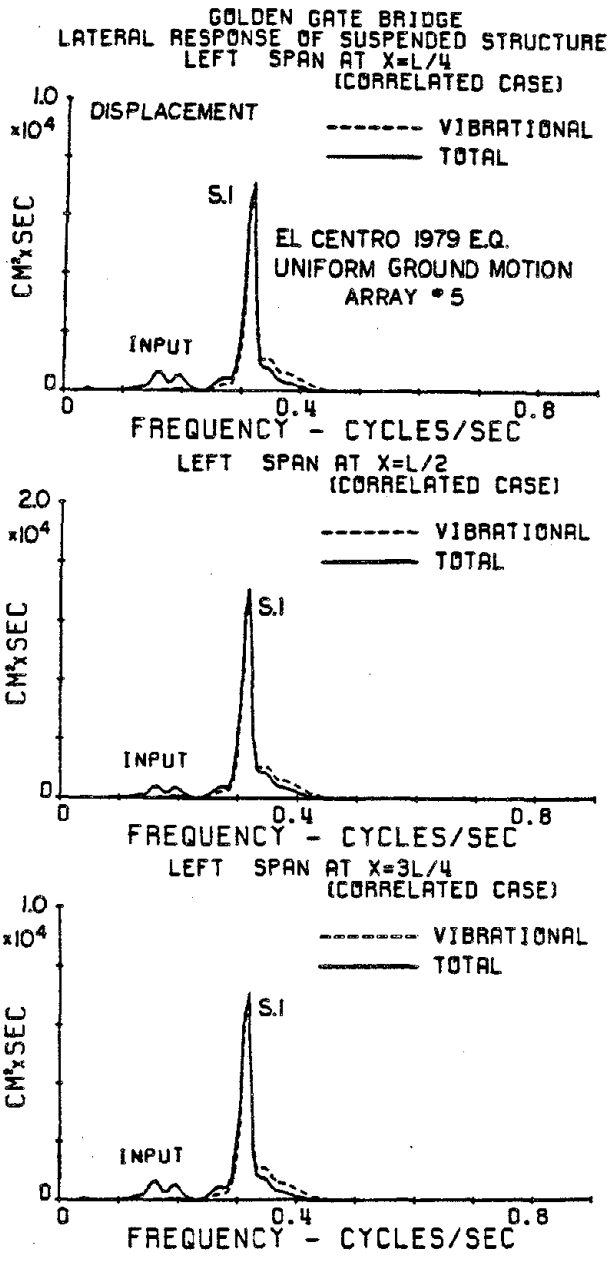

Fig. IV-10a Autospectra of the suspended structure displacement; uniform ground motion (left side span).

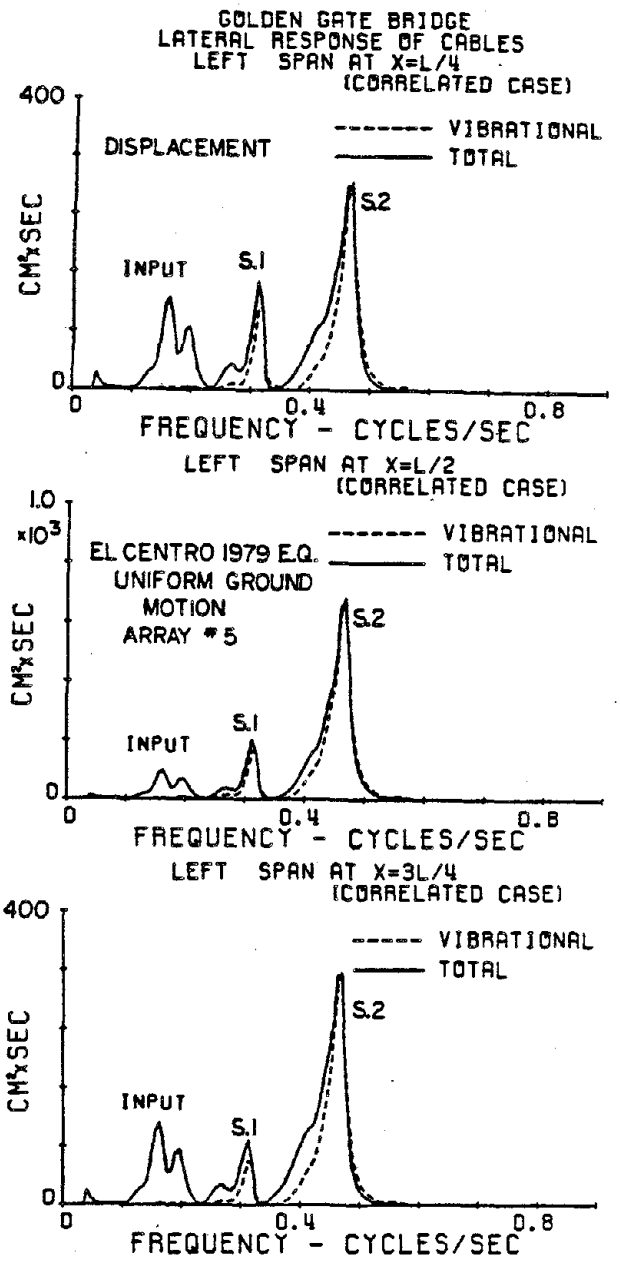

Fig. IV-10b Autospectra of the cables' displacement; uniform ground motion (left side span).

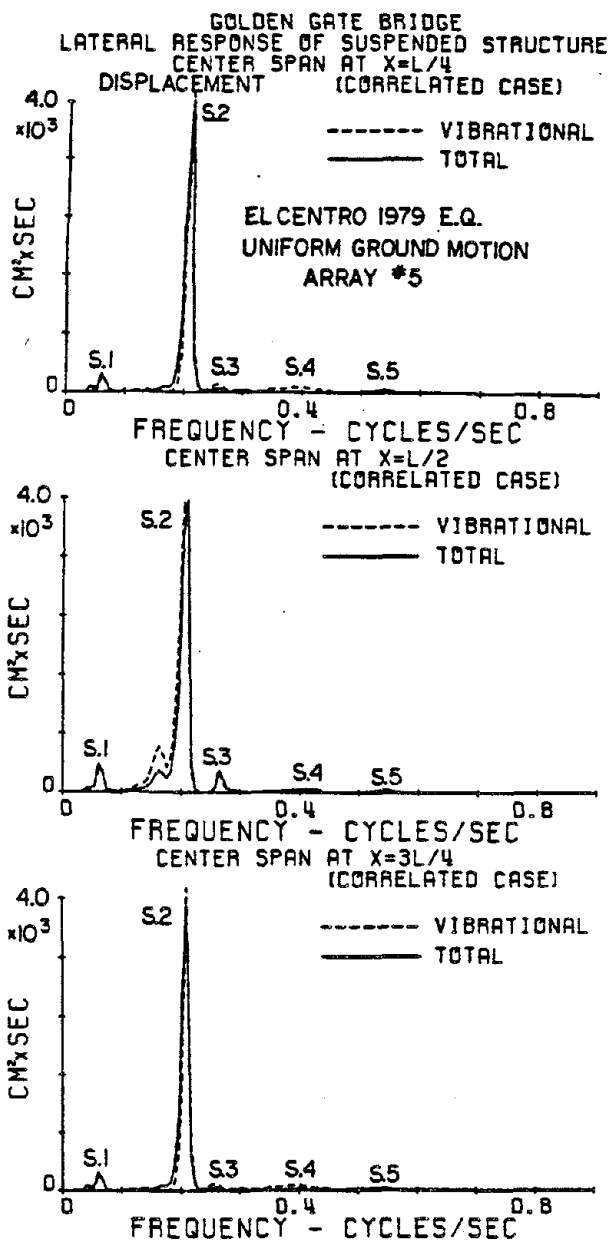

Fig. IV-10c Autospectra of the suspended structure displacement; uniform ground motion (center span).

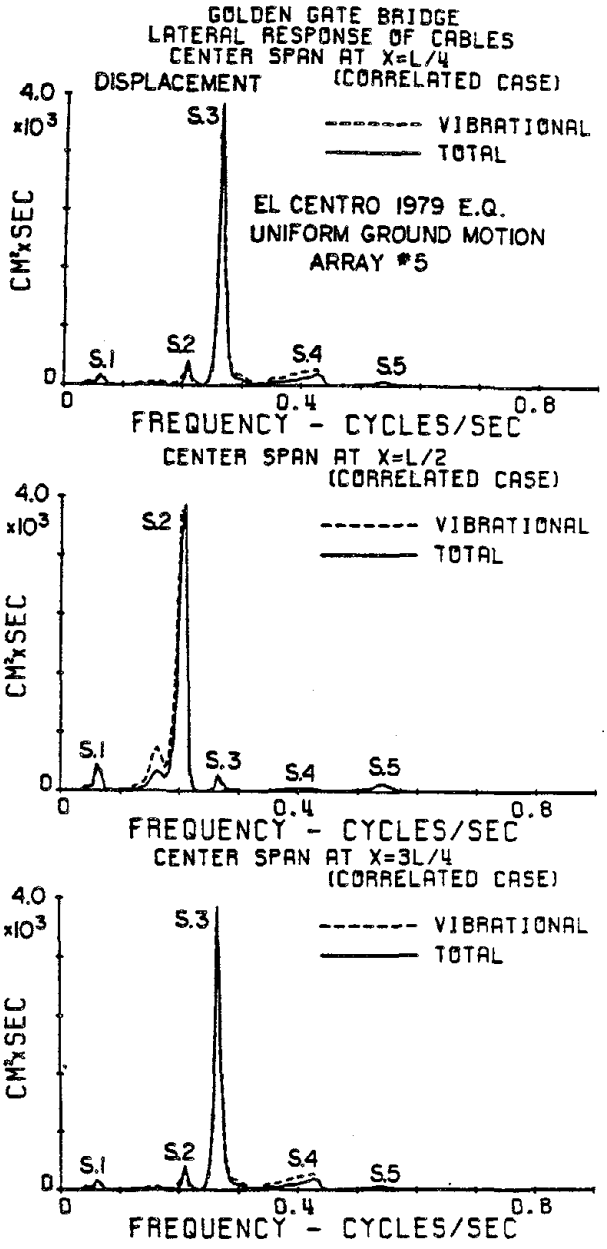

Fig. IV-10d Autospectra of the cables' displacement; uniform ground motion (center span).

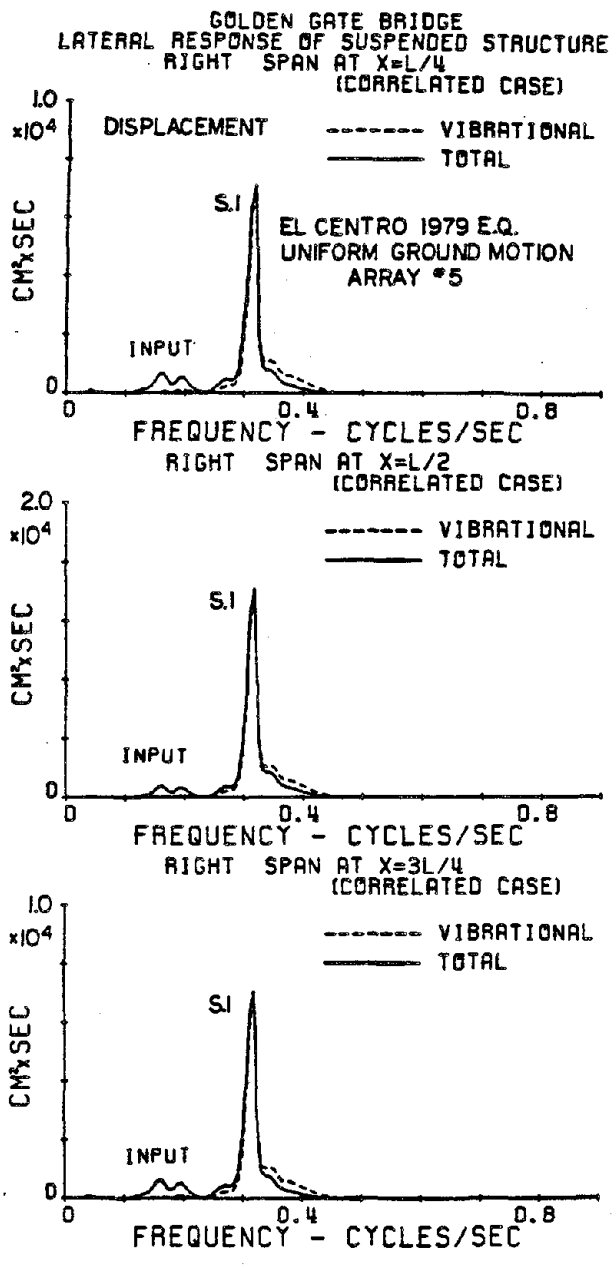

Fig. IV-10e Autospectra of the suspended structure displacement; uniform ground motion (right side span).

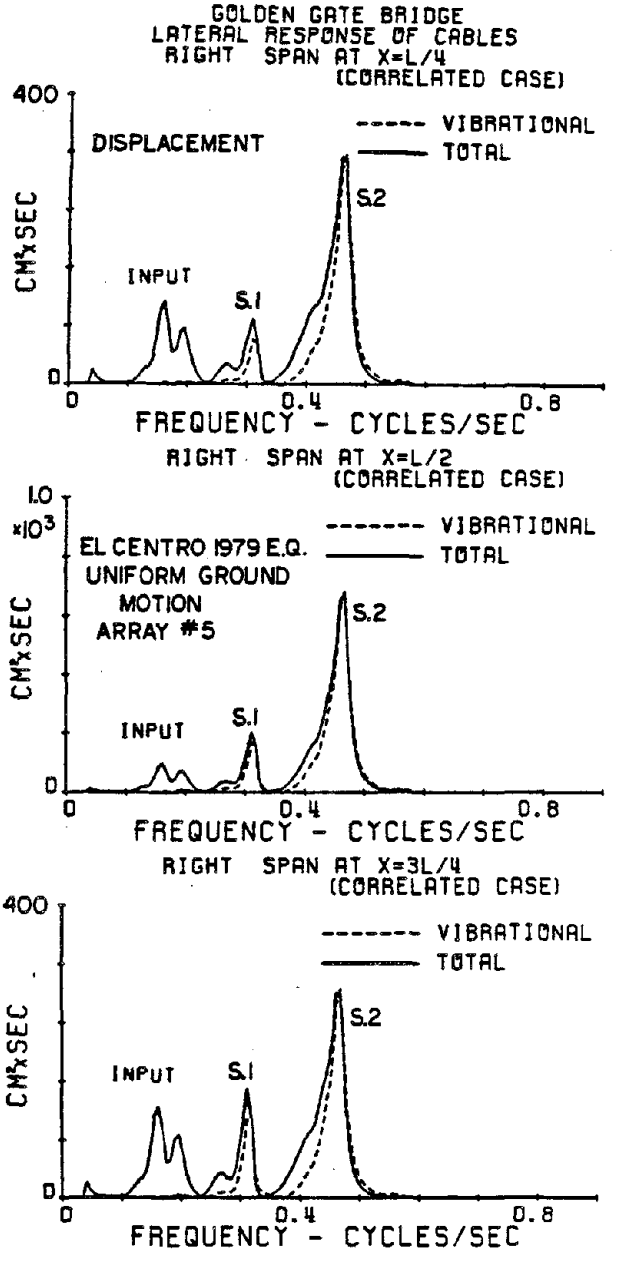

Fig. IV-10f Autospectra of the cables' displacement; uniform ground motion (right side span).

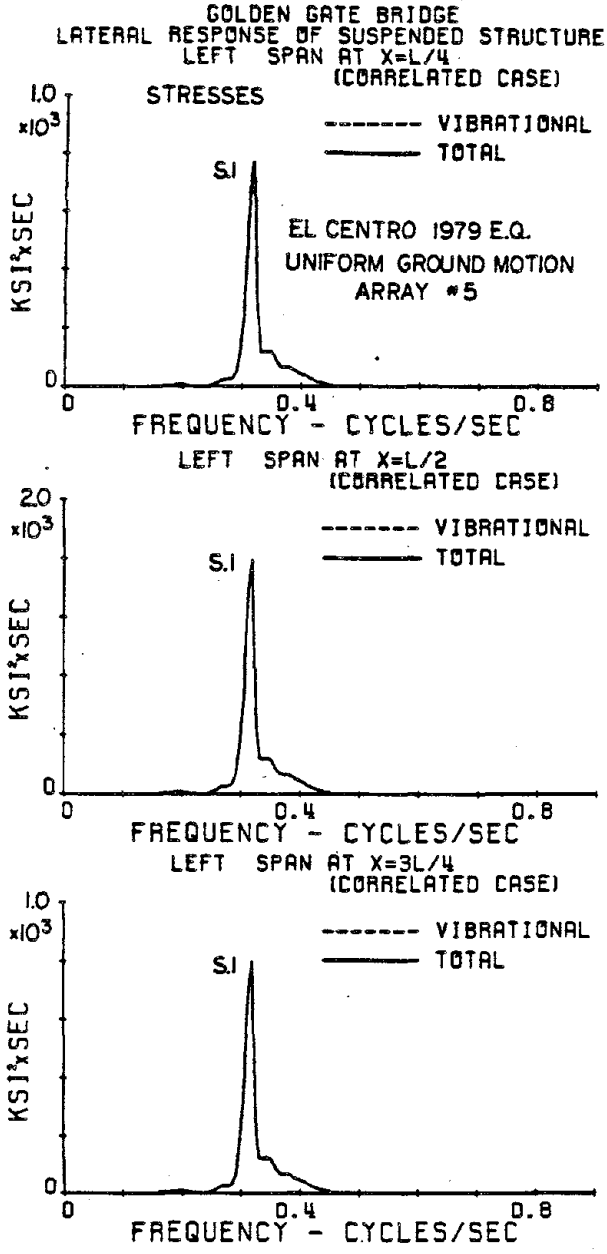

Fig. IV-11a Autospectra of the suspended structure stresses; uniform ground motion (left side span).

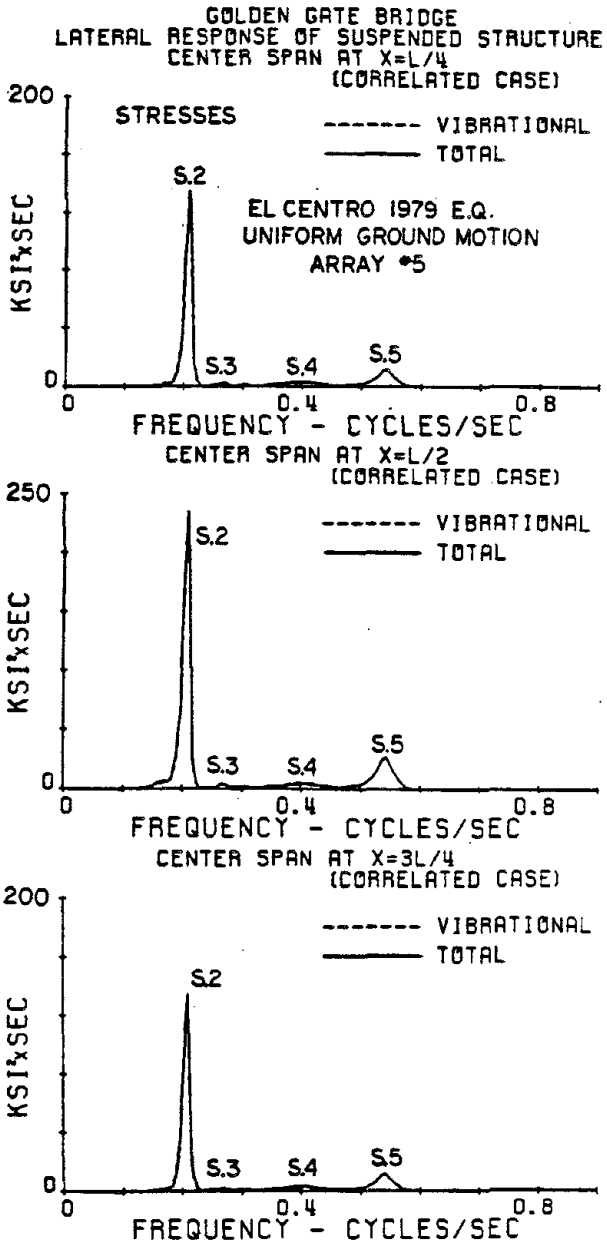

Fig. IV-11b Autospectra of the suspended structure stresses; uniform ground motion (center span).

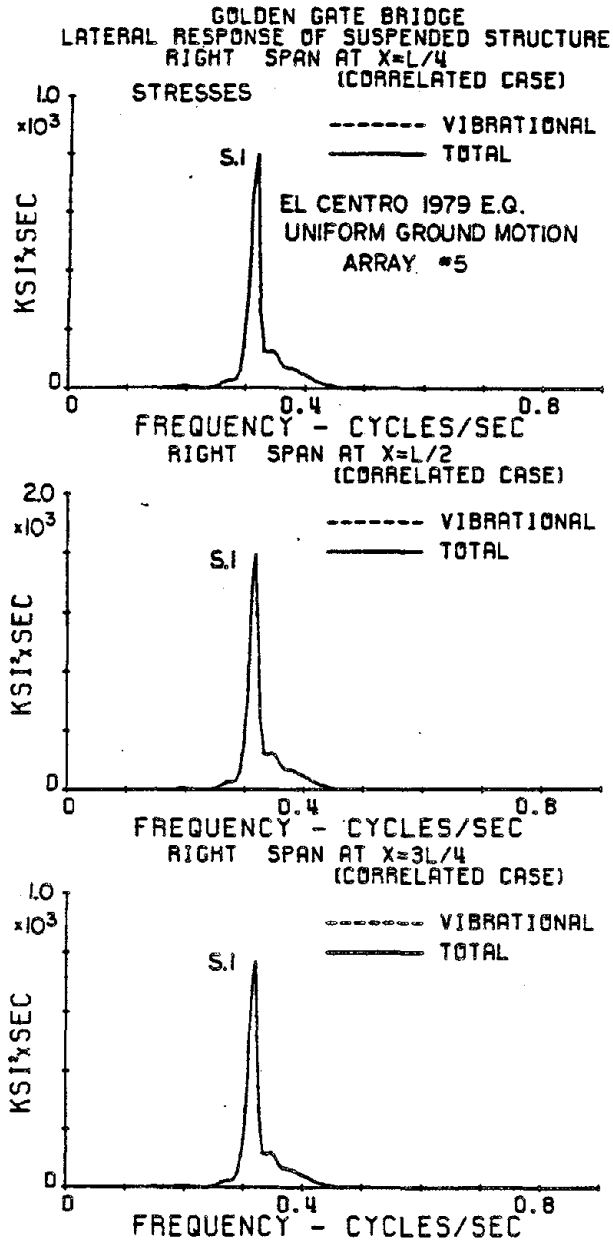

Fig. IV-11c Autospectra of the suspended structure stresses; uniform ground motion (right side span).

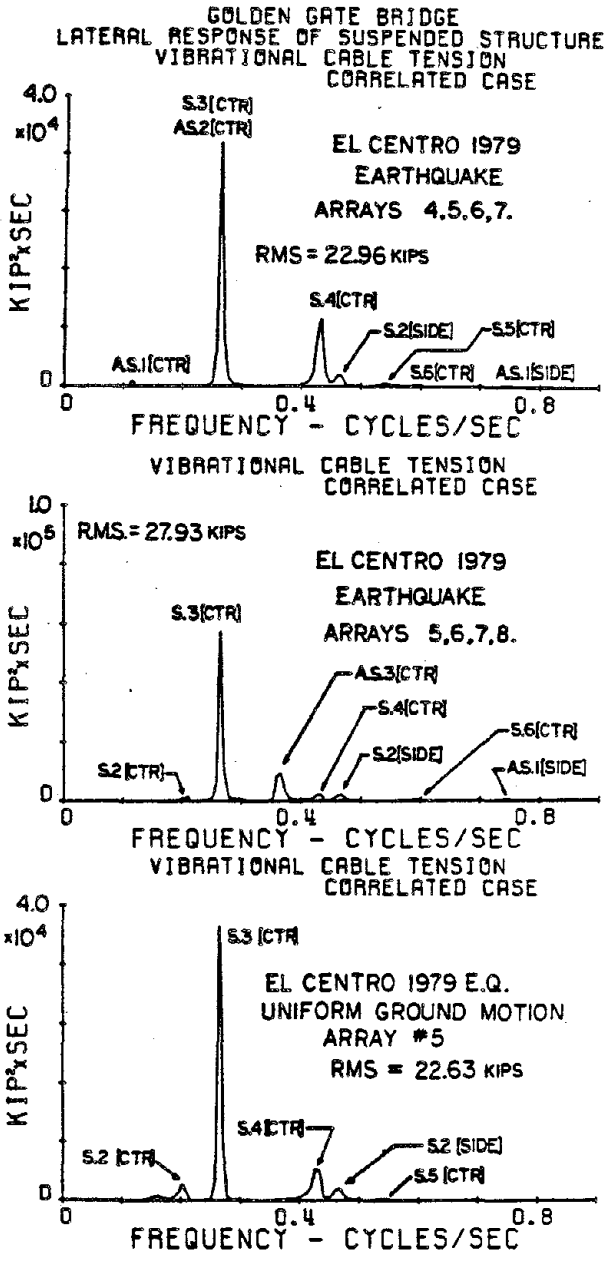

Fig. IV-12 Autospectra of the additional horizontal component of cable tension.

Table IV-4

GOLDEN GATE SUSPENSION BRIDGE

R.M.S. LATERAL DISPLACEMENT (in cm) DUE TO THE 1979 EL CENTRO EARTHQUAKE (Correlated Case)

	Suspended Structure																	
	Left Span						Center Span						Right Span					
Array	1/4 point		1/2 point		3/4 point		1/4 point		1/2 point		3/4 point		1/4 point		1/2 point		3/4 point	
No.	Vib.	Total	Vib.	Total	Vib.	Total	Vib.	Total	Vib.	Total	Vib.	Total	Vib.	Total	Vib.	Total	Vib.	Total
4,5,6,7	4.73	5.51	6.70	7.27	4.75	6.01	7.46	6.32	4.31	4.37	8.31	7.24	21.02	21.62	29.65	29.98	20.92	21.27
5,6,7,8	19.05	18.98	26.99	26.76	19.14	19.11	9.21	8.28	8.03	8.14	8.10	7.49	10.41	11.65	14.68	15.76	10.36	11.64
Uniform Array No. 5	14.46	15.13	20.49	20.88	14.53	15.20	8.35	8.32	10.46	9.72	8.35	8.32	14.53	15.20	20.49	20.88	14.46	15.13
							Cable											
4,5,6,7	2.83	3.16	3.66	4.05	3.23	4.24	9.93	9.32	4.58	4.68	9.63	9.18	5.09	5.98	6.48	6.91	5.05	5.46
5,6,7,8	5.19	5.89	7.55	7.98	5.32	6.10	10.77	10.46	7.94	8.08	9.05	8.73	3.29	4.03	2.67	3.27	3.39	4.03
Uniform Array No. 5	3.86	5.08	5.80	6.57	3.93	5.10	8.91	8.32	10.36	9.65	8.91	8.32	3.93	5.10	5.80	6.57	3.86	5.08

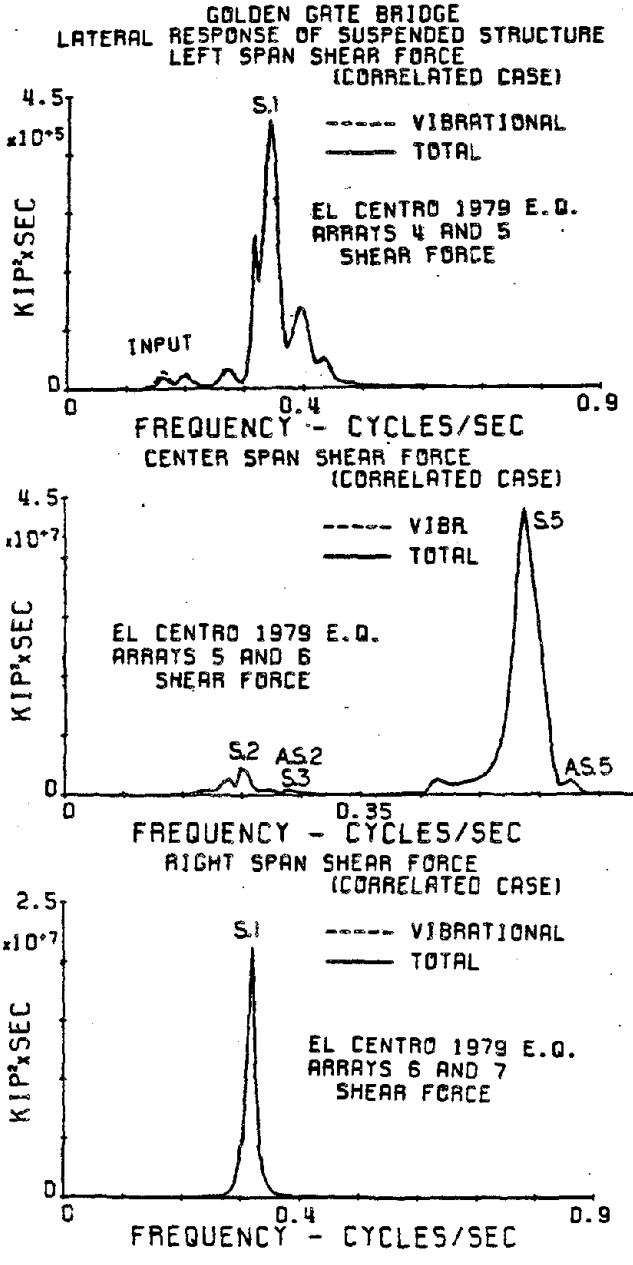

Fig. IV-13a Autospectra of the lateral shear force (Arrays 4, 5, 6, 7).

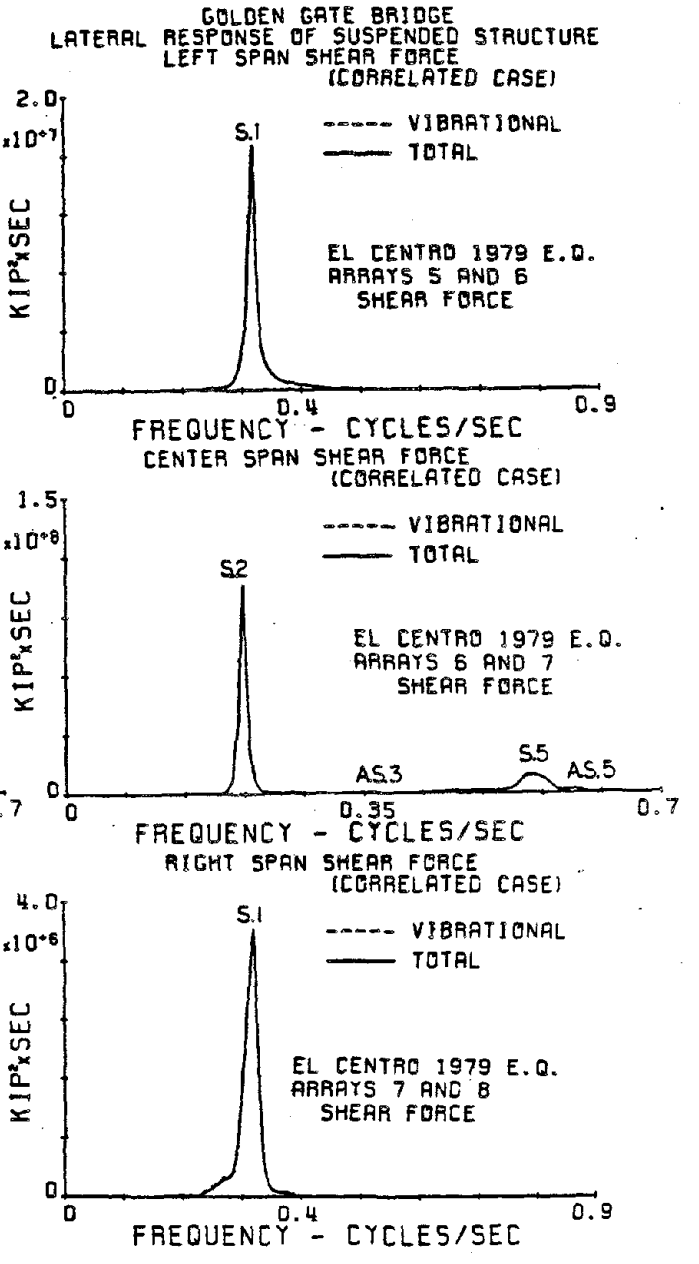

Fig. IV-13b Autospectra of the lateral shear force (Arrays 5, 6, 7, 8).

Table IV-5

GOLDEN GATE SUSPENSION BRIDGE

LATERALLY-INDUCED FLEXURAL SEISMIC STRESSES AND SHEAR FORCES, EL CENTRO 1979 EARTHQUAKE (Correlated Case)

	STRESSES (KSI)																	
	Left Span						Center Span						Right Span					
Array	$\frac{1}{4}$ point		$\frac{1}{2}$ point		$\frac{3}{4}$ point		$\frac{1}{4}$ point		$\frac{1}{2}$ point		$\frac{3}{4}$ point		$\frac{1}{4}$ point		$\frac{1}{2}$ point		$\frac{3}{4}$ point	
No.	Vib.	Total	Vib.	Total	Vib.	Total	Vib.	Total	Vib.	Total	Vib.	Total	Vib.	Total	Vib.	Total	Vib.	Total
4,5,6,7	1.56	1.57	2.24	2.25	1.60	1.60	1.21	1.23	1.61	1.60	1.36	1.39	7.05	7.05	9.93	9.93	6.92	6.92
5,6,7,8	6.30	6.31	9.04	9.05	6.42	6.43	1.59	1.61	2.01	2.00	1.45	1.47	3.49	3.49	4.91	4.91	3.43	3.42
Uniform Array No. 5	4.78	4.79	6.86	6.86	4.88	4.88	1.67	1.67	2.31	2.32	1.67	1.67	4.88	4.88	6.86	6.86	4.78	4.79

	SHEAR FORCE (KIPS)					
Array No.	Left Span at Anchorage		Center Span at Left Tower		Right Span at Anchorage	
	Vib.	Total	Vib.	Total	Vib.	Total
4,5,6,7	152.2	152.2	1405	1405	675.9	675.8
5,6,7,8	615.0	616.5	1361	1361	334.9	333.0

The frequency domain random vibration analysis results in root mean square (R.M.S.) response values. From a practical point of view, the parameter of most interest to the design and analyst engineers is the expected peak value of the response, which is compared with the allowable yield limit. The estimation of appropriate peak factors, based upon the response spectral moments, was described in Section II.10 of this report. Table IV-6 summarizes the estimation of peak factors for two of the center span lateral displacement response cases. The peak factors proposed by Vanmarcke and Der Kiureghian seem to indicate that a peak factor of about 3.5 would be appropriate to convert root mean square values to expected peak responses. However, from the results of a time domain analysis, shown in Fig. IV-14 and summarized in Table IV-6, it is seen that the predicted peak factors deviate considerably from the actual time domain (convolution integral) results, up to a factor of almost 2.0 in some response cases. This could possibly be due to the nonstationarity and/or non-Gaussian character of the inputs. (Vanmarcke's and Der Kiureghian's analyses assume stationary Gaussian inputs), or due to the separation of the displacement into quasi-static and vibrational portions for analysis.

IV.11.2 Uncorrelated Case

The uncorrelated calculations involve assuming the lateral inputs to be independently applied and unrelated. Under such assumptions, all input cross-spectral terms vanish. Two lateral uncorrelated response cases are studied for the Golden Gate Bridge. In the first case, the lateral input motions, $F_1(t)$, $F_2(t)$, $F_3(t)$, $F_4(t)$, at the bridge's support points correspond to the S40°E components of horizontal ground

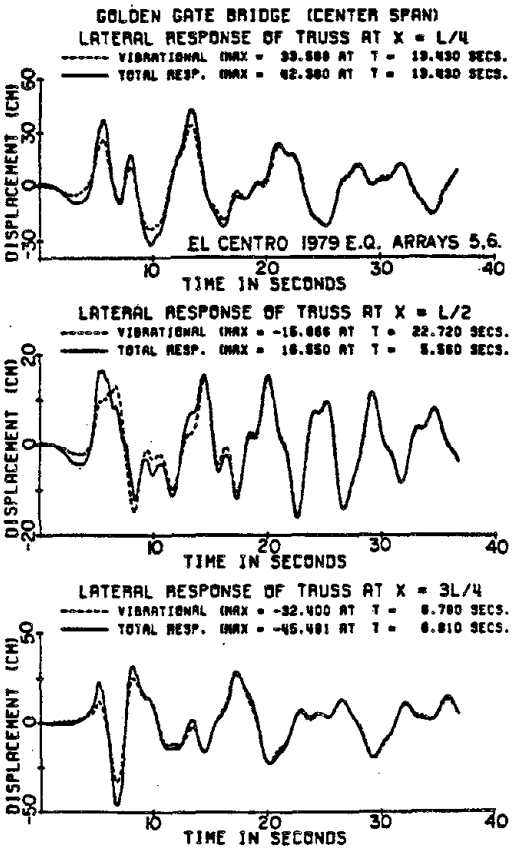

Fig. IV-14a Time domain displacement response of suspended structure (center span).

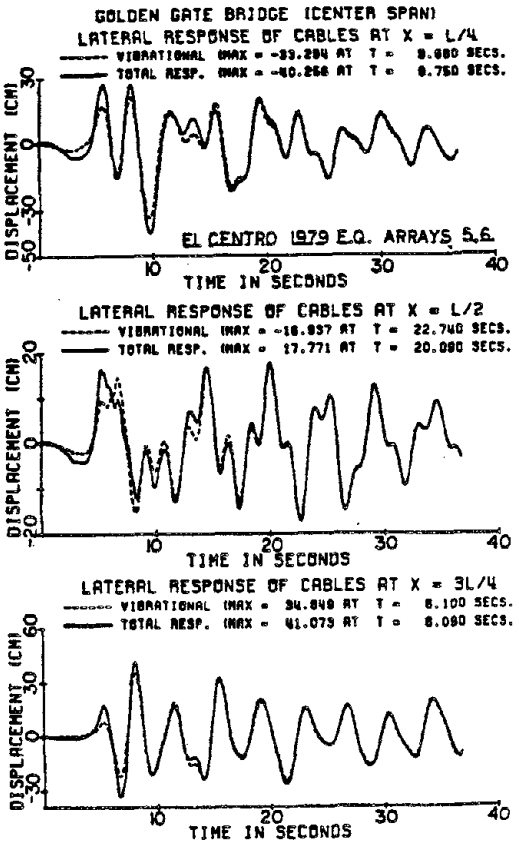

Fig. IV-14b Time domain displacement response of cables (center span).

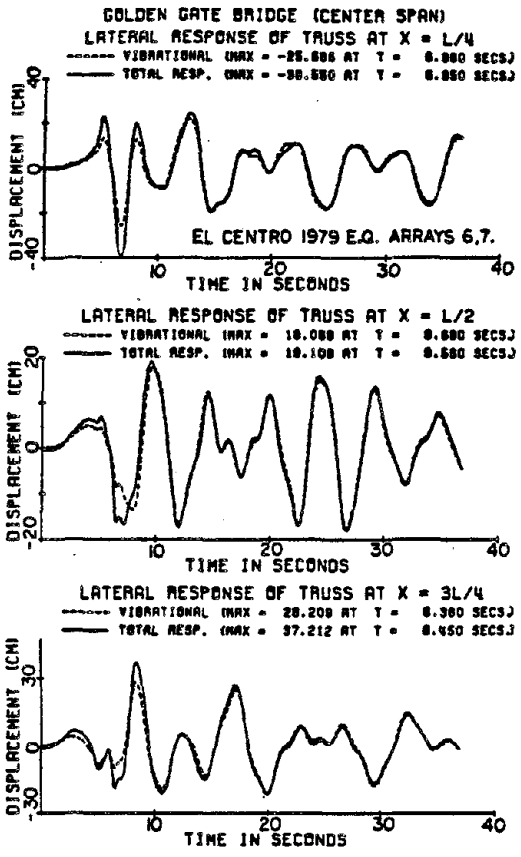

Fig. IV-14c Time domain displacement response of suspended structure (center span).

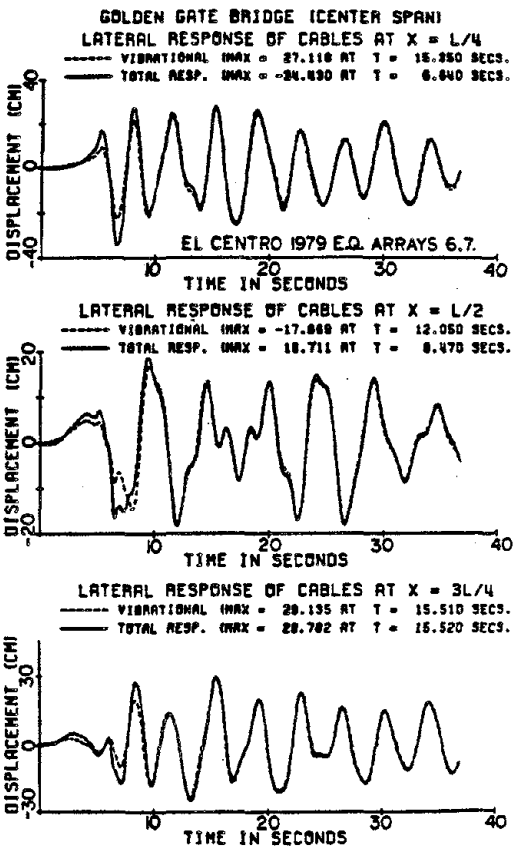

Fig. IV-14d Time domain displacement response of cables (center span).

Table IV-6

EXPECTED PEAK LATERAL RESPONSE GOLDEN GATE BRIDGE (Center Span) -- CORRELATED CASE

Response Case (Correlated Cases)	R.M.S. Response (Frequency Domain Analysis)	Peak Response (Time Domain Analysis)	Peak/R.M.S.	Vanmarcke Peak Factor	Der Kiureghian (*)		
					$\mu/\sqrt{\lambda_o}$	$\sigma/\sqrt{\lambda_o}$	$1/\sqrt{\lambda_o}\ (\mu + 2\sigma)$
Arrays 5, 6							
cable at L/4	9.32	40.3	4.32	3.37	2.51	0.50	3.51
cable at L/2	4.68	17.8	3.80	3.47	2.65	0.48	3.61
cable at 3L/4	9.18	41.1	4.48	3.35	2.48	0.50	3.48
truss at L/4	6.32	42.4	6.71	3.34	2.51	0.50	3.51
truss at L/2	4.37	16.6	3.80	3.42	2.58	0.49	3.56
truss at 3L/4	7.24	45.5	6.28	3.33	2.48	0.50	3.48
Arrays 6, 7							
cable at L/4	10.5	34.4	3.28	3.31	2.42	0.52	3.46
cable at L/2	8.08	18.7	2.31	3.29	2.39	0.52	3.43
cable at 3L/4	8.73	29.8	3.41	3.30	2.40	0.52	3.44
truss at L/4	8.28	39.6	4.78	3.23	2.30	0.54	3.38
truss at L/2	8.14	19.1	2.35	3.23	2.32	0.53	3.38
truss at 3L/4	7.49	37.2	4.97	3.23	2.30	0.54	3.38

(*) It appears that the mean plus two standard deviations will be a good peak factor.

motion recorded at Arrays No. 4, 5, 6, and 7 of the El Centro Arrays, respectively; while the second case involves similar correspondences with Arrays No. 5, 6, 7, and 8.

The autospectra of lateral displacement of the cables and suspended structure at the quarter points in each span are shown in Figs. IV-15 for input arrays 4, 5, 6, and 7. The response is separated into vibrational (relative or modal) response shown in dotted lines, and the total response, which includes quasi-static contributions, shown in solid lines. Similar autospectra of lateral displacement are shown in Fig. IV-16 for input arrays 5, 6, 7, and 8, while the autospectra of response stresses for both sets of arrays are shown in Fig. IV-17. The responses obtained for each set of input arrays are seen to be different in magnitude due to the different frequency content of each input. Figure IV-18 shows the autospectra of the lateral shear force occurring at the left side of each span for both sets of input arrays. Table IV-7 summarizes the root mean square displacements for both input cases for the uncorrelated case, while Table IV-8 is a similar table corresponding to R.M.S. laterally induced flexural stresses and shear forces. Based upon a peak factor of 3.5 (Chapter II), the maximum expected stress, for the uncorrelated case, is seen to occur at the midpoint of the right side span, and is approximately $3.5 \times 7.18 \simeq 25$ ksi, which is a significant live load condition in a suspension bridge when compared to the yield stress of 50.5 ksi. The maximum expected shear force, for the uncorrelated case, is seen to occur at the ends of the center span with approximate magnitude of $3.5 \times 1254 \simeq 4390$ kips, which appears to be significant.

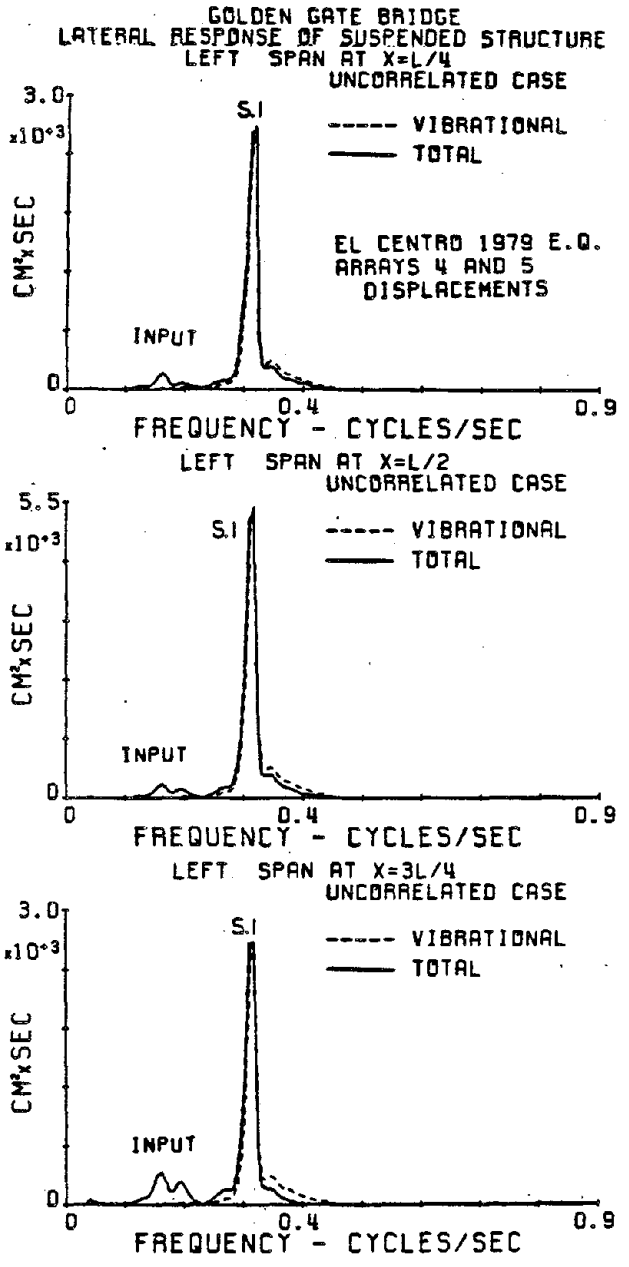

Fig. IV-15a Autospectra of the suspended structure displacement (left side span).

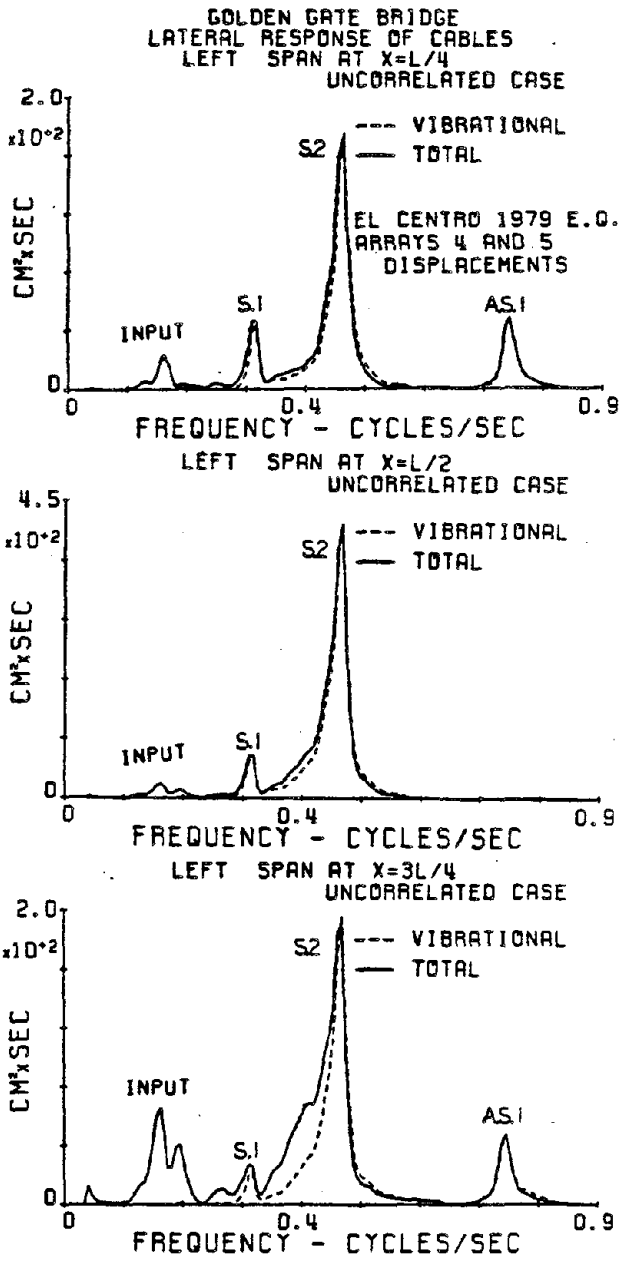

Fig. IV-15b Autospectra of the cables' displacement (left side span).

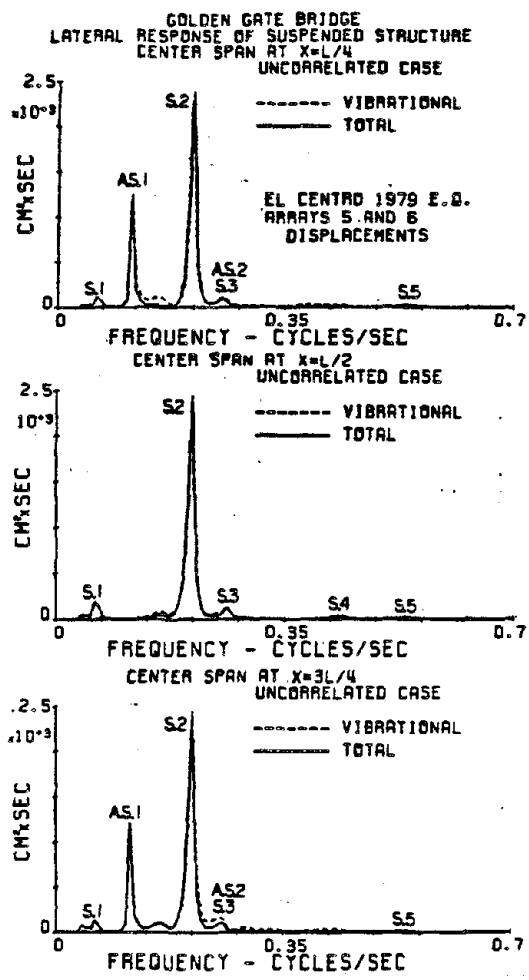

Fig. IV-15c Autospectra of the suspended structure displacement (center span).

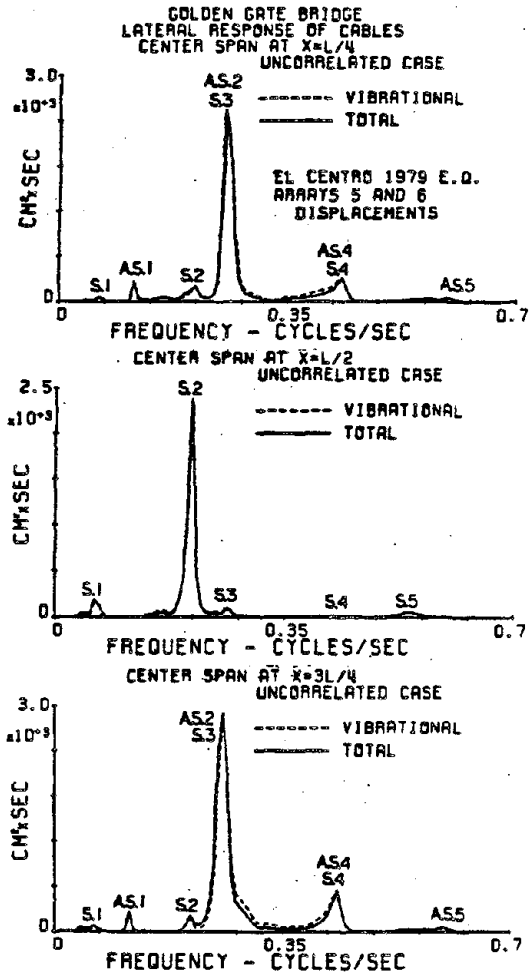

Fig. IV-15d Autospectra of the cables' displacement (center span).

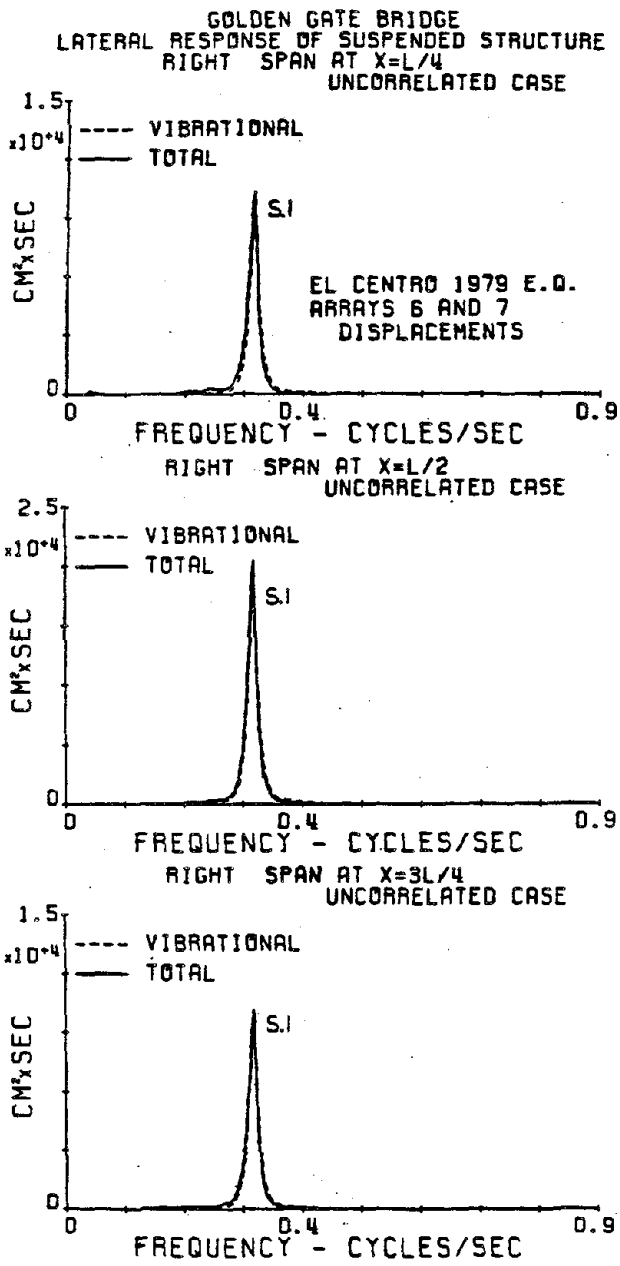

Fig. IV-15e Autospectra of the suspended structure displacement (right side span).

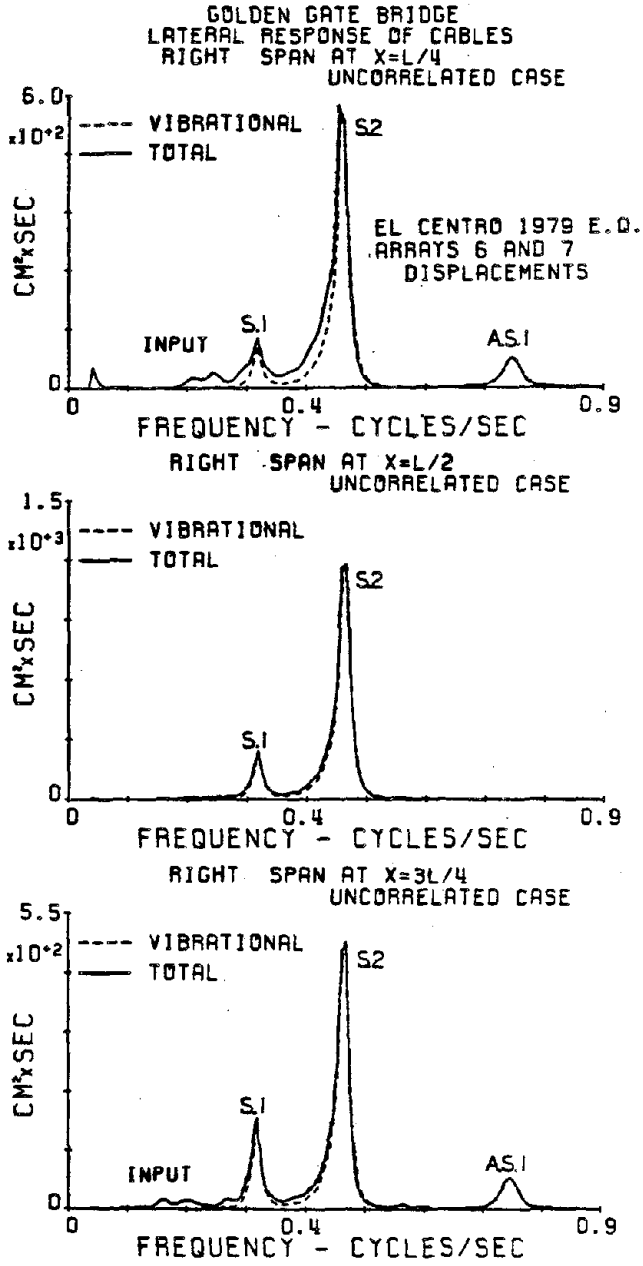

Fig. IV-15f Autospectra of the cables' displacement (right side span).

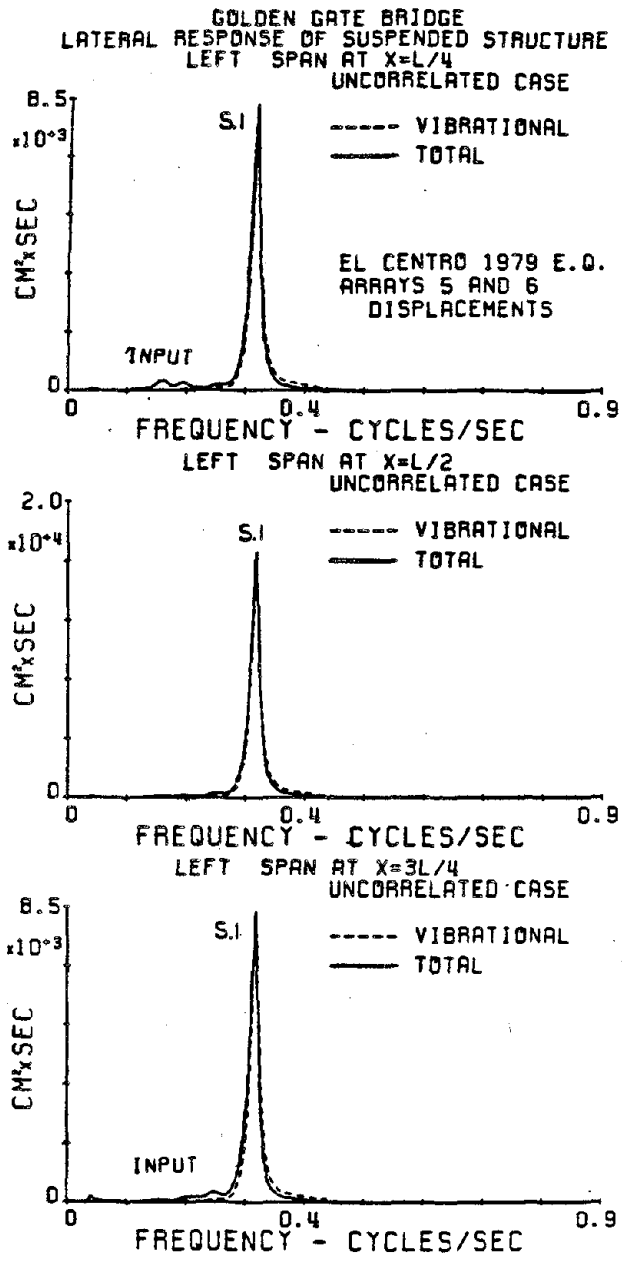

Fig. IV-16a Autospectra of the suspended structure displacement (left side span).

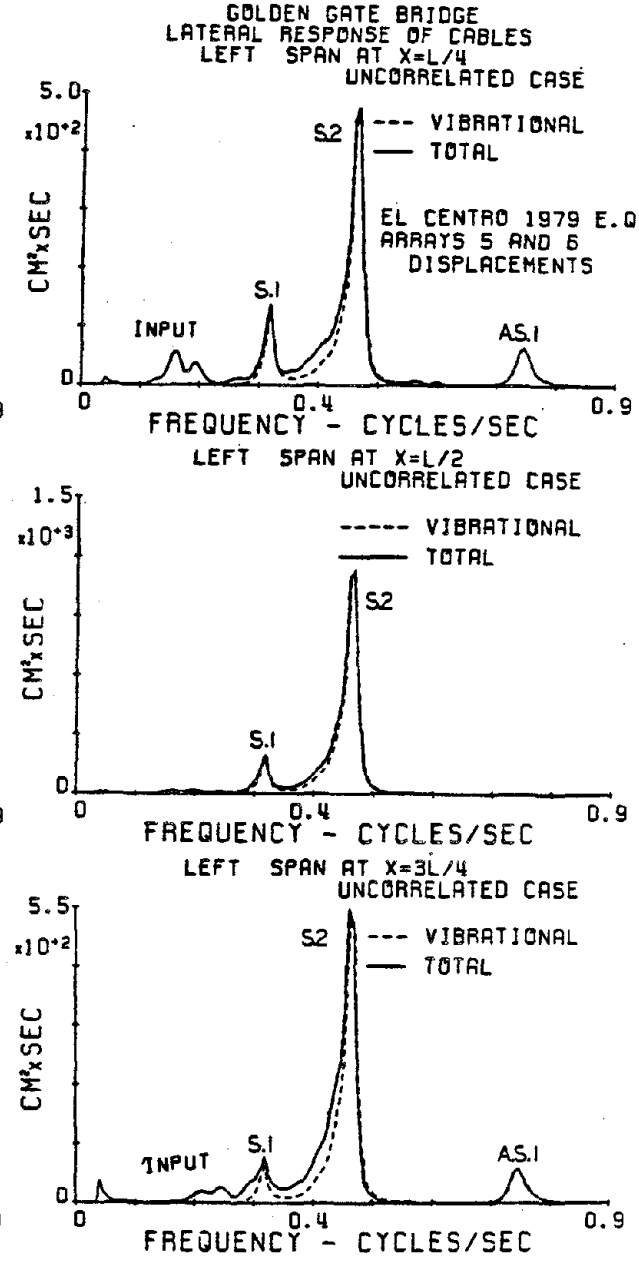

Fig. IV-16b Autospectra of the cables' displacement (left side span).

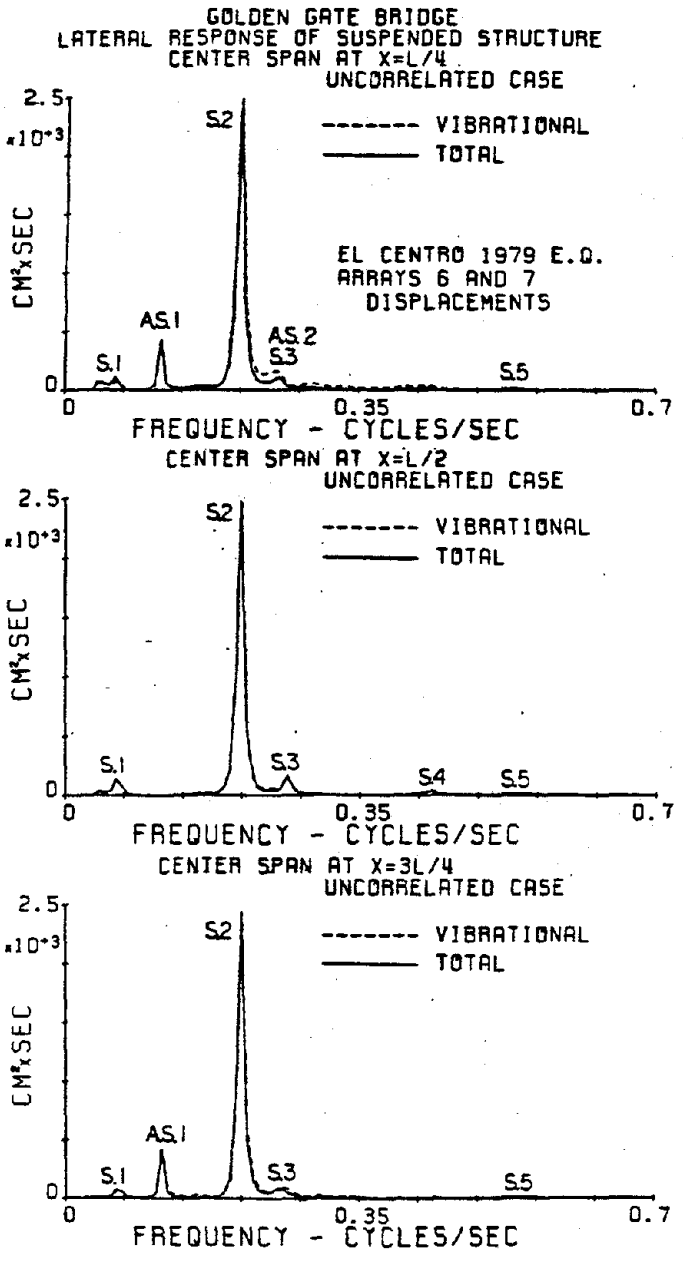

Fig. IV-16c Autospectra of the suspended structure displacement (center span).

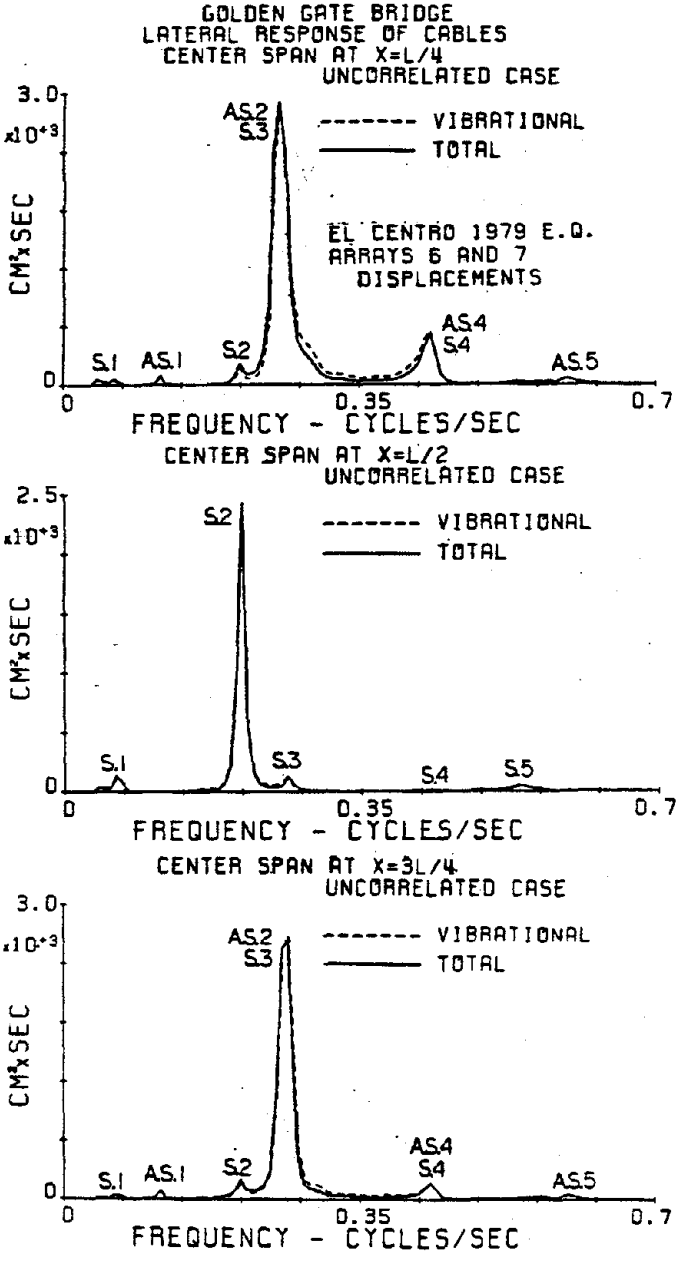

Fig. IV-16d Autospectra of the cables' displacement (center span).

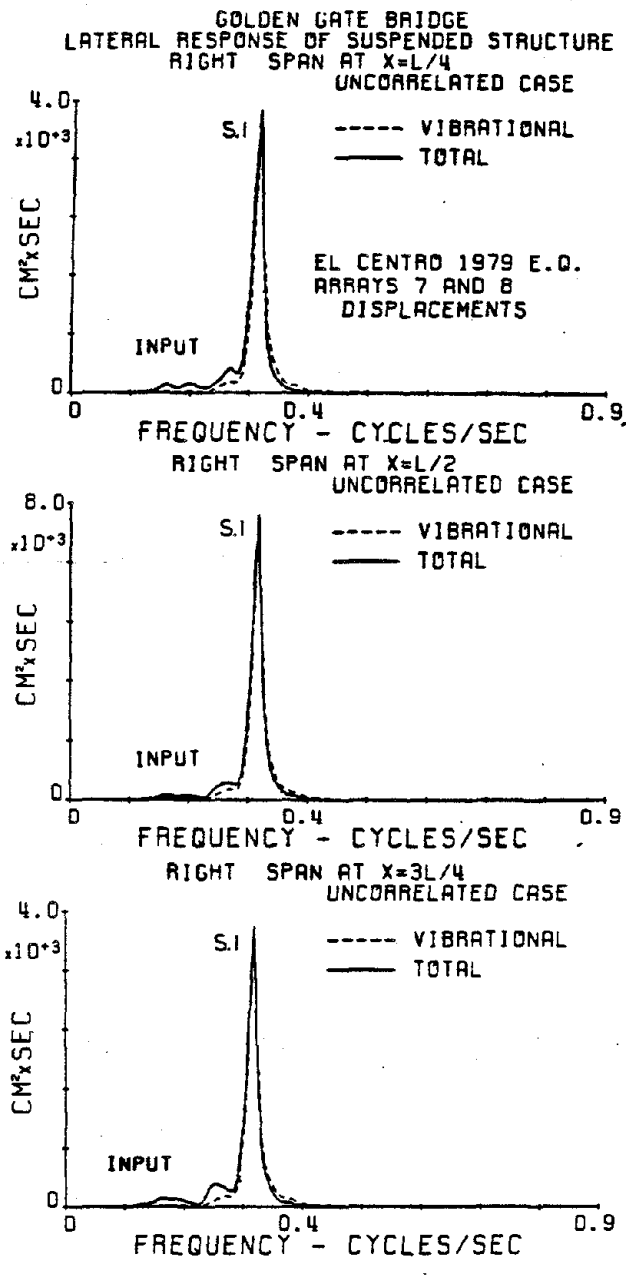

Fig. IV-16e Autospectra of the suspended structure displacement (right side span).

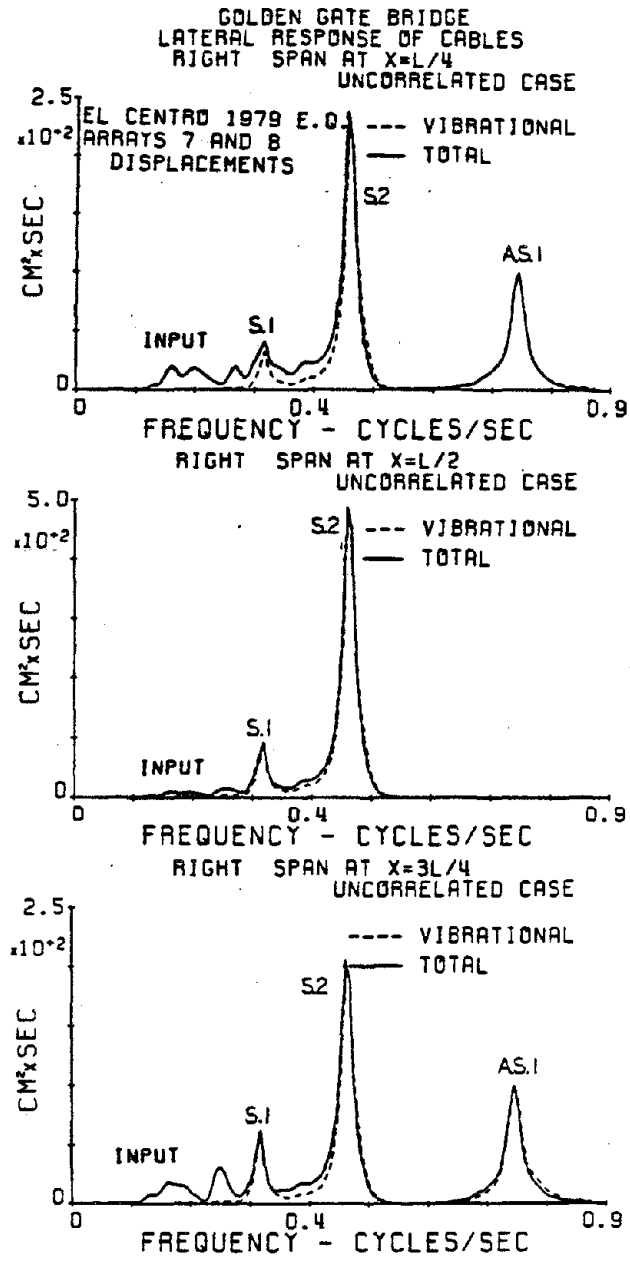

Fig. IV-16f Autospectra of the cables' displacement (right side span).

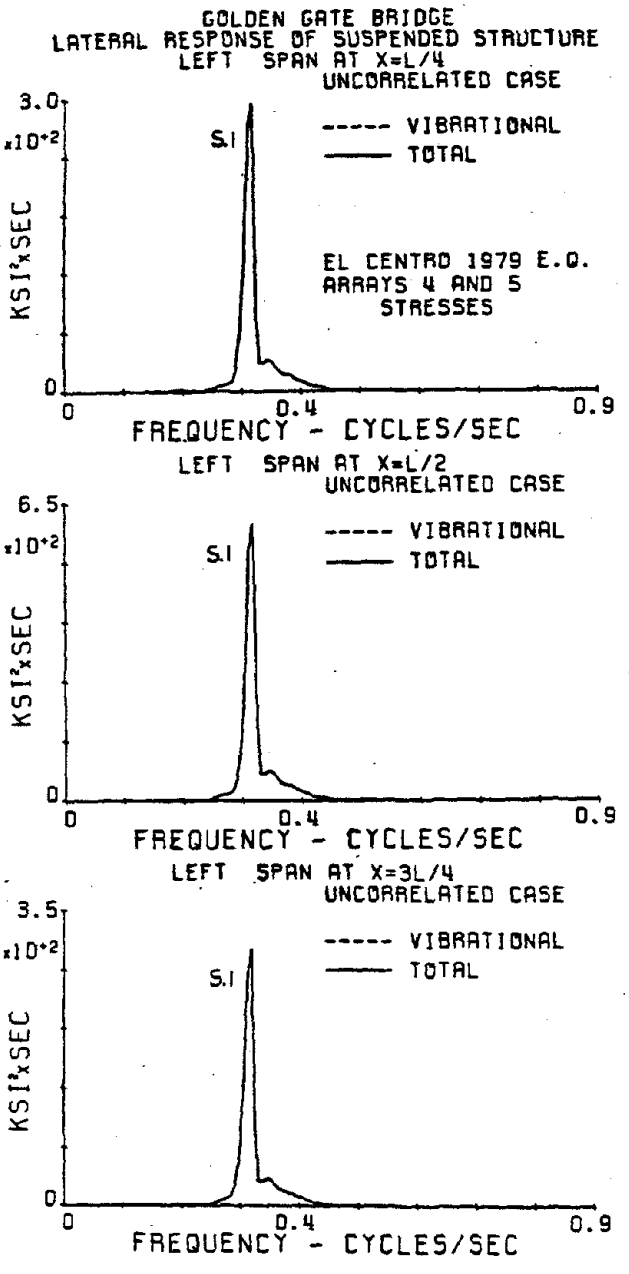

Fig. IV-17a Autospectra of the suspended structure stresses (left side span).

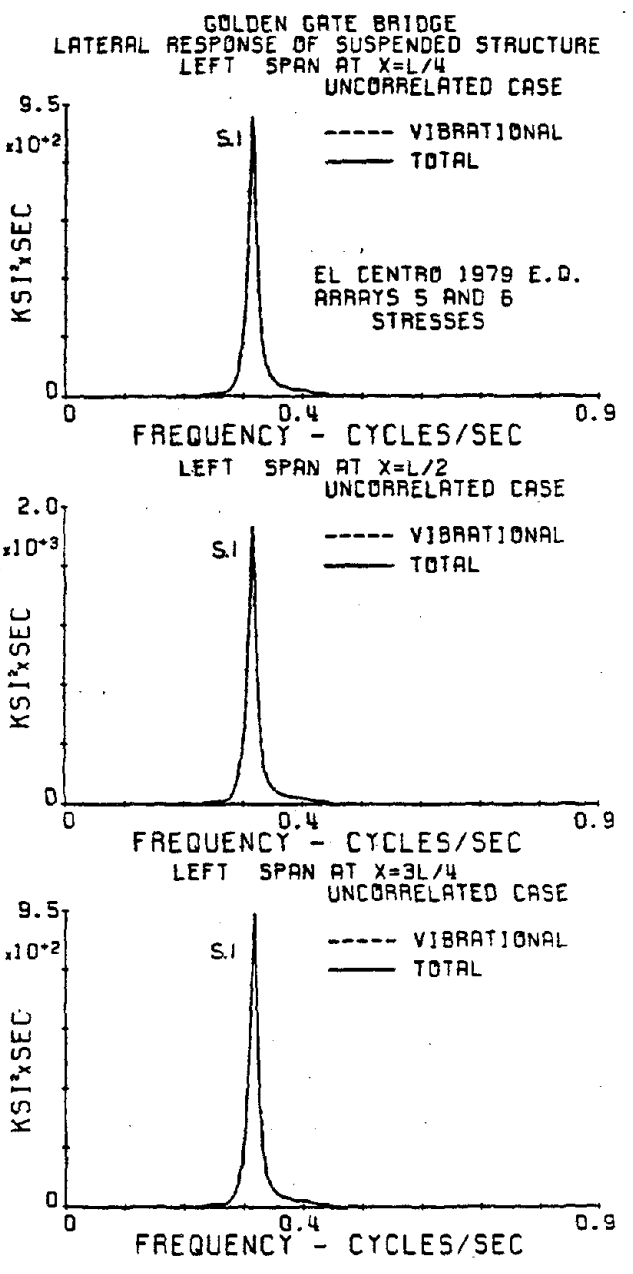

Fig. IV-17b Autospectra of the suspended structure stresses (left side span).

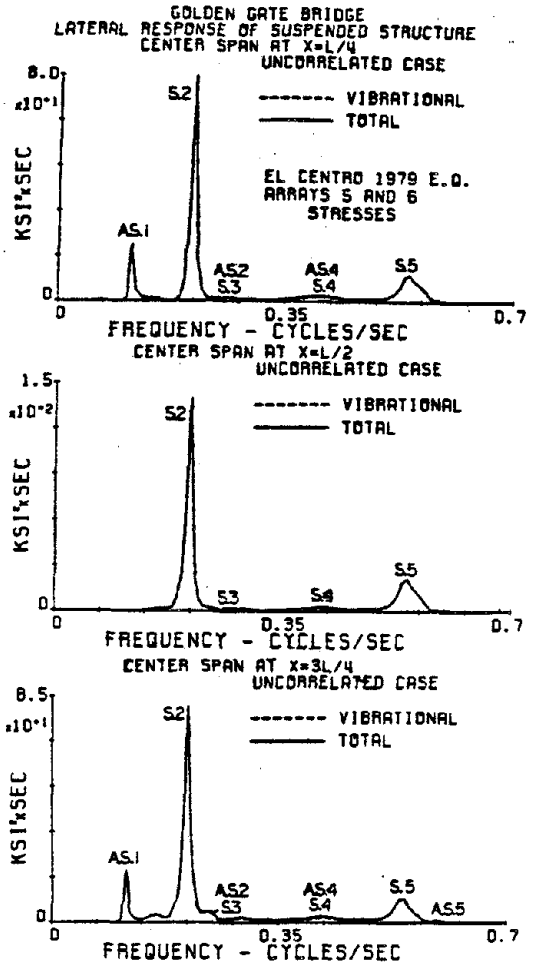

Fig. IV-17c Autospectra of the suspended structure stresses (center span).

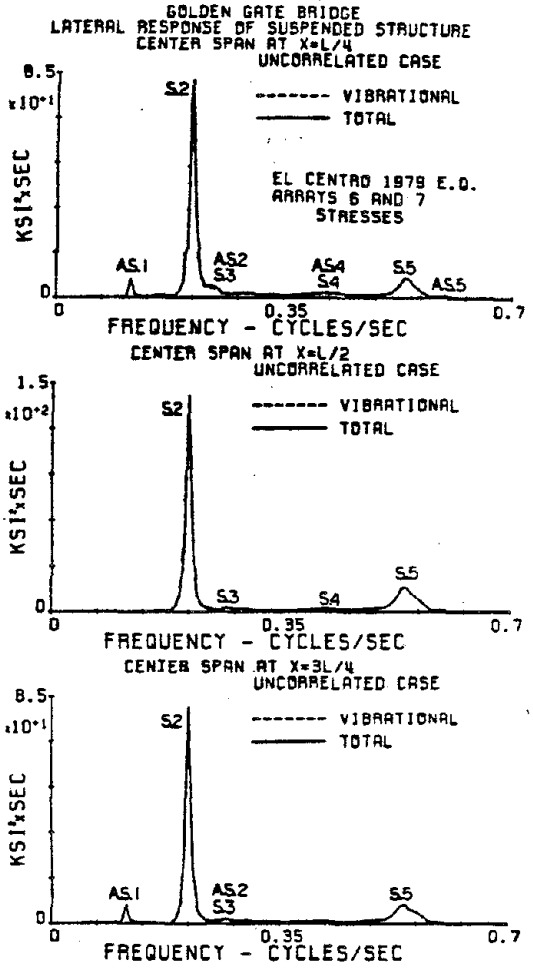

Fig. IV-17d Autospectra of the suspended structure stresses (center span).

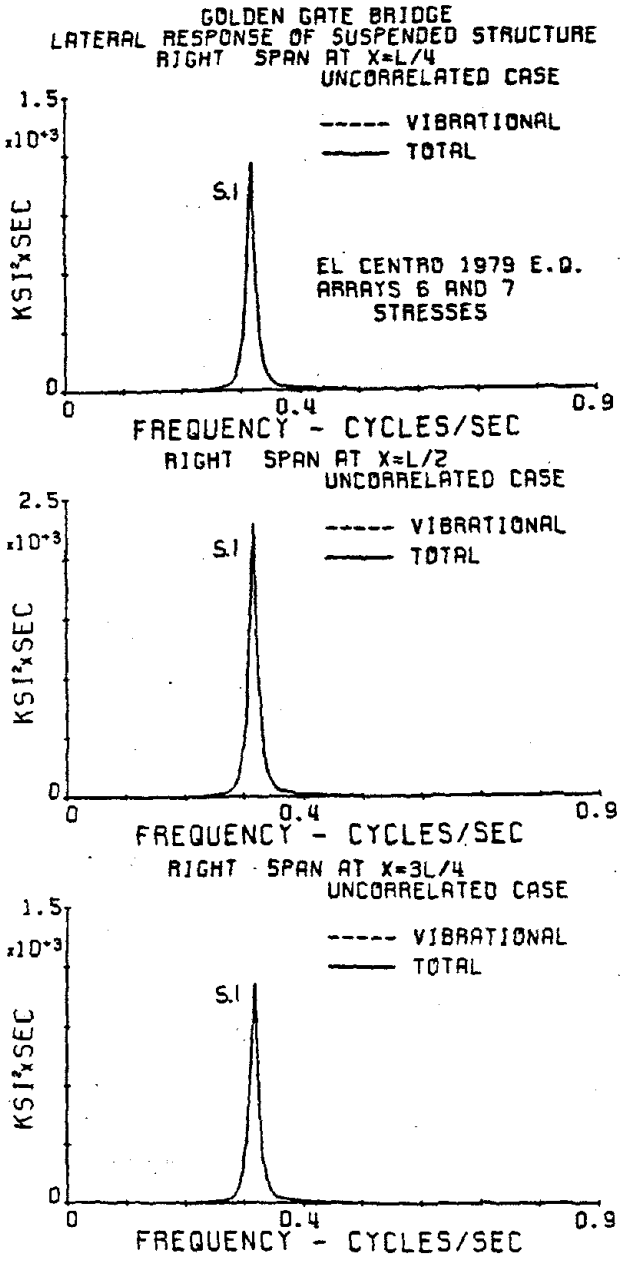

Fig. IV-17e Autospectra of the suspended structure stresses (right side span).

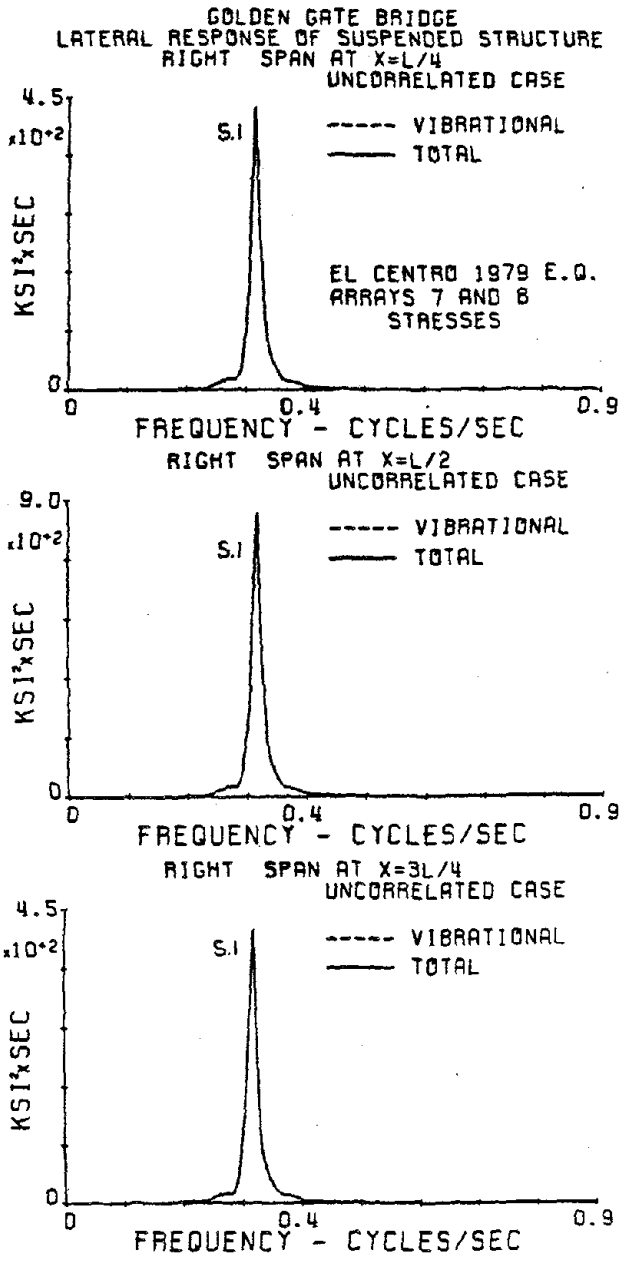

Fig. IV-17f Autospectra of the suspended structure stresses (right side span).

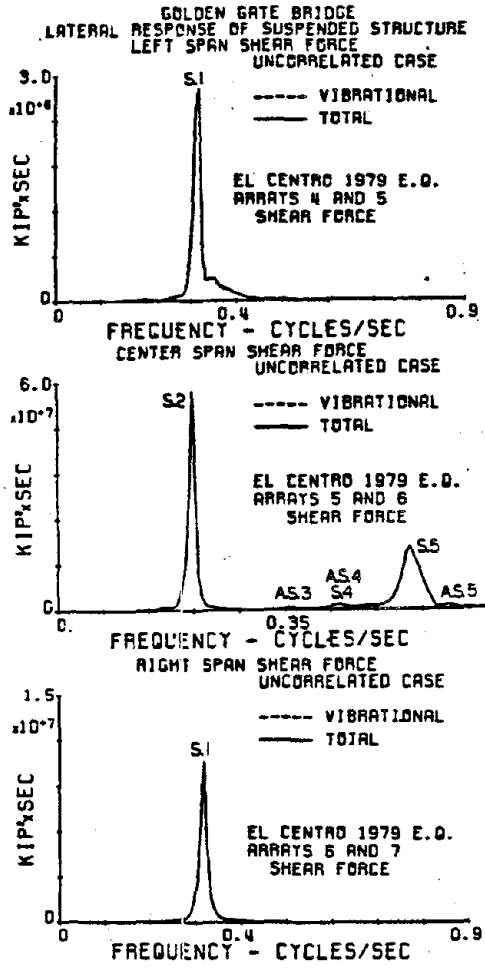

Fig. IV-18a Autospectra of the lateral shear force (Arrays 4, 5, 6, 7).

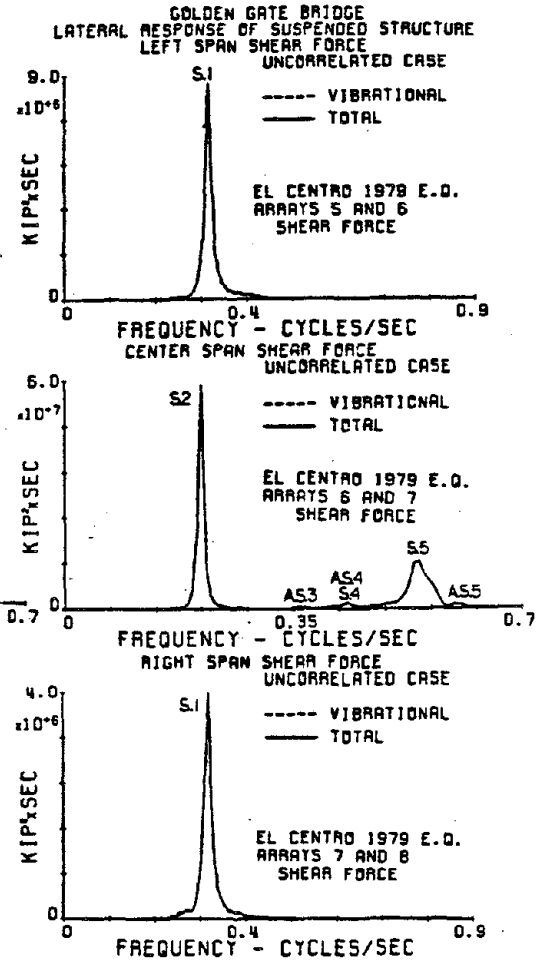

Fig. IV-18b Autospectra of the lateral shear force (Arrays 5, 6, 7, 8).

Table IV-7

GOLDEN GATE SUSPENSION BRIDGE

R.M.S. LATERAL DISPLACEMENT (in cm) USED TO THE 1979 EL CENTRO EARTHQUAKE (Uncorrelated Case)

	SUSPENDED STRUCTURE																	
	Left Span						Center Span						Right Span					
Array Number	1/4 Point		1/2 Point		3/4 Point		1/4 Point		1/2 Point		3/4 Point		1/4 Point		1/2 Point		3/4 Point	
	Vib.	Tot.	Vib.	Tot.	Vib.	Tot.	Vib.	Tot.	Vib.	Tot.	Vib.	Tot.	Vib.	Tot.	Vib.	Tot.	Vib.	Tot.
4,5,6,7	8.52	8.89	12.08	12.38	8.56	9.34	7.38	6.97	6.74	6.62	7.96	7.50	15.21	15.56	21.45	2.159	15.14	15.42
5,6,7,8	14.01	14.44	19.86	20.00	14.08	14.44	7.07	6.55	6.32	6.26	6.56	6.23	9.99	10.51	14.09	14.43	9.95	10.51
	CABLE																	
4,5,6,7	3.14	3.36	4.41	4.66	3.40	4.26	8.98	8.71	6.72	6.60	10.32	10.11	4.83	5.54	6.66	6.91	4.74	5.08
5,6,7,8	4.74	5.32	6.64	6.96	4.80	5.53	10.36	10.15	6.29	6.23	9.00	8.75	3.66	4.13	4.40	4.61	3.63	4.02

Table IV-8

GOLDEN GATE SUSPENSION BRIDGE

LATERALLY-INDUCED FLEXURAL SEISMIC STRESSES AND SHEAR FORCES, EL CENTRO 1979 EARTHQUAKE (Uncorrelated Case)

Root Mean Square of the Response

	STRESSES (KSI)																	
	Left Span						Center Span						Right Span					
Array Number	1/4 Point		1/2 Point		3/4 Point		1/4 Point		1/2 Point		3/4 Point		1/4 Point		1/2 Point		3/4 Point	
	Vib.	Tot.	Vib.	Tot.	Vib.	Tot.	Vib.	Tot.	Vib.	Tot.	Vib.	Tot.	Vib.	Tot.	Vib.	Tot.	Vib.	Tot.
4,5,6,7	2.82	2.82	4.04	4.04	2.87	2.87	1.33	1.34	1.77	1.77	1.46	1.49	5.10	5.10	7.18	7.18	5.01	5.01
5,6,7,8	4.64	4.64	6.65	6.65	4.72	4.72	1.33	1.36	1.68	1.67	1.25	1.26	3.35	3.35	4.72	4.72	3.29	3.29

	SHEAR FORCE (KIPS)					
	Left Span at Anchorage		Center Span at Left Tower		Right Span at Anchorage	
Array Number	Vib.	Total	Vib.	Total	Vib.	Total
4,5,6,7	275.5	275.5	1255	1254	489.3	489.8
5,6,7,8	452.8	454.6	1172	1172	321.4	321.5

It should be noted that with reference to the vertical vibration (Chapter II) it was found that the uncorrelated calculation is usually conservative in nature. However, by examining Figs. IV-7 through IV-18 as well as Tables IV-4 through IV-8, it can be seen that this is not necessarily the case in lateral vibration.

Appendix IV-a

Details of Mass and Stiffness Matrices

The general procedure as outlined by Abdel-Ghaffar (1) involves discretizing each span into elements (Fig. III-2). Each element, as shown, has six degrees of freedom; two corresponding to the cables' deflections (modeled as a string element) and four corresponding to the suspended structure's deflections and rotations (modeled as a beam element). Linear interpolation functions are used to model the cables, while hermite polynomials are utilized in modeling the beam elements. The mass and stiffness matrices can be set up on the element level, and then assembled into the global mass and stiffness matrices. The global mass and stiffness matrices are symmetric, positive-definite, banded matrices.

The mass matrix has two contributions, one arising from the kinetic energy of the suspended structure and one arising from the kinetic energy of the cables, that is

$$[M] = [M_s] + [M_c]$$
$$= \sum_{e=1}^{n_{el}} [m_s]_e + \sum_{e=1}^{n_{el}} [m_c]_e \qquad \text{(IV-a-1)}$$

where $[M_s]$ is the contribution from the suspended structure to the global mass matrix; $[M_c]$ is the contribution from the cables to the global mass matrix; $[m_s]_e$ and $[m_c]_e$ are the corresponding matrices on the element level; and the summation over the number of elements (n_{el}) involves assembling each element mass matrix into the global mass matrix in its proper position.

The element mass matrices are (1)

$$[m_S]_e = \frac{\overset{*}{m}_S L}{420} \begin{bmatrix} 156 & -22L & 0 & 54 & 13L & 0 \\ -22L & 4L^2 & 0 & -13L & -3L^2 & 0 \\ 0 & 0 & 0 & 0 & 0 & 0 \\ 54 & -13L & 0 & 156 & 22L & 0 \\ 13L & -3L^2 & 0 & 22L & 4L^2 & 0 \\ 0 & 0 & 0 & 0 & 0 & 0 \end{bmatrix}$$

(IV-a-2)

where $\overset{*}{m}_S$ is the mass of the suspended structure per unit span length and L is the length of the element and

$$[m_c]_e = \frac{\overset{*}{m}_c L}{6} \begin{bmatrix} 0 & 0 & 0 & 0 & 0 & 0 \\ 0 & 0 & 0 & 0 & 0 & 0 \\ 0 & 0 & 2 & 0 & 0 & 1 \\ 0 & 0 & 0 & 0 & 0 & 0 \\ 0 & 0 & 0 & 0 & 0 & 0 \\ 0 & 0 & 1 & 0 & 0 & 2 \end{bmatrix}$$

(IV-a-3)

The stiffness matrix has four contributions, one arising from the elastic stiffness of the suspended structure, denoted $[K_{SE}]$; one arising from the elastic stiffness of the cables denoted $[K_{CE}]$; one arising from the gravity stiffness of the suspended structure, denoted $[K_{SG}]$; and one arising from the gravity stiffness of the cables, denoted $[K_{CG}]$, that is

$$[K] = [K_{SE}] + [K_{SG}] + [K_{CE}] + [K_{CG}]$$

$$= \sum_{e=1}^{n_{el}} ([k_{SE}]_e + [k_{SG}]_e + [k_{CE}]_e + [k_{CG}]_e) \qquad \text{(IV-a-4)}$$

where $[k_{SE}]_e$, $[k_{SG}]_e$, $[k_{CE}]_e$, and $[k_{CG}]_e$ are the corresponding matrices on the element level; and the summation over the number of elements (n_{el}) involves assembling each element stiffness into the global stiffness matrix in its proper position.

The element stiffness matrices are as follows (1):

$$[k_{SE}]_e = \frac{E_S I_S}{L^3} \begin{bmatrix} 12 & -6L & 0 & -12 & -6L & 0 \\ -6L & 4L^2 & 0 & 6L & 2L^2 & 0 \\ 0 & 0 & 0 & 0 & 0 & 0 \\ -12 & 6L & 0 & 12 & 6L & 0 \\ -6L & 2L^2 & 0 & 6L & 4L^2 & 0 \\ 0 & 0 & 0 & 0 & 0 & 0 \end{bmatrix} \qquad \text{(IV-a-5)}$$

$$[k_{SG}]_e = \frac{w_S^* L}{420\, h_e} \begin{bmatrix} 156 & -22L & -147 & 54 & 13L & -63 \\ -22L & 4L^2 & 21L & -13L & -3L^2 & 14L \\ -147 & 21L & 140(1 + \frac{h_e}{y_e}) & -63 & -14L & 70(1 + \frac{h_e}{y_e}) \\ 54 & -13L & -63 & 156 & 22L & -147 \\ 13L & -3L^2 & -14L & 22L & 4L^2 & -21L \\ -63 & 14L & 70(1 + \frac{h_e}{y_e}) & -147 & -21L & 140(1 + \frac{h_e}{y_e}) \end{bmatrix} \qquad \text{(IV-a-6)}$$

$$[k_{CE}]_e = \frac{2H_w}{L}\begin{bmatrix} 0 & 0 & 0 & 0 & 0 & 0 \\ 0 & 0 & 0 & 0 & 0 & 0 \\ 0 & 0 & 1 & 0 & 0 & -1 \\ 0 & 0 & 0 & 0 & 0 & 0 \\ 0 & 0 & 0 & 0 & 0 & 0 \\ 0 & 0 & 1 & 0 & 0 & 1 \end{bmatrix}$$

$$+ \frac{\overset{*}{w}_s + \overset{*}{w}_c}{6\, y_e}\begin{bmatrix} 0 & 0 & 0 & 0 & 0 & 0 \\ 0 & 0 & 0 & 0 & 0 & 0 \\ 0 & 0 & 2 & 0 & 0 & 1 \\ 0 & 0 & 0 & 0 & 0 & 0 \\ 0 & 0 & 0 & 0 & 0 & 0 \\ 0 & 0 & 1 & 0 & 0 & 2 \end{bmatrix} \qquad \text{(IV-a-7)}$$

$$[k_{CG}]_e = \frac{\overset{*}{w}_c L}{6\, y_e}\begin{bmatrix} 0 & 0 & 0 & 0 & 0 & 0 \\ 0 & 0 & 0 & 0 & 0 & 0 \\ 0 & 0 & 2 & 0 & 0 & 1 \\ 0 & 0 & 0 & 0 & 0 & 0 \\ 0 & 0 & 0 & 0 & 0 & 0 \\ 0 & 0 & 1 & 0 & 0 & 2 \end{bmatrix} \qquad \text{(IV-a-8)}$$

where h_e and y_e are element cable ordinates defined in Fig. IV-2; H_w is the initial (dead-load) horizontal component of cable tension; $\overset{*}{w}_s$ and $\overset{*}{w}_c$ are the dead weights of the suspended structure and cables, respectively; E_s and I_s are the modulus of elasticity and lateral

moment of inertia of the suspended structure, respectively; and L is the length of the element.

Appendix IV-b

Orthogonality of Lateral Mode Shapes

The n^{th} lateral mode shape, $\{\phi_n\}$, satisfies the equation

$$\omega_n^2[M_{SS}]\{\phi_n\} = [K_{SS}]\{\phi_n\} \qquad n = 1, 2, 3 \ldots \qquad \text{(IV-b-1)}$$

The m^{th} lateral mode shape, $\{\phi_m\}$, satisfies a similar equation, that is

$$\omega_m^2[M_{SS}]\{\phi_m\} = [K_{SS}]\{\phi_m\} \qquad m = 1, 2, 3 \ldots \qquad \text{(IV-b-2)}$$

Premultiplying Eq. IV-b-1 by $\{\phi_m\}^T$, premultiplying Eq. IV-b-2 by $\{\phi_n\}^T$ and subtracting gives

$$\omega_n^2\{\phi_m\}^T[M_{SS}]\{\phi_n\} - \omega_m^2\{\phi_n\}^T[M_{SS}]\{\phi_m\} = \{\phi_m\}^T[K_{SS}]\{\phi_n\}$$

$$- \{\phi_n\}^T[K_{SS}]\{\phi_m\}$$

$$n = 1, 2, 3 \ldots$$

$$m = 1, 2, 3 \ldots \qquad \text{(IV-b-3)}$$

Because the stiffness and mass matrices resulting from the finite element method are symmetric and positive-definite, Eq. IV-b-3 reduces to

$$(\omega_n^2 - \omega_m^2)\{\phi_m\}^T[M_{SS}]\{\phi_n\} = 0$$

$$m = 1, 2, 3 \ldots$$

$$n = 1, 2, 3 \ldots \qquad \text{(IV-b-4)}$$

which yields modal orthogonality, with respect to mass matrix weighting, of the form

$$\{\phi_m\}^T[M_{SS}]\{\phi_n\} = 0 \qquad m \neq n \qquad \text{(IV-b-5)}$$

REFERENCES OF CHAPTER IV

1. Abdel-Ghaffar, Ahmed M., "Dynamic Analysis of Suspension Bridge Structures," Report No. EERL 76-01, Earthquake Engineering Research Laboratory, College of Engineering, California Institute of Technology, Pasadena, May, 1976.

2. Abdel-Ghaffar, Ahmed M., "Free Lateral Vibrations of Suspension Bridges," Journal of the Structural Division, ASCE, Vol. 104, No. ST3, Proc. Paper 13609, March 1978, pp. 503-525.

3. Baron, F., Arikan, M., and Hamati, E., "The Effects of Seismic Disturbances on the Golden Gate Bridge," Report No. EERC 76-31, Earthquake Engineering Research Center, College of Engineering, University of California, Berkeley, November 1976.

4. Bendat, Julius S., and Piersol, Allan G., Engineering Applications of Correlation and Spectral Analysis, John Wiley and Sons, New York, 1980.

5. Bleich, F., McCullough, C.B., Rosecrans, R., and Vincent, G.S., The Mathematical Theory of Vibration in Suspension Bridges, U.S. Bureau of Public Roads, Government Printing Office, Washington 25, D.C., 1950.

6. Brady, A.G., Perez, V. and Mork, P.N., "The Imperial Valley Earthquake, October 15, 1979: Digitization and Processing of Accelerograph Records," U.S. Geological Survey, Seismic Engineering Branch, Open-File Report 80-703, April 1980, Menlo Park, California.

7. Mindlin, R.D., and Goodman, L.E., "Beam Vibrations with Time-Dependent Boundary Conditions," Journal of Applied Mechanics, ASME, Vol. 17, 1950, pp. 377-380.

8. Pugsley, A.G., The Theory of Suspension Bridges, Edward Arnold, London, 1957.

9. Steinman, D.B., "Modes and Natural Frequencies of Suspension Bridge Oscillations," ASCE, pp. 148-173, September 1959.

10. Vanmarcke, Erik H., "Structural Response to Earthquakes," Chapter 8, from Seismic Risk and Engineering Decisions, Edited by C. Lomnitz and E. Rosenblueth, Elsevier Publishing Company, Amsterdam, London, New York, 1976.

CHAPTER V

LONGITUDINAL RESPONSE OF SUSPENSION BRIDGE TOWER-PIER SYSTEMS TO EARTHQUAKE GROUND MOTION

V.1 INTRODUCTION

Analytical and numerical dynamic analyses of free vibration of suspension bridges (1,4,15) show that modes of the structure can be divided into two groups, one in which the suspended structure and cables dominate and the other where the displacement of the tower dominates. Thus, the tower can be separated from the rest of the structure at least in an approximate fashion and its earthquake response can be studied separately. While the transverse response analysis of suspension bridge tower-pier systems is quite conventional, being simply a free-standing beam supported by the soil elastic halfspace, the longitudinal response analysis methodology is more difficult. This difficulty results from the cable restraint in the longitudinal direction at the top of the tower. This chapter presents the dynamic analysis methodology for earthquake-induced longitudinal vibrations of suspension bridge tower-pier systems. The method accounts for the underlying and surrounding soil flexibility, as well as its geometric and hysteretic damping characteristics. The effect of surrounding water is taken into account using the concept of the added mass (or virtual mass) which intends to represent that quantity of water which vibrates along with the pier. The analysis is carried out in the time domain and

compared to the frequency domain (random vibration) results in order to determine appropriate peak factors for the tower-pier vibration problem.

Finally, the longitudinal response of the Golden Gate's San Francisco tower-pier system is investigated in order to estimate its earthquake response characteristics. The San Francisco tower-pier system is partially embedded, and is also partially submerged so that the effect of surrounding water must be taken into account. The soil stiffness and damping for rocking, translation, and coupled translation-rocking of the pier are calculated using existing techniques (13), and are converted to equivalent modal damping and generalized modal stiffness (18). Because the underlying and surrounding soil characteristics may change under high amplitude vibration, a parametric study is performed in this chapter using four different soil conditions. The first case involves the pier being completely fixed at its base, hereafter referred to as the "fixed-base case." The second case corresponds to the pier being founded on rock type soil; the "rock case." The third case corresponds to a "moderately stiff soil," while the fourth case corresponds to "soft soil."

Three different earthquake ground motion records are applied longitudinally at the base of the Golden Gate's San Francisco pier. These correspond to the S50W component of El Centro's (1979) Array No. 5 (see Appendix II-e), the S16°E component of the 1971 Pacoima Dam Record (see Appendix V-c or Ref. 11), and an artificially generated earthquake ground motion (see Appendix II-e or Ref. 10). The longitudinal displacement response is compared for each earthquake at selected points on the tower as well as the resulting stresses and shear forces.

V.2 COORDINATE SYSTEM

The coordinate system used for the general longitudinal tower-pier vibration problem is shown in Fig. V-1. For the purpose of studying the longitudinal vibration of the tower-pier system, the following is considered:

1. The x-axis is defined as the vertical line passing through the base of the pier.
2. The y-axis is defined as the horizontal line measured in the longitudinal direction of the bridge passing through the base of the pier.
3. The longitudinal vibration of the centerline of the tower $u(x,t)$ is measured horizontally in the longitudinal direction of the bridge.
4. As will be shown at a later point, the longitudinal vibration of the tower-pier system is excited by the longitudinal component of ground motion acting at the pier's base. In Fig. V-1, this ground motion displacement is denoted as $f(t)$.

V.3 FUNDAMENTAL ASSUMPTIONS

The following assumptions and approximations are made for simplifying the tower vibration analysis (1):

1. All stresses in the tower remain within the elastic limit and therefore obey Hooke's law.
2. To stay within the linear theory, small vibrational longitudinal displacements are assumed.
3. The soil flexibility may be represented by equivalent rotational and translational soil springs, whose determination is discussed in Appendix V-b.

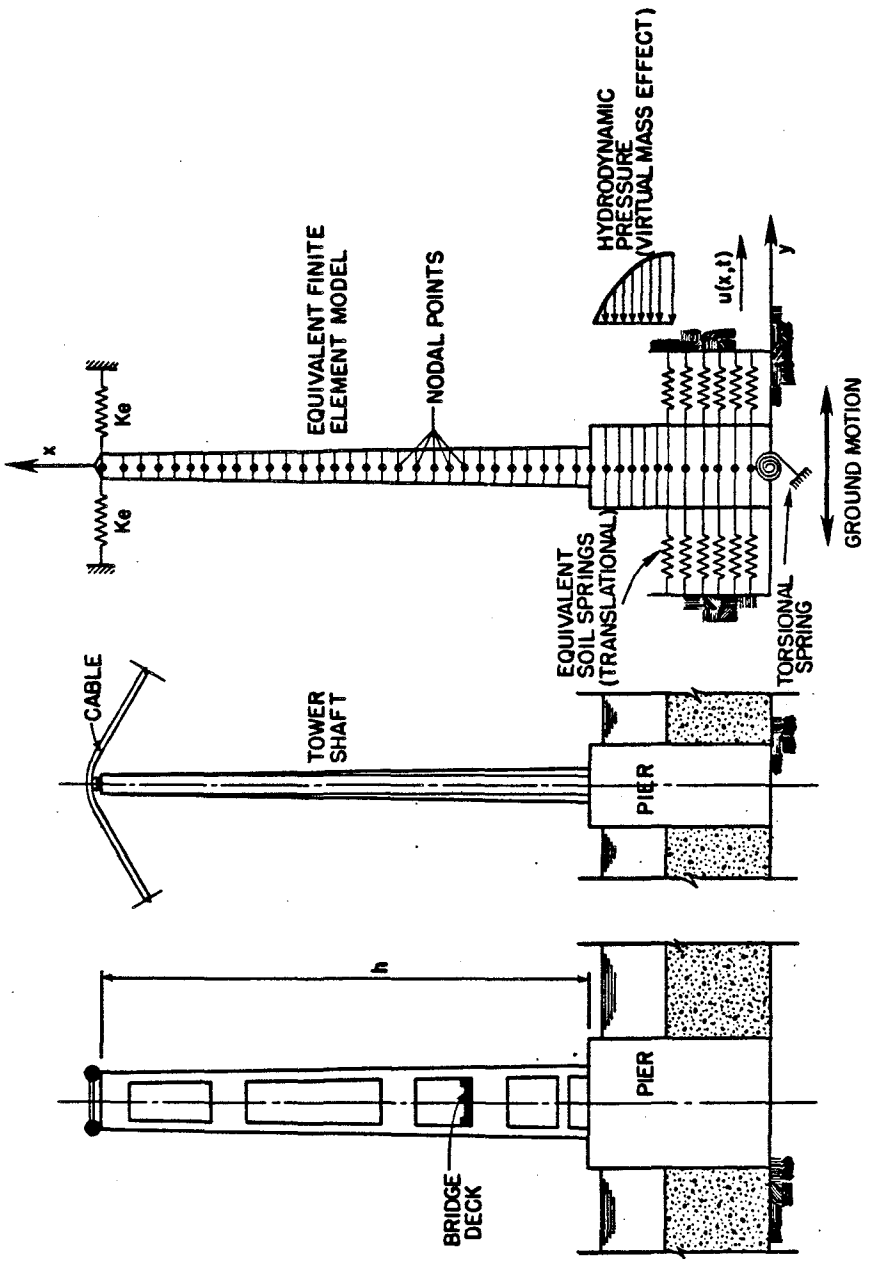

Fig. V-1 TYPICAL SUSPENSION BRIDGE TOWER-PIER SYSTEM ; DEFINITION DIAGRAM

4. The elastic restraint by the cables at the top of the tower can be simulated by a spring of stiffness k_e, whose determination is discussed in Appendix V-e.
5. The effect of the mass of the suspended structure which vibrates along with the tower is neglected.
6. The additional axial force P(t) at the top of tower arising from the vertical component of the additional (vibrational) cable tension is small with respect to the dead load axial force P_w and is thus neglected.
7. The only excitation included is the ground motion input at the base of the tower. The effect of anchorage inputs is neglected.

V.4 EQUATION OF MOTION GOVERNING LONGITUDINAL TOWER-PIER VIBRATION

Under the previous assumptions, the linearized equation of motion governing the longitudinal vibration of the tower-pier of a suspension bridge is given by (1)

$$[M]\{\ddot{u}\} + [C]\{\dot{u}\} + [K]\{u\} = 0 \tag{5.1}$$

where [M] is the mass matrix which includes the masses of the tower vertical elements, diagonals and struts as well as the masses of the pier elements and the virtual mass of water surrounding the pier, the details of which appear in Appendix V-a; [K] is the stiffness matrix which includes the stiffness contribution from the elastic flexural deformation as well as the geometric stiffness arising from the axial component of the dead load cable tension, P_w, and the soil springs and equivalent cable spring restraints, the details of which appear in Appendix V-a, and [C] is the damping matrix.

Equation 5.1 may be written in partitioned form as (3)

$$\begin{bmatrix} M_{gg} & M_{gs} \\ M_{sg} & M_{ss} \end{bmatrix} \begin{Bmatrix} \ddot{u}_g \\ \ddot{u}_s \end{Bmatrix} + \begin{bmatrix} C_{gg} & C_{gs} \\ C_{sg} & C_{ss} \end{bmatrix} \begin{Bmatrix} \dot{u}_g \\ \dot{u}_s \end{Bmatrix} + \begin{bmatrix} K_{gg} & K_{gs} \\ K_{sg} & K_{ss} \end{bmatrix} \begin{Bmatrix} u_g \\ u_s \end{Bmatrix} = \begin{Bmatrix} 0 \\ 0 \end{Bmatrix} \quad , \tag{5.2}$$

in which the subscript "g" designates the degrees of freedom which correspond to the points of application of ground motions, that is, the ends of the two translational soil spring elements (Fig. V-1). The subscript "s" corresponds to all other structural degrees of freedom of the tower-pier system.

V.5 GENERAL SOLUTION

In order to handle the statical indeterminacy of the structural model, and its associated time-dependent boundary conditions, the nodal displacements may be decomposed into quasi-static (or pseudo-static) displacements and relative (or vibrational) displacements. Quasi-static displacements are those resulting from the static application of support displacements (degrees of freedom with subscript g) at any time t. Thus the displacement can be written as

$$\begin{Bmatrix} u_g \\ u_s \end{Bmatrix} = \begin{Bmatrix} u_{pg} \\ u_{ps} \end{Bmatrix} + \begin{Bmatrix} 0 \\ u_{vs} \end{Bmatrix} \tag{5.3}$$

where the subscript "p" denotes the pseudo-static displacements and the subscript "v" denotes the vibrational displacements.

The pseudo-static displacement vector can be expressed as

$$\begin{Bmatrix} u_{pg} \\ u_{ps} \end{Bmatrix} = \begin{Bmatrix} g_{pg} \\ g_{ps} \end{Bmatrix} f(t) \tag{5.4}$$

where g_{ps} is the quasi-static function that results from unit displacement of the ground surrounding the pier; $f(t)$ is the longitudinal input ground-motion displacement; and g_{pg} is a vector whose dimension is equal to the number of soil translation springs taken in the model (equal to two in the case of the Golden Gate Bridge Tower; Fig. V-2), and whose elements are all equal to unity.

Substituting Eqs. 5.4 and 5.3 into Eq. 5.2 gives

$$[M_{ss}]\{\ddot{u}_{vs}\} + [C_{ss}]\{\dot{u}_{vs}\} + [K_{ss}]\{u_{vs}\} =$$

$$-\left([M_{sg}\ M_{ss}]\ddot{f}(t) + [C_{sg}\ C_{ss}]\dot{f}(t) + [K_{sg}\ K_{ss}]f(t)\right)\begin{Bmatrix} g_{pg} \\ g_{ps} \end{Bmatrix} \tag{5.5}$$

The previous equation can be simplified by noting that for an unloaded tower-pier system with a static condition of support displacement, one has

$$[K_{sg}\ K_{ss}]\begin{Bmatrix} u_{pg} \\ u_{ps} \end{Bmatrix} = \{0\} \tag{5.6}$$

Substituting Eq. 5.4 into Eq. 5.6 yields

$$[K_{sg}\ K_{ss}]\begin{Bmatrix} g_{pg} \\ g_{ps} \end{Bmatrix} = \{0\} \tag{5.7}$$

Thus, the quasi-static vector can be defined in the following manner:

$$\{g_{ps}\} = -[K_{ss}]^{-1}[K_{sg}]\{g_{pg}\} \tag{5.8}$$

and the equation governing the tower's vibrational response (Eq. 5.5) reduces to

$$[M_{ss}]\{\ddot{u}_{vs}\} + [C_{ss}]\{\dot{u}_{vs}\} + [K_{ss}]\{u_{vs}\} =$$

$$- \left([M_{sg}\ M_{ss}]\ddot{f}(t) + [C_{sg}\ C_{ss}]\dot{f}(t)\right)\begin{Bmatrix} g_{pg} \\ g_{ps} \end{Bmatrix} \tag{5.9}$$

Note that the previous equation is excited by ground acceleration and velocity terms. As indicated by Baron (3,4), the contribution to the total response from velocity terms is small; therefore the velocity terms are neglected hereafter in this analysis.

V.6 EIGENVALUE PROBLEM - FREE VIBRATIONS

The solution to Eq. 5.9 is obtained by modal superposition, that is the vibrational displacement is taken to be

$$\{u_{vs}\} = \sum_{n=1}^{N} \{\phi_n\} q_n(t) \tag{5.10}$$

where $\{\phi_n\}$ is the n^{th} longitudinal tower vibration mode shape; $q_n(t)$ is the n^{th} generalized coordinate; and N corresponds to the number of degrees of freedom in the finite element model. Usually, the number of modes necessary for an accurate response analysis will be significantly less than the number of degrees of freedom N, which is an inherent advantage of using the modal superposition method. The longitudinal tower-pier mode shapes and corresponding natural circular frequencies, ω_n, are obtained from the solution of the matrix eigenvalue problem

$$(-\omega_n^2[M_{ss}] + [K_{ss}])\{\phi_n\} = \{0\} \qquad n=1,2,3... \qquad (5.11)$$

It should be noted that the stiffness matrix $[K_{ss}]$ includes the translational and rotational soil stiffnesses (see Appendices V-a, V-b). Therefore, as one varies the soil parameters, the mode shapes and associated natural frequencies of vibration of the tower-pier will change accordingly.

V.7 MODAL SOLUTIONS - FORCED VIBRATIONS

After neglecting input velocity terms, substituting Eq. 5.10 into Eq. 5.9 results in

$$\sum_{n=1}^{N} \left([M_{ss}]\{\phi_n\}\ddot{q}_n(t) + [C_{ss}]\{\phi_n\}\dot{q}_n(t) + [K_{ss}]\{\phi_n\}q_n(t) \right) =$$

$$- [M_{sg}\ M_{ss}] \begin{Bmatrix} g_{pg} \\ g_{ps} \end{Bmatrix} \ddot{f}(t) \qquad (5.12)$$

Now multiplying Eq. 5.12 by $\{\phi_m\}^T$, using modal orthogonality of the undamped vibration modes (see Appendix V-d), that is,

$$\{\phi_m\}^T[M_{ss}]\{\phi_n\} = 0 \qquad n \neq m \qquad (5.13)$$

and using the procedure presented in Appendix V-c for determining the equivalent modal damping ratio ζ_n^{eq}, combining structural damping with soil geometric and hysteretic damping, yields the equation governing the response for the n^{th} generalized coordinate

$$\ddot{q}_n(t) + 2\zeta_n^{eq}\omega_n\dot{q}_n(t) + \omega_n^2 q_n(t) = \alpha_n\ddot{f}(t) \qquad n=1,2,3... \qquad (5.14)$$

where the modal participation coefficient α_n is given by

$$\alpha_n = \frac{-\{\phi_n\}^T [M_{sg} \; M_{ss}] \begin{Bmatrix} g_{pg} \\ g_{ps} \end{Bmatrix}}{\{\phi_n\}^T [M_{ss}] \{\phi_n\}} \qquad n=1,2,3... \qquad (5.15)$$

The solution to Eq. 5.15, assuming quiescent initial conditions is given by the convolution (Duhamel) integral

$$q_n(t) = \frac{\alpha_n}{\omega_{nd}} \int_0^t \ddot{f}(\tau) e^{-\zeta_n^{eq} \omega_n (t-\tau)} \sin \omega_{nd}(t-\tau) d\tau \qquad n=1,2,3... \qquad (5.16)$$

where ω_{nd} is the damped natural circular frequency of the n^{th} longitudinal tower mode, given by

$$\omega_{nd} = \omega_n \sqrt{1 - (\zeta_n^{eq})^2} \qquad n=1,2,3... \qquad (5.17)$$

The total longitudinal tower displacement response is obtained as the sum of quasi-static and relative responses, that is

$$\begin{Bmatrix} u_g \\ u_s \end{Bmatrix} = \begin{Bmatrix} g_{pg} \\ g_{ps} \end{Bmatrix} f(t) + \sum_{n=1}^{N} \begin{Bmatrix} 0 \\ \phi_n \end{Bmatrix} q_n(t) \qquad (5.18)$$

For the purpose of calculating dynamically induced bending moments, flexural stresses, and shear forces in the tower, it is necessary to utilize the second and third space derivatives of the quasi-static functions and mode shapes. For example, the dynamic bending moment about the tower's lateral axis may be written as

$$\{M_s\} = \{E_{te} I_{te} g_{ps}''\} f(t) + \sum_{n=1}^{N} \{E_{te} I_{te} \phi_n''\} q_n(t) \qquad (5.19)$$

where $\{M_s\}$ is the vector of dynamic bending moments corresponding to the structural degrees of freedom; E_{te} is the modulus of elasticity of the tower elements; I_{te} is the area moment of inertia of the tower elements about its lateral axis; and the double prime denotes the second spacewise derivatives (of the quasi-static functions and mode shapes).

Similarly, the total dynamic longitudinal shearing force at any point in the tower may be calculated as

$$\{V_s\} = \{E_{te}I_{te}g_{ps}'''\}f(t) + \sum_{n=1}^{N} \{E_{te}I_{te}\phi_n'''\}q_n(t) \tag{5.20}$$

where $\{V_s\}$ is the vector of shearing forces corresponding to the structural degrees of freedom; and the triple prime denotes the third spanwise derivatives (of the quasi-static functions and mode shapes).

Furthermore, the dynamically induced longitudinal flexural stresses may be related to the moments by the following flexural relation

$$\{\sigma_s\} = \left\{\frac{b_e}{2I_{te}} M_s\right\} \tag{5.21}$$

where $\{\sigma_s\}$ is the vector of induced flexural stresses in the tower; and b_e is the longitudinal width of the tower at the particular element cross-section of interest.

V.8 FREQUENCY-DOMAIN, RANDOM VIBRATION APPROACH

In order to study the longitudinal dynamic behavior of suspension bridge tower-piers when subjected to earthquake excitations, a random vibration approach is utilized (5). For the ground motion displacement input at the pier base, there are complex frequency response functions associated with each vibration mode. To determine these functions

$f(t)$ is taken equal to $\exp(i\omega t)$, where $i = \sqrt{-1}$, and the response of the n^{th} generalized coordinate is assumed to be of the form

$$q_n(t) = H_n(\omega)\exp(i\omega t) \qquad n=1,2,3... \tag{5.22}$$

where $H_n(\omega)$ is the n^{th} complex frequency response due to input displacement $f(t)$. Now substituting Eq. 5.22 into Eq. 5.14 yields

$$H_n(\omega) = \frac{-\omega^2\alpha_n}{(\omega_n^2 - \omega^2) + i(2\zeta_n^{eq}\omega_n\omega)} \qquad \begin{matrix} n=1,2,3,... \\ i = \sqrt{-1} \end{matrix} \tag{5.23}$$

Taking the finite Fourier transform of Eq. 5.10 over the time duration of the ground motion input displacement, T_1, yields the Fourier transform of the vibrational response

$$\{U_{vs}(\omega)\} = \int_0^{T_1} \{u_{vs}\}e^{-i\omega t}\,dt = \sum_{n=1}^{N} \{\phi_n\}Q_n(\omega) \tag{5.24}$$

where $Q_n(\omega)$ is the finite Fourier transform of the generalized coordinate $q_n(t)$, given by

$$Q_n(\omega) = \int_0^{T_1} q_n(t)e^{-i\omega t}\,dt \qquad n=1,2,3... \tag{5.25}$$

A similar Fourier transformation of Eq. 5.14 yields

$$[(\omega_n^2 - \omega^2) + i(2\zeta_n^{eq}\omega_n\omega)]Q_n(\omega) = -\omega^2\alpha_n F(\omega) \qquad n=1,2,3... \tag{5.26}$$

in which $F(\omega)$ is the finite Fourier transform of the displacement input $f(t)$, given by

$$F(\omega) = \int_0^{T_1} f(t)e^{-i\omega t}\,dt \tag{5.27}$$

It follows from Eqs. 5.23 and 5.26 that the Fourier transform of the generalized coordinate can be expressed as

$$Q_n(\omega) = H_n(\omega)F(\omega) \qquad n=1,2,3... \tag{5.28}$$

Now substituting Eq. 5.28 into Eq. 5.24 enables the Fourier transform of the vibrational response to be expressed as

$$\{U_{vs}(\omega)\} = \sum_{n=1}^{N} \{\phi_n\}H_n(\omega)F(\omega) \tag{5.29}$$

The relative-displacement power-spectral density function is given by

$$\{G_{uvs}(\omega)\} = \lim_{T_1\to\infty} \frac{2}{T_1} E[\{\overset{*}{U}_{vs}(\omega)\}\{U_{vs}(\omega)\}] \tag{5.30}$$

where $E[\cdot]$ represents the expected value of the term inside the brackets and the superposed asterisk denotes complex conjugate. An estimate of $\{G_{uvs}(\omega)\}$ can be obtained by simply omitting the limiting and expectation operations in Eq. 5.30, hence

$$\{G_{uvs}(\omega)\} \simeq \frac{2}{T_1} [\{\overset{*}{U}_{vs}(\omega)\}\{U_{vs}(\omega)\}^T] \tag{5.31}$$

Substituting Eq. 5.29 into Eq. 5.31 yields

$$\{G_{uvs}(\omega)\} = \sum_{n=1}^{N} \sum_{m=1}^{N} \{\phi_n\}\{\phi_m\}^T\left(\overset{*}{H}_n(\omega)\right)\left(H_m(\omega)\right)G(\omega) \tag{5.32}$$

where $G(\omega)$ is the power spectrum of the displacement input $f(t)$, given by

$$G(\omega) = \lim_{T_1\to\infty} \frac{2}{T_1} E[\overset{*}{F}(\omega) \cdot F(\omega)] \simeq \frac{2}{T_1} |F(\omega)|^2 \tag{5.33}$$

It should again be noted, as in previous chapters, that the double summation appearing in Eq. 5.32 accounts for modal interaction. The complex frequency response functions $H_n(\omega)$ peak in amplitude at their associated natural frequencies ω_n, and have much lower amplitudes elsewhere along the frequency band. Therefore, when the natural frequencies of the tower are well separated and damping ratios are small, the effect of cross-terms ($n \neq m$) in Eq. 5.32 becomes less significant than the diagonal terms ($n = m$), and may be neglected. However, in this analysis all modal interaction terms will be retained, in order to obtain an accurate representation of the response, even under the possibility of closely-spaced modes.

The mean square value of the relative tower-displacement response $\{\Psi^2_{uvs}\}$ is given by the integration of $\{G_{uvs}(\omega)\}$ over the entire frequency range, that is

$$\{\Psi^2_{uvs}\} = \frac{1}{2\pi} \int_0^\infty \{G_{uvs}(\omega)\} d\omega \tag{5.34}$$

and the square root of Eq. 5.34 is the root mean square (R.M.S.) relative tower-displacement response.

The power spectral density of the total longitudinal tower-displacement response can be obtained by multiplying Eq. 5.18 by its complex conjugate and by $(2/T_1)$ which leads to

$$\begin{Bmatrix} G_{ug} \\ G_{us} \end{Bmatrix} = \sum_{n=1}^{N} \sum_{m=1}^{N} \begin{Bmatrix} 0 \\ \phi_n \end{Bmatrix} \begin{Bmatrix} 0 \\ \phi_m \end{Bmatrix}^T \left(\overset{*}{H}_n(\omega)\right)\left(H_m(\omega)\right) G(\omega)$$

$$+ \sum_{n=1}^{N} \begin{Bmatrix} 0 \\ \phi_n \end{Bmatrix} \begin{Bmatrix} g_{pg} \\ g_{ps} \end{Bmatrix}^T \left(\overset{*}{H}_n(\omega) + H_n(\omega)\right) G(\omega) + \begin{Bmatrix} g_{pg} \\ g_{ps} \end{Bmatrix} \begin{Bmatrix} g_{pg} \\ g_{ps} \end{Bmatrix}^T G(\omega) \tag{5.35}$$

The integration of $\{G_{ug}\}$ and $\{G_{us}\}$ over the frequency domain provides the mean square total longitudinal tower-displacement response, $\{\psi_u^2\}$

$$\begin{Bmatrix} \psi_{ug}^2 \\ \psi_{us}^2 \end{Bmatrix} = \frac{1}{2\pi} \int_0^\infty \begin{Bmatrix} G_{ug} \\ G_{us} \end{Bmatrix} d\omega \tag{5.36}$$

whose square root is the root mean square (R.M.S.) total longitudinal tower-displacement response.

The procedure outlined in the above section may be used to evaluate the power spectral density of the vibrationally-induced bending moment in the tower by simply replacing the mode shapes, $\{\phi_n\}$, and quasi-static functions $\{g_{ps}\}$ by $\{E_{te}I_{te}\phi_n''\}$ and $\{E_{te}I_{te}g_{ps}''\}$ respectively, where $E_{te}I_{te}$ are the tower element flexural rigidities, and the double prime denotes the second space derivative. Similarly, the power spectral density of the vibrationally-induced shearing force in the tower may be obtained by replacing the modes and quasi-static functions by $\{E_{te}I_{te}\phi_n'''\}$ and $\{E_{te}I_{te}g_{ps}'''\}$ respectively. In addition, the autospectra of maximum tower stresses due to longitudinal vibration is given by the following flexural stress relation.

$$\{G_\sigma\} = \left\{ \left(\frac{b_e}{2I_{te}} \right)^2 G_M \right\} \tag{5.37}$$

where $\{G_M\}$ is the autospectra of tower bending moments, $\{G_\sigma\}$ is the autospectra of tower maximum stresses; b_e is the width of the tower at the particular element cross-section of interest, and I_{te} is the moment of inertia of the tower at the same point.

Mean square bending moments, shearing forces, and bending stresses are obtained by using Eq. 5.36 with the mode shapes and quasi-static functions replaced as described above.

V.9 LONGITUDINAL SEISMIC BEHAVIOR OF THE GOLDEN GATE BRIDGE'S SAN FRANCISCO TOWER-PIER SYSTEM

The analysis outlined in this chapter is applied to the Golden Gate's San Francisco Tower-Pier system, in California, in order to estimate its longitudinal response characteristics. The finite element model of this tower-pier system is shown in Fig. V-2, while the structural properties of the tower-pier elements appear in Appendix V-a. The longitudinal tower-pier quasi-static functions are shown in Fig. V-3 for unit ground motion displacement at the base of the pier. The first five longitudinal mode shapes also appear in Fig. V-3, while their natural periods of vibration appear in Table V-1, and their associated participation coefficients, α_n, appear in Table V-2. It should be noted that the behavior of the soil under high amplitude earthquake excitation is fairly difficult to model. As the amplitude of vibration increases, the soil behaves in a softer or yielding manner. In order to account for this behavior, four different cases are examined which are intended to represent the complete spectrum of soil properties. The first case involves the pier being completely fixed at its base, hereafter referred to as the "fixed-base" case. The second case corresponds to the pier overlying rock, the "rock case". The third case corresponds to a "moderately stiff soil," while the fourth case corresponds to a "soft soil". The soil properties appear in Appendix V-b. The effect of soil flexibility upon the mode shapes can be

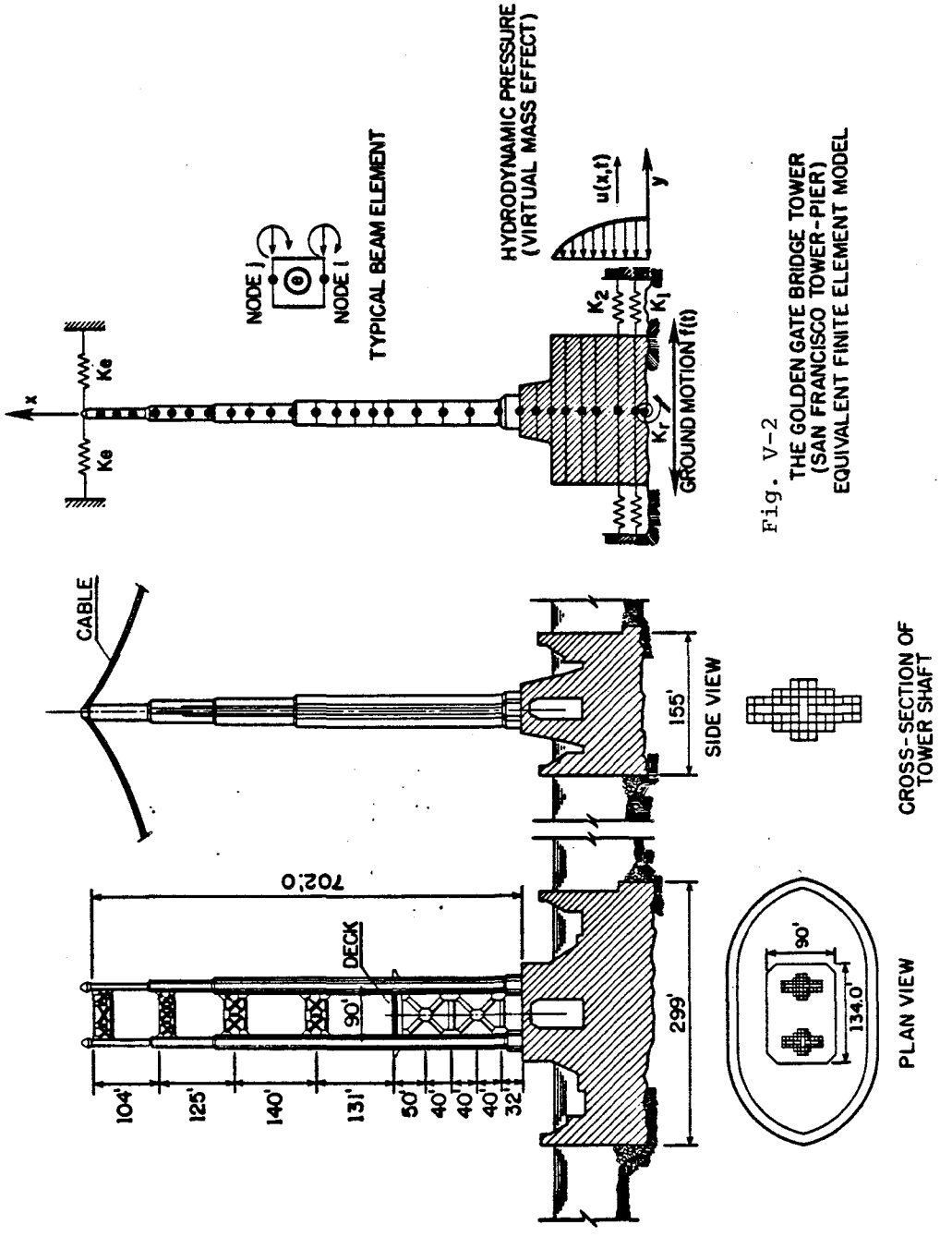

Fig. V-2
THE GOLDEN GATE BRIDGE TOWER
(SAN FRANCISCO TOWER-PIER)
EQUIVALENT FINITE ELEMENT MODEL

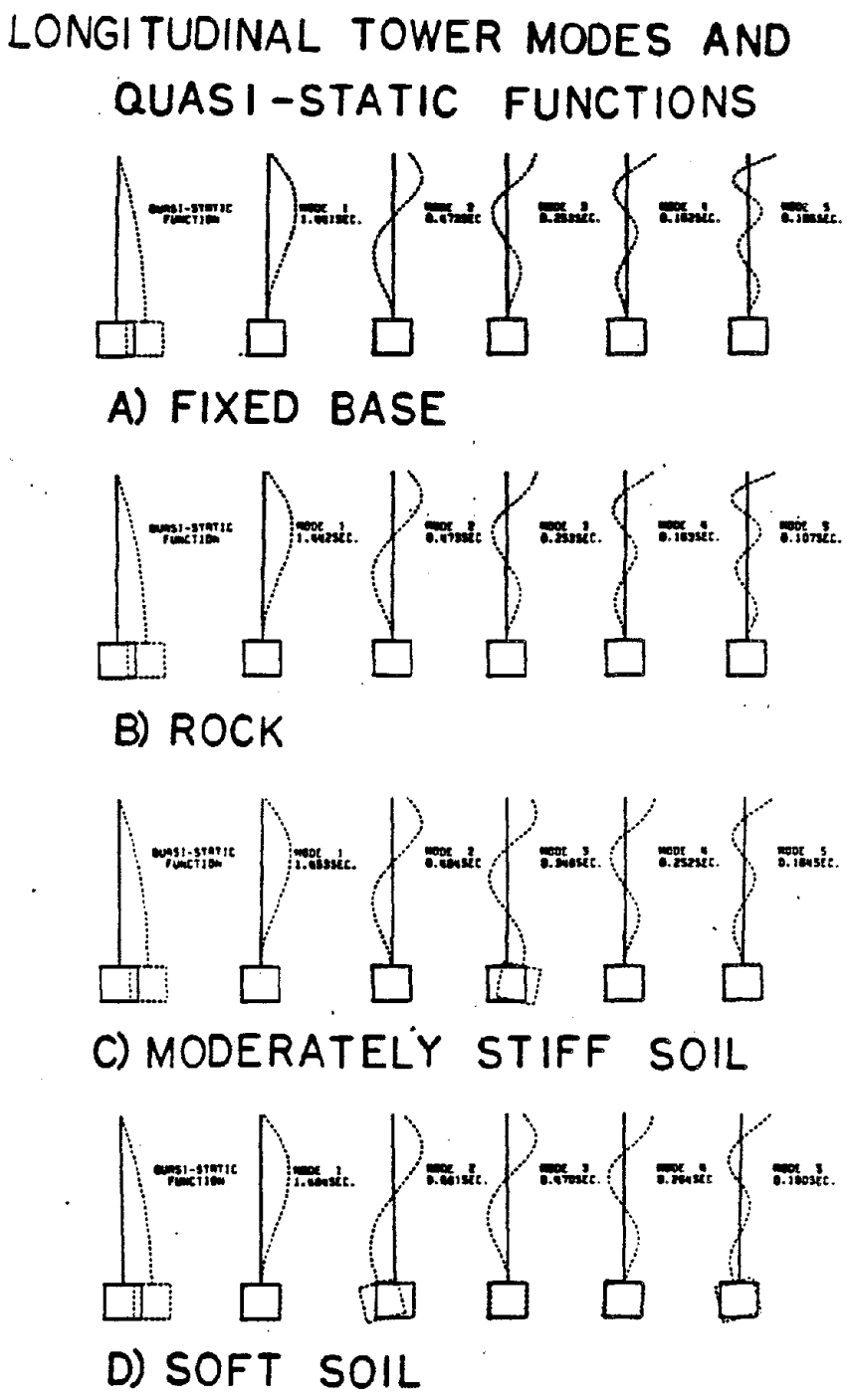

Fig. V-3 Longitudinal tower modes and quasi-static functions of the Golden Gate Bridge.

Table V-1

NATURAL PERIODS OF LONGITUDINAL TOWER VIBRATION (sec.)

	SOIL TYPE			
MODE ORDER	FIXBASE (a)	ROCK (b)	MODERATELY STIFF SOIL (c)	SOFT SOIL (d)
1	1.441	1.442	1.453	1.484
2	0.473	0.473	0.484	0.661*
3	0.253	0.253	0.348*	0.470
4	0.162	0.163	0.252	0.264
5	0.106	0.107	0.164	0.190
6	0.072	0.095*	0.112	0.150*
7	0.052	0.072	0.095*	0.103
8	0.039	0.052	0.070	0.071
9	0.031	0.040	0.051	0.051
10	0.020	0.031	0.039	0.039

* indicates a mode whose counterpart does not exist in the fixed-base case, and which involves significant rocking of the pier.

(a) $C_s = \infty$ ft/sec (shear wave velocity)

(b) $C_s = 5900$ ft/sec

(c) $C_s = 1900$ ft/sec

(d) $C_s = 1076$ ft/sec

Table V-2

PARTICIPATION FACTORS α_n OF LONGITUDINAL TOWER VIBRATION

	TYPE OF SOIL* SURROUNDING AND UNDERLYING PIER			
MODE ORDER	FIXBASE[a]	ROCK[b]	MODERATELY STIFF SOIL[c]	SOFT SOIL[d]
1	-0.8641	-0.8735	-0.9923	-1.338
2	0.5974	0.6439	1.777	2.107
3	0.5902	-0.7648	-2.351	-1.757
4	0.6479	1.229	1.708	0.9438
5	-0.5072	-3.474	-1.075	-1.061
6	0.3994	3.595	1.1680	0.5972
7	-0.3573	-1.159	-0.8629	-0.1309
8	0.3267	0.5536	0.2093	0.0350
9	-0.2784	-0.4782	-0.0673	-0.0149
10	-0.2368	0.6469	0.0294	0.0073

(a) G = ∞ ksf (shear modulus)

(b) G = 172,800 ksf

(c) G = 12,960 ksf

(d) G = 3,600 ksf

clearly seen from Fig. V-3. Also, as the soil becomes softer, additional modes emerge whose counterparts do not exist in the fixed-base case, and which involve significant rocking of the pier.

The frequency response functions $H_n(\omega)$ for the first five longitudinal tower-pier modes are shown in Fig. V-4 as a function of soil type, while their associated equivalent damping ratios (structural plus soil damping are summarized in Table V-3 (see also Appendix V-c). These frequency response functions measure the magnification (or gain) factor corresponding to a unit harmonic input upon the generalized coordinate $q_n(t)$.

Three longitudinal tower-pier response cases are studied for the Golden Gate Bridge. The first case utilizes the S50°W component of El Centro's (1979) Array No. 5 (see Appendix II-e) as base excitation; the second case involves an artificially generated earthquake ground motion (type B-1; see Appendix II-e; Ref. 10); and the third case uses the S16°E component of the 1971 Pacoima Dam record as input (see Appendix V-f; Ref. 11).

The displacement, bending-stress, and shear force responses of the tower are calculated at discrete points along the tower, namely at 0.0h, 0.2h, 0.4h, 0.6h, 0.8h, and 1.0h where h = the height of the tower, along with the rocking motion of the pier. Calculations are performed in both the time and frequency domains for the fixed-base case as well as for the three soil types in order to estimate appropriate peak factors for the tower-pier vibration problem. Peak displacements flexural stresses, and shear forces are summarized in tabular form in Tables V-4, V-5, and V-6 and in graphical form in Figs. V-5, V-6, and V-7 for the three different applied base excitations. The complete

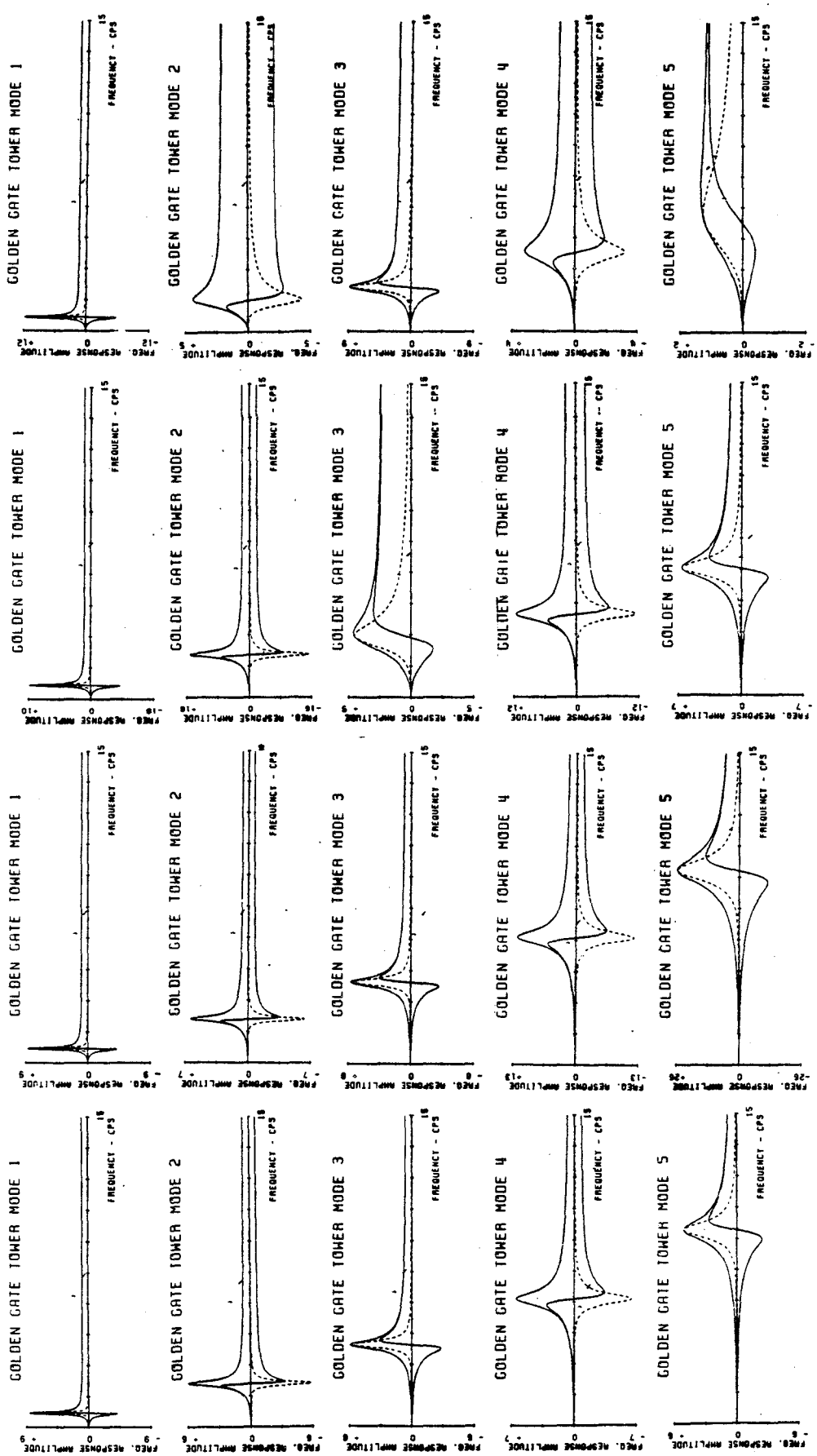

Fig. V-4 Frequency response functions for the first five longitudinal tower modes of the Golden Gate Bridge.

Table V-3

Composite Damping Ratios ζ_n^{eq} (Based on Ref. 18)

	SOIL-FOUNDATION TYPE			
MODE ORDER	FIXED BASE	ROCK	MODERATELY STIFF SOIL	SOFT SOIL
1	0.0500	0.0501	0.0508	0.0533
2	0.0500	0.0501	0.0584	0.2479
3	0.0500	0.0502	0.2651	0.0955
4	0.0500	0.0508	0.0744	0.1498
5	0.0500	0.0679	0.0814	0.4444

Table V-4

Displacement Response (cm)

RESPONSE CASE	PEAK (Time Domain)						R.M.S. (Freq. Domain)						PEAK FACTOR					
	0.0h	0.2h	0.4h	0.6h	0.8h	1.0h	0.0h	0.2h	0.4h	0.6h	0.8h	1.0h	0.0h	0.2h	0.4h	0.6h	0.8h	1.0h
El Centro Array 5, S5OW																		
o fixbase	51.9	48.4	39.2	28.7	18.4	2.07	11.7	10.9	9.08	6.78	3.95	0.377	4.45	4.43	4.31	4.24	4.66	5.50
o rock	51.8	48.3	39.1	28.7	18.7	2.44	11.6	10.9	9.07	6.77	3.97	0.405	4.45	4.42	4.31	4.24	4.71	6.04
o mod. stiff	51.2	47.5	39.7	29.4	23.6	5.06	11.5	10.7	8.94	6.76	4.19	0.651	4.45	4.42	4.44	4.35	5.63	7.77
o soft	46.9	46.0	41.1	28.4	17.4	3.87	11.2	10.3	8.65	7.01	4.69	0.628	4.19	4.46	4.75	4.05	3.71	6.17
Artificial E:/Q.B-1																		
o fixbase	29.4	28.1	26.8	25.7	19.6	2.76	7.49	7.12	6.74	6.74	5.19	0.699	3.93	3.95	3.98	3.81	3.76	3.94
o rock	29.4	27.9	26.9	25.9	19.9	2.88	7.49	7.11	6.76	6.78	5.25	0.741	3.93	3.93	3.98	3.81	3.79	3.88
o mod. stiff	28.0	27.8	28.6	27.0	23.7	4.88	7.41	7.08	7.05	7.41	6.06	1.13	3.78	3.92	4.05	3.65	3.91	4.30
o soft	28.3	30.1	31.7	33.6	29.6	4.60	7.28	7.11	8.01	9.36	7.72	1.12	3.89	4.24	3.96	3.59	3.83	4.09
Pacoima Dam, S16E																		
o fixbase	37.5	40.2	48.4	54.4	42.4	5.45	9.49	9.14	9.60	10.8	8.73	1.19	3.96	4.40	5.05	5.05	4.85	4.60
o rock	37.5	40.2	48.9	54.9	42.8	6.37	9.49	9.13	9.64	10.9	8.82	1.26	3.96	4.40	5.07	5.06	4.85	5.07
o mod. stiff	38.7	47.1	57.8	59.3	49.5	11.2	9.39	9.17	10.3	12.0	10.1	1.79	4.12	5.14	5.63	4.94	4.90	6.25
o soft	41.4	43.1	58.0	75.5	64.2	9.61	9.21	9.29	12.1	15.4	12.9	1.78	4.49	4.64	4.78	4.89	4.96	5.41

Table V-5

Response Stresses (ksi)

RESPONSE CASE	PEAK (Time Domain)						R.M.S. (Freq. Domain)						PEAK FACTOR					
	0.0h	0.2h	0.4h	0.6h	0.8h	1.0h	0.0h	0.2h	0.4h	0.6h	0.8h	1.0h	0.0h	0.2h	0.4h	0.6h	0.8h	1.0h
El Centro Array 5,																		
o fixbase	8.89	7.76	4.93	3.69	4.57	0.0	1.60	1.60	0.781	1.02	1.22	0.0	5.57	4.86	6.31	3.62	3.74	---
o rock	9.30	7.78	5.61	3.84	5.51	0.0	1.71	1.55	0.851	1.03	1.26	0.0	5.45	5.00	6.59	3.73	4.37	---
o mod. stiff	12.6	9.07	11.5	5.75	10.5	0.0	1.93	1.67	1.27	1.22	1.70	0.0	6.52	5.43	9.08	4.73	6.19	---
o soft	11.5	9.14	8.79	5.40	9.84	0.0	2.02	1.82	1.03	1.62	2.00	0.0	5.69	5.01	8.53	3.34	4.92	---
Artificial E./Q.B-1																		
o fixbase	8.42	7.17	4.24	7.13	8.85	0.0	2.13	1.79	0.849	1.98	2.40	0.0	3.96	4.02	4.99	3.59	3.68	---
o rock	9.08	7.78	4.39	7.32	9.36	0.0	2.22	1.82	0.931	2.02	2.46	0.0	4.08	4.27	4.71	3.63	3.81	---
o mod. stiff	12.3	8.14	7.29	8.95	13.1	0.0	2.79	2.08	1.81	2.37	3.17	0.0	4.39	3.91	4.03	3.77	4.14	---
o soft	11.6	10.0	7.78	11.4	15.5	0.0	3.18	2.54	1.64	3.12	3.80	0.0	3.66	3.94	4.76	3.65	4.08	---
Pacoima Dam, S16E																		
o fixbase	15.6	13.4	8.06	16.9	18.8	0.0	3.52	2.91	1.32	3.45	4.16	0.0	4.42	4.60	6.10	4.89	4.51	---
o rock	17.1	14.3	9.66	17.6	18.8	0.0	3.64	2.99	1.50	3.51	4.25	0.0	4.70	4.77	6.43	5.02	4.43	---
o mod. stiff	22.7	15.5	19.7	19.4	23.9	0.0	4.53	3.35	2.75	4.06	5.24	0.0	5.01	4.64	7.18	4.77	4.56	---
o soft	22.1	20.3	13.3	23.8	30.3	0.0	5.20	4.03	2.26	5.29	6.28	0.0	4.25	5.04	5.89	4.50	4.83	---

Table V-6

Response Shear Force ($x10^3$ kips)

RESPONSE CASE	PEAK (Time Domain)						R.M.S. (Freq. Domain)						PEAK FACTOR					
	0.0h	0.2h	0.4h	0.6h	0.8h	1.0h	0.0h	0.2h	0.4h	0.6h	0.8h	1.0h	0.0h	0.2h	0.4h	0.6h	0.8h	1.0h
El Centro Array 5, S50W																		
o fixbase	7.75	6.67	3.29	2.54	1.69	2.84	1.24	1.13	0.678	0.377	0.294	0.517	6.26	5.91	4.85	6.74	5.73	5.50
o rock	10.8	7.00	3.69	3.74	1.88	3.35	1.62	1.18	0.693	0.494	0.356	0.555	6.68	5.92	5.33	7.60	5.29	6.04
o mod. stiff	16.9	11.6	5.07	7.17	2.72	6.94	2.21	1.65	0.832	0.816	0.412	0.893	7.65	7.06	6.10	8.78	6.59	7.77
o soft	14.7	10.2	4.30	5.05	2.42	5.31	1.96	1.63	1.02	0.629	0.485	0.861	7.50	6.24	4.23	8.03	4.99	6.17
Artificial E./Q-B-1																		
o fixbase	7.61	6.49	4.12	2.33	2.05	3.79	1.84	1.70	1.14	0.561	0.572	0.959	4.13	3.81	3.63	4.15	3.58	3.94
o rock	10.7	6.96	4.53	3.17	2.75	3.95	2.28	1.77	1.21	0.708	0.657	1.02	4.71	3.92	3.74	4.49	4.18	3.88
o mod. stiff	15.1	11.9	5.87	5.39	3.50	6.69	3.45	2.62	1.42	1.29	0.789	1.55	4.39	4.54	4.14	4.17	4.44	4.30
o soft	13.6	10.4	6.43	4.86	3.11	6.31	3.25	2.74	1.72	1.05	0.883	1.54	4.17	3.80	3.73	4.62	3.52	4.09
Pacoima Dam, S16E																		
o fixbase	13.7	12.0	9.08	7.33	5.17	7.47	2.94	2.78	1.93	0.900	0.970	1.63	4.65	4.32	4.71	8.14	5.33	4.60
o rock	22.9	12.7	10.3	11.0	6.49	8.74	3.53	2.86	2.06	1.20	1.12	1.73	6.49	4.44	5.03	9.11	5.78	5.07
o mod. stiff	34.1	25.6	11.9	12.7	7.51	15.4	5.13	4.18	2.32	1.94	1.29	2.45	6.66	6.13	5.12	6.54	5.84	6.25
o soft	22.7	19.8	13.4	9.15	6.71	13.2	4.72	4.31	2.80	1.40	1.46	2.44	4.80	4.58	4.79	6.52	4.60	5.41

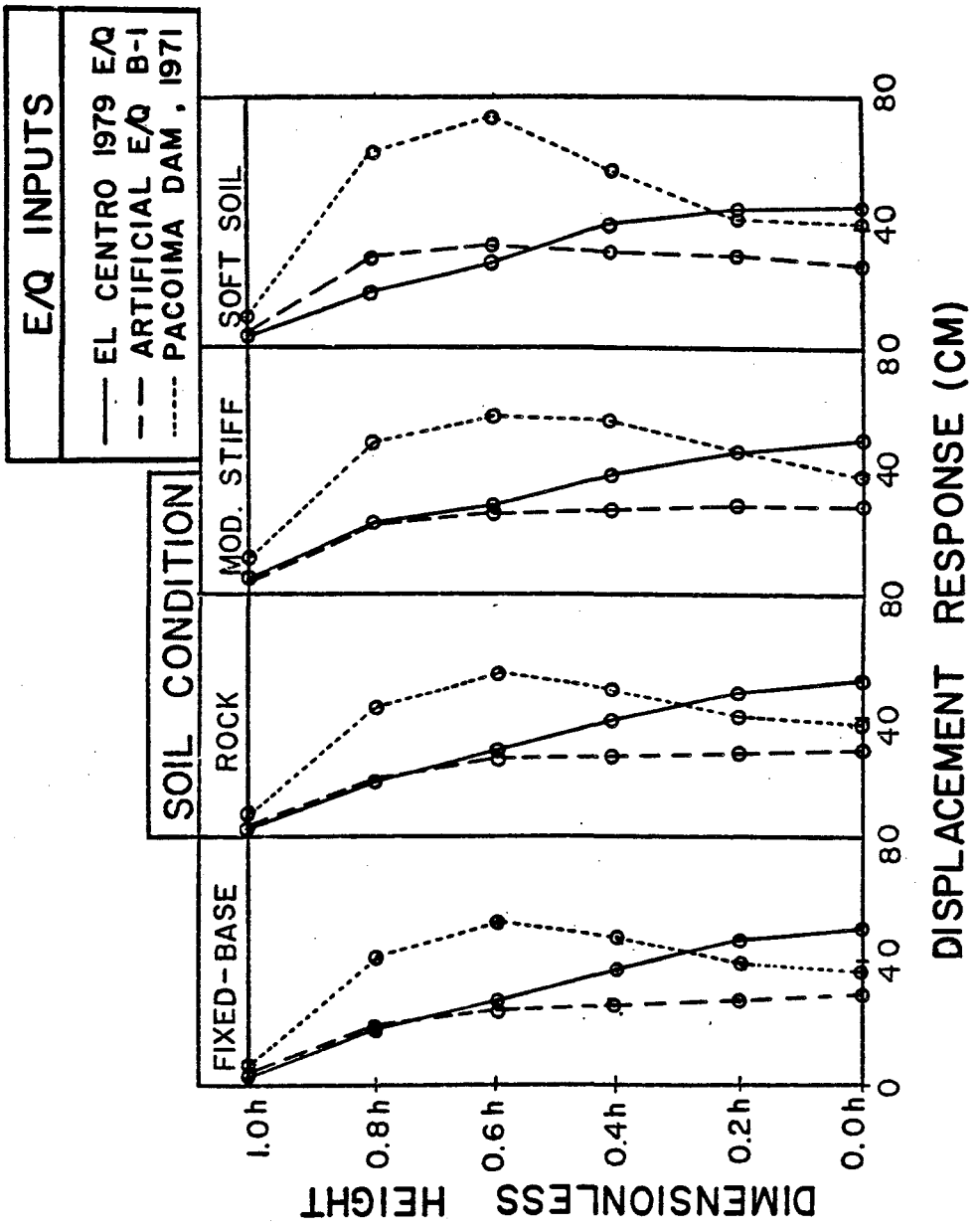

Fig. V-5 Time domain displacement response summary along the height of the Golden Gate tower.

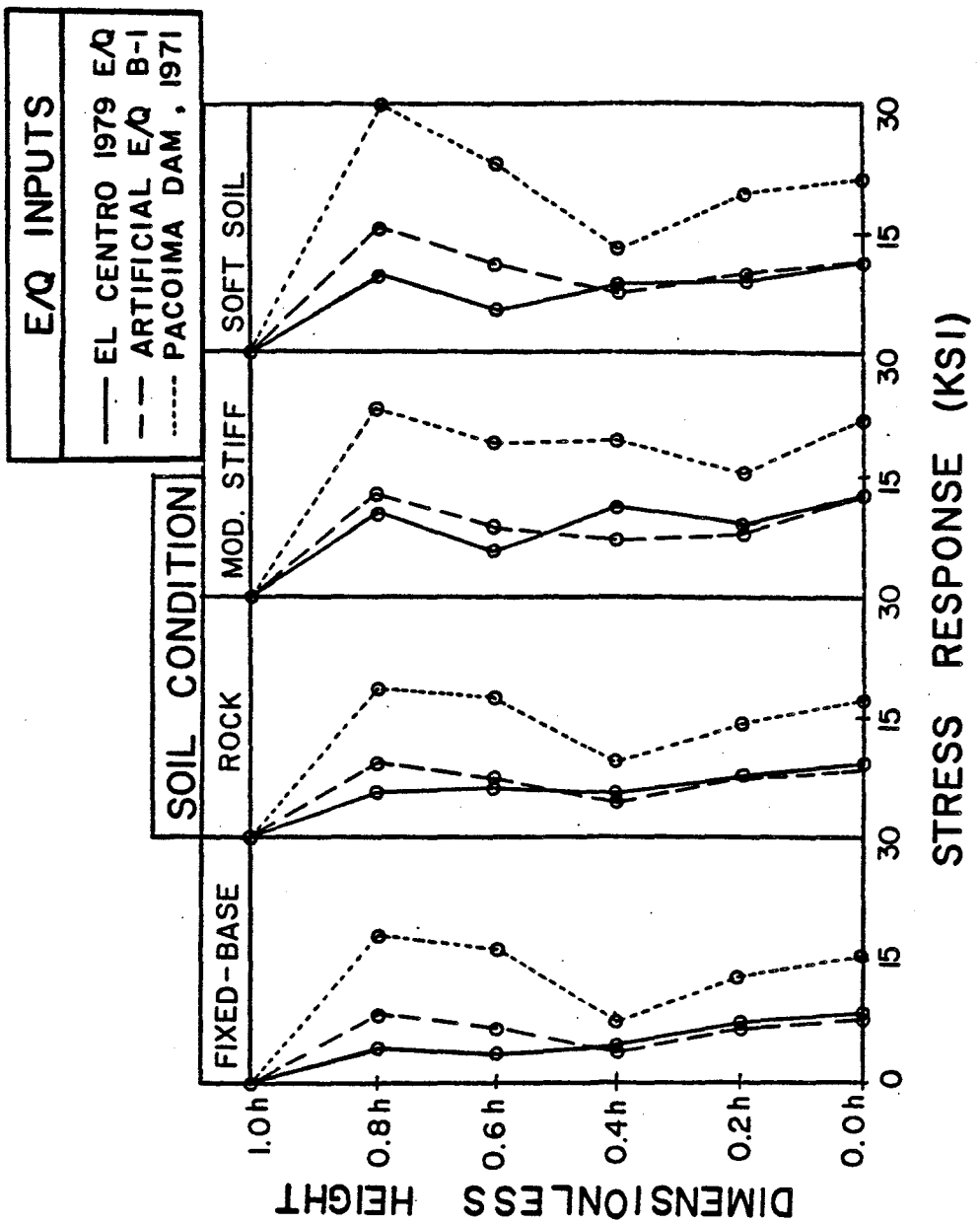

Fig. V-6 Time domain stress response summary along the height of the Golden Gate tower.

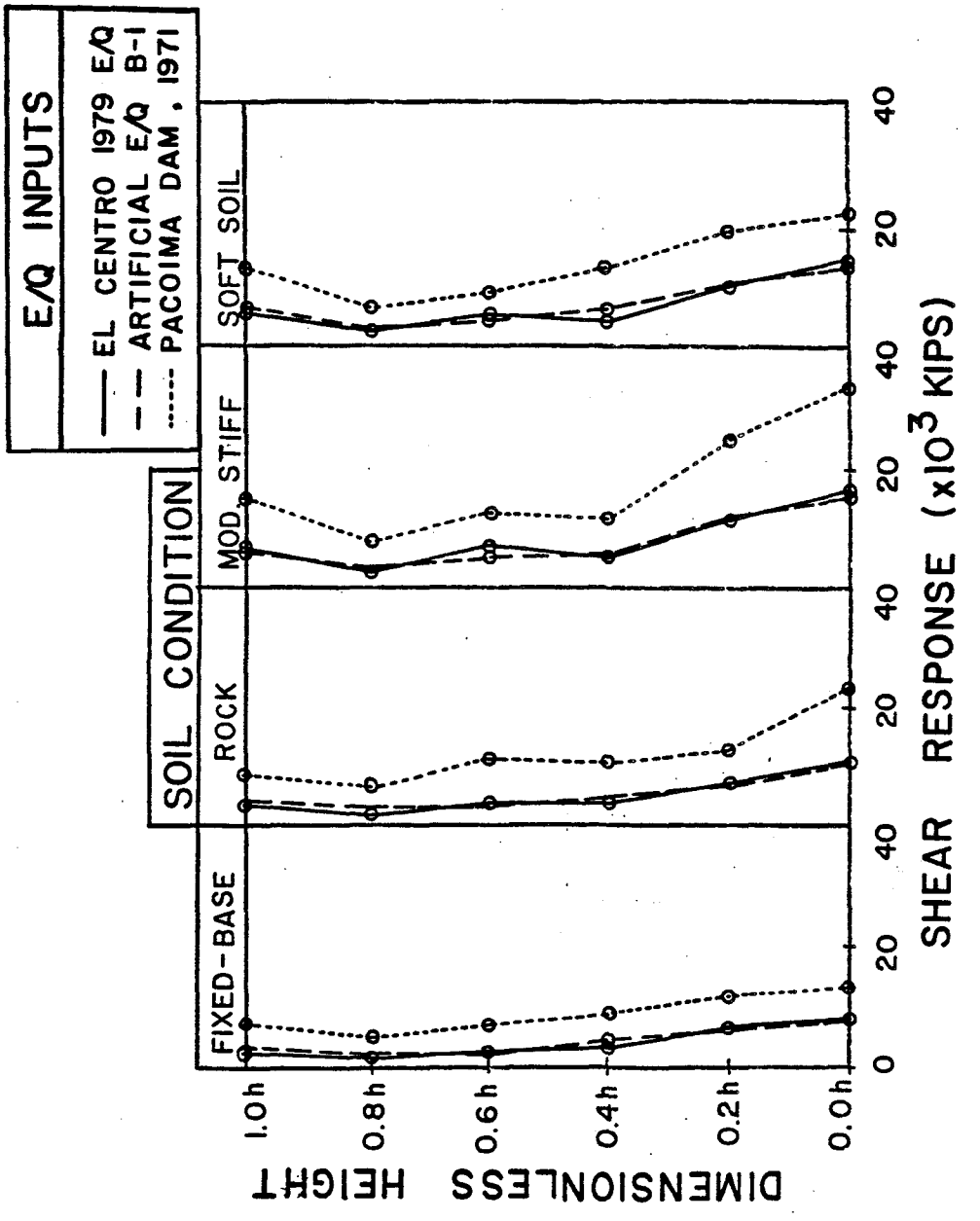

Fig. V-7 Time domain shear force response summary along the height of the Golden Gate tower.

time history responses appear in Appendices V-g, V-h, and V-i as a function of soil type, while the autospectra (frequency domain) responses appear in Appendices V-j, V-k, V-l, as a function of soil type. It is seen from these plots that the displacement near the bottom of the tower is mostly quasi-static (i.e., identical to ground displacement). Towards the top of the tower, the vibrational portion of the displacement becomes more important. It seems that the 1971 Pacoima Dam record excites the tower-pier's displacement response more strongly than the 1979 El Centro input record, both being stronger than the artificial earthquake (type B-1) input. The influence of soil condition upon the displacement response is not as dramatic as in the flexural stress and shear force response cases, however it still indicates that softer soil will tend to increase the tower-pier response. For the purpose of analyzing the response, five modes were utilized. However, the tower-pier appears to respond predominantly in its first two natural modes of longitudinal vibration. The flexural stress response (Appendix V-h) is almost totally vibrational in nature. It seems that the 1971 Pacoima Dam input gives higher stresses than the artificial earthquake earthquake (type B-1) input, both being stronger than the 1979 El Centro input case. The softness of the soil results in increased tower flexural stresses, as can be seen in these figures. The maximum stress of 30.3 ksi, occurring at 0.8h in the soft soil case, is a significant live load condition, but is well below the average yield value of 52.4 ksi for the silicon steel used in the tower (27). Even after adding the dead load stress of 7.93 ksi (21), stresses are still below the yield value. The longitudinal shear force response (Appendix V-i) is greatest at the base of the tower and decreases progressing up

the tower. The vibrational portion of the shear force dominates the response. It seems that the moderately stiff soil is critical, as far as the shear force is concerned, with a maximum base shear (1971 Pacoima Dam record) of 34,100 kips.

The corresponding root mean square (R.M.S.) results obtained from the random vibration frequency domain approach appear in Tables V-4, V-5, and V-6. By dividing the peak responses obtained in the time domain by these R.M.S. values, the estimation of peak factors may be examined. It can be seen that the peak factors range from 3.5 to 9.1, which is quite a large variation. The artificial earthquake input, which is designed to be Gaussian in nature, possesses peak factors which range from 3.5 to 5.0 which seem more realistic. The real earthquake inputs develop peak factors which are wider distributed in range. This may be due to the fact that they are real non-Gaussian inputs. The nature of the problem, that is the necessity for separation of the total response into quasi-static and vibrational parts, may also be partly responsible for the large peak factors.

Appendix V-a

Details of Mass and Stiffness Matrices

The general procedure as outlined by Abdel-Ghaffar (1) involves discretizing the tower-pier into elements (Figs. V-1, V-2). For simplicity, beam elements are used to model both the tower and the pier, with the moment of inertia of the pier elements set very high to accomodate only rigid body motion of the pier. Each beam element, as shown, has four degrees of freedom corresponding to end deflections and end rotations. The classic hermite polynomials are used as interpolation functions for the beam elements. The mass and stiffness matrices can be set up on the element level, and then assembled into the global mass and stiffness matrices. Concentrated masses arising from the tower struts and from the virtual mass of water surrounding the pier, and the distributed mass of water internal to the pier may also be added to the global mass matrix. Also, the effects of the elastic restraint of the cables and the soil stiffnesses can be added to the global stiffness matrix in the form of spring elements, as will be discussed. The resulting global mass and stiffness matrices are symmetric, positive-definite, banded matrices.

The mass matrix of the tower, arising from the kinetic energy of longitudinal vibration, can be written as

$$[M] = \sum_{e=1}^{N_{el}} [m_t]_e + \sum_{i=1}^{N_{ST}} m_{ST} + \sum_{j=1}^{2} m_{oj} \qquad \text{(V-a-1)}$$

where $[m_t]_e$ are the mass matrices on the element level; m_{ST} are the concentrated masses of the struts which vibrate longitudinally with the

tower; m_{oj} are the concentrated masses added at two of the pier nodes in order to represent the virtual mass of the surrounding water which vibrates with the pier; and the summation over the number of elements (N_{el}) and over the number of struts (N_{ST}) involves assembling each element mass matrix and each concentrated mass into the global mass matrix in its proper position.

The element mass matrices are (1)

$$[m_t]_e = \frac{m_{te}L}{420}\begin{bmatrix} 156 & -22L & 54 & 13L \\ -22L & 4L^2 & -13L & -3L^3 \\ 54 & -13L & 156 & 22L \\ 13L & -3L^2 & 22L & 4L^2 \end{bmatrix} \qquad \text{(V-a-2)}$$

where m_{te} is the distributed mass of the tower-pier element per unit length and L is the length of the element. The distributed masses, m_{te}, appear in Table V-a-1 for the Golden Gate's San Francisco Tower-Pier.

The added strut masses are calculated from the strut's dimensions, and are concentrated at the nodes at which the struts are located (nodes 9, 11, 13, 17, 21, 24, and 27; see Fig. V-2). These concentrated masses appear in Table V-a-2 for the Golden Gate's San Francisco Tower-Pier.

The added virtual mass of water can be computed by a simplified procedure (9, 17) which involves taking as added mass a cylindrical volume of water whose diameter is equal to the width of the pier (measured in the lateral direction; equals 299 ft for the Golden Gate) and whose length is equal to the depth of submergence of the pier.

Table V-a-1

Tower-Pier Element Properties (E=29000 ksi = 4,176,000 ksf)

ELEMENT	MASS/FT ($k sec^2/ft^2$)	INERTIA (ft^4)	LENGTH (ft)
1,2	168.7	∞	27.0
3	165.1	∞	10.0
4	144.8	∞	17.0
5	94.3	∞	18.0
6	32.7	∞	20.0
7	38.2	∞	24.0
8	2.067	34000	32.08
9,10	2.376	14436	40.16, 40.17
11,12	2.376	14436	40.17
13,14,15,16	2.067	14436	35.0
17,18,19,20	1.717	8131	32.5
21,22,23	1.415	5305	36.7, 36.7, 36.6
24,25,26	1.142	3073	33.0
27	1.142	3073	30.25

Table V-a-2

Additional Concentrated Masses

(Added Water Virtual Mass and Mass of Tower Struts)

NODE	MASS ($ksec^2/ft$)	
3	1889	water
4	71	
9	7.006	struts
11	7.006	
13	9.979	
17	11.04	
21	8.280	
24	8.492	
27	7.006	

A correction factor is then applied to this resulting mass based upon the ratio of the submerged depth to the diameter. The location of the centroid of this added mass is determined in a similar manner and is at a distance of approximately H/3, where H is the submerged depth in the case of the San Francisco Tower-Pier. In order to account for this added mass in the finite element model, it is sufficient (since the pier is assumed to move as a rigid body) to add two nodal concentrated masses whose values are adjusted so that the added mass and its centroidal location are both properly represented. In the case of the Golden Gate, these equivalent nodal masses (at nodes 3 and 4) appear in Table V-a-2.

The stiffness matrix has three contributions, one arising from the elastic stiffness of the tower, into which the elastic restraint of the cable and the soil's rotational (rocking) stiffness can be encorporated, one arising from the geometric-stiffness due to the compressive dead load cable tension, P_w, and one arising from the soil's translational stiffness, that is

$$[K] = \sum_{e=1}^{N_{el}} ([k_{te}]_e + [k_{tg}]_e) + \sum_{i=1}^{N_{TR}} [k_{TR}]_i \qquad \text{(V-a-3)}$$

where $[k_{te}]_e$ are the elastic stiffness matrices on the element level; $[k_{tg}]$ are the geometric stiffness matrices on the element level; $[k_{TR}]$ are the stiffness matrices resulting from the translational soil springs; and the summation over the number of elements (N_{el}) and over the number of translational soil springs (N_{TR}) involves assembling each element stiffness matrix into the global stiffness in its proper position.

The element elastic stiffness matrices, excepting the matrices for the uppermost tower element and the lowermost pier element, are as follows (1):

$$[k_{te}]_e = \frac{E_{te}I_{te}}{L^3}\begin{bmatrix} 12 & -6L & -12 & -6L \\ -6L & 4L^2 & 6L & 2L^2 \\ -12 & 6L & 12 & 6L \\ -6L & 2L^2 & 6L & 4L^2 \end{bmatrix} \qquad \text{(V-a-4)}$$

where $E_{te}I_{te}$ is the flexural rigidity of the individual element; and L is the element length (see Table V-a-1).

For the uppermost tower element, the elastic stiffness becomes

$$[k_{te}]_e = \frac{E_{te}I_{te}}{L^3}\begin{bmatrix} 12 & -6L & -12 & -6L \\ -6L & 4L^2 & 6L & 2L^2 \\ -12 & 6L & 12+k_e & 6L \\ -6L & 2L^2 & 6L & 4L^2 \end{bmatrix} \qquad \text{(V-a-5)}$$

where k_e is the spring stiffness arising from the elastic restraint of the cable estimated by Konishi and Yamada (Refs. 15, 16), and proven in Appendix V-e, to have a value of:

$$k_e = \frac{E_c A_c}{L_{e1}} + \frac{E_c A_c}{L_{e2}} \qquad \text{(v-a-6)}$$

where E_c is the cable's modulus of elasticity; A_c is the cable's cross-sectional area; and L_{e1}, L_{e2} are the virtual lengths defined as (1)

$$L_{ei} = \int_o^{\ell_i} \left(\frac{d_{si}}{d_{xi}}\right)^3 dx_i \qquad i = 1, 2 \qquad \text{(V-a-7)}$$

where s_i is a coordinate measured along the cable in the i^{th} span of the suspension bridge, and ℓ_i is the length of the i^{th} span.

For the lowermost pier element, the elastic stiffness becomes

$$[k_{te}]_e = \frac{E_{te} I_{te}}{L^3} \begin{bmatrix} 12+k_r & -6L & -12 & -6L \\ -6L & 4L^2 & 6L & 2L^2 \\ -12 & 6L & 12 & 6L \\ -6L & 2L^2 & 6L & 4L^2 \end{bmatrix} \qquad \text{(V-a-8)}$$

where k_r is a rotational spring at the pier's base (see Fig. V-2) which accounts for a portion of the rocking stiffness of the soil, the other portion being taken by the combination of translational springs. The equivalent structural springs shown in Fig. V-2 can be calculated from the soil stiffnesses k^o_{xx}, $k^o_{x\phi}$, $k^o_{\phi\phi}$ by the following relations

$$\left.\begin{aligned} k_1 + k_2 &= k^o_{xx} \\ (27\ \text{ft})k_2 &= k^o_{x\phi} \\ k_r + (27\ \text{ft})^2 k_2 &= k^o_{\phi\phi} \end{aligned}\right\} \qquad \text{(V-a-9)}$$

A summary of the values of k_1, k_2 and k_r appear in Table V-a-3 for the Golden Gate's San Francisco Tower-Pier system, based upon the soil stiffness k^o_{xx}, $k^o_{x\phi}$, $k^o_{\phi\phi}$ appearing in Table V-b-2 (Appendix V-b).

The element geometric stiffness matrices are as follows (1)

$$[k_{tg}]_e = \frac{-P_w}{30L} \begin{bmatrix} 36 & -3L & -36 & -3L \\ -3L & 4L^2 & 3L & -L^2 \\ -36 & 3L & 36 & 3L \\ -3L & -L^2 & 3L & 4L^2 \end{bmatrix} \qquad \text{(V-a-10)}$$

Table V-a-3

Equivalent Structural Springs

SOIL TYPE	k_1 (kips/ft)	k_2 (kips/ft)	k_r (kft/rad)
ROCK (G=172800 ksf)	7.527×10^7	2.933×10^7	8.242×10^{11}
MODERATELY STIFF SOIL (G=12960 ksf)	5.679×10^6	2.213×10^6	6.279×10^{10}
SOFT SOIL (G=3600 ksf)	1.627×10^6	6.341×10^5	1.892×10^{10}

where P_w is the compressive load arising from the vertical component of dead load of the cables (P_w = 123,000 kips).

The equivalent structural springs k_1 and k_2 (which represent the soil stiffness) give rise to stiffness matrices of the form

$$[k_{TR}]_i = \begin{bmatrix} k_i & -k_i \\ -k_i & k_i \end{bmatrix} \qquad i = 1, 2 \qquad \text{(V-a-11)}$$

where k_i appears in Table V-a-3 for the Golden Gate's San Francisco Tower-Pier.

Appendix V-b

Calculation of Soil Stiffness and Soil Damping

For the purpose of calculating the soil stiffness and damping values, it is first necessary to convert the elliptical cross-section of the pier to an equivalent circular cross-section. In order to calculate the equivalent radius for translation, R_t, it is sufficient to set the area of the ellipse equal to the area of the circle, that is

$$\pi R_t^2 = 0.7854(2A)(2B) \qquad \text{(V-b-1)}$$

where 2A is the major axis of the ellipse and 2B is the minor axis of the ellipse. For the Golden Gate Bridge's San Francisco tower, 2A = 299 ft and 2B = 155 ft which results in the equivalent circular radius for translation, R_t = 107.6 ft.

In order to calculate the equivalent circular radius for rocking, R_r, it is sufficient to set the second moment of inertia of the circle equal to that of the ellipse, that is

$$\frac{\pi}{4} R_r^4 = \frac{\pi}{4} AB^3 \qquad \text{(V-b-2)}$$

For the Golden Gate Bridge's San Francisco tower the equivalent circular radius for rocking, R_r = 91.3 ft.

For the purpose of calculating the soil stiffness and soil damping, the following equations are used by Kausel (13)

$$\left.\begin{aligned} k_{xx} &= k^o_{xx}\,(k_{11} + ia_o c_{11})(1 + 2i\beta) \\ k_{x\phi} &= k^o_{x\phi}(k_{12} + ia_o c_{12})(1 + 2i\beta) \\ k_{\phi\phi} &= k^o_{\phi\phi}(k_{22} + ia_o c_{22})(1 + 2i\beta) \end{aligned}\right\} \qquad \text{(V-b-3)}$$

where k^o_{xx}, $k^o_{\phi\phi}$, $k^o_{x\phi}$ are the static stiffness in translation, rocking, and coupled rocking-translation respectively; β is a measure of the internal hysteretic damping in the soil (taken to be 0.05 in this report); $i = \sqrt{-1}$; and a_o is the dimensionless frequency = $\omega R/c_s$; where ω is the circular frequency of the exciting motion, R is the radius of the foundation slab, and c_s is the shear wave velocity; k_{ij} and c_{ij} are frequency dependent coefficients normalized with respect to the static stiffness and obtained via halfspace solutions or modified halfspace solutions. The coefficients c_{ij} express energy loss by radiation.

For the static case, $k_{11} = k_{12} = k_{22} = 1$ (13) and

$$\left.\begin{aligned} k^o_{xx} &= \frac{8GR_t}{2-\nu}\left(1+\frac{1}{2}\frac{R_t}{H}\right)\left(1+\frac{2}{3}\frac{E}{R_t}\right)\left(1+\frac{5}{4}\frac{E}{H}\right) \\ k^o_{x\phi} &= k^o_{xx}\, R_r\left(\frac{2}{5}\frac{E}{R_r}-0.03\right) \\ K^o_{\phi\phi} &= \frac{8GR_r^3}{3(1-\nu)}\left(1+\frac{1}{6}\frac{R_r}{H}\right)\left(1+2\frac{E}{R_r}\right)\left(1+0.71\frac{E}{H}\right) \end{aligned}\right\} \qquad \text{(V-b-4)}$$

where G is the shear modulus of the soil; R is the radius of the foundation; E is the depth of embedment; H is the depth to bedrock; and ν = Poisson's ratio. The stiffness and damping coefficients k_{ij} and c_{ij} appear in graphical form in Ref. 13 and will not be repeated here.

In order to use modal analysis, frequency independent stiffness and damping values are utilized. Since the stiffness coefficients k_{ij} are slowly varying functions of the dimensionless frequency a_o, (13) it appears appropriate to calculate the longitudinal

tower modes using the static stiffness values (Eq. V-b-4). Once the tower modes and associated natural frequencies are obtained, the damping coefficients c_{ij} may be computed for each mode from knowledge of the dimensionless frequency $a_o = \omega_n R/C_s$ where ω_n is the natural circular of the n^{th} tower mode. The total damping is the sum of internal hysteretic damping and radiation damping, as follows:

$$\left.\begin{aligned} c_{xx} &= k^o_{xx}(a_o c_{11} + 2\beta) \\ c_{x\phi} &= k^o_{x\phi}(a_o c_{12} + 2\beta) \\ c_{\phi\phi} &= k^o_{\phi\phi}(a_o c_{22} + 2\beta) \end{aligned}\right\} \qquad \text{(V-b-5)}$$

The above methodology was used for three different soil types, corresponding to rock, moderately stiff soil, and soft soil. A summary of the soil parameters is shown in Table V-b-1 (14). The resulting soil stiffnesses are shown in Table V-b-2 which are computed using Eqs. V-b-4. The soil damping values are shown in Table V-b-3 as a function of soil type and natural mode (of the Golden Gate Tower-Pier), which are computed using Eqs. V-b-5.

Table V-b-1

Soil Properties (Based on Ref. 13)

MATERIAL PROPERTY	ROCK	MODERATELY STIFF SOIL	SOFT SOIL
C_s = shear wave velocity (ft/sec)	5900	1900	1076
ν = Poisson's ratio	0.34	0.35	0.40
G = modulus (ksf)	172800	12960	3600

Table V-b-2

Soil Stiffnesses (Based on Ref. 13)

SOIL TYPE	k°_{xx} (kips/ft)	$k^{\circ}_{x\phi}$ (kips)	$k^{\circ}_{\phi\phi}$ (ft kips/rad)
Rock	1.046×10^{8}	7.920×10^{8}	8.456×10^{11}
Moderately Stiff Soil	7.892×10^{6}	5.976×10^{7}	6.440×10^{10}
Soft soil	2.261×10^{6}	1.712×10^{7}	1.938×10^{10}

Table V-b-3

Soil Damping (Based on Ref. 13)

SOIL TYPE/ MODE ORDER	C_{xx} ($\times 10^6$ ksec/ft)	$C_{x\phi}$ ($\times 10^6$ ksec)	$C_{\phi\phi}$ ($\times 10^9$ kftsec/rad)
Rock			
Mode 1	2.411	18.26	19.12
Mode 2	0.8244	6.242	6.319
Mode 3	0.5742	4.348	3.887
Mode 4	1.370	10.37	3.414
Mode 5	1.277	9.669	3.602
Moderately Stiff Soil			
Mode 1	0.1914	1.449	1.478
Mode 2	0.3181	2.409	0.8066
Mode 3	0.3010	2.279	0.8426
Mode 4	0.2890	2.188	0.9143
Mode 5	0.2781	2.106	0.9974
Soft Soil			
Mode 1	0.0604	0.4849	0.5072
Mode 2	0.1540	1.166	0.4410
Mode 3	0.1472	1.115	0.4790
Mode 4	0.1397	1.058	0.5370
Mode 5	0.1371	1.038	0.5524

Appendix V-c

Calculation of Equivalent Modal Damping Ratios

An approximate energy method is utilized here to convert the soil damping values obtained in Appendix V-b to equivalent modal damping ratios, in order to proceed directly with a modal analysis approach. The following procedure was proposed by Novak (18).

Assuming that the undamped vibration modes of the tower have been determined with the soil stiffnesses taken into account, the total work done by the soil damping during a period T, as the pier undergoes harmonic motion in the n^{th} natural mode, is given by (18)

$$W = \int_o^T C_{xx} u_n^2 \omega_n^2 \cos^2 \omega_n t \, dt + \int_o^T C_{\phi\phi} \phi_n^2 \omega_n^2 \cos^2 \omega_n t \, dt$$

$$+ 2 \int_o^T C_{x\phi} \phi_n u_n \omega_n^2 \cos^2 \omega_n t \, dt \qquad \text{(V-c-1)}$$

which reduces to

$$W = \pi \omega_n (C_{xx} u_n^2 + C_{\phi\phi} \phi_n^2 + 2 C_{x\phi} u_n \phi_n) \qquad \text{(V-c-2)}$$

where C_{xx}, $C_{x\phi}$, $C_{\phi\phi}$ are the soil damping values (see Appendix V-b); ω_n is the natural circular frequency of the n^{th} longitudinal tower mode; and u_n and u_ϕ are modal translational and rotational displacement at the pier's base, respectively, taken in arbitrary scale.

The maximum potential energy for the complete tower vibrating in its n^{th} mode can be calculated as the maximum kinetic energy and is given by (18)

$$L = \sum_{i=1}^{n} \frac{1}{2} \{\phi_n\}^T [M] \{\phi_n\} \qquad \text{(V-c-3)}$$

where [M] is the mass matrix for the entire tower-pier; and $\{\phi_n\}$ represents the n^{th} mode shape for the tower-pier.

The damping ratio of the structure, due to the geometric and hysteric damping of the soil, in the n^{th} mode, can then be calculated as $\xi_n^{soil} = W/(4\pi L)$ which is

$$\xi_n^{soil} = \frac{1}{2\omega_n M_n} (C_{xx} u_n^2 + C_{\phi\phi} \phi_n^2 + 2C_{x\phi} u_n \phi_n) \qquad \text{(V-c-4)}$$

where M_n is the generalized modal mass

$$M_n = \{\phi_n\}^T [M] \{\phi_n\} \qquad \text{(V-c-5)}$$

The total damping ratio is the sum of the structural damping ratio (taken as 0.05 in all modes) and the damping ratio derived from the underlying soil (Eq. V-c-4), that is

$$\xi_n^{eq} = \xi_n^{st} + \xi_n^{soil} \qquad \text{(V-c-6)}$$

This approximate approach is quite accurate since the damping is very important only in the resonant range. Hence, as long as damping is small and natural frequencies are well separated, the method works fairly well (Ref. 18). This energy method is equivalent to neglecting the off-diagonal terms in the generalized damping matrix $\{\phi_n\}^T [C] \{\phi_n\}$. Table V-c-1 summarized the damping ratios of the Golden Gate San Francisco Tower-Pier for the three soil types as compared to the case of a com-

Table V-c-1

Composite Damping Ratios ξ_n^{eq} (Based on Ref. 18)

	SOIL-FOUNDATION TYPE			
MODE ORDER	FIXED BASE	ROCK	MODERATELY STIFF SOIL	SOFT SOIL
1	0.0500	0.0501	0.0508	0.0533
2	0.0500	0.0501	0.0584	0.2479
3	0.0500	0.0502	0.2651	0.0995
4	0.0500	0.0508	0.0744	0.1498
5	0.0500	0.0679	0.0814	0.4444

pletely fixed base pier, where only structural damping is present (estimated to be 5%).

Appendix V-d

Orthogonality of Longitudinal Tower Mode Shapes

The n^{th} longitudinal tower mode shape, $\{\phi_n\}$, satisfies the equation

$$\omega_n^2[M_{ss}]\{\phi_n\} = [K_{ss}]\{\phi_n\} \qquad n = 1, 2, 3... \qquad \text{(V-d-1)}$$

The m^{th} longitudinal tower mode shape, $\{\phi_m\}$, satisfies a similar equation, that is

$$\omega_m^2[M_{ss}]\{\phi_m\} = [K_{ss}]\{\phi_m\} \qquad m = 1, 2, 3... \qquad \text{(V-d-2)}$$

Premultiplying Eq. V-d-1 by $\{\phi_m\}^T$, premultiplying Eq. V-d-2 by $\{\phi_n\}^T$ and subtracting gives

$$\omega_n^2\{\phi_m\}^T[M_{ss}]\{\phi_n\} - \omega_m^2\{\phi_n\}^T[M_{ss}]\{\phi_m\}$$

$$= \{\phi_m\}^T[K_{ss}]\{\phi_n\} - \{\phi_n\}^T[K_{ss}]\{\phi_m\}$$

$$n = 1, 2, 3 \ldots \qquad m = 1, 2, 3 \ldots$$

(V-d-3)

Because the stiffness and mass matrices resulting from the finite element method are symmetric and positive-definite, Eq. V-d-3 reduces to

$$(\omega_n^2 - \omega_m^2)\{\phi_m\}^T[M_{ss}]\{\phi_n\} = 0$$

$$n = 1, 2, 3 \ldots \qquad m = 1, 2, 3 \ldots \qquad \text{(V-d-4)}$$

which yields modal orthogonality, with respect to mass matrix weighting, of the form

$$\{\phi_m\}^T[M_{ss}]\{\phi_n\} = 0 \qquad m \neq n \qquad \text{(V-d-5)}$$

Appendix V-e

Derivation of Equivalent Spring Constant k_e

The idea of assuming an equivalent spring of stiffness k_e at the tower top (to simulate the elastic restraint of the cables) was explained by Abdel-Ghaffar (28).

The elastic strain energy stored in the cable due to change in tension associated with $H_i(t)$ $(i = 1, 2, 3)$ can be written as

$$V_{ce}(t) = \frac{1}{2} \sum_{i=1}^{3} \frac{H_i^2(t)\, L_{ei}}{E_c A_c} \qquad \text{(V-e-1)}$$

where E_c is the cable's modulus of elasticity; A_c is the cable's cross-sectional area and L_{ei} are the virtual lengths defined as (1)

$$L_{ei} = \int_0^{\ell_i} \left(\frac{ds_i}{dx_i}\right)^3 dx_i \qquad i = 1, 2, 3 \qquad \text{(V-e-2)}$$

where s_i is a coordinate measured along the cable in the i^{th} span of the suspension bridge, and ℓ_i is the length of the i^{th} span.

For any tower, the energy stored in the cable in the two adjacent spans is

$$V_{ce}(t) = \frac{1}{2} \frac{H_1^2(t) L_{ei}}{E_c A_c} + \frac{1}{2} \frac{H_2^2(t) L_{e2}}{E_c A_c} \qquad \text{(V-e-3)}$$

Each term of Eq. V-e-3 is similar to the elastic energy in an axially loaded truss member which is of the form

$$V(t) = \frac{1}{2} \frac{F^2(t)L}{EA} \qquad \text{(V-e-4)}$$

where $\frac{EA}{L}$ is the axial rigidity (or stiffness) of the truss member.

Thus, the equivalent stiffness at the tower top can be approximated by

$$k_e \simeq \frac{E_c A_c}{L_{e1}} + \frac{E_c A_c}{L_{e2}} = k_{e1} + k_{e2} \qquad \text{(V-e-5)}$$

APPENDIX V-f

PACOIMA DAM RECORD INPUTS

(1971 San Fernando Earthquake)

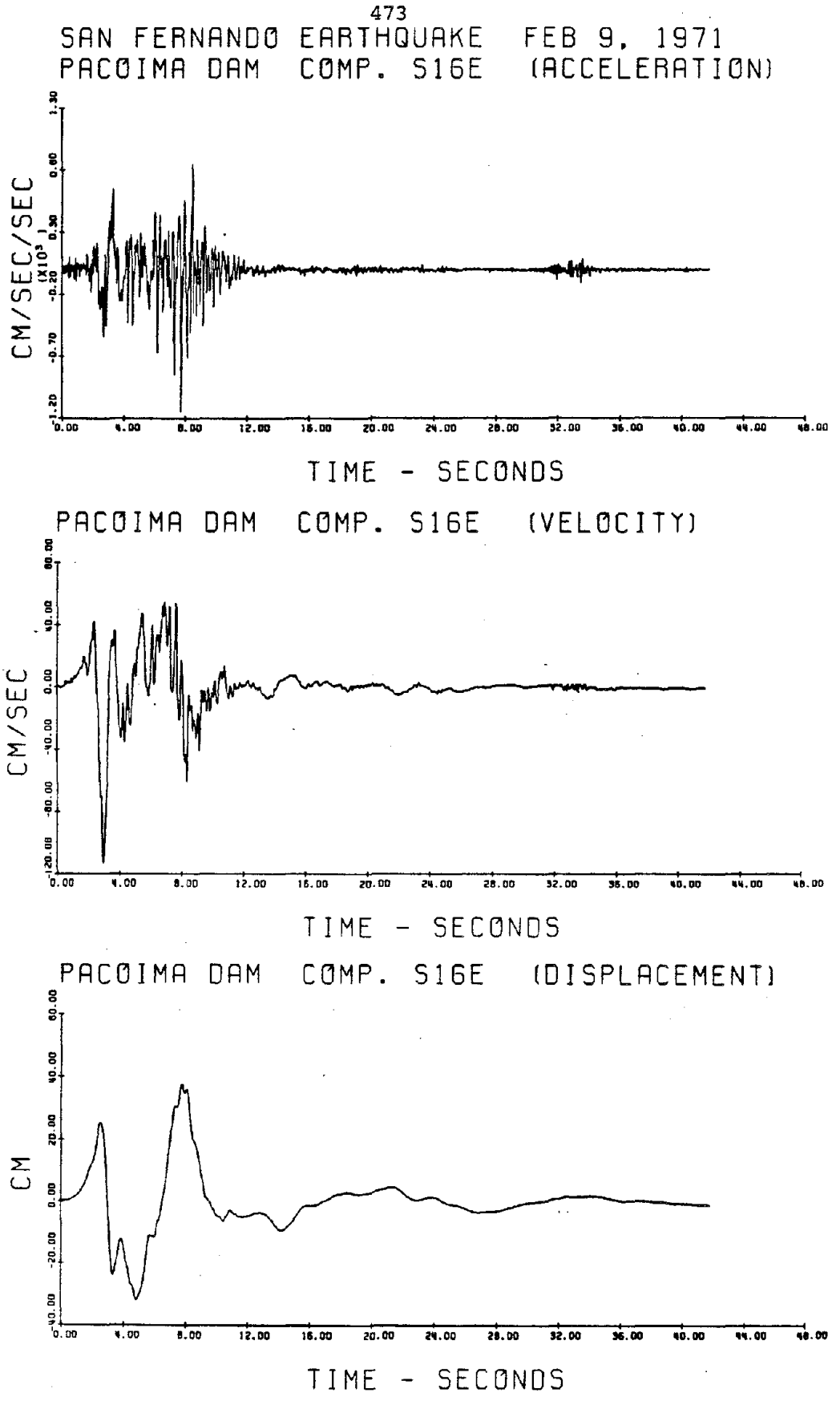

Fig. V-f-1 Time history of Pacoima Dam component S16E record (San Fernando 1971 Earthquake).

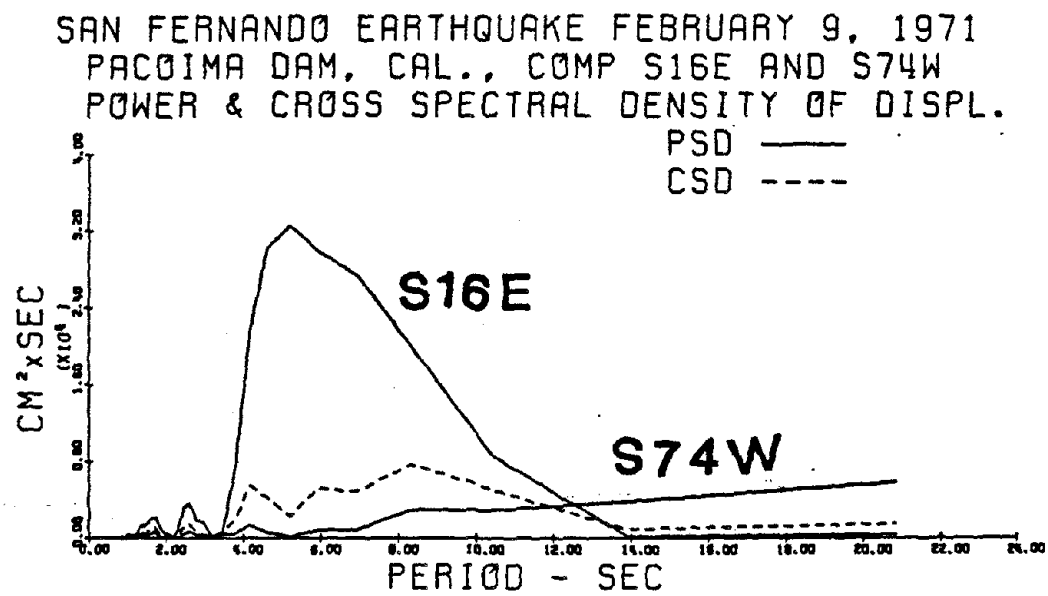

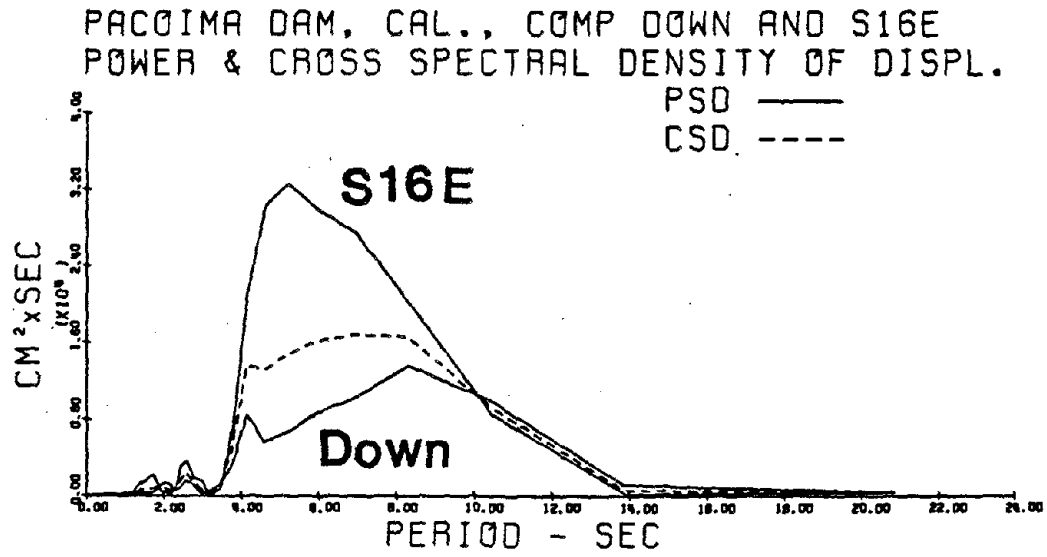

Fig. V-f-2 Power and cross-spectra of the Pacoima Dam Records (San Fernando 1971 Earthquake)

APPENDIX V-g

TIME DOMAIN DISPLACEMENT RESPONSE OF THE GOLDEN GATE TOWER-PIER SYSTEM

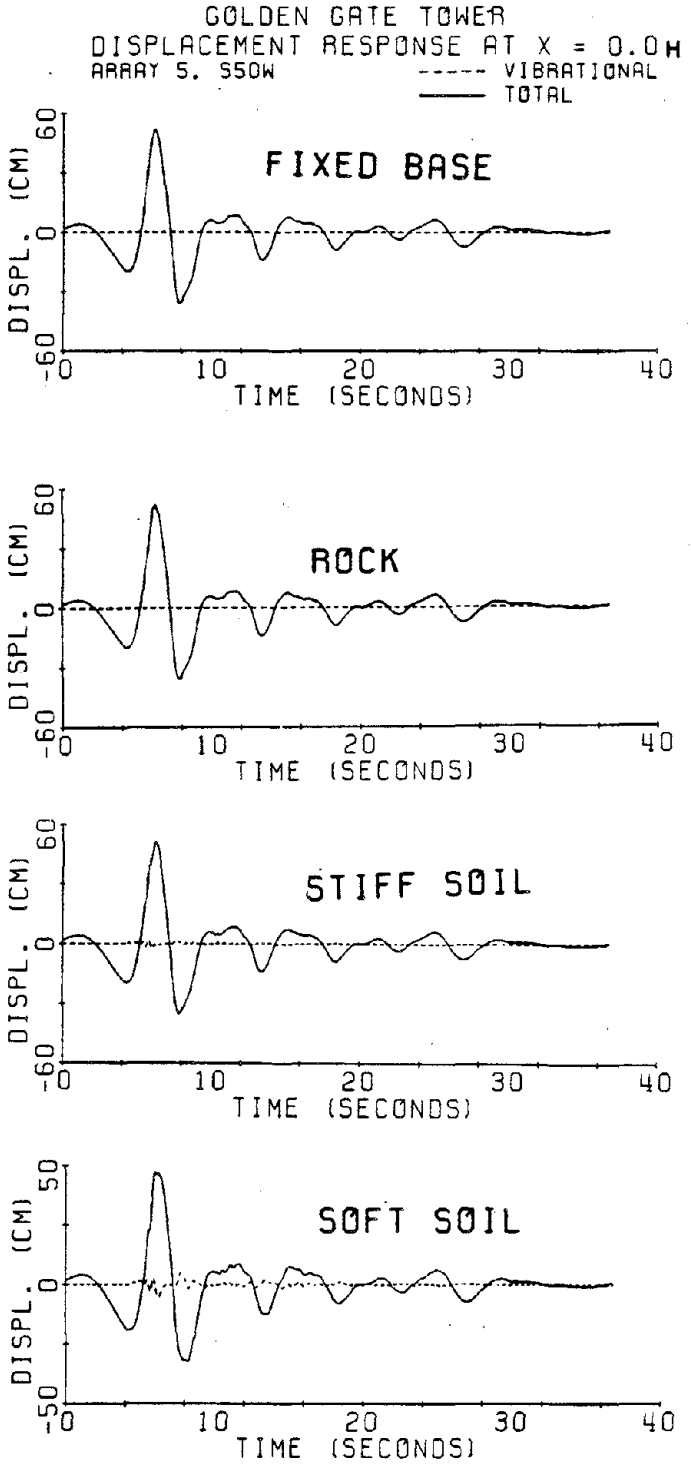

Fig. V-g-1 Time history displacement response at bottom of tower to 1979 El Centro Array 5 input.

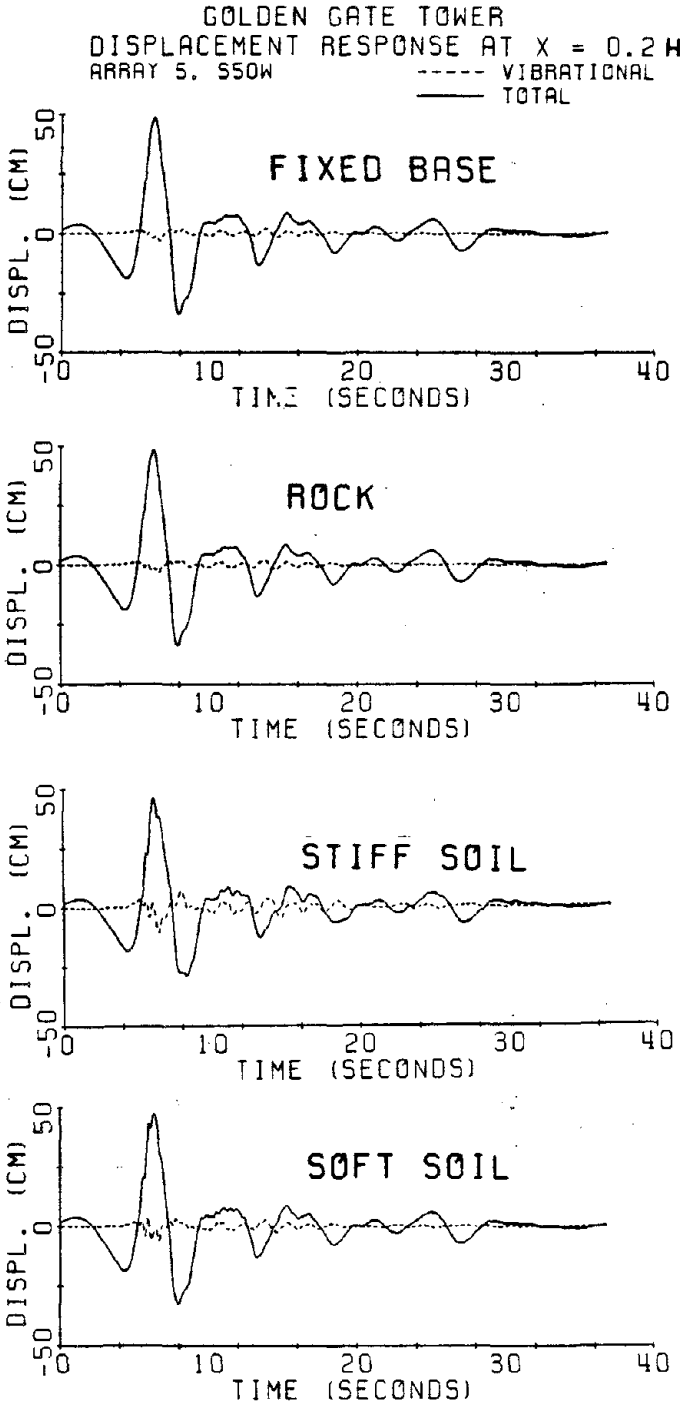

Fig. V-g-2 Time history displacement response at x = 0.2h to 1979 El Centro Array 5 input.

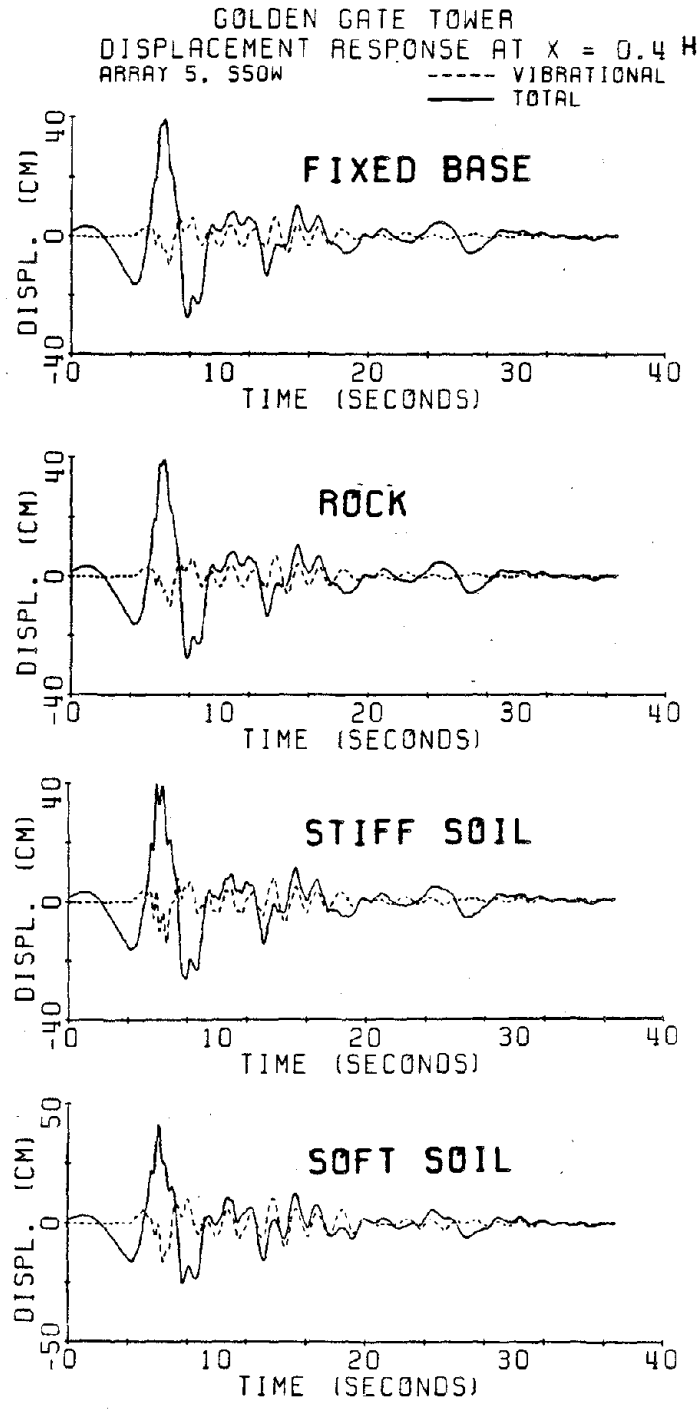

Fig. V-g-3 Time history displacement response at x = 0.4h to 1979 El Centro Array 5 input.

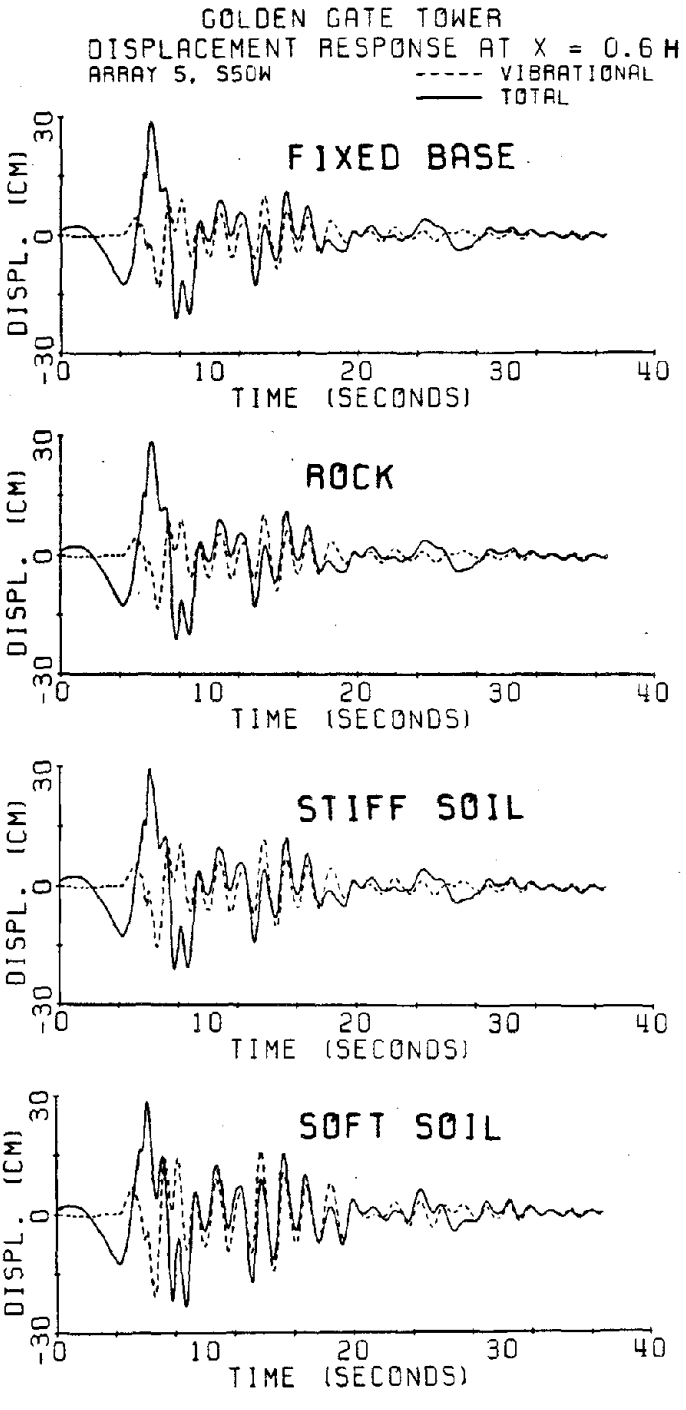

Fig. V-g-4 Time history displacement response at x = 0.6h to 1979 El Centro Array 5 input.

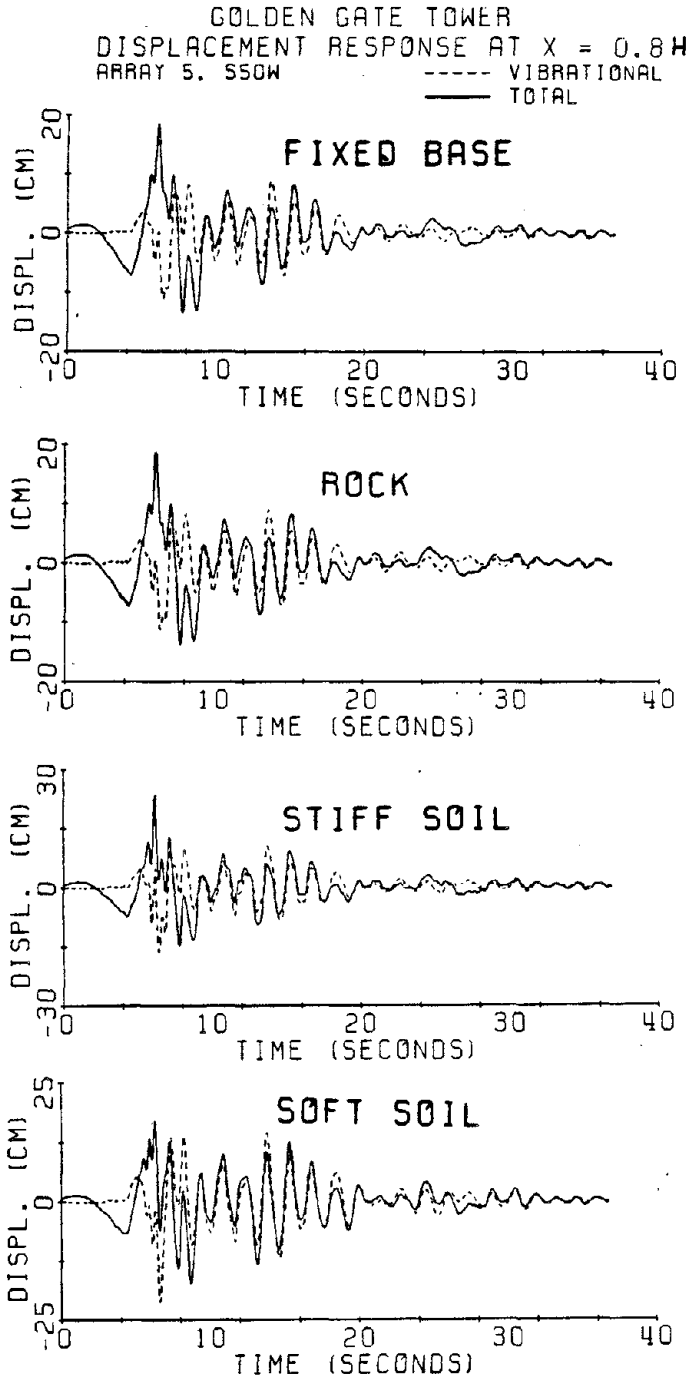

Fig. V-g-5 Time history displacement response at x = 0.8h to 1979 El Centro Array 5 input.

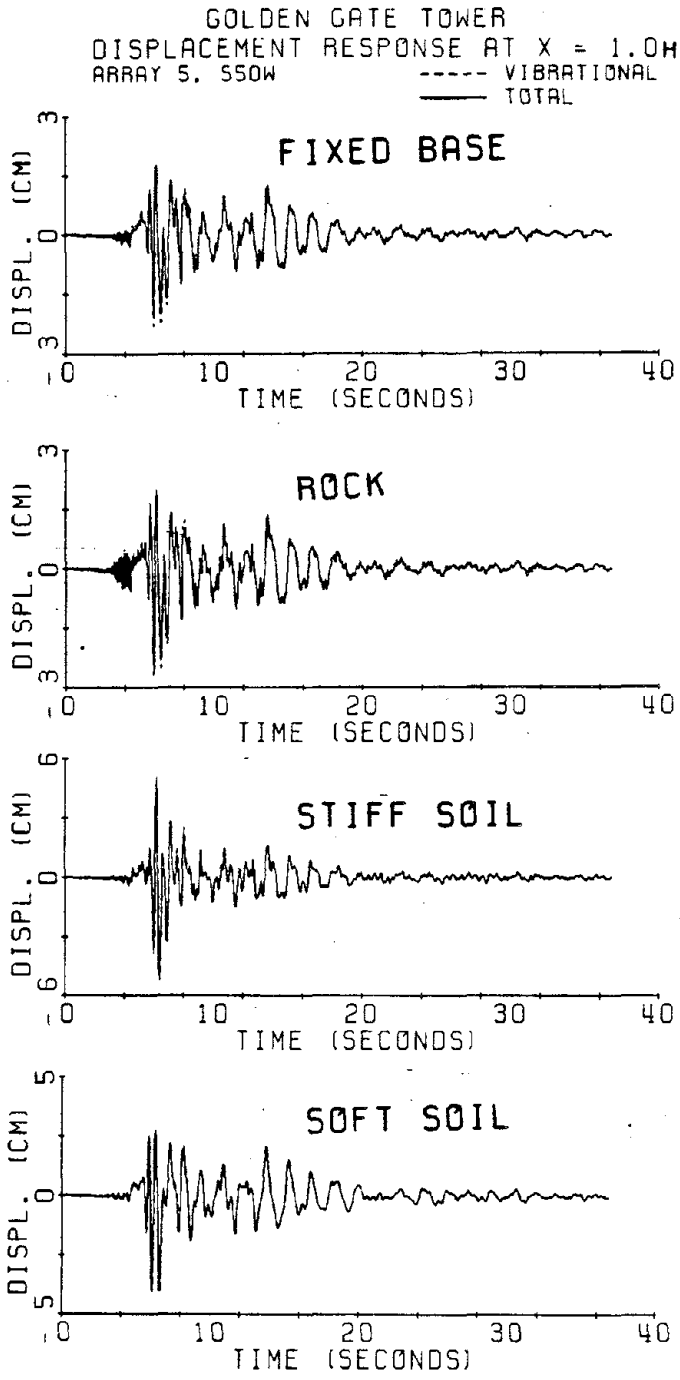

Fig. V-g-6 Time history displacement response at top of tower to 1979 El Centro Array 5 input.

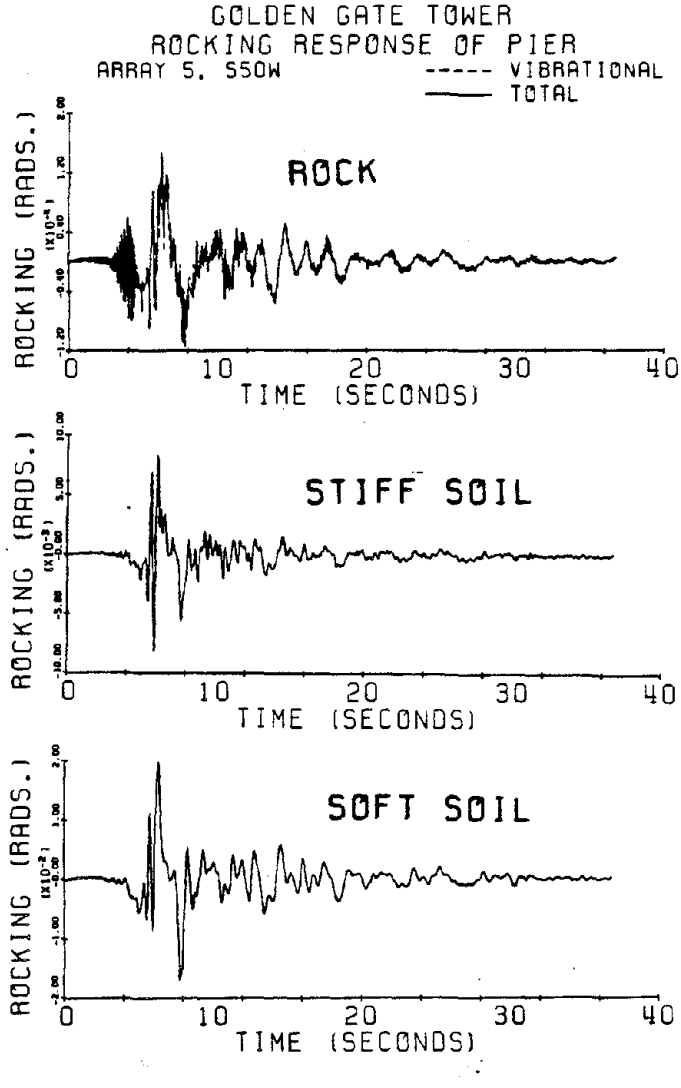

Fig. V-g-7 Time history rocking response of pier to 1979 El Centro Array 5 input.

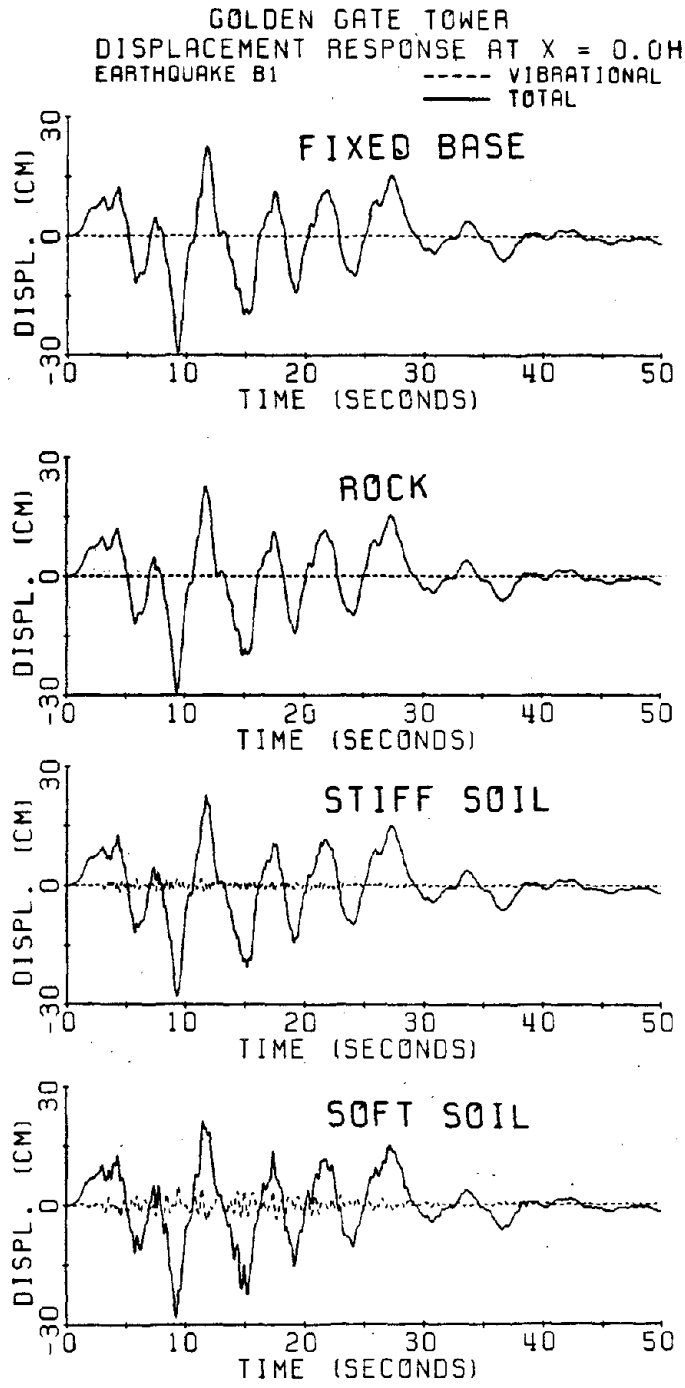

Fig. V-g-8 Time history displacement response at bottom of tower to artificial earthquake B-1 input.

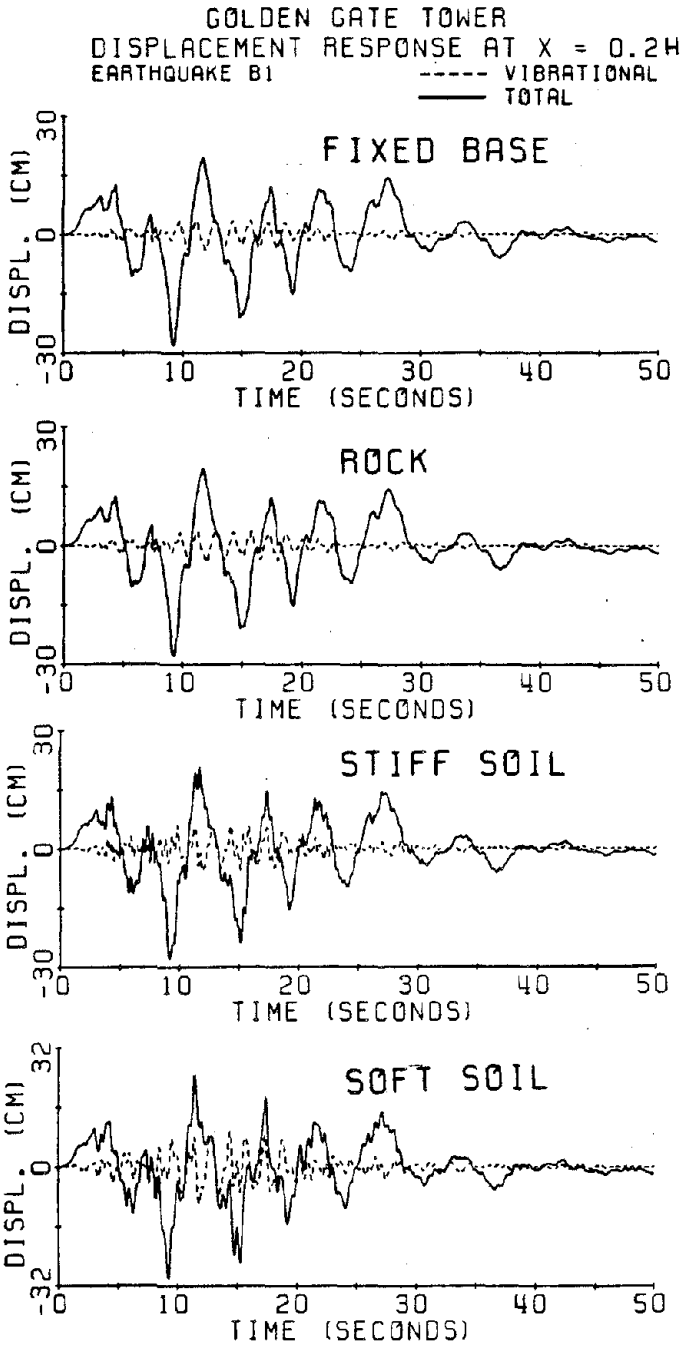

Fig. V-g-9 Time history displacement response at x = 0.2h to artificial earthquake B-1 input.

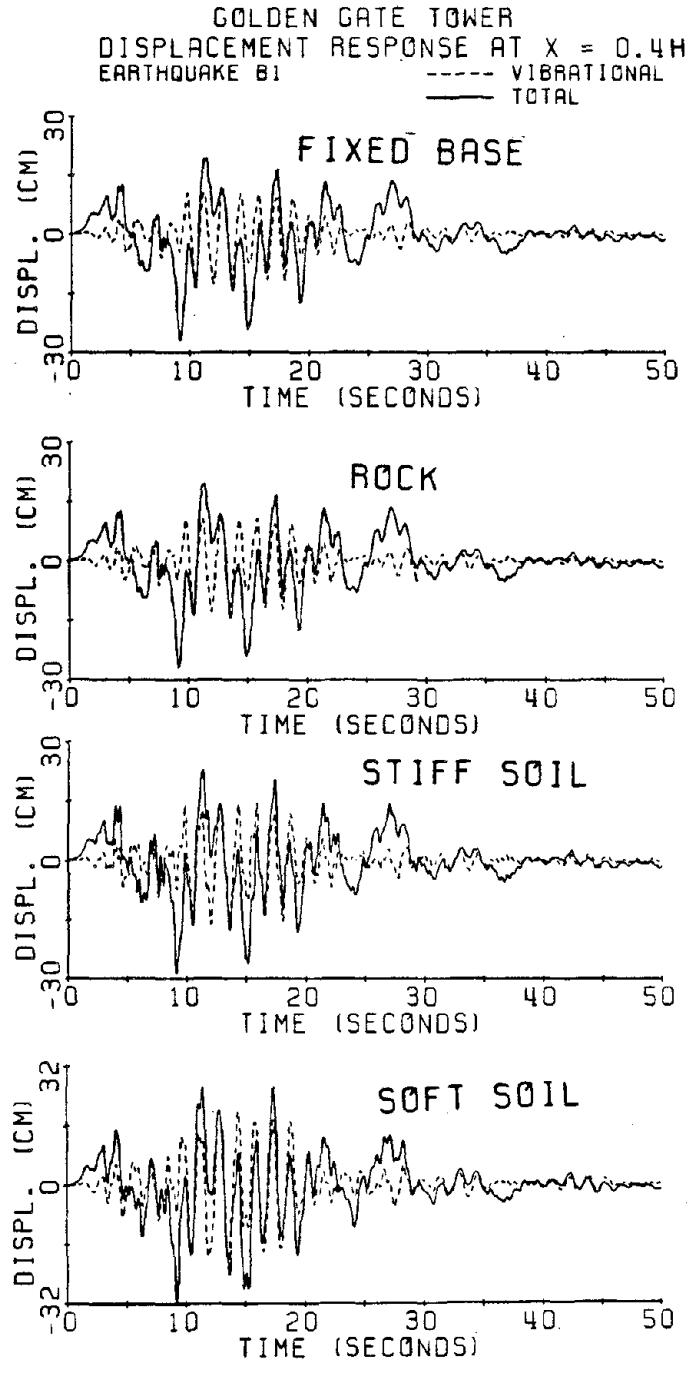

Fig. V-g-10 Time history displacement response at x = 0.4h to artificial earthquake B-1 input.

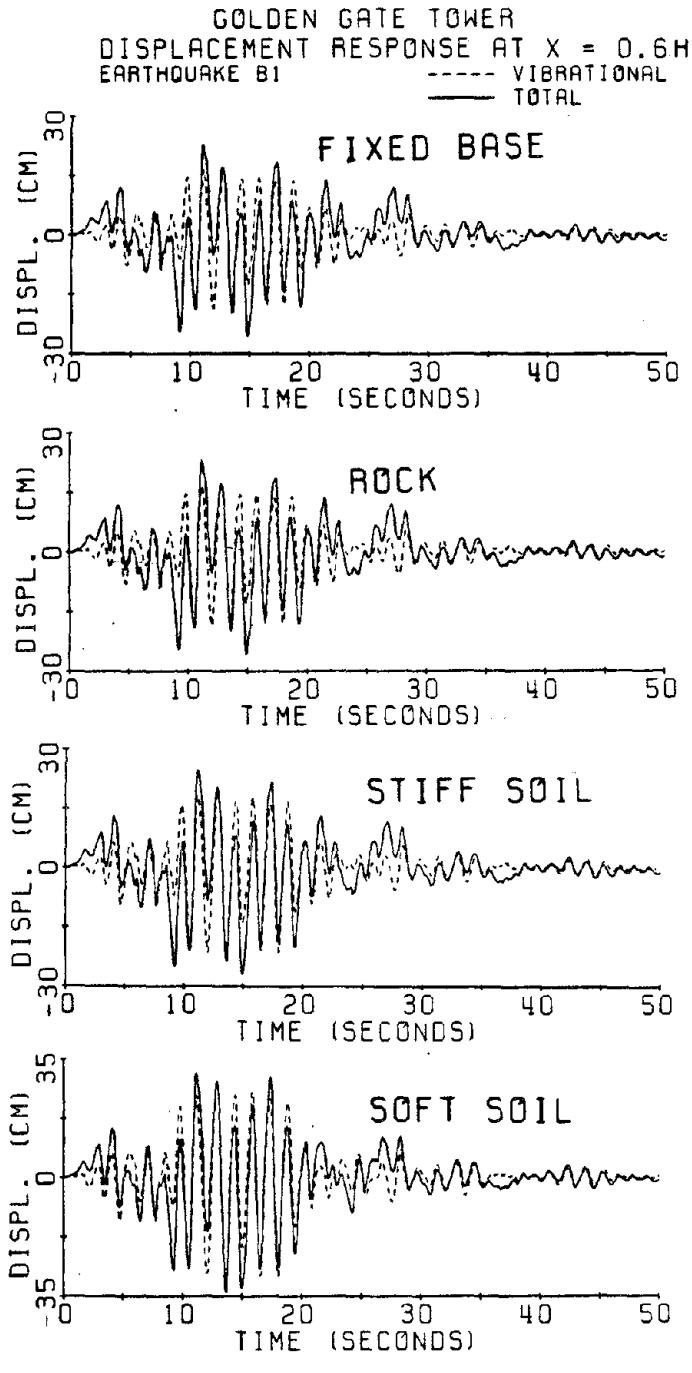

Fig. V-g-11 Time history displacement response at x = 0.6h to artificial earthquake B-1 input.

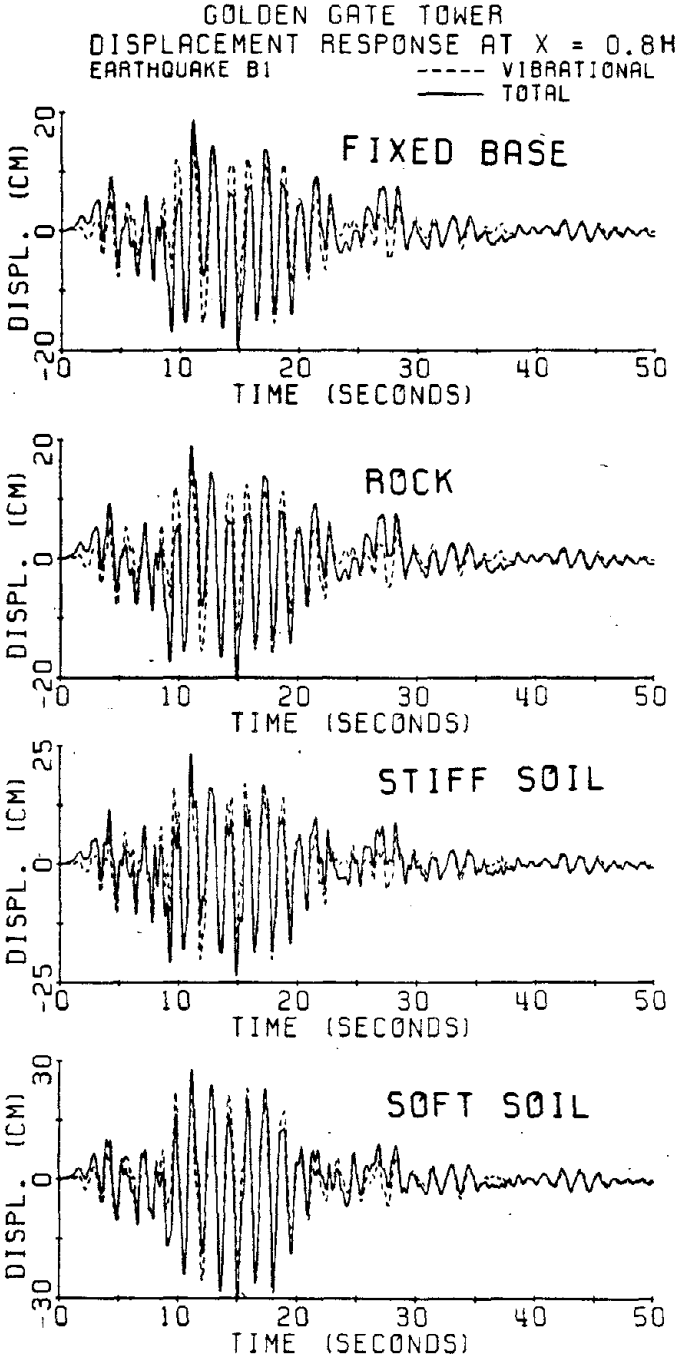

Fig. V-g-12 Time history displacement response at x = 0.8h to artificial earthquake B-1 input.

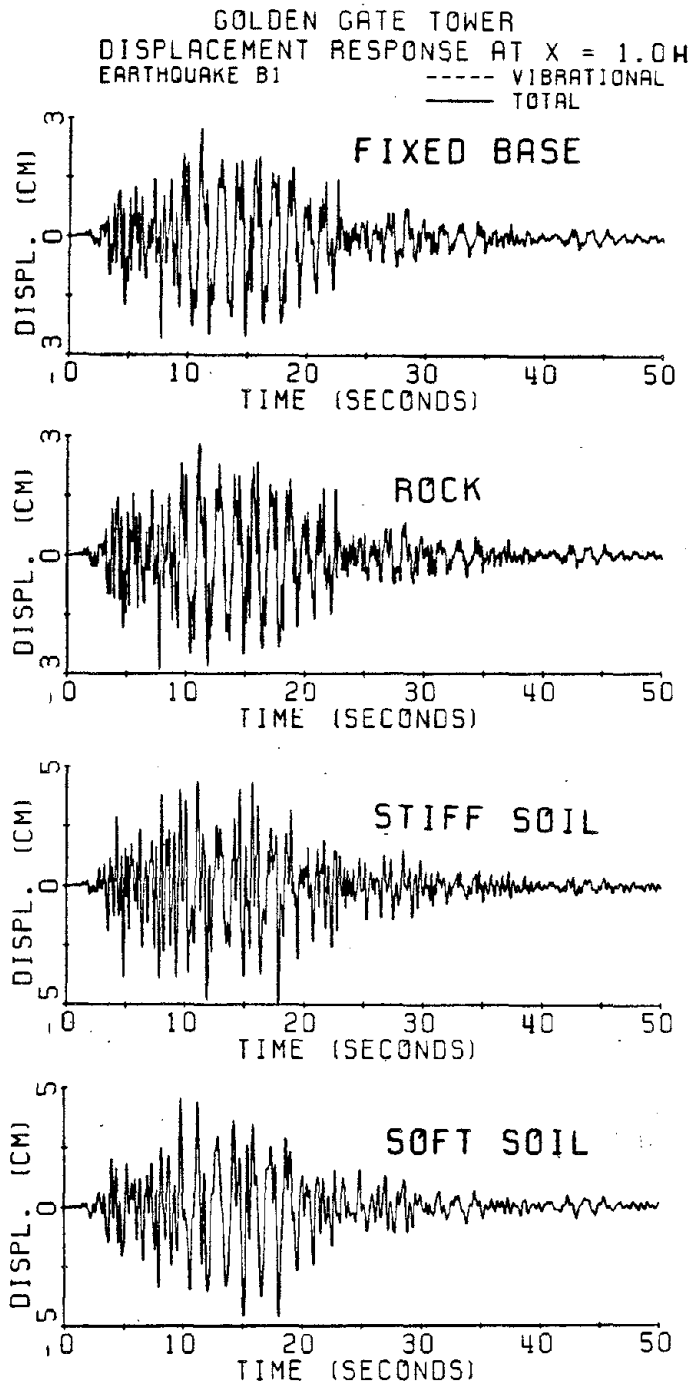

Fig. V-g-13 Time history displacement response at top of tower to artificial earthquake B-1 input.

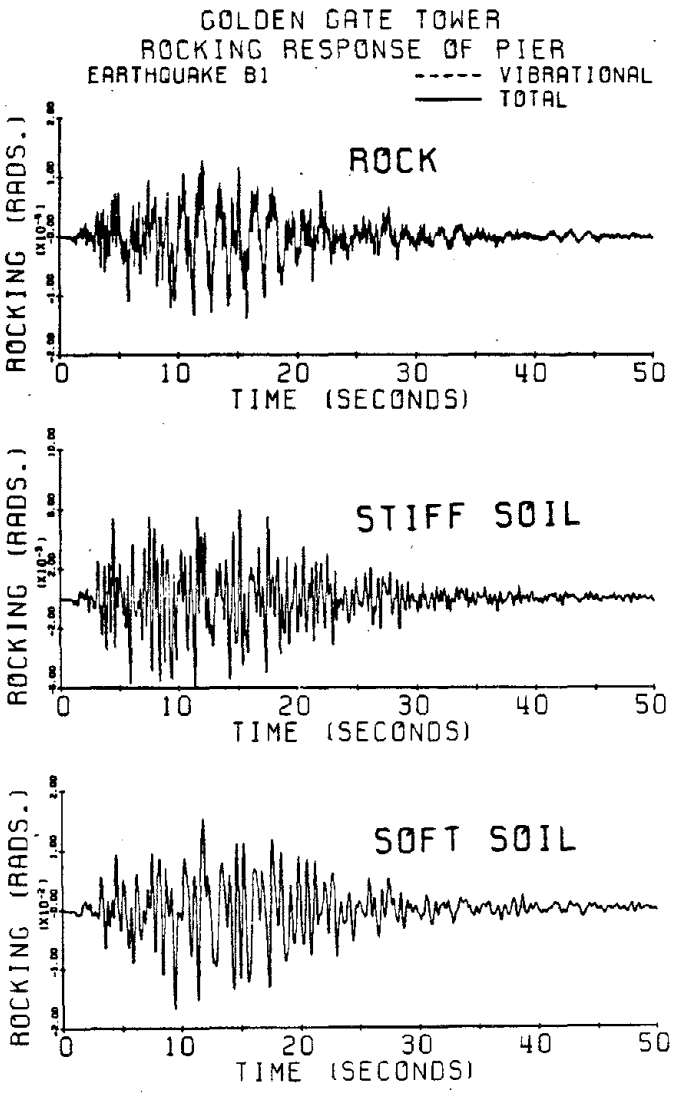

Fig. V-g-14 Time history rocking response of pier to artificial earthquake B-1 input.

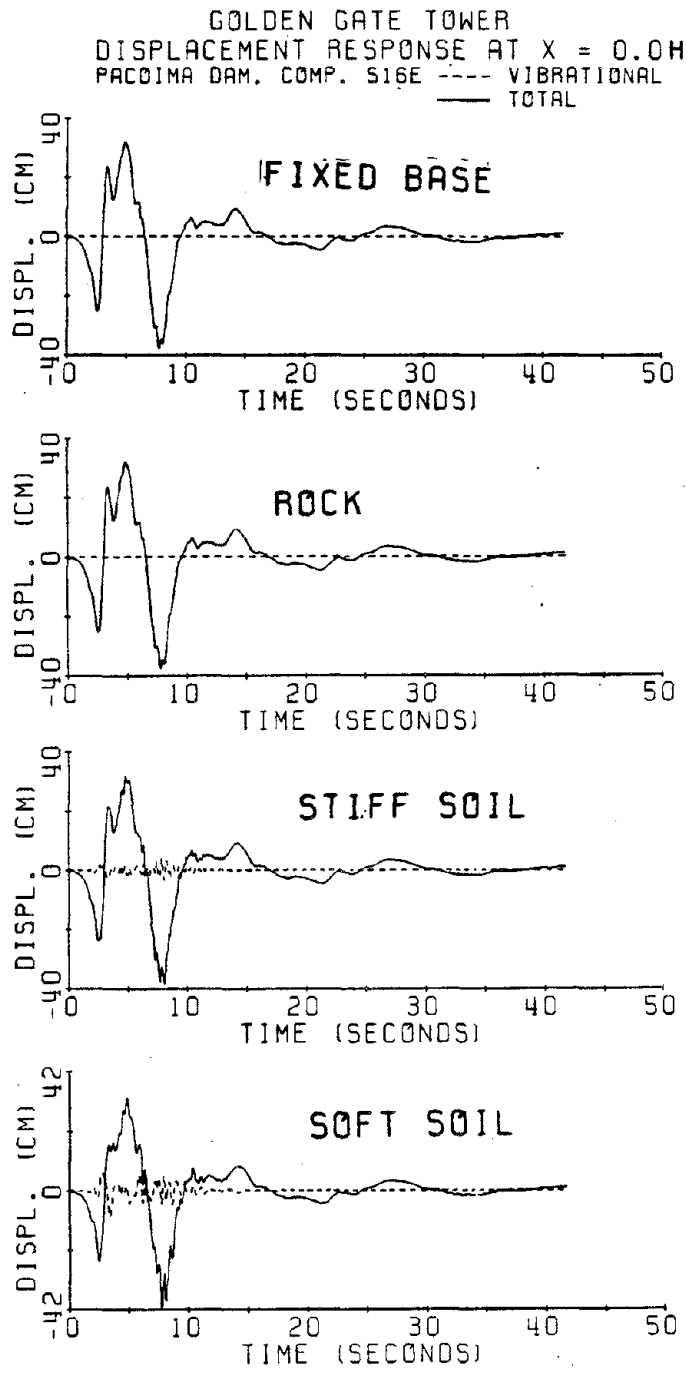

Fig. V-g-15 Time history displacement response at bottom of tower to 1971 Pacoima Dam input record.

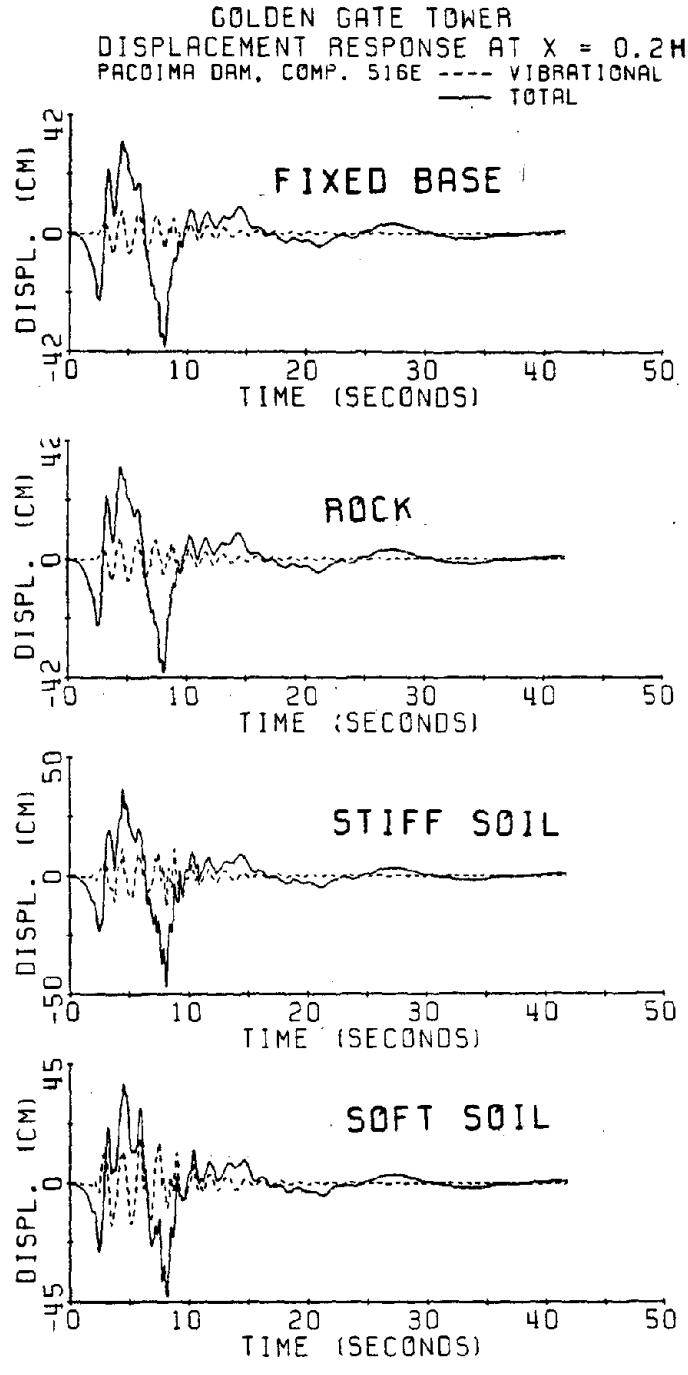

Fig. V-g-16 Time history displacement response at x = 0.2h to 1971 Pacoima Dam input.

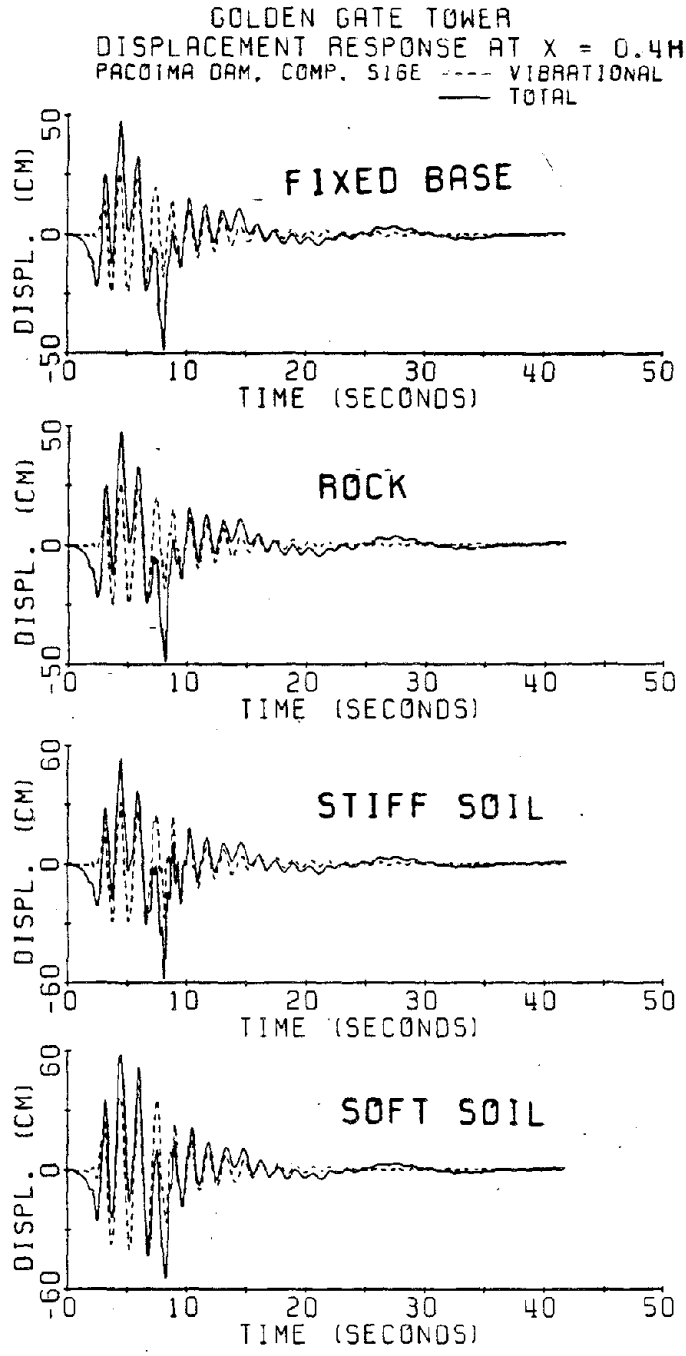

Fig. V-g-17 Time history displacement response at 0.4h to 1971 Pacoima Dam input.

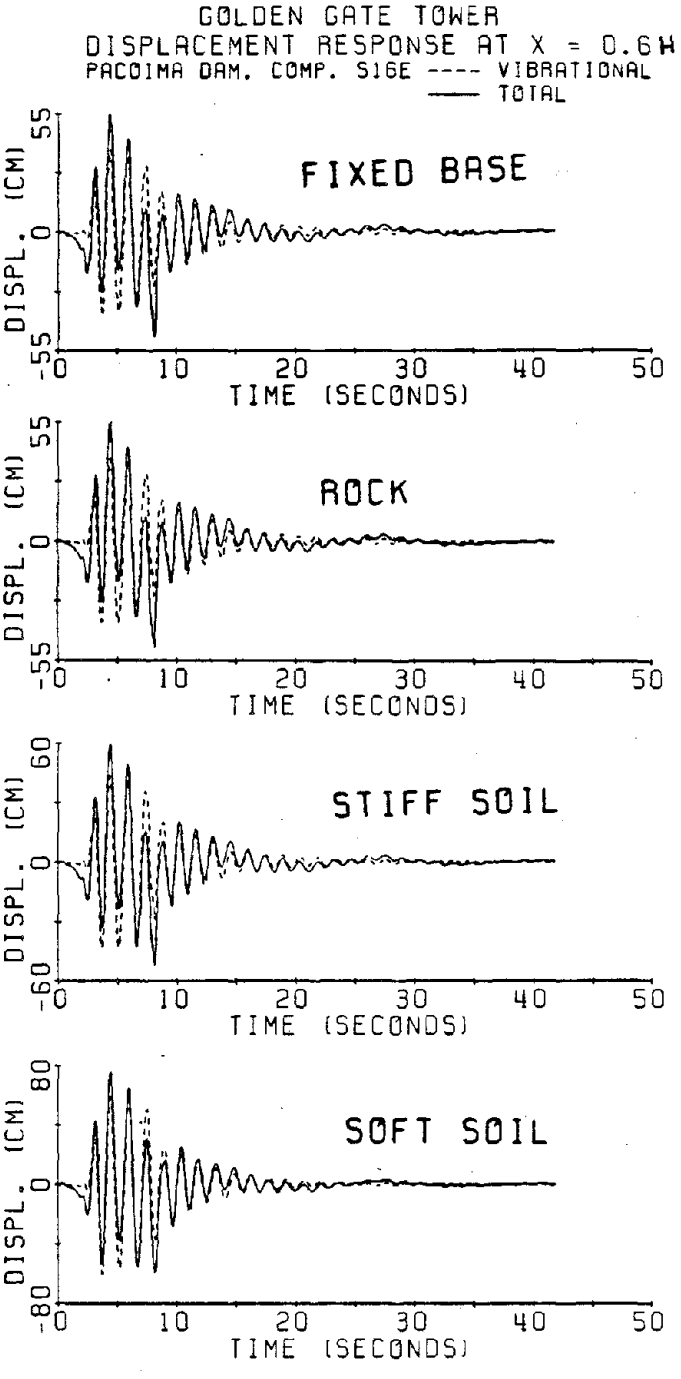

Fig. V-g-18 Time history displacement response at x = 0.6h to 1971 Pacoima Dam input.

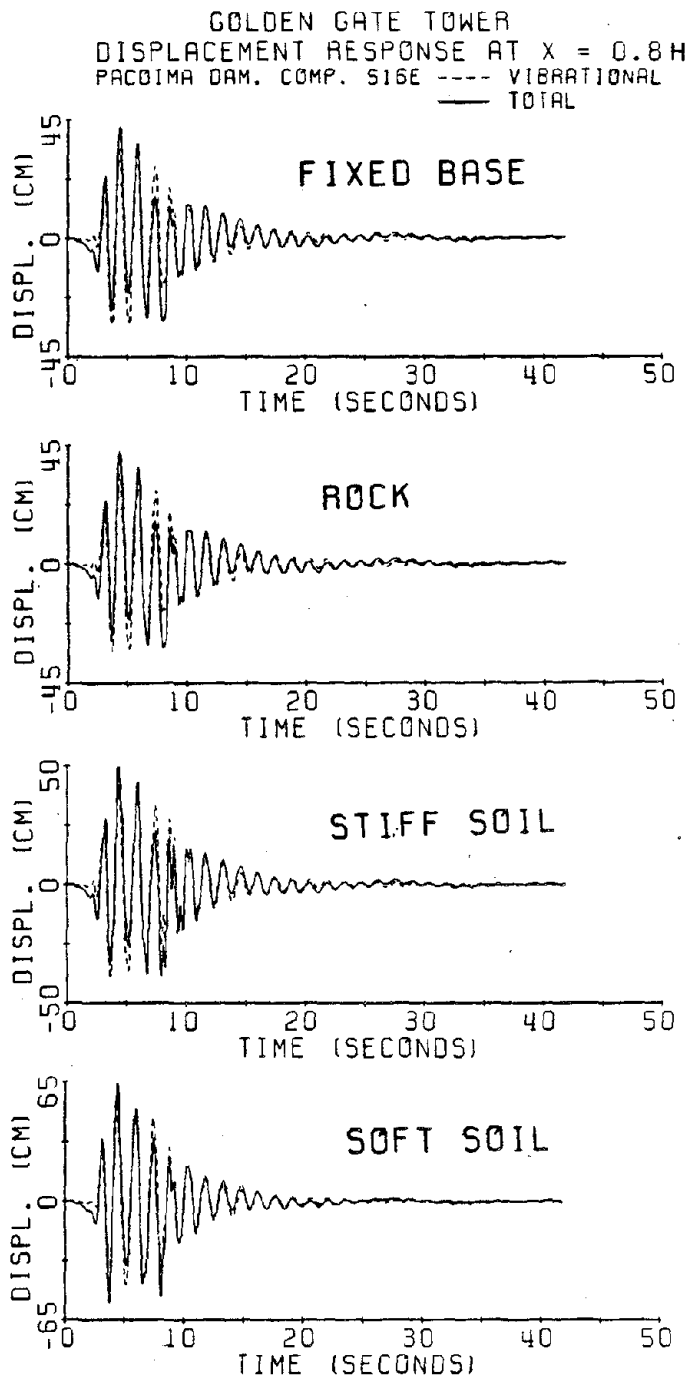

Fig. V-g-19 Time history displacement response at x = 0.8h to 1971 Pacoima Dam input.

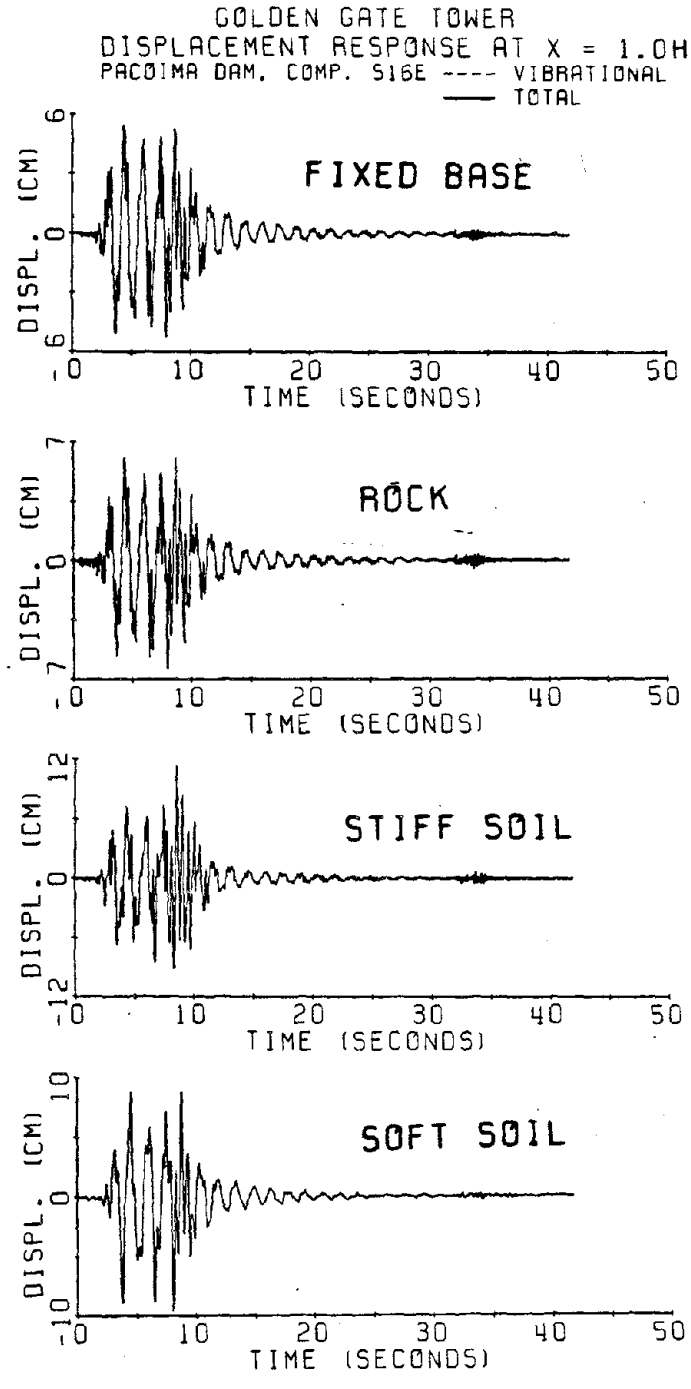

Fig. V-g-20 Time history displacement response at top of tower to 1971 Pacoima Dam input.

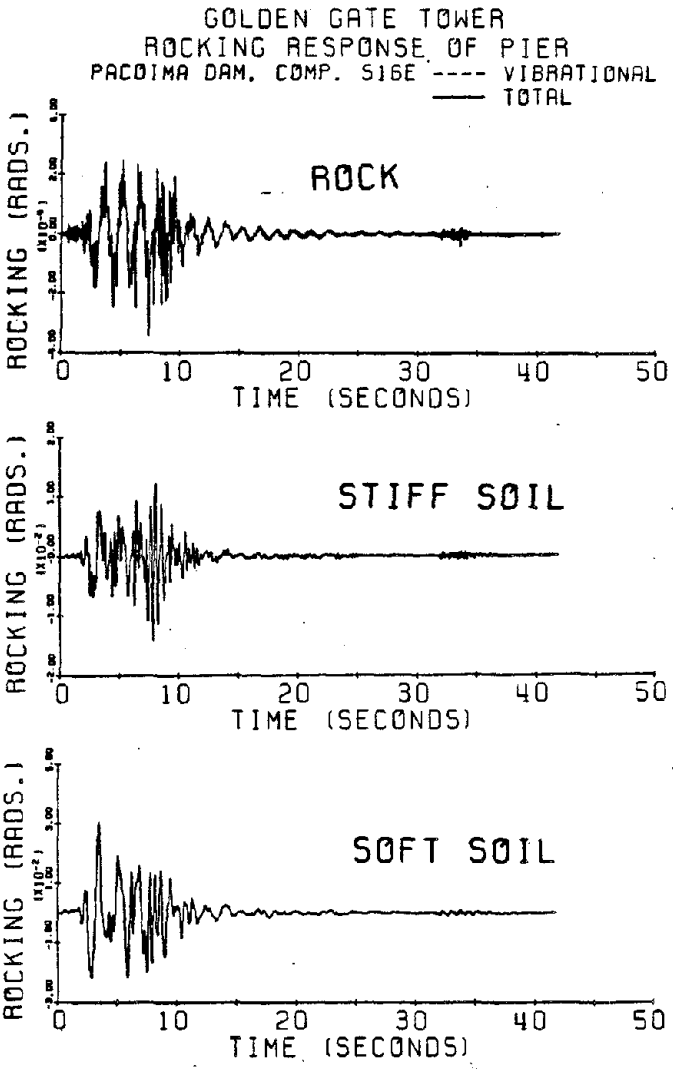

Fig. V-g-21 Time history rocking response of pier to 1971 Pacoima Dam input.

APPENDIX V-h

TIME DOMAIN FLEXURAL (BENDING) STRESS RESPONSE OF THE GOLDEN GATE TOWER PIER SYSTEM

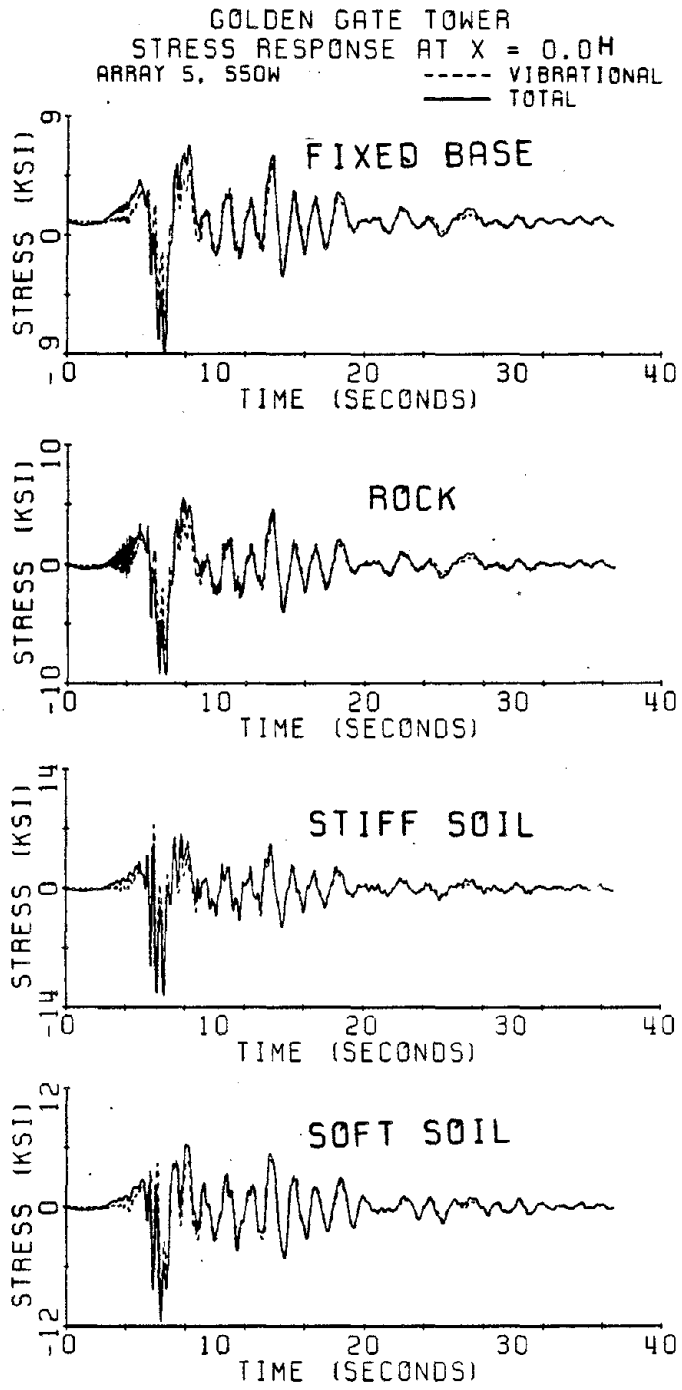

Fig. V-h-1 Time history stress response at bottom of tower to 1979 El Centro Array 5 input.

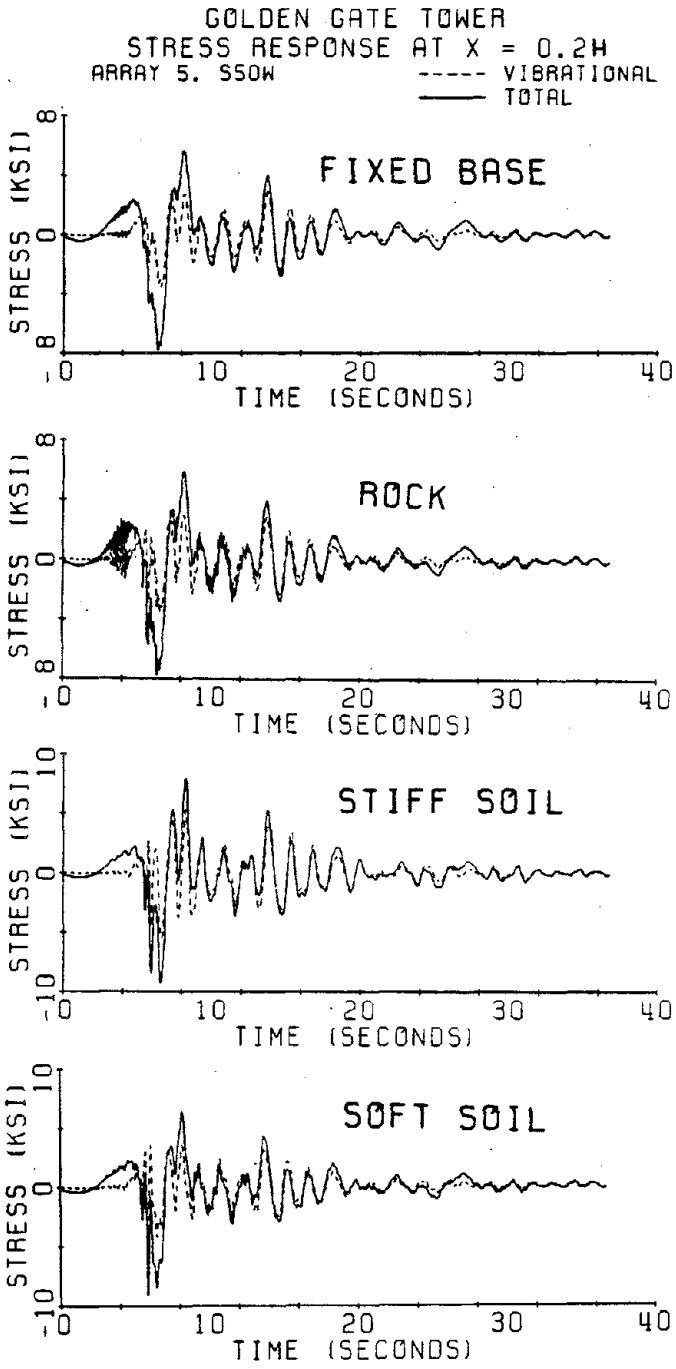

Fig. V-h-2 Time history stress response at x = 0.2h to 1979 El Centro Array 5 input.

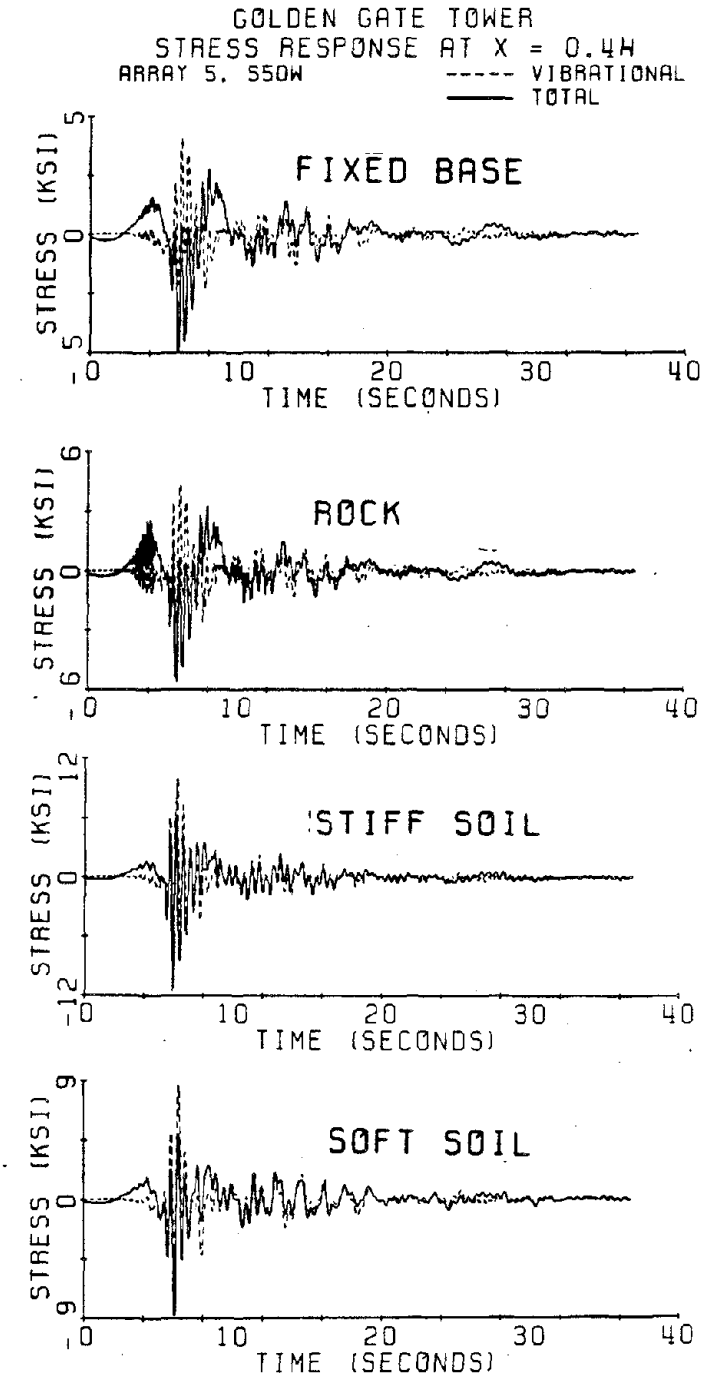

Fig. V-h-3 Time history stress response at x = 0.4 h to 1979 El Centro Array 5 input.

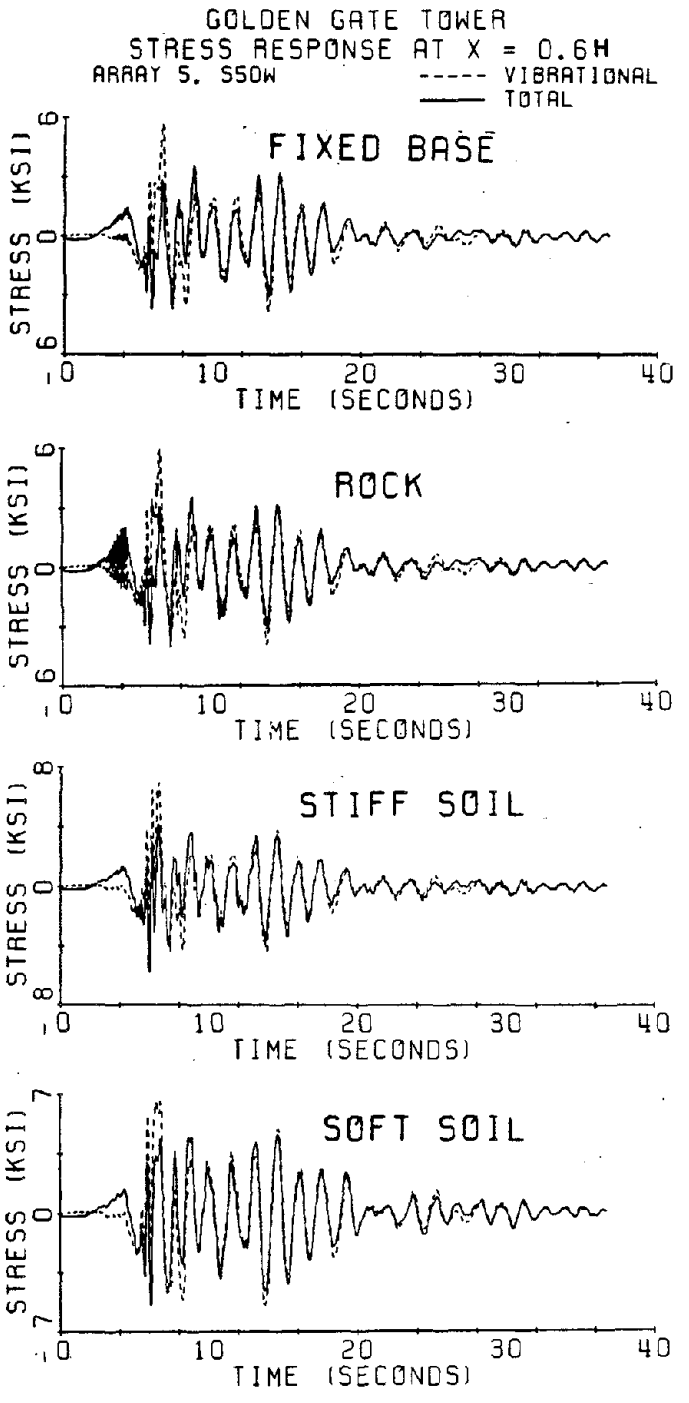

Fig. V-h-4 Time history stress response at x = 0.6h to 1979 El Centro Array 5 input.

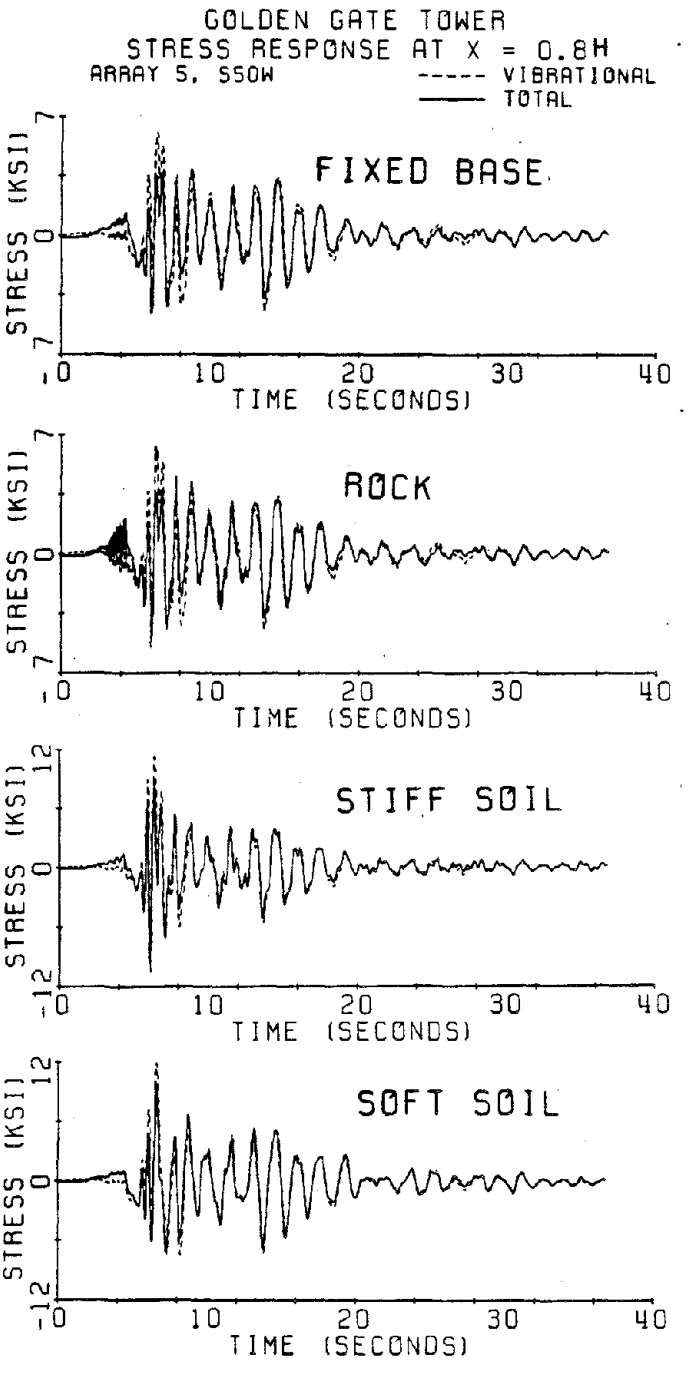

Fig. V-h-5 Time history stress response at x = 0.8h to 1979 El Centro Array 5 input.

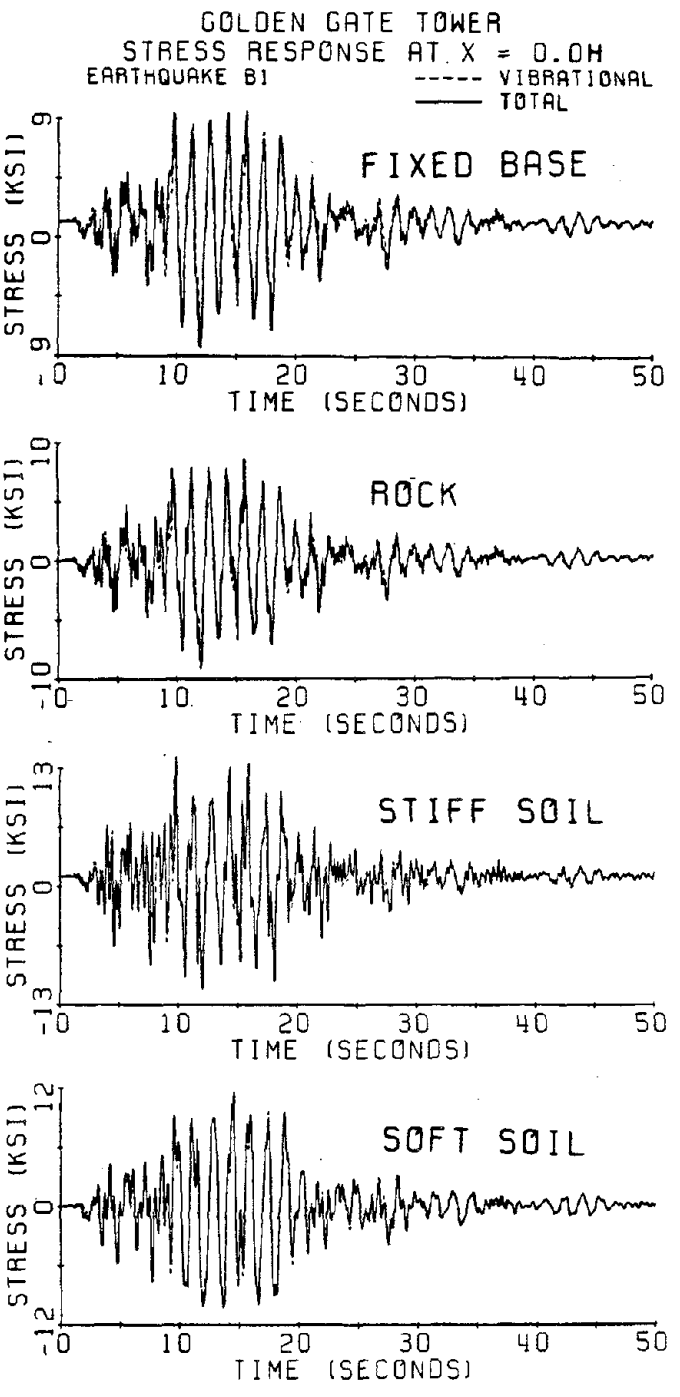

Fig. V-h-6 Time history stress response at bottom of tower to artificial earthquake B-1 input.

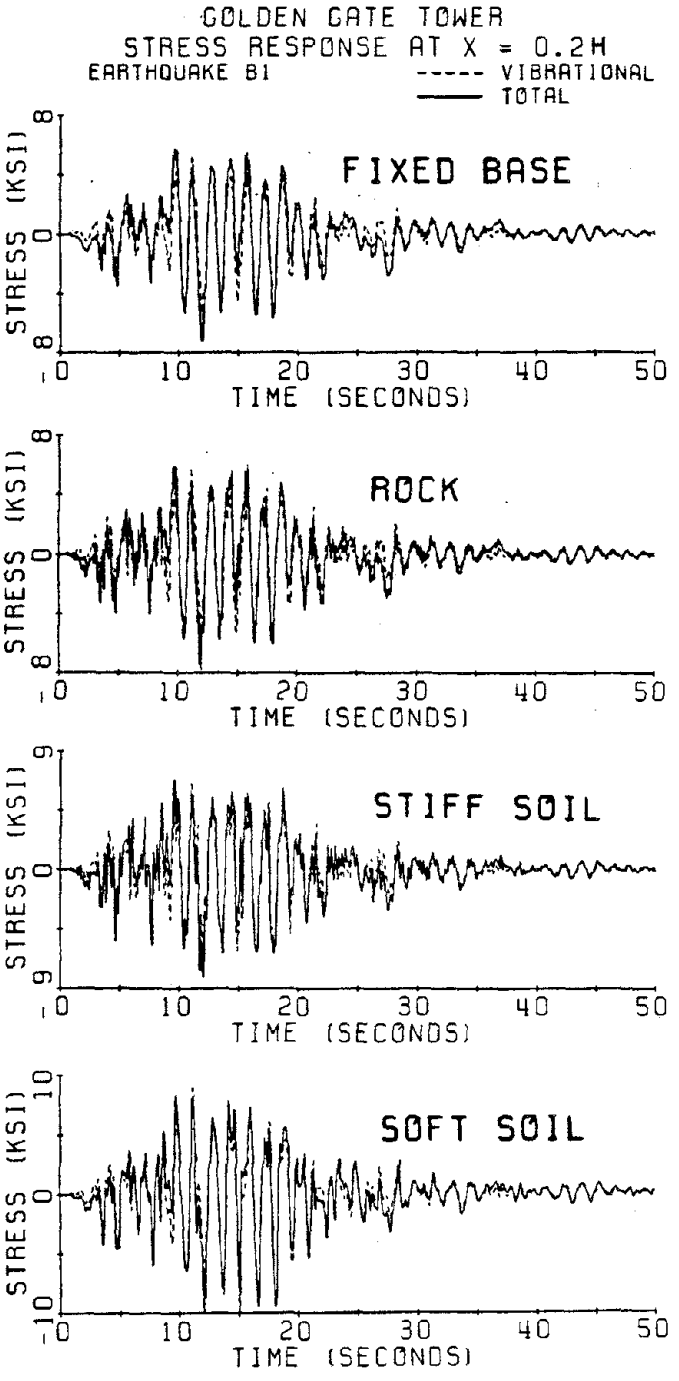

Fig. V-h-7 Time history stress response at x = 0.2h to artificial earthquake B-1 input.

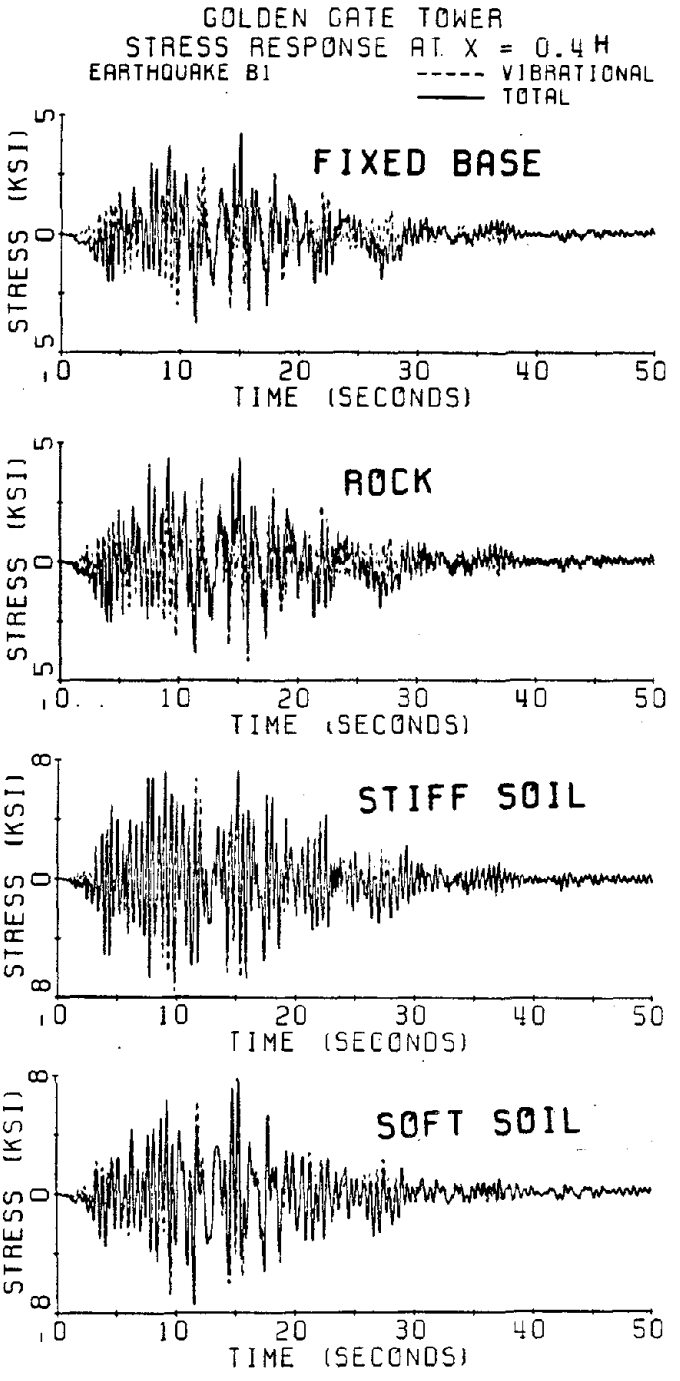

Fig. V-h-8 Time history stress response at x = 0.4h to artificial earthquake B-1 input.

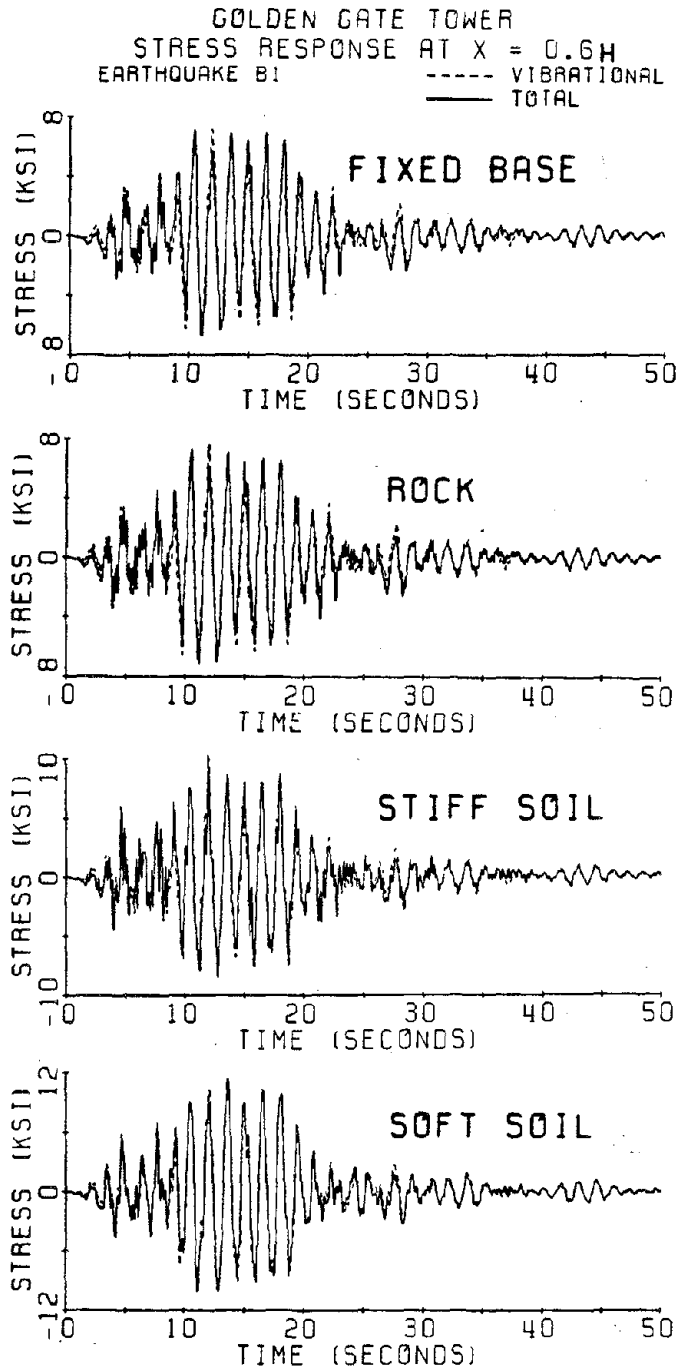

Fig. V-h-9 Time history stress response at x = 0.6h to artificial earthquake B-1 input.

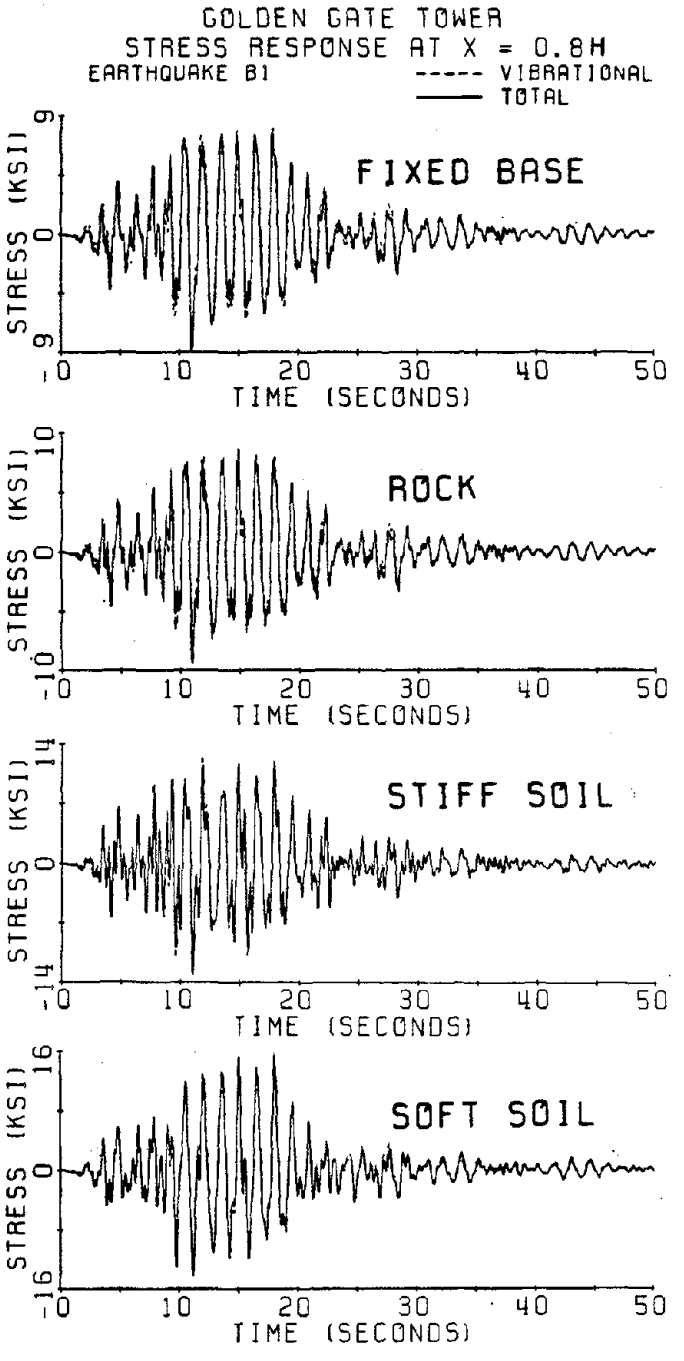

Fig. V-h-10 Time history stress response at x = 0.8h to artificial earthquake B-1 input.

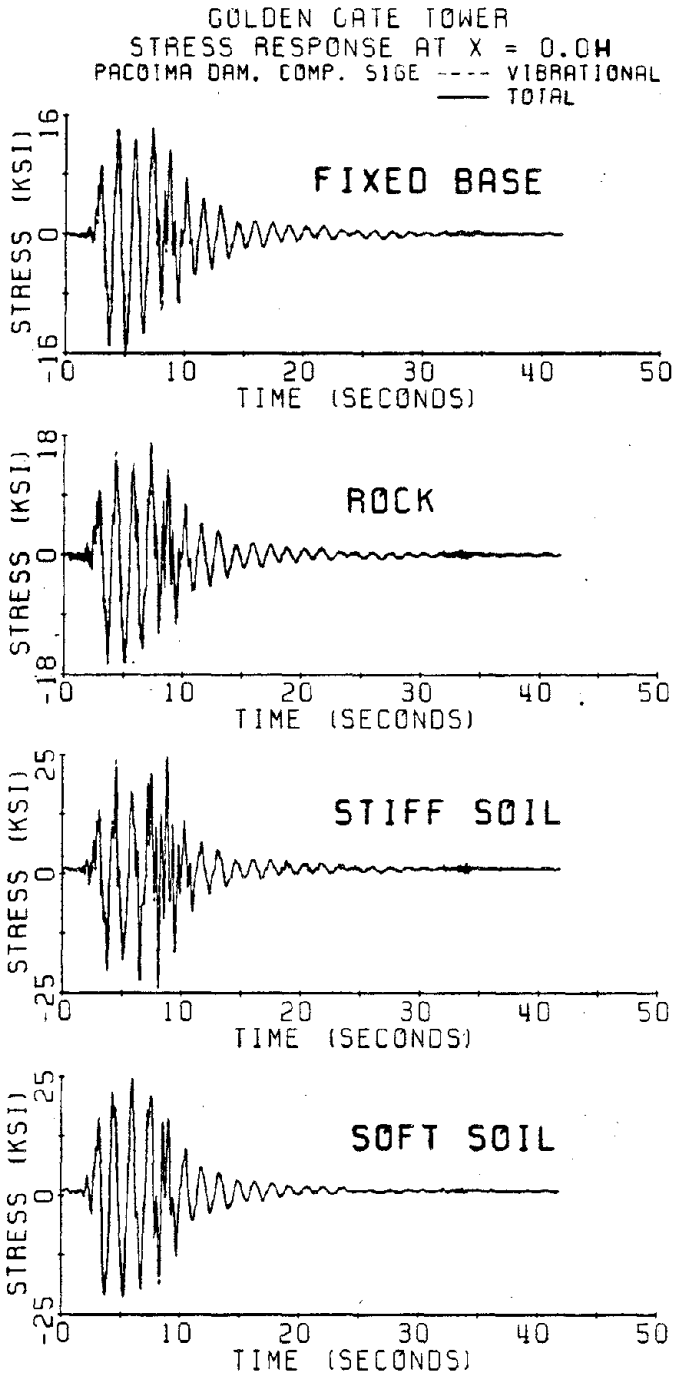

Fig. V-h-11 Time history stress response at bottom of tower to 1971 Pacoima Dam input record.

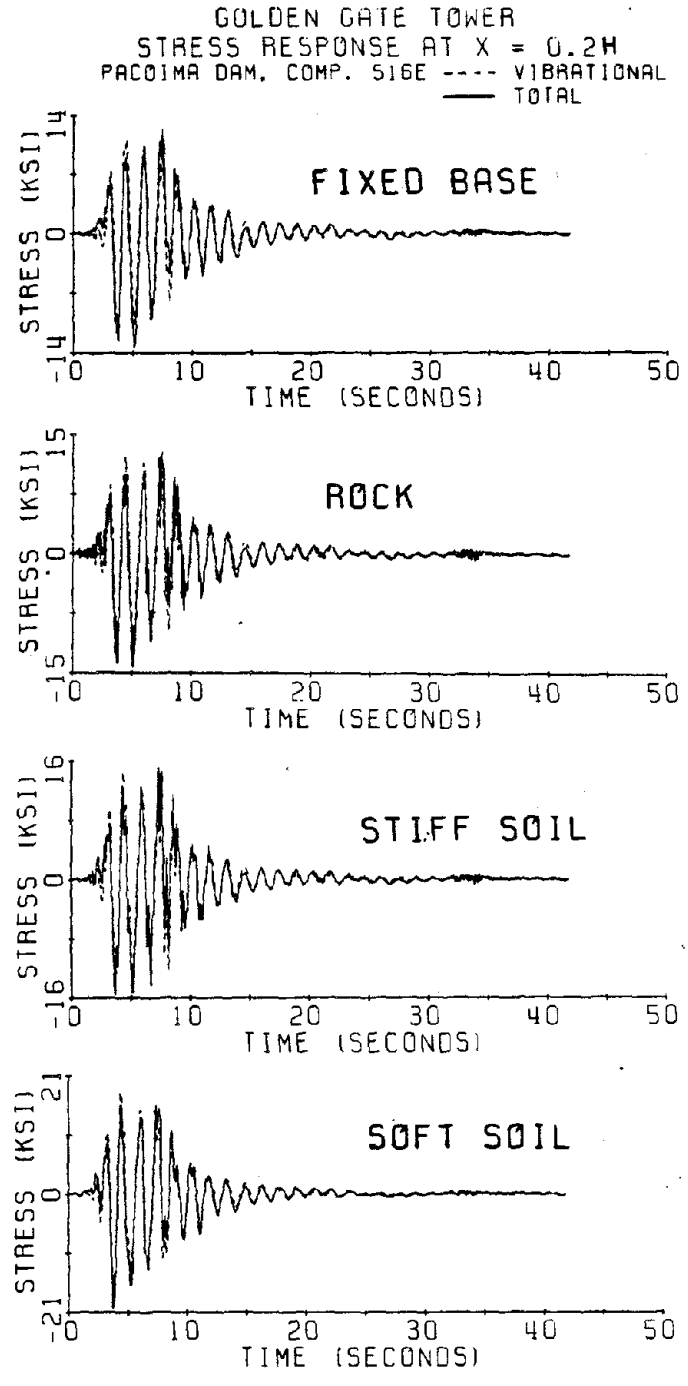

Fig. V-h-12 Time history stress response at x = 0.2h to 1971 Pacoima Dam input record.

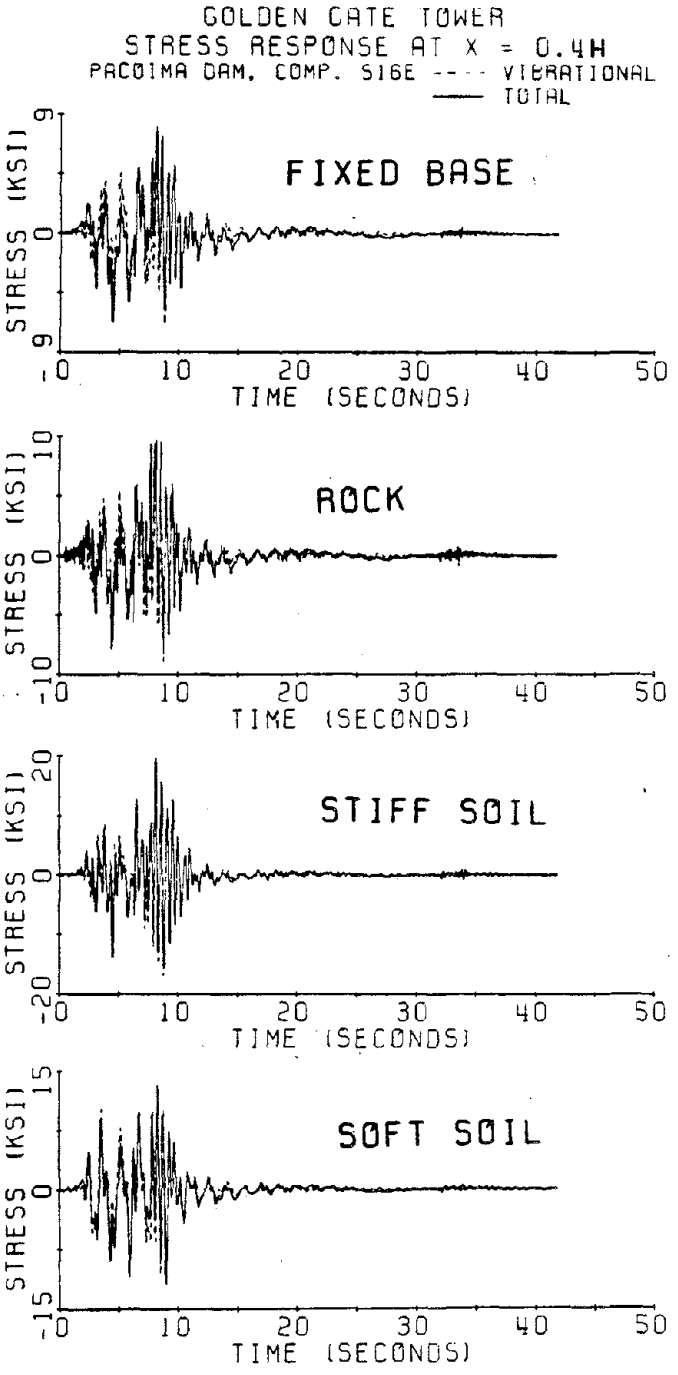

Fig. V-h-13 Time history stress response at x = 0.4h to 1971 Pacoima Dam input record.

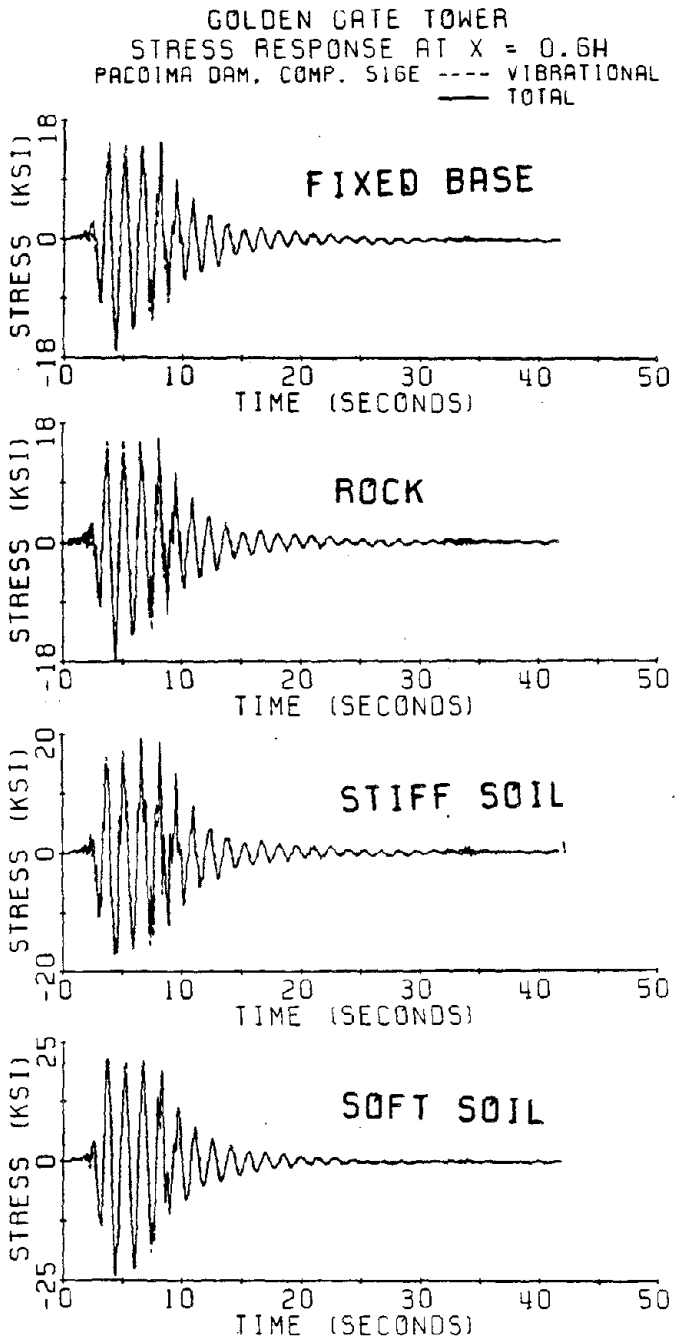

Fig. V-h-14 Time history stress response at x = 0.6h to 1971 Pacoima Dam input record.

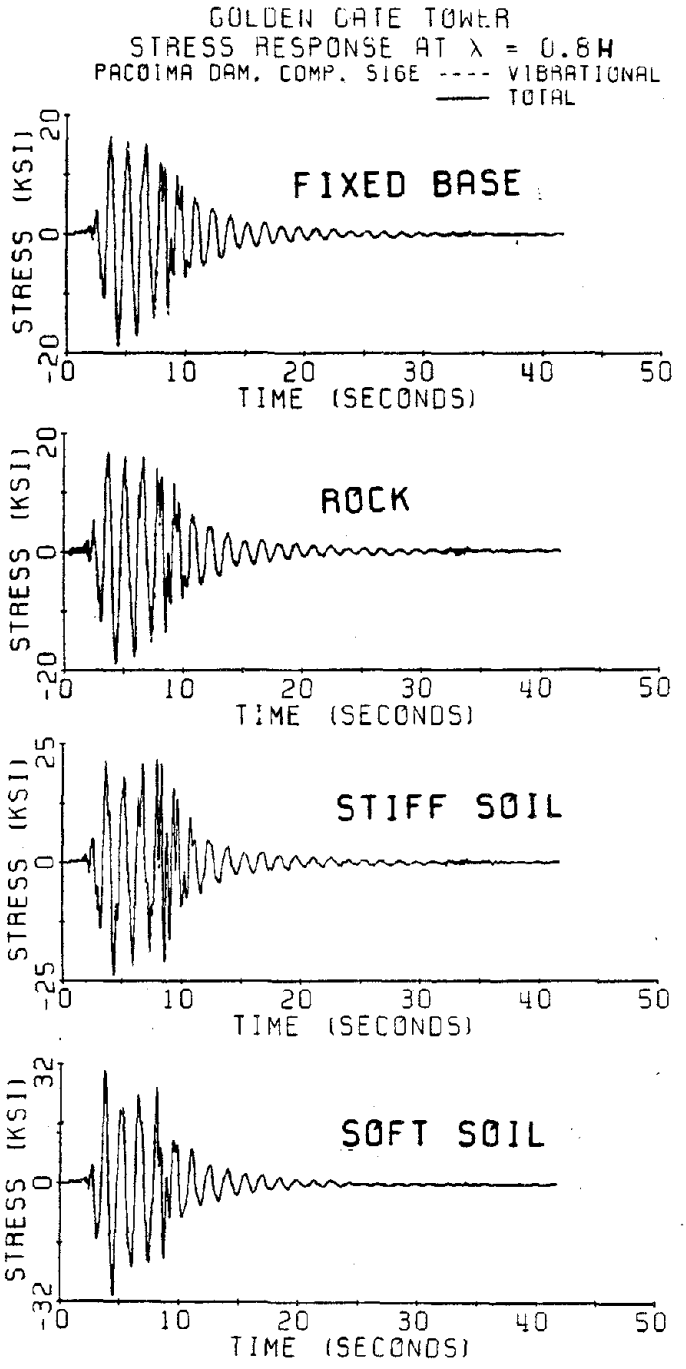

Fig. V-h-15 Time history stress response at x = 0.8h to 1971 Pacoima Dam input record.

APPENDIX V-i

TIME DOMAIN DYNAMIC SHEAR FORCE RESPONSE OF THE GOLDEN GATE BRIDGE TOWER-PIER SYSTEM

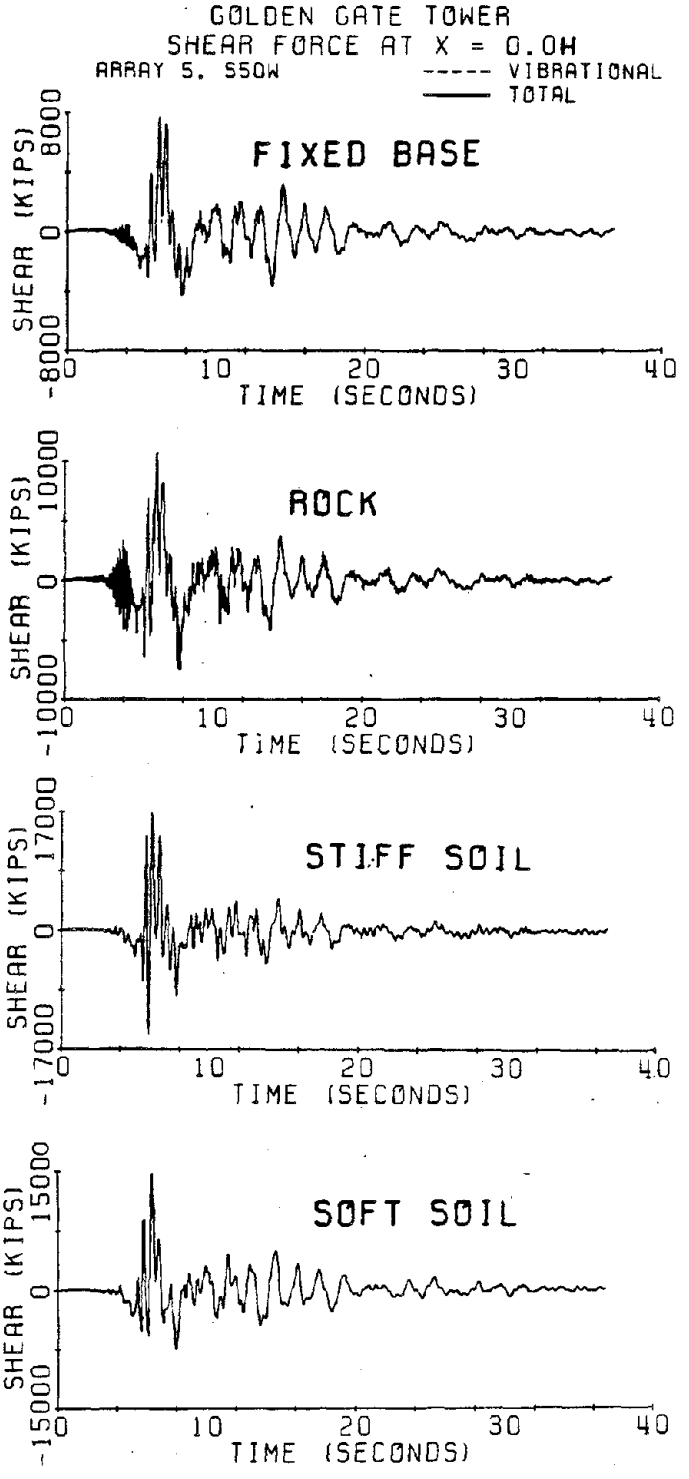

Fig. V-i-1 Time history shear force response at bottom of tower to 1979 El Centro Array 5 input.

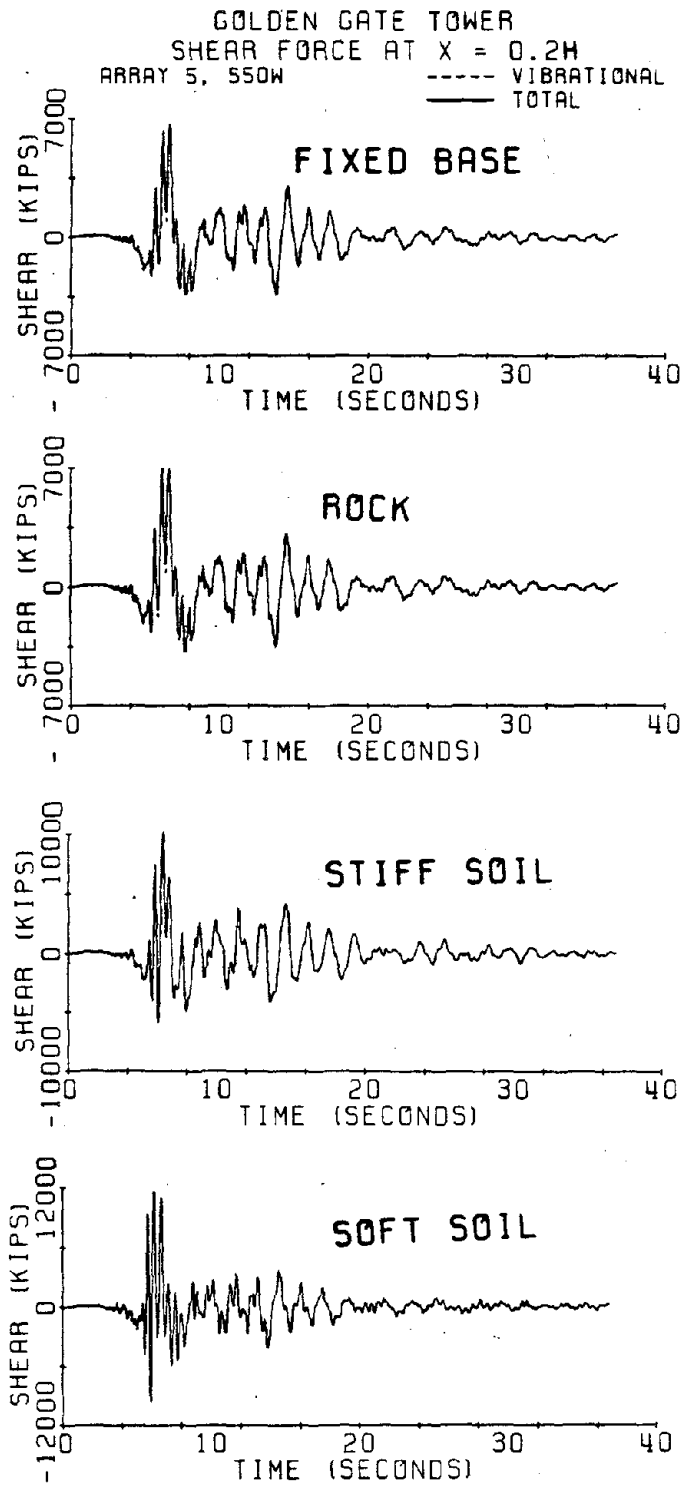

Fig. V-i-2 Time history shear force response at x = 0.2h to 1979 El Centro Array 5 input.

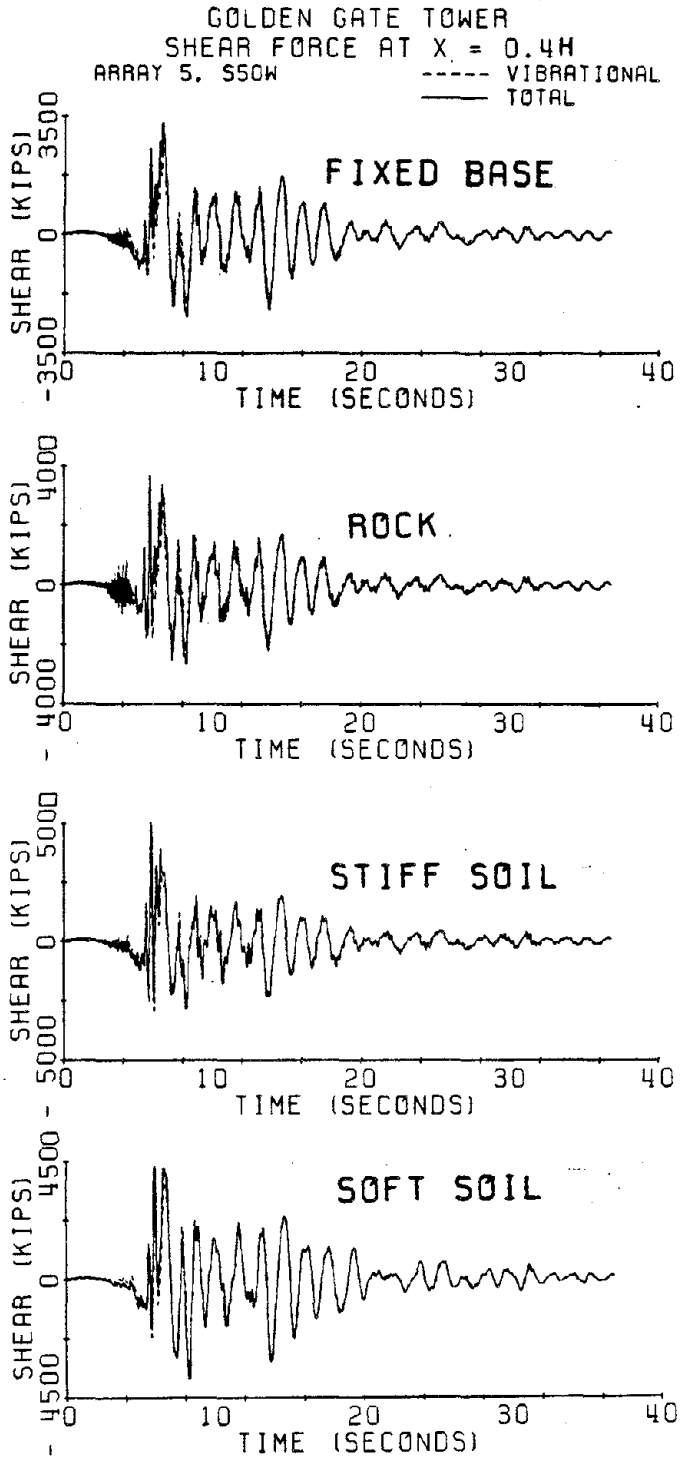

Fig. V-i-3 Time history shear force response at x = 0.4h to 1979 El Centro Array 5 input.

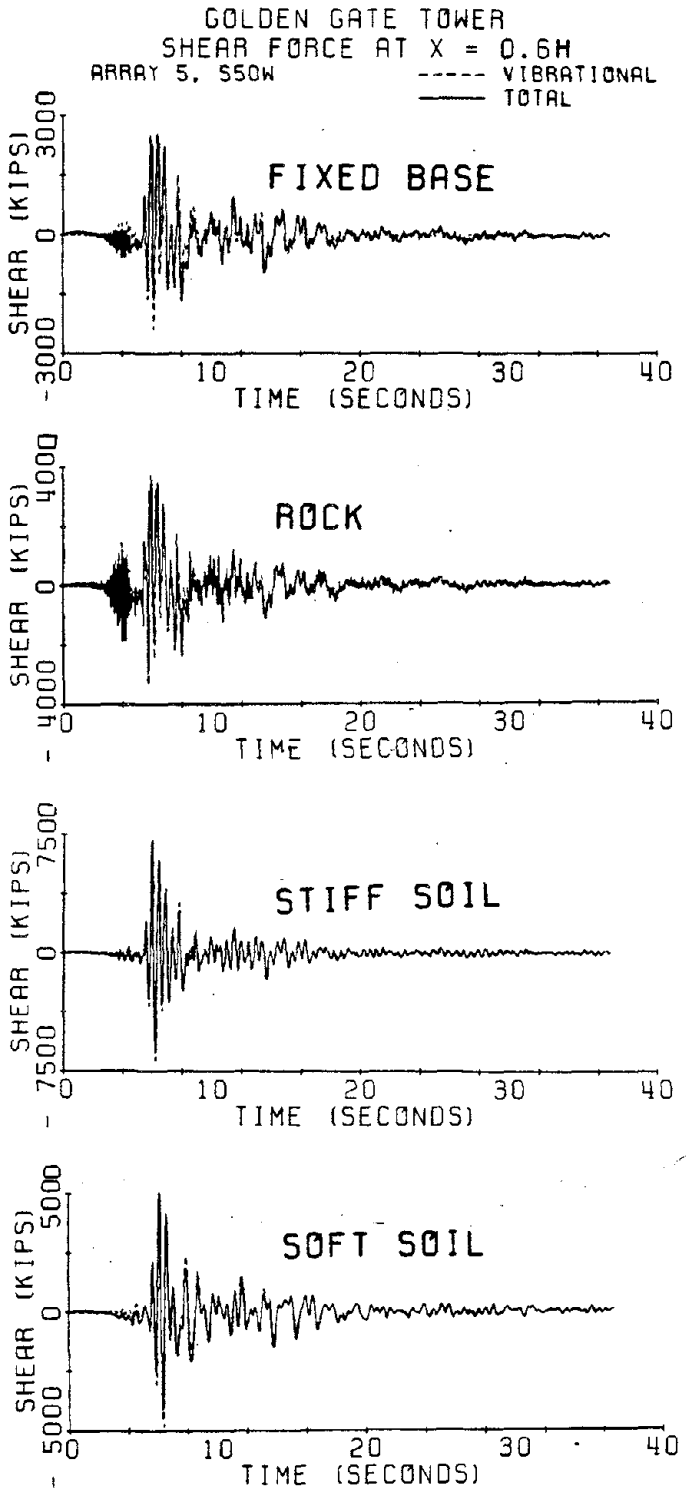

Fig. V-i-4 Time history shear force response at x = 0.6h to 1979 El Centro Array 5 input.

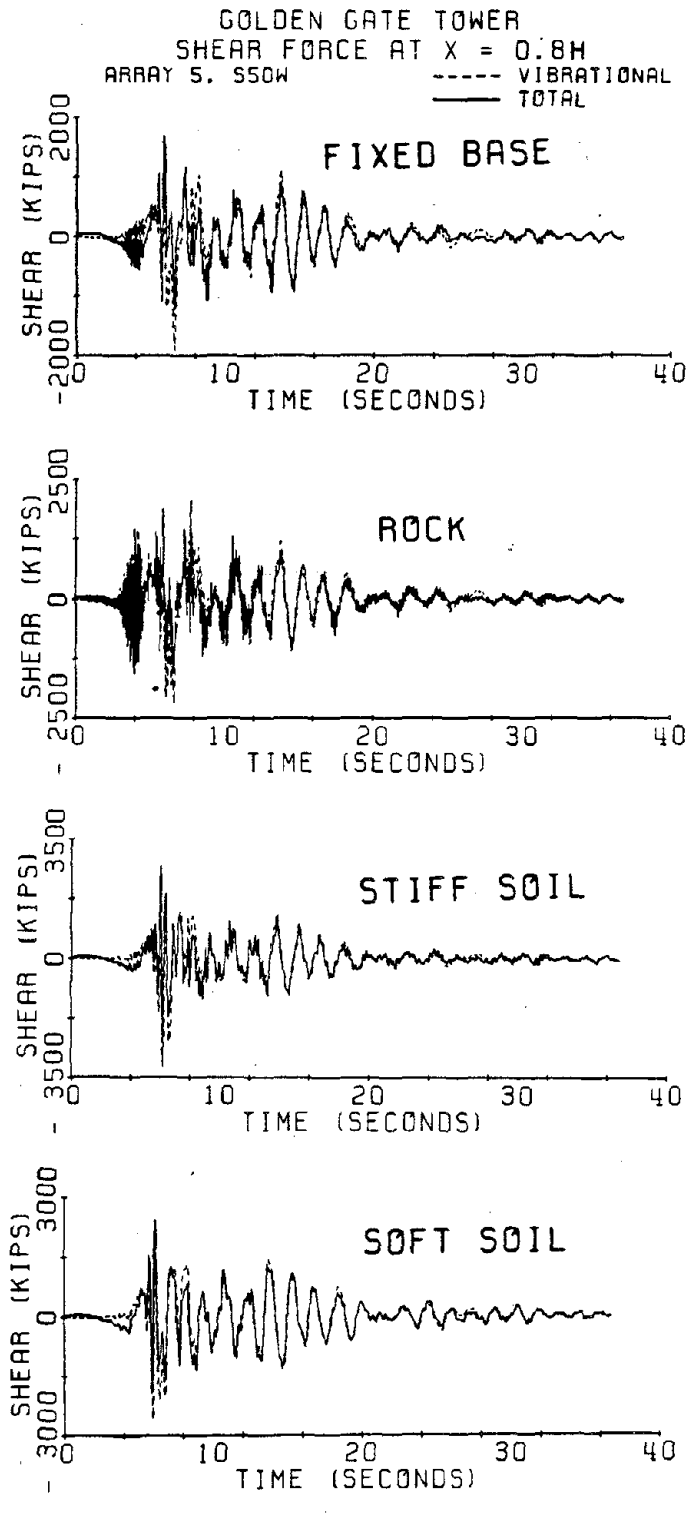

Fig. V-i-5 Time history shear force response at x = 0.8h to 1979 El Centro Array 5 input.

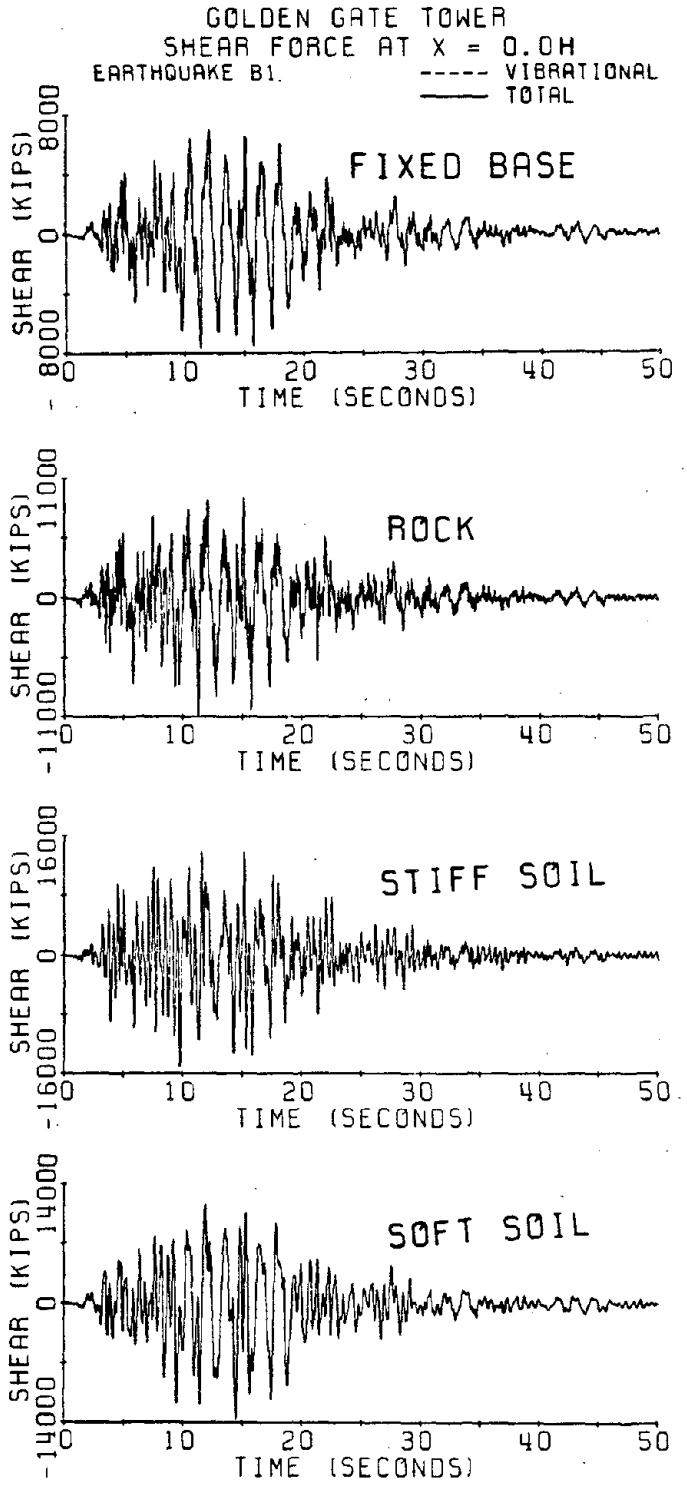

Fig. V-i-6 Time history shear force response at bottom of tower to artificial earthquake B-1 input.

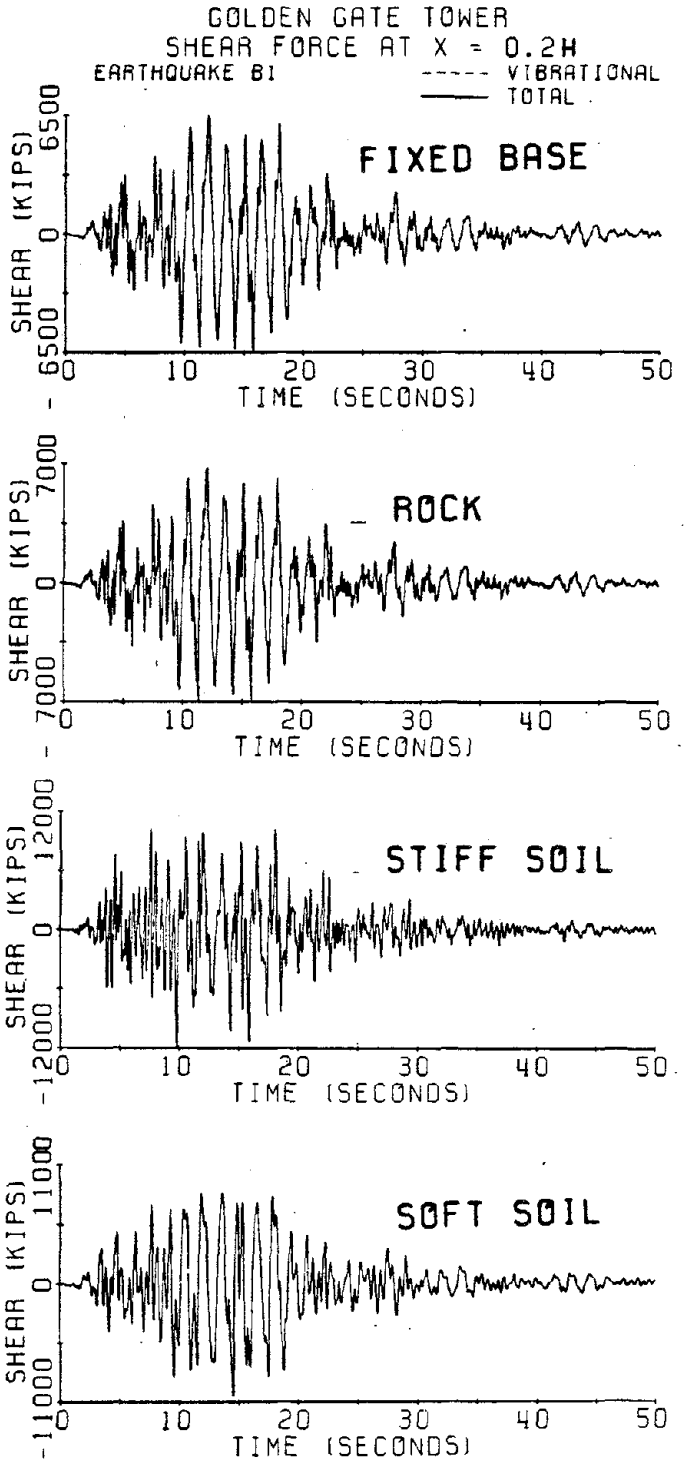

Fig. V-i-7 Time history shear force response at x = 0.2h to artificial earthquake B-1 input.

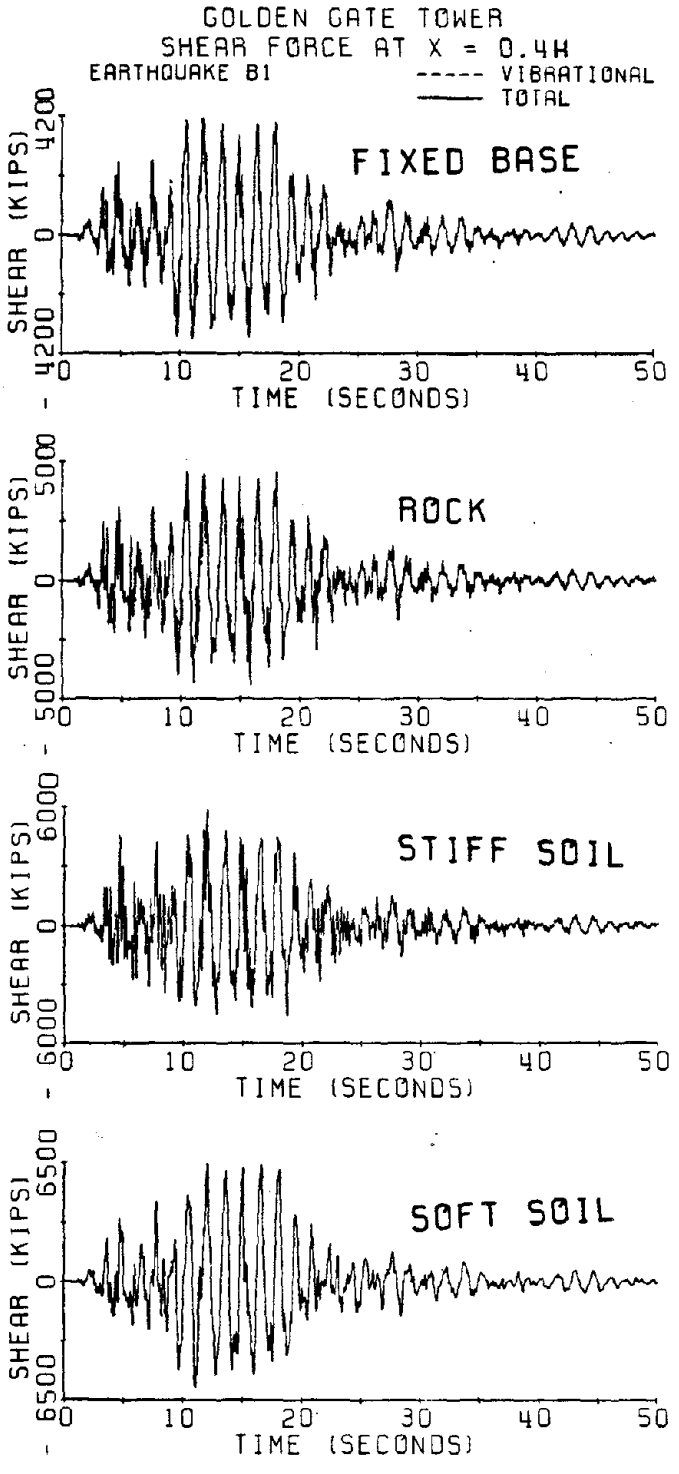

Fig. V-i-8 Time history shear force response at x = 0.4h to artificial earthquake B-1 input.

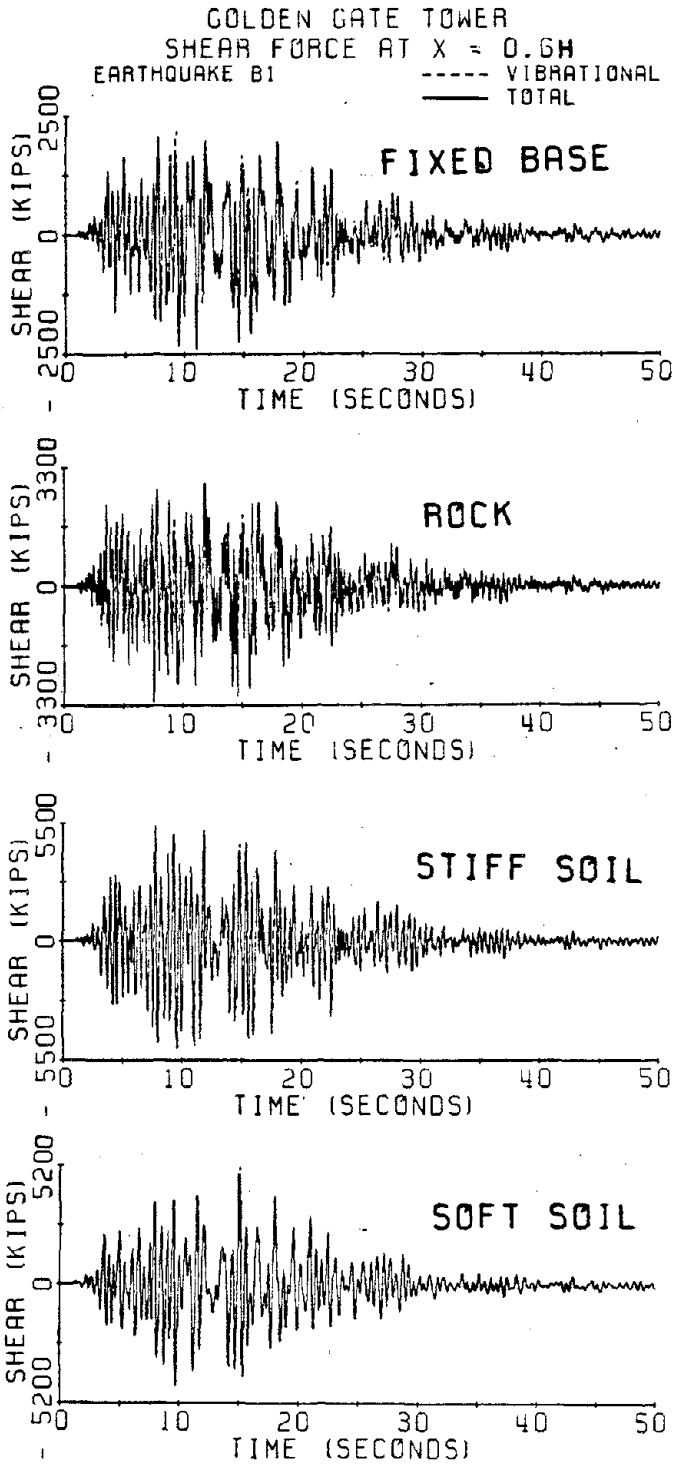

Fig. V-i-9 Time history shear force response at x = 0.6h to artificial earthquake B-1 input.

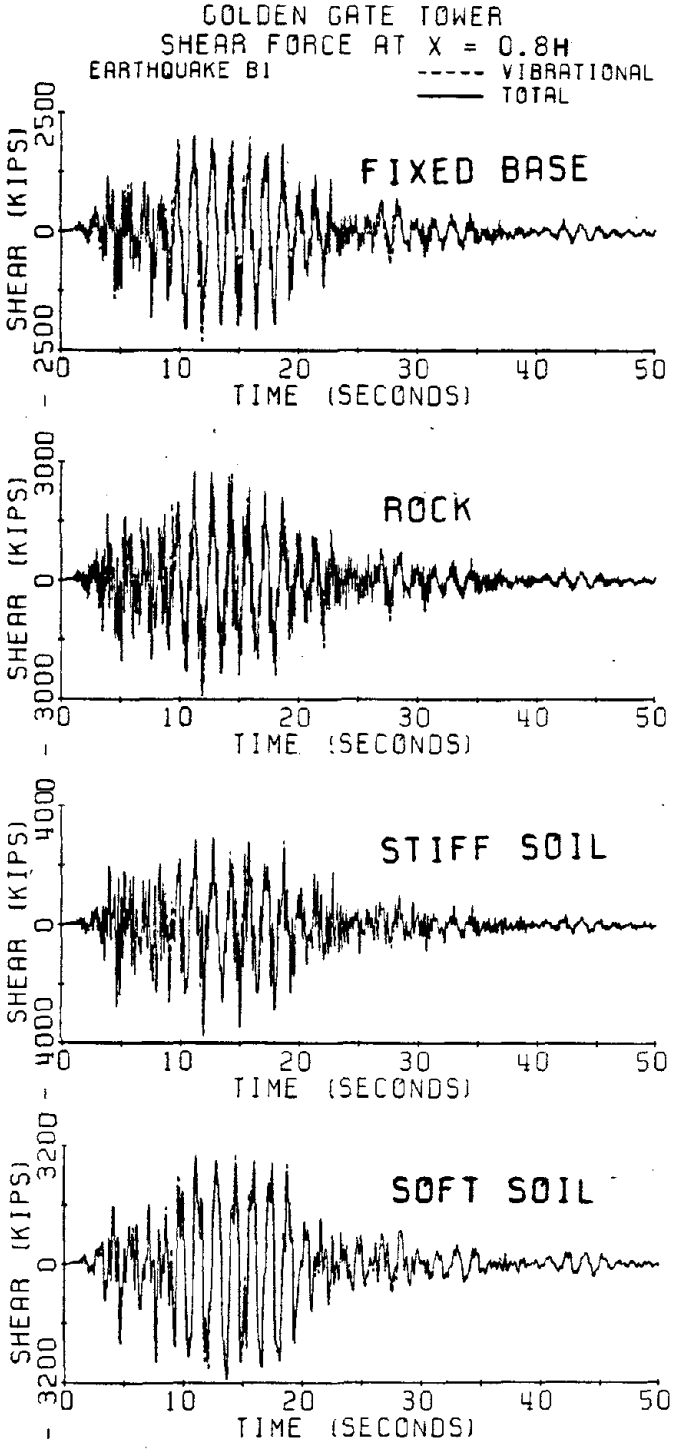

Fig. V-i-10 Time history shear force response at x = 0.8h to artificial earthquake B-1 input.

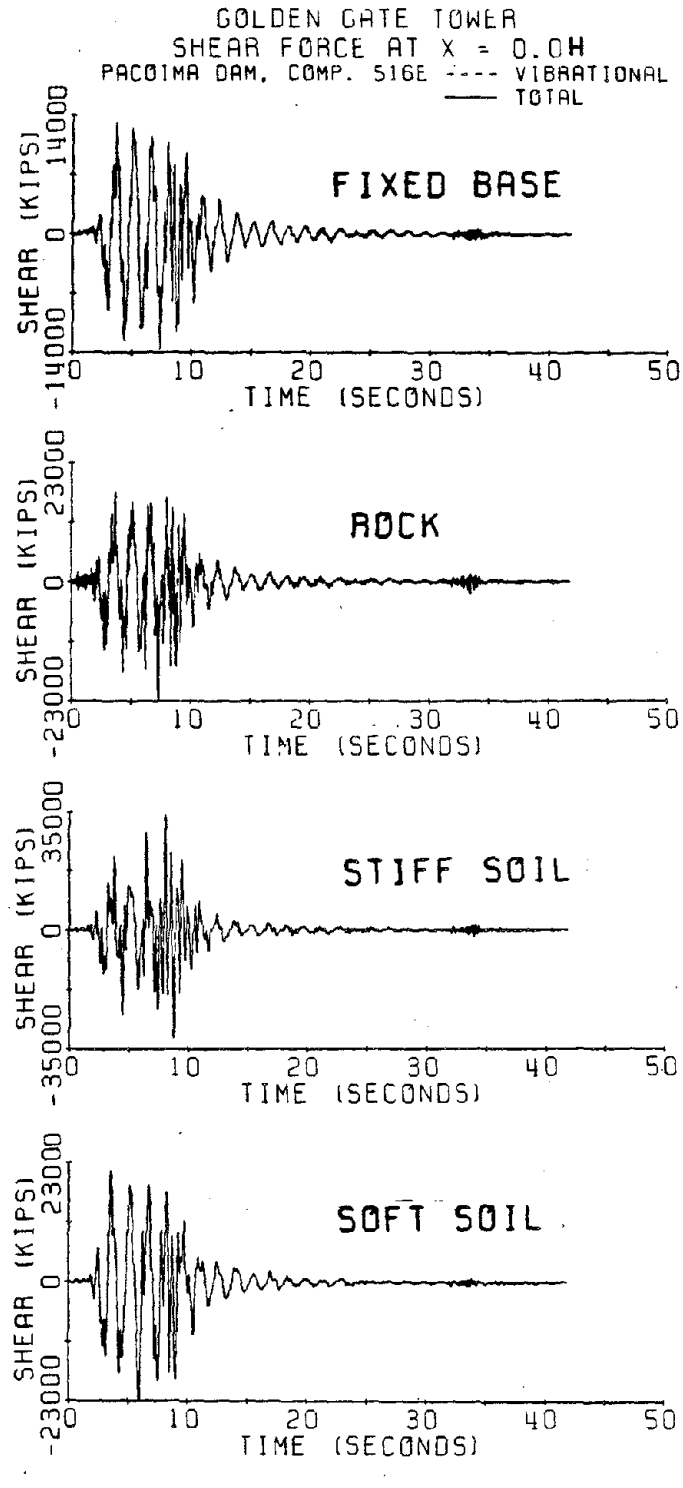

Fig. V-i-11 Time history shear force response at bottom of tower to 1971 Pacoima Dam input record.

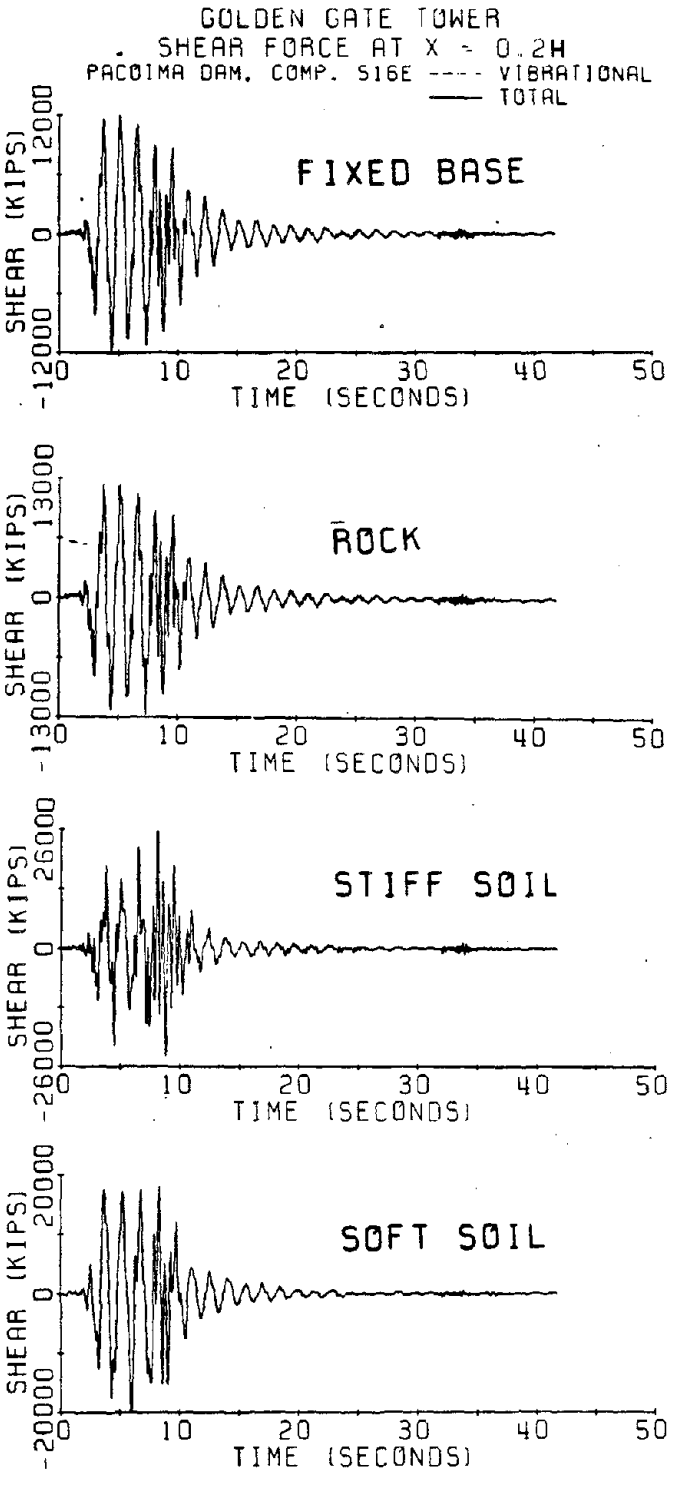

Fig. V-i-12 Time history shear force response at x = 0.2h to 1971 Pacoima Dam input.

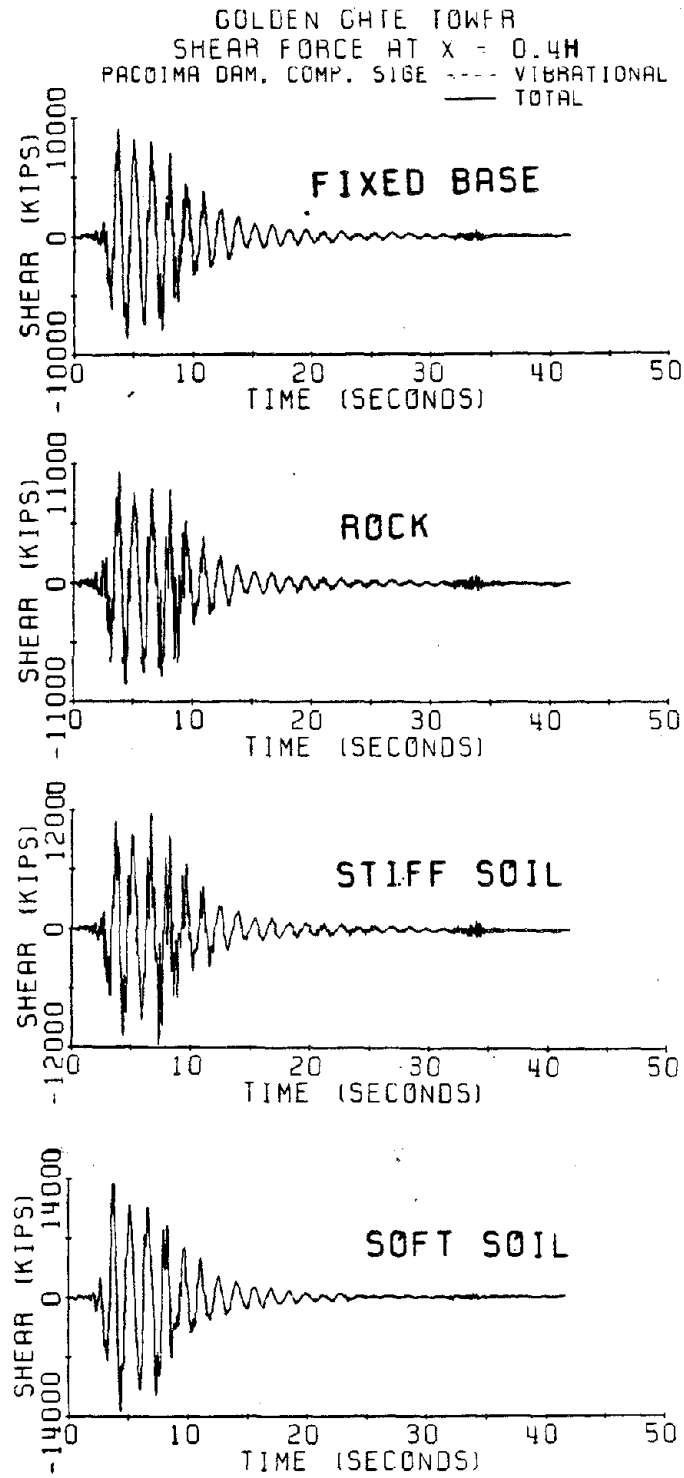

Fig. V-i-13 Time history shear force response at x = 0.4h to 1971 Pacoima Dam input record.

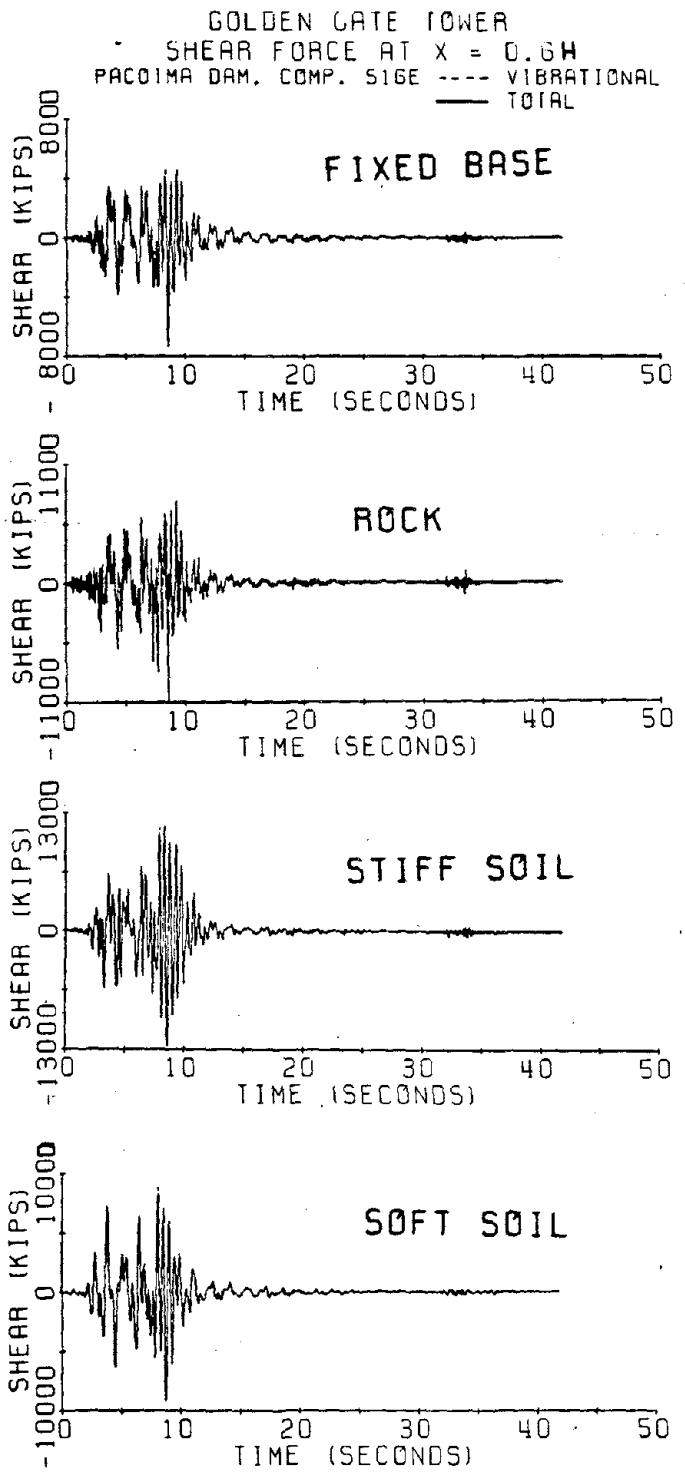

Fig. V-i-14 Time history shear force response at x = 0.6h to 1971 Pacoima Dam input record.

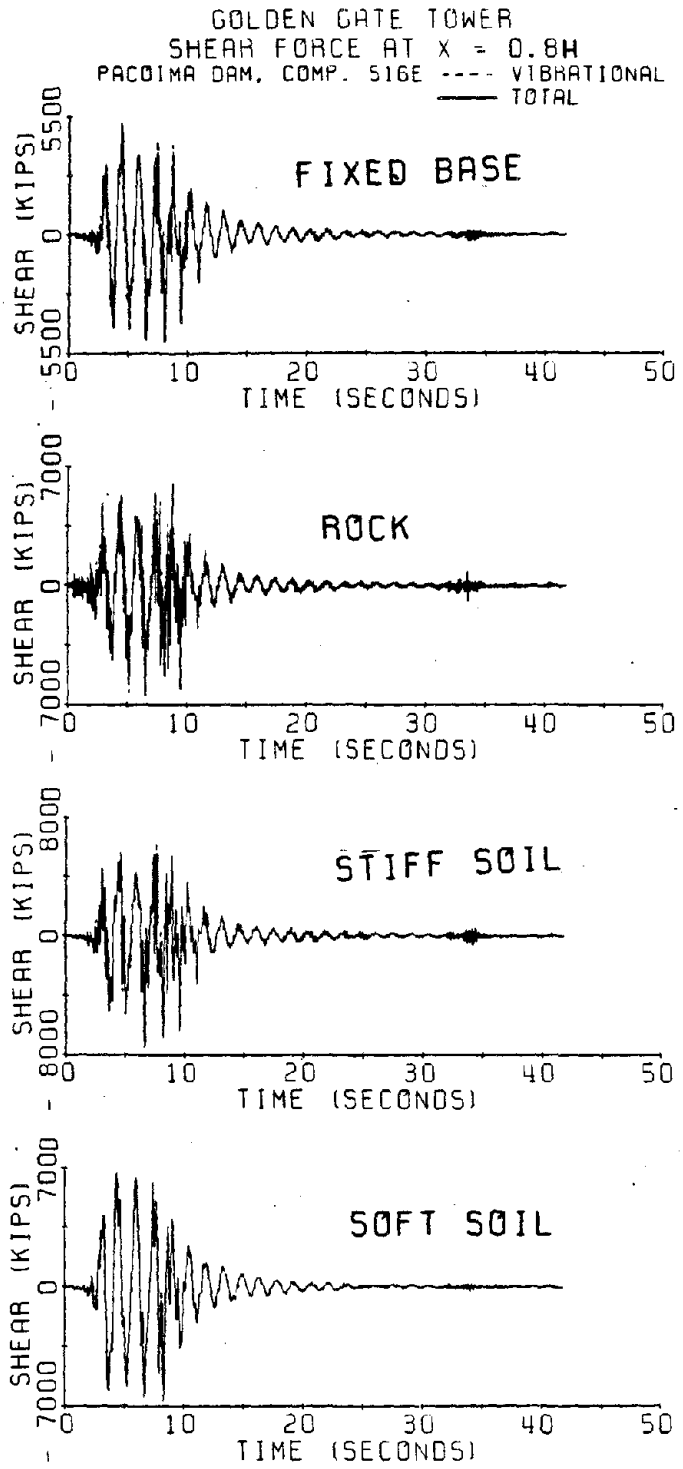

Fig. V-i-15 Time history shear force response at x = 0.8h to 1971 Pacoima Dam input record.

APPENDIX V-j

FREQUENCY DOMAIN DISPLACEMENT RESPONSE OF THE GOLDEN GATE TOWER-PIER SYSTEM

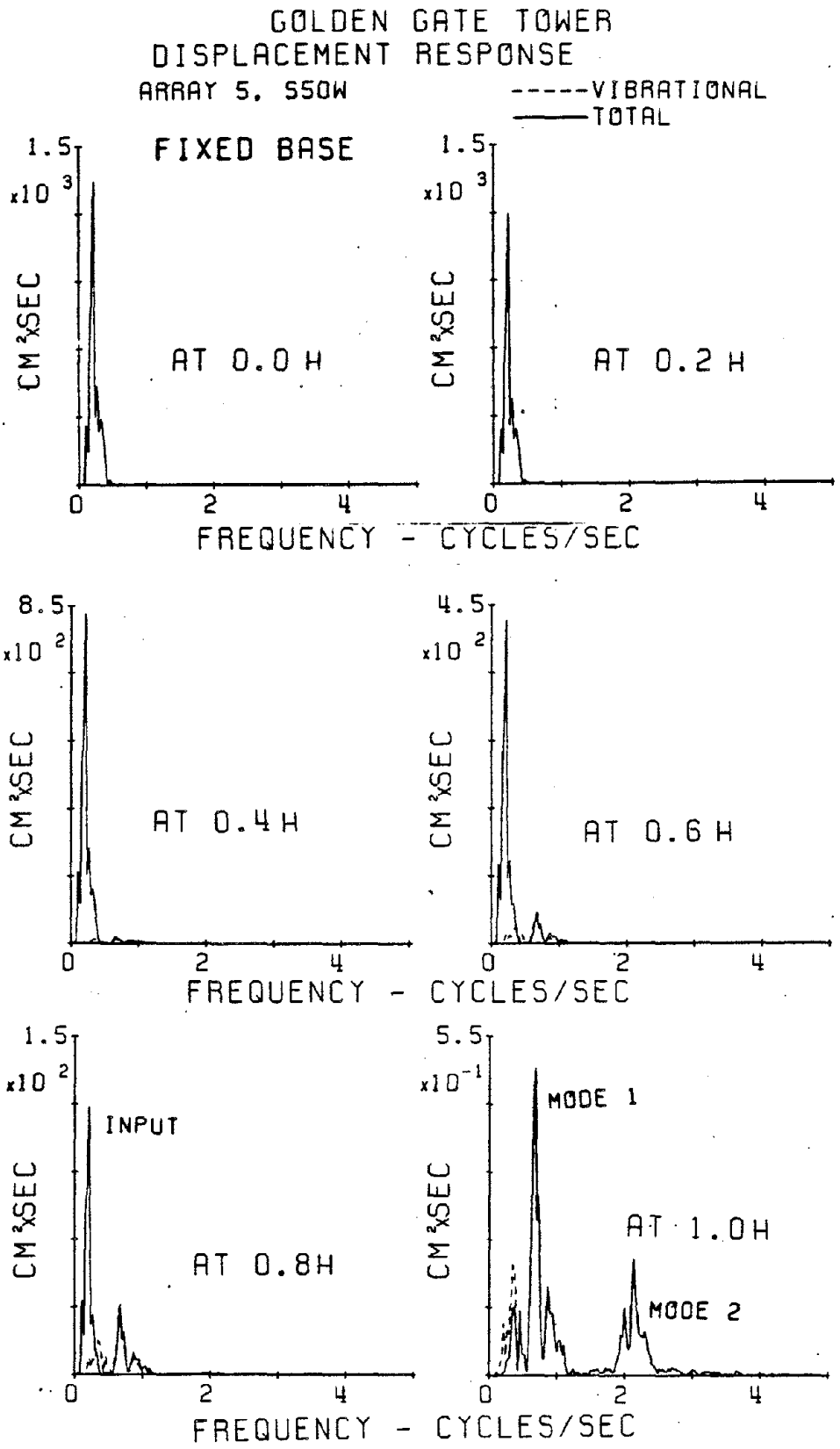

Fig. V-j-1 Power spectra of response displacements to 1979 El Centro Array 5 input (fixed base case).

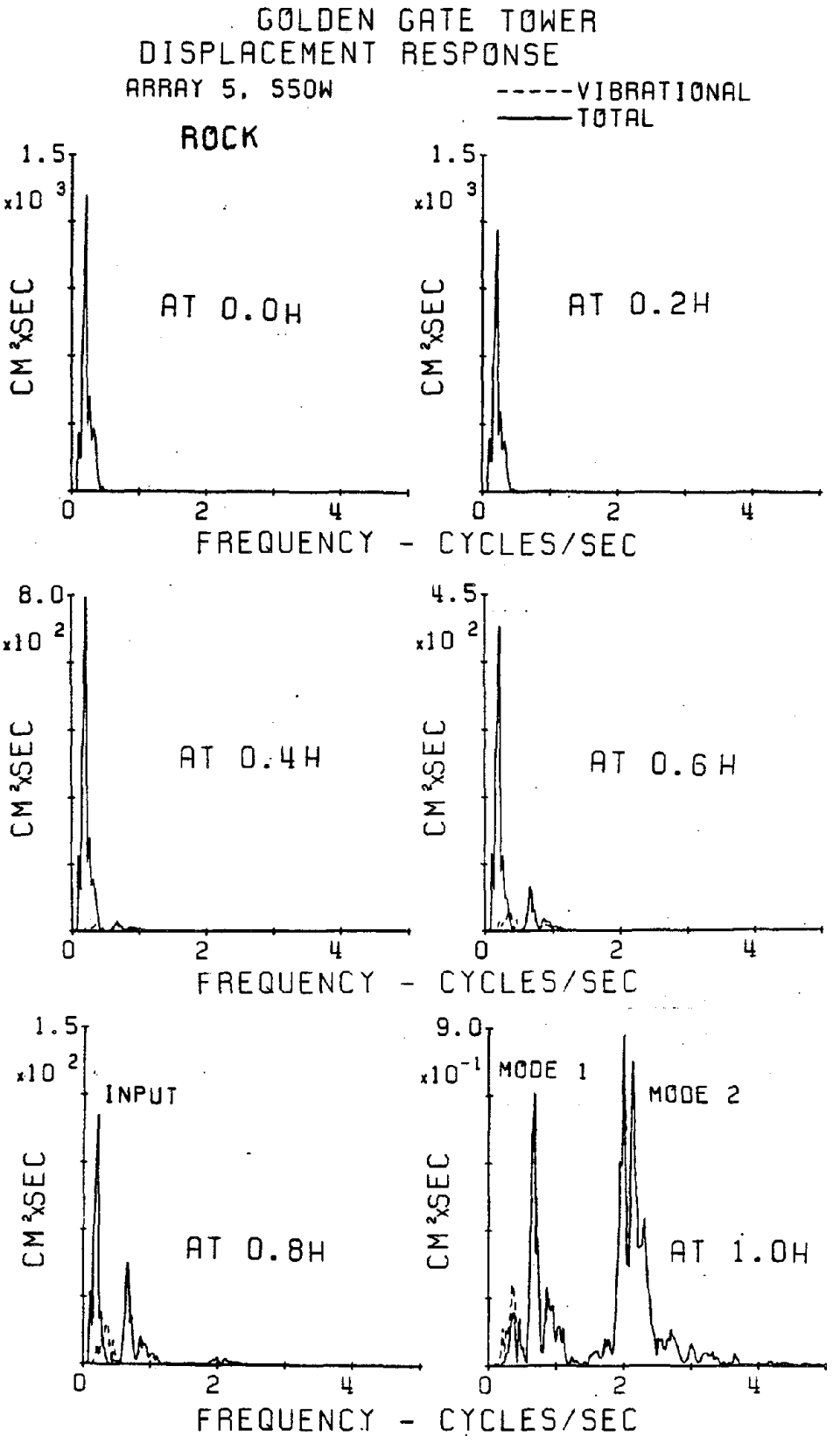

Fig. V-j-2 Power spectra of response displacements to 1979 El Centro Array 5 input (Rock Soil Case).

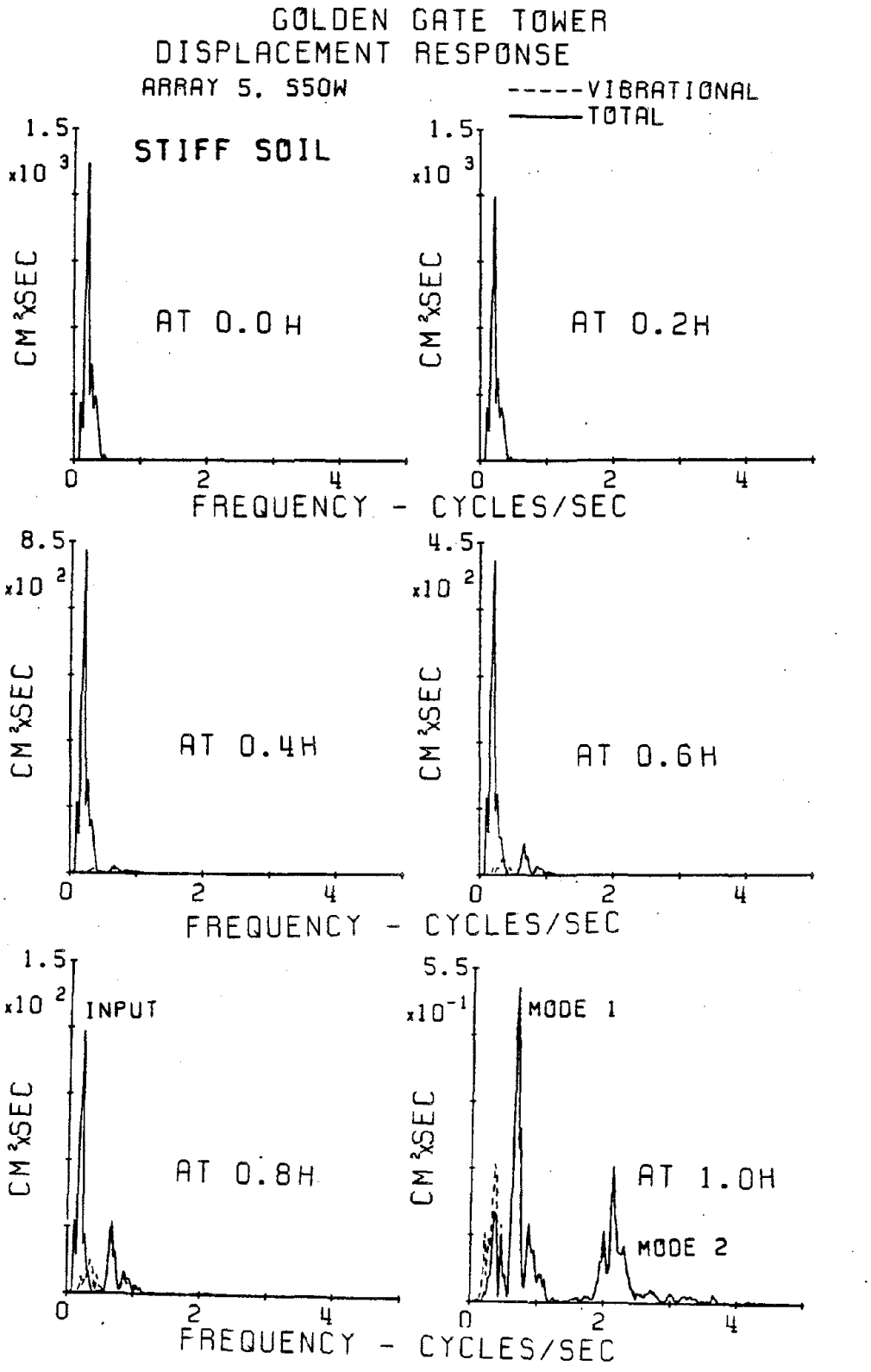

Fig. V-j-3 Power spectra of response displacements to 1979 El Centro Array 5 input (moderately Stiff Soil Case).

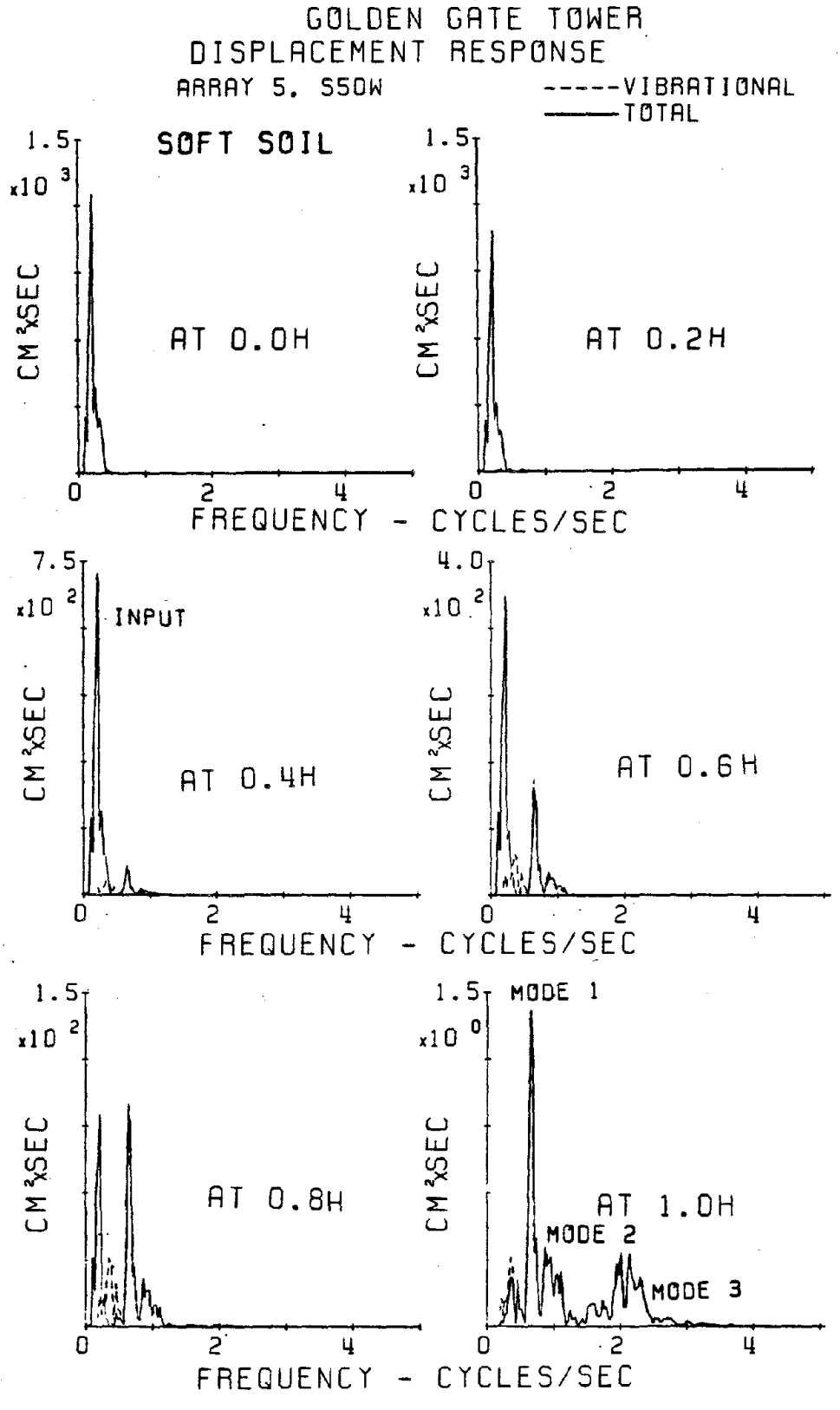

Fig. V-j-4 Power spectra of response displacements to 1979 El Centro Array 5 input (Soft Soil Case).

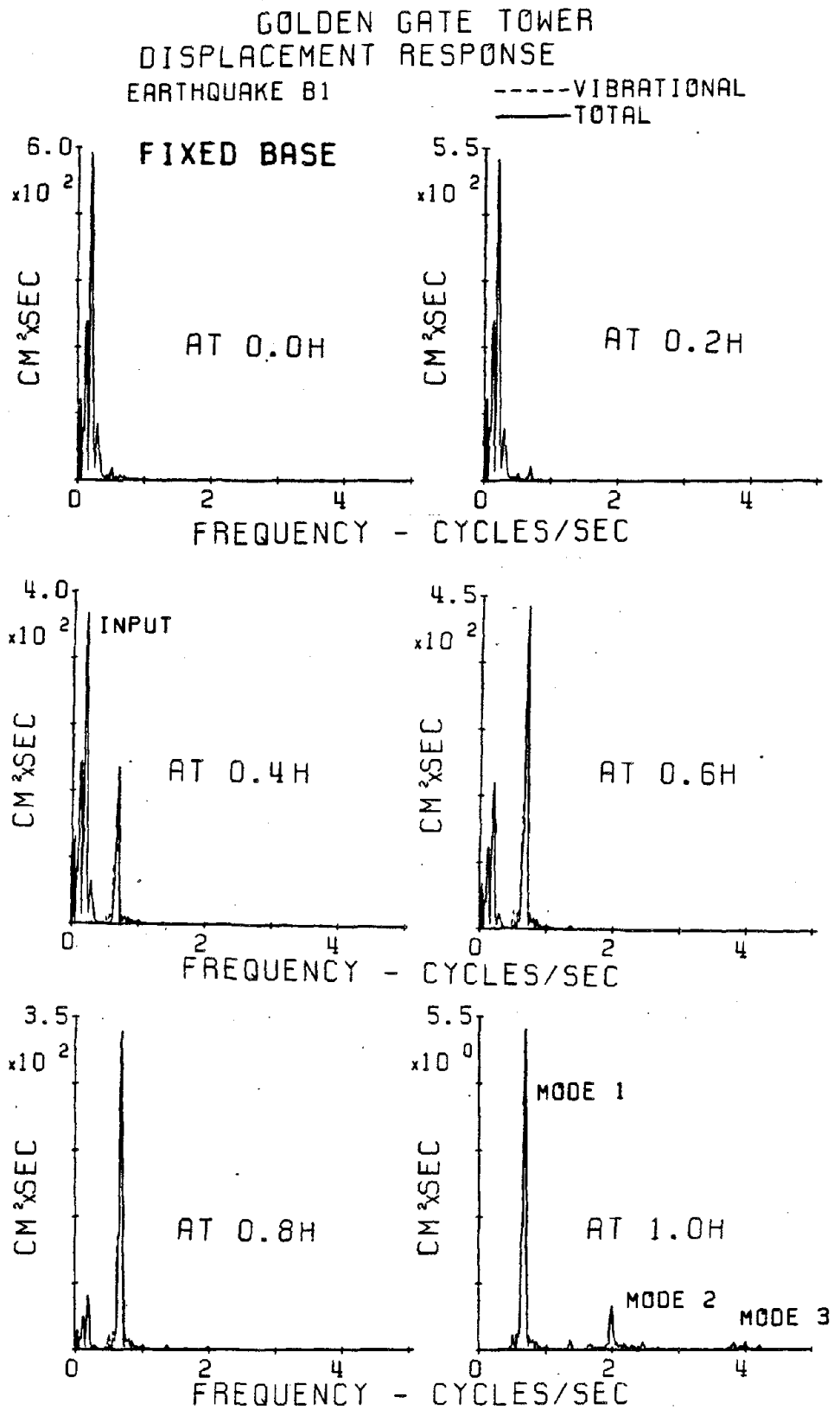

Fig. V-j-5 Power spectra of response displacements to artificial earthquake B-1 input (Fixed Base Case).

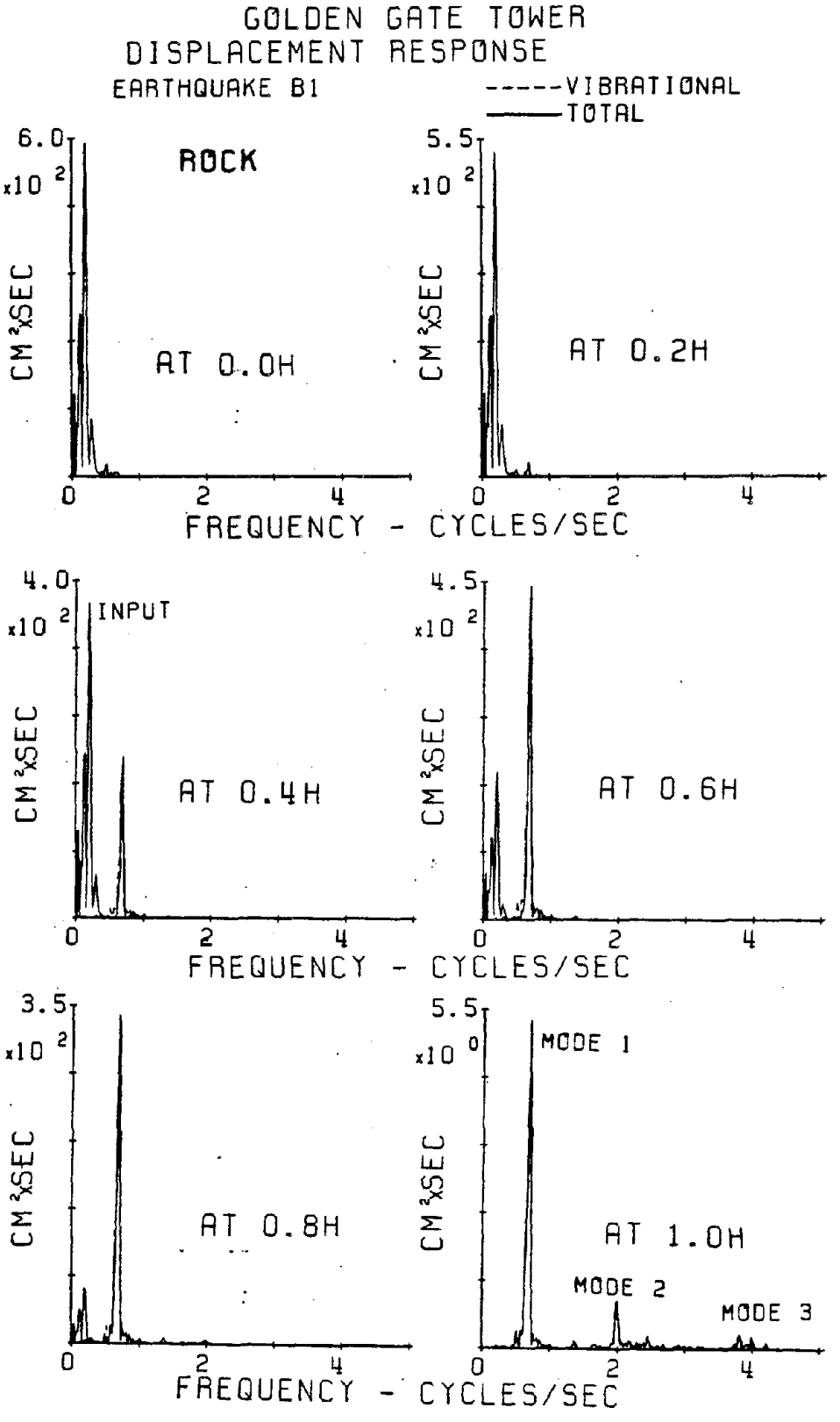

Fig. V-j-6 Power spectra of response displacements to artificial earthquake B-1 input (Rock Soil Case).

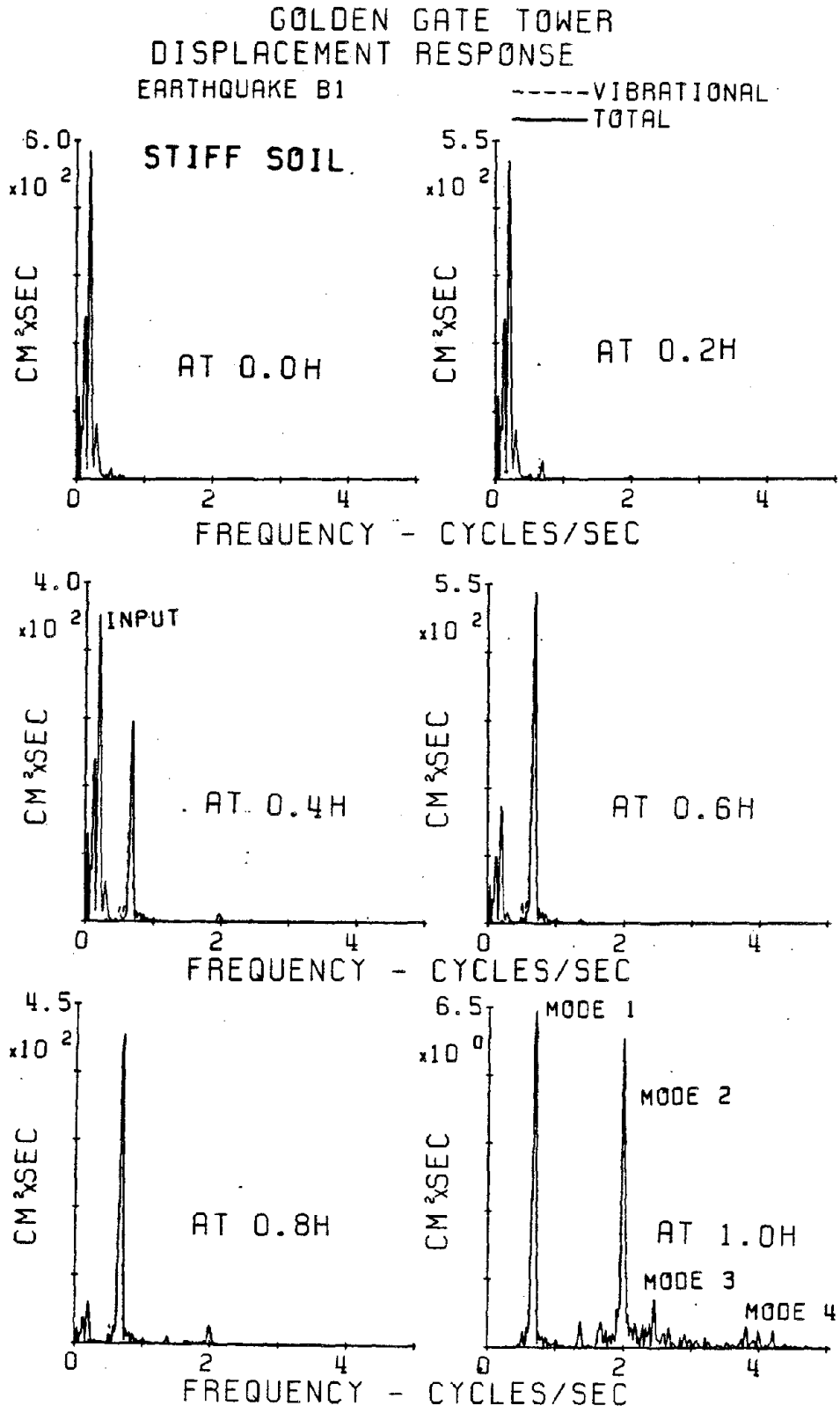

Fig. V-j-7 Power spectra of response displacements to artificial earthquake B-1 input (Moderately Stiff Soil Case).

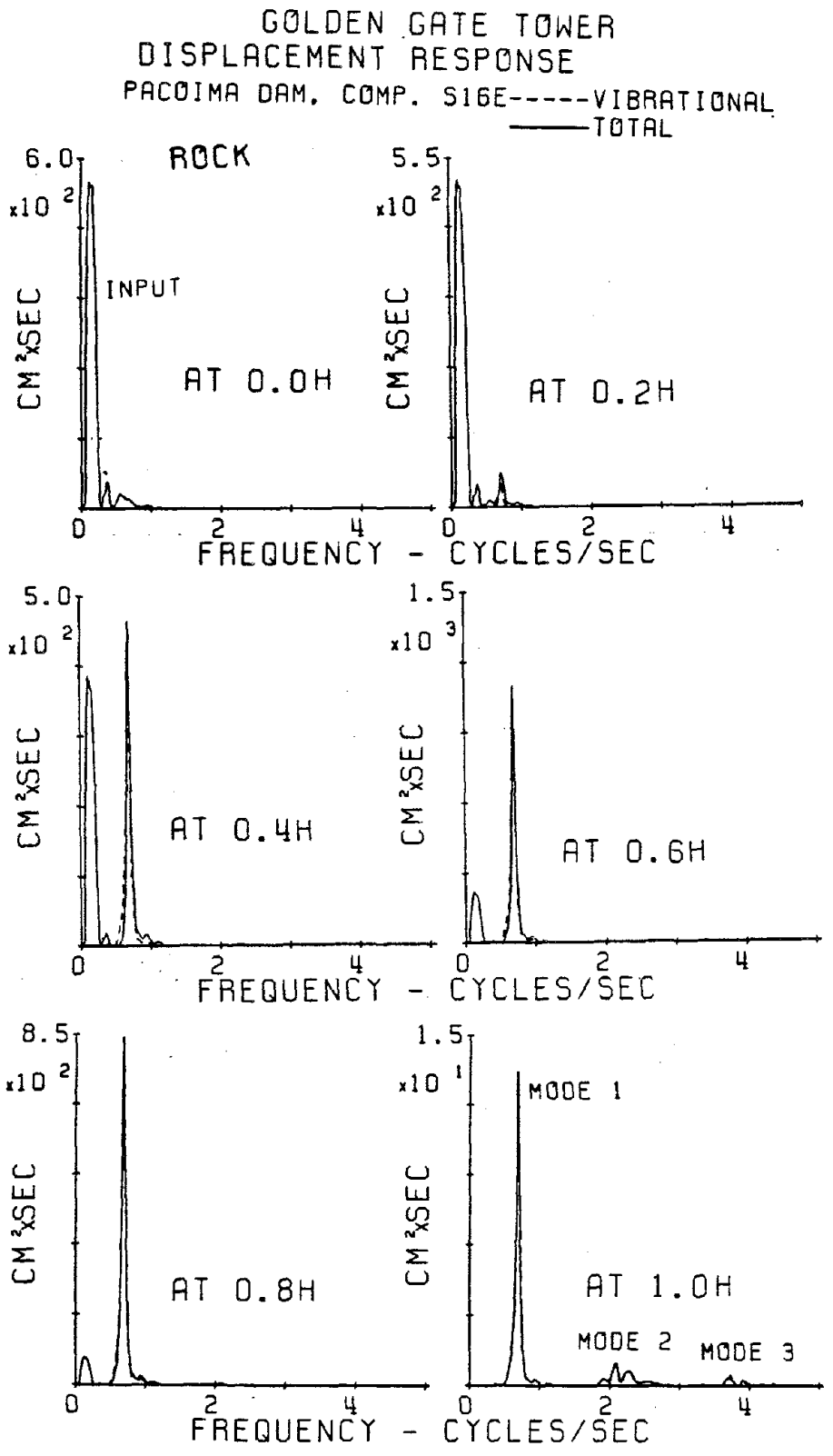

Fig. V-j-10 Power spectra of response displacements to 1971 Pacoima Dam input (Rock Soil Case).

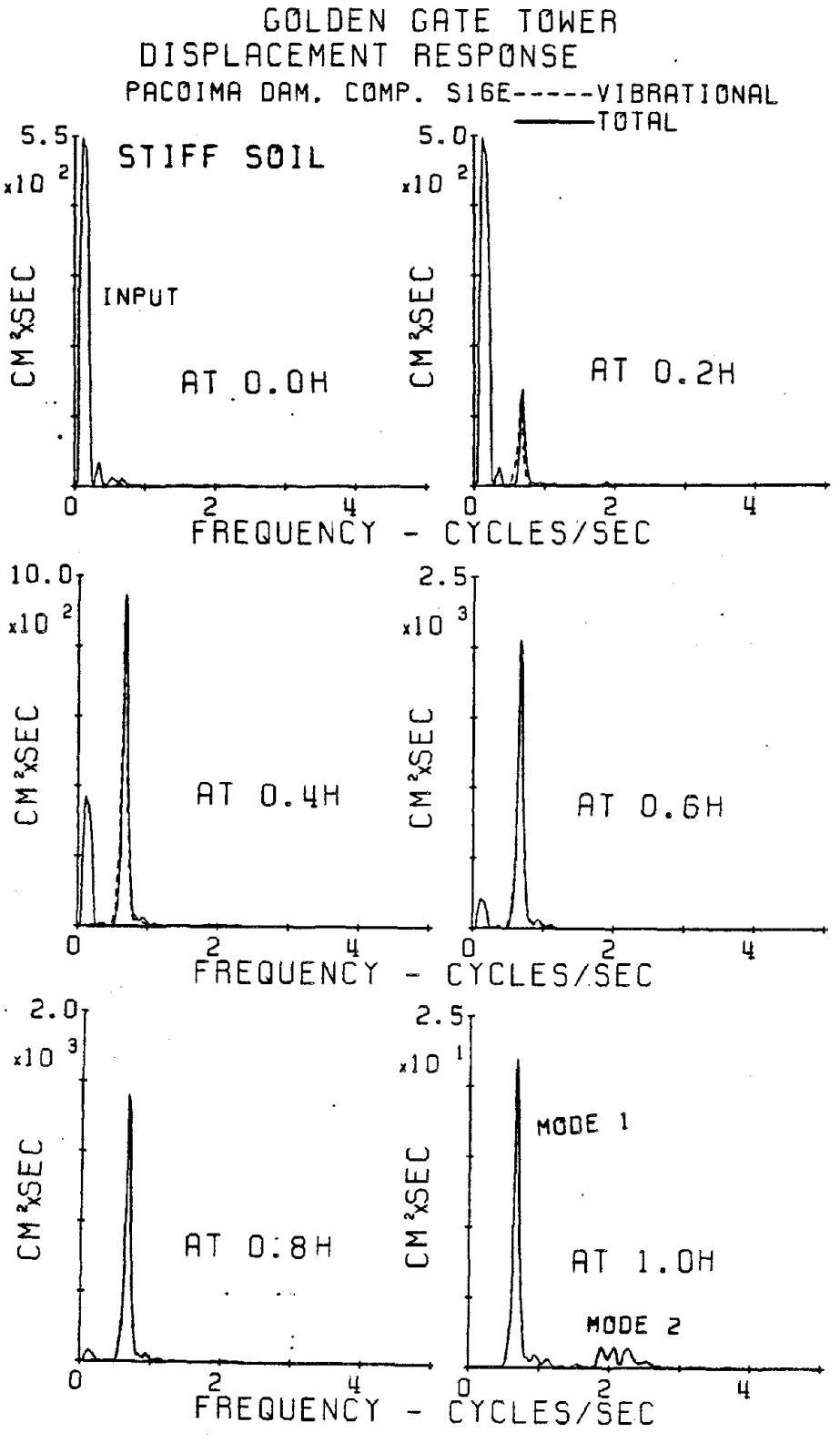

Fig. V-j-11 Power spectra of response displacements to 1971 Pacoima Dam input (Moderately Stiff Soil Case).

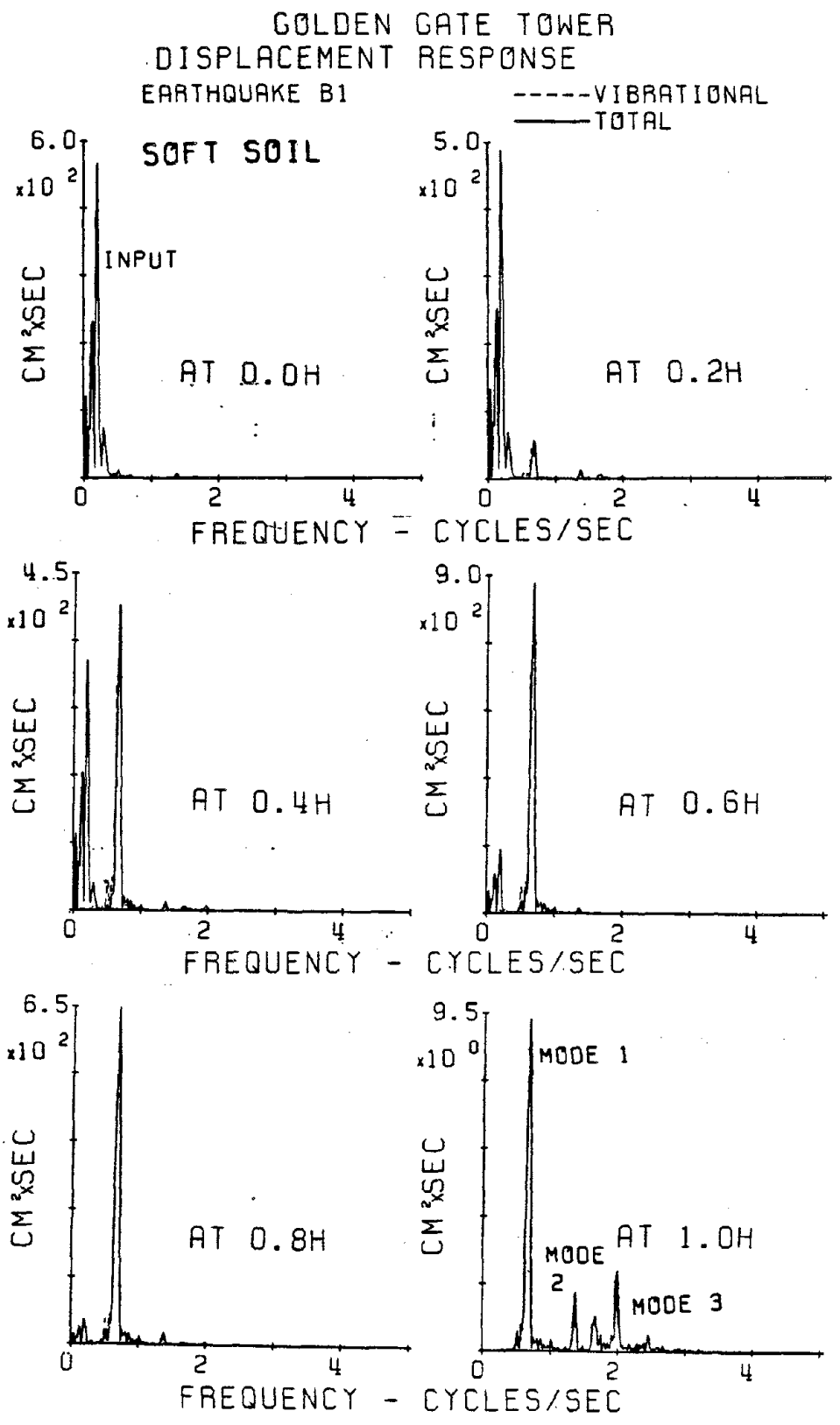

Fig. V-j-8 Power spectra of response displacements to artificial earthquake B-1 input (Soft Soil Case).

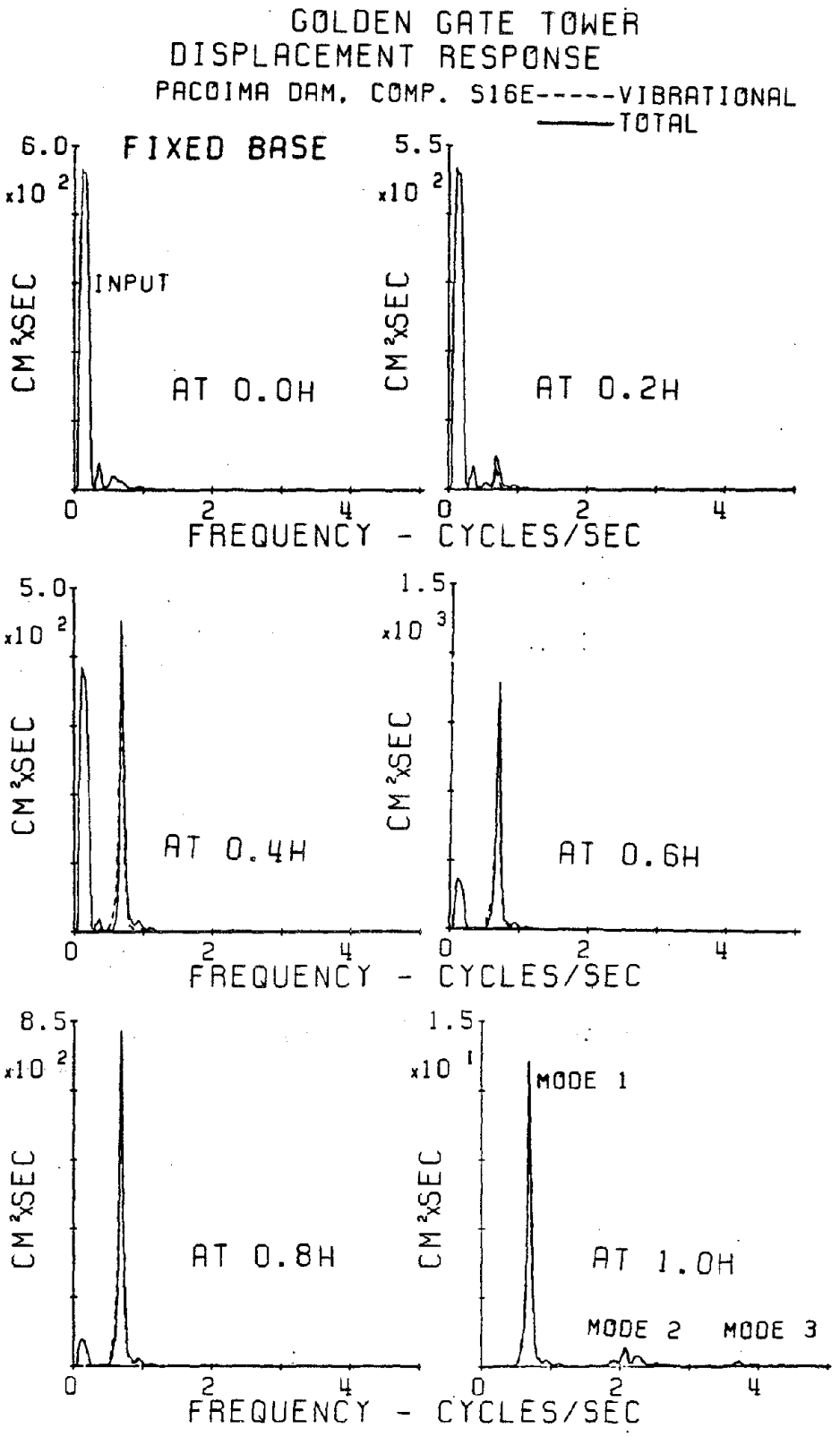

Fig. V-j-9 Power spectra of response displacements to 1971 Pacoima Dam input (Fixed Base Case).

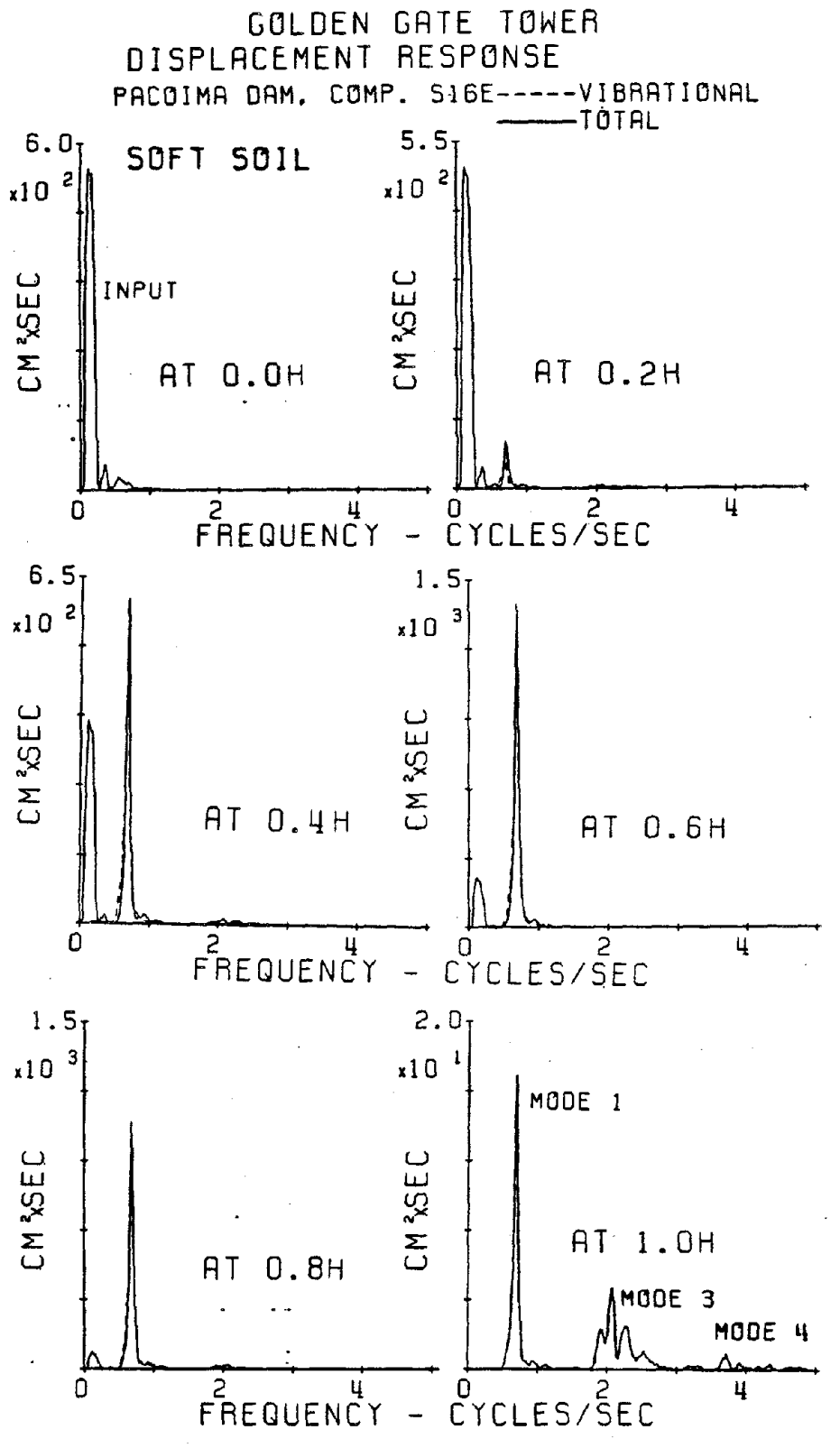

Fig. V-j-12 Power spectra of response displacements to 1971 Pacoima Dam input (Soft Soil Case).

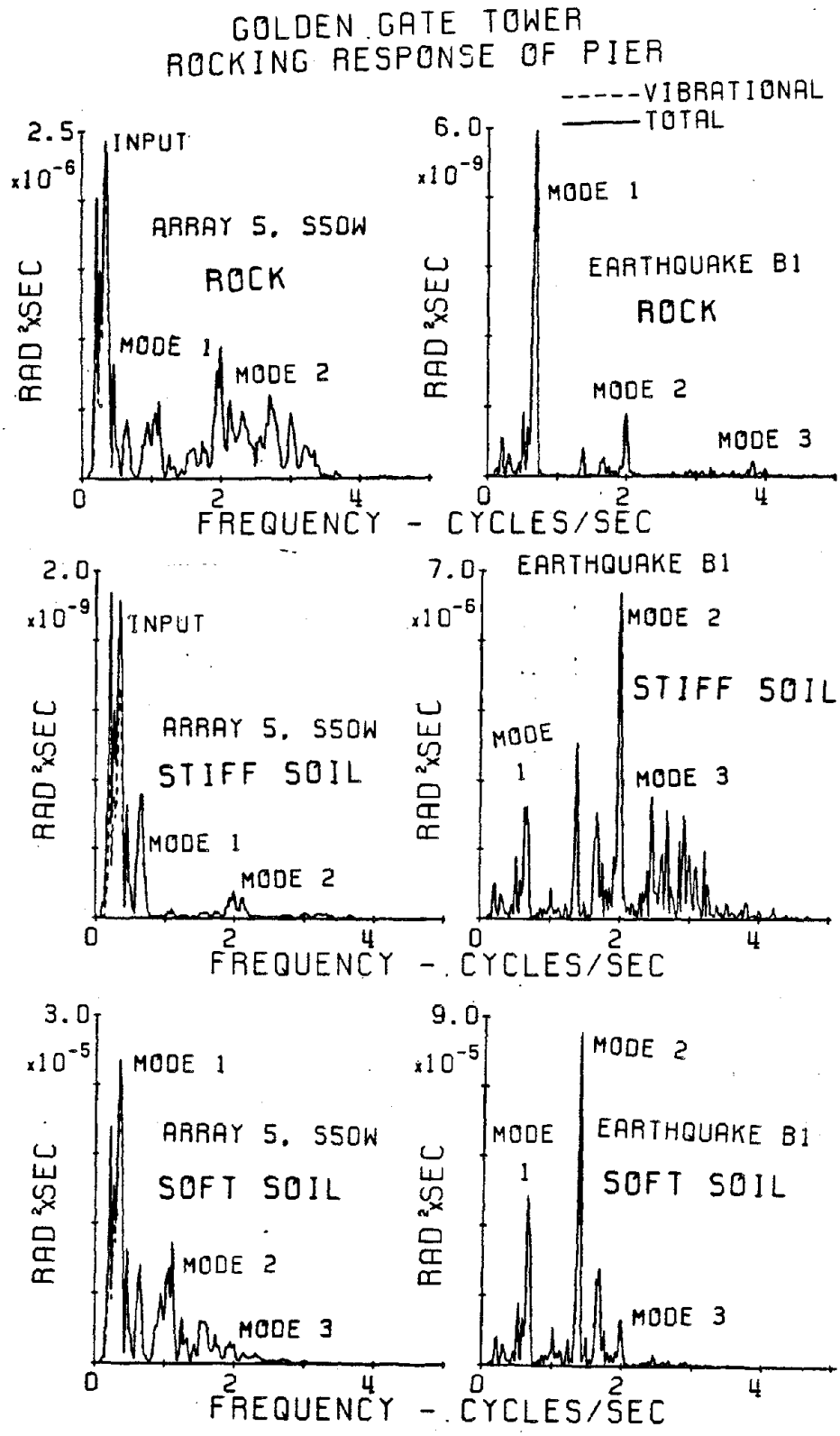

Fig. V-j-13a Power spectra of pier rocking response.

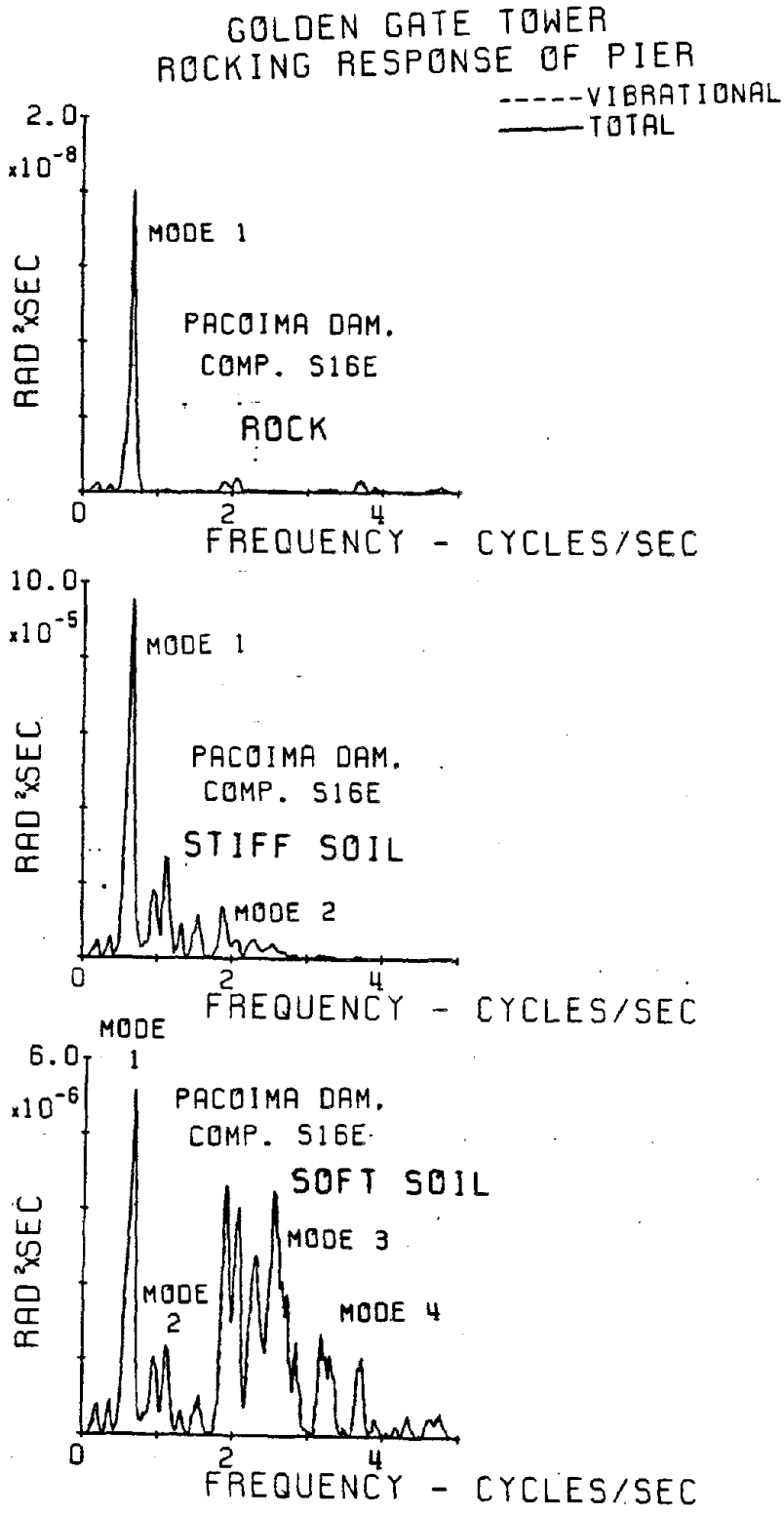

Fig. V-j-13b Power spectra of pier rocking response.

APPENDIX V-k

FREQUENCY DOMAIN FLEXURAL (BENDING) STRESS RESPONSE OF THE GOLDEN GATE TOWER-PIER SYSTEM

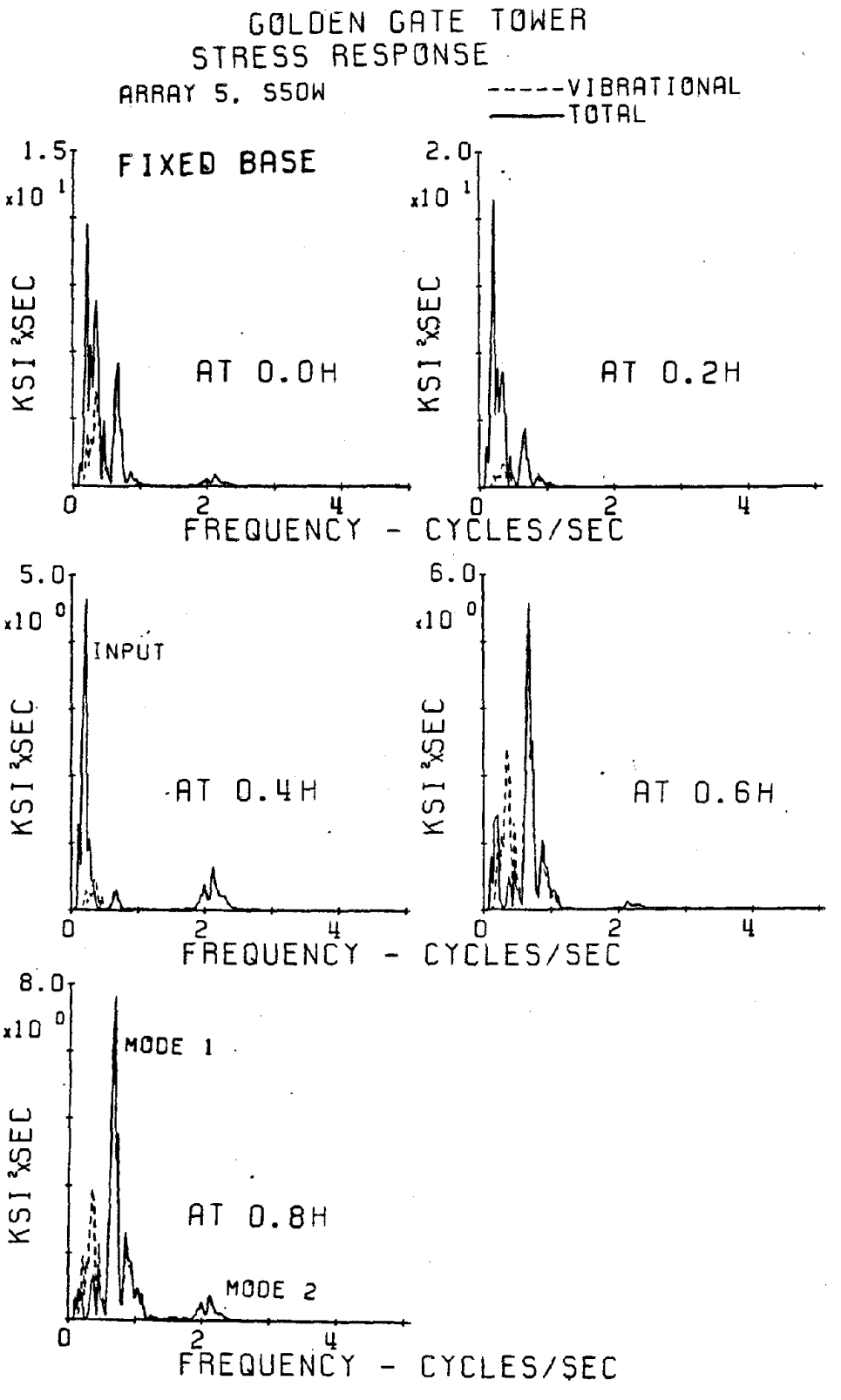

Fig. V-k-1 Power spectra of responses stresses to 1979 El Centro Array 5 input (Fixed Base Case).

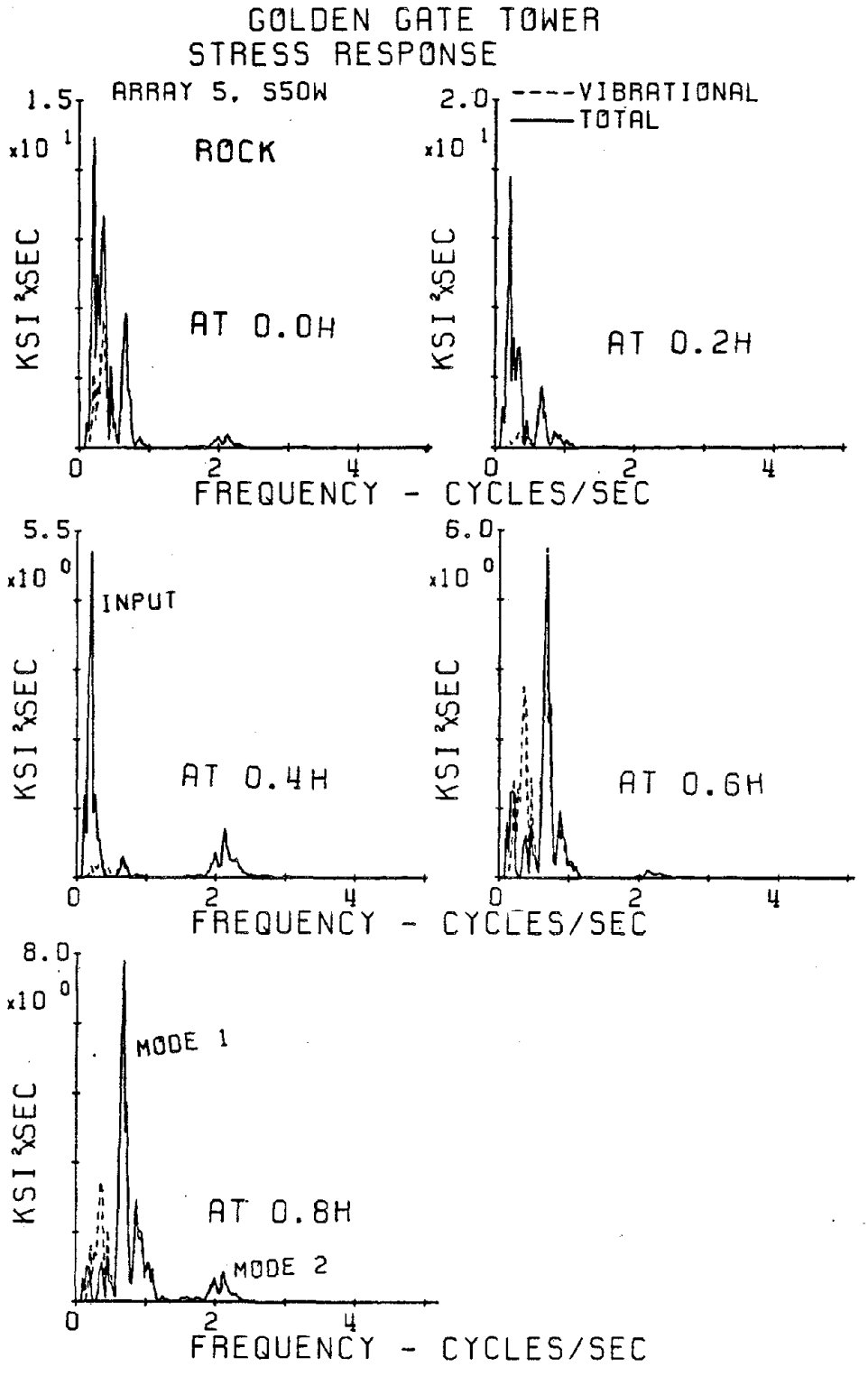

Fig. V-k-2 Power spectra of response stresses to 1979 El Centro Array 5 input (Rock Soil Case).

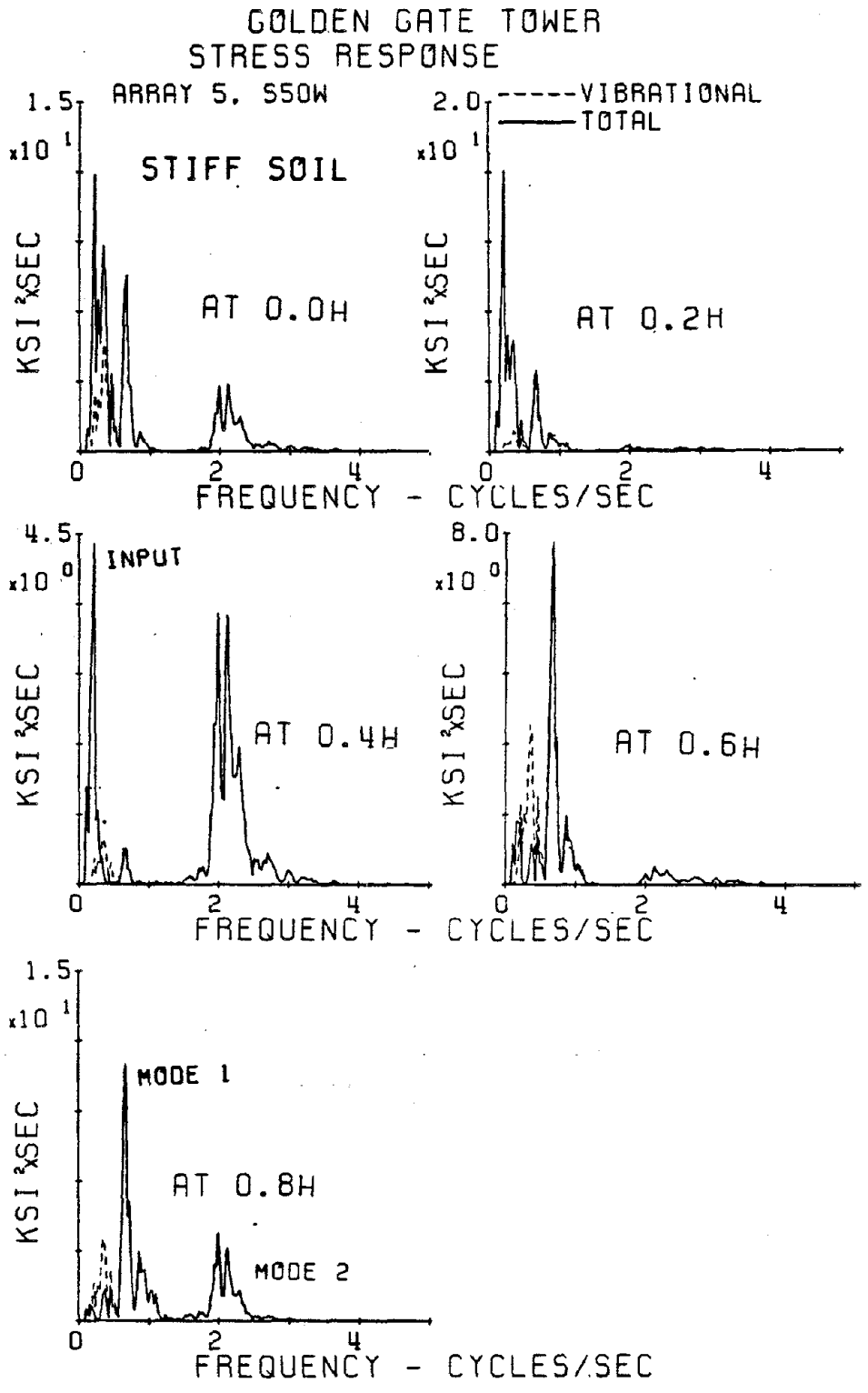

Fig. V-k-3 Power spectra of response stresses to 1979 El Centro Array 5 input (Moderately Stiff Soil Case).

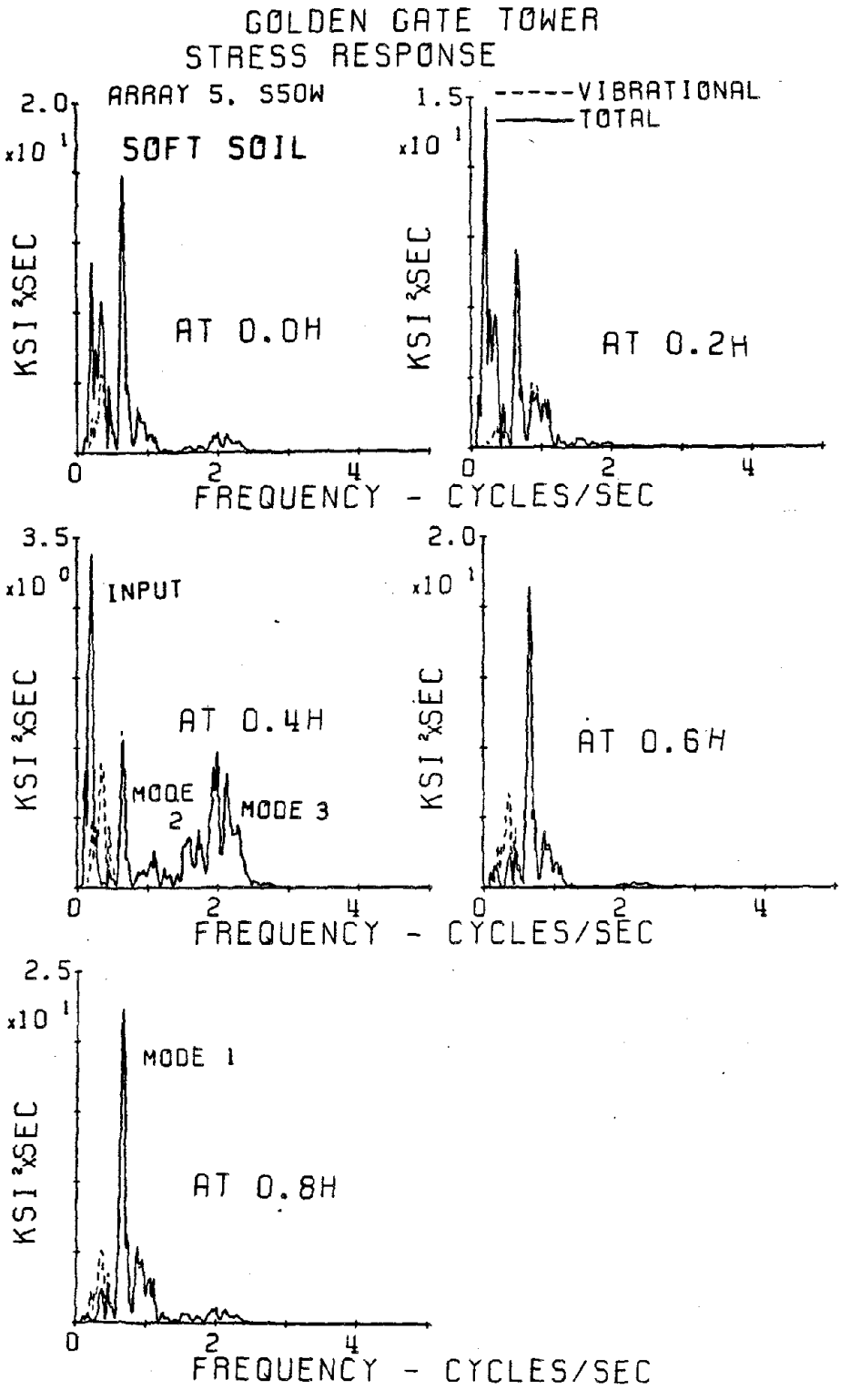

Fig. V-k-4 Power spectra of response stresses to 1979 El Centro Array 5 input (Soft Soil Case).

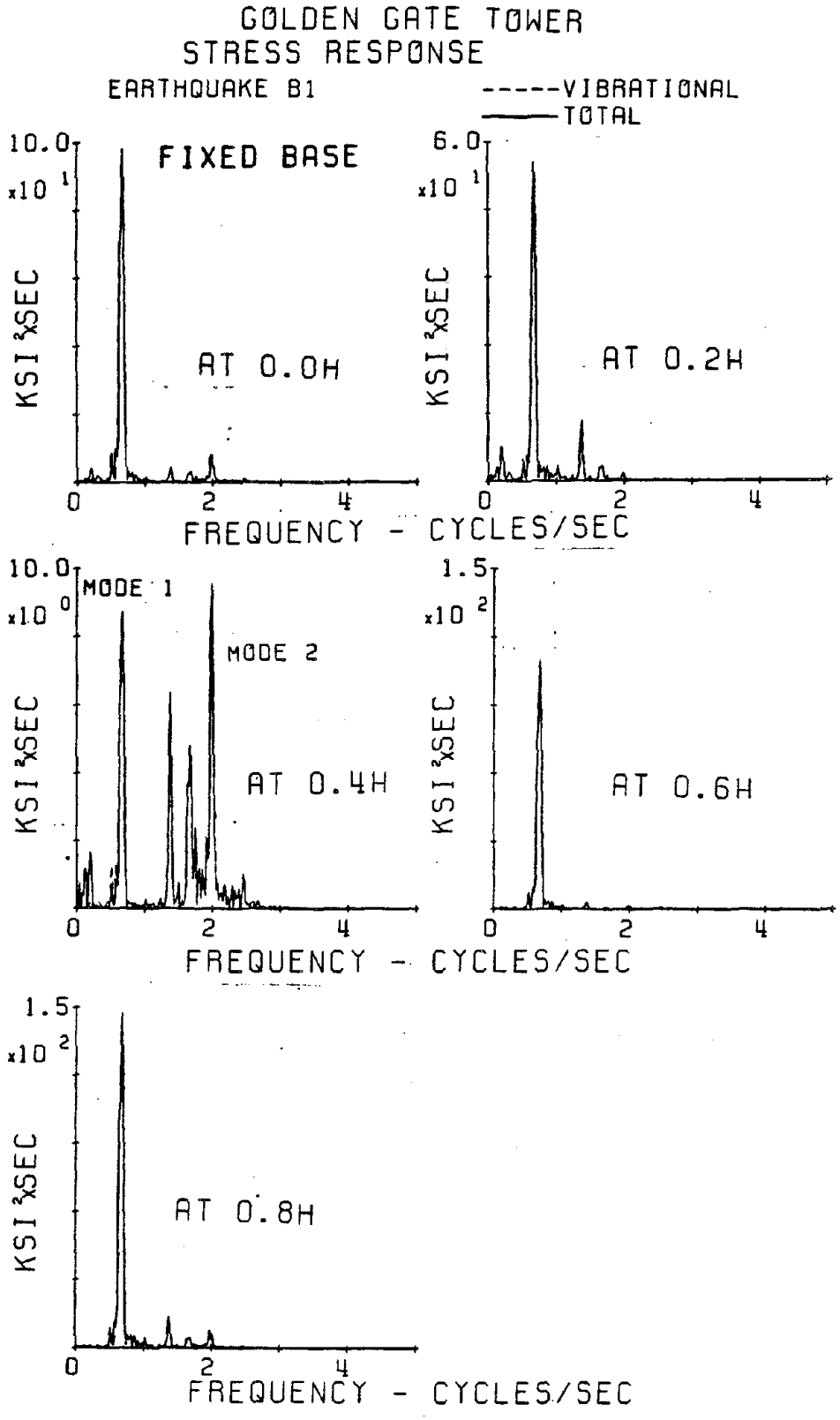

Fig. V-k-5 Power spectra of response stresses to artificial earthquake B-1 input (Fixed Base Case).

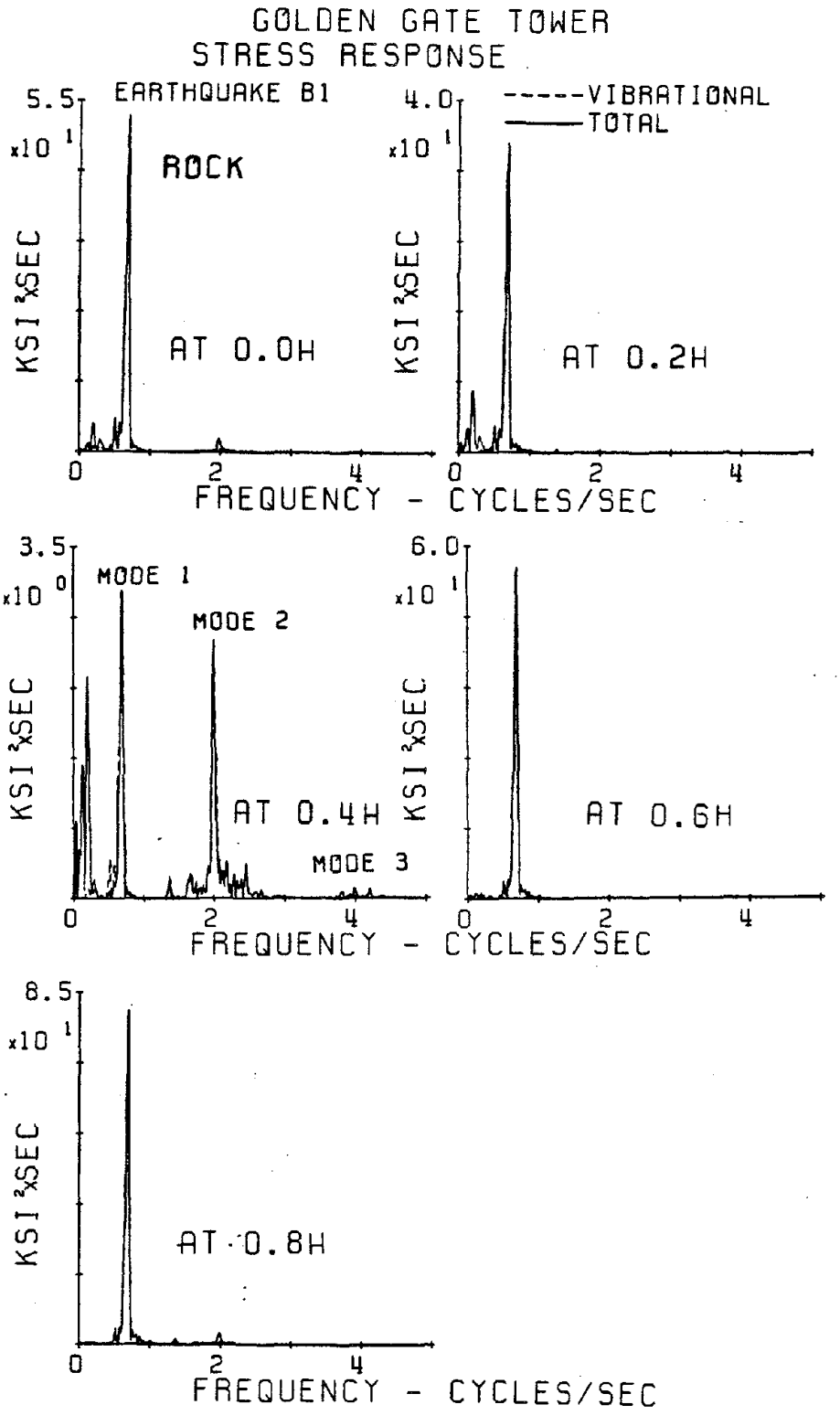

Fig. V-k-6 Power spectra of response stresses to artificial earthquake B-1 input (Rock Soil Case).

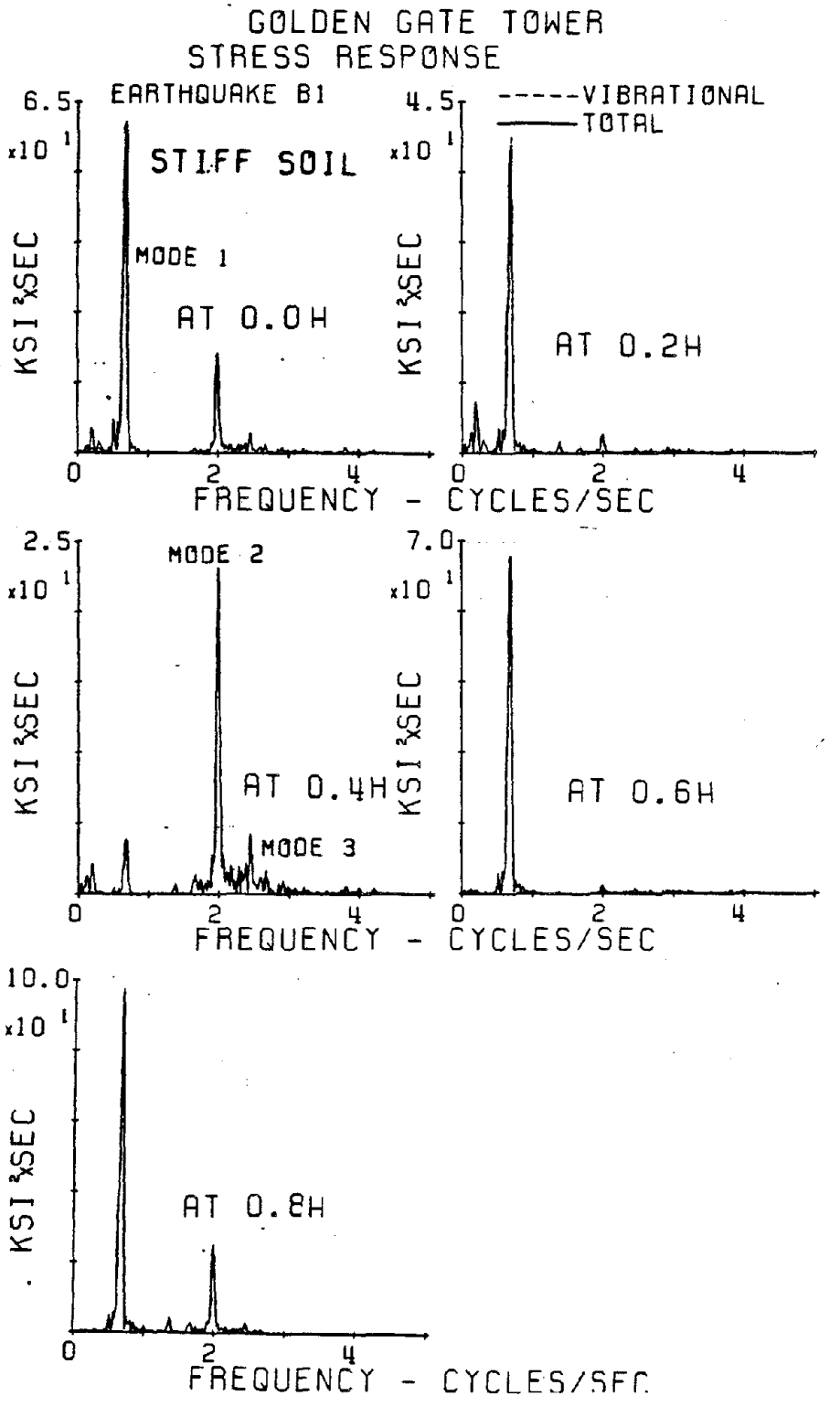

Fig. V-k-7 Power spectra of Response stresses to artificial earthquake B-1 input (Moderately Stiff Soil Case).

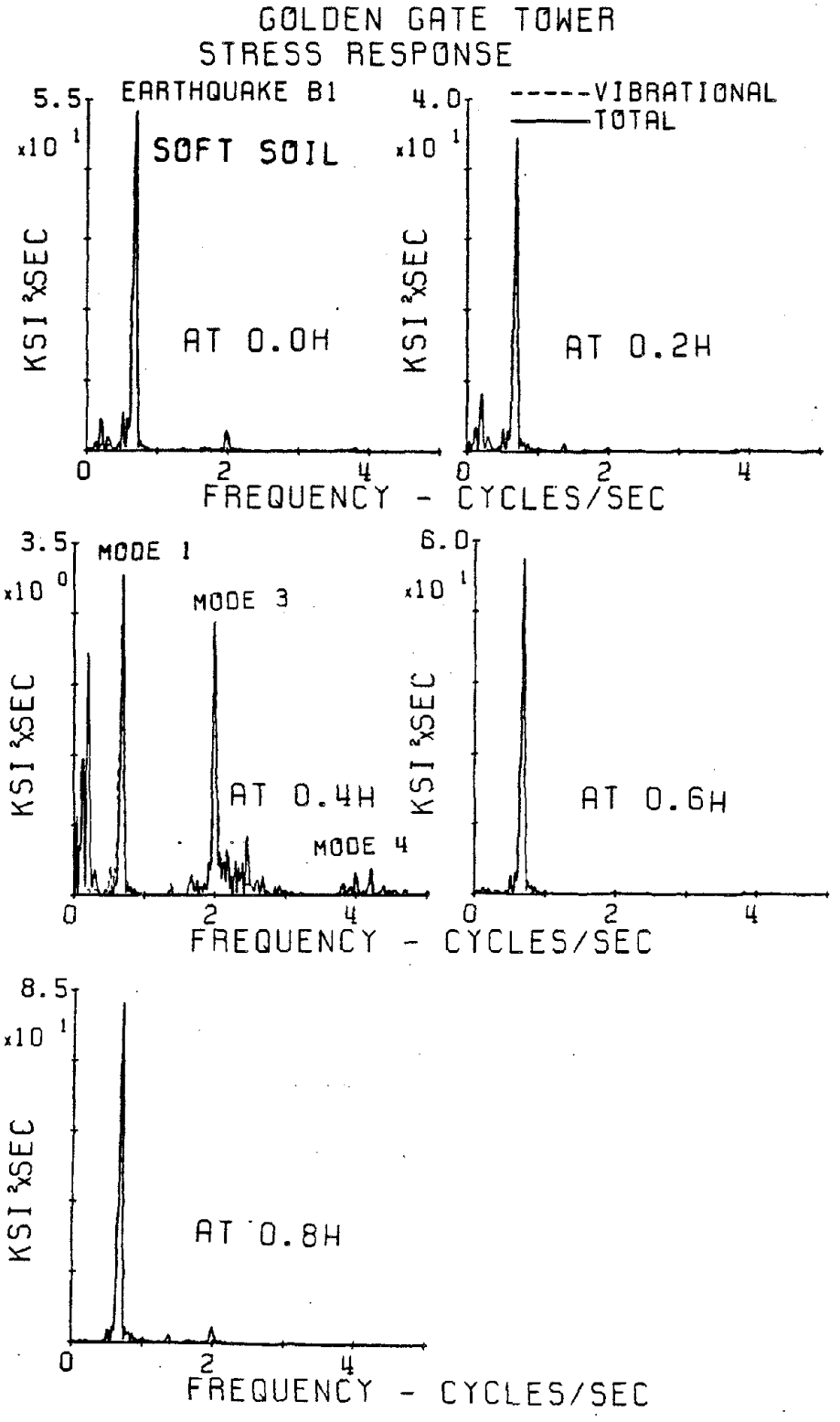

Fig. V-k-8 Power spectra of response stresses to artificial earthquake B-1 input (Soft Soil Case).

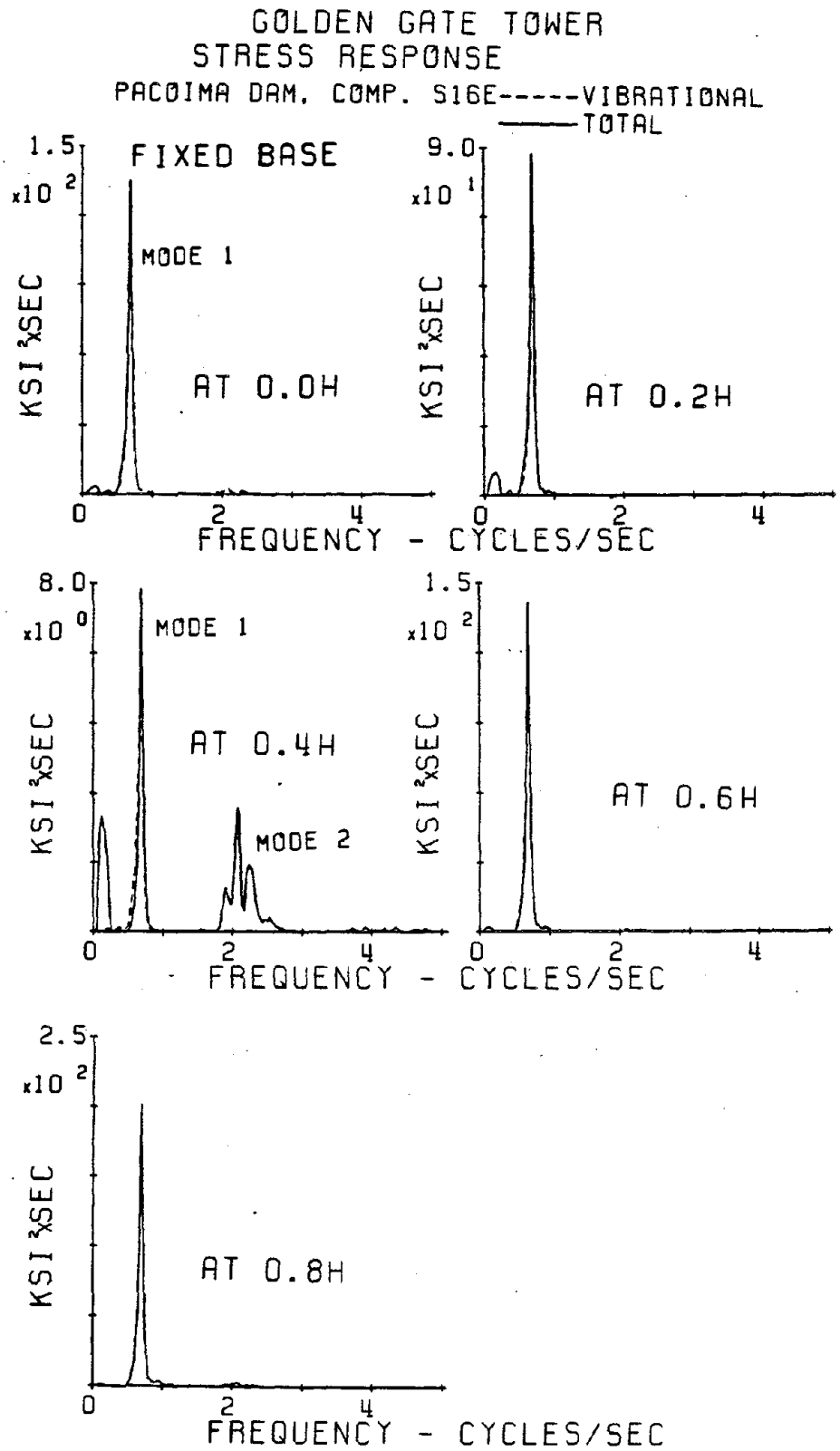

Fig. V-k-9 Power spectra of response stresses to 1971 Pacoima Dam input (Fixed Base Case).

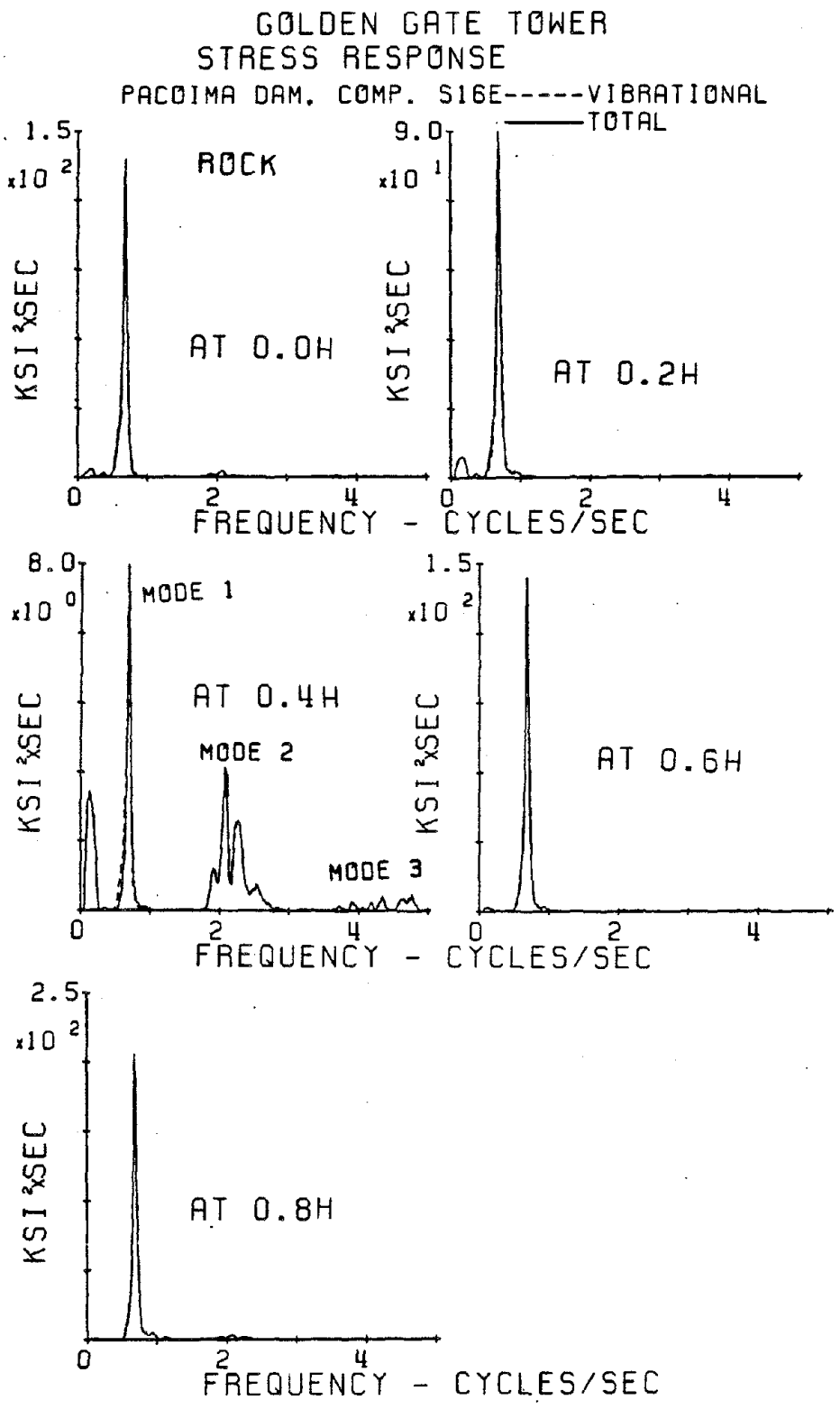

Fig. V-k-10 Power spectra of response stresses to 1971 Pacoima Dam input (Rock Soil Case).

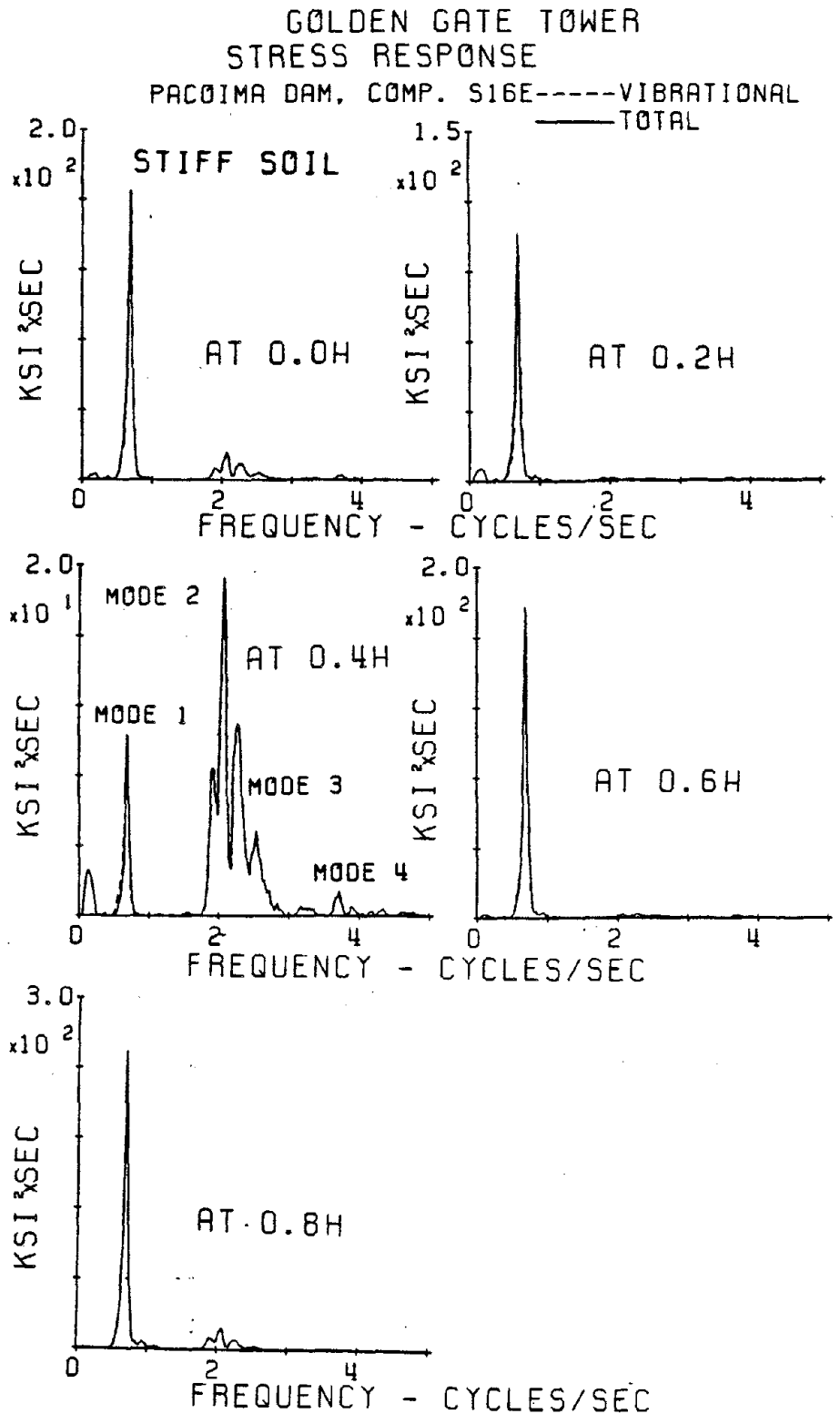

Fig. V-k-11 Power spectra of response stresses to 1971 Pacoima Dam input (Moderately Stiff Soil).

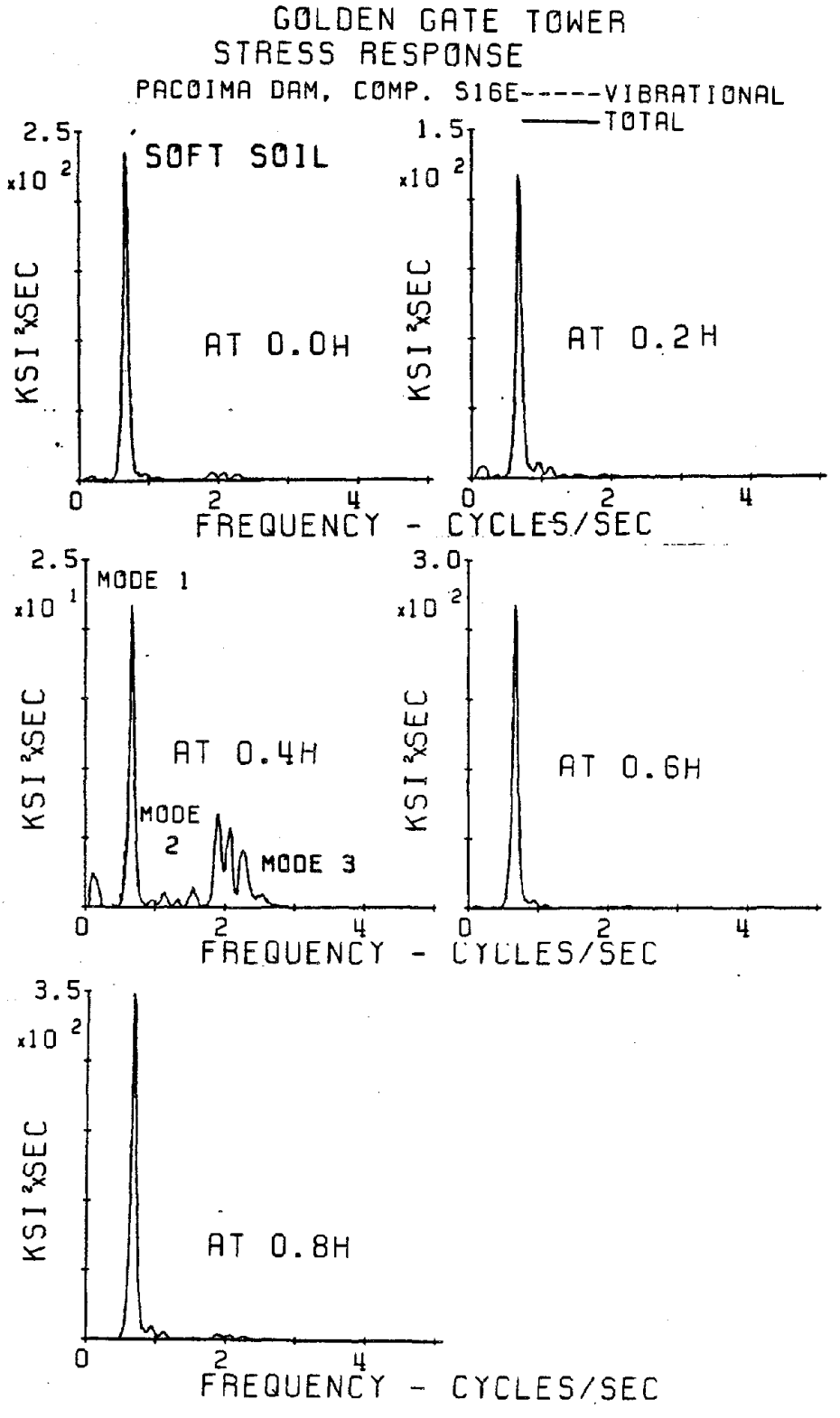

Fig. V-k-12 Power spectra of response stresses to 1971 Pacoima Dam input (Soft Soil Case).

APPENDIX V-1

FREQUENCY DOMAIN SHEAR FORCE RESPONSE OF THE GOLDEN GATE BRIDGE TOWER-PIER SYSTEM

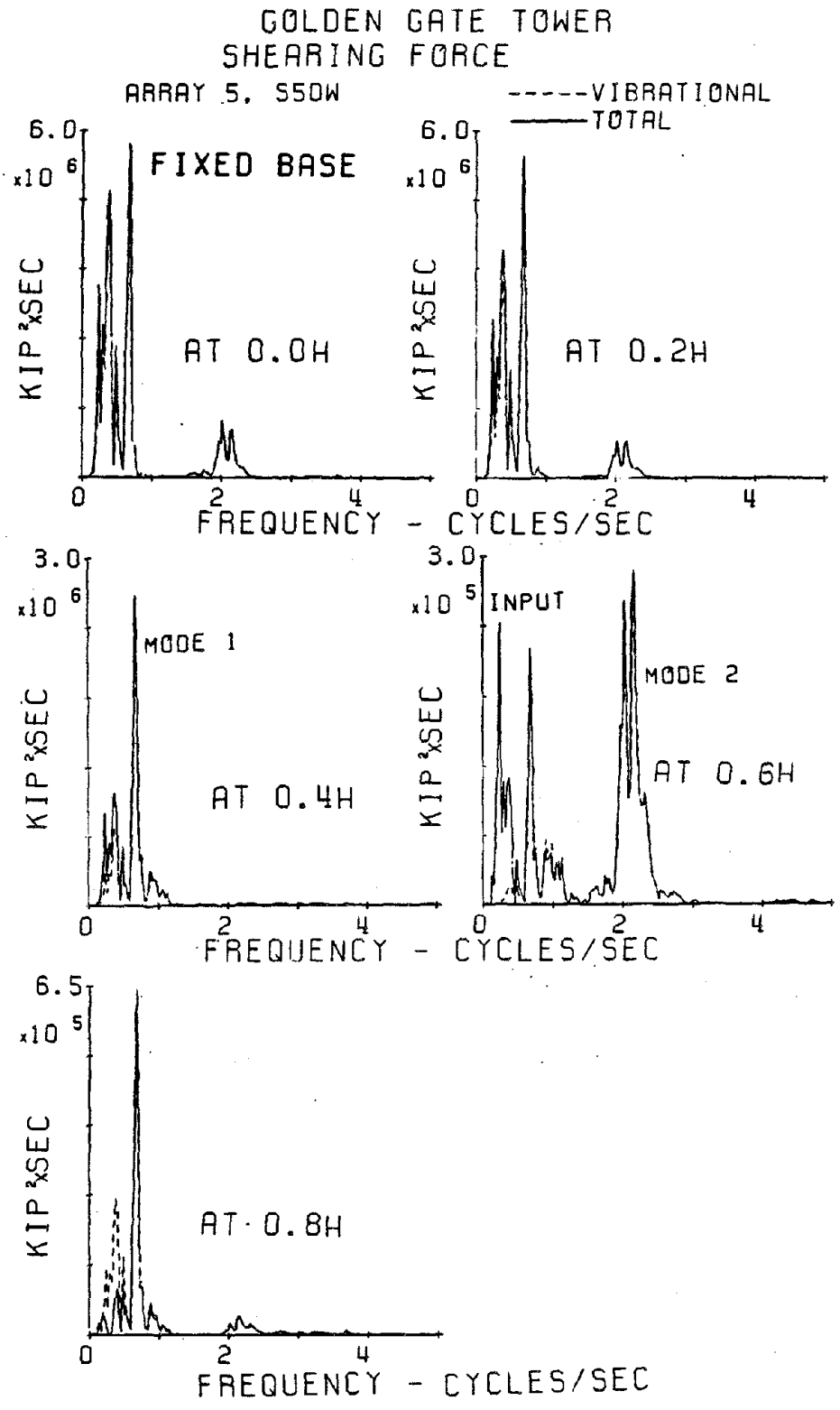

Fig. V-1-1 Power spectra of response shear forces to 1979 El Centro Array 5 input (Fixed Base Case).

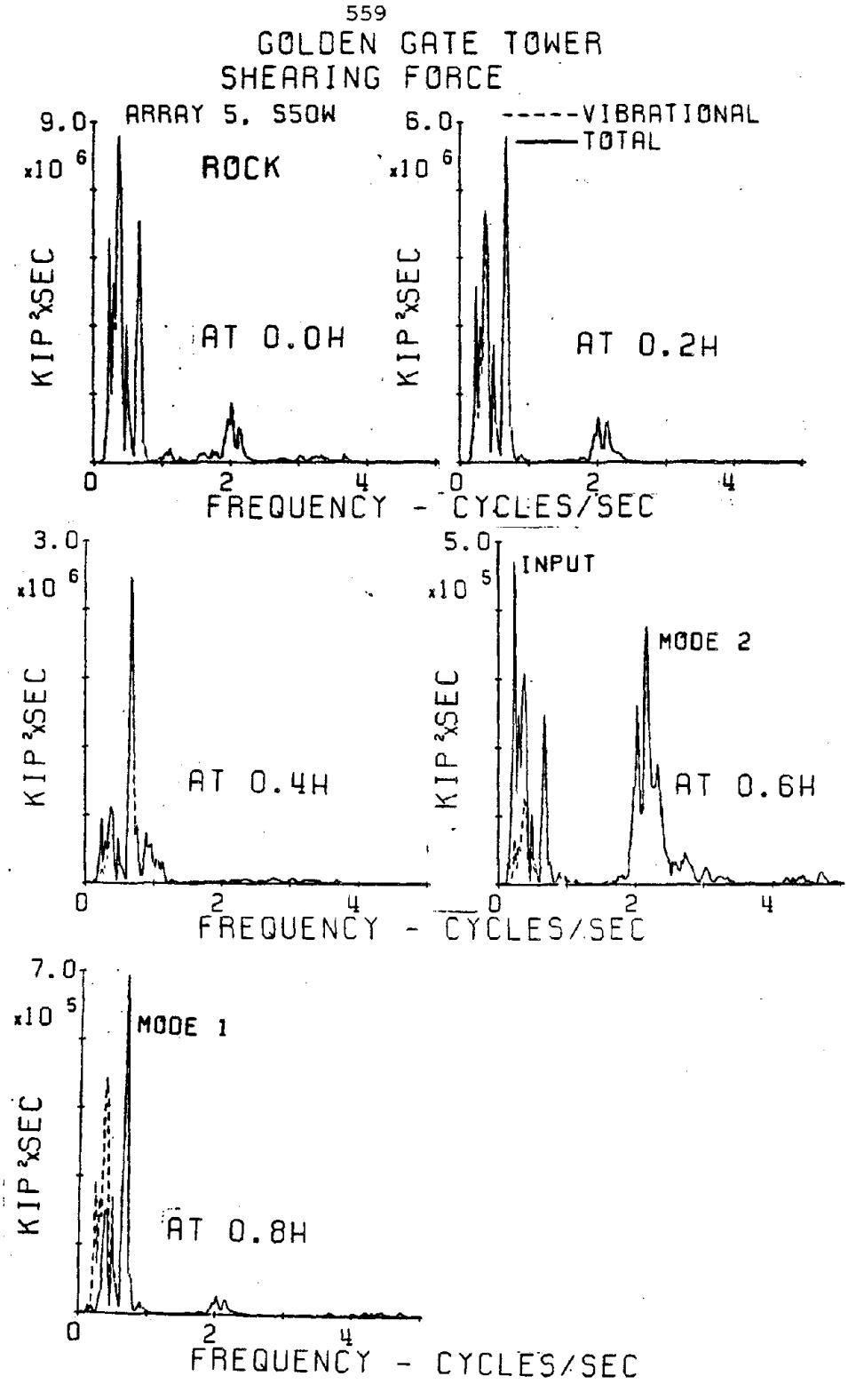

Fig. V-1-2 Power spectra of response shear forces to 1979 El Centro Array 5 input (Rock Soil Case).

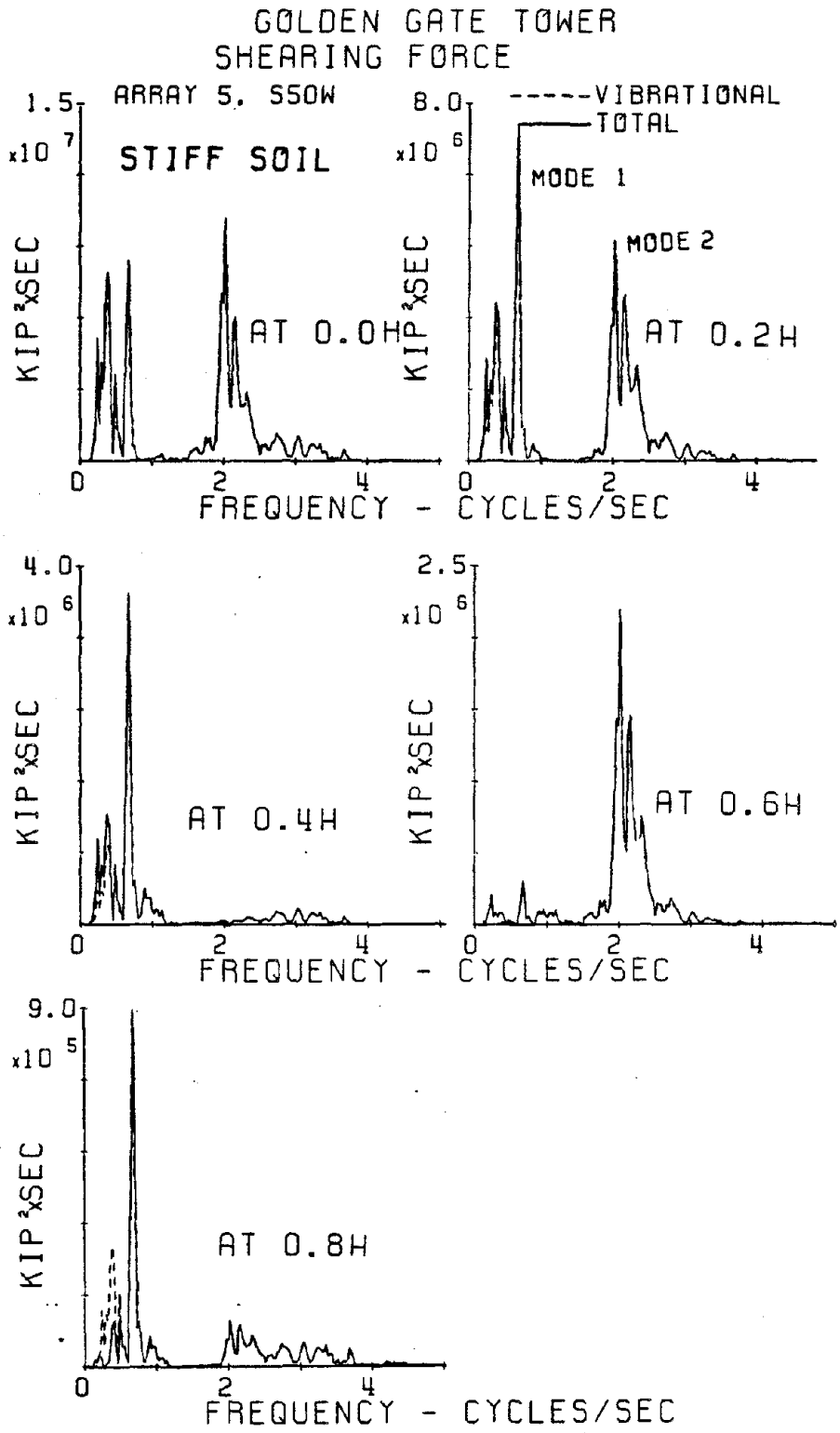

Fig. V-1-3 Power spectra of response shear forces to 1979 El Centro Array 5 input (Moderately Stiff Soil Case).

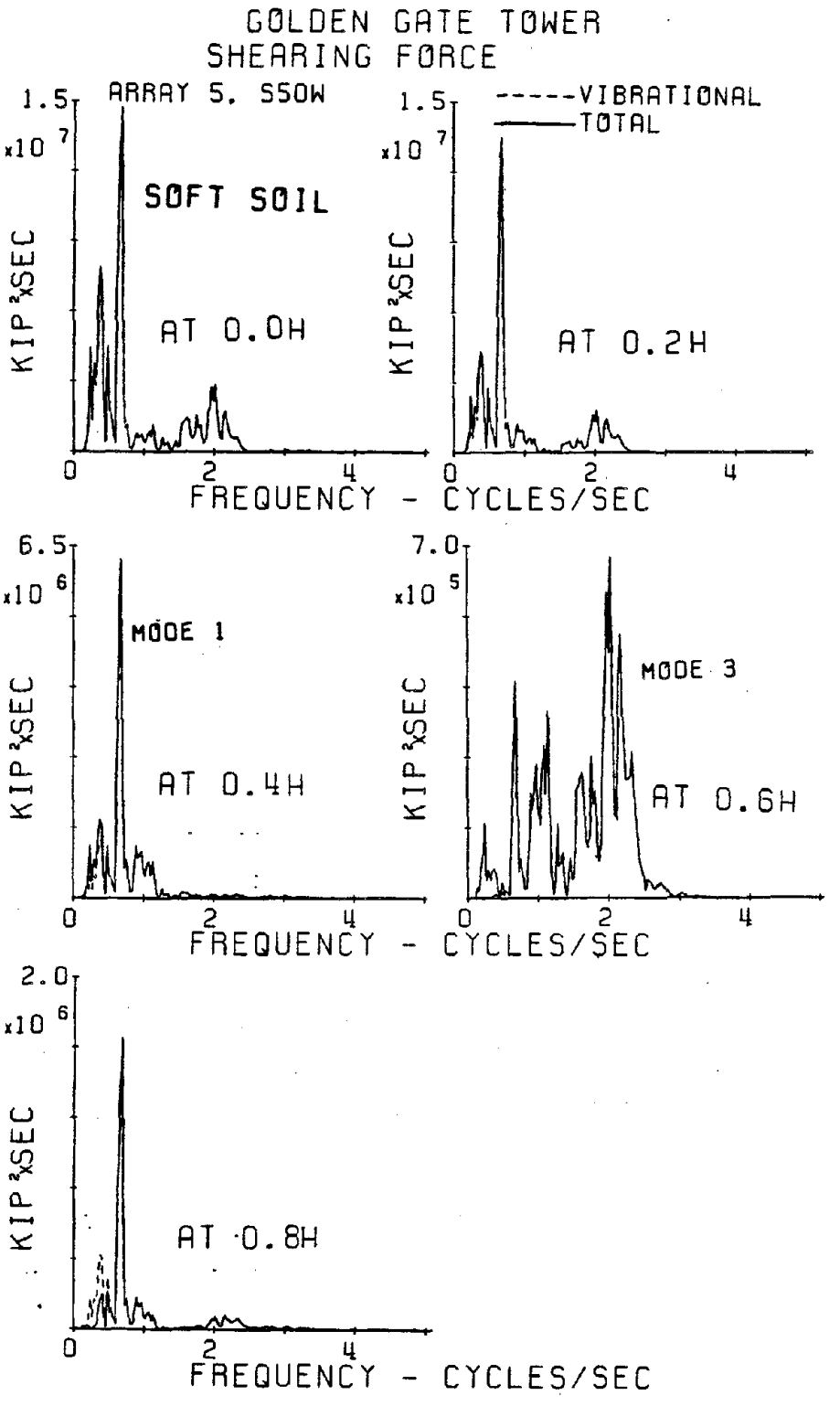

Fig. V-1-4 Power spectra of response stresses to 1979 El Centro Array 5 input (Soft Soil Case).

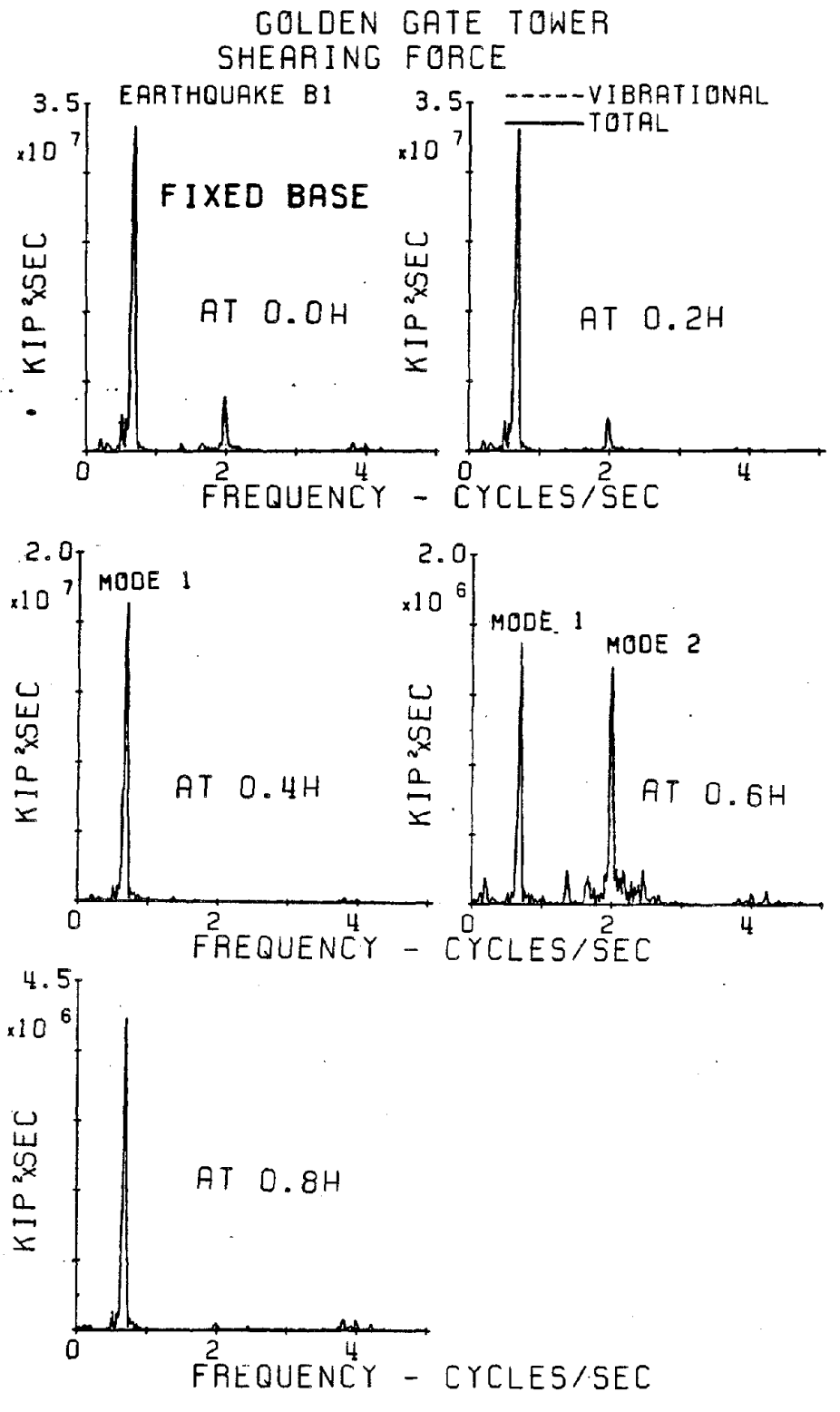

Fig. V-1-5 Power spectra of response shear forces to artificial earthquake B-1 input (Fixed Base Case).

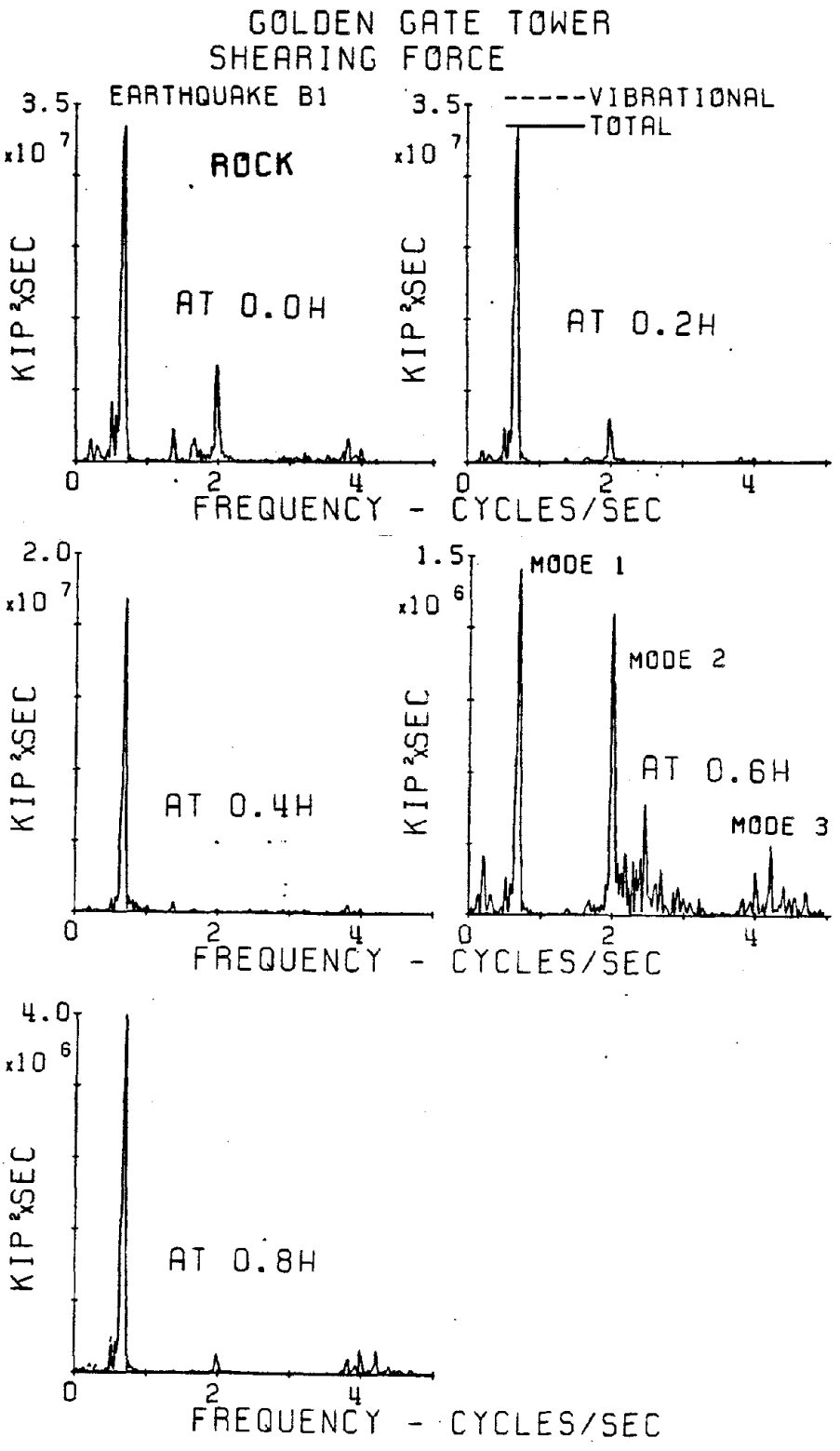

Fig. V-1-6 Power spectra of response shear forces to artificial earthquake B-1 input (Rock Soil Case).

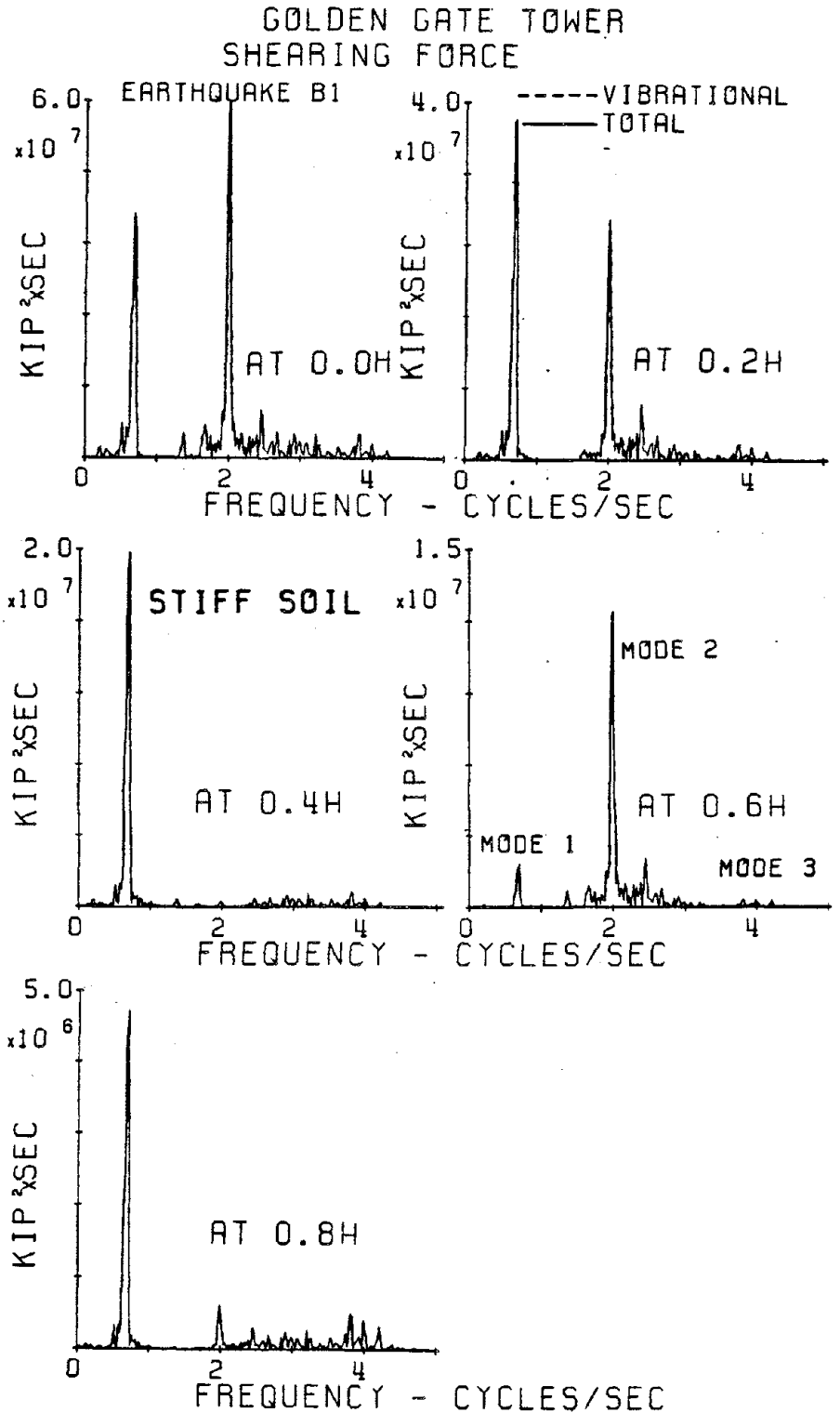

Fig. V-1-7 Power spectra of response shear forces to artificial earthquake B-1 input (Moderately Stiff Soil Case).

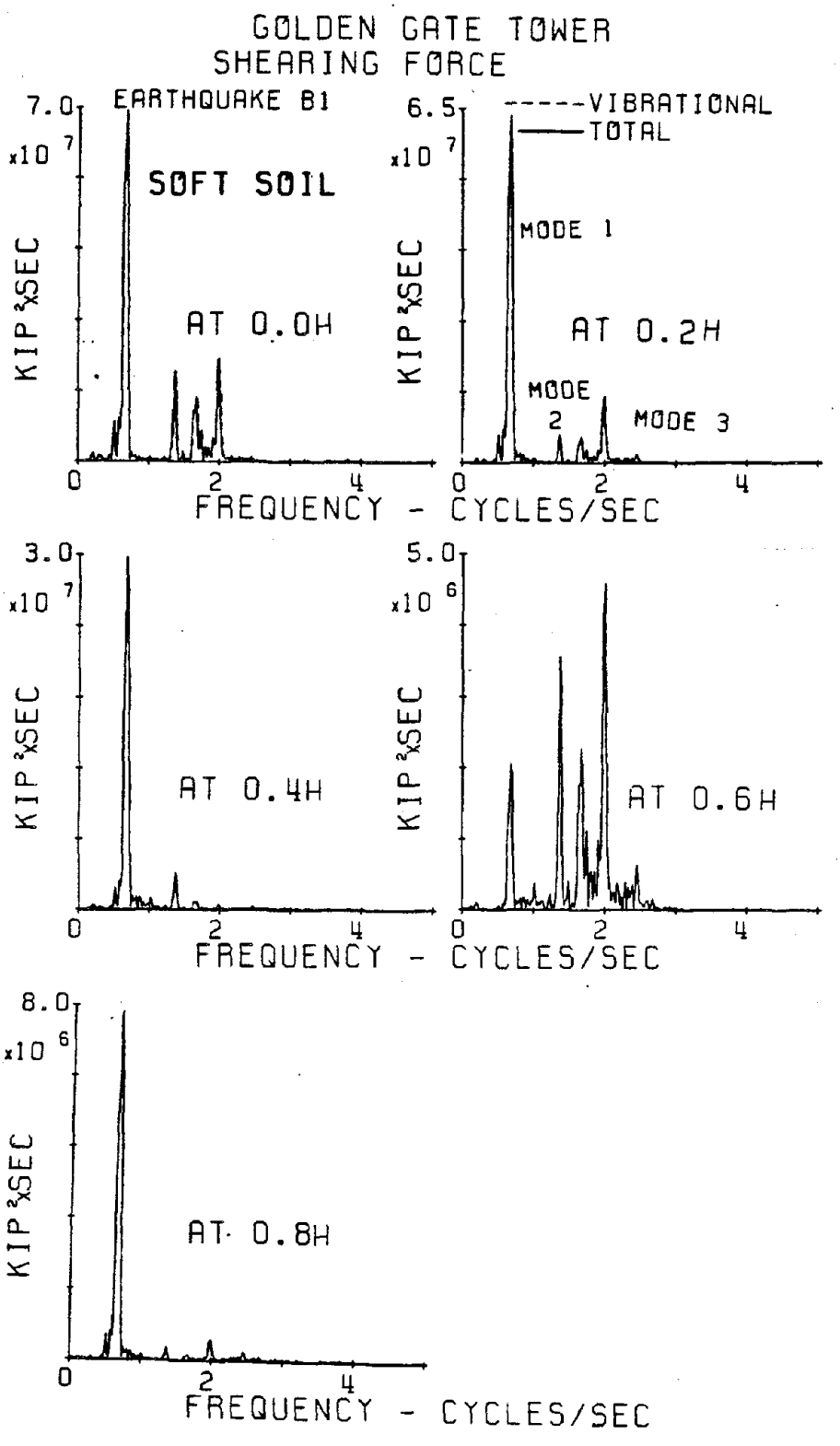

Fig. V-1-8 Power spectra of response shear forces to artificial earthquake B-1 input (Soft Soil Case).

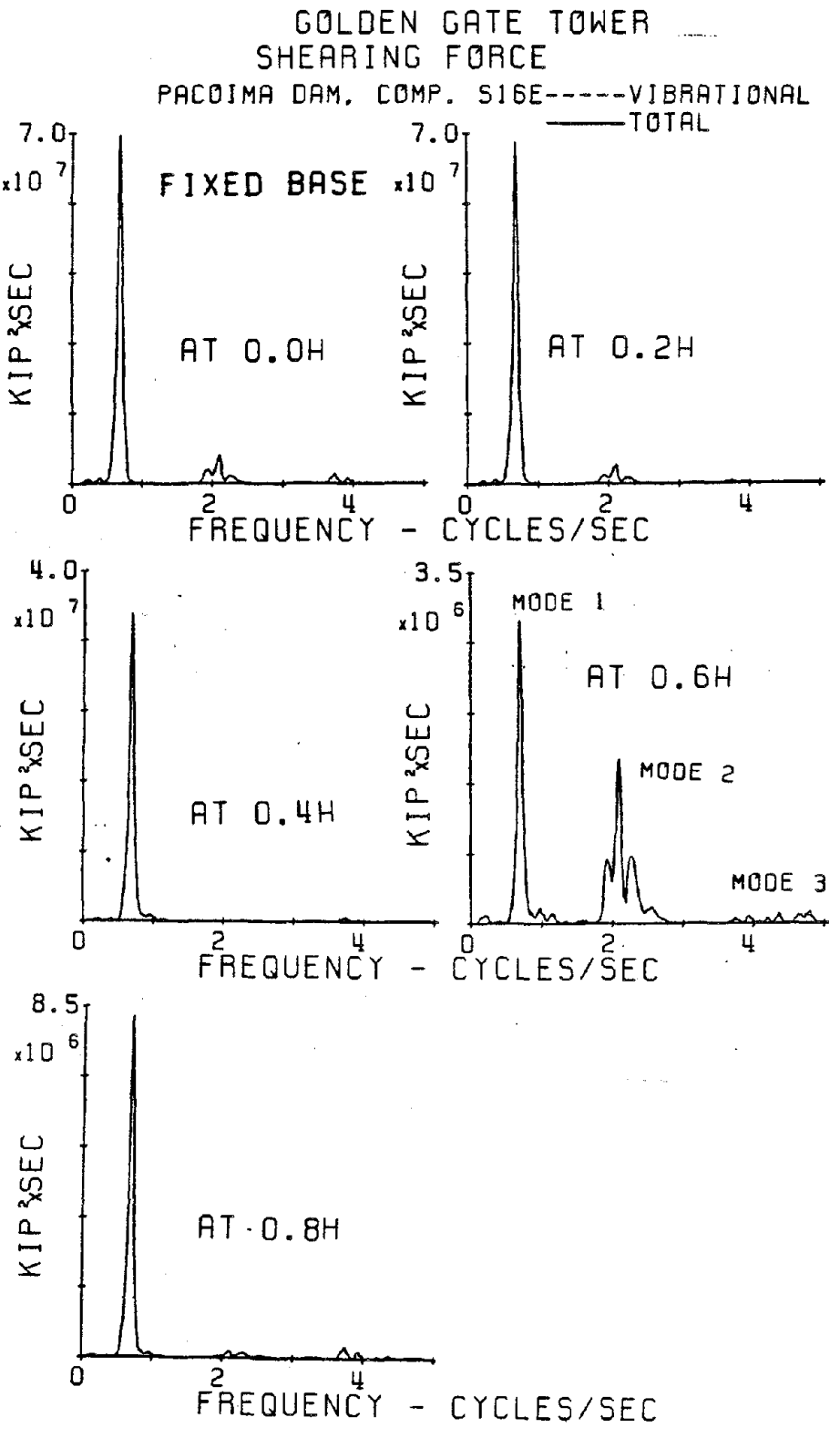

Fig. V-1-9 Power spectra of response shear forces to 1971 Pacoima Dam input (Fixed Base Case).

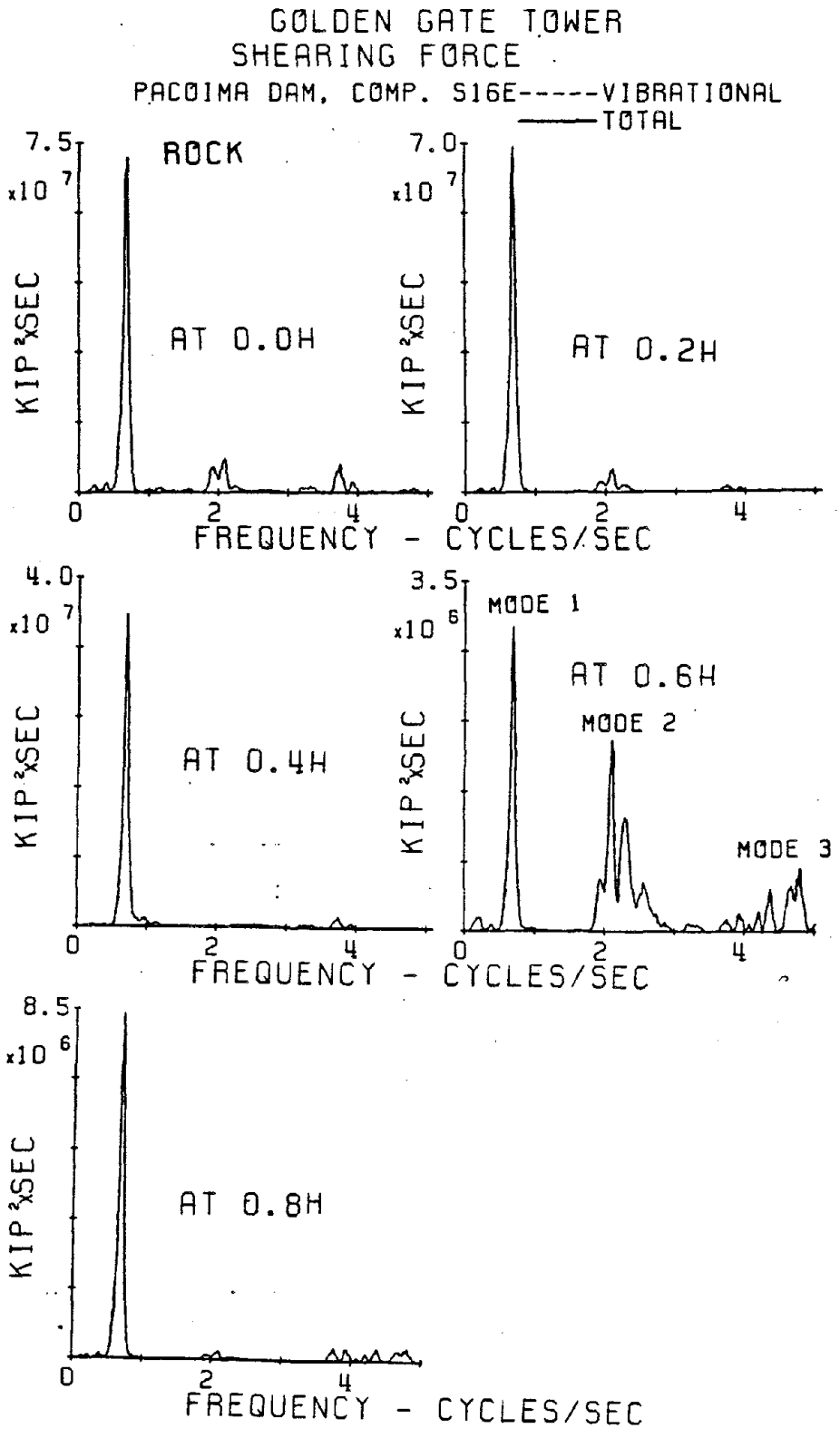

Fig. V-1-10 Power spectra of response shear forces to 1971 Pacoima Dam input (Rock Soil Case).

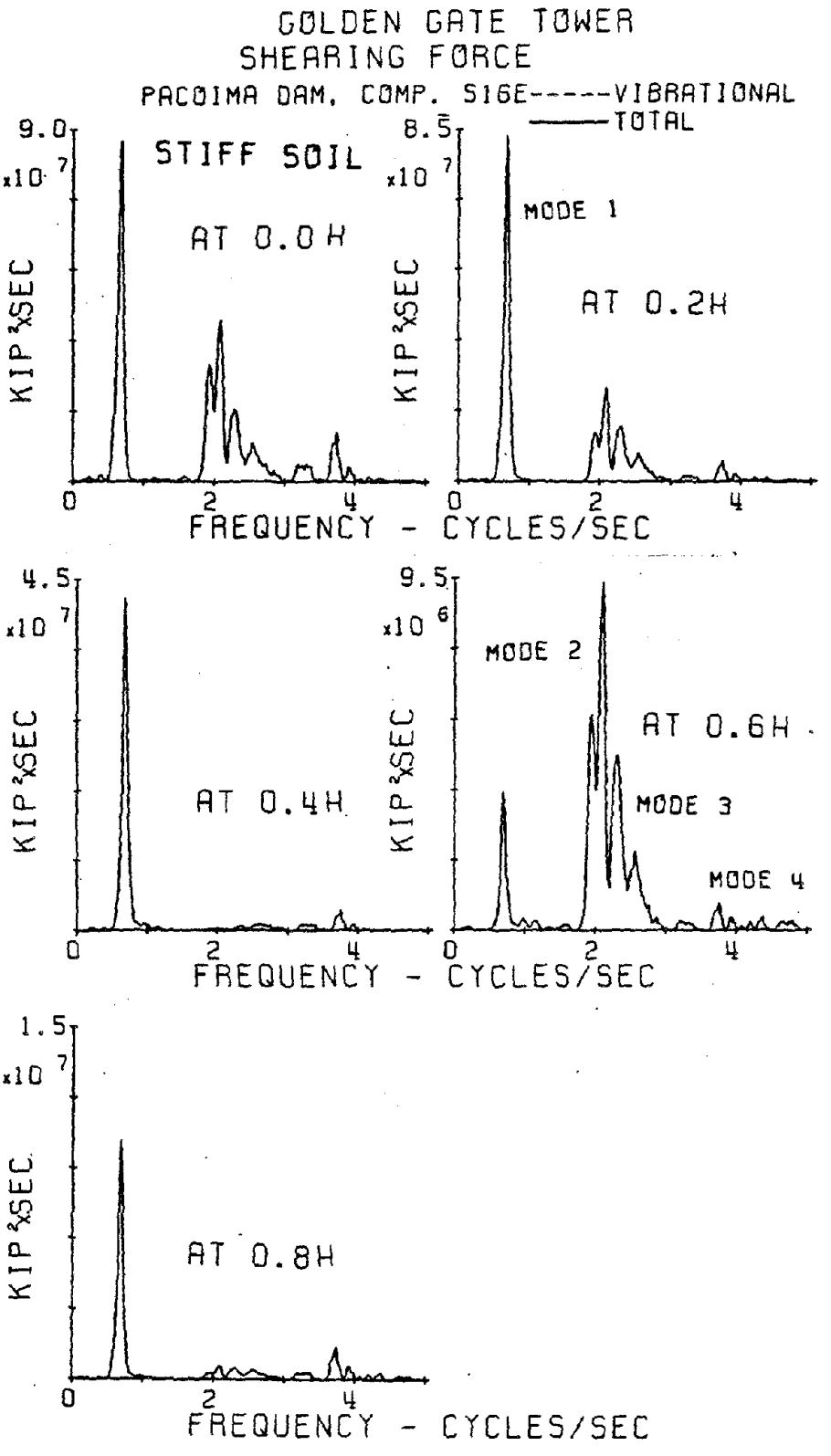

Fig. V-1-11 Power spectra of response shear forces to 1971 Pacoima Dam input (Moderately Stiff Soil Case).

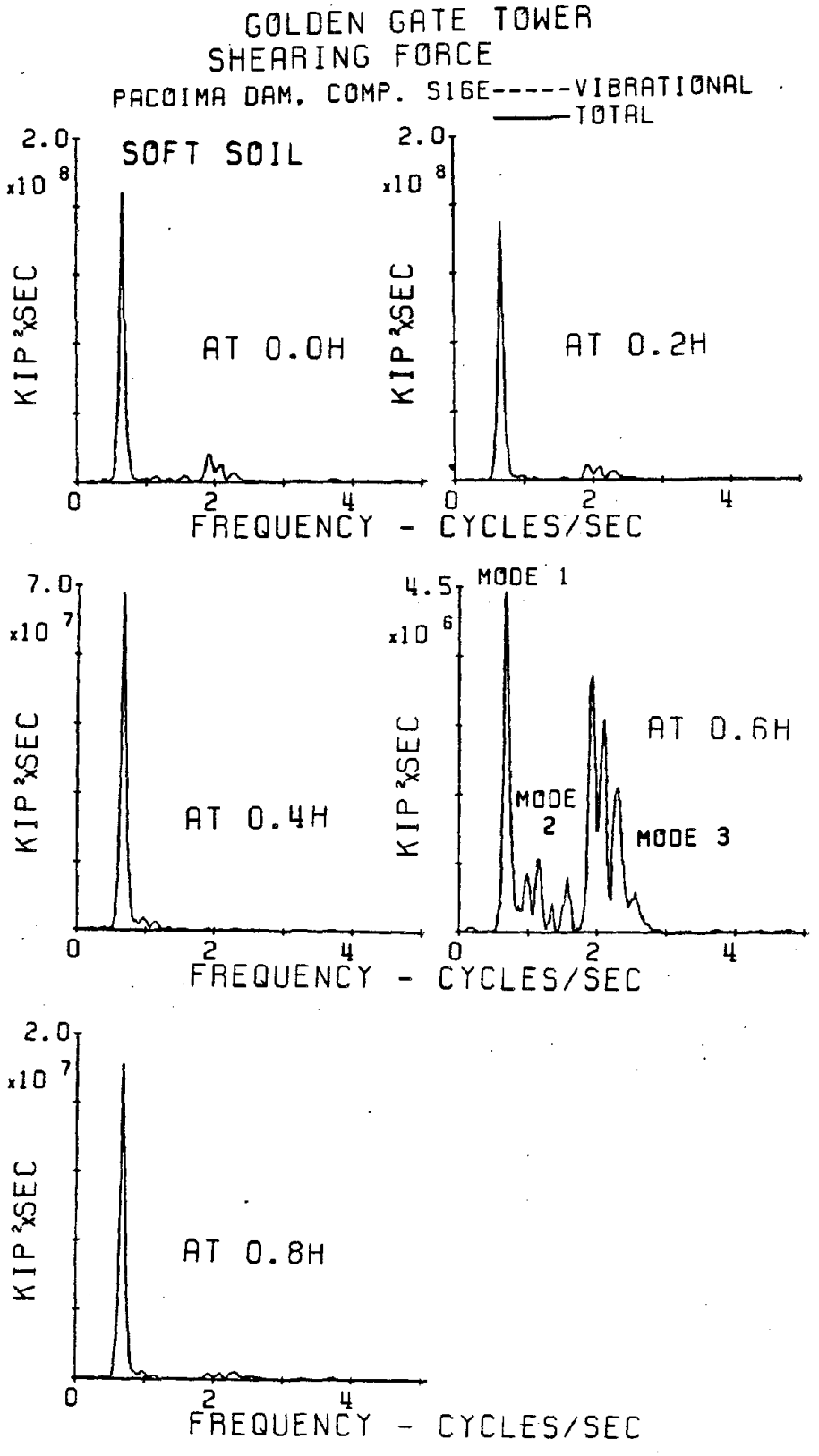

Fig. V-1-12 Power spectra of response shear forces to 1971 Pacoima Dam input (Soft Soil Case).

REFERENCES FOR CHAPTER V

1. Abdel-Ghaffar, Ahmed M., "Dynamic Analysis of Suspension Bridge Structures," Report No. EERL 76-01, Earthquake Engineering Research Laboratory, College of Engineering, California Institute of Technology, Pasadena, May 1976.

2. Abdel-Ghaffar, Ahmed M. and Rood, Joel D., "Simplified Earthquake Analysis of Suspension Bridge Towers," Journal of the Engineering Mechanics Division, ASCE, Vol. 108, No. EM2, April 1982, pp. 291-308.

3. Baron, F. and Hamati, E., "Effect of Non-Uniform Seismic Disturbances on the Dumbarton Bridge Replacement Structure," Report No. EERC 76-19, Earthquake Engineering Research Center, College of Engineering, University of California, Berkeley, July 1976.

4. Baron, F., Arikan, M., and Hamati, E., "The Effects of Seismic Disturbances on the Golden Gate Bridge," Report No. EERC 76-31, Earthquake Engineering Research Center, College of Engineering, University of California, Berkeley, November 1976.

5. Bendat, Julius S., and Piersol, Allan G., Engineering Applications of Correlation and Spectral Analysis, John Wiley and Sons, Inc., New York, 1980.

6. Beredugo, Y.O., "Modal Analysis of Coupled Motion of Horizontally Excited Embedded Footings," Earthquake Engineering and Structural Dynamics, Vol. 4, 1976, pp. 403-410.

7. Beredugo, Y.O. and Novak, M., "Coupled Horizontal and Rocking Vibration of Embedded Footings," Canadian Geotechnical Journal, Vol. 9, 1972, pp. 477-479.

8. Brady, A.G., Perez, V. and Mork, P.N., "The Imperial Valley Earthquake, October 15, 1979: Digitization and Processing of Accelerograph Records," U.S. Geological Survey, Seismic Engineering Branch, Open-File Report 80-703, April 1980, Menlo Park, California.

9. Jacobsen, Lydik S., "Impulsive Hydrodynamics of Fluid Inside a Cylindrical Tank and of a Fluid Surrounding a Cylindrical Pier," Bulletin of the Seismological Society of America, Vol. 39, 1949. pp. 189-204.

10. Jennings, P.C., Housner, G.W., and Tsai, N.C., "Simulated Earthquake Motions," Earthquake Engineering Research Laboratory, College of Engineering, California Institute of Technology, Pasadena, April 1968.

11. Jennings, P.C., "Engineering Features of the San Fernando Earthquake of February 9, 1971," Earthquake Engineering Research Laboratory Report No. EERL 71-02, College of Engineering, California Institute of Technology, Pasadena, California, June 1971.

12. Kausel, Eduardo, and Roesset, Jose M., "Dynamic Stiffness of Circular Foundations," Journal of the Engineering Mechanics Division, ASCE, Vol. 101, No. EM6, Proc. Paper 11800, December 1975, pp. 771-785.

13. Kausel, Eduardo, Whitman, Robert V., Morray, Joseph P., and Elsabee, Farid, "The Spring Method for Embedded Foundations," Nuclear Engineering and Design, Vol. 48, 1978, pp. 377-392.

14. Kennedy, R.P., et. al., "Non-linear Soil-Structure Interaction Due to Base Slab Uplift on the Seismic Response of HTGR Plant," Transactions of the 3rd International Conference on Structural Mechanics in Reactor Technology, Vol. 4, Paper K 3/5, 16, 1975.

15. Konishi, Ichiro, and Yamada, Yoshikazu, "Earthquake Response and Earthquake Resistant Design of Long Span Suspension Bridges," Proc. of III WCEE, Vol. III, IV-312, 1965.

16. Konishi, Ichiro, and Yamada, Yoshikazu, "Studies on the Earthquake Resistant Design of Suspension Bridge Tower and Pier Systems," Proc. of IV WCEE, 1969.

17. Newmark, N.M. and Rosenblueth, E., Fundamentals of Earthquake Engineering, Prentice-Hall, Englewood Cliffs, New Jersey, 1971. Chapter 6.

18. Novak, M., "Effect of Soil on Structural Response to Wind and Earthquake," Earthquake Engineering and Structural Dynamics, Vol. 3, 1974, pp. 79-96.

19. Novak, M., and Sachs, K., "Torsional and Coupled Vibrations of Embedded Footings," Earthquake Engineering and Structural Dynamics, Vol. 2, 1973, pp. 11-33.

20. Roesset, J.M., "Stiffness and Damping Coefficients of Foundations," Dynamic Response of Pile Foundations; Analytical Aspects, ASCE, O'Neill and Dobry, Editors, October 30, 1980, pp. 1-31.

21. Rood, Joel D., "Suspension Bridge Towers: Modeling for Seismic Design," Senior Thesis, Princeton University, Department of Civil Engineering, Structures and Mechanics Program, Princeton, New Jersey, April 1980.

22. Schonberg, William P., "Dynamic Response Characteristics of Embedded Tower-Foundation Systems," Senior Thesis, Princeton University, Department of Civil Engineering, Structures and Mechanics Program, Princeton, New Jersey, April 1981.

23. Takaoka, Nobuyoshi and Sato, Yuhji, "Influence of Rocking Motion of Tower Piers on the Earthquake Response of Long Span Suspension Bridge Towers," Transactions of the JSCE, Vol. 1, Part 2, 1969.

24. Yamada, Y., Takemiya, H., and Kawano, K., "Random Response Analysis of a Non-Linear Soil-Suspension Bridge Pier," Earthquake Engineering and Structural Dynamics, Vol. 7, 1979, pp. 31-47.

25. Yamada, Yoshikazu, and Takemiya, Hirokazu, "Studies on the Responses of Multi-Degree of Freedom Systems Subjected to Random Excitation with Applications to the Tower and Pier Systems of Long Span Suspension Bridges," Transactions of the JSCE, Vol. 1, Part 1, 1969.

26. The Golden Gate Bridge, Report of the Chief Engineer to the Board of Directors of the Golden Gate Bridge and Highway District, California. Published and copywrited by the Golden Gate Bridge and Highway District, January 1938.

27. "A Review of 'The Effects of Seismic Disturbances on the Golden Gate Bridge,' Report No. 76-31 by Frank Baron, Metin Arikan and Raymond E. Hamati, College of Engineering, University of California, Berkeley," by Amman and Whitney Consulting Engineers, December 1977.

28. Private correspondence from H.M. Irvine (University of Auckland, New Zealand, Civil Engineering Department) to A.M. Abdel-Ghaffar (California Institute of Technology, Pasadena, California), letter dated February 21, 1978.